PERFORMANCE OF MULTIPLE CORROSION PROTECTION SYSTEMS FOR REINFORCED CONCRETE BRIDGE DECKS

BY

Matthew O'Reilly

Submitted to the graduate degree program in Civil Engineering
and the Graduate Faculty of the University of Kansas in partial fulfillment
of the requirements for the degree of Doctor of Philosophy.

_____
Chairperson

_____

_____

_____

_____
Committee Members

Date Defended:_____

The Dissertation Committee for Matthew O'Reilly
certifies that this is the approved version of the following dissertation:

PERFORMANCE OF MULTIPLE CORROSION PROTECTION SYSTEMS FOR REINFORCED CONCRETE BRIDGE DECKS

_____
Chairperson

Date approved:_____

ABSTRACT

The performance of corrosion protection systems for reinforcing steel in concrete is evaluated. In addition to conventional and conventional epoxy-coated reinforcement, the corrosion protection systems tested include epoxy coatings with improved adhesion to the underlying steel, conventional and conventional epoxy-coated reinforcement used in conjunction with concrete containing one of three corrosion inhibitors, DCI-S, Rheocrete 222+, or Hycrete, epoxy-coated reinforcement with a microencapsulated calcium nitrite primer, multiple-coated reinforcement with a layer of zinc between the epoxy and steel, and pickled 2205 duplex stainless steel. The systems are evaluated using bench-scale and field tests. Two bridges in Kansas, cast with 2205 stainless steel, are monitored using corrosion potential mapping. Epoxy-coated and multiple-coated bars are evaluated to determine the effect of corrosion loss and time on the disbondment of the epoxy coating. Conventional, galvanized, and epoxy-coated reinforcement are evaluated using impressed current to determine the corrosion loss required to crack concrete for each system. A finite element model is developed to represent general and localized corrosion, and the results are used to develop a relationship between concrete cover, bar diameter, and area of bar corroding, and the corrosion loss required to crack concrete. An analysis of pore solutions expressed from cement pastes containing corrosion inhibitors is performed, with pH and selected ion concentrations measured from solutions collected one and seven days after casting. The results obtained from bench-scale and field test specimens are used to estimate cost effectiveness for each system under a 75-year service life.

The results show epoxy coatings significantly reduce the corrosion rate compared to conventional reinforcement. Corrosion inhibitors significantly reduce corrosion rates in uncracked concrete. In cracked concrete, corrosion inhibitors also reduce corrosion rates, but their relative effectiveness is reduced. Specimens containing Hycrete exhibit the lowest corrosion rates; however, field specimens containing Hycrete also show signs of scaling. Epoxies with improved adhesion exhibit no improvement over conventional epoxy-coated reinforcement in terms of corrosion rate or disbondment of the epoxy coating. Multiple-coated

reinforcement exhibits significantly less disbondment than epoxy-coated reinforcement. Pickled 2205 reinforcement exhibits the least corrosion among all systems tested.

Testing of conventional and galvanized reinforcement indicates galvanized reinforcement requires more than twice as much corrosion loss to crack the surrounding concrete compared to conventional reinforcement.

An analysis of pore solution extracted from cement pastes containing inhibitors indicates an elevated sulfate content in pore solution collected from specimens containing Hycrete. Increased sulfate levels may explain the reduced strength and critical chloride corrosion threshold observed in concrete containing Hycrete. Elevated sulfate levels are also observed in pore solutions collected 7 days after casting from cement paste containing Rheocrete.

An economic analysis of a 0.216-m (8.5-in.) thick bridge deck over a 75-year design life indicates that corrosion protection systems using either coated or stainless steel reinforcement are significantly more cost-effective than any of the systems containing conventional reinforcement..

Keywords: chlorides, concrete, corrosion, cracking, disbondment, epoxy-coated reinforcement, galvanized reinforcement, inhibitors, pore solution

ACKNOWLEDGEMENTS

I would like to sincerely thank my advisors, Dr. David Darwin and Dr. JoAnn Browning for their guidance and support, without which this research would not be possible. I would also like to thank my other committee members, Dr. Carl Locke, Dr. Stan Rolfe, and Dr. Adolfo Matamoros for their time and advice.

Special thanks to Dr. Ted Peltier for his assistance with the ion chromatography analysis, and to our laboratory technicians, Jim Weaver and Matt Maksimowicz, for their help and their time.

Funding for this research comes from the Federal Highway Administration and Kansas Department of Transportation. Material support is provided by LRM Industries (now Midwest Concrete Materials), Concrete Steel Reinforcing Institute, Valspar Corp., DuPont Powder Coatings, 3M Corporation, BASF Construction Chemicals, W. R. Grace & Co., Hycrete Technologies, and Western Coating, Inc. Many thanks to all of them.

I am grateful for all the graduate and undergraduate coworkers and friends whom I had the pleasure to work with over the course of this project. The best of luck to all of you. Last, but not least, thank you to all my friends and family for their continuing support.

TABLE OF CONTENTS

LIST OF TABLES

LIST OF FIGURES

CHAPTER 1

INTRODUCTION

1.1 GENERAL

Bridges are a vital part of the U.S. transportation system. As of 2007, there were 599,766 bridges in the United States. However, degradation from corrosion and other effects threaten the integrity of these structures. The damage caused by corrosion is significant; 72,524 bridges are classified as structurally deficient in the United States (FHWA 2007). Half of these bridges are deemed structurally deficient due to corrosion-related damage, with direct maintenance and repair costs estimated at $8.3 billion annually (Koch 2002). Indirect costs are estimated to be as much as ten times direct costs (Koch 2002).

Rapid increases in corrosion-related damage to bridge decks were noted in the early 1970s when the increasing use of deicing salts required maintenance to be performed in as few as 10 years (Manning 1996). To extend service life, designs were changed to incorporate increased concrete cover, higher quality concrete, and steel with an epoxy coating. After initial studies identified feasible coating materials (Clifton, Beeghly, and Mathey 1975), the introduction of epoxy-coated reinforcement was rapid, becoming the predominant corrosion protection system in the United States by 1981 (Ramniceanu 2008). With the changes, service life was extended to approximately 40 years (Weyers, Pyc, and Sprinkel 1998, Koch 2002), but epoxy-coated reinforcement remains far from the ideal solution (Koch 2002). Some doubts remain as to whether epoxy-coated reinforcement alone can achieve a 75 year target service life. Over time, the epoxy layer can degrade and lose adhesion to the underlying steel (a process known as disbondment), allowing underfilm corrosion to occur (Manning 1996, Ramniceanu 2008). This corrosion mechanism has caused premature damage to some structures. Several bridge piers in the Florida Keys built in the early 1980s suffered corrosion-related damage due to poorly applied epoxy (Manning 1996) and a bridge deck on I-81 in

Virginia suffered a closure strip failure due to localized corrosion of epoxy-coated reinforcement at a crack (Weyers, Ramniceanu, and Weyers 2009), although in the latter case it appears a particular design detail would have resulted in poor performance for any type of reinforcement.

As a result of the actual and perceived shortcomings of epoxy-coated reinforcement, corrosion protection systems continue to be developed with the goal of extending the service life of reinforced concrete bridge decks. These include improved adhesion of epoxy coatings to the reinforcing steel to minimize disbondment, the use of chemical admixtures that decrease the permeability of concrete and thus increase the time it takes for moisture and chlorides to reach the underlying steel, the use of corrosion inhibiting admixtures that interfere with the corrosion process, and corrosion resistant stainless steels. In general, these systems work by decreasing the permeability of concrete or increasing the resistance of the reinforcing steel to corrosion. The corrosion protection systems studied for this report are discussed in Section 1.7.

1.2 CORROSION MECHANISMS OF STEEL IN CONCRETE

Corrosion is a destructive chemical reaction between a metal and its environment (Jones 1996). For corrosion to occur, four components are required; an anode, a cathode, an electrical connection, and an ionic connection or electrolyte.

For reinforcing steel in concrete, corrosion begins with some site on the reinforcing steel acting as an anode. Here, solid iron is oxidized to its ionic form, releasing electrons.

$$Fe \rightarrow Fe^{2+} + 2e^{-} \quad (1.1)$$

The electrons given off by this reaction flow through the reinforcing steel to another location on the reinforcement. This location serves as the cathode and may be located on the same bar as the anode or a different bar if form ties and contact provide an

electrical connection. If oxygen and moisture are present at the cathode, oxygen is reduced producing hydroxyl ions.

$$2H_2O + O_2 + 4e^- \rightarrow 4OH^- \quad (1.2)$$

The hydroxyl ions migrate through the pore solution to the anode where they react with the ferrous ions [Eq. (1.1)] to form ferrous hydroxide.

$$Fe^{2+} + 2OH^- \rightarrow Fe(OH)_2 \quad (1.3)$$

In the high pH environment provided by concrete pore solution, steel is protected from further corrosion by the formation of a tightly-adhering γ-ferric oxyhydroxide layer [Eq. (1.4)]. This layer acts as a passive barrier against corrosion (Verbeck 1975).

$$4\ Fe(OH)_2 + O_2 \rightarrow 4\ \gamma\text{-}FeOOH + 2H_2O \quad (1.4)$$

This passive layer, however, can be disrupted through carbonation of the concrete or penetration by chlorides. The penetration of carbon dioxide into the concrete lowers the pH by neutralizing hydroxides in the pore solution (Verbeck 1975). If the pore solution pH becomes sufficiently low, the passive layer [Eq. (1.4)] will not form. Instead, ferrous hydroxide rapidly oxidizes in the presence of oxygen to form ferric oxide, or rust.

$$4Fe(OH)_2 + 2H_2O + O_2 \rightarrow 4Fe(OH)_3 \quad (1.5)$$

$$2Fe(OH)_3 \rightarrow 2Fe_2O_3 \cdot H_2O + 2H_2O \quad (1.6)$$

In the presence of chlorides, breakdown of the passive layer can occur, even in concrete with a high pH. Chlorides combine with the iron in the passive layer, forming a Fe-Cl complex [Eq. (1.7)]. This complex combines with water to form ferrous hydroxide [Eq. (1.8)], which forms ferric oxide [Eqs. (1.5) and (1.6)] and releases chloride ions that are again free to react with other ferrous ions, a process known as depassivation.

$$Fe^{2+} + 4Cl^- \rightarrow (FeCl_4)^{2-} \quad (1.7)$$

$$(FeCl_4)^{2-} + 2H_2O \rightarrow Fe(OH)_2 + 2H^+ + 4Cl^- \quad (1.8)$$

Research has shown that corrosion takes the form of either general or pitting corrosion on bare reinforcing steel and underfilm or crevice corrosion on epoxy-coated

steel (Weyers et al. 1998, Draper et al. 2009). For epoxy-coated reinforcement, the buildup of positively charged ferrous ions under disbonded portions of the epoxy coating is balanced by the migration of negatively charged chloride ions to the crevice. Corrosion can then occur under areas of disbonded coating in the absence of oxygen by reaction with water, with chlorides working to destabilize the passive layer.

$$[Fe^{2+}Cl_2^{2-}] + 2H_2O \rightarrow Fe(OH)_2 + 2[H^+Cl^-] \quad (1.9)$$

The production of hydrogen ions under the coating [Eq. (1.9)] makes the local environment acidic allowing the corrosion process to continue (Weyers et al. 1998).

Rust occupies several times the volume of solid steel (Verbeck 1975, Suda, Misra, and Motohashi 1993). When rust forms, it causes tensile stresses in the surrounding concrete, eventually leading to spalling and cracking.

The service life of a reinforced concrete bridge deck may be broken into two stages; the initiation phase and the corrosion phase. During the first phase, no corrosion occurs. Chlorides penetrate the concrete until they reach a level sufficient to depassivate the steel. Once this occurs, the steel will begin corroding. Eventually, the volume of the corrosion products will be sufficient to crack and spall the concrete cover, at which point maintenance or replacement of the bridge deck will be required. The chloride concentration needed to initiate corrosion and the corrosion losses needed to crack concrete are discussed in more detail in Sections 1.3 and 1.4, respectively.

1.3 CRITICAL CHLORIDE CORROSION THRESHOLD

The depassivation process shown in Eq. (1.7) and (1.8) requires a minimum concentration of chloride ions at the surface of the steel. This concentration is known as the critical chloride corrosion threshold. Research by Hartt and Nam (2008) and others (Hope and Ip 1987, Balma et al. 2005, Ann and Song 2007, Darwin et al. 2009, Draper et al. 2009, Xing, Darwin, and Browning 2010) show the threshold for corrosion initiation varies greatly and depends on many factors. Cement content and type, specifically

tricalcium aluminate (C_3A) content, has been found to have a strong impact on critical chloride threshold, with an increase in C_3A corresponding with an increase in critical chloride corrosion threshold (Hussain, Al-Gahtani, and Rasheeduzzafar 1996, Oh, Yang, and Shin 2003). The availability of oxygen and moisture at the level of the reinforcement also affects corrosion initiation, with a lack of these elements delaying the onset of corrosion (ACI Committee 222 2001). The critical chloride threshold also increases as the alkalinity of the concrete increases (Hartt and Nam 2008). Research indicates that corrosion preferentially initiates at air voids adjacent to the reinforcing steel in the concrete (Ryou and Ann 2008); as such, the presence of significant air voids can lower the measured critical corrosion threshold. Ryou and Ann (2008) also found that the use of supplementary cementious materials, such as fly ash, ground granulated blast furnace slag, or silica fume lowered the critical chloride threshold; however, for ground granulated blast furnace slag, other research has shown improvements in the critical chloride threshold level (Schiessl and Breit 1996).

Several methods exist for both measuring and reporting the critical chloride corrosion threshold. Because chlorides do not progress uniformly through concrete, the sampling and analysis methods used impact the value obtained. As most aggregates are impermeable to chlorides, aggregate particles will halt the ingress of chlorides, which then must move around the aggregate to continue advancing (Yu and Hartt 2007b). As a result, the aggregate distribution near the chloride sampling site will alter the chloride level measured. Ji, Darwin, and Browning (2005) took twenty samples of concrete at the depth of reinforcement from each of three prismatic beam specimens containing conventional reinforcement and found that chloride contents at corrosion initiation varied by as much as a factor of four. Furthermore, the reinforcing steel itself has been found to act as a barrier to chloride ingress, causing chlorides to build up over the top of the reinforcement (Kranc, Sagues, and Presuel-Moreno 2002, Yu and Hartt 2007a). Yu and Hartt (2007a) found the chloride concentration over the top of reinforcing bars to be 1.9

to 3.8 times greater than chloride levels at the same depth away from the bar. Thus, cores taken to determine chloride levels will underestimate the level of chlorides at the bar. In spite of this observation, chloride contents away from the reinforcement still provide valuable information about the condition of the concrete and can serve as a measure of the corrosion threshold. As a result, critical chloride corrosion thresholds are frequently measured using prismatic beam specimens with chloride levels sampled away from the reinforcement (Ann and Song 2007). Studies that attempt to find critical chloride corrosion thresholds for steel subjected to a uniform chloride content, either using bare bars in simulated pore solution or chloride internally mixed into the concrete, generally report values greater than those obtained when chlorides are applied externally and diffuse through the concrete (Ann and Song 2007, Ryou and Ann 2008). These greater values are unconservative; admixed chlorides more readily bind with C_3A in plastic concrete and chloride addition to a simulated pore solution does not reflect the buildup of chlorides over the reinforcing bar that affects field measurements.

Chloride levels in concrete may be expressed in terms of free or total chloride content, also known as water-soluble and acid soluble content, respectively. As chlorides enter the concrete, some percentage will bind with C_3A in the cement matrix. Chlorides bound in this manner are not able to depassivate the reinforcement and do not contribute to the corrosion process while bound. The remaining unbound chlorides are free to react with the passive layer on the reinforcement (Ann and Song 2007). The free chloride content represents only those chlorides that are not bound by the cement matrix. Total chloride content, or acid-soluble chloride content, includes both bound and unbound chlorides. Data presented in this report will be based on the water soluble (free) chloride content.

Numerous studies have been undertaken to determine the critical chloride corrosion threshold for steel in concrete. In early work, Hausmann (1967) expressed the critical chloride threshold in terms of the ratio of chloride ions to hydroxyl ions and

obtained a value of 0.6. Ann and Song (2007) analyzed results from numerous studies and found critical chloride corrosion thresholds in terms of the $[Cl^-]/[OH^-]$ ratio ranging from 0.3 to 63. Ann and Song claimed this wide variation was a result the inability of the $[Cl^-]/[OH^-]$ ratio to account for the changing binding capacity of the concrete as the pH varies.

Ann and Song also collected results from studies reporting chloride contents as a percentage of cement mass. In seven studies based on water soluble chloride content, values of the critical chloride corrosion threshold ranged from 0.07 to 0.36 percent, with most values falling between 0.1 and 0.2 percent by mass of cement. For a typical concrete mixture containing 360 kg/m^3 (600 lb/yd^3) of cement, this represents a free chloride content ranging from 0.36 to 0.72 kg/m^3 (0.6 to 1.2 lb/yd^3). Ann and Song also analyzed nineteen studies reporting acid soluble chloride content and found values for the critical chloride corrosion threshold ranging from 0.1 to 2.9 percent by mass of cement, with most values falling between 0.5 and 1.5 percent. Research by Balma et al. (2005) compared water-soluble and acid-soluble chloride contents for 45 chloride samples. For chloride contents greater than 0.6 kg/m^3 (1 lb/yd^3), the ratio of measured water-soluble chloride content to measured acid-soluble chloride content was very consistent, with an average ratio of 0.96 and values ranging between 0.9 and 1.0. For samples with chloride contents less than 0.6 kg/m^3 (1 lb/yd^3), the ratio of measured water-soluble chloride content to measured acid-soluble chloride content ranged from 0.52 to 1.31 with an average of 0.8. At the lower chloride contents, a large percentage of the chlorides were introduced during the mixing process – chloride contents after mixing were found to be as high as 0.3 kg/m^3 (0.5 lb/yd^3). Internally mixed chlorides are more easily bound by C_3A, leading to an increase in bound or acid soluble chlorides and a greater difference between water-soluble and acid-soluble chloride contents. At higher concentrations, most of the chloride was from external sources, with a lower percentage binding to C_3A.

Chloride contents presented in this report are expressed in terms of kg/m^3 (lb/yd^3) of concrete.

1.4 CORROSION LOSS FOR CONCRETE CRACKING

The high volume of corrosion products compared to uncorroded steel causes tensile stresses in the surrounding concrete, eventually cracking and spalling the concrete cover. The amount of corrosion loss required to spall concrete depends on many factors, including the concrete cover over the reinforcement, the reinforcement diameter, bar spacing, the tensile strength and elastic modulus of the concrete (Cady and Weyers 1992), and the length of the corroding region (Torres-Acosta and Saguez 2004). A number of studies have been performed to determine the relative importance of these factors in a relationship with the corrosion loss required to crack concrete.

Research by Alonso et al. (1997) used two series of prism specimens. The Series 1 specimens were 150 x 150 x 380 mm (6 x 6 x 15 in.). Bar diameters ranged from 3 to 16 mm (0.125 to 0.625 in.), and concrete cover ranged from 10 to 70 mm (0.40 to 2.75 in.). Calcium chloride (3% by weight of cement) was added to the concrete to depassivate the steel, and a current density of 100 μA/cm^2 was applied to the test bar to drive corrosion. The average corrosion loss along the full length of the bar at crack initiation was compared to the cover-to-bar diameter ratio, which was considered to be the most important factor in crack initiation. The results yielded the relationship

$$x_{crit} = 7.53 + 9.32 \, c/\phi \tag{1.10}$$

where

x_{crit} = corrosion loss at crack initiation, μm

c = concrete cover, mm (in.)

ϕ = bar diameter, mm (in.)

Most structures have a cover-to-bar diameter ratio between 2 and 3. Experimental results from specimens tested with cover-to-bar diameter ratios in this range had critical corrosion losses ranging from 15 to 35 μm. The derived expression, Eq. (1.10), predicts critical corrosion losses of 28 μm for a cover-to-bar diameter ratio of 2 to 35 μm for a cover-to-bar diameter ratio of 3 (Alonso et al. 1997), indicating a reasonably good fit between the derived formula and the experimental results.

Alonso also studied the effect of corrosion rate and concrete quality on the critical corrosion loss using a second series of slab specimens 300 mm (12 in.) on a side. The concrete cover over the bars was 25 mm (1 in.), and the bar diameter was 16 mm (0.625 in.). Applied corrosion current densities of 100 $\mu A/cm^2$, 10 $\mu A/cm^2$, and 3 $\mu A/cm^2$ were used; the latter two current densities are in the range observed in in-service structures subject to corrosion. To vary concrete quality, water/cement ratios between 0.52 and 0.65 were used. Alonso found that neither corrosion rate nor concrete quality had any effect on the corrosion loss required to initiate a crack. The observation that corrosion rate did not affect crack initiation is not a surprise because the tensile stress needed to crack concrete is a function of the buildup of corrosion products around the reinforcement, independent of rate of formation. Concrete quality is also expected to have little effect on crack initiation; research by Darwin et al. (2001) found that the fracture energy of concrete, the energy required to form a crack of unit area, is independent of concrete strength and water/cement ratio. After initiation, however, both corrosion rate and concrete quality had an effect on the rate of crack growth. Specimens with greater applied current densities showed less crack growth at a given corrosion loss than specimens with lower applied current densities. Alonso believed this behavior to be analogous to that observed in tensile testing, where a greater rate of load application results in a greater resistance. Alonso also found that as the water/cement ratio increased, the rate of crack growth decreased. This was attributed to the increased porosity of the higher water/cement ratio concrete providing more room for the corrosion products to

expand into. Furthermore, the lower modulus of elasticity of lower strength concrete results in greater compliance (lower stiffness) of the concrete, which would result in increased local deformation and a lower tendency to crack.

Maaddawy and Soudki (2003) also found that the corrosion rate has no effect on the corrosion loss required for crack initiation. However, contrary to Alonso, Maaddawy and Soudki found that greater current densities increased crack width at a given mass loss. This research used current densities that were greater than those used by Alonso (100-500 $\mu A/cm^2$), possibly explaining the discrepancy.

Alonso's work focused on the general corrosion of a bare steel bar in concrete; however, when epoxy-coated reinforcement corrodes, the corrosion is limited to small damage sites on the bar. Torres-Acosta and Sagues (2004) studied the effects of localized steel corrosion on the corrosion loss required to crack concrete. Two series of specimens were tested. The first series consisted of cylindrical specimens with a 21 mm (0.875 in.) test bar centered along the axis of the cylinder, providing uniform cover on all sides of the bar. Localized exposed metal lengths ranged from 19.1 to 346 mm (0.75 to 13.5 in.) and concrete cover ranged from 27.6 to 65.7 mm (1.1 to 2.6 in.). The second series consisted of 140 mm x 140 mm x 406 mm (5.5 in. x 5.5 in. x 16 in.) prismatic specimens with 6 mm or 13 mm (0.25 in. or 0.5 in.) test bars. Exposed lengths of steel ranged from 8 to 390 mm (0.3 to 15.4 in.) and cover ranged from 13 to 45 mm (0.5 to 1.75 in.). An applied current density of 100 $\mu A/cm^2$ was used.

Based on the results from the 36 specimens in the study as well as 31 specimens from other studies, Torres-Acosta and Sagues derived an expression relating bar cover, bar diameter, and localized corrosion length with the corrosion loss required for crack initiation.

$$x_{crit} = 11.0 \frac{c}{\phi}\left(\frac{c}{l}+1\right)^2 \tag{1.11}$$

where

x_{crit} = corrosion loss at crack initiation, μm

c = cover, mm

Φ = bar diameter, mm

l = length of exposed steel, mm

It should be noted that the smallest exposed length tested was 8 mm (0.3 in.), much larger than the size of a typical defect or holiday on epoxy-coated reinforcement. Holidays are defined by ASTM A775 as defects not visible to a person with normal or corrected vision. ASTM A775 also sets a limit on visible defects at 1 percent of bar area and requires these defects to be patched. Miura, Itabashi, and Iwaki (1997) studied the size of defects on epoxy-coated reinforcement measured after a bridge deck was constructed in Japan and found that with rough handling, the maximum defect size was 60 mm^2 (0.093 $in.^2$), equivalent to a 8.7 mm (0.34 in.) diameter hole. When reinforcing bars were handled with the care typically afforded epoxy-coated bars, defect size did not exceed 20 mm^2 (0.031 $in.^2$), equivalent to a 5.0 mm (0.20 in.) diameter hole (Miura et al. 1997), much smaller than the damage region examined by Torres-Acosta and Saguez. Regardless, it is clear from the above equation that localized corrosion requires a greater material loss on the exposed area to cause cracking than a bar experiencing general corrosion.

In the limiting case of general corrosion where the exposed length is large compared to cover, Eq. (1.11) reduces to

$$x_{crit} = 11.0\, c/\phi \tag{1.12}$$

For cover to bar-diameter ratios between 2 and 3, Eq. (1.12) predicts critical corrosion losses between 22 μm and 33 μm, similar to the Alonso model.

1.5 EFFECT OF CRACKS IN CONCRETE ON CORROSION

In most bridge decks, cracks first form in the concrete as the result of causes other than corrosion-related damage. Drying shrinkage, settlement, and thermal changes can all induce cracks in a bridge deck (Lindquist et al. 2006). These cracks are of concern because they provide a direct path for oxygen, moisture, and chlorides to reach the reinforcement and initiate corrosion. A study of Kansas bridge decks has shown that, while the chloride content at the level of reinforcement in uncracked concrete remained below the critical chloride corrosion threshold after 12 years of service for most decks, the critical chloride corrosion threshold for conventional steel was exceeded in cracked concrete within two years, and often within the first year (Lindquist et al. 2006). This can result in the immediate onset of corrosion, sometimes to a severe extent. The failure of a closure strip on a bridge deck on I-81 was attributed to the corrosion of epoxy-coated reinforcement at the site of a crack, with some epoxy-coated bars exhibiting up to 84 percent section loss (Weyers et al. 2009). In this case, a poor closure strip design allowed relative movement of the concrete on either side of the closure pour. This allowed chlorides and moisture to directly reach the reinforcement through a gap exceeding 0.25 mm (0.010 in.) between the closure strip and the remainder of the bridge deck resulting in severe attack on a localized area of reinforcement. A study of 80 bridge decks in Iowa built with epoxy-coated reinforcement included an evaluation of cores containing reinforcement from both cracked and uncracked concrete (Fanous and Wu 2005). While no bars from uncracked concrete showed signs of corrosion, many bars located where the concrete cover had cracked did. Furthermore, it was discovered that epoxy-coated reinforcement in cracked concrete showed a greater rate of adhesion loss than reinforcement in uncracked concrete.

Even narrow cracks may pose a significant problem if they reach the level of reinforcing steel. Rodriguez and Hooton (2003) observed that for smooth and rough-

walled cracks ranging in width from 0.08 mm to 0.68 mm (0.0031 to 0.0268 mils), the rate of chloride diffusion is independent of crack width or roughness.

1.6 CORROSION MONITORING AND MEASUREMENTS

Corrosion monitoring of reinforcing steel in concrete structures poses unique challenges. The reinforcing steel is hidden from direct view, making direct visual inspection of the reinforcement impossible. Surfaces may be monitored for signs of staining and spalling, but by the time these become visible at the surface, significant corrosion damage will have already occurred. As such, other methods are needed to monitor corrosion. Corrosion monitoring methods used in this study are described below.

1.6.1 Corrosion Potential

Corrosion of metal is the oxidation of the metal to an ionic form. The tendency for the oxidation process to occur depends on the thermodynamic stability of the base metal relative to its ionic form. The difference in stability for a given metal in a specific environment is the corrosion potential. For a given set of environmental conditions, a more negative corrosion potential indicates a greater tendency for corrosion.

Corrosion potentials are measured with respect to an electrode of known properties, known as a reference electrode. The standard reference electrode is a standard hydrogen electrode (SHE), which consists of purified hydrogen gas bubbled over platinum foil in a 0.5 molar sulfuric acid solution. The need for a purified hydrogen source and a strong acid, however, make the standard hydrogen electrode impractical for most measurements. Two common electrodes used in the lab and field are the saturated calomel electrode (SCE) and the copper-copper sulfate electrode (CSE). The saturated calomel electrode consists of mercurous chloride on a liquid mercury pool in a saturated potassium chloride solution. Readings with a SCE will be 0.241 volts more negative than readings taken with a standard hydrogen electrode. A copper-copper sulfate electrode consists of a copper rod immersed in a saturated copper sulfate solution and is favored for

field use due to its simple and durable design (Jones 1996). Readings taken with a copper-copper sulfate electrode will be 0.318 volts more negative than readings taken with a standard hydrogen electrode.

It is important to note that corrosion potential measurements only reveal the likelihood of corrosion; they do not provide information on corrosion rate. ASTM C876 provides guidelines for taking and interpreting corrosion potential measurements on uncoated reinforcing steel in the field. The guidelines provided by ASTM C876 for interpreting corrosion potentials are summarized in Table 1.1 below.

Table 1.1: ASTM C876 Corrosion Potential Interpretation

Measured Potential (V)		**Corrosion Activity**
SCE	**CSE**	
> –0.125	> –0.200	>90% probability corrosion is not occurring
–0.125 to –0.275	–0.200 to –0.350	corrosion activity uncertain
<–0.275	<–0.350	>90% probability corrosion is occurring

Potential measurements may be affected by interference from both stray currents and high concrete resistivity (Jones 1996). Factors such as the presence of chloride ions in the concrete, the moisture content of the concrete, and the presence of oxygen can cause variations in potential readings as large as 0.150 V (Schiegg, Buchler, and Brem 2009). Variations can be minimized by taking steps to decrease resistivity, such as wetting the concrete prior to readings. Epoxy-coated reinforcement by design will have a high resistivity and as such the values in Table 1.1 are not applicable to epoxy-coated steel.

1.6.2 Macrocell Corrosion Rate

The corrosion process requires an electrical connection between the anode and the cathode and involves the flow of electrons between the two. If the anode and cathode are on different reinforcing bars, the result is macrocell corrosion. If the anode and cathode are located on the same bar, the result is termed microcell corrosion and will be discussed in the next section.

The flow of electrons from the anode to the cathode creates a current that may be measured to determine corrosion rate. Corrosion may be expressed as a current density ($\mu A/cm^2$) or as a loss of material at the surface (μm/year). Faraday's Law may be used to convert between current density and material loss:

$$R = k\frac{ia}{nF\rho} \tag{1.13}$$

where

R = corrosion rate, μm/year

k = conversion factor, $315360\ \frac{A \cdot \mu m \cdot s}{\mu A \cdot cm \cdot yr}$

i = current density, $\mu A/cm^2$

a = atomic weight of the corroding metal, g/mol

n = number of electrons lost per atom of metal oxidized

F = Faraday's constant, 96,485 Coulombs/equivalent

ρ = density of metal, g/cm^3

For iron, a = 55.85 g/mol, n = 2, and ρ = 7.87 g/cm^3. Eq. (1.13) simplifies to

$$R = 11.6i \tag{1.14}$$

For zinc, a = 65.38 g/mol, n = 2, and ρ = 7.13 g/cm^3. Eq. (1.13) simplifies to

$$R = 15.0i \tag{1.15}$$

By measuring the current flowing between the cathode and the anode, the macrocell corrosion rate of the reinforcement may be determined. This is usually impractical for bridge decks; numerous electrical connections exist where mats of steel touch, either directly or through bar ties or chairs, and all connections would need to be monitored to determine total current flow. In a laboratory, however, such a measurement becomes practical. Typically, the anode bar will be kept in a corrosion-inducing environment, whereas the cathode will be placed in an inert environment. This may be accomplished by many means; a common method used in ASTM G109 and other tests involves using top and bottom mats of steel in a concrete slab. Chloride, applied via the top surface, reaches the top mat of steel while the bottom mat remains passive. An electrical connection is established via external wiring through which current may be measured. To measure current, a resistor is placed in series between the anode and cathode and the voltage drop across the resistor measured. The corrosion current density can be calculated using Ohm's Law [Eq. (1.16)].

$$i_{\text{corr}} = 10^{-6} \times \frac{V}{RA} \tag{1.16}$$

where

i_{corr} = current density, μA/cm^2

V = measured voltage drop across resistor, volts

R = resistance, ohms

A = surface area of anode, cm^2

Macrocell corrosion rate as a measure of corrosion has its limitations. It can only be used in laboratory specimens where electrical connections can be easily monitored. It also will not detect corrosion where the anode and cathode are on the same bar, as electrons will not flow through the resistor.

1.6.3 Linear Polarization Resistance (LPR)

Linear polarization resistance (LPR) provides a method for determining the total corrosion rate (macrocell and microcell) of a metal by measuring its response to an applied voltage (polarization). With no externally applied voltage, a metal will corrode with a current density i_{corr} and a potential E_{corr}. Forcing the potential to shift by an amount $\Delta\varepsilon$ will cause the current to shift by some amount Δi. The polarization resistance is defined as the slope of the potential-current function, also known as the polarization curve (Jones 1996).

$$R_p = \left[\frac{\Delta\varepsilon}{\Delta i}\right]_{\varepsilon\to 0} \tag{1.17}$$

where

R_p = polarization resistance

$\Delta\varepsilon$ = imposed potential change

Δi = current density change caused by $\Delta\varepsilon$

For small changes in potential, the polarization curve is linear. In this region, the polarization resistance is inversely proportional to the corrosion current density.

$$i_{corr} = \frac{\beta_a \beta_c}{2.3R_p(\beta_a + \beta_c)} \tag{1.18}$$

where

β_a, β_c = anodic and cathodic Tafel constants, V/decade

R_p = polarization resistance

The polarization resistance may be determined by taking a series of current density measurements at a range of potential shifts and measuring the resultant current, or by applying a range of currents to the sample and measuring the resultant voltage shifts. Plotting the data and finding the slope of the linear region yields R_p [Eq. (1.15)]. The corrosion current density may then be found using Eq. (1.18). Values of 0.12 V/decade

for both the anodic and cathodic Tafel constants β_a and β_c have been shown to give a linear region for the polarization curve over a region of approximately ±10 mV with respect to E_{corr}. Using these values in Eq. (1.18) yields

$$i_{corr} = \frac{0.026}{R_p} \tag{1.19}$$

This form [Eq. (1.19)] is used to determine corrosion current densities for all LPR data presented in this report.

1.7 CORROSION PROTECTION SYSTEMS

The onset of corrosion may be delayed by using deicers without chlorides, applying protective coatings to the steel, using membranes on the concrete surface, increasing concrete cover, decreasing concrete permeability, and using corrosion-resistant reinforcement (Vassie 1996, Kepler, Darwin, and Locke 2000). The corrosion protection systems used in this study are discussed below.

1.7.1 Epoxy-Coated Reinforcement (ECR)

Epoxy-coated reinforcement (ECR) was first investigated as a potential corrosion protection system in the mid-1970s in response to the rapid deterioration of numerous bridge decks exposed to deicing salts. Clifton et al. (1975) examined 47 different coatings, 36 of which were epoxy. The coatings were tested for chemical resistance, durability, flexibility, consistency of application, and effect on bond strength. The study found that powder-based epoxies provided better overall performance than either liquid-based epoxies or other plastic coatings and deemed them a viable corrosion control system.

Epoxy coatings protect the steel from corrosion in multiple ways. First, coatings are nonconductive, preventing an electrical connection from forming between bars. It should be noted, however, that microcell corrosion is still possible. Second, epoxy

coatings act as a barrier to oxygen, moisture, and chlorides, preventing them from reaching the underlying steel.

The corrosion performance of epoxy-coated reinforcement has been generally positive. A study by Treadaway and Davies (1989) showed that epoxy-coated reinforcement performed significantly better than conventional reinforcement. Slabs with chlorides added to the plastic concrete were exposed to atmospheric conditions for five years and examined at end of life. The slabs containing conventional steel exhibited moderate cracking over reinforcement and corrosion potentials of all the bars indicated active corrosion. The slabs containing epoxy-coated reinforcement exhibited no cracking and most bars had corrosion potentials more positive than the threshold for active corrosion. Other studies have shown similar results, with epoxy-coated reinforcement significantly improving the service life of structures compared to uncoated bars (McDonald et al. 1996, Fanous and Wu 2005). Research has shown epoxy-coated reinforcement with a damaged coating exhibits less than 1 percent of the corrosion loss exhibited by conventional steel (Draper et al. 2009).

Two concerns have been raised with the use of epoxy-coated reinforcement: damage to the epoxy coating and the loss of adhesion of the epoxy. Epoxy coatings often have small imperfections in the coating called holidays. These holidays expose a very small area of the underlying steel, allowing localized corrosion to occur. The coating may also be damaged during shipment and placement of the reinforcement. A study (Samples 1998) found epoxy-coated reinforcement sustained an average of 40 defects per meter (12.2 defects per foot) of bar from shipping, bar placement, and concrete placement, with an average of 75 percent of those defects being introduced during the concrete placement. Defects are difficult to properly repair once the reinforcement has been placed (Reed et al. 2003) and impossible to repair after concrete is in place; thus every bridge deck using epoxy-coated reinforcement will have coating defects. These damage sites will act as small anodes, leading to underfilm corrosion and, in some cases,

blistering. Corrosion at these damage sites has, in some cases, led to poor performance of epoxy-coated reinforcement (Manning 1996).

Studies have also shown that epoxy-coated reinforcement is subject to a loss of adhesion of the epoxy layer to the steel, causing disbondment (Manning 1996, Weyers et al. 1998, Ramniceanu 2008, Draper et al. 2009). Bridges constructed in the Florida Keys with the first generation of epoxy-coated reinforcement began cracking and spalling as early as seven years after construction (Manning 1996). The cause of this damage was found to be disbonded epoxy coatings, aggravated by bending of the epoxy-coated bars and local damage sites. Disbonded coatings can allow crevice or underfilm corrosion to occur. The pH of the solution under the epoxy can drop to as low as 5, further accelerating the corrosion of the underlying steel (Weyers et al. 1998). A study estimating the service life of bridges constructed with epoxy-coated reinforcement in Virginia estimated that only 5 percent of the bridge decks in that state would benefit from epoxy-coated reinforcement due to disbondment of the epoxy coating after 6 to 13 years of service (Weyers et al. 1998). A survey of six bridge decks with epoxy-coated reinforcement in Indiana, however, found no signs of disbondment after 18 years of service (Hasan, Ramirez, and Cleary 1995).

In this study, epoxy-coated reinforcement is evaluated and compared with conventional steel. Three types of reinforcement designed to have increased adhesion between the epoxy and steel are also evaluated: bars that received a chromate pretreatment prior to coating and bars with proprietary coatings from DuPont and Valspar.

1.7.2 Galvanized and Multiple-Coated Reinforcement

Zinc coatings can be used to protect steel. Like an epoxy-coating, zinc acts as a barrier to moisture and chlorides; however, no electrical insulation is provided. Zinc is also thermodynamically more active than iron; as a result it will corrode preferentially to iron. In a corrosive environment, zinc will act as a sacrificial anode, providing cathodic

protection to the steel even if the underlying steel is exposed due to damage to the zinc coating.

In concrete, zinc reacts with the highly alkaline pore solution in concrete (Freedman 1970), forming a calcium zincate salt and hydrogen gas.

$$Zn + Ca(OH)_2 + 2H_2O \rightarrow CaZn(OH)_4 + H_2 \quad (1.20)$$

The behavior of the zincate salt depends on the pH of the concrete (Macias and Andrade 1987). Below a pH of 13.3, the zincate salt forms a stable passive layer. Above a pH of 13.3, the zincate forms large crystals that do not protect the reinforcing steel. In either case, evolution of hydrogen gas can increase the permeability of the surrounding concrete. Therefore, most galvanized bars are treated with chromate or coated with an organic coating both to prevent hydrogen formation and to protect the zinc in high pH environments (Freedman 1970). The presence of chlorides will cause the passive layer to break down in a manner similar to that of iron.

Studies examining the effectiveness of galvanized bars in preventing corrosion have been mixed. The study by Treadaway and Davies (1989) mentioned earlier also examined galvanized reinforcement and found that slabs cast with galvanized reinforcement exhibited significantly more cracking than slabs cast with conventional steel. Research by Saraswathy and Song (2005), in which four types of galvanized reinforcement were tested in accordance with ASTM G109, found only one performed better than conventional steel. However, Haran et al. (2000) showed that, while the corrosion rate of the zinc layer of galvanized reinforcement in the presence of chlorides was greater than that of conventional steel, the corrosion of the underlying reinforcement was delayed. A study examining the critical chloride corrosion threshold of galvanized reinforcement found that galvanized steel had an average critical chloride corrosion threshold of 1.52 kg/m^3 (2.57 lb/yd^3) compared to 0.97 kg/m^3 (1.63 lb/yd^3) for conventional reinforcement (Darwin et al. 2009).

Limited research has been done on multiple-coated reinforcement with a layer of zinc underneath a layer of epoxy. A study comparing ECR and multiple-coated bars in simulated pore solution (Lau and Sagues 2009) found that after an initial period of high corrosion rates, multiple-coated bars showed corrosion rates comparable to ECR, with slightly less disbondment of the multiple-coated bars at the end of the test.

The performance of multiple-coated reinforcement is evaluated in this study. In addition, the corrosion loss of galvanized reinforcement required to crack concrete is evaluated and compared to conventional steel.

1.7.3 Corrosion Inhibitors

Admixtures, both inorganic and organic, have been developed with the goal of delaying the onset of corrosion or slowing the corrosion rate. These admixtures work in one of three ways: interfering with the anodic reaction [(Eqs. (1.5) and (1.6)], interfering with the cathodic reaction [Eq. (1.2)], or slowing the rate of chloride and moisture ingress by decreasing the permeability of the concrete. The corrosion inhibitors used in this study are described below.

1.7.3.1 Calcium Nitrite (Darex Corrosion Inhibitor-DCI)

Calcium nitrite is a corrosion inhibitor that helps stabilize the passive layer of steel. The nitrite ions encourage the formation of the γ-ferric oxyhydroxide layer as shown in Eq. (1.21) (Civjan et al. 2003).

$$Fe^{2+} + OH^- + NO_2^- \rightarrow \gamma\text{-}FeOOH + NO \qquad (1.21)$$

In addition to forming a passive layer, calcium nitrite competes with chloride ions for ferrous ions, preventing them from being converted to ferric oxide [Eqs (1.5) and (1.6)]. Calcium nitrite is effective in reasonably small amounts; research in the late 1980s (Hope and Ip 1989) established a threshold chloride to nitrite ion ratio between 11.1 and 14.3, above which corrosion will proceed.

The effectiveness of calcium nitrite does not appear to be based on the pH of the pore solution because research has shown that calcium nitrite lowers the pH of the pore

solution in concrete (Li, Sagues, and Poor 1999). In the study, the pH of the pore solution in specimens with and without calcium nitrite was monitored over time. Specimens were cured at 100% relative humidity for 9 days, after which holes were drilled into the specimens, 0.4 mL deionized water injected into the holes, and the holes stoppered. Pore solution leached into the water allowing the pH to be monitored over time. The pore solution of specimens with no calcium nitrite had an average pH of 13.0 after curing for nine days, with a peak pH of 13.5 at day 25 of the test. The pore solution of specimens with calcium nitrite had a pH of 12.8 after curing with a peak pH of 13.2 at 25 days.

Studies examining the effectiveness of calcium nitrite have yielded positive results. One study examined five reinforced concrete piers in Hawaii cast with a calcium nitrite inhibitor (Bola and Newtson 2005). Dosages of calcium nitrite (concentration not specified in the paper) ranged from 12.4 to 22.3 L/m^3 (2.5 to 4.5 gal/yd^3). Polarization resistance measurements on each pier indicated high corrosion rates (> 1µA/cm^2) on less than 5 percent of the surface area for all structures, with the majority of the surface area of the structures exhibiting low to no corrosion. The pier receiving the highest dosage of calcium nitrite showed no regions of high corrosion, despite being subjected to the worst exposure conditions. Other research used simulated pore solution and slabs designed to simulate bridge decks and piers to compare the effectiveness of calcium nitrite and other inhibitors (Pyc et al. 1999). Specimens containing calcium nitrite exhibited significant increases in the time to corrosion initiation, 70 weeks compared to 37 weeks for control specimens. A study by Xing et al. (2010) found specimens with a calcium nitrite inhibitor had a critical chloride corrosion threshold of 1.59 kg/m^3 (2.69 lb/yd^3) compared to 0.96 kg/m^3 (1.62 lb/yd^3) for specimens with no inhibitor.

In addition to serving as a corrosion inhibitor, calcium nitrite acts as a set accelerator. To counteract this, calcium nitrite based inhibitors are often combined with a set retarder. For this study, the performance of Darex Corrosion Inhibitor (DCI-S), a

calcium nitrite inhibitor with a set retarder manufactured by W.R. Grace, is examined. Epoxy-coated reinforcement with a primer containing microencapsulated calcium nitrite under the epoxy is also evaluated. In addition, a pore press analysis of cement pastes containing DCI and other inhibitors in this study is performed.

1.7.3.2 Rheocrete 222+

Rheocrete 222+ is a water-based organic corrosion inhibitor composed of amines and esters. Rheocrete protects steel by adsorption of the amines on the surface of the reinforcement, where it forms a protective film. The esters in Rheocrete react [Eqs (1.22) and (1.23)] to form insoluble salts that decrease the permeability of concrete (Soylev and Richardson 2008). R and R' represent different hydrocarbon chains.

$$RCOOR' \text{ (ester)} + OH^- \rightarrow RO_2^- + CR'OH \quad (1.22)$$

$$2\ RO_2^- + Ca(OH)_2 \rightarrow Ca(RO_2)_2 + 2\ OH^- \quad (1.23)$$

The formation of the insoluble calcium salt [Eq. (1.22)] blocks the pores in concrete which, in turn, decreases the rate of chloride penetration, increasing the time until the critical chloride corrosion threshold is reached (Nmai, Farrington, and Bobrowski 1992).

Research involving Rheocrete 222+ is limited and has had mixed results. Pyc et al. (1999) tested Rheocrete and other inhibitors in a simulated pore solution and in concrete slabs with 25 mm (1 in.) cover ponded with a 6% NaCl solution. Rheocrete was used at a rate of 5 L/m^3 (1 gal/yd^3). Reinforcement was oriented both vertically and horizontally to simulate reinforcement in bridge piers and decks. Specimens containing Rheocrete showed no improvement in critical chloride threshold or time to corrosion initiation compared to control specimens, with corrosion initiating at 30 weeks for specimens with Rheocrete inhibitor compared to 37 weeks for control specimens. In another study, Rheocrete was tested at a dosage rate of 5 L/m^3 (1 gal/yd^3) in Southern Exposure and cracked beam tests (discussed in Chapter 2). In this case, Rheocrete increased the time to corrosion initiation from 63 to 252 days in uncracked concrete and from 5 to over 180 days in cracked concrete (Nmai et al. 1992). An analysis of research

by Soylev and Richardson (2008) found that while Rheocrete and other organic inhibitors delayed the onset of corrosion, there was no significant effect on corrosion rate; however they noted that other studies contradicted this finding (Nmai et al. 1992, Batis, Pantazopoulou, and Routoulas 2003). Nmai et al. (1992) and Xing et al. (2010) noted a reduction in strength of approximately 10 percent for concrete containing Rheocrete compared to concrete with no inhibitor. No other significant adverse effects on material properties were observed.

1.7.3.3 Hycrete DSS

Hycrete DSS (disodium tetrapropenyl succinate) is an organic inhibitor marketed by Hycrete, Inc. The mechanism of corrosion protection is similar to that of Rheocrete. The polar end of the molecule attaches to the steel and stabilizes the passive layer, while a hydrophobic hydrocarbon repels water, decreasing the tendency for moisture to enter the concrete (Wojakowski and Distlehorst 2009).

Hycrete DSS was first evaluated in the laboratory by Goodwin, Frantz, and Stephens (2000). Test specimens consisted of 76 x 152 mm (3 x 6 in.) cylinders with a No. 13 (No. 4) reinforcing bar centered in the cylinder. The Hycrete dosage rate ranged from 0.5 to 2 percent by weight of cement. The cylinders were subjected to alternating ponding and drying cycles, with 4 days submerged in a 15% salt solution followed by 3 days of drying. After 100 days, uncracked specimens containing Hycrete (all dosages) showed almost no chlorides at the level of reinforcement. Uncracked specimens with no inhibitor showed over 1 percent chlorides by weight of cement at the level of reinforcement, above the critical chloride corrosion threshold for conventional steel. No corrosion was observed for uncracked specimens containing Hycrete, and corrosion rates for cracked specimens with Hycrete were significantly reduced compared to similar specimens without Hycrete. A reduction in compressive strength was observed for all specimens containing Hycrete, ranging from 12 percent for specimens with 0.5 percent by weight of cement to 31 percent for specimens with 2 percent by weight of cement.

Other research (Gong, Darwin, and Browning 2006, Xing et al. 2010) noted reductions in strength of 52 percent for specimens with 2.5 percent Hycrete by weight of cement. Xing et al. (2010) noted a significant reduction in critical chloride corrosion threshold, with specimens with Hycrete having a critical chloride corrosion threshold of 0.37 kg/m^3 (0.63 lb/yd^3) compared to 0.96 kg/m^3 (1.62 lb/yd^3) for specimens with no inhibitor. The time to corrosion initiation, however, was significantly increased, with specimens containing Hycrete initiating corrosion at 28.5 weeks compared to 14.2 weeks for specimens with no inhibitor.

Other research using Southern Exposure and cracked beam specimens showed similar results (Civjan et al. 2003). Hycrete was dosed at 0.5 percent by weight of cement, and the specimens were tested for 108 weeks. In uncracked concrete, both Hycrete and calcium nitrite showed significant improvements compared to control specimens; in cracked concrete, however, only Hycrete had a significant effect. A negative impact on strength was noted in this study as well.

Based on these results, the Kansas Department of Transportation investigated the use of Hycrete DSS in a bridge deck in Elk County, Kansas (Wojakowski and Distlehorst 2009). Trial batches showed that while the early-age strength of the concrete containing Hycrete was comparable to similar concrete without Hycrete, the long-term strength was significantly reduced (Figure 1.1). The strength of the Hycrete mix did, however, exceed the design strength of 27 MPa (4000 psi).

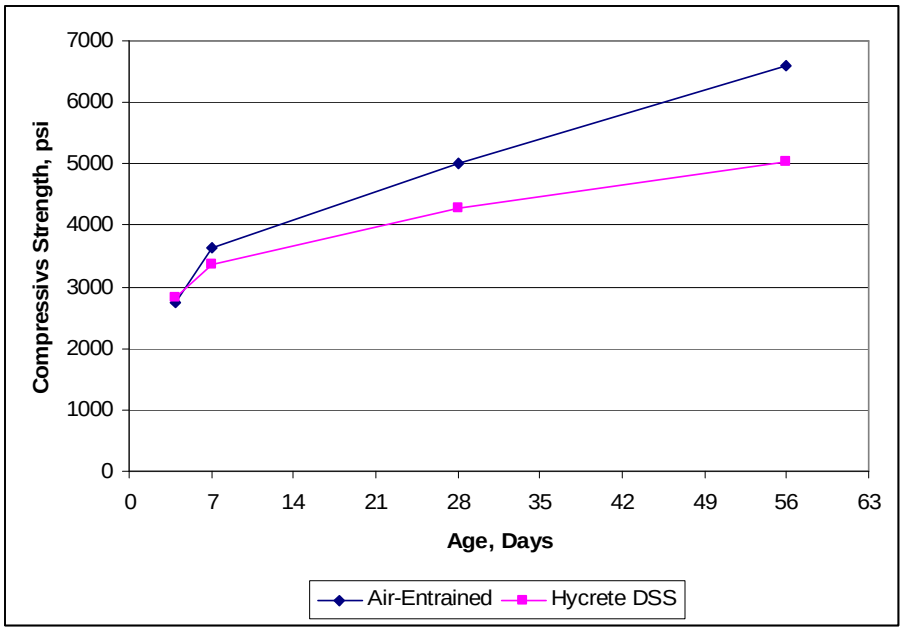

Figure 1.1: Compressive Strength of Concrete with Hycrete Inhibitor and Control Mix

Two bridge decks, one with and one without Hycrete, were cast in Elk County in late August and early September 2004. Bridge dimensions were similar. To more rapidly obtain corrosion data, uncoated conventional steel test bars designed to have 25 mm (1 in.) cover were placed in both bridge decks in addition to the epoxy-coated reinforcement [designed with 50 mm (2 in.) cover]. Actual cover over the test bars in the control bridge averaged 35 mm (1.4 in.), while cover over the test conventional bars on the bridge with Hycrete inhibitor averaged 45 mm (1.75 in.). Cover over the epoxy-coated reinforcement exceeded 63 mm (2.5 in.). Corrosion potentials of the bars showed that the bars in concrete containing Hycrete had more positive potentials than the bars in the control deck, although neither showed signs of active corrosion after 4 years of service. In the control bridge deck, significant cracking was observed parallel to and above the test bars, likely due to the decreased cover. In the bridge with Hycrete inhibitor, significant transverse cracking was observed in negative moment regions. KDOT estimated at the time of formwork removal the compressive strength of the concrete in the bridge deck containing Hycrete to be less than 14 MPa (2000 psi).

1.7.4 Stainless Steels

Stainless steels are steels alloyed with a minimum of 11 percent chromium (ASTM A955). Chromium forms a thin stable passive layer on the surface of the steel. The stability of this layer is further improved with the addition of nickel. To encourage the formation of the passive layer, it is common practice to wash the steel in an acid solution to cause oxidation of the metal, a process called pickling. Stainless steels are classified based on their grain structure as martinsitic, austenitic, ferritic, or duplex (austenite and ferrite).

Stainless steels, particularly austenitic stainless steels, have performed very well in corrosion tests in concrete. One study tested Type 405 (12% Cr, < 0.5% Ni) and 430 (17% Cr, < 0.75% Ni) ferritic stainless steel reinforcement as well as Type 316 (17% Cr, 12% Ni) austenitic stainless steel reinforcement, using concrete prisms containing 0.96% and 3.2% chlorides added by weight of cement (Treadaway, Cox, and Brown 1989). The ferritic stainless steels showed modest improvements in corrosion resistance compared to conventional steel, with earliest pitting in concrete with 0.96% added chlorides after 1 year and moderate pitting after 3 years. However, Type 316 steel exhibited no visible corrosion after 10 years, even in the concrete with 3.2% chlorides by weight of cement.

Duplex steels have also been shown to perform very well. Tests of duplex 2101 (21% Cr, 1% Ni) and 2205 (22% Cr, 5% Ni) reinforcing steel in Southern Exposure, cracked beam, and simulated pore solution tests (Balma et al. 2005) showed that, in the pickled state, both duplex steels exhibited average corrosion losses between 0.3% and 1.3% of those observed in conventional steel. Without pickling, the 2205 bars performed slightly worse than pickled 2205 steel, but the 2101 bars without pickling performed significantly worse, with corrosion losses between 6.5% and 8.5% of those observed in conventional steel. Further testing of pickled 2101 and 2205 stainless steel bars using Southern Exposure and cracked beam specimens sought to establish a critical chloride corrosion threshold (Ji et al. 2005). The 2101 steel exhibited a critical chloride corrosion

threshold of 14.0 kg/m^3 (23.5 lb/yd^3). No pickled 2205 specimens had initiated corrosion at the writing of the report, so it could only be established that the critical chloride corrosion threshold exceeded 12.5 kg/m^3 (22.6 lb/yd^3).

One major drawback limiting the use of stainless steels in bridge decks is initial cost. When the Missouri Department of Transportation constructed a bridge deck with stainless steel in 2003, they found the cost of stainless steel reinforcement was three times that of epoxy-coated reinforcement and four times that of black steel (Wenzlick and Yin 2003).

To reduce the cost, stainless clad reinforcement – conventional steel with a stainless steel cladding – has become available. Like all bars with coatings, clad stainless steel is subject to damage that can detrimentally affect corrosion resistance. Hartt et al. (2009) tested solid and clad stainless steel (Type 316) in concrete prisms under a cyclic 1 week ponding–1 week drying cycle using 15% NaCl solution. The clad bars were tested in an undamaged condition as well as with damage caused by bending the bar and by intentionally drilling holes through the cladding. The undamaged clad bars performed similarly to solid stainless steel; neither initiated corrosion during the test period (994 days). Bars with holes in the cladding in cracked concrete initiated corrosion immediately. Bent bars cast in uncracked concrete with no cap protecting the cut end of reinforcement, leaving conventional steel exposed, initiated corrosion between 130 and 239 days, with corrosion initiating at the cut end. An earlier study by Darwin et al. (1999) had similar results. In that study, Type 304 clad stainless steel and conventional steel bars were tested in a simulated concrete pore solution with a 1.6 m ion sodium chloride solution. No. 19 (No. 6) bars were tested bare and encased in mortar cylinders, 30 to 33 mm (1.18 to 1.5 in.) in diameter. Corrosion rates for undamaged 304 clad steel with the cut ends protected were 1% to 5% that of conventional steel. However, in cases where the cut end was exposed to the chlorides, the behavior of 304 clad steel was similar to conventional steel. Darwin et al. (2007) tested stainless clad reinforcement using

Southern Exposure and cracked beam specimens. The clad reinforcement was tested in the undamaged condition, as well two damaged conditions: one with four 3-mm (0.125-in.) diameter holes drilled through the cladding and one with the clad bar bent 180 degrees about a 51-mm (2-in.) pin. In uncracked and cracked concrete, undamaged stainless steel clad reinforcement exhibited no measurable corrosion loss. Damaged clad bars, however, exhibited active corrosion in both uncracked and cracked concrete, with corrosion losses ranging from 1.5 to 4.5 percent of those observed in specimens with conventional reinforcement.

In this study, solid pickled 2205 reinforcement is evaluated.

1.8 OBJECTIVES AND SCOPE

The purpose of this study is to evaluate the effectiveness of multiple corrosion protection systems and compare their performance to corrosion protection systems used in current practice. The following systems are included in this study:

1. Conventional steel and conventional epoxy-coated reinforcement, serving as controls.
2. Corrosion inhibitors added to the concrete in conjunction with conventional steel reinforcement. The corrosion inhibitors tested are calcium nitrite with a set retarder (DCI-S), Rheocrete 222+, and Hycrete.
3. Corrosion inhibitors added to the concrete in conjunction with epoxy-coated reinforcement. Corrosion inhibitors tested are as listed above. In addition, an epoxy-coated reinforcement with a primer containing microencapsulated calcium nitrite under the epoxy coating was tested in concrete with no added inhibitor.
4. Multiple-coated steel reinforcement – epoxy-coated reinforcement with a 0.05-mm (2-mil) thick coating consisting of 98% zinc and 2% aluminum underneath the epoxy coating.

5. Epoxy-coated reinforcement with increased adhesion between the reinforcement and epoxy. Three types of bars are tested: bars that received a chromate pretreatment prior to coating and bars with proprietary coatings from DuPont and Valspar.
6. Epoxy-coated reinforcement with increased adhesion in conjunction with concrete with DCI-S inhibitor.
7. Galvanized reinforcement.
8. 2205 pickled stainless steel.

The epoxy coating on all epoxy-coated reinforcement is 3M™ Scotchkote™ 413 fusion-bonded epoxy, except the epoxy coating used on multiple coated bars, which is DuPont 8-2739 (flex west blue).

The performance of the corrosion protection systems is evaluated using Southern Exposure, cracked beam, field test specimens, and bridge deck surveys. Tests to monitor corrosion are described in Chapter 2. Corrosion activity is monitored using macrocell corrosion rate readings (1.6.2) and corrosion potential (1.6.1). Selected specimens are monitored using linear polarization resistance measurements (1.6.3). Mat-to-mat resistance and chloride contents are also recorded.

In addition, the corrosion loss required to cause cracking for conventional, galvanized, and epoxy-coated reinforcement is evaluated using test methods described in Chapter 4. Analysis of pore solution expressed from cement pastes containing corrosion inhibitors is discussed in Chapter 5.

CHAPTER 2

EXPERIMENTAL WORK

2.1 GENERAL

Corrosion protection systems examined for this study were tested using Southern Exposure (SE), cracked beam (CB), corrosion initiation beam (B), field test (FTS) and rapid macrocell (M) specimens. Pickled 2205 duplex stainless steel is also being evaluated in two bridge decks in Kansas; bridge no. 7-22-18.21(004) in Doniphan County (DCB) and bridge no. 4-89-4.58(281) in Mission Creek (MCB). This work is the continuation of earlier research reported by Ji et al. (2005), Guo, Darwin, and Browning (2006), Gong et al. (2006), Draper et al. (2009), and Xing et al. (2010).

A description of each test method, including fabrication and testing procedures, appears in the following sections. In addition, Southern Exposure and field test specimens were sampled for chlorides. Sampling procedures for chloride analysis are described in Section 2.3.6.

2.2 SYSTEMS STUDIED

A detailed list of corrosion protection systems, including reinforcing bars and corrosion inhibitors, appears below.

2.2.1 Reinforcement

Conv. – Conventional steel, first heat. Chemistry and mechanical properties appear in Tables 2.1 and 2.2, respectively.

Conv.2 – Conventional steel, second heat. Chemistry and mechanical properties for this heat of steel are not available.

ECR – Epoxy-coated reinforcement

ECR(Ca(NO$_2$)$_2$) – ECR with a microencapsulated calcium nitrite primer applied to the base metal prior to the application of epoxy

ECR(Valspar) – ECR with increased adhesion to the base steel, developed by Valspar

ECR(DuPont) – ECR with increased adhesion to the base steel, developed by DuPont

ECR(Chromate) – ECR with increased adhesion to the base steel, accomplished via a chromate pretreatment applied prior to application of the epoxy.

MC – Multiple-coated reinforcement; reinforcement with a 0.05 mm (2 mil) layer of 98% zinc, 2% aluminum underneath a layer of DuPont 8-2737 (flex west blue) epoxy.

Zn – Galvanized reinforcement, average thickness 0.150 mm (6 mil), without a chromate treatment.

2205p – Pickled 2205 duplex stainless steel reinforcement. Chemistry and mechanical properties appear in Table 2.1 and 2.2, respectively.

Except as noted above, coating on all epoxy-coated reinforcement is 3M™ Scotchkote™ 413 fusion-bonded epoxy.

Table 2.1 – Chemical compositions of pickled 2205 (2205p) stainless steel and conventional steel.

Steel[a]	Bar No.	Heat No.	C	Mn	Si	P	S	CR	Ni	Mo	Cu	N	B
DCB-2205p	16 (5)	150694	0.02	1.72	0.41	0.021	0.001	21.53	4.85	2.60	0.19	0.16	-
DCB-2205p	13 (4)	150692	0.02	1.80	0.47	0.023	0.004	21.30	4.67	2.65	0.22	0.16	-
MCB-2205p	16 (5)	150876	0.02	1.75	0.47	0.024	0.003	21.55	4.75	2.59	0.26	0.16	0.0025
MCB-2205p	13 (4)	150863	0.02	1.73	0.42	0.027	0.003	21.54	4.72	2.59	0.22	0.18	0.0027
Conv.	16 (5)	231159	0.43	0.95	0.21	0.014	0.046	0.200	0.17	0.038	0.49	-	0.0005

[a] DCB-2205p = 2205 pickled stainless steel for the Doniphan County Bridge.
MCB-2205p = 2205 pickled stainless steel for the Mission Creek Bridge.
Conv. = conventional steel.

Table 2.2 – Mechanical properties of 2205p stainless steel and conventional steel

Stee[a]	Bar No.	Heat No.	Yield Strength		Tensile Strength		Elongation (%)
			(MPa)	(ksi)	(MPa)	(ksi)	in 203 mm (8 in.)
DCB-2205p	16 (5)	150694	632	91.5	1255	182.0	28.0
DCB-2205p	13 (4)	150692	655	95.0	848	123.0	25.0
MCB-2205p	16 (5)	150876	627	91.0	848	123.0	25.0
MCB-2205p	13 (4)	150863	717	104.0	883	128.0	25.0
Conv.	16 (5)	231159	442.7	64.2	713.6	103.5	15.0

[a] DCB-2205p = 2205 pickled stainless steel for the Doniphan County Bridge.
MCB-2205p = 2205 pickled stainless steel for the Mission Creek Bridge.
Conv. = conventional steel.

2.2.2 Corrosion Inhibitors

DCI – Darex Corrosion Inhibitor (DCI-S), a calcium nitrite inhibitor manufactured by W.R. Grace. A set retarder in added to counteract the effects of calcium nitrite as an accelerator. Dosage rate = 15 L/m^3 (3 gal/yd^3). Designation DCI.

Rheocrete – Rheocrete 222+, a water-based solution of esters and amines manufactured by BASF, Inc. Dosage rate = 5 L/m^3 (1 gal/yd^3). Designation RH.

Hycrete – Hycrete DSS (disodium tetrapropenyl succinate), manufactured by Hycrete, Inc. Dosage rate = 2.25% by weight of cement, equivalent to 7.6 L/m^3 (1.54 gal/yd^3). Designation HY.

2.2.3 Concrete Mix Design and Aggregate Properties

Materials used for concrete mixtures:

Water – Municipal tap water from the City of Lawrence.

Cement – Type I/II portland cement.

Coarse Aggregate – Crushed limestone from Fogle quarry. Nominal maximum size = 19 mm (0.75 in.), bulk specific gravity (SSD) = 2.58, absorption = 2.3%, unit weight = 1536 kg/m^3 (95.9 lb/ft^3).

Fine Aggregate – Kansas River sand. Bulk specific gravity (SSD) = 2.62, absorption = 0.8%, fineness modulus = 2.51.

Air Entraining Agent – Daravair 1400, a saponified rosin-based air entraining agent manufactured by W.R. Grace.

Inhibitors – Listed above.

The mixture proportions used for Southern Exposure, cracked beam, and field test specimens are shown in Table 2.3. The water-cement ratio was 0.45 with a target slump of 75 ± 13 mm (3 ± 0.5 in.) and a target air content of 6 ± 1%. The Doniphan County and Mission Creek bridges are discussed in Section 2.7.

Table 2.3: Mix Proportions for Lab and Field Specimens

Mix	Water kg/m^3 (lb/yd^3)	Cement kg/m^3 (lb/yd^3)	Coarse Aggregate kg/m^3 (lb/yd^3)	Fine Aggregate kg/m^3 (lb/yd^3)	Air-entraining Agent mL/m^3 (oz/yd^3)	Inhibitor L/m^3 (gal/yd^3)
Conv.	160 (269)	355 (598)	880 (1484)	851 (1435)	90 (2.33)	-
DCI	148 (248)	355 (598)	880 (1484)	851 (1435)	140 (3.62)	15 (3.03)
Rheocrete	156 (262)	355 (598)	880 (1484)	851 (1435)	300 (7.74)	5 (1.01)
Hycrete	154 (259)	355 (598)	880 (1484)	851 (1435)	35 (1.18)	7.6 (1.54)

2.3 SOUTHERN EXPOSURE (SE) AND CRACKED BEAM (CB) TESTS

2.3.1 Description

The Southern Exposure (SE) and cracked beam (CB) tests use alternating cycles of elevated temperature and exposure to a salt solution to expose the reinforcing steel in the specimens to high chloride concentrations during the course of the tests. The Southern Exposure specimens (Figure 2.1) are 305 × 305 × 178 mm (12 × 12 × 7 in.) concrete prisms. Two mats of No. 16 (No. 5) reinforcing bars are cast in the specimen, a top mat, consisting of two 305-mm (12-in.) long No. 16 (No. 5) bars with 25-mm (1-in.) concrete clear cover, and a bottom mat, consisting of four 305-mm (12-in.) long No. 16 (No. 5) bars placed with 25-mm (1-in.) clear cover above the specimen base. Bars in each mat are spaced at 64 mm (2.5 in.) and centered within the prism. The bars in the top and bottom mats are electrically connected via external wiring through a terminal box across a 10-ohm resistor to allow for macrocell corrosion rate measurements. A 19-mm (0.75-in.) concrete dam is cast integrally with the specimen to allow for ponding of the salt solution.

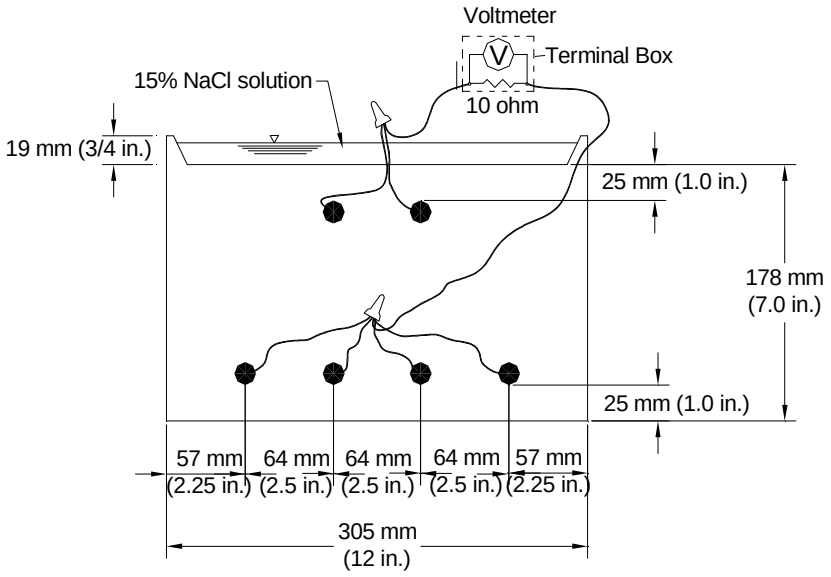

Figure 2.1 – Southern Exposure (SE) specimen

Cracked beam specimens are half the width of the Southern Exposure specimens. The top mat of steel consists of a single No. 16 (No. 5) bar and the bottom mat consists of two No. 16 (No. 5) bars. Prior to casting, a 0.3-mm (12-mil) by 151-mm (6-in.) stainless steel shim is inserted into the mold, centered on and in contact with the top bar. This shim is removed 12 hours after casting, creating a 151-mm (6-in.) long crack in the concrete exposing the top mat of steel. The cracked beam specimen is shown in Figure 2.2.

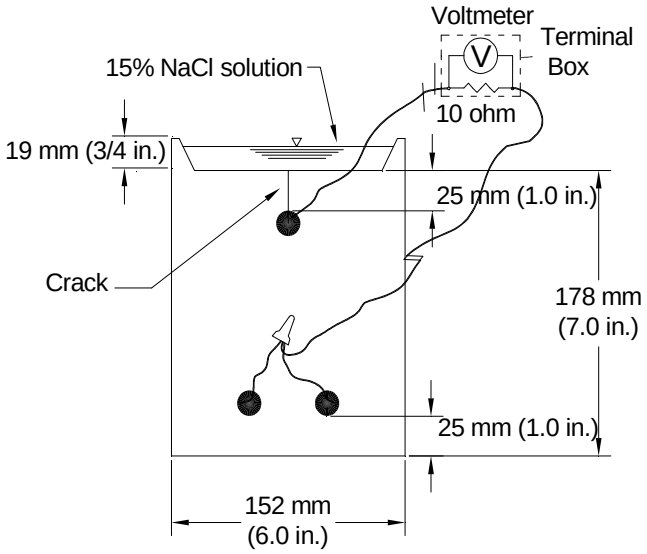

Figure 2.2 – Cracked Beam (CB) specimen

2.3.2 Materials and Equipment

The following materials and equipment are used for the Southern Exposure and cracked beam tests.

Wire – External specimen connections from each mat of steel to the terminal box are made with 16-gauge multi-strand copper wire.

Terminal Box – The terminal box provides an electrical connection between the top and bottom mats of steel and simplifies corrosion measurements. Each SE and CB specimen has its own station in the terminal box. A station consists of a red binding post, a black binding post, a single pole single throw switch and a 10-ohm resistor. The resistor and switch are connected in series and connect the red and black binding posts. Internal terminal box connections are made with 22-gauge solid copper wire. The connections are housed within the terminal box to protect them from inadvertent salt expose, leaving only the face of the switch and binding posts exposed. The bottom mat of steel is connected to the black binding post and the top mat of steel to the red binding post, allowing the voltage drop across the 10-ohm resistor to be measured and used to determine macrocell corrosion rate, as

discussed in Section 1.6.2. The switch allows for interruption of the circuit to permit mat-to-mat resistance, corrosion potential, and linear polarization resistance measurements.

Voltmeter – The voltmeter is used to obtain macrocell voltage drop and corrosion potential measurements. The voltmeter used for this study was a Keithley model 2182A nanovoltmeter.

Ohmmeter – The ohmmeter is used to measure mat-to-mat resistance of SE and CB specimens. For this study, an Agilent 4338B milliohmmeter was used.

Reference Electrode – Used for corrosion potential measurements. A saturated calomel electrode (SCE) was used for the SE and CB readings in this study.

Epoxy – Epoxy is used to prevent ingress of chlorides from the sides of the specimen and to prevent corrosion of electrical connections. Sewer Guard HBS 100 Epoxy, manufactured by BASF, was used for this study.

Stainless Steel Screws/Washers – Used to hold reinforcement in place in formwork and to connect wires to specimens during testing. Parts are specified in Section 2.3.4.

Salt Solution – Salt solution is used to pond specimens. A 15% by weight NaCl solution is prepared and applied to specimens, as described in Section 2.3.5.

Wet/Dry Vacuum – The wet/dry vacuum is used for removal of salt solution from specimens, as described in Section 2.3.5.

Heat Tent – Heat tents are used to expose specimens to an elevated temperature, as described in Section 2.3.4. The tents used in this study were 2.44 m (8 ft) long by 1.22 m (4 ft) wide by 1.07 m (3.5 ft) high. The faces and roof of the tent are fabricated from 19 mm (0.75 in.) plywood with six 2 x 4 studs bracing the tent. Two sheets of plastic sheeting cover the space between studs. Heat is provided by three 250-watt heat lamps spaced evenly along the roof of the tent. These lamps sit 0.45 m (1.5 ft) above the surface of the SE and CB specimens. Temperature is

controlled with a thermostat set to maintain specimens at 38 ± 2° C (100 ± 3° F). A schematic of the tent is shown in Figure 2.3.

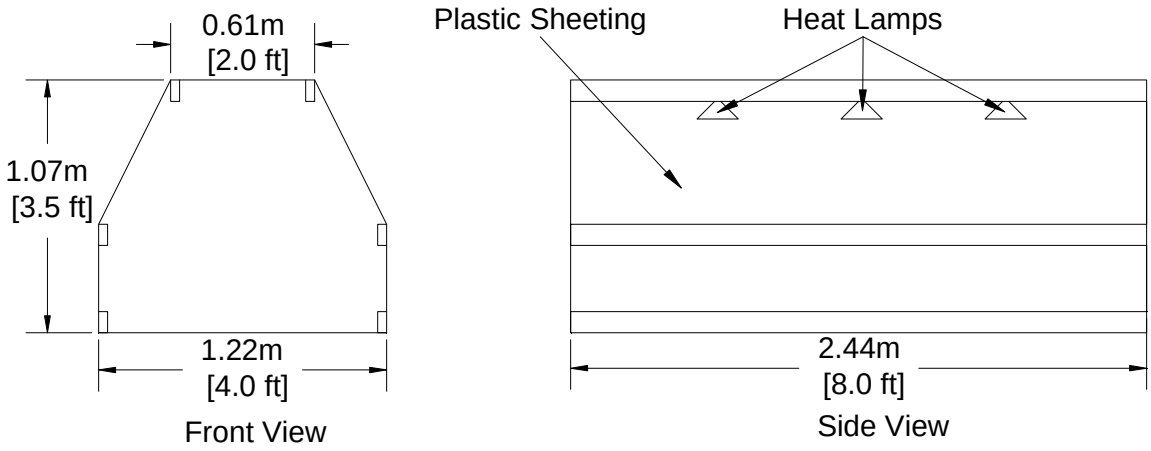

Figure 2.3: Heat tent dimensions.

2.3.3 Formwork

Formwork for SE and CB specimens is constructed from 19 mm (0.75 in.) plywood treated with polyurethane and consists of four face pieces and a base. Specimens are cast upside-down. The SE formwork base has a tapered 267 × 267 × 19 mm (10.5 × 10.5 × 0.75 in.) plywood insert affixed to create the concrete dam used to hold ponding solution on the specimen. The CB formwork insert measures 114 × 267 × 19 mm (4.5 × 10.5 × 0.75 in.) and has a slot centered and cut in the insert to accommodate the 0.3-mm (12-mil) shim. Holes are drilled on two opposing faces to allow the reinforcement to be held in place during casting. The faces and base are held together with threaded inserts in the side of the plywood and 32-mm (1.25-in.) long 10-24 stainless steel machine screws. Prior to reinforcement placement, all interior surfaces are coated with mineral oil and the 0.3-mm (12-mil) stainless steel shim is placed into position for CB specimens.

2.3.4 Fabrication

Specimen fabrication for Southern Exposure and cracked beam specimens proceeds as follows:

1. Reinforcing bars are cut to 305 mm (12 in.) with a band saw.
2. Both ends of each bar are drilled and tapped to a 19-mm (0.75-in.) depth with 10-24 threading.
3. Epoxy-coated reinforcement is intentionally damaged using a 3-mm (0.125-in.) diameter four-flute drill bit. A milling machine is used to penetrate the epoxy surface to a depth of 0.4 mm (15 mils), just deep enough to expose the underlying steel. Bars were damaged with a total of four or ten holes, with two or five holes spaced evenly on each side of the bar. Some multiple-coated (MC) reinforcement is damaged in the same manner to expose the underlying steel. Other MC bars are damaged using a soldering gun set to 205° C (493° F), hot enough to melt the epoxy but below the melting point of zinc, to expose the zinc layer without exposing the underlying steel. The exposed area is controlled by first marking the epoxy surface using a 3-mm (0.125-in.) diameter four-flute drill bit.
4. Epoxy-coated bars are cleaned with warm soapy water, rinsed and allowed to dry. Bare steel bars are soaked in acetone for a minimum of two hours and scrubbed to remove any oil.
5. The reinforcement is placed into the assembled formwork described in Section 2.3.3 and held in place with 32-mm (1.25-in.) long 10-24 threaded stainless steel machine screws. Epoxy-coated reinforcement is aligned such that the holes in the coating face the top and bottom of the specimen.
6. Specimens are cast with concrete using the mixture proportions in Table 2.3. Specimens are filled in two layers. For each layer, the concrete is consolidated using a 60-Hz, 0.15-mm (6-mil) amplitude vibrating table for 30 seconds. The free surface of the concrete (the bottom of the specimen) is finished with a float.
7. Specimens are cured for 24 hours in the formwork at room temperature. Wet burlap and plastic are used to minimize evaporation. Stainless steel shims are removed from CB specimens after the concrete has set.

8. Formwork is removed after 24 hours.
9. Specimens are kept for an additional two days in a plastic bag with deionized water, then air cured for 25 days.
10. Prior to testing, wire leads are connected to all test bars using 10-24 × 13 mm (0.5 in.) stainless steel screws and a No. 10 stainless steel washer. Two coats of Sewer Guard HBS 100 Epoxy are applied to the four sides of all specimens, leaving the top and bottom uncoated. The top surface is lightly sanded to remove the outer layer of cement paste.
11. Both SE and CB specimens begin testing 28 days after casting. Top and bottom mats of steel are connected to the terminal box. Terminal box switches are left connected except as required to take readings (See Section 2.3.5). Specimens are placed on 2 x 2 studs to allow air flow under the specimens.

2.3.5 Southern Exposure and Cracked Beam Test Procedure

The Southern Exposure and cracked beam tests take 96 weeks. The test alternates between two cycles for the duration of the test. The two cycles are described next.

2.3.5.1: Test Cycles

Ponding and Drying Cycles:

On day 1, a 15% NaCl solution is ponded on the surface of the specimens. SE specimens receive 600 mL of solution; CB specimens receive 300 mL of solution. Specimens are covered with plastic sheeting to minimize evaporation. On day 4, readings are taken. Corrosion measurements are described in Section 2.3.5.2. After readings are completed, the salt solution is removed from all specimens using a shop vacuum and a heat tent is placed over the specimens. The heat tent keeps the specimens at 38 ± 2° C (100 ± 3° F) for three days, completing one full week. The tent is removed and the cyclic wetting and dry cycles are repeated for 12 weeks.

Ponding Cycle:

After the heat tent is removed after 12 weeks of ponding and drying cycles, specimens are ponded for 12 weeks with the appropriate amount of 15% NaCl solution and covered with plastic sheeting. Readings continue to be taken on a weekly basis, but the ponding solution is not vacuumed from the surface of the specimens and the heat tent is not used. If excessive evaporation occurs during this time, deionized water is added to the surface to maintain moisture. No additional salt solution is added during this time. After 12 weeks, the specimens are again subjected to the weekly ponding and drying cycles. The two 12-week exposure regimes are repeated three more times for a total of 96 weeks of testing.

2.3.5.2 Corrosion Measurements

Measurements taken during Southern Exposure and cracked beam testing include macrocell voltage drop, mat-to-mat resistance, corrosion potential, and linear polarization resistance. On a weekly basis, the voltage drop across the 10-ohm resistor is taken to measure macrocell corrosion rate. The top and bottom mats are then electrically disconnected at the terminal box and the mat-to-mat resistance for each specimen is recorded. Specimens remain disconnected for a minimum of two hours to allow the corrosion potentials of the top and bottom mats to stabilize. The corrosion potentials are then measured with respect to a saturated calomel electrode, and the top and bottom mats are reconnected via the switch at the terminal box to allow corrosion to continue.

Linear polarization resistance (LPR) readings are taken every four weeks for both top and bottom mats. LPR readings are taken just prior to the corrosion potential readings.

Linear polarization measurements are taken on one SE and one CB specimen for each corrosion protection system. Readings are taken using a PC4/750 Potentiostat and DC105 computer-controlled corrosion measurement system. Potentiostatic LPR is measured; the PC4/750 forces the corrosion specimen away from the equilibrium

potential and the resulting change in current is measured. The bars in the test specimen act as the working electrode, a saturated calomel electrode acts as the reference electrode, and a solid platinum wire acts as the counter electrode. The input window with fields populated for the top mat of a SE specimen, is shown in Figure 2.4. An explanation of terms appears below.

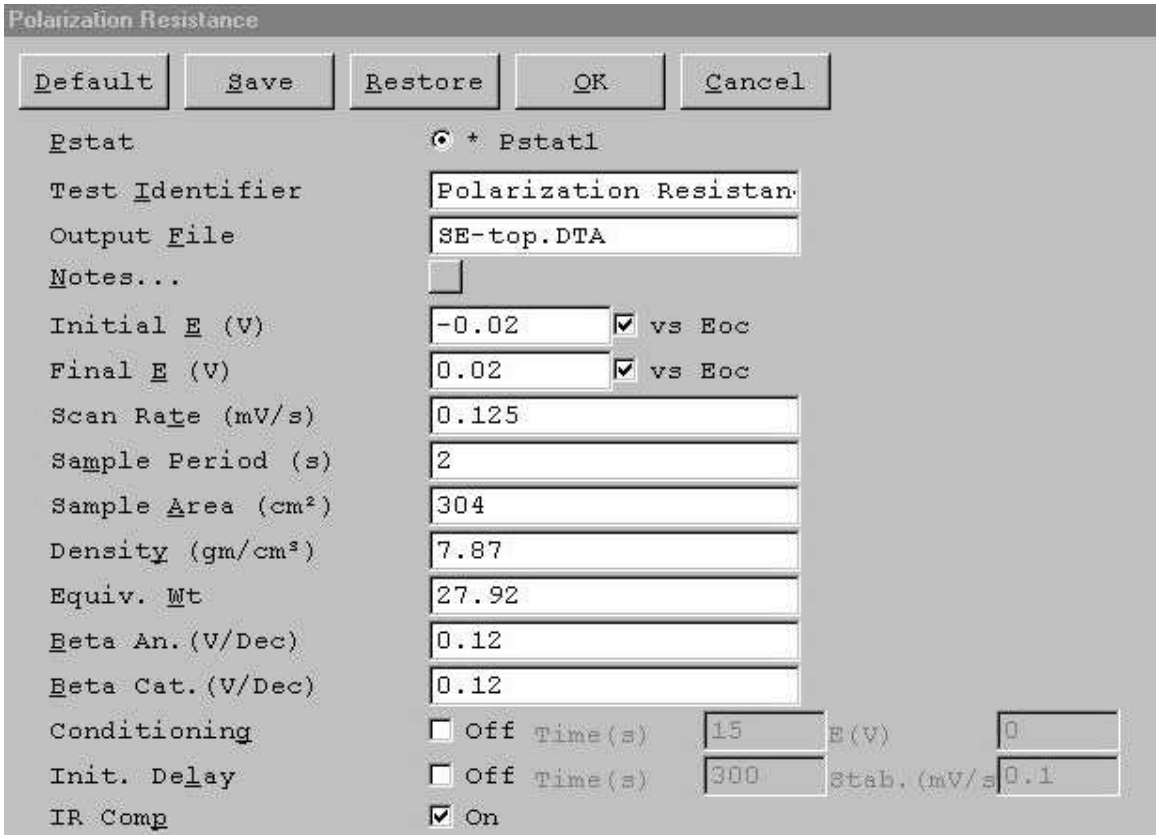

Figure 2.4: LPR input window.

The range of the scan is defined by Initial E and Final E. The range is taken with respect to the equilibrium potential of the reinforcing bar; this is measured by the software at the start of the test. A range of –20 mV to 20 mV is used for data collection; the linear region of –10 mV to 10 mV is used to determine the polarization resistance. Scan rate defines the rate at which the applied potential is shifted. At a rate of 0.125 mV/s, it takes 320 seconds to cover the entire sample range. The sample period defines how frequently a data point is collected; every 2 seconds (160 data points) over the full range. The sample area is the surface area of the mat of steel. A single 308 mm (12 in.)

No. 16 (No. 5) bar has a surface area of 152 cm^2. Density and equivalent weight are metal-specific properties, where equivalent weight is the atomic weight of the metal divided by the number of electrons lost when the metal oxidizes. Anodic and cathodic Tafel constants are set to 0.12, as discussed in Section 1.6.3. The polarization resistance is used to determine current density [Eq. (1.19)] and corrosion rate [Eq. (1.13)].

2.3.6 Chloride Sampling for SE Specimens

Southern Exposure specimens are sampled for chlorides at the initiation of corrosion, at 48 weeks, and at the end of the 96-week test. Cracked beam specimens are not sampled for chlorides. The chloride content at corrosion initiation gives the critical chloride corrosion threshold, and sampling at 48 and 96 weeks allows for tracking the rate of chloride ingress into the concrete. The onset of corrosion is defined as occurring when the measured macrocell corrosion rate exceeds 0.3 µm/yr or the corrosion potential becomes more negative than –0.275 V with respect to a saturated calomel electrode.

2.3.6.1 Chloride Sampling Procedure

Prior to chloride sampling, the specimen is cleaned on all four sides with soapy water, and then rinsed with tap water followed by a deionized water rinse. After drying, the specimens are marked for drilling. Samples are taken from the side of the specimen with a 6.4-mm (0.25-in.) masonry drill bit aligned such that the top of the bit is level with the top of the top mat of reinforcing steel, as shown in Figure 2.5. Three samples are taken from each side of the specimen for a total of six samples. Sample sites are chosen at random along the side of the specimen; however no samples are taken within 38 mm (1.5 in.) of the specimen edge.

At each sample site, the hole is initially drilled to a depth of 13 mm (0.5 in.). The bit is then removed, rinsed with deionized water and the powder discarded. The bit is reinserted with drilling proceeding to a depth of 89 mm (3.5 in.). The powdered concrete sample is collected and transferred to a plastic bag and labeled for analysis. Each sample provides about 4 grams of material. The drill bit is cleaned with deionized water in

preparation for the next sample. If the specimen is to be returned to testing after sampling, the drill holes are filled with modeling clay.

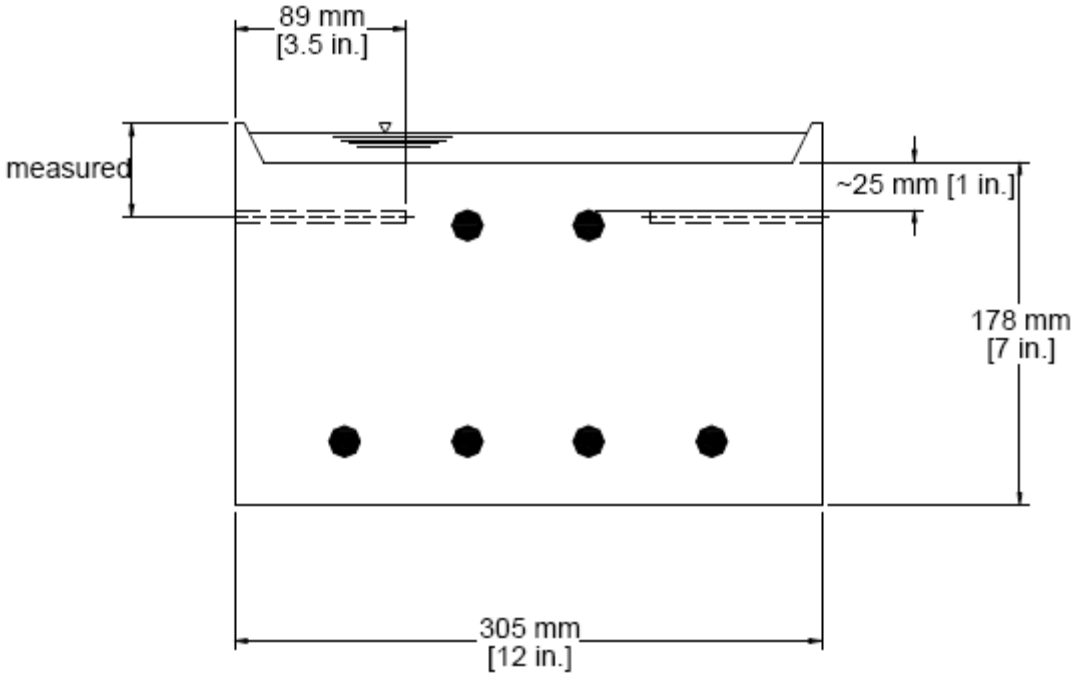

Figure 2.5: Southern Exposure chloride sampling.

2.3.6.2 Chloride Analysis

Concrete samples are analyzed for water-soluble chloride content using Procedure A from AASHTO T 260-94, "Standard Method of Test for Sampling and Testing for Chloride Ion in Concrete and Concrete Raw Materials." Samples are boiled in deionized water to free any water soluble chlorides. The solution is filtered, acidified with nitric acid and titrated with silver nitrate. The potential of a chloride ion-selective electrode is monitored throughout the titration. The change in potential with respect to volume of silver nitrate is calculated with the endpoint indicated by the inflection point of the potential-volume curve – the point at which the greatest change in potential for a given incremental addition of silver nitrate is observed. This procedure gives chloride ion concentration in terms of percent chloride by mass (weight) of concrete. In this study, values are presented in kg/m^3 (lb/yd^3) by multiplying by the unit weight of concrete, taken as 2246 kg/m^3 (3786 lb/yd^3).

2.3.7 End of Life Autopsy

At the end of testing, specimens are visually inspected for signs of surface staining or cracking. Specimens are then broken using a sledgehammer or by loading the specimen laterally using a compression testing machine. Reinforcement is marked to indicate the top side prior to autopsy. Each bar is removed and photographed to document corrosion on the bars. Epoxy-coated bars also undergo a disbondment test, described next. For Southern Exposure and cracked beam specimens, one bar each is selected from the top and bottom mats to evaluate disbondment.

2.3.7.1 Disbondment Test

Disbondment tests are performed at sites of intentional damage in the epoxy. At each site to be tested, a sharp utility knife is used to make two cuts through the epoxy at 45° from the axis of the bar, forming an 'X' centered about the damage site. The knife is then used to remove any disbonded epoxy. All disbonded epoxy is removed; epoxy adhering to the steel cannot be removed without considerable force and is left on the bar. The distance from the edge of the initial hole to the edge of the disbonded area is measured in four directions along and perpendicular to the axis of the bar. If this average distance exceeds 12.7 mm (0.5 in.), the epoxy is considered to have undergone total disbondment. For purposes of plotting, bars with total disbondment are assigned a disbonded area of 677 mm^2 (1.05 $in.^2$), the area of a rectangle extending 12.7 mm (0.5 in.) from the initial hole in the longitudinal direction and to the longitudinal ribs on either side of the hole. For bars without total disbondment, a transparent film marked with a square 2.54-mm (0.1-in.) grid is placed over the surface of the bar and the disbonded area measured by counting the squares on the grid within the disbonded area, excluding the area of the initial hole. Disbondment tests are performed at three sites on each bar evaluated; two on the upper surface of the bar as it was oriented in the specimen and one on the underside of the bar.

2.3.8 Southern Exposure and Cracked Beam Test Program

As part of the current study, Draper et al. (2009) included test results for 96 Southern Exposure and 87 cracked beam specimens evaluating the effect of corrosion inhibitors used in conjunction with ECR. Due to low overall corrosion rates associated with all ECR specimens, it was difficult to determine any differences in performance among the inhibitors. In the current study, twelve additional SE and CB specimens were cast; three each for concrete containing DCI, Rheocrete, and Hycrete with conventional reinforcement and three specimens for concrete without a corrosion inhibitor with conventional reinforcement to serve as a control (Table 2.2). The heat of steel used for these tests, designated *Conv.2*, is different from that used in other tests for this study.

Table 2.4: SE and CB Test Program

Southern Exposure		
Specimen Designation	**No. of Tests**	**LPR Specimen No.**
SE-Conv.2	3	1
SE-Conv.2-DCI	3	1
SE-Conv.2-RH	3	1
SE-Conv.2-HY	3	1
Cracked Beam		
Specimen Designation	**No. of Tests**	**LPR Specimen No.**
CB-Conv.2	3	1
CB-Conv.2-DCI	3	1
CB-Conv.2-RH	3	1
CB-Conv.2-HY	3	1

2.4 CORROSION INITIATION BEAM (B) TESTS

The corrosion initiation beam (B) is used to determine the critical chloride corrosion threshold of a corrosion protection system. While this data is also obtained from Southern Exposure specimens, corrosion initiation beam tests are terminated at the onset of corrosion, allowing more chloride samples to be collected. A corrosion initiation beam specimen is identical to a cracked beam specimen with the exception that no intentional crack is placed above the reinforcement. The initiation beam specimen is shown is Figure 2.6.

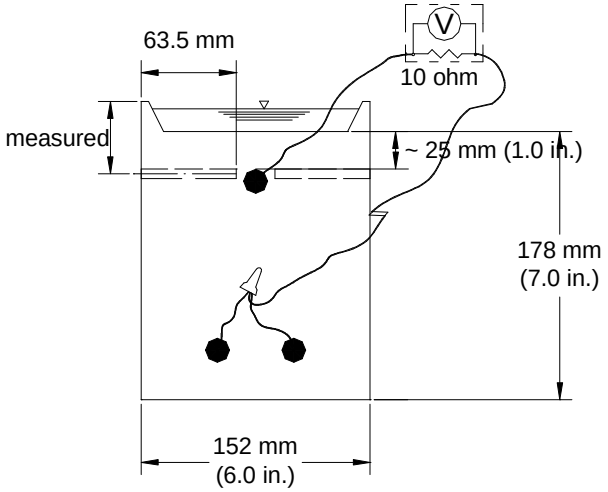

Figure 2.6: Corrosion initiation beam specimen

The materials, fabrication, and testing procedures for corrosion initiation beams are identical those used for Southern Exposure and cracked beam specimens, as outlined in Section 2.3, with the exception of test duration. Once corrosion initiation occurs, defined as a measured macrocell corrosion greater than 0.3 µm/yr or a corrosion potential more negative than –0.275 V with respect to a saturated calomel electrode, testing is halted and chloride samples are taken. A total of twenty samples are obtained from each beam; ten from each side starting 40 mm (1.5 in.) from the edge, spaced at 25-mm (1-in.) intervals, as shown in Figure 2.7. The drill is placed such that the top of the drill bit is level with the top of the top bar of steel. Sampling and analysis otherwise proceeds as outlined in Section 2.3.6.

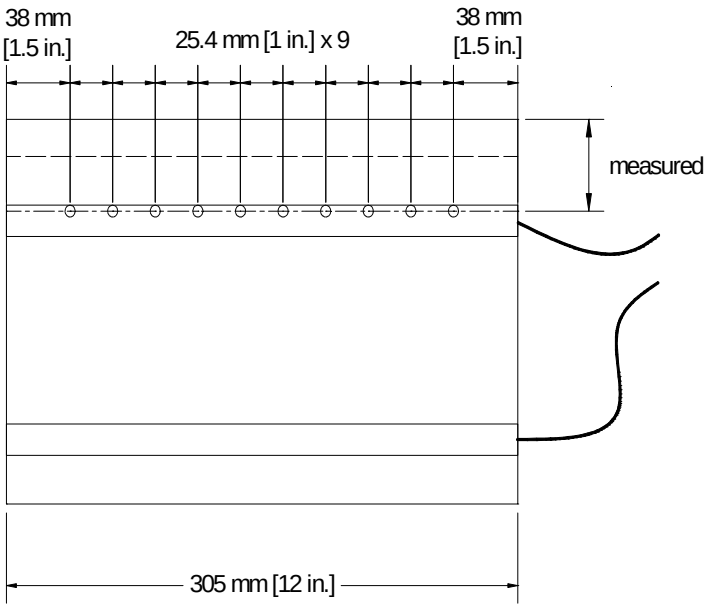

Figure 2.7: Sampling locations for initiation beam specimens

2.4.1 Test Program

Xing et al. (2010) tested eighteen corrosion initiation beams; six each with DCI, Rheocrete, and Hycrete inhibitor. Critical chloride corrosion thresholds and time to initiation, as reported by Xing et al., are summarized in Table 2.5. Twelve additional specimens, six conventional steel specimens with Hycrete inhibitor in the concrete and six control specimens, were tested in this study, cast to verify the low critical chloride corrosion threshold for specimens with Hycrete inhibitor reported by Xing et al. (2010).

Table 2.5: Critical Chloride Corrosion Threshold for concrete with Corrosion Inhibitors (Xing et al. 2010)

Specimen Designation	Average Age at Initiation (weeks)	Average Chloride Content, kg/m^3, (lb/yd^3)
B-Conv.	14.2	0.96 (1.62)
B-DCI	26.5	1.59 (2.67)
B-RH	19.5	1.23 (2.07)
B-HY	28.5	0.37 (0.62)

2.5 FIELD TEST SPECIMENS

2.5.1 Description

Field test specimens are designed to evaluate the performance of corrosion protection systems when subjected to seasonal weather and environmental changes. The specimens measure 1.22 × 1.22 × 0.17 m (48 × 48 × 6.5 in.) and are shown in Figure 2.8.

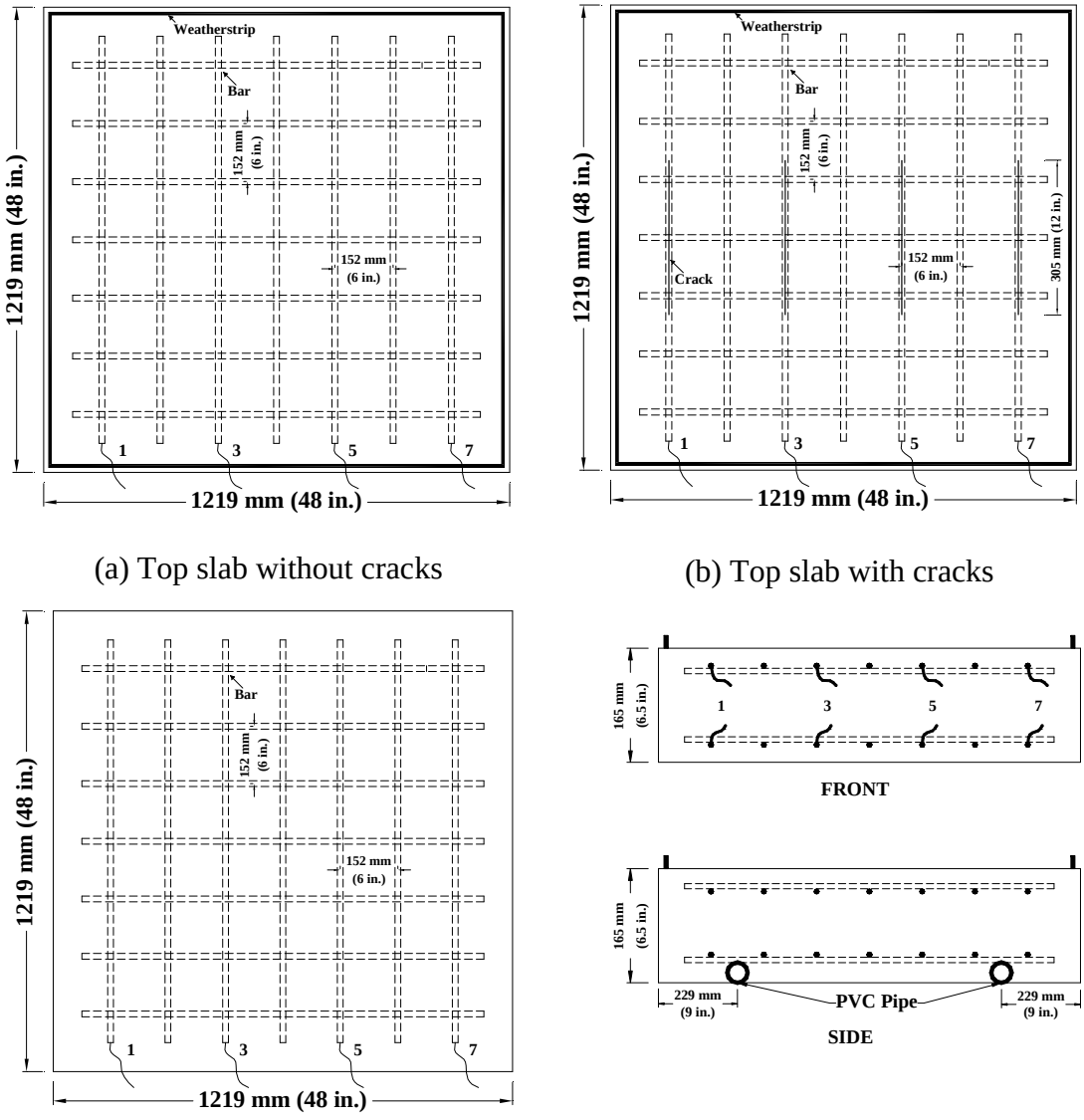

(a) Top slab without cracks

(b) Top slab with cracks

(c) Bottom slab

(d) Front and side views

Figure 2.8: Field test specimen setup

Each specimen has two mats of No. 16 (No. 5) reinforcing steel. Each mat consists of two layers of seven 1.07-m (42-in.) long No. 16 (No. 5) bars spaced 0.15 m (6 in.) on center. The bars in the upper layer of each mat run perpendicular to those in the lower layer. Reinforcement is tied with form ties selected to match the type of reinforcement being used, and plastic chairs are used to provide 25-mm (1-in.) clear cover to both the top and bottom mats of steel. Specimens are tested in both the cracked and uncracked condition, and weather stripping is used on the top surface to allow for ponding of a 10 percent salt solution. Two or four bars from the top mat are electrically connected across a 10-ohm resistor to the equivalent bar in the bottom mat. Concrete for the field test specimens is supplied by a local ready-mix concrete plant following the mixture proportions outlined in Table 2.3.

2.5.2 Materials and Equipment

The materials and equipment used for the field test specimens are identical to those used for the Southern Exposure specimens outlined in Section 2.3.2 except as follows:

Salt Solution – A 10% by weight NaCl solution is prepared and applied to specimens as specified in Section 2.5.5.

Epoxy – The sides of field test specimens are not treated with epoxy. Electrical connections are protected with 3M Scotchkote^{TM} rebar patch kit.

Heat Tent – No heat tent is used for field test specimens.

Weather Stripping – High density foam, 12.7 × 9.5 mm (0.5 × 0.375 in.). Used to form a dam on the surface of field test specimens to allow for ponding of salt solution.

Silicone Caulk – Applied to the underside of the weather stripping to bond the weather stripping to the specimen surface.

Heat-shrink Tubing – Used to protect electrical connections in the specimen. 19 mm (0.75 in.) expanded diameter, 9.5 mm (0.375 in.) shrunk diameter.

Reference Electrode – A copper/copper sulfate electrode is used for all potential readings.

PVC Pipe – 1.37-m (54-in.) long, 3/4-in. Schedule 80 PVC pipe, inside diameter 18.3 mm (0.722 in.). Used to aid in moving specimens.

2.5.3 Formwork

Formwork for field test specimens is constructed using 19-mm (0.75-in.) plywood. Specimens are cast upright. The faces and base of the formwork are held together with external clamps and wood screws. 25-mm (1-in.) diameter holes are drilled 229 mm (9 in.) on center from the edge of the form to allow the insertion of two 1.73-m (54-in.) long PVC pipes (see Figure 2.8 d). These pipes allow for the insertion and removal of No. 16 (No. 5) reinforcement to allow the specimen to be lifted and moved. Mats of reinforcing steel are held in place with plastic chairs. A 76-mm (3-in.) clear cover is provided on all sides, and a 25-mm (1-in.) clear cover is provided at the upper and lower faces of the specimens.

For specimens with simulated cracks, four 0.3 mm by 304 mm (0.012 in. by 12 in.) stainless steel shims are placed parallel to and directly above four test bars in the top mat of steel. Bars are held in place with a plywood shim holder attached to the formwork.

2.5.4 Fabrication

Specimen fabrication for field test specimens, as reported by Guo et al. (2006), proceeds as follows:

1. Reinforcing bars are cut to 1.07 m (42 in.) with a band saw.
2. One end of each bar is drilled and tapped to a 19 mm (0.75 in.) depth with 10-24 threading.
3. Epoxy-coated reinforcement is intentionally damaged using a 3-mm (0.125-in.) diameter four-flute drill bit. A milling machine is used to penetrate the epoxy surface to a depth of 0.4 mm (15 mils), just deep enough to expose the underlying steel. The coating of the bar is damaged with a total of sixteen holes, with eight holes spaced evenly on each side of the reinforcement.

4. Epoxy-coated bars are cleaned with warm soapy water, rinsed and allowed to dry. Bare steel bars are cleaned with acetone.
5. A 0.9-m (36-in.) long, 16-gauge insulated multi-strand copper wire is attached to the tapped end of each test bar using a 13-mm (0.5-in.) 10-24 stainless steel machine screw. Most specimens had four test bars, numbered 1, 3, 5 and 7 in Figure 2.8. Some specimens only had two test bars; numbered 3 and 5 in Figure 2.8.
6. The electrical connection and all cut ends of the epoxy-coated reinforcement are coated with rebar patch epoxy. Electrical connections are fitted with heat-shrink tubing, holding the wire in place upon shrinking.
7. The reinforcement is placed into the assembled formwork described in Section 2.5.3 and held in place with plastic chairs. Epoxy-coated reinforcement is aligned such that the holes in the coating face the top and bottom of the specimen. Mats are held in position horizontally via tie wires. Shims are inserted into specimens that require cracked concrete.
8. Specimens are cast with ready-mix concrete using the mixture proportions shown in Table 2.3. Consolidation was achieved with internal vibrators. Batch information appears in Table 2.6, with plastic and hardened concrete properties, as reported by Guo et al. (2006), in Tables 2.7 and 2.8, respectively.
9. Shims are removed from cracked specimens after 12 hours.
10. Specimens are covered with wet burlap and plastic sheeting and cured for seven days.
11. Specimens are demolded and air cured outside for three months.
12. Seven days prior to testing, specimens are moved to the outdoor test site (University of Kansas Adams Campus). Specimens are placed on concrete blocks to keep them approximately 203 mm (8 in.) above the ground.

13. 9.5-mm (0.375-in.) wide, 12.7-mm (0.5 in.) thick weather stripping is applied around the top edge of all specimens to allow for ponding with salt solution.

Table 2.6: Field Test Specimen Batch Schedule (Guo et al. 2006).

Batch No.	Steel Designation[a]	Number of Specimens	Total Number of Specimens
1	Conv.	2	6
	ECR	2	
	ECR(Valspar)	2	
2	ECR(DuPont)	2	6
	ECR(Chromate)	2	
	MC	2	
3	ECR(primer/Ca$(NO_2)_2$)	2	6
	Conv.	2	
	ECR	2	
4	ECR(Valspar)	2	6
	ECR(DuPont)	2	
	ECR(Chromate)	2	
5	MC	2	4
	ECR(primer/Ca$(NO_2)_2$)	2	
6	ECR(DCI)	4	4
7	ECR(DCI)	2	2
8	ECR(Rheocrete)	4	4
9	ECR(Hycrete)	4	4

[a] Conv. = conventional steel. ECR = conventional epoxy-coated reinforcement. All epoxy-coated bars are penetrated with 16 surface holes.
MC = multiple coated bars. Multiple coated bars have both the zinc and epoxy layers penetrated.
ECR(Chromate) = ECR with the chromate pre-treatment.
ECR(DuPont) = ECR with high adhesion DuPont coating. ECR(Valspar) = ECR with high adhesion Valspar coating.
ECR(DCI) = ECR in concrete with DCI inhibitor. ECR(Hycrete) = ECR in concrete with Hycrete inhibitor.
ECR(Rheocrete) = ECR in concrete with Rheocrete inhibitor.
ECR(primer/Ca(NO2)2) = ECR with a primer containing calcium nitrite.

Table 2.7: Field Test Specimen Plastic Concrete Properties

Batch No.	*w/c*	Slump mm (in.)	Temp. °C (°F)	Unit Weight kg/m^3 (lb/ft^3)	Air content (%)	
					(Pressure)	(Volumetric)
1	0.39	100 (4)	19 (66)	2219 (138.4)	7.00	6.25
2	0.43	100 (4)	19 (67)	2319 (144.7)	6.20	5.00
3	0.41	50 (2)	28 (82)	2307 (143.9)	5.30	4.00
4	0.42	125 (5)	24 (75)	2296 (143.2)	7.80	5.75
5	0.44	110 (4.25)	23 (73)	2291 (142.9)	6.40	5.25
6	0.48	210 (8.25)	22 (72)	2255 (140.7)	11.00	7.25
7	0.40	25 (1)[a]	21 (70)	-	-	5.50
8	0.44	165 (6.5)	23 (73)	2295 (143.2)	7.00	5.50
9	0.41	185 (7.25)	16 (61)	2216 (138.2)	-	5.65

[a] A slump of 150 mm (6 in.) slump was obtained at the Lawrence Ready Mix Plant before transporting concrete to the lab.

Table 2.8: Field Test Specimen Hardened Concrete Properties

Batch No.	Average Concrete Compressive Strength[a] MPa (psi)		
	Curing Tank	Curing Room	With Specimens
1	-	28.4 (4110)	30.6 (4440)
2	-	35.7 (5180)	37.4 (5430)
3	-	34.4 (4990)	36.9 (5350)
4	-	32.5 (4710)	32.9 (4780)
5	32.8 (4760)	32.6 (4730)	33.2 (4810)
6	35.3 (5110)	30.9 (4480)	29.6 (4290)
7	36.8 (5340)	35.9 (5210)	-
8	29.1 (4220)	28.5 (4130)	28.1 (4080)
9	15.0 (2170)	13.5 (1960)	13.1 (1900)

[a] Average of three cylinders.

2.5.5 Test Procedure

2.5.5.1 Salting Procedure

Field test specimens are left in the field for 250 to 254 weeks. In addition to exposure to the weather, specimens are ponded with 3.3 L (0.87 gal) of a 10% rock salt solution every four weeks, consisting of 0.33 kg (0.73 lb) of rock salt every four weeks for a total average salt application of 3.93 kg (8.64 lb). This application rate comes from work by Guo et al. (2006). Guo found the average annual salt usage on roadways in Kansas was 0.66 kg/m^2 (0.14 lb/ft^2). However, as bridge decks have a lower temperature

than the surrounding pavement, they are salted more frequently and with an increased application of salt compared to the surrounding pavement. As a result, a typical bridge deck in Kansas will see four to five times the average annual salt application for a roadway, resulting in an average annual salt application of 2.64 kg/m^2 (0.54 lb/ft^2). Using this application rate on a field test specimen with a surface area of 1.49 m^2 (16 ft^2) results in an annual salt application of 3.93 kg (8.64 lb).

2.5.5.2 Corrosion Measurements

Measurements taken on field test specimens include macrocell voltage drop, mat-to-mat resistance, and corrosion potential. Polarization resistance was not taken on a regular basis. Readings were taken every four weeks until specimens reached 96 weeks, after which readings were taken every eight weeks.

Each field test specimen has either two or four test bars wired to allow for macrocell voltage drop and potential readings. Other epoxy-coated bars in the mat are electrically isolated from the test bars. No effort was made to electrically isolate bars in conventional steel specimens. The number of test bars in each specimen is shown in Table 2.9. Voltage drop and mat-to-mat resistance readings were taken for each test bar. Three corrosion potential measurements were taken for each test bar. Locations of potential readings are shown in Figure 2.9 with the total number of potential readings per mat listed in Table 2.9. Potentials were taken on both the top and bottom mat with respect to a copper/copper sulfate electrode. The potential of a copper/copper sulfate electrode varies with temperature (Roberge 2008); a correction factor [Eq. (2.1)] is applied to all potential measurements taken in the field to compensate for this variation.

$$E = E_o + 0.5(T - 72) \tag{2.1}$$

where:

T = temperature, °F

E_o = uncorrected corrosion potential reading, mV

E = temperature corrected corrosion potential reading, mV

Table 2.9: Field Test Specimen Test Program

Without Cracks			With Cracks		
Steel Designation[a]	**Number of Test Bars[b]**	**Number of Potential Test Points**	**Steel Designation[a]**	**Number of Test Bars[b]**	**Number of Potential Test Points**
Control					
Conv. (1)	2	12	Conv. (1)	2	12
Conv. (2)	2	12	Conv. (2)	2	12
ECR (1)	2	6	ECR (1)	2	6
ECR (2)	4	12	ECR (2)	4	12
Task 3 Corrosion Inhibitors					
ECR($Ca(NO_2)_2$) (1)	4	12	ECR($Ca(NO_2)_2$) (1)	4	12
ECR($Ca(NO_2)_2$) (2)	4	12	ECR($Ca(NO_2)_2$) (2)	4	12
ECR(DCI) (1)	4	12	ECR(DCI) (1)	4	12
ECR(DCI) (2)	4	12	ECR(DCI) (2)	4	12
ECR(DCI) (3)	4	12	ECR(DCI) (3)	4	12
ECR(RH) (1)	4	12	ECR(RH) (1)	4	12
ECR(RH) (2)	4	12	ECR(RH) (2)	4	12
ECR(HY) (1)	4	12	ECR(HY) (1)	4	12
ECR(HY) (2)	4	12	ECR(HY) (2)	4	12
Task 4 Multiple Coated Bars					
MC (1)	2	6	MC (1)	2	6
MC (2)	4	12	MC (2)	4	12
Task 5 Increased Adhesion					
ECR(Valspar) (1)	2	6	ECR(Valspar) (1)	2	6
ECR(Valspar) (2)	4	12	ECR(Valspar) (2)	4	12
ECR(DuPont) (1)	2	6	ECR(DuPont) (1)	2	6
ECR(DuPont) (2)	4	12	ECR(DuPont) (2)	4	12
ECR(Chromate) (1)	2	6	ECR(Chromate) (1)	2	6
ECR(Chromate) (2)	4	12	ECR(Chromate) (2)	4	12

[a] Conv. = conventional steel. ECR = normal epoxy-coated reinforcement. All epoxy-coated bars are penetrated with 16 surface holes. Multiple coated bars have both the zinc and epoxy layers penetrated.
ECR(primer/$Ca(NO_2)_2$) = ECR with a calcium nitrite primer. MC = multiple coated bars.
ECR(Chromate) = ECR with the zinc chromate pretreatment. ECR(DuPont) = high adhesion DuPont bars.
ECR(Valspar) = high adhesion Valspar bars.
ECR(DCI) = normal ECR in concrete with DCI inhibitor. ECR(Rheocrete) = normal ECR in concrete with Rheocrete inhibitor. ECR(Hycrete) = normal ECR in concrete with Hycrete inhibitor.

[b] Total number of test bars in each specimen

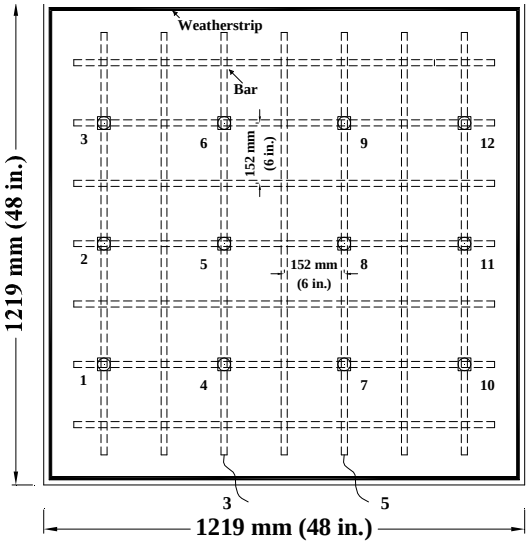

(a) Conventional steel specimen

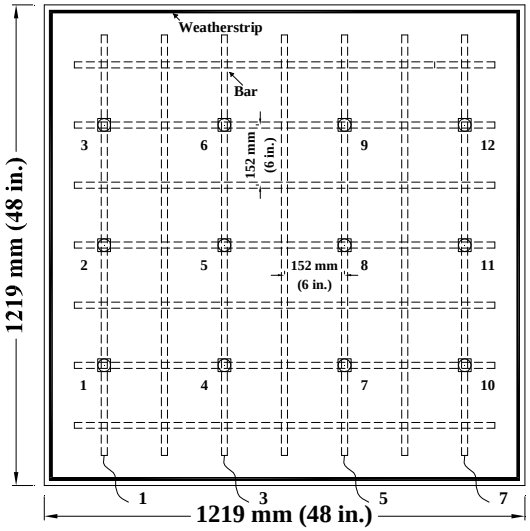

(b) Epoxy-coated bar specimen with four test bars

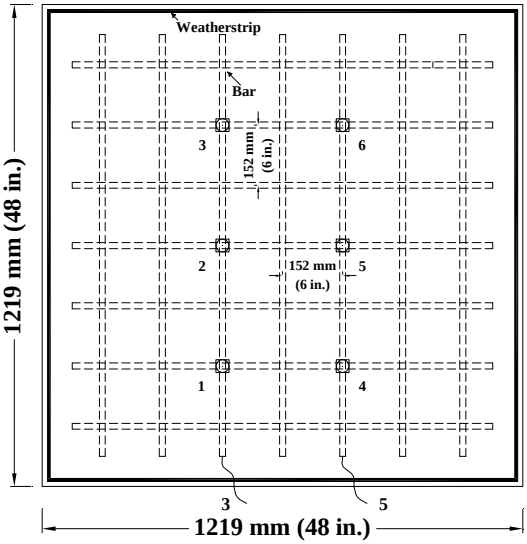

(c) Epoxy-coated bar specimen with two test bars

Figure 2.9: Field Test Specimen Corrosion Potential Locations

2.5.6 Chloride Sampling for Field Test Specimens

Chloride samples for field test specimens were obtained from most specimens at the end of the testing period. Samples were not obtained from cracked or uncracked specimens Conv.-1, ECR-1, ECR(primer/$Ca(NO_2)_2$)-1, MC-1, ECR(Valspar)-1, or ECR(Chromate)-1 as these specimens were autopsied prior to the decision to sample specimens for chlorides was made.

2.5.6.1 Sampling Procedure

Samples for chloride analysis were obtained from concrete cores taken from field test specimens at end of life. A total of four cores were taken from each specimen using an 89-mm (3.5-in.) diameter core drill bit and core drill. Cores were taken at the corners, 230 mm (9 in.) from the edges of the specimens. Cores with reinforcement in them were not analyzed to avoid an increased reading from chloride buildup over the reinforcement (Yu and Hartt 2007a). Cores were stored at -18° C (0° F) to minimize chloride ion migration prior to chloride sampling.

Concrete powder for sampling was obtained from cores using a milling machine and a 32-mm (1.25-in.) diamond grit hole saw. Photos of the milling setup are shown in Figures 2.10 and 2.11. Cores were mounted on a rotary table and positioned with the hole saw off-center from the core such that when the table was rotated, the hole saw would cut a 44-mm (2.5-in.) diameter circle in the core. This avoided sampling from the edge of the core where water from the core drill may have affected chloride content. The milling machine was used to obtain samples from different depths and to produce a depth profile of chloride content. The powder obtained from the top 4 mm (0.15 in.) of the core was discarded due to possible contamination from the core drill water. Samples were collected from 4–8 mm (0.15–0.30 in.), 8–13 mm (0.3–0.5 in.), 13–19 mm (0.5–0.75 in.), 19–25 mm (0.75–1.0 in.), 25–29 mm (1–1.125 in.), 29–32 mm (1.125–1.25 in.), and 38–41 mm (1.5–1.625 in.) with the aid of a vacuum filter collection system. A milled core appears in Figure 2.12.

Figure 2.10: Milling Setup for Core Sampling

Figure 2.11: Sampling Chlorides from Concrete Core

Figure 2.12: Core After Milling

2.5.6.2 Chloride Analysis

The chloride content of the samples is determined as described in Section 2.3.6.2.

In addition to the chloride content at the depth of reinforcement, a chloride depth profile allows apparent surface chloride content and the diffusion coefficient to be determined. The diffusion of chlorides into concrete may be modeled using Fick's Second Law.

$$\frac{\partial C(x,t)}{\partial t} = D\frac{\partial^2 C(x,t)}{\partial x^2} \tag{2.2}$$

where:

C(x,t) = Chloride concentration at some depth *x* and time *t*, kg/m^3 (lb/yd^3)

x = Depth, mm (in.)

t = Time, days

D = *D*iffusion coefficient, mm^2/day (in^2/day)

Crank's solution to Fick's Second Law is often used to calculate an effective diffusion coefficient from a chloride depth profile (Lindquist et. al 2006).

$$C(x,t) = C_o\left[1 - erf\,\frac{x}{2\sqrt{t \times D_{eff}}}\right] \tag{2.3}$$

where:

C_o = Apparent surface chloride concentration, kg/m^3 (lb/yd^3)

D_{eff} = Effective diffusion coefficient, mm^2/day (in^2/day)

erf = Error function

Equation (2.3) is the result of several assumptions, including a constant apparent surface chloride concentration, a constant diffusion coefficient, homogeneous concrete properties and one-dimensional diffusion behavior into the concrete. To solve for the apparent surface chloride concentration C_o and diffusion coefficient D_{eff}, Eq. (2.3) is fitted to the chloride depth profile obtained from the chloride analysis for each core and a

nonlinear least-square error analysis is used to determine values of C_o and D_{eff} (McLeod et al. 2009).

2.5.7 End of Life Autopsy

At the end of testing, specimens are cored for chlorides prior to autopsy. Bars are then removed using a jackhammer and sledgehammer.

2.5.7.1 Disbondment Tests

Disbondment tests are performed on every test bar of every specimen. In addition, disbondment tests are performed on electrically isolated bars from the top mat of steel from uncracked specimens to determine the effect of electrically connecting the bars. The disbondment tests are performed as described in Section 2.3.7.1.

2.5.8 Field Test Specimen Test Program

The FTS test program is listed in Table 2.9. Earlier results for the field test specimens were reported by Guo et al. (2006) and Xing et al. (2010).

2.6 RAPID MACROCELL TEST

2.6.1 Description

The rapid macrocell test, developed at the University of Kansas, is described in Annex A2 of ASTM A955 (ASTM A955-09). The rapid macrocell test is used to measure macrocell corrosion rates and corrosion potentials of reinforcing steel in a simulated concrete pore solution. The test allows chloride ions direct contact with the steel surface, resulting in the early initiation of corrosion. The rapid macrocell specimen is shown in Figure 2.13. Specimens consist of a single 127-mm (5-in.) long No. 16 (No. 5) reinforcing bar in a container with simulated concrete pore and salt solution with an electrical and ionic connection to two 127-mm (5-in.) long No. 16 (No. 5) reinforcing bars in a second container with simulated pore solution. Air, scrubbed to remove CO_2, is bubbled to the pore solution in the second container to provide oxygen. The test duration

is increased from the 15 weeks specified in ASTM A955 to 40 weeks, with specimens removed from testing for disbondment at five week intervals.

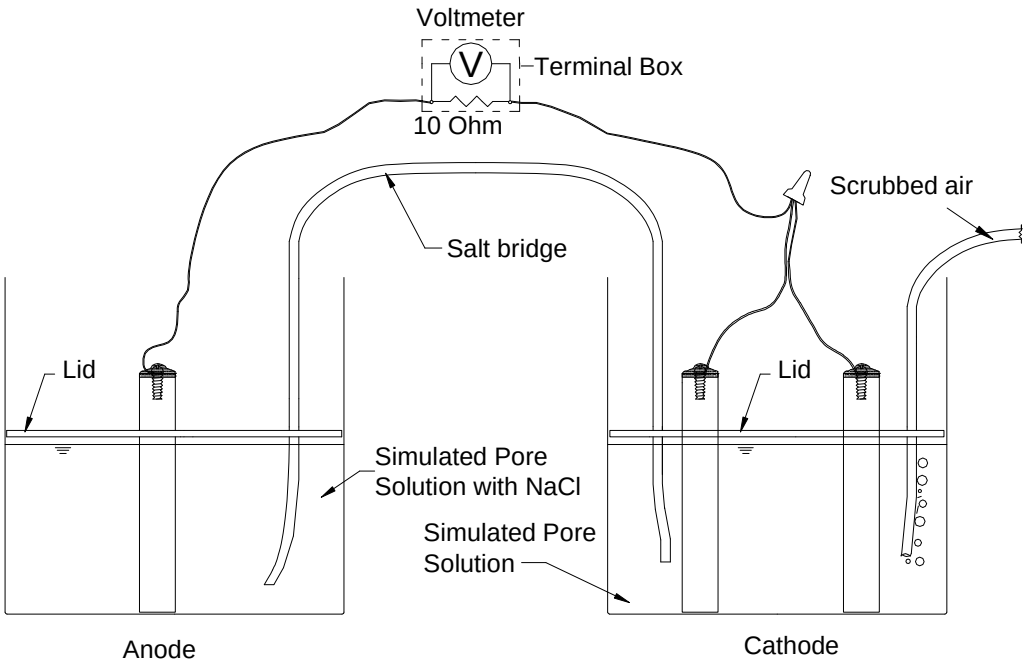

Figure 2.13: Rapid Macrocell Specimen

2.6.2 Materials and Equipment

The following materials and equipment are needed for rapid macrocell test:

Wire – Electrical connections from bar to the terminal box are made with 16 gauge multi-strand copper wire.

Terminal Box – The terminal box is identical to that used for SE and CB specimens described in Section 2.3.2.

Caps – Vinyl caps with an inner diameter of 16 mm (0.627 in.) and a height of 13 mm (0.5 in.) are used to protect the cut ends of epoxy-coated reinforcement from salt solution.

Voltmeter – The voltmeter is used to obtain macrocell voltage drop and corrosion potential measurements. The voltmeter used for this study was a Keithley model 2182A nanovoltmeter.

Reference Electrode – Used for corrosion potential measurements. A saturated calomel electrode (SCE) was used for rapid macrocell readings in this study.

Epoxy – Electrical connections are protected with a rebar patch epoxy by 3M.

Stainless Steel Screws/Washers – Used to connect wire to specimens during testing. Parts are as described in Section 2.6.4.

Containers – Used to hold specimens in pore solution. Containers are 3.8-L (1-gal) high density polyethylene food storage containers. Lids are cut and fitted to rest just above the solution level to minimize evaporation.

Pore solution – Simulates the pore solution in concrete. Based on an analysis by Farzammehr (1985), one liter of simulated pore solution contains 974.8 g of distilled water, 18.81 g of KOH and 17.87 g of NaOH.

Pore Solution with Salt – Simulates pore solution with chloride contamination. A 6.04 molal ion (15%) NaCl solution is used in this study. To obtain this concentration, 172.1 g of NaCl is added to one liter of pore solution.

Salt Bridge – The salt bridge provides an ionic connection between the anode and cathode. To prepare salt bridges, 4.5 g agar and 30 g potassium chloride are dissolved in 100 g of deionized water and heated over a hot plate until the solution begins to congeal. The mixture is used to fill 0.61-m (2-ft) long sections of vinyl tubing with an inner diameter of 6.4 mm (0.25 in.) and an outer diameter of 9.5 mm (0.375 in.). The ends of the tubing are tied together with a rubber band, forming a teardrop shape. The bridges are then kept in boiling water for one hour with cut ends above the water surface. After cooling, rubber bands are removed and the ends of the tubing cut such that continuous gel is exposed. Bridges with internal voids are not used in testing.

Air Scrubber – The air scrubber removes CO_2 from the air bubbled to the cathode to prevent carbonation of the solution. A compressed air supply with a regulator feeds air into a 19-L (5-gal) airtight container via a barbed fitting and vinyl

tubing. Inside the container, a 1.8-m (6-ft) long perforated vinyl tube is used to bubble the air through a 1 N NaOH solution. One end of this tube is sealed and the other end connected to the air inlet tube via the barbed fitting. The tubing is coiled and weighted to keep the perforations submerged. Another barbed fitting, located above the level of the NaOH solution, serves as the air outlet, delivering air scrubbed of CO_2 to the macrocell specimens via vinyl tubing. Barbed plastic T-fittings are used to distribute the air to multiple specimens with small C-clamps used to regulate flow to individual specimens. Care is taken not to over pressurize the 19-L (5-gal) container. The solution in the container is changed as needed.

2.6.3 Macrocell Container Setup

Setup for the containers for the rapid macrocell tests proceeds as follows:

1. Containers are prepared for use as described in Section 2.6.2. Each macrocell specimen requires two buckets – one to hold the pore solution with salt and the anode and one to hold the cathode bars in pore solution. A mark is placed 76 mm (3 in.) above the container base to indicate the fill level of solution. Lids are drilled to allow for the reinforcement, salt bridge, air scrubber line and reference electrode to be inserted into the solution. Containers are labeled “Salt” and “Pore” to avoid inadvertent chloride contamination on future tests.
2. Pore solution with and without salt are prepared as described above and added to a depth of 76 mm (3 in.) to the appropriate container.
3. A salt bridge is inserted with one end in the pore solution and the other end in the pore solution with salt.
4. The air output line from the air scrubber is inserted into the pore solution bucket. The flow rate is adjusted to give a steady flow of air to the cathode.

2.6.4 Fabrication

Specimen fabrication for rapid macrocell specimens proceeds as follows:

1. Reinforcing bars are cut to 127 mm (5 in.) with a band saw. Sharp edges are removed with a grinding wheel.
2. One end of each bar is drilled and tapped to a 19 mm (0.75 in.) depth with 10-24 threading.
3. Epoxy-coated reinforcement is intentionally damaged using a 3 mm (0.125 in.) diameter four-flute drill bit. A milling machine is used to penetrate the epoxy surface to a depth of 0.4 mm (15 mils), just deep enough to expose the underlying steel. Bars are damaged with a total of four holes. Each side has two holes, placed 25 mm (1 in.) and 51 mm (2 in.) away from the untapped end of the bar.
4. Epoxy-coated bars are cleaned with warm soapy water, rinsed and allowed to dry. Bare steel bars are cleaned with acetone.
5. A 16 gauge insulated multi-strand copper wire is attached to the tapped end of each bar using a 13 mm (0.5 in.) 10-24 stainless steel machine screw and a No. 10 stainless steel washer.
6. The electrical connection and all cut ends of epoxy-coated reinforcement are coated with rebar patch epoxy. After drying, a second coat of epoxy is applied to the untapped cut end as well as the interior of a vinyl cap. The cap is immediately pressed on the cut end of the bar and the epoxy allowed to dry.
7. A single test bar is placed in the pore solution with salt as the anode and two bars are placed in the pore solution without salt as the cathode. Bars are held upright with the lid and are electrically connected across a 10-ohm resistor via the terminal box.

2.6.5 Rapid Macrocell Test Procedure

The rapid macrocell tests run for five to forty weeks. The rapid macrocell test as outlined in Annex A1 of ASTM A955-09 specifies a 15 week test; the test duration is varied in this study to track disbondment as a function of corrosion loss and time. Every five weeks the pore solutions with and without salt are changed to counteract carbonation

from atmospheric CO_2. Macrocell corrosion rate and corrosion potential measurements were taken daily for the first week and once a week thereafter. Linear polarization resistance readings are taken for six specimens.

2.6.6 End of Life Autopsy

At the end of testing, specimens are removed from the solutions and photographed to document visible corrosion products. Disbondment tests are performed at all four holes in the epoxy coating. The disbondment test procedure is similar to that described in Section 2.3.7.1 with the exception that disbonded area is measured for all bars, including those considered to have total disbondment. The small size of the rapid macrocell specimens made it possible to measure the actual total disbonded area measurements rather than limiting the maximum value to 677 mm^2 (1.05 $in.^2$) as done for Southern Exposure, cracked beam, and field test specimens, as described in Section 2.3.7.1.

2.6.7 Rapid Macrocell Test Program

A total of forty-eight rapid macrocell test specimens were examined for this study – 24 ECR specimens and 24 MC specimens. The purpose of these tests was to determine the disbondment of the epoxy coating on both types of bar as a function of corrosion loss and time. Specimens consisted of a single ECR or MC bar as the anode and two bare steel bars as the cathode. Every five weeks, three specimens were pulled from testing and a disbondment test performed on the anode. The schedule of testing is shown in Table 2.10. Five control specimens of each type were soaked in simulated pore solution with no chlorides to track disbondment in the absence of chlorides.

Table 2.10: Rapid Macrocell Test Program

ECR		MC	
Specimen Designation	**Weeks Tested**	**Specimen Designation**	**Weeks Tested**
M-ECR-1	5	M-MC-1	5
M-ECR-2	5	M-MC-2	5
M-ECR-3	5	M-MC-3	5
M-ECR-4	10	M-MC-4	10
M-ECR-5	10	M-MC-5	10
M-ECR-6	10	M-MC-6	10
M-ECR-7[a]	15	M-MC-7	15
M-ECR-8	15	M-MC-8	15
M-ECR-9	15	M-MC-9	15
M-ECR-10	20	M-MC-10	20
M-ECR-11	20	M-MC-11	20
M-ECR-12	20	M-MC-12	20
M-ECR-13[a]	40	M-MC-13	25
M-ECR-14	25	M-MC-14	25
M-ECR-15	25	M-MC-15	25
M-ECR-16	25	M-MC-16	30
M-ECR-17	30	M-MC-17	30
M-ECR-18	30	M-MC-18	30
M-ECR-19[a]	40	M-MC-19	35
M-ECR-20	30	M-MC-20	35
M-ECR-21	35	M-MC-21	35
M-ECR-22	35	M-MC-22[a]	40
M-ECR-23	35	M-MC-23[a]	40
M-ECR-24	40	M-MC-24[a]	40
M-ECR-A[b]	10	M-MC-A[b]	10
M-ECR-B[b]	20	M-MC-B[b]	20
M-ECR-C[b]	25	M-MC-C[b]	30
M-ECR-D[b]	30	M-MC-D[b]	35
M-ECR-E[b]	35	M-MC-E[b]	40

[a] LPR tests performed on this specimen

[b] Control specimen kept in simulated pore solution (no salt)

2.7 DONIPHAN COUNTY AND MISSION CREEK BRIDGE TESTS

2.7.1 Description

In 2004, two bridges in Kansas were cast with pickled 2205 stainless steel to study the corrosion resistance of stainless steel on full scale bridge decks. Both bridges were fitted with test bars electrically connected to the stainless steel mats to allow for

corrosion potential mapping. In addition, Southern Exposure and cracked beam specimens were cast with pickled 2205 stainless steel and field test specimens were cast with pickled 2205 stainless steel, epoxy-coated reinforcement and conventional steel. This report continues prior research reported by Guo et al. (2006) and Xing et al. (2010).

The Doniphan County Bridge (DCB) is a 75.8-m (249-ft) long three span continuous composite steel girder bridge on Highway K-7 spanning the Wolf River in Doniphan County, Kansas. The bridge was cast on February 26, 2004. The Mission Creek Bridge (MCB) is a 27.5-m (90-ft) long single span composite steel girder bridge on Highway K-4 spanning Mission Creek in Shawnee County, Kansas. The bridge was cast on August 25, 2004. Both bridge decks are monolithic. Full details for each bridge are shown in Table 2.11.

Table 2.11: DCB and MCB Specifications (Guo et al. 2006)

Bridge			**DCB**	**MCB**
Bridge No.			7-22-18.21 (004)	4-89-4.58 (281)
Bridge Deck Cast Date [a]			February 26, 2004	August 25, 2004
Length m (ft)			75.8 (249)	27.45 (90)
Deck Width m (ft)			8 (26)	11 (36)
Number of Girders			5	6
Type of Girder			Composite	Composite
Number of Spans			3	1
Abutment			Integral	Integral
Deck Type			Monolithic	Monolithic
Deck Depth mm (in.)			210 (8.3)	210 (8.3)
Top Clear Cover mm (in.)			65 (2.6)	65 (2.6)
Bottom Clear Cover mm (in.)			30 (1.2)	30 (1.2)
Reinforcement [b]	Direction	Bar Size	Spacing[d] mm (in.)	
Top	Longitudinal	No.16 (No.5)	290 (11.4)	300 (11.8)
	Transverse	No.16 (No.5)	170 (6.7)	170 (6.7)
Bottom	Longitudinal	No.16 (No.5)	260 (10.2)	250 (9.8)
	Transverse	No.16/13 (No.5/4) [c]	170 (6.7)	170 (6.7)

[a] Bridge deck replacement for DCB, and new construction for MCB.

[b] Reinforcement in midspan region.

[c] No.16 (No.5) and No.13 (No.4) bars are alternated.

[d] Spacing in the midspan region. Over the piers, spacing of the top longitudinal reinforcement is reduced to half.

2.7.2 Mix Design and Concrete Properties

The mixture proportions used for the bridges are shown in Table 2.12. Concrete properties as provided by KDOT are shown in Tables 2.13 and 2.14. For bench scale and field test specimens, trial-batch concrete from the ready mix plant handling the bridge pour was used for the fabrication of test specimens. Concrete was held in trucks prior to casting to simulate transit times from the ready mix plant to the bridge site.

Table 2.12: Mixture Proportions for DCB and MCB

Bridge		**DCB**	**MCB**
Water	kg/m^3 (lb/yd^3)	143 (241)	129 (217)
Cement	kg/m^3 (lb/yd^3)	357 (602)	357 (602)
CA	kg/m^3 (lb/yd^3)	883 (1487)	893 (1504)
FA	kg/m^3 (lb/yd^3)	883 (1487)	893 (1504)
AE	mL/m3 (oz/yd^3)	290 (7.5)	154 (4)
Design *w*/*c*		0.40	0.36
Design Slump	mm (in.)	75 (2.95)	55 (2.25)
Design Air Content	(%)	6.5	6.5
Design Unit Weight	kg/m^3 (lb/ft^3)	2267 (141.37)	2272 (141.70)

Table 2.13: Concrete Properties for Doniphan County Bridge

Sample Location	**Slump mm (in.)**	**Unit Weight kg/m^3 (lb/ft^3)**	**Air Content[a] (%)**	**Air Temp. °C (°F)**	**Conc. Temp. °C (°F)**	**Compressive Strength[b] MPa (psi)**
Pump	90 (3.5)	2313 (144.26)	2.5	7 (45)	11 (52)	41.9 (6080)
Pump	100 (4.0)	2333 (145.28)	2	9 (49)	16 (60)	41.0 (5950)
Pump	90 (3.5)	2321 (144.74)	1	12 (53)	21 (70)	40.8 (5920)
Deck	90 (3.5)	2177 (135.78)	8	12 (53)	21 (70)	35.6 (5160)
Deck	75 (3.0)	2174 (135.59)	9	12 (53)	21 (70)	-
Deck	75 (3.0)	2200 (137.22)	6.5	12 (53)	21 (70)	-
Deck	75 (3.0)	2171 (135.41)	8	12 (53)	21 (70)	-
Deck	75 (3.0)	2170 (135.41)	8	12 (53)	21 (70)	-
Deck	75 (3.0)	2177 (135.78)	8	12 (53)	21 (70)	-

[a] Pressure method was used to test concrete air content.

[b] Average of three cylinders.

Table 2.14: Concrete Properties for Mission Creek Bridge

Sample Location	Slump mm (in.)	Unit Weight kg/m^3 (lb/ft^3)	Air Content[a] (%)	Air Temp. °C (°F)	Conc. Temp. °C (°F)	Compressive Strength[b] MPa (psi)
East Abutment	100 (4.0)	2269 (141.52)	6.1	27 (81)	31 (88)	-
West Abutment	90 (3.5)	2253 (140.52)	5.25	25 (77)	34 (92)	-
Bridge Deck	75 (3.0)	2304 (143.70)	4.25	28 (82)	32 (89)	42.7 (6190)
Bridge Deck	50 (2.0)	2293 (143.00)	5	25 (77)	33 ((91)	42.1 (6110)
Bridge Deck	65 (2.5)	2264 (141.19)	6	25 (77)	35 (94)	-
North Handrail	50 (2.0)	2294 (143.11)	5.5	25 (77)	30 (86)	-
South Handrail	145 (5.75)	2253 (140.52)	5	18 (64)	28 (82)	-

[a] Pressure method was used to test concrete air content.

[b] Average of three cylinders.

2.7.3 Bridge Potential Mapping

2.7.3.1 Bridge Preparation

To allow for bridge potential mappings, stainless steel test bars were prepared and electrically connected to the reinforcing mats, providing an electrical connection to the entire mat of steel. Test bars were prepared in a manner similar to that used for the field test specimens described in Section 2.5.4. Test bar lengths and locations are given in Tables 2.15 and 2.16 for DCB and MCB, respectively. The Doniphan County Bridge had two sets of test bars 11.5 and 23 m (37.8 and 75.5 ft) from the east abutment. Each set of test bars consists of three bars attached to the top mat of steel and two bars attached to the bottom mat of steel. The Mission Creek Bridge had a single set of test bars 3 m (9.8 ft) from the east abutment, consisting of three bars on both the top and bottom mats. Wire leads from the test bars were fed through a hole in the formwork located near the east abutment of each deck, as shown in Figures 2.14 and 2.15 respectively.

Table 2.15: DCB Test Bar Locations (Guo et al. 2006)

Position	Location	No.	Wire Color	Bar Length cm (ft)	Bar Location
Pier #2	Top	1	Blue	183 (6)	East
		2	Blue	183 (6)	Center
		3	Blue	183 (6)	West
	Bottom	4	Black	46 (1.5)	East
		5	White	46 (1.5)	West
Midspan	Top	6	Yellow	183 (6)	East
		7	Green	183 (6)	Center
		8	Black	183 (6)	West
	Bottom	9	White	46 (1.5)	East
		10	Black	46 (1.5)	West

Table 2.16: MCB Test Bar Locations (Guo et al. 2006)

Position	Location	No.	Wire Color	Bar Length cm (ft)	Bar Location
About 3 m (10 ft) away from the east abutment	Top	1	Black	91 (3)	West
		2	Black	91 (3)	Center
		3	Black	91 (3)	East
	Bottom	4	Yellow	91 (3)	West
		5	Yellow	91 (3)	Center
		6	Yellow	91 (3)	East

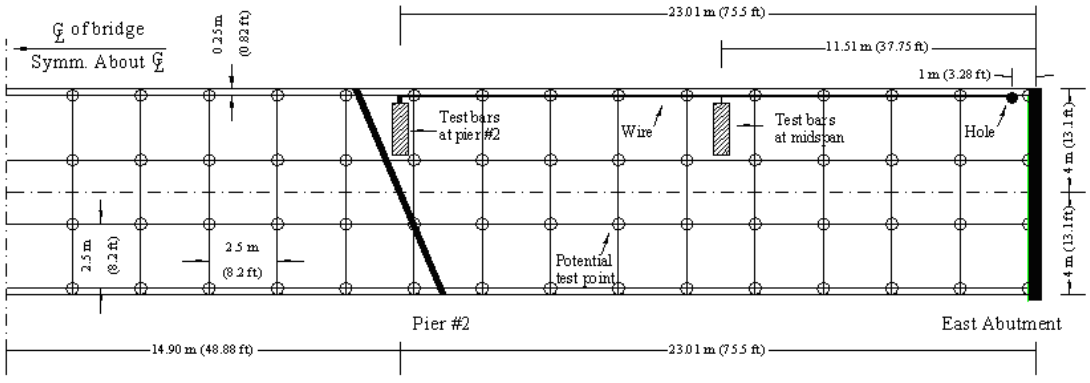

Figure 2.14: DCB Test Bar Layout (Guo et al. 2006)

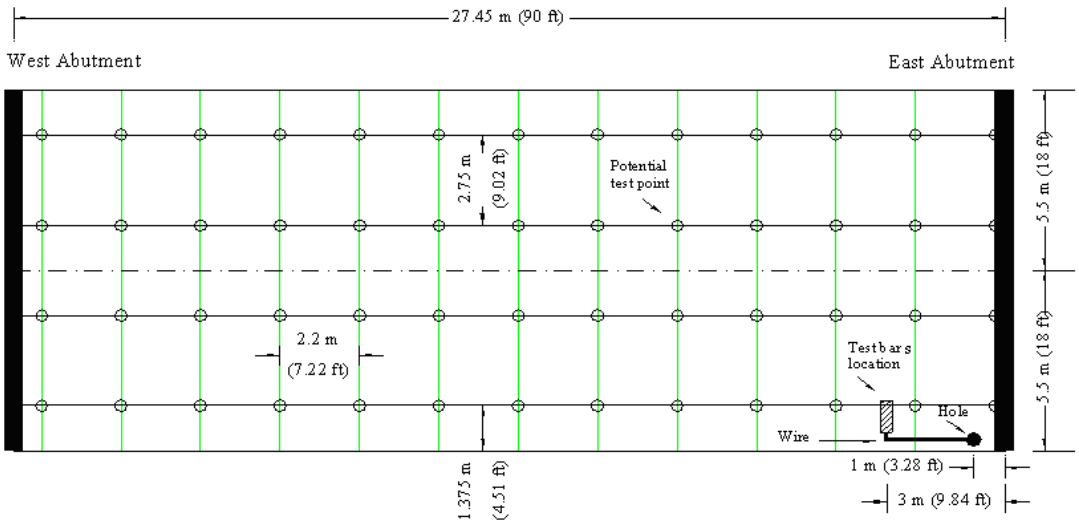

Figure 2.15: MCB Test Bar Layout (Guo et al. 2006)

2.7.3.2 Potential Mapping Procedure

Corrosion potentials are measured and mapped every six months (April and October) on both bridges using a copper/copper sulfate electrode and a voltmeter. Testing proceeds as follows:

1. One hour prior to testing, the bridge is soaked using a water tank truck to reduce concrete resistance.
2. Grid points are marked on the bridge using crayon or chalk. For DCB, grid points are spaced 2.5 × 2.5 m (8.2 × 8.2 ft) along the bridge deck for a total of four rows of 36 points. For MCB, grid points are spaced 2.75 × 2.2 m (9.0 × 7.2 ft) for a total of four rows of 13 points.
3. The positive voltmeter lead is connected to the lead wires from the test bars. The negative lead is connected to the copper/copper sulfate electrode. The electrode is fitted with a damp sponge to improve electrical contact with the bridge.
4. The electrode is placed in contact with the bridge deck at each grid point and the potential recorded.
5. Potential is plotted on a two-dimensional contour plot for ease of analysis.

2.7.4 Bench-Scale Specimens

Southern Exposure and cracked beam specimens were cast at the ready-mix plants using trial batch concrete for both the Doniphan County and Mission Creek bridges. Concrete was consolidated using an internal vibrator as opposed to a shaker table and the test duration was extended due to the corrosion resistant nature of stainless steel. Other than the exceptions noted above, specimen fabrication and testing is identical to that discussed in Section 2.3. The test program is outlined in Table 2.17.

Table 2.17: SE and CB Test Program for KDOT specimens

Bridge	Steel Desiganation[a]	Number of Test Specimens
Southern Exposure (SE) Test		
DCB	SE-2205p	6
MCB	SE-2205p	5
Cracked Beam (CB) Test		
DCB	CB-2205p	3
MCB	SE-2205p	6

[a] 2205p = Pickled 2205 stainless steel used in the bridges decks.

2.7.5 Field Test Specimens

For each bridge, a total of six field test specimens were cast at ready-mix plants using trial batch concrete for the Doniphan County and Mission Creek Bridges. For the Doniphan County Bridge, two each specimens containing 2205p stainless steel, ECR without holes in the epoxy, and conventional reinforcement were cast, all without simulated cracks. For the Mission Creek Bridge, two each specimens containing 2205p stainless steel, ECR with holes through the epoxy as described in Section 2.5.4, and conventional reinforcement were cast. For each pair of specimens, one contained uncracked concrete and one had a simulated crack over four reinforcing bars. Cracks were formed in the manner described in Section 2.5.4.

The reinforcement for the field test specimens for the two bridges is shown in Figures 2.16 and 2.17. Tie wire matching the composition of the reinforcement was used in all specimens. Specimens were cured outside for seven days under wet burlap prior to being demolded and moved to the Adams Campus testing site, where they air cured for three months prior to testing.

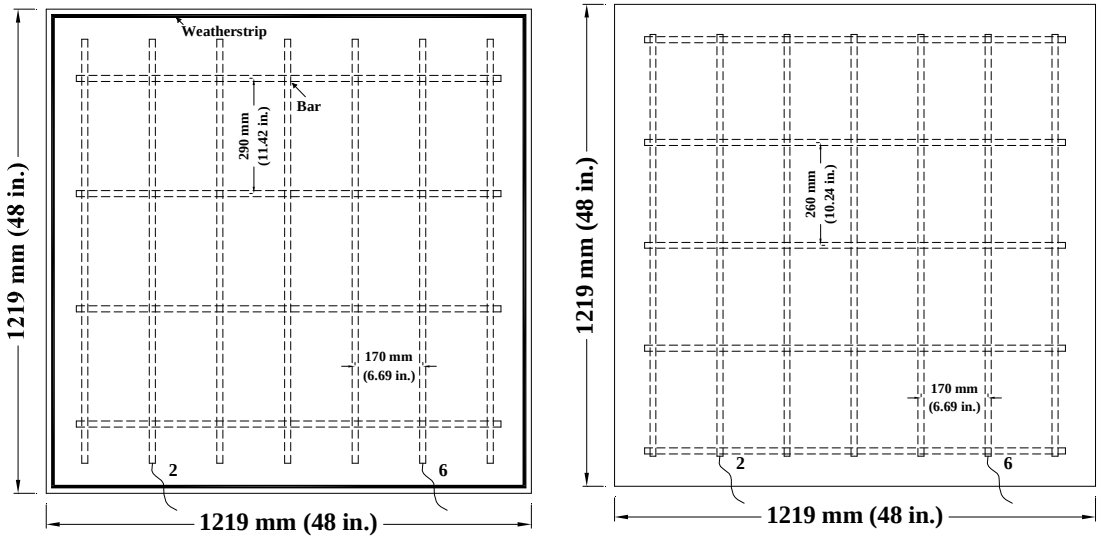

(a) Top slab

(b) Bottom slab

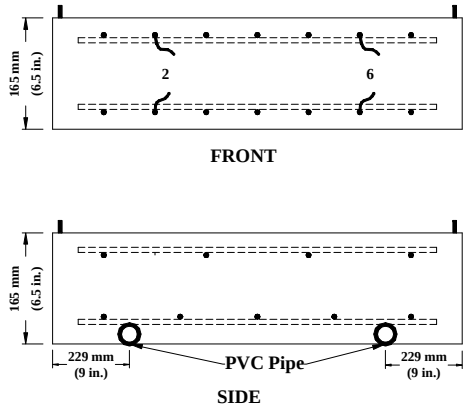

(c) Front and side views

Figure 2.16: DCB Field Test Specimen Dimensions

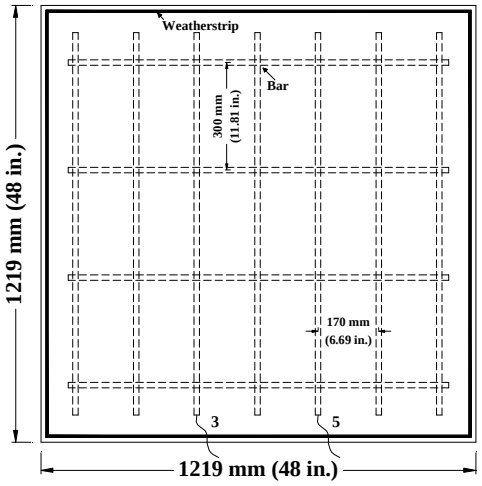

(a) Top slab without cracks

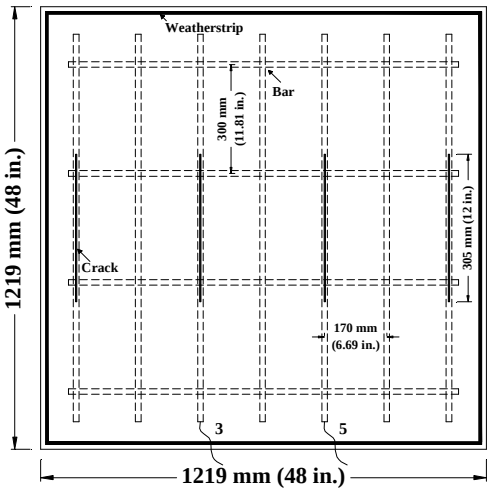

(b) Top slab with cracks

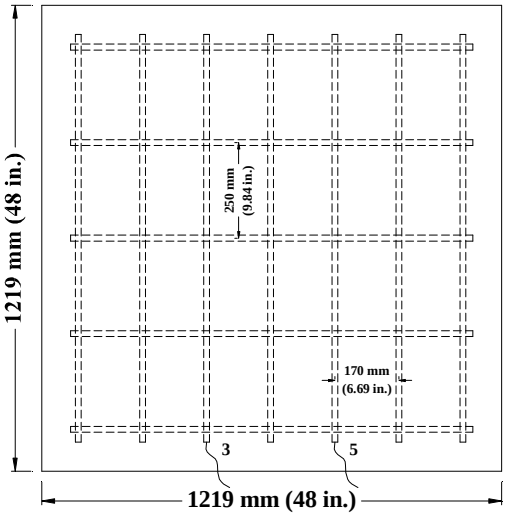

(c) Bottom slab

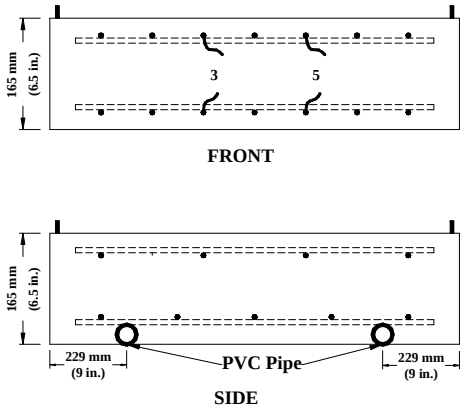

(d) Front and side views

Figure 2.17: MCB Field Test Specimen Dimensions

Concrete properties for the field test specimens are shown in Table 2.18. The lower compressive strength of the concrete used in the Doniphan County Bridge compared to that used in the Mission Creek Bridge is principally due to the low temperature during the winter casting of DCB [7° C (45° F)] compared to the summer casting of MCB [(35° C (95° F)] (Guo et al. 2006).

The test procedure for field test specimens is identical to the procedure outlined in Section 2.5.5. Potential reading points are shown in Figures 2.18 and 2.19, and the test program is summarized in Table 2.19.

Table 2.18: Concrete Properties for Field Test Specimens

Bridge	**DCB**	**MCB**
Specimen Cast Date [a]	January 16, 2004	July 15, 2004
Simulated Haul Time (min.) [b]	55	30
Slump mm (in.)	55 (2.25)	50 (2)
Air Content (%) [c]	5	5.25
Air Temp. °C (°F)	7 (45)	35 (95)
Concrete Temp. °C (°F)	20 (68)	27 (80)
Unit Weight kg/m^3 (lb/ft^3)	2292 (142.96)	2261 (141.04)
Concrete Compressive Strength MPa (psi) [d]		
Curing Room	32.8 (4750)	35.4 (5140)
With Field Specimens	28.9 (4190)	38.2 (5540)

[a] Bridge trial-batch concrete were used for field test specimens.

[b] DCB specimens were cast at Builder Choice Concrete (St. Joseph, MO);
MCB specimens were cast at Meier's Ready Mix, Inc. (Topeka, KS).

[c] Pressure method was used for DCB and Volumetric method was used for MCB.

[d] Average of three cylinders.

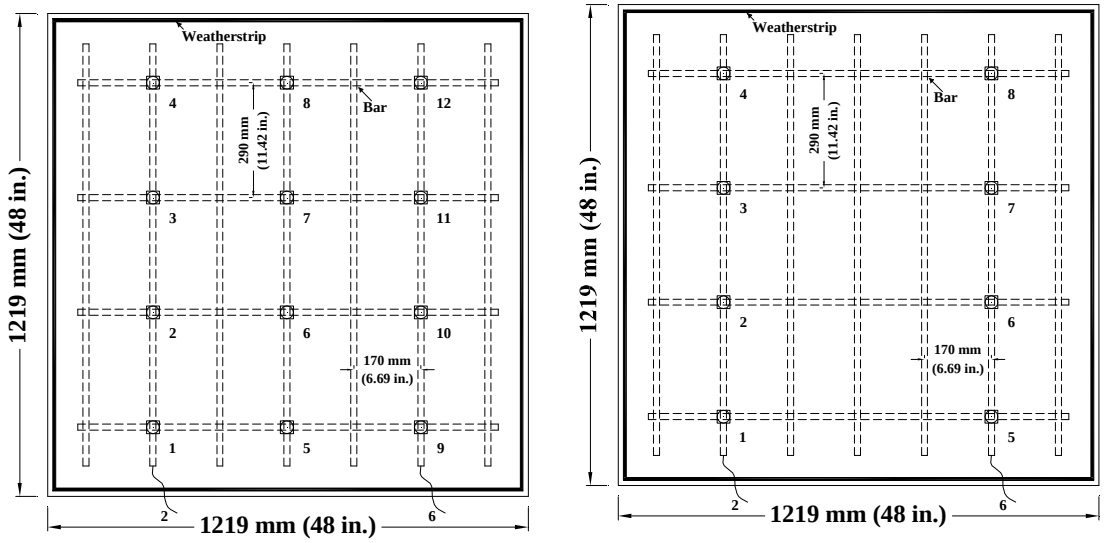

(a) Conventional and stainless steel

(b) Epoxy-coated reinforcement

Figure 2.18: DCB Potential Reading Points

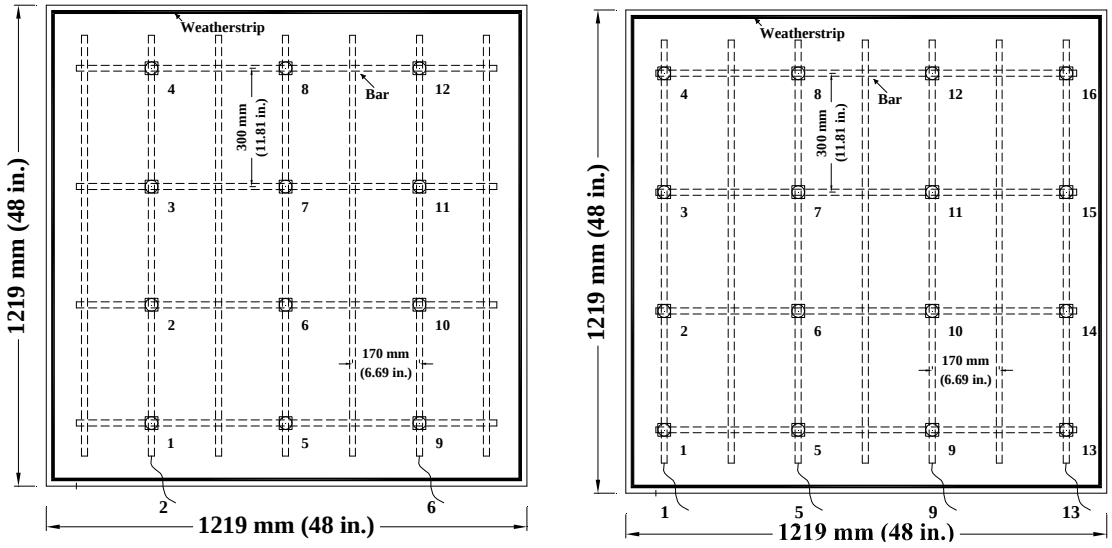

(a) Conventional or stainless steel

(b) Epoxy-coated reinforcement

Figure 2.19: MCB Potential Reading Points

Table 2.19: Test Program for DCB and MCB Field Test Specimens

Bridge	Steel Designation[a]	Number of Test Bars	Potential Test Points	Notes
DCB	Conv. (1)	2	12	
	Conv. (2)	2	12	
	ECR (1)	2	8	
	ECR (2)	2	8	
	2205p (1)	2	12	
	2205p (2)	2	12	
MCB	Conv. (1)	2	12	
	Conv. (2)	2	12	with cracks
	ECR (1)	4	16	with 16 drilled holes
	ECR (2)	4	16	with cracks and 16 drilled holes
	2205p (1)	2	12	
	2205p (2)	2	12	with cracks

[a] Conv. = conventional steel.
ECR = conventional epoxy-coated reinforcement.
2205p = 2205 pickled stainless steel used in the bridge decks.

CHAPTER 3

RESULTS – BENCH SCALE, FIELD TEST, AND BRIDGE POTENTIAL MAPPING

In this chapter, the test results from the Southern Exposure, cracked beam, corrosion initiation beam, field, and rapid macrocell tests, and the bridge potential mappings are presented. The corrosion protection systems evaluated using the Southern Exposure and cracked beam tests include conventional reinforcement with and without corrosion inhibitors and specimens with pickled 2205 stainless steel (2205p) reinforcement. Corrosion initiation beams tested include conventional reinforcement with and without Hycrete to verify earlier work reported by Xing et al. (2010). Field test specimens include conventional and epoxy-coated reinforcement, epoxy-coated reinforcement with increased adhesion, epoxy-coated reinforcement with corrosion inhibitors, multiple-coated reinforcement, and 2205p stainless steel. Rapid macrocell test specimens include epoxy-coated and multiple-coated reinforcement. Results from all specimens with 2205p steel are presented with the bridge potential mappings in Section 3.5.

The results presented in this chapter include macrocell corrosion rate, corrosion loss, mat-to-mat resistance, corrosion potentials of the anode and cathode, microcell corrosion rate, as measured by linear polarization resistance, chloride content, and disbondment. Corrosion loss is determined by integrating the measured corrosion rate over time. Corrosion potentials are measured with respect to a copper-copper sulfate electrode (CSE) for Southern Exposure, cracked beam, corrosion initiation beam, and field test specimens, as well as for bridge potential mappings. Corrosion potentials are measured with respect to a saturated calomel electrode (SCE) for rapid macrocell specimens. Chloride contents are determined for Southern Exposure, corrosion initiation beams, and field test specimens and are presented in terms of water-soluble chloride

content. Disbondment tests are performed on all epoxy-coated and multiple-coated bars at the end of the tests.

As described in Section 2.3.4, most epoxy-coated reinforcement in this study is damaged prior to testing to simulate damage incurred during the handling and placement of reinforcement. It is therefore possible to calculate two corrosion rates (and losses) for epoxy-coated reinforcement: a rate based on the entire surface area of the bar (total area) and a rate based only on the damaged area of the bar (exposed area). Results for specimens with epoxy-coated reinforcement are usually presented in terms of the latter to account for differences in exposed area between specimens. Exceptions include comparing epoxy-coated reinforcement to conventional reinforcement and presenting rapid macrocell readings. The corrosion rate and loss based on total area are related to the rate and loss based on exposed area by the ratio of total area to damaged area. The total area, exposed area, and ratio for each test specimen appear in Table 3.1.

Table 3.1: Bar Areas and Ratios of Total to Exposed Area

Test Specimen[a]	No. of Test Bars	Bar Length, mm (in.)	Total Area, mm^2 ($in.^2$)	Exposed Area, mm^2 ($in.^2$)	Ratio
SE					
4 holes	2	305 (12)	30,400 (47.1)	63.3 (0.098)	480
10 holes	2	305 (12)	30,400 (47.1)	158.3 (0.245)	192
CB					
4 holes	1	305 (12)	15,200 (23.6)	31.7 (0.049)	480
10 holes	1	305 (12)	15,200 (23.6)	79.2 (0.123)	192
FTS					
16 holes	1	991 (39)	49,400 (76.6)	126.7 (0.196)	390

[a] SE =Southern Exposure, CB = cracked beam, FTS = field test specimen

While measuring the voltage drop across the 10-ohm resistor to determine the macrocell corrosion rate, it was observed that voltages near zero could vary by as much as 0.003 mV due to interference from outside sources. To account for this variation, any reading in the range from –0.003 mV to +0.003 mV is treated as a voltage drop of zero. For Southern Exposure, cracked beam, and field test specimens, a voltage drop of 0.003 mV corresponds to a corrosion rate of 0.011, 0.023, and 0.007 µm/yr, respectively.

These values are several orders of magnitude less than the corrosion rates observed in conventional reinforcement and an order of magnitude less than the corrosion rates seen in specimens containing ECR, indicating the rounding described above has little effect on overall results.

With the exception of field test specimens, the test specimens are designed so that the mat of steel acting as the cathode has twice the surface area as the mat acting as the anode. This design choice was made so the corrosion rate would not be limited by the cathodic reaction [Eq. (1.2)]. During active corrosion at the anode, current flows from the cathode (bottom mat of steel) to the anode (top mat) because, by definition, current flows in the opposite direction of electron movement. The resulting corrosion rate is defined as positive. Some readings indicate a current flow from top mat to bottom mat, which is defined as a "negative" corrosion rate. Although the presence of a negative corrosion rate can indicate corrosion on the bottom mat of steel or the connecting wires, it is usually the result of a small current drift from the cathode to the anode due to the difference in surface area.

Results from Southern Exposure and cracked beam specimens are presented in Section 3.1. Results from corrosion initiation beams are presented in Section 3.2. Field test specimen results are presented in Section 3.3. Rapid macrocell results are presented in Section 3.4. Results for 2205 pickled stainless steel, including bench scale specimens, field test specimens, and bridge potential mappings are presented in Section 3.5. Comparisons between disbondment and corrosion loss and disbondment and time are presented in Chapter 6. In addition, the performance of corrosion protection systems among the different test methods and with respect to each other is analyzed. Prior work by Draper et al. (2009) and Xing et al. (2010) is summarized and used in the comparisons.

3.1 SOUTHERN EXPOSURE AND CRACKED BEAM TESTS

The results from the benchscale test programs are presented in this section. Macrocell corrosion rate, corrosion loss, corrosion potentials, and mat-to-mat resistance are discussed in Section 3.1.1. The autopsy results are discussed in Section 3.1.2. The chloride concentration for each specimen is presented in Section 3.1.3, and the total corrosion loss, as measured by linear polarization resistance, is presented in Section 3.1.4.

A total of 12 Southern Exposure and 12 cracked beam specimens are tested to determine the effectiveness of corrosion inhibitors in conjunction with conventional reinforcement. Three Southern Exposure and three cracked beam specimens have no corrosion inhibitor and serve as control specimens (Conv.2); three Southern Exposure and cracked beam specimens are cast with each of the inhibitors tested: calcium nitrite (DCI), Rheocrete 222+ (RH), and Hycrete (HY). The heat of steel used for this series of tests is different than the heat of steel used in the other series of tests; the designation Conv.2 is used to indicate the difference. A water-cement ratio of 0.45 is used for all specimens.

3.1.1 Corrosion Rates, Losses, and Potentials

Figure 3.1 shows average corrosion rates for Southern Exposure specimens with and without corrosion inhibitors. The specimens with no corrosion inhibitor (Conv.2) first show signs of corrosion at week 15, with a peak average corrosion rate of 14.6 µm/yr at week 93. All corrosion inhibitors delay the onset of corrosion and reduce the corrosion rate compared to control specimens. Specimens containing DCI show the earliest initiation and greatest corrosion rate among those containing a corrosion inhibitor, with the first signs of corrosion activity observed at week 22 and a peak corrosion rate of 9.30 µm/yr at week 35. Specimens containing Rheocrete exhibit the latest corrosion initiation, with the first signs of corrosion observed at 26 weeks, and a peak corrosion rate of 3.94 µm/yr observed at week 70. Specimens containing Hycrete

exhibited corrosion initiation at week 25 with a peak corrosion rate of 2.31 µm/yr at week 28.

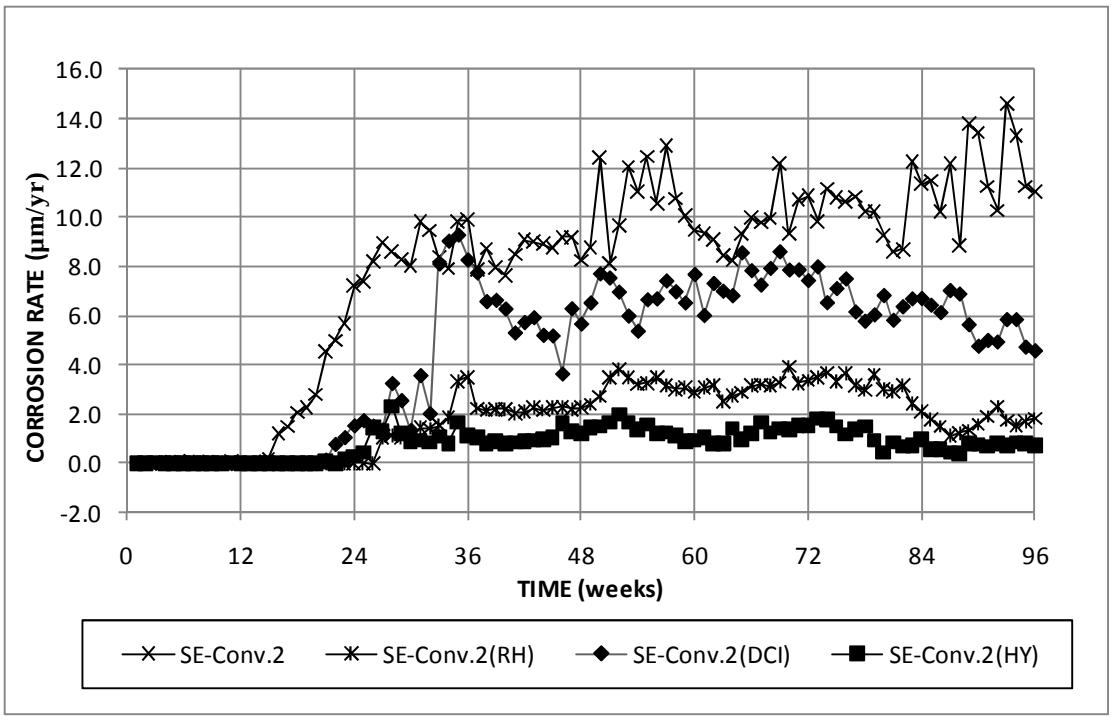

Figure 3.1: Southern Exposure test. Average corrosion rates for specimens with conventional steel, with and without corrosion inhibitors.

Figure 3.2 shows average corrosion losses for the Southern Exposure specimens. Table 3.2 summarizes individual corrosion losses at 96 weeks. The specimens with no corrosion inhibitor (Conv.2) exhibit the greatest corrosion loss, with an average corrosion loss of 14.4 µm at week 96. The specimens containing DCI exhibit slightly more than half the corrosion loss of specimens without corrosion inhibitors, with an average loss of 8.6 µm. Specimens containing Rheocrete exhibit an average corrosion loss of 3.40 µm, and specimens containing Hycrete exhibit an average corrosion loss of 1.55 µm at week 96.

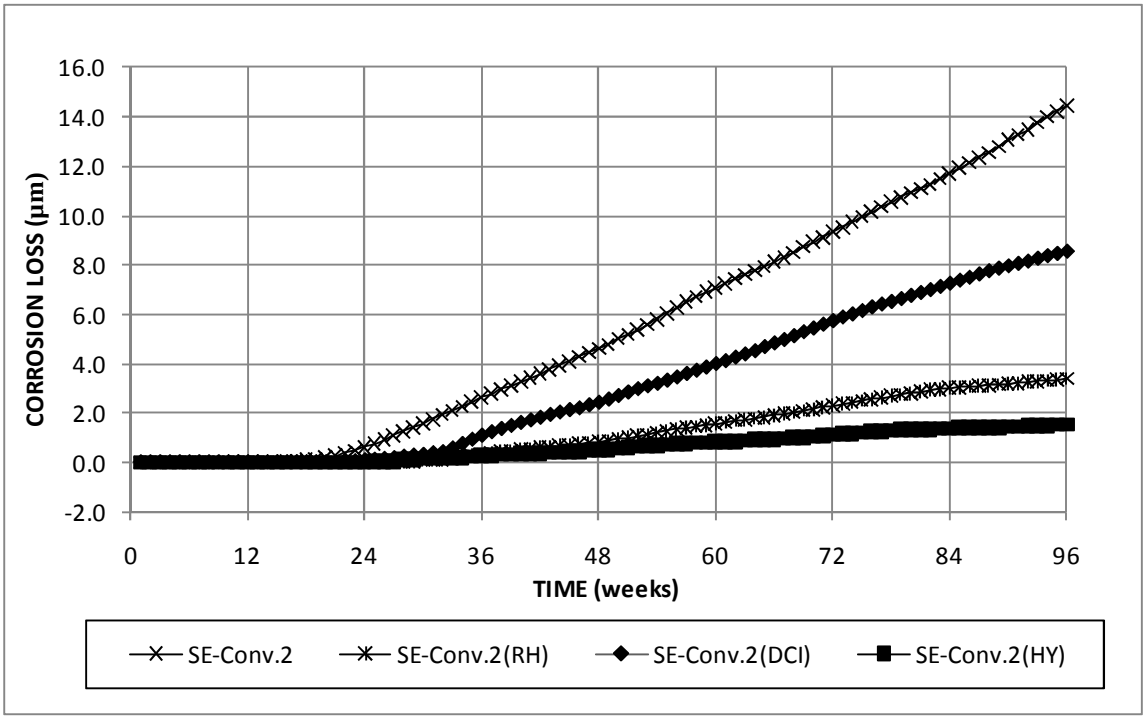

Figure 3.2: Southern Exposure test. Average corrosion losses for specimens with conventional steel, with and without corrosion inhibitors.

Table 3.2: Southern Exposure test. Individual corrosion losses (µm) at 96 weeks for specimens with conventional steel, with and without corrosion inhibitors.

Steel Designation	Specimen			Average	Standard Deviation
	1	2	3		
Conv.2	14.3	13.8	15.2	14.4	0.731
Conv.2(RH)	3.11	2.29	4.79	3.40	1.28
Conv.2(DCI)	9.63	7.28	8.88	8.60	1.20
Conv.2(HY)	1.24	1.59	1.82	1.55	0.292

Average top and bottom mat potentials measured with respect to a copper-copper sulfate electrode (CSE) are shown in Figures 3.3a and 3.3b, respectively. On an individual basis (Figures A1 through A8, Appendix A), the onset of corrosion is marked by both an increase in corrosion rate and a drop in top mat potential to a value more negative than –0.350 V, indicating a greater than 90 percent probability of active corrosion (ASTM C876). On an average basis, a potential drop is observed that

correlates with the first observed spike in corrosion rate (Figure 3.1), but the average corrosion potential does not drop below –0.350 V until all three specimens are corroding.

For specimens with no corrosion inhibitor, the first observed drop in top mat potential (Figure 3.3a) occurs at week 15. The average top mat potential becomes more negative than –0.350 V at week 24 and continues to decrease, approaching –0.600 V at week 57 and remaining there for the remainder of the test. All specimens with corrosion inhibitors show somewhat less negative top mat potentials after initiation. No difference in potential is observed prior to corrosion initiation. The first drop in potential for specimens containing DCI is observed at week 19, with the average top mat potential exceeding –0.350 V at week 24. The corrosion potential continues to drop, reaching –0.500 V at week 48 and remaining there for the remainder of the test. Specimens with Rheocrete show the first corrosion potential drop at week 27. The average top mat potential reaches a value of –0.350 V at week 48. The corrosion potential drops to –0.400 V at week 52 and remains there for the remainder of the test. A drop in corrosion potential is first observed for specimens containing Hycrete at week 26. The average corrosion potential becomes more negative than –0.350 V at week 48, but does not decrease beyond that point. At week 76, the average corrosion potential for specimens containing Hycrete becomes more positive than –0.350 V and remains there for the remainder of the test. Figure 3.1 shows a slight drop in corrosion rate for specimens containing Hycrete around this age, but corrosion activity does not cease.

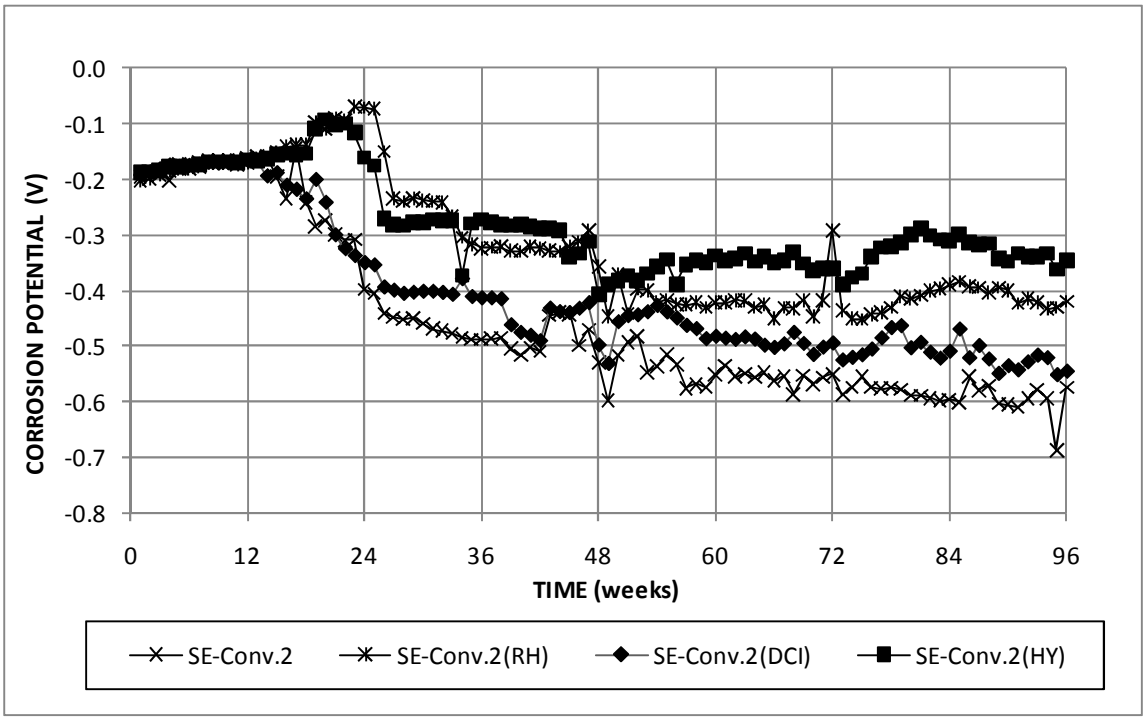

Figure 3.3a: Southern Exposure test. Average top mat potential with respect to CSE for specimens with conventional steel, with and without corrosion inhibitors.

The bottom mat potentials for Southern Exposure specimens are shown in Figure 3.3b. A drop in potential for all specimens is observed at week 49, possibly due to a problem with equipment or interference. The potentials otherwise remain around –0.200 V for all specimens for the duration of the test.

The average mat-to-mat resistances for Southern Exposure specimens are shown in Figure 3.4. All specimens show an increase in resistance from the start of the test to 84 weeks, after which the resistances remain constant or declines. Specimens containing Rheocrete show resistances comparable to control specimens. Specimens containing DCI exhibit somewhat greater resistances than control specimens. Specimens with Hycrete show the greatest mat-to-mat resistance throughout the test.

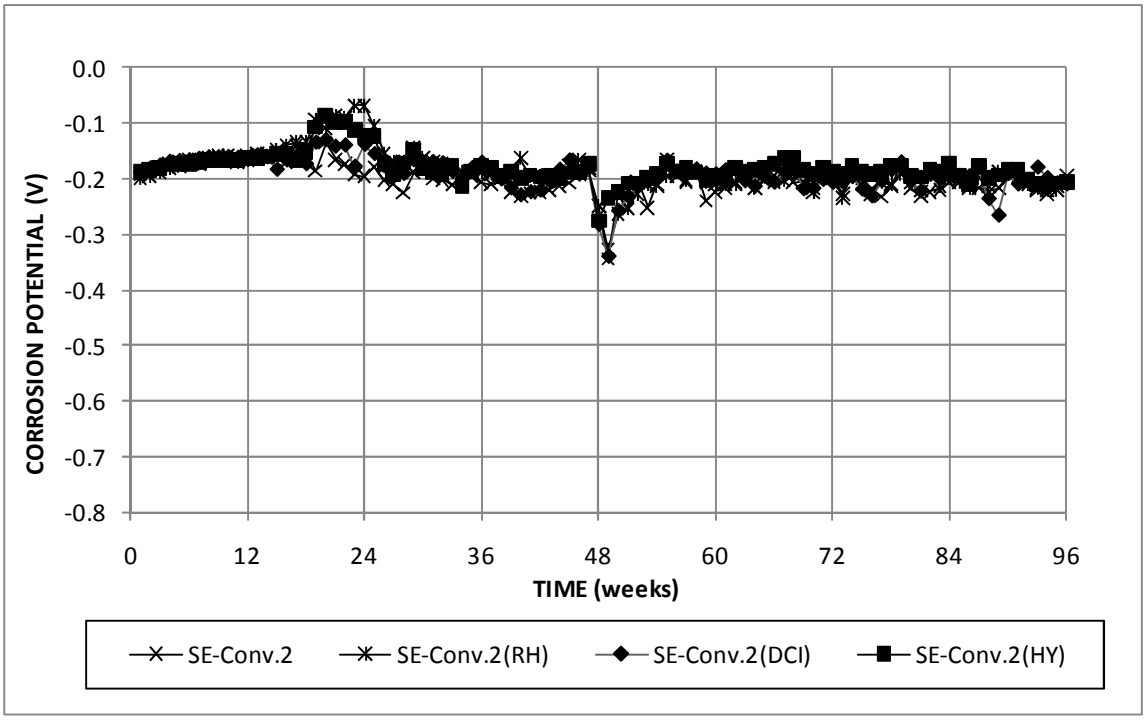

Figure 3.3b: Southern Exposure test. Average bottom mat potential with respect to CSE for specimens with conventional steel, with and without corrosion inhibitors.

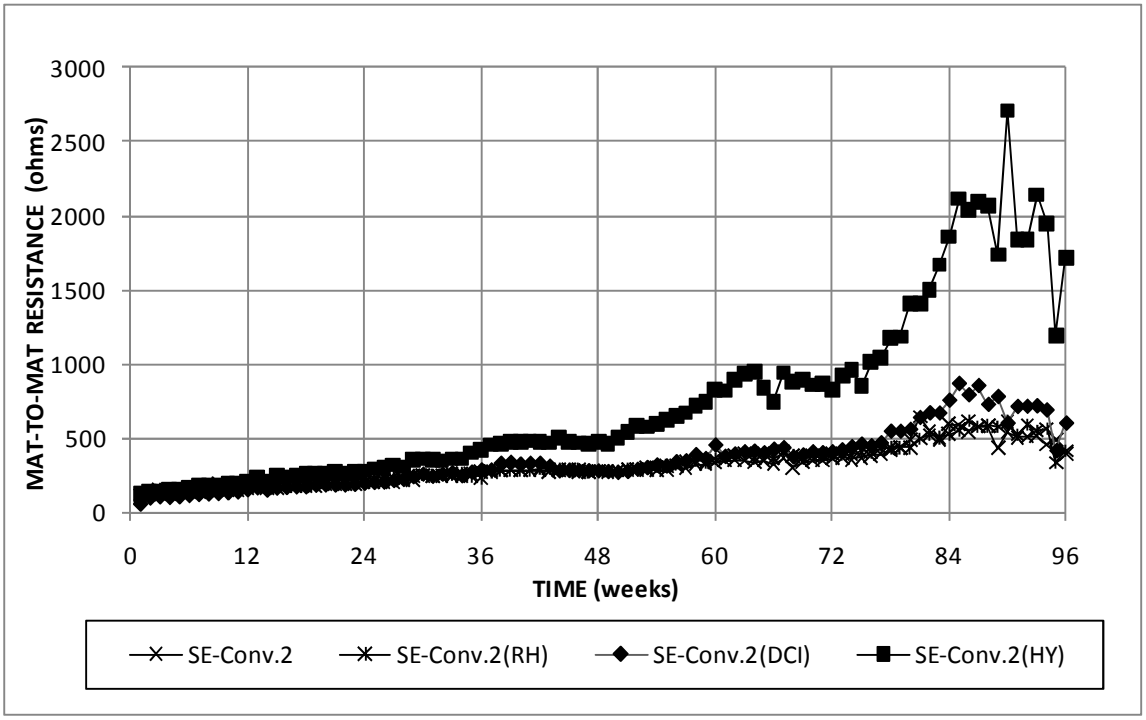

Figure 3.4: Southern Exposure test. Average mat-to-mat resistance for specimens with conventional steel, with and without corrosion inhibitors.

After 96 weeks, heavy staining is observed on two of the three Southern Exposure specimens with no inhibitor (Figure 3.5), with moderate staining on the third specimen. Two of the three specimens containing DCI show moderate staining, and two of the three specimens containing Rheocrete and Hycrete show light staining (Figure 3.6). No staining is observed on the remaining Southern Exposure specimens.

Autopsy results show moderate staining on the top mat of steel for all specimens without corrosion inhibitors, with limited to no corrosion products on the bottom mat of steel (Figure 3.7). Similar results are observed for specimens containing DCI (Figure 3.8) and Rheocrete (Figure 3.9). The specimens containing Hycrete inhibitor show slightly less corrosion on the top bars than bars from specimens with other inhibitors (Figure 3.10).

Figure 3.5: Specimen SE-Conv.2-2, 96 weeks, showing heavy staining on the surface.

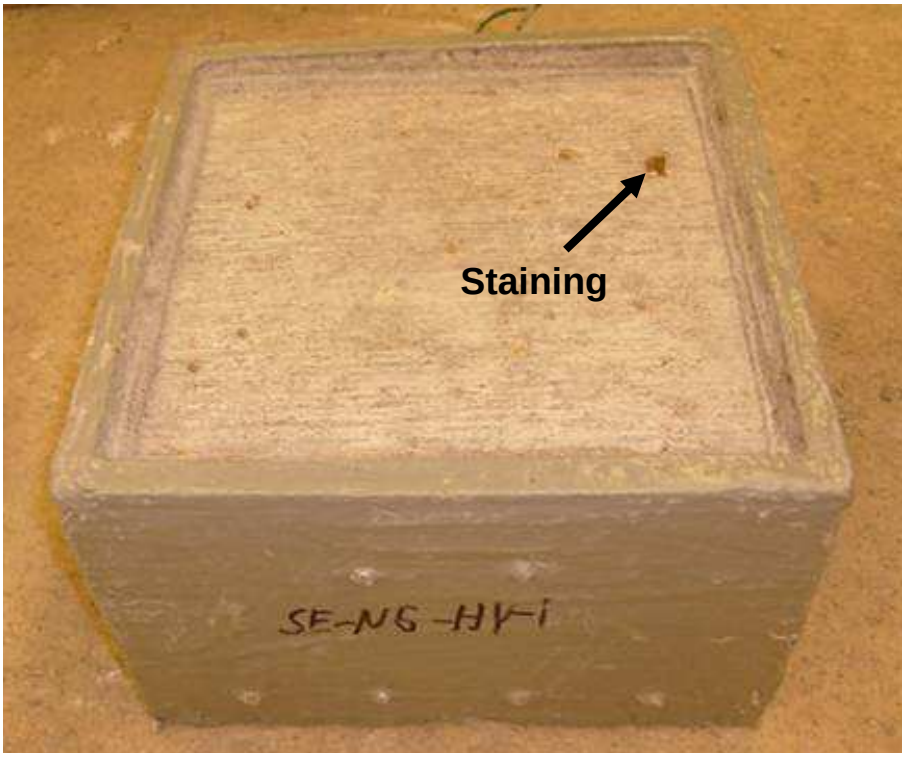

Figure 3.6: Specimen SE-Conv.2-HY-1, 96 weeks, showing light staining on the surface.

Figure 3.7: Specimen SE-Conv.2-1, 96 weeks. Steel in top mat (above label) and bottom mat (below label).

Figure 3.8: Specimen SE-Conv.2-DCI-1, 96 weeks. Steel in top mat (above label) and bottom mat (below label).

Figure 3.9: Specimen SE-Conv.2-RH-2, 96 weeks. Steel in top mat (above label) and bottom mat (below label).

Figure 3.10: Specimen SE-Conv.2-HY-3, 96 weeks. Steel in top mat (above label) and bottom mat (below label).

Figure 3.11 shows average corrosion rates for the cracked beam specimens with and without corrosion inhibitors. The corrosion rates, losses, and potentials for individual specimens are shown in Figures A.9 through A.16 of Appendix A. All specimens exhibit active corrosion by the second week of testing. The specimens with no corrosion inhibitor exhibit a peak average corrosion rate of 29.3 µm/yr at week 11. The corrosion rate drops to around 20 µm/yr at week 13, further dropping to between 10 and 15 µm/yr at week 47. The specimens containing DCI show the greatest corrosion rate among those with a corrosion inhibitor. After early corrosion rates between 15 and 20 µm/yr, corrosion activity drops to approximately 10 µm/yr between week 27 and week 50. After week 50, the specimens containing DCI exhibit corrosion rates greater than the rates observed in control specimens, exceeding 15 µm/yr for several weeks, with a peak corrosion rate of 20.50 µm/yr at week 66. The specimens containing Rheocrete exhibit average corrosion rates similar to the rates observed in specimens containing DCI for the

first 50 weeks. The average corrosion rate for the specimens containing Rheocrete remains between 10 and 15 µm/yr between week 50 and week 84, dropping below 10 µm/yr for most of the last 12 weeks of the test. The peak corrosion rate, 18.6 µm/yr, is observed at week 8. The specimens containing Hycrete show the lowest average corrosion rate; the average corrosion rate does not exceed 5 µm/yr after week 32. The peak corrosion rate of 11.5 µm/yr occurs at week 11.

As shown in Figure 3.11, all specimens exhibit early high corrosion rates that decrease with time; with the exception of specimens containing DCI, all specimens exhibit their peak corrosion rate during the first 12 weeks. The increase in corrosion rate observed after week 50 for specimens containing DCI could be due to a depletion of calcium nitrite around the reinforcing bar.

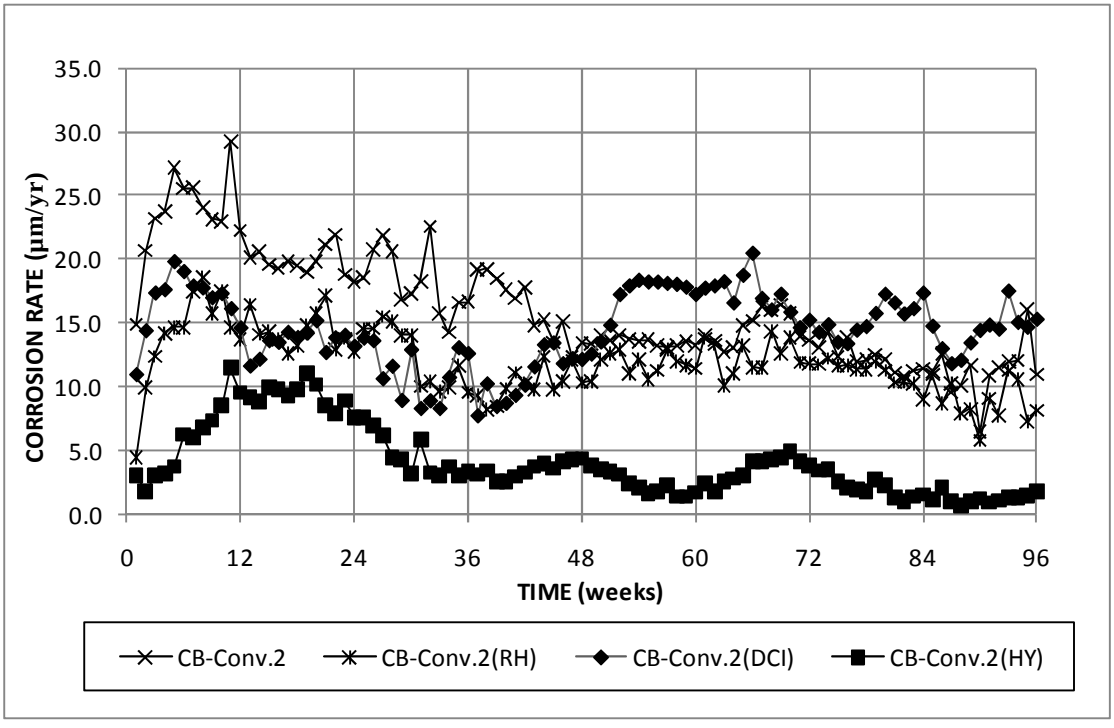

Figure 3.11: Cracked beam test. Average corrosion rates for specimens with conventional steel, with and without corrosion inhibitors.

Figure 3.12 shows the average corrosion losses for cracked beam specimens. Table 3.3 summarizes the individual corrosion losses at 96 weeks. The specimens with no corrosion inhibitor exhibit the greatest corrosion loss, with an average corrosion loss of 29.9 µm at week 96, with one specimen showing a corrosion loss of 44.4 µm. The specimens containing DCI exhibit corrosion losses just below those observed in the specimens without corrosion inhibitors, with an average loss of 26.7 µm at week 96. The specimens containing Rheocrete exhibit a 27 percent reduction in corrosion loss compared to control specimens, with losses of 21.8 µm at week 96. The specimens containing Hycrete exhibit the lowest average corrosion loss, 7.60 µm at week 96.

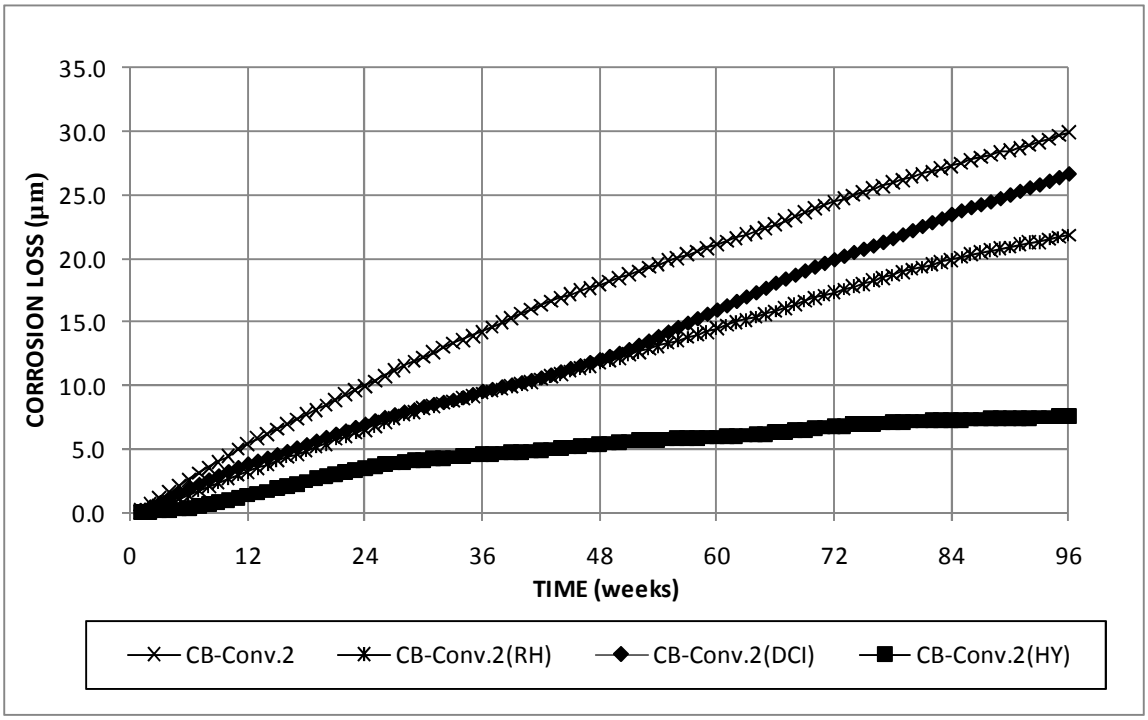

Figure 3.12: Cracked beam test. Average corrosion losses for specimens with conventional steel, with and without corrosion inhibitors.

Table 3.3: Cracked beam test. Individual corrosion losses (µm) at 96 weeks for specimens with conventional steel, with and without corrosion inhibitors.

Steel Designation	Specimen			Average	Standard Deviation
	1	2	3		
Conv.2	44.4	22.7	22.6	29.9	12.5
Conv.2-RH	24.6	18.3	22.6	21.8	3.24
Conv.2-DCI	32.1	26.4	21.6	26.7	5.27
Conv.2-HY	8.64	6.31	7.84	7.60	1.18

Table 3.4 presents the corrosion loss for the Southern Exposure and cracked beam specimens with corrosion inhibitors as a fraction of the corrosion loss in the specimens without inhibitors. All inhibitors show reduced effectiveness in cracked concrete. The specimens containing Rheocrete show the greatest drop in effectiveness; the corrosion losses in uncracked concrete are 24 percent of those in the control specimens, compared to 73 percent of control specimen losses in cracked concrete. The specimens containing DCI show corrosion losses that are 60 percent of those in the control specimens in uncracked concrete compared to 89 percent in cracked concrete. For the specimens containing Hycrete, corrosion losses are 11 percent of the losses observed in the control specimens in uncracked concrete and 25 percent in cracked concrete.

Table 3.4: Southern Exposure and cracked beam tests. Corrosion loss at 96 weeks for specimens with conventional steel with corrosion inhibitors expressed as a fraction of corrosion loss in specimens without inhibitors.

Steel Designation	Southern Exposure		Cracked Beam	
	Loss, µm	Fraction of Control Specimen Loss	Loss, µm	Fraction of Control Specimen Loss
Conv.2	14.4	1.00	29.9	1.00
Conv.2-RH	3.4	0.24	21.8	0.73
Conv.2-DCI	8.6	0.60	26.7	0.89
Conv.2-HY	1.5	0.11	7.6	0.25

The average top mat potentials measured with respect to a copper-copper sulfate electrode (CSE) are shown in Figure 3.13a. The specimens with no inhibitor exhibit average top mat potentials below –0.350 V during the first week of testing. By week 6,

the corrosion potentials approach –0.600 V and, with the exception of a slight increase in corrosion potential at week 49, remain near –0.600 V for the duration of the test. The corrosion potential for specimens containing DCI is similar to the corrosion potential for specimens with no inhibitor. The average corrosion potential is more negative than –0.350 V at the start of the test. The corrosion potential reaches –0.500 V by week 5 and remains there until week 39, at which time it drops to –0.600 V over a four week period. The specimens containing Rheocrete show corrosion potentials more negative than –0.350 V at week 2. The corrosion potential reaches –0.500 V by week 7 and, with the exception of two readings around –0.400 V at weeks 25 and 26, remains near –0.500 V until week 36, at which time it drops to –0.600 V over a six week period. The specimens containing Hycrete first show an average top mat corrosion potential more negative than –0.350 V at week 4. The average corrosion potential reaches –0.500 V at week 18 and varies between –0.400 V and –0.550 V for the remainder of the test.

The bottom mat potentials for cracked beam specimens are shown in Figure 3.13b. Specimens with no inhibitor show average bottom mat potentials more negative than –0.350 V for multiple time periods of limited duration (1 to 3 weeks) during the test. Potentials otherwise start around –0.200 V and gradually decrease to –0.300 V over the duration of the test. The specimens containing Rheocrete show isolated drops in bottom mat potential at weeks 23, 25, and 26, but otherwise remain between –0.200 V and –0.300 V. The specimens containing DCI and Hycrete exhibit bottom mat corrosion potentials more positive than –0.300 V throughout the test.

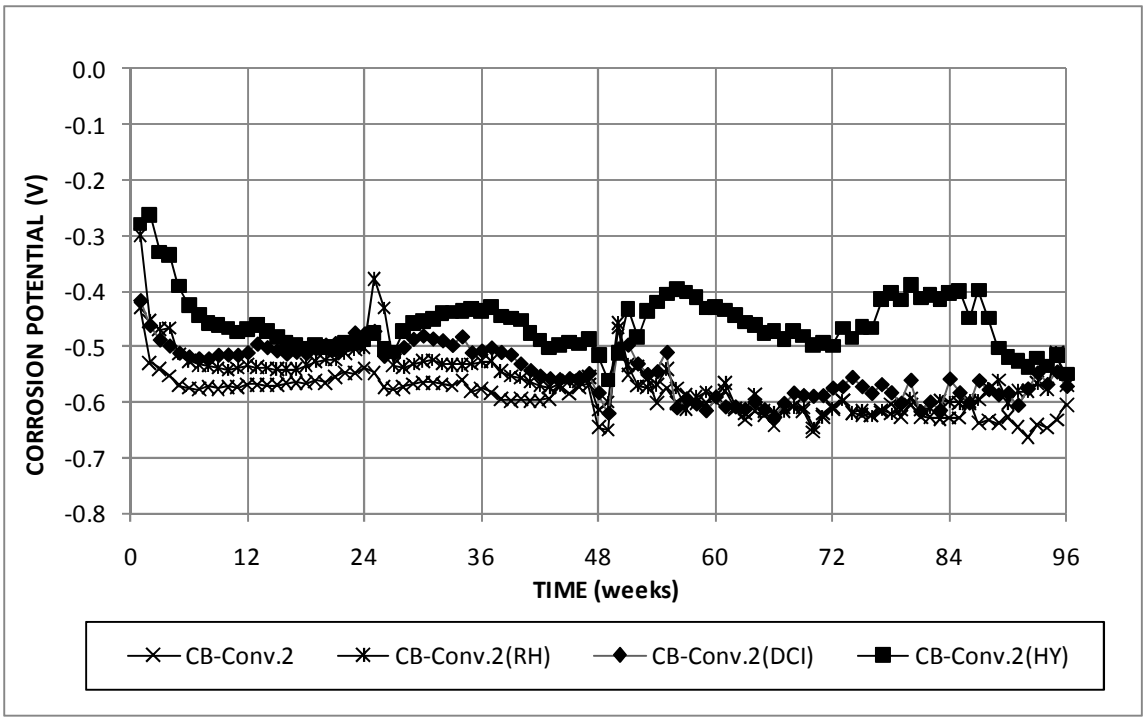

Figure 3.13a: Cracked beam test. Average top mat potential with respect to CSE for specimens with conventional steel, with and without corrosion inhibitors.

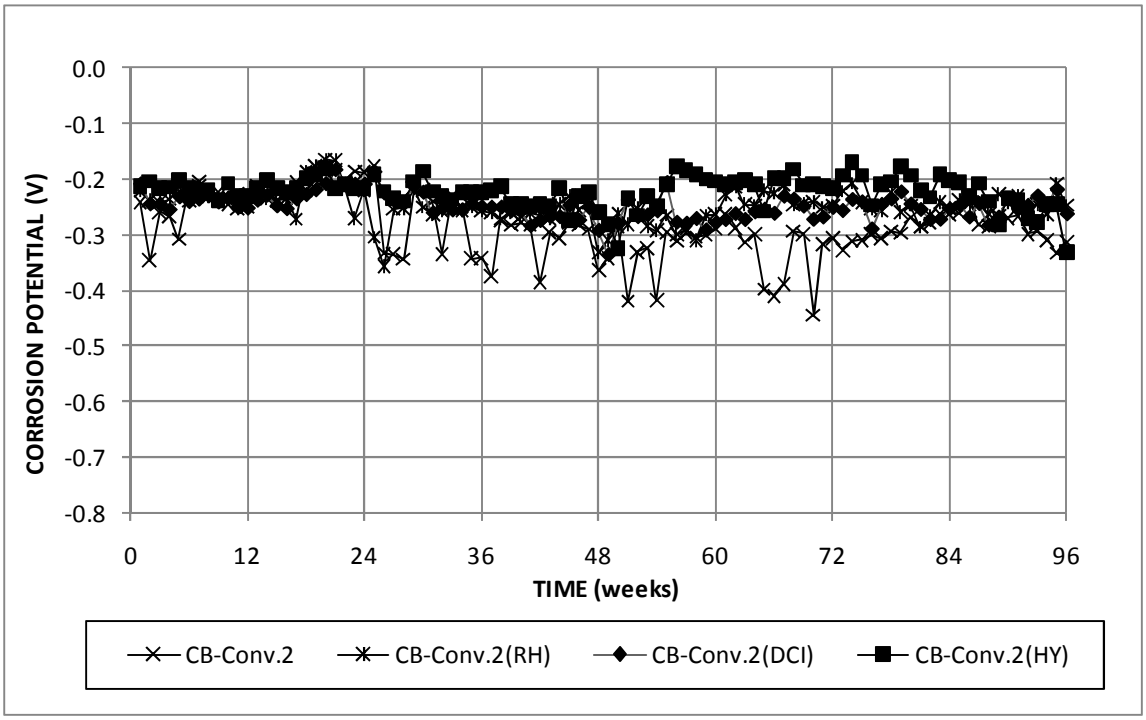

Figure 3.13b: Cracked beam test. Average bottom mat potential with respect to CSE for specimens with conventional steel, with and without corrosion inhibitors.

Figure 3.14 shows the average mat-to-mat resistance for the cracked beam specimens with and without corrosion inhibitors. In general, resistances for cracked beam specimens are two to three times the measured resistance for Southern Exposure specimens (Figure 3.4). This is expected, as the top and bottom mats of steel in cracked beam specimens have half the surface area of the top and bottom mats of steel in Southern Exposure specimens. For all specimens, the resistance tends to increase with time, with an approximately constant resistance near the end of the test. The specimens with no inhibitor and the specimens containing Rheocrete and DCI exhibit similar values of mat-to-mat resistance. The specimens containing Hycrete, however, exhibit a significant increase in resistance compared to the other specimens, with a measured resistance exceeding five times the resistance of other specimens after 84 weeks.

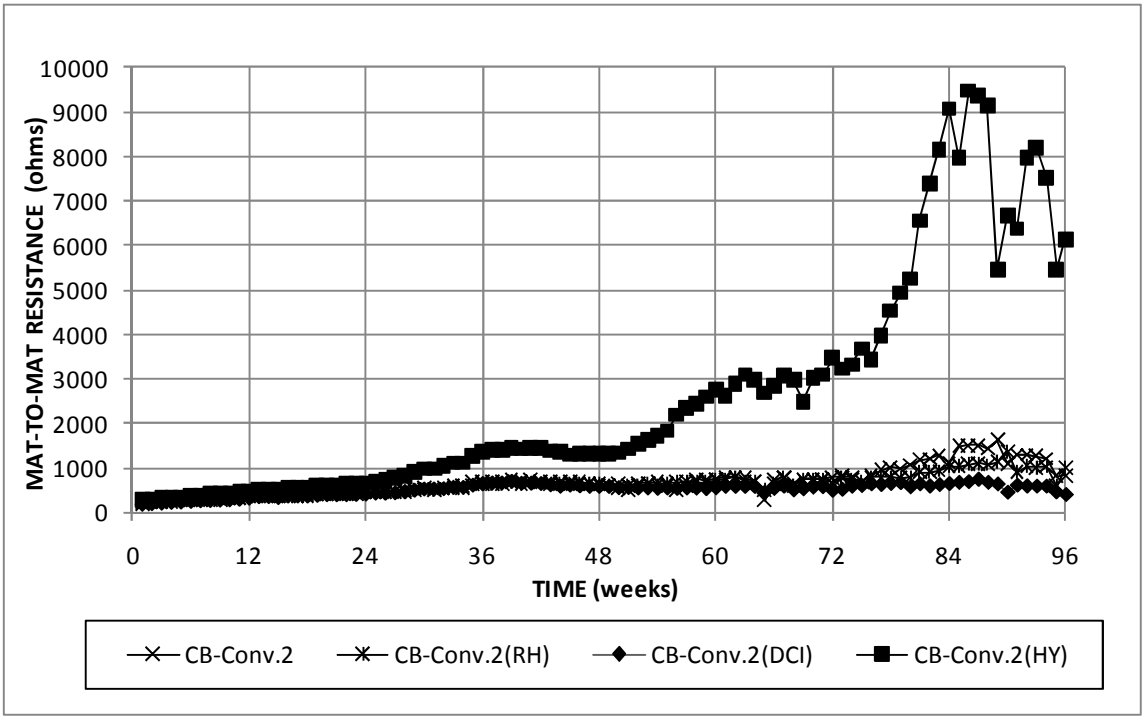

Figure 3.14: Cracked beam test. Average mat-to-mat resistance for specimens with conventional steel, with and without corrosion inhibitors.

3.1.2 Autopsy Results

After 96 weeks, heavy staining is observed on all cracked beam specimens. One specimen with no corrosion inhibitor shows cracking of the concrete cover (Figure 3.15a) in addition to surface staining (Figure 3.15b). Cracking of the concrete is also observed on all three of the specimens containing DCI (Figure 3.16), two of the three specimens containing Rheocrete, and one specimen containing Hycrete.

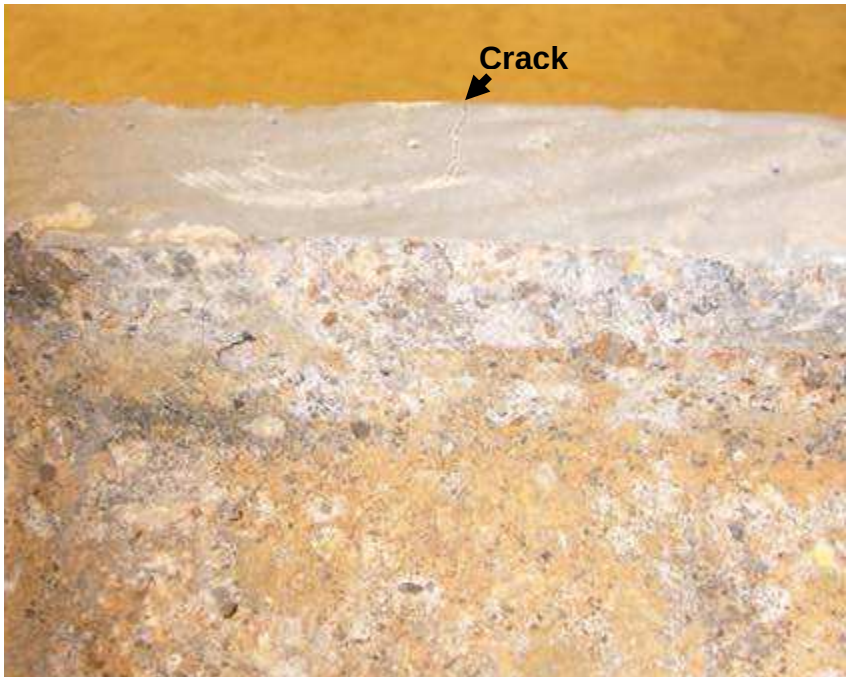

Figure 3.15a: Specimen CB-Conv.2-2 (top surface detail), 96 weeks, showing cracking of the concrete.

Figure 3.15b: Specimen CB-Conv.2-2, 96 weeks, showing staining on the surface.

Figure 3.16: Specimen CB-Conv.2-DCI-2, 96 weeks, showing cracking of the concrete.

The autopsy results show heavy staining on the top bars in all specimens without inhibitors, with light corrosion products on the bottom bars (Figure 3.17). Similar results are observed for specimens with corrosion inhibitors, with heavy corrosion products on the top mat of steel and limited to no corrosion products on the bottom mat of steel (Figure 3.18). One specimen containing Rheocrete shows highly localized corrosion under the crack, with losses of several millimeters at this location (Figure 3.19).

Figure 3.17: Specimen CB-Conv.2-3, 96 weeks. Heavy corrosion on top mat (above label), light corrosion on bottom mat (below label).

Figure 3.18: Specimen CB-Conv.2-DCI-3, 96 weeks. Heavy corrosion on top mat (above label), light corrosion on bottom mat (below label).

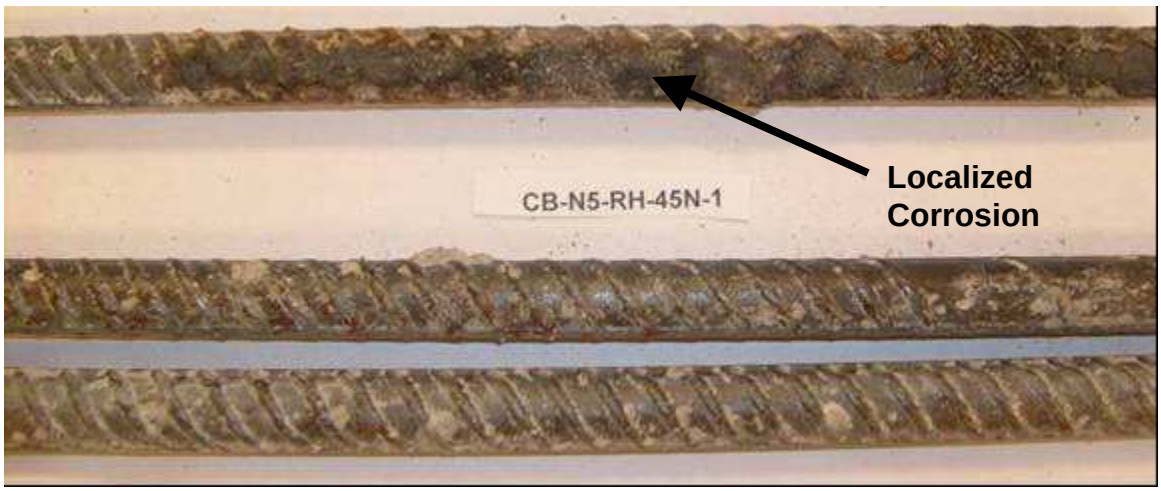

Figure 3.19: Specimen CB-Conv.2-RH-1, 96 weeks. Heavy localized corrosion (arrow) on top mat (above label), light corrosion on bottom mat (below label).

3.1.3 Linear Polarization Resistance (LPR) Results

Linear polarization resistance tests were performed on one Southern Exposure and cracked beam specimen for each inhibitor type and one SE and CB control specimen. The LPR (microcell) corrosion loss and macrocell corrosion loss for each specimen is presented in Table 3.5. For Southern Exposure specimens, the specimen with no corrosion inhibitor shows the greatest microcell corrosion loss, 20.46 µm at 96 weeks. All specimens with inhibitors show decreased corrosion losses compared to control specimens; the specimen containing DCI exhibits microcell losses of 12.15 µm at 96 weeks, while specimens containing Rheocrete and Hycrete show microcell losses at 96 weeks of 4.61 µm and 2.61 µm, respectively.

The cracked beam specimen without a corrosion inhibitor shows a microcell corrosion loss of 49.16 µm at 96 weeks. The specimens containing DCI and Rheocrete inhibitors show greater microcell corrosion losses than the control specimen; 132.8 µm and 62.12 µm, respectively. Only the specimen containing Hycrete shows less microcell corrosion loss at 96 weeks than control specimens, with a loss of 27.38 µm.

Table 3.5: Microcell and Macrocell Corrosion Loss for Individual Specimens

Specimen	Southern Exposure Test		Cracked Beam Test	
	Microcell	Macrocell	Microcell	Macrocell
Conv.2-1	20.46	14.31	49.16	44.39
Conv.2-RH-1	4.61	3.11	62.12	24.58
Conv.2-DCI-1	12.15	9.63	132.8	32.09
Conv.2-HY-1	2.61	1.24	27.38	8.64

The ratio of the microcell corrosion loss for the single specimen to the average macrocell corrosion loss for these specimens for each specimen type is shown in Table 3.6. With the exception of the specimens with no inhibitor, the ratio of microcell to macrocell corrosion loss is greater for the cracked beam specimens than for the Southern Exposure specimens. This indicates that significant differences in environment exist in the vicinity of the crack, resulting in localized corrosion, with cathodes located on the top bar away from the crack.

Table 3.6: Ratio of Microcell to Macrocell Corrosion Loss-SE and CB Specimens.

Specimen	Ratio: Microcell Loss to Macrocell Loss	
	Southern Exposure	Cracked Beam
Conv.2-1	1.43	1.11
Conv.2-RH-1	1.48	2.53
Conv.2-DCI-1	1.26	4.14
Conv.2-HY-1	2.11	3.17

3.1.4 Chloride Content

All Southern Exposure specimens were sampled for chloride content at corrosion initiation, at 48 weeks, and at 96 weeks. The values of chloride content at 48 weeks are presented in Appendix C. Chloride contents at corrosion initiation and at 96 weeks are discussed in this section. Cracked beam specimens were not sampled for chlorides.

Table 3.7 gives the average age and chloride content at corrosion initiation for the Southern Exposure specimens. The specimens with no inhibitor had an average time to corrosion initiation of 20.7 weeks, at an average chloride content of 0.88 kg/m^3 (1.48

lb/yd^3). All of the corrosion inhibitors extended the time to corrosion initiation. The specimens containing Rheocrete show the greatest time to corrosion initiation, initiating corrosion at 37.3 weeks at an average chloride content of 2.16 kg/m^3 (3.63 lb/yd^3). The specimens containing DCI initiated corrosion at an average age of 29.3 weeks and an average chloride content of 3.72 kg/m^3 (6.26 lb/yd^3). The specimens containing Hycrete initiated corrosion at an average age of 31.3 weeks and an average chloride content of 1.19 kg/m^3 (2.00 lb/yd^3); however, this average is heavily influenced by the high chloride content measured in specimen Conv.2-HY-45-1, 2.14 kg/m^3 (3.62 lb/yd^3). The latter value differs markedly from that measured in the other specimens, 0.82 and 0.62 kg/m^3 (1.39 and 1.05 lb/yd^3), and the values measured in the corrosion initiation beams described in Section 3.2.

Table 3.7: Southern Exposure Test. Chloride Content at Corrosion Initiation

Specimen	Age At Initiation (weeks)	Water Soluble Cl^- Content, kg/m^3						Average, kg/m^3	Standard Deviation, kg/m^3	Coefficient of Variation
		1	2	3	4	5	6			
SE-Conv.2-45-1	23	1.84	1.01	1.46	2.66	0.53	-	1.50	0.81	0.54
SE-Conv.2-45-2	23	0.71	0.30	0.83	0.79	0.68	-	0.66	0.21	0.32
SE-Conv.2-45-3	16	0.53	0.56	0.64	0.60	0.30	0.23	0.48	0.17	0.36
SE-Conv.2 Avg.	20.7							0.88	0.64	0.73
SE-Conv.2-RH-45-1	34	2.61	1.73	1.90	1.71	1.39	2.49	1.97	0.48	0.24
SE-Conv.2-RH-45-2	51	2.24	1.13	2.44	2.81	2.68	-	2.26	0.67	0.30
SE-Conv.2-RH-45-3	27	1.20	1.74	1.18	3.26	2.76	3.28	2.24	0.98	0.44
SE-Conv.2-RH Avg.	37.3							2.16	0.71	0.33
SE-Conv.2-DCI-45-1	33	2.05	3.52	3.64	3.71	1.95	2.37	2.87	0.83	0.29
SE-Conv.2-DCI-45-2	22	4.95	2.19	3.60	4.54	1.39	1.46	3.02	1.56	0.52
SE-Conv.2-DCI-45-3	33	3.00	5.40	4.28	6.94	6.68	-	5.26	1.65	0.31
SE-Conv.2-DCI Avg.	29.3							3.72	1.69	0.45
SE-Conv.2-HY-45-1	45	2.66	1.63	-	2.13	-	1.93	2.14	0.44	0.20
SE-Conv.2-HY-45-2	26	1.15	0.72	1.05	1.02	0.36	0.63	0.82	0.30	0.37
SE-Conv.2-HY-45-3	23	1.13	0.41	0.90	0.39	0.34	0.53	0.62	0.32	0.52
SE-Conv.2-HY Avg.	31.3							1.19	0.70	0.59

Table 3.8 gives the average chloride contents at 96 weeks for Southern Exposure specimens. The specimens with no inhibitor have an average chloride content of 11.59 kg/m^3 (19.5 lb/yd^3) at 96 weeks. The specimens containing DCI show a greater average chloride content than control specimens at 96 weeks, 14.49 kg/m^3 (24.4 lb/yd^3). The

specimens containing Rheocrete and Hycrete show decreased chloride contents at 96 weeks, 5.83 and 3.77 kg/m^3 (9.83 and 6.35 lb/yd^3), respectively.

Table 3.8: Southern Exposure Test. Chloride Content at 96 Weeks

Specimen	Water Soluble Cl^- Content, kg/m^3						Average, kg/m^3	Standard Deviation, kg/m^3	Coefficient of Variation
	1	2	3	4	5	6			
SE-Conv.2-45-1	11.52	9.04	11.74	9.23	10.95	8.55	10.17	1.39	0.14
SE-Conv.2-45-2	10.31	8.10	8.63	12.34	12.79	11.21	10.56	1.92	0.18
SE-Conv.2-45-3	16.44	14.10	8.21	21.73	13.65	10.01	14.02	4.80	0.34
	SE-Conv.2 Avg.						11.59	3.62	0.31
SE-Conv.2-RH-45-1	4.95	5.93	7.95	4.76	4.50	5.36	5.58	1.27	0.23
SE-Conv.2-RH-45-2	6.38	6.78	6.19	3.79	7.35	-	6.10	1.37	0.22
SE-Conv.2-RH-45-3	-	3.71	5.48	8.63	4.37	6.90	5.82	1.98	0.34
	SE-Conv.2-RH Avg.						5.83	1.46	0.25
SE-Conv.2-DCI-45-1	-	-	-	-	-	-	-	-	-
SE-Conv.2-DCI-45-2	13.35	18.04	10.69	14.96	16.91	15.23	14.86	2.61	0.18
SE-Conv.2-DCI-45-3	13.84	19.13	-	11.36	12.15	-	14.12	3.49	0.25
	SE-Conv.2-DCI Avg.						14.49	2.83	0.20
SE-Conv.2-HY-45-1	1.54	1.95	-	4.31	-	6.34	2.60	2.23	0.86
SE-Conv.2-HY-45-2	1.98	5.05	1.39	3.56	3.30	7.01	3.71	2.06	0.55
SE-Conv.2-HY-45-3	7.39	3.03	5.29	4.20	4.84	5.18	4.99	1.44	0.29
	SE-Conv.2-HY Avg.						3.77	1.89	0.50

3.1.5 Summary

In uncracked concrete, all corrosion inhibitors tested improve the corrosion resistance of conventional reinforcement. The specimens containing DCI exhibit approximately half the corrosion loss of specimens without a corrosion inhibitor. The specimens containing Rheocrete and Hycrete exhibit approximately 25 and 10 percent corrosion losses, respectively, compared to the specimens containing no corrosion inhibitor.

In cracked concrete, all corrosion inhibitors are less effective than in uncracked concrete. The specimens containing DCI exhibit corrosion losses comparable to those observed in specimens without corrosion inhibitors. The specimens containing Rheocrete exhibit a 27 percent reduction in corrosion loss compared to the control specimens, and the specimens containing Hycrete exhibit a reduction in corrosion loss of approximately 75 percent compared to the control specimens.

3.2 CORROSION INITIATION BEAMS

A total of 12 corrosion initiation beams were tested to verify the low critical chloride corrosion threshold for concrete containing Hycrete reported by Xing et al. (2010). Six beams were cast with concrete containing Hycrete and six beams were cast with no inhibitor as a control. Corrosion initiation was missed on specimens B-Conv.2-5 and B-Conv.2(HY)-2; results from these specimens are not presented.

Figure 3.20 shows the corrosion rates for each of the five specimens without inhibitors in the concrete. Corrosion initiation, defined as a corrosion rate exceeding 0.3 µm/yr generally accompanied by a drop in corrosion potential, occurs between 16 and 28 weeks for specimens without a corrosion inhibitor. For specimens 1, 2, and 4, the corrosion rate increases from zero to above the corrosion threshold in a single week. Specimen B-Conv.2-6 exhibits a negative corrosion rate between 10 and 20 weeks before initiating corrosion at week 23. The corrosion rate of specimen B-Conv.2-3 increases from zero to above the corrosion threshold over a two week period.

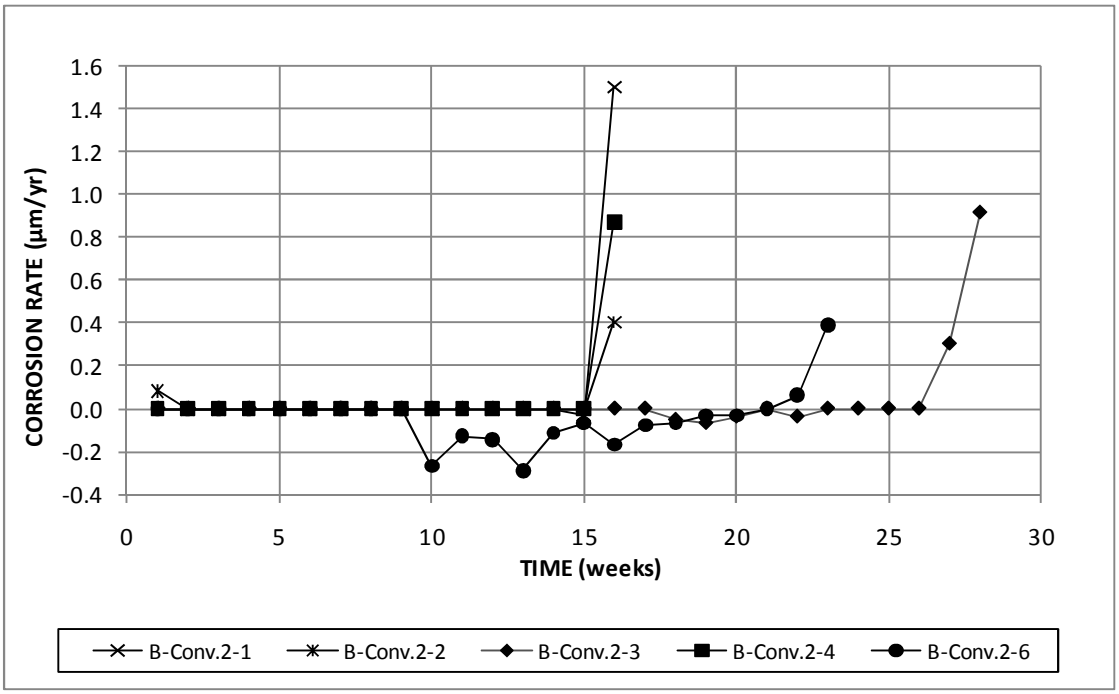

Figure 3.20: Corrosion initiation beam test. Individual corrosion rates for specimens with conventional reinforcement with no corrosion inhibitor.

Figure 3.21 shows the top mat corrosion potentials for each of the five initiation beam specimens without inhibitors. Specimen B-Conv.2-1 shows a drop in corrosion potential one week before the corresponding jump in corrosion rate. For all other specimens, a drop in corrosion potential occurs at the same time as the increase in corrosion rate.

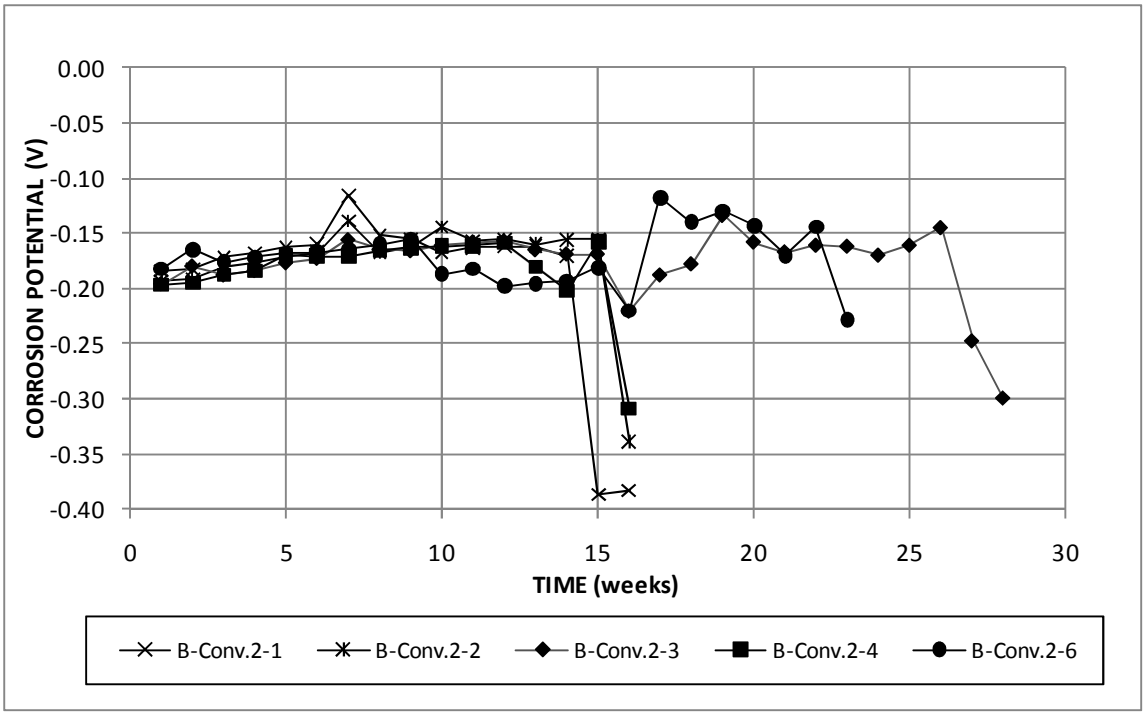

Figure 3.21: Corrosion initiation beam test. Individual top mat corrosion potentials with respect to CSE for specimens with conventional reinforcement with no corrosion inhibitor.

Figure 3.22 shows the corrosion rates for each of the five specimens containing Hycrete. Corrosion initiation occurs between 24 and 68 weeks. For all specimens with Hycrete, the corrosion rate increases from zero to a value greater than 0.3 μm/yr in a single week.

Figure 3.23 shows the top mat corrosion potentials for each of the five initiation beam specimens containing Hycrete. Specimen B-Conv.2(HY)-5 does not show a drop

in corrosion potential when the corrosion rate increases. For all other specimens, a drop in corrosion potential occurs at the same time as the increase in corrosion rate.

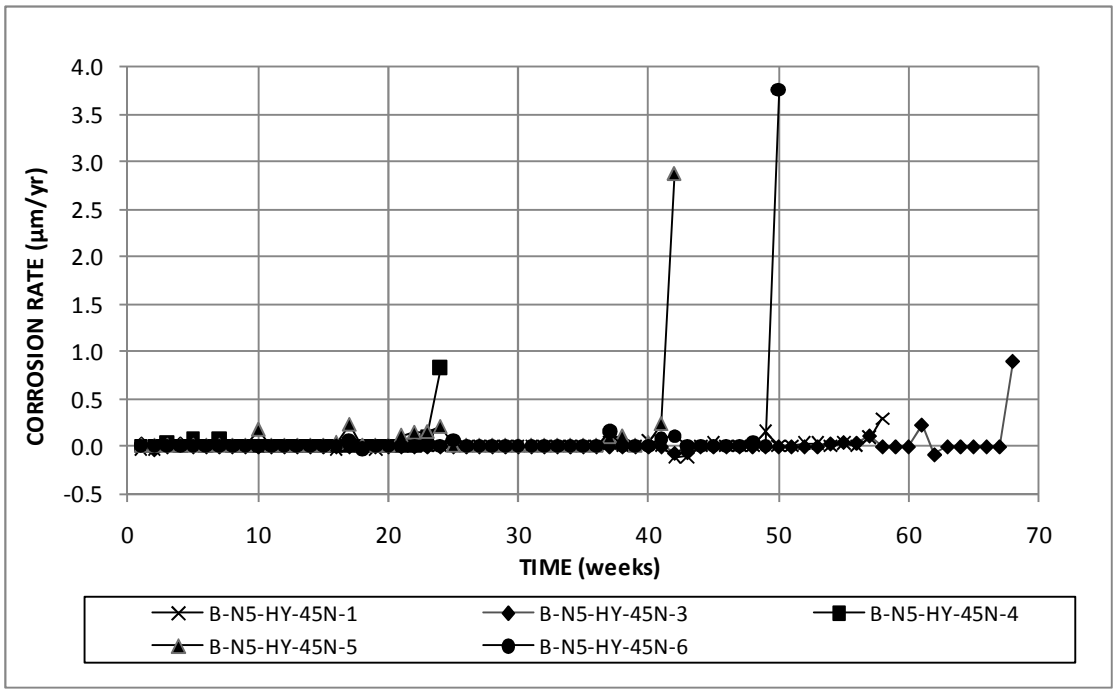

Figure 3.22: Corrosion initiation beam test. Individual corrosion rates for specimens with conventional reinforcement in concrete containing Hycrete.

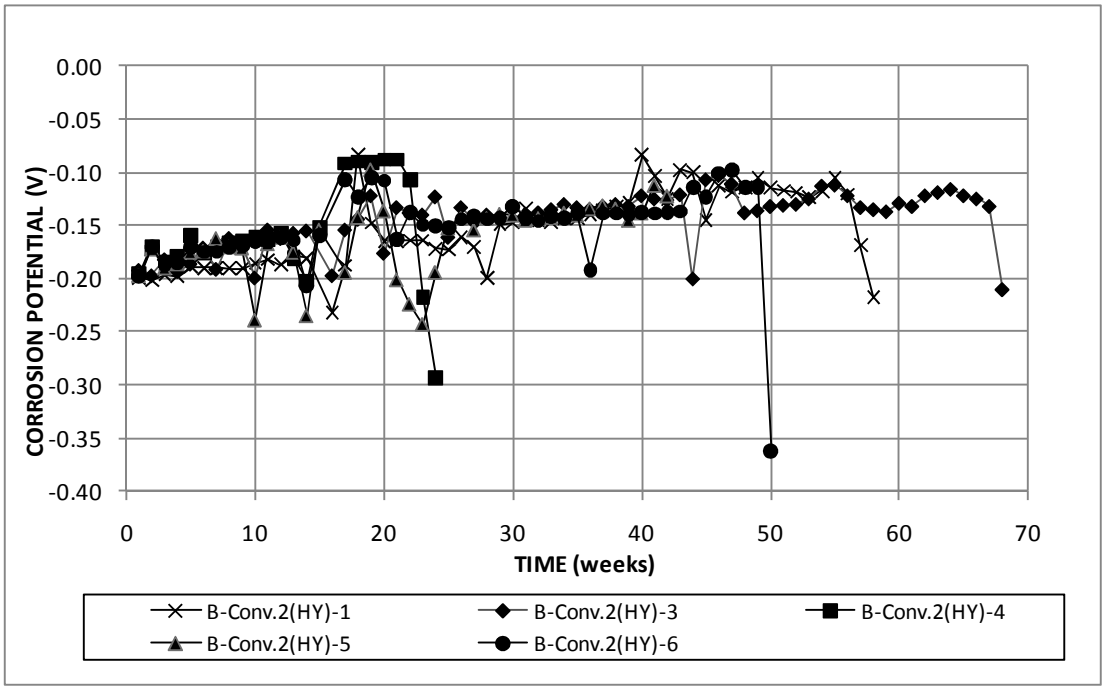

Figure 3.23: Corrosion initiation beam test. Individual top mat corrosion potentials with respect to CSE for specimens with conventional reinforcement in concrete containing Hycrete.

The autopsy results for the specimens without an inhibitor and with Hycrete are shown in Figures 3.24 and 3.25, respectively. All specimens show isolated corrosion products on the top side of the top bar.

(a)

(b)

Figure 3.24: Initiation beam test. Specimen B-Conv.2-1 (a) Top and bottom bars after autopsy, (b) detail of corrosion on top bar.

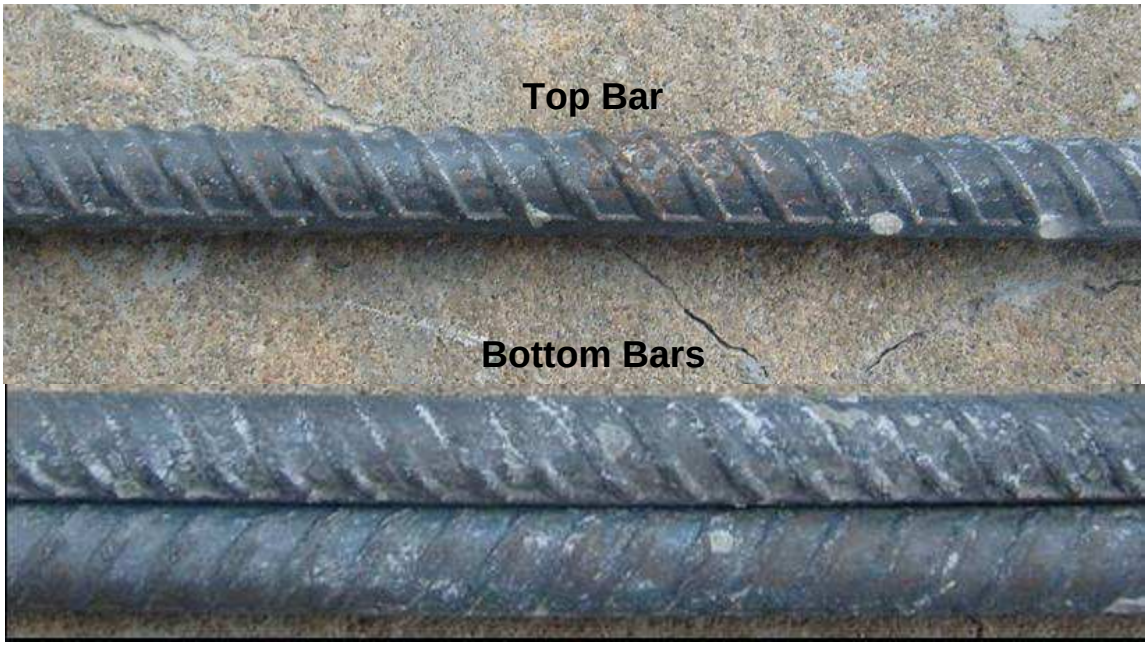

(a)

(b)

Figure 3.25: Initiation beam test. Specimen B-Conv.2(HY)-6 (a) Top and bottom bars after autopsy, (b) detail of corrosion on top bar.

Table 3.9 shows the individual and average chloride contents for specimens without a corrosion inhibitor. For specimens with no inhibitor, corrosion initiated at an average age of 19.8 weeks. The average critical chloride corrosion threshold of conventional reinforcement without an inhibitor is 1.00 kg/m^3 (1.68 lb/yd^3). Average specimen values range from 0.54 to 1.45 kg/m^3 (0.91 to 2.44 lb/yd^3). The coefficient of variation for the entire data set is 0.92, with coefficients of variation for individual specimens ranging from 0.71 to 1.16.

Table 3.10 shows the individual and average chloride contents for specimens with concrete containing Hycrete. Corrosion initiated at an average age of 48.4 weeks, compared to 19.8 weeks for the control specimens. The average critical chloride corrosion threshold of conventional reinforcement in concrete containing Hycrete is 0.51 kg/m^3 (0.88 lb/yd^3), approximately half the value observed in control specimens. Average specimen values range from 0.34 to 0.69 kg/m^3 (0.57 to 1.16 lb/yd^3). The coefficient of variation for the entire data set is 0.60, with coefficients of variation for individual specimens ranging from 0.48 to 0.72.

The results in Tables 3.9 and 3.10 confirm the earlier findings by Xing et al. (2010), summarized, along with the results from this study, in Table 3.11. Critical chloride corrosion thresholds for concrete containing Rheocrete and DCI are also included for reference. The critical chloride corrosion thresholds found in this study for specimens with and without Hycrete are 0.51 and 1.00 kg/m^3, respectively, similar to the results reported by Xing et al. (2010), 0.37 and 0.96 kg/m^3 (1.62 and 0.63 lb/yd^3), respectively, for a different heat of steel.

Table 3.9: Critical Chloride Corrosion Threshold for Conventional Reinforcement in Concrete without a Corrosion Inhibitor.

Specimen[a]	Side[b]	Initiation time (weeks)	Corrosion rate (μm/yr)	Corrosion potential (V)	Water soluble Cl^- (kg/m^3)			
					1	2	3	4
B-Conv.2-1	1	16	1.50	-0.383	0.19	0.19	0.34	0.83
	2				0.79	0.34	0.75	0.83
B-Conv.2-2	1	16	0.404	-0.339	1.24	0.60	0.86	0.75
	2				0.41	0.75	0.71	0.38
B-Conv.2-3	1	28	0.922	-0.300	0.64	0.38	0.56	0.26
	2				[d]	[d]	[d]	[d]
B-Conv.2-4	1	16	0.869	-0.309	1.24	2.55	1.31	5.10
	2				0.23	0.23	0.34	0.26
B-Conv.2-5[e]	1							
	2							
B-Conv.2-6	1	23	0.389	-0.229	0.45	1.09	0.41	0.53
	2				0.26	1.73	0.30	1.09
Average		19.8						

Specimen[a]	Side[b]	Water soluble Cl- (kg/m3)						Average (kg/m^3)	SD[c]	COV[c]
		5	6	7	8	9	10			
B-Conv.2-1	1	1.61	1.09	0.98	0.90	0.56	0.75	1.23	1.09	0.89
	2	2.10	4.46	3.34	2.18	1.69	0.71			
B-Conv.2-2	1	[d]	2.36	1.35	0.71	0.83	2.55	0.93	0.66	0.71
	2	0.75	1.80	0.68	0.19	0.45	0.34			
B-Conv.2-3	1	3.53	0.68	0.41	1.13	0.26	0.56	0.84	0.98	1.16
	2	[d]	[d]	[d]	[d]	[d]	[d]			
B-Conv.2-4	1	1.99	0.41	2.06	0.38	0.34	0.23	1.45	1.44	1.00
	2	1.24	0.71	2.36	4.95	1.50	1.54			
B-Conv.2-5[e]	1									
	2									
B-Conv.2-6	1	0.30	0.23	0.19	1.13	0.34	0.23	0.54	0.41	0.76
	2	0.41	0.23	0.26	0.53	0.71	0.41			
						Average		1.00	0.92	0.92

[a] Beam specimens with *w/c* = 0.45

[b] 10 chloride samples were taken from each side of the bar in one specimen

[c] SD = standard deviation; COV = coefficient of variation

[d] Data not available

[e] Initiation missed

Table 3.10: Critical Chloride Corrosion Threshold for Conventional Reinforcement in Concrete Containing Hycrete.

Specimen[a]	Side[b]	Initiation time (weeks)	Corrosion rate (μm/yr)	Corrosion potentials (V)	Water soluble Cl^- (kg/m^3)			
					1	2	3	4
B-Conv.2(HY)-1	1	58	0.137	-0.218	1.13	0.71	0.60	0.64
	2				2.12	0.49	0.11	0.41
B-Conv.2(HY)-2[d]	1							
	2							
B-Conv.2(HY)-3	1	68	0.899	-0.21	0.53	0.04	0.08	0.04
	2				1.09	0.49	0.60	0.41
B-Conv.2(HY)-4	1	24	0.823	-0.294	0.11	0.04	0.04	1.13
	2				0.26	0.49	0.56	0.19
B-Conv.2(HY)-5	1	42	2.87	-0.222	0.60	0.23	0.26	0.15
	2				0.15	0.24	0.38	0.74
B-Conv.2(HY)-6	1	50	3.76	-0.362	0.75	0.98	0.41	0.45
	2				0.56	0.45	0.53	0.53
Average		48.4						

Specimen[a]	Side[b]	Water soluble Cl- (kg/m3)						Average (kg/m^3)	SD[c]	COV[c]
		5	6	7	8	9	10			
B-Conv.2(HY)-1	1	0.26	0.34	0.79	0.90	0.38	0.56	0.67	0.43	0.64
	2	0.60	0.60	0.53	0.79	1.13	0.38			
B-Conv.2(HY)-2[d]	1									
	2									
B-Conv.2(HY)-3	1	0.04	0.64	0.51	0.30	0.79	0.53	0.49	0.35	0.71
	2	0.75	0.75	[e]	0.53	0.04	1.20			
B-Conv.2(HY)-4	1	0.53	0.53	0.41	0.53	0.26	0.34	0.34	0.25	0.72
	2	0.15	0.30	0.30	0.19	0.26	0.23			
B-Conv.2(HY)-5	1	0.43	[e]	[e]	[e]	[e]	[e]	0.34	0.18	0.53
	2	0.23	0.34	0.21	0.23	0.30	0.56			
B-Conv.2(HY)-6	1	0.45	0.56	0.38	0.53	0.86	1.76	0.69	0.33	0.48
	2	0.38	1.05	0.90	0.64	0.90	0.71			
						Average		0.51	0.31	0.60

[a] Beam specimens with *w/c* = 0.45

[b] 10 chloride samples were taken from each side of the bar in one specimen

[c] SD = standard deviation; COV = coefficient of variation

[d] Data not available

[e] Initiation missed

Table 3.11: Average Critical Chloride Corrosion Threshold for Conventional Reinforcement in Concrete With and Without Inhibitors.

Specimen	Initiation Age (weeks)	Average Chloride Content (kg/m^3)	COV
Current Study			
B-Conv.2	19.8	1.00	0.92
B-Conv.2(HY)	48.4	0.51	0.60
Xing et al. (2010)			
B-Conv.	14.2	0.96	0.38
B-Conv.(RH)	19.5	1.23	0.47
B-Conv.(DCI)	26.5	1.59	0.27
B-Conv.(HY)	28.5	0.37	0.55

3.3 FIELD TEST SPECIMENS

The results from the field test program are presented in this section. Macrocell corrosion rate, corrosion loss, corrosion potentials, and mat-to-mat resistance are discussed in Section 3.3.1. The autopsy results are discussed in Section 3.3.2.1, the disbondment results are discussed in Section 3.3.2.2, and the chloride concentration for each specimen is presented in Section 3.3.2.3.

A total of 42 field test specimens, 21 with cracks and 21 without cracks, were tested to determine the effectiveness of increased adhesion epoxies, corrosion inhibitors, and multiple-coated reinforcement. Four field test specimens, two with cracks (C) and two without cracks (U), are tested with conventional steel (FTS-Conv.); an additional four specimens, two each cracked and uncracked, are tested with conventional epoxy-coated reinforcement (FTS-ECR). These specimens serve as controls. Three epoxies with increased adhesion, obtained via a chromate pretreatment (FTS-ECR(Chromate)) or via proprietary coatings from DuPont (FTS-ECR(DuPont)) and Valspar (FTS-ECR(Valspar)) are also tested; each epoxy is tested in two specimens with cracks and two specimens without cracks. For specimens with corrosion inhibitors used in conjunction with ECR, two each cracked and uncracked specimens are tested for Rheocrete (FTS-ECR(RH)), Hycrete (FTS-ECR(HY)), and epoxy with a microencapsulated calcium

nitrite primer (FTS-ECR(primer/$Ca(NO_2)_2$)), and three each specimens with and without cracks are tested for calcium nitrite (DCI) (FTS-ECR(DCI)). Two each cracked and uncracked specimens are tested with multiple-coated reinforcement (FTS-ECR(MC)).

3.3.1 Corrosion Rate, Loss, and Potential and Mat-to-Mat Resistance

3.3.1.1 Control Specimens

Figure 3.26 shows the individual corrosion rates based on total area for the conventional and epoxy-coated reinforcement specimens without cracks. The corrosion rates for each specimen represent the average corrosion rate of all test bars within the specimen; data for individual test bars are presented in Figures A17 through A24 of Appendix A. Specimen FTS-Conv.-U-1 exhibits corrosion initiation at week 81, with a peak corrosion rate of 2.47 µm/yr at week 237. The corrosion rate drops to zero between weeks 161 and 169 and at week 213. Specimen FTS-Conv.-2 initiates corrosion at week 40; corrosion rates remain low until week 127, with a peak corrosion rate of 1.34 µm/yr at week 153. The specimens with epoxy-coated reinforcement show negligible corrosion rates based on total area.

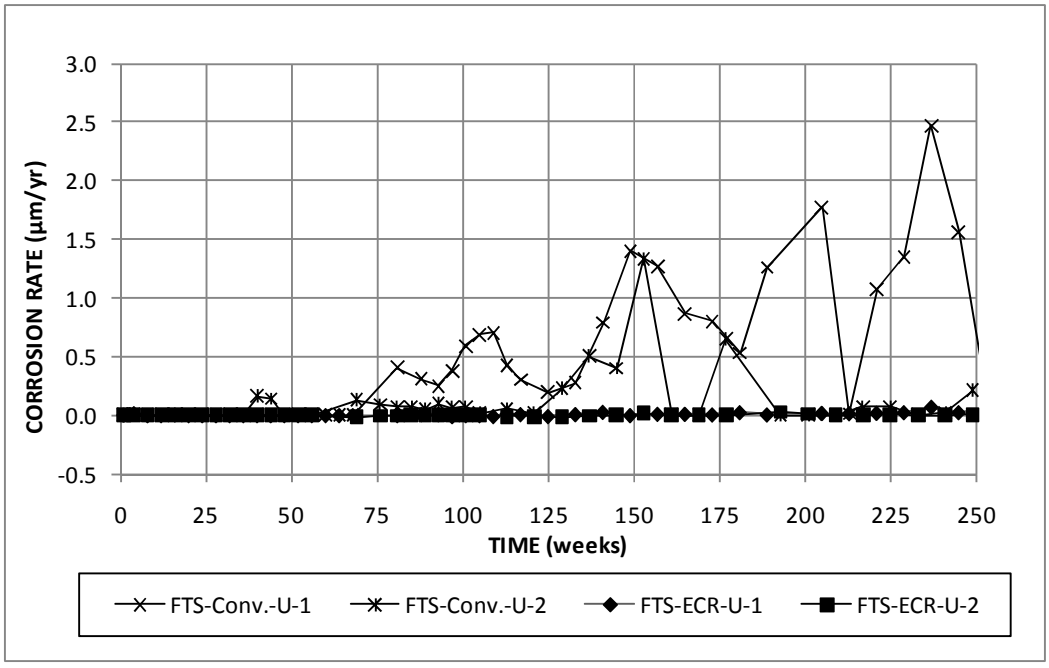

Figure 3.26: Field test specimens, uncracked concrete. Individual corrosion rates based on total area for specimens with conventional steel and epoxy-coated reinforcement.

Figure 3.27 shows corrosion rates for the conventional and epoxy-coated specimens with cracks. Specimen FTS-Conv.-1 exhibits corrosion initiation at week 40, with a peak corrosion rate of 4.32 µm/yr at week 237. Specimen FTS-Conv.-2 exhibits corrosion initiation at week 16, with a peak corrosion rate of 2.17 µm/yr at week 249. The specimens with epoxy-coated reinforcement show negligible corrosion rates based on total area.

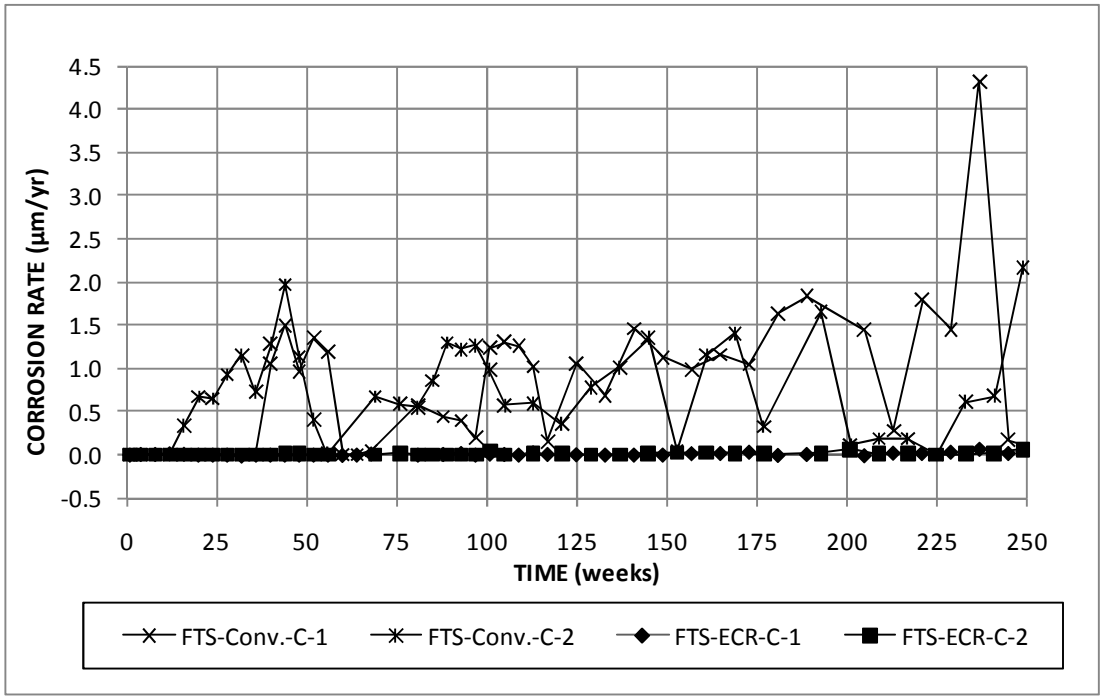

Figure 3.27: Field test specimens, cracked concrete. Individual corrosion rates based on total area for specimens with conventional steel and epoxy-coated reinforcement.

Figure 3.28 shows individual corrosion rates based on exposed area for the specimens with epoxy-coated reinforcement in both cracked and uncracked concrete. For the uncracked concrete specimens, specimen FTS-ECR-U-1 has a peak corrosion rate based on exposed area of 26.5 µm/yr at week 237. Specimen FTS-ECR-U-2 generally exhibits lower corrosion rates than specimen FTS-ECR-U-1, with a peak corrosion rate based on exposed area of 10.3 µm/yr at week 193. For the cracked concrete specimens,

the peak corrosion rates for specimens FTS-ECR-C-1 and FTS-ECR-C-2 are 26.1 µm/yr at week 237 and 23.8 µm/yr at week 249, respectively.

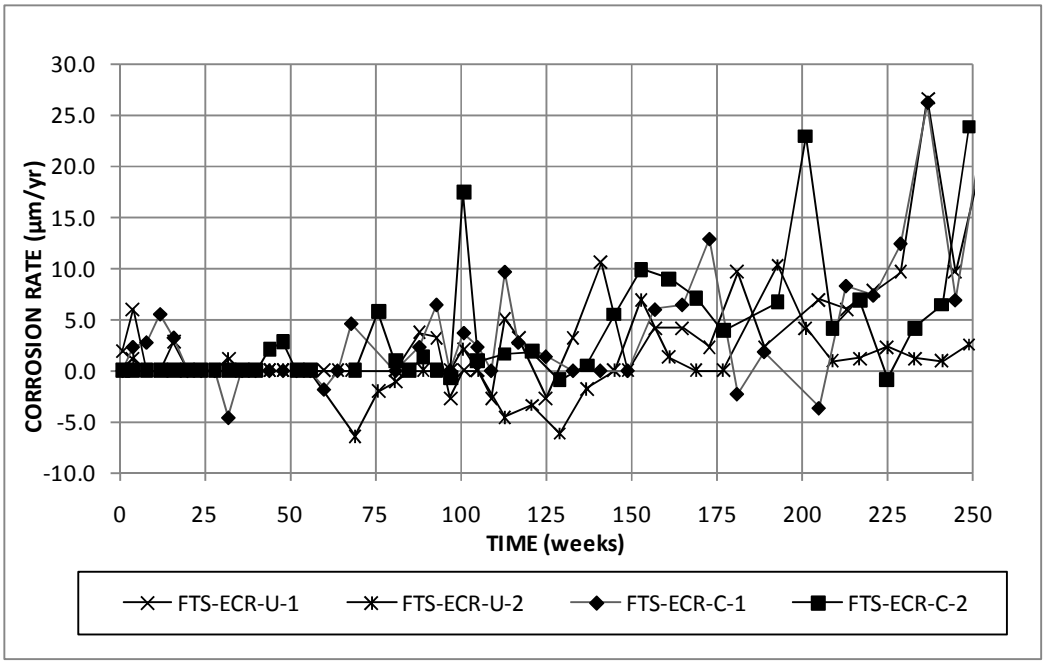

Figure 3.28: Field test specimens. Individual corrosion rates based on exposed area for specimens with epoxy-coated reinforcement.

Figures 3.29 and 3.30 show the average corrosion losses for conventional and epoxy-coated reinforcement based on total area and exposed area, respectively. Individual corrosion loss data at the end of testing are shown in Table 3.11. Some epoxy-coated bars exhibit a slight negative corrosion rate, resulting in a negative corrosion loss at the end of testing (Figures A21 and A23, Appendix A). Negative corrosion losses are the result of current drift between top and bottom mat of steel and do not necessarily indicate corrosion on the bottom mat. Individual bars with zero or negative corrosion loss at the end of testing are excluded from the average corrosion loss. Other epoxy-coated bars exhibit negative corrosion rates early in testing, before corrosion initiates. After initiation, the corrosion rate becomes positive. These bars are included in the average corrosion loss; however, the negative corrosion rates on these bars prior to

corrosion initiation result in an average negative corrosion loss before corrosion initiation, as observed between weeks 75 and 150 in Figure 3.30.

For conventional reinforcement (Figure 3.29), the specimens in cracked concrete show the greatest average corrosion loss, 4.07 µm based on total area. The specimens with conventional reinforcement in uncracked concrete show average corrosion losses of 1.87 µm, approximately half the value observed in specimens with conventional reinforcement in cracked concrete. Conventional reinforcement in cracked concrete first initiates corrosion at 25 weeks, compared to 75 weeks for the first initiation of corrosion for conventional reinforcement in uncracked concrete. In both cracked and uncracked concrete, the average corrosion rate (the slope of the corrosion loss plot) remains constant throughout the test, with similar rates in cracked and uncracked concrete.

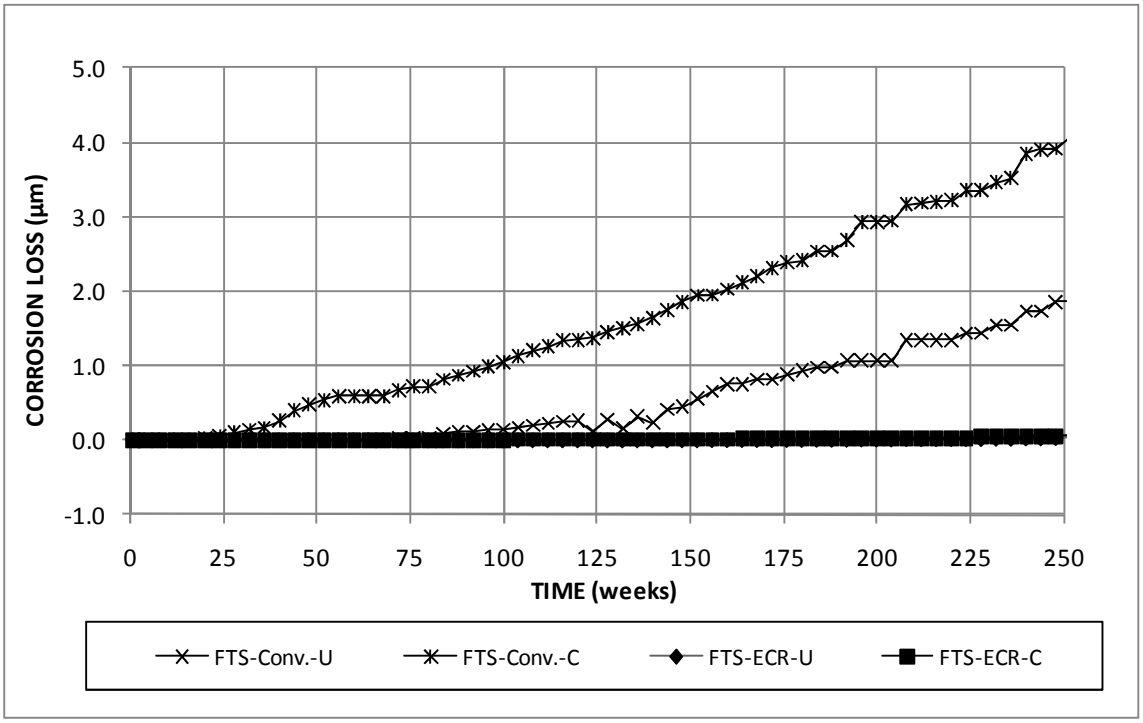

Figure 3.29: Field test specimens. Average corrosion losses based on total area for specimens with conventional and epoxy-coated reinforcement.

For all specimens with epoxy-coated reinforcement, the corrosion losses based on total area are less than 0.1 µm (Figure 3.29, Table 3.12). Based on exposed area, the specimens with epoxy-coated reinforcement in cracked concrete show the greatest average corrosion losses, 23.0 µm at the end of testing. The specimens with epoxy-coated reinforcement in uncracked concrete exhibit slightly less than half the average corrosion loss of specimens with cracked concrete, averaging 10.9 µm at the end of testing (Figure 3.28). In uncracked concrete, the corrosion loss remains zero or negative for 75 weeks, after which the corrosion loss increases. The corrosion rate in uncracked concrete increases slightly near 250 weeks. In cracked concrete, the corrosion loss remains zero or negative for 75 weeks, after which the corrosion loss steadily increases until 150 weeks. After 150 weeks, corrosion loss continues at an increased rate. The corrosion loss data for individual bars are shown in Table 3.12. With the exception of test bar 3 in specimen FTS-ECR-U-2, all bars show positive corrosion losses at the end of testing (Figure A.21, Appendix A).

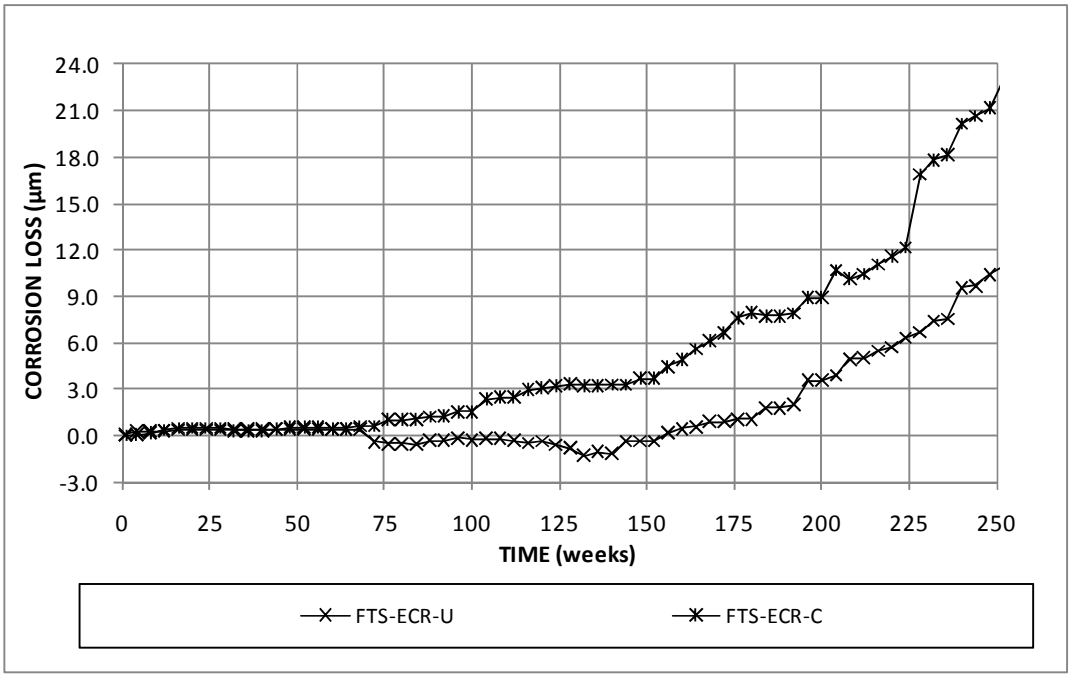

Figure 3.30: Field test specimens. Average corrosion losses based on exposed area for specimens with epoxy-coated reinforcement.

Table 3.12: Corrosion Losses (µm) Based on Total Area for Field Test Specimens with Conventional and Epoxy-Coated Reinforcement.

Steel Designation[a]	Exposure time (weeks)	Test Bar 1	2	3	4	Average[b]	Standard Deviation
Uncracked Concrete							
FTS-Conv.-U-1	250	3.67	2.49			3.08	0.833
FTS-Conv.-U-2	254	0.142	1.17			0.657	0.728
FTS-ECR-U-1	250	0.024	0.069			0.046	0.032
FTS-ECR-U-2	254	0.016	0.008	-0.005	0.004	0.010	0.009
Cracked Concrete							
FTS-Conv.-C-1	250	2.26	6.71			4.49	3.14
FTS-Conv.-C-2	254	4.01	3.34			3.68	0.475
FTS-ECR-C-1	250	0.015	0.065			0.040	0.035
FTS-ECR-C-2	254	0.056	0.171	0.044	0.042	0.078	0.062

[a] Conv. = conventional steel. ECR = normal epoxy-coated reinforcement. All epoxy-coated bars are penetrated with 16 surface holes.
[b] Excludes bars with 0 or negative losses

The average corrosion potentials for the control specimens are shown in Figure 3.31 (top mat) and Figure 3.32 (bottom mat). The individual corrosion potentials are provided in Figures A18, A20, A22, and A24 of Appendix A. For the top mat of steel, all of the specimens shown begin the test with a corrosion potential between –0.100 V and –0.200 V with respect to CSE. The top mat corrosion potential for specimens with conventional reinforcement in cracked concrete drops to approximately –0.400 V at week 16 and remains more negative than –0.350 V for the duration of the test. For specimens with conventional reinforcement in uncracked concrete, the corrosion potential of the top mat of steel gradually drops from –0.200 V to –0.350 V between 44 and 84 weeks. The corrosion potential remains more negative than –0.300 V for much of the remainder of the test, becoming more positive than –0.300 V at week 212 before dropping again at week 236. The corrosion potential of the top mat of steel for specimens with epoxy-coated reinforcement in cracked concrete also drops gradually from –0.200 V at week 50 to below –0.350 V at week 75. The corrosion potential varies between approximately –0.300 to –0.450 V for much of the test duration. The potential returns to –0.200 V at

week 220, however, corrosion continues to occur (Figure 3.30). The specimens with epoxy-coated reinforcement in uncracked concrete exhibit top mat corrosion potentials between –0.100 V and –0.300 V for the duration of the test. On the bottom mat of steel (Figure 3.32), the corrosion potentials for all specimens remain between –0.100 V and –0.300 V for most of the test, with isolated readings more negative than –0.350 V.

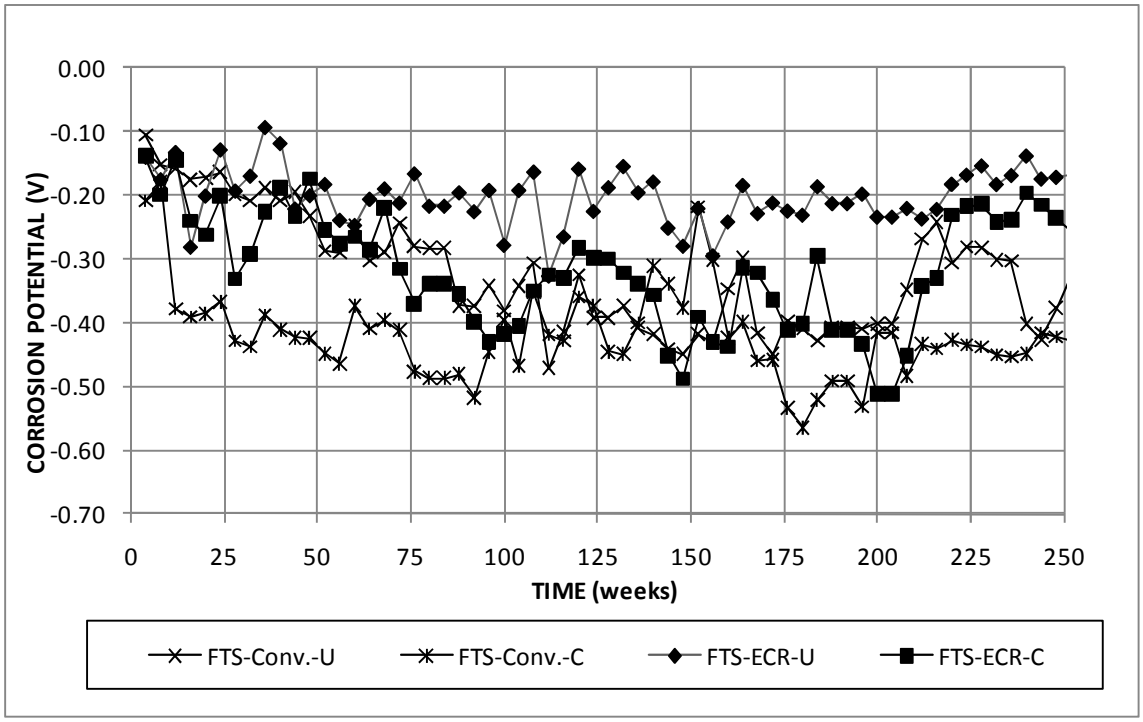

Figure 3.31: Average top mat potential (CSE) for field test specimens with conventional and epoxy-coated reinforcement in cracked and uncracked concrete.

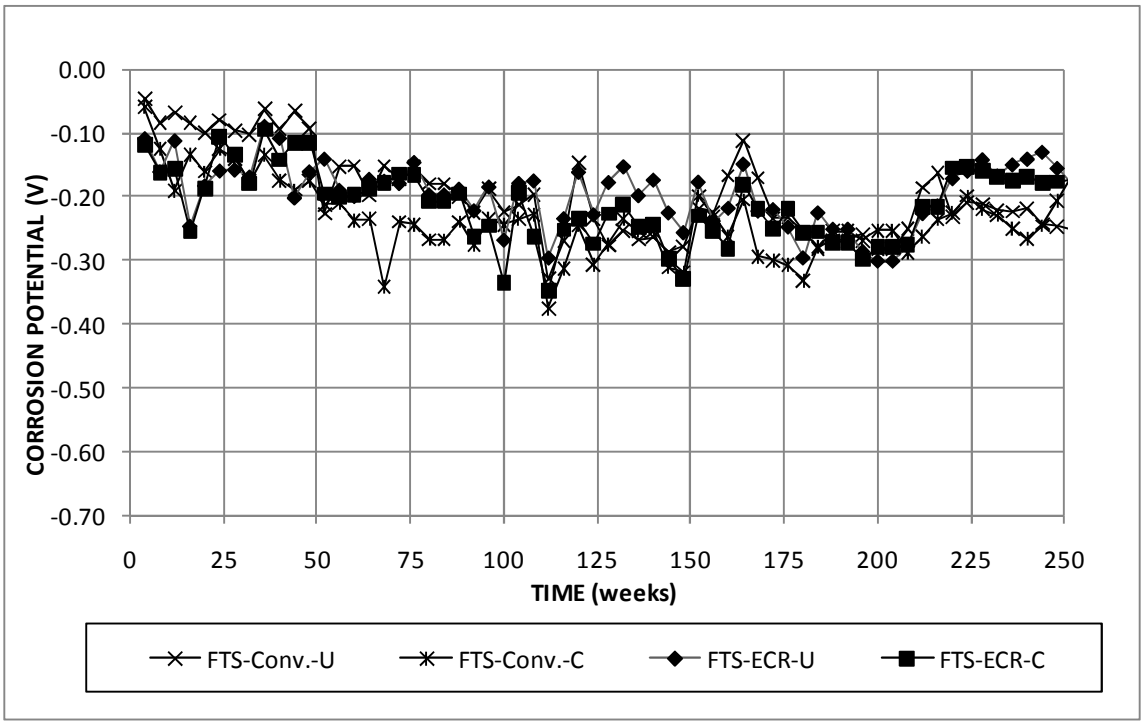

Figure 3.32: Average bottom mat potential (CSE) for field test specimens with conventional and epoxy-coated reinforcement in cracked and uncracked concrete.

The average mat-to-mat resistances for control specimens are shown in Figure 3.33. The specimens with conventional reinforcement show a low mat-to-mat resistance, with a value of less than 100 ohms at the start of the test. The mat-to-mat resistances for conventional reinforcement in uncracked concrete remain low for the duration of the test. In cracked concrete, the mat-to-mat resistance increases to 2200 ohms at week 121 and remains between 1000 and 2500 ohms for the duration of the test. The increased resistance compared to specimens with uncracked concrete is likely due to the increased quantity of corrosion products on the conventional steel in cracked concrete. The specimens with epoxy-coated reinforcement in cracked concrete show significantly greater values of mat-to-mat resistance compared to conventional reinforcement because of the epoxy coating. The mat-to-mat resistances for cracked and uncracked concrete specimens are approximately equal for most of the test, with a drop in the measured

resistance in the specimens with epoxy-coated reinforcement in uncracked concrete after 200 weeks.

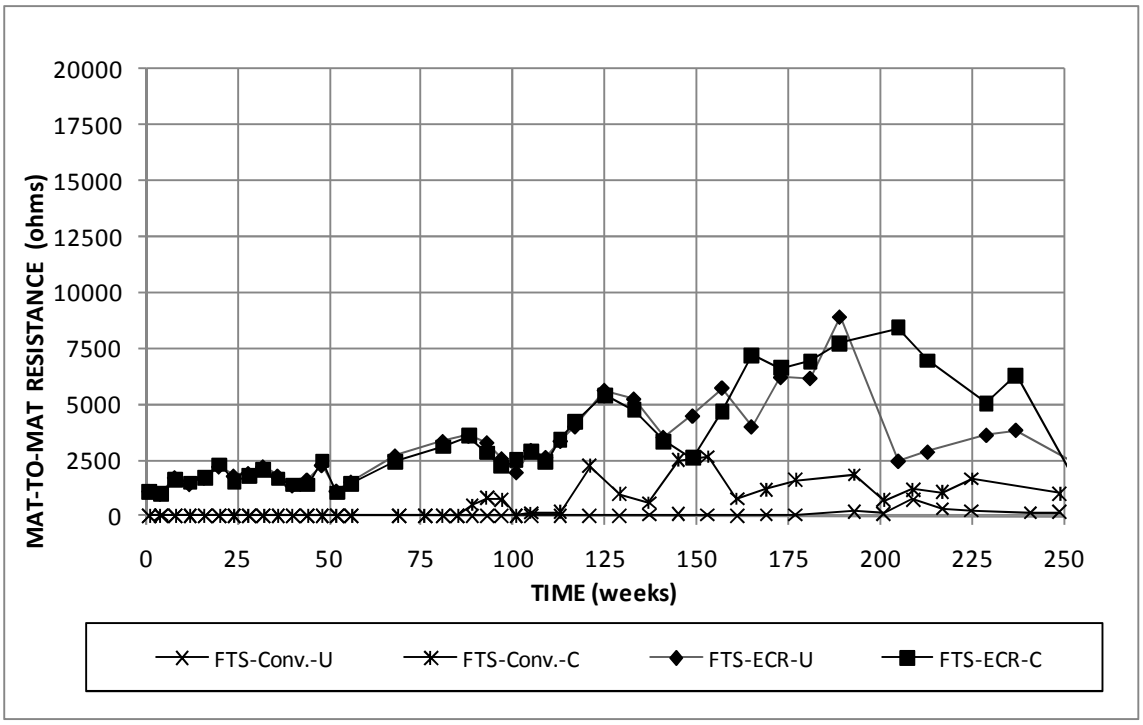

Figure 3.33: Field test specimens. Average mat-to-mat resistance for specimens with conventional and epoxy-coated reinforcement in cracked and uncracked concrete.

3.3.1.2 Increased Adhesion Epoxies

Figures 3.34 and 3.35 show the average corrosion rates based on exposed area for epoxies with increased adhesion in uncracked and cracked concrete, respectively. In uncracked concrete, conventional ECR has the highest peak corrosion rate, 13.9 μm/yr at week 237. FTS-ECR(Valspar) has the next highest peak corrosion rate, 12.0 μm/yr at week 93. FTS-ECR(DuPont) and FTS-ECR(Chromate) have peak corrosion rates of 11.1 μm/yr at week 215 and 10.3 μm/yr at week 207, respectively. In cracked concrete (Figure 3.35), FTS-ECR(Valspar) has the highest peak corrosion rate, 56.8 μm/yr at week 229. FTS-ECR(DuPont) has a peak corrosion rate of 27.9 μm/yr at week 151, followed by FTS-ECR(Chromate) and FTS-ECR with peak corrosion rates of 25.1 μm/yr at week 175 and 16.3 μm/yr at week 237, respectively.

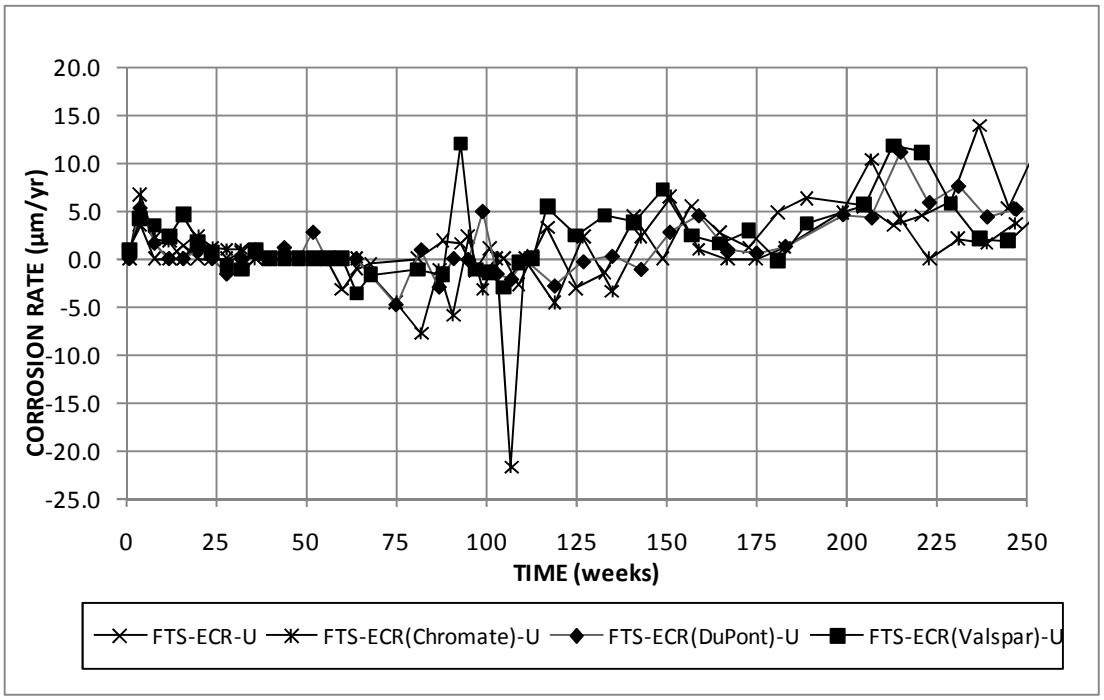

Figure 3.34: Field test specimens, uncracked concrete. Average corrosion rates based on exposed area for specimens with epoxy-coated reinforcement with increased adhesion.

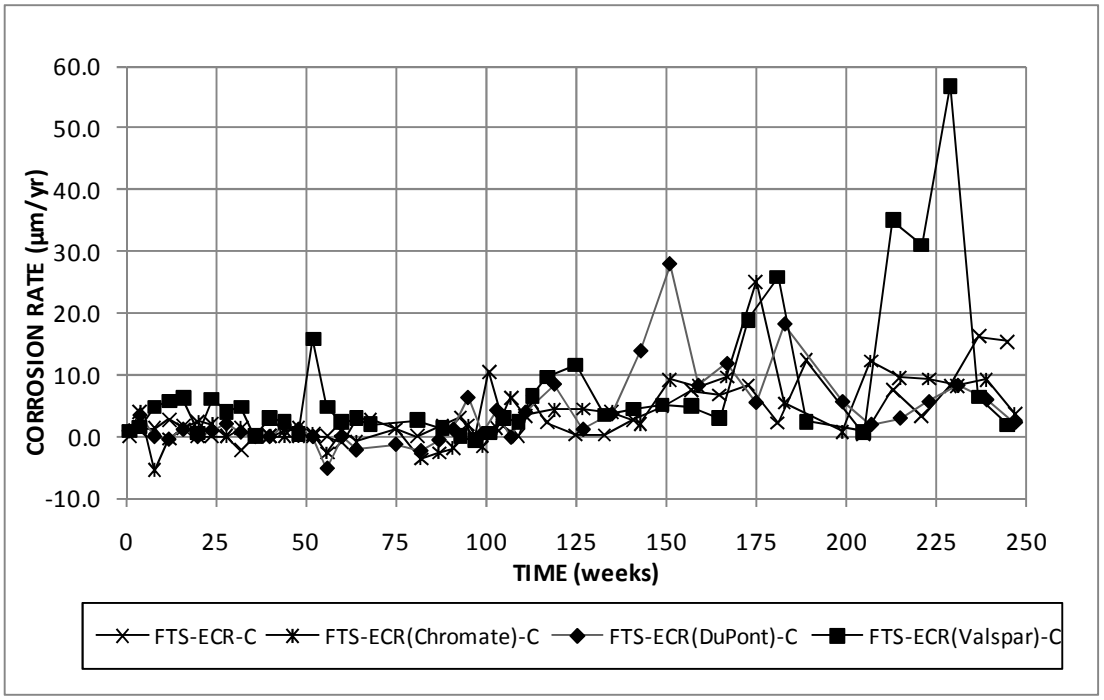

Figure 3.35: Field test specimens, cracked concrete. Average corrosion rates based on exposed area for specimens with epoxy-coated reinforcement with increased adhesion.

Figures 3.36 and 3.37 show the average corrosion losses based on exposed area for epoxy-coated reinforcement with increased adhesion in uncracked and cracked concrete, respectively. Individual corrosion loss data at the end of testing are summarized in Table 3.13. In uncracked concrete (Figure 3.36), bars with increased adhesion exhibit behavior similar to conventional ECR. Epoxy-coated bars with Valspar begin corroding at 125 weeks, slightly earlier than conventional ECR. Bars with DuPont epoxy and bars with a chromate pretreatment begin corroding around 150 weeks, similar to conventional ECR. All bars with increased adhesion exhibit corrosion rates similar to conventional ECR after corrosion initiation. At the end of testing (250 weeks), FTS-ECR(Valspar) exhibits the greatest average corrosion loss, 12.5 µm. Conventional ECR shows the next highest corrosion loss at 250 weeks, 10.9 µm, followed by FTS-ECR(Chromate) and FTS-ECR(DuPont) with losses of 9.79 µm and 7.68 µm, respectively. Among individual specimens with increased adhesion epoxy in uncracked concrete (Table 3.13), FTS-ECR(Valspar)-U-2 shows the greatest corrosion losses, 18.7 µm, followed by ECR(Chromate)-U-2 with 14.2 µm. All specimens, except FTS-ECR-U-2, show corrosion losses based on exposed area greater than 5.0 µm. The wide variation in performance between FTS-ECR-U-1 and FTS-ECR-U-2 is likely due to variations in the quality of concrete between batches. Negative corrosion losses are observed on test bar 3 from specimen FTS-ECR-U-2, test bar 2 from FTS-ECR(Valspar)-U-2, and test bars 2 and 3 from specimen FTS-ECR(Chromate)-U-2 (Figures A17, A25, and A33, Appendix A); these test bars are excluded from the averages in Table 3.13.

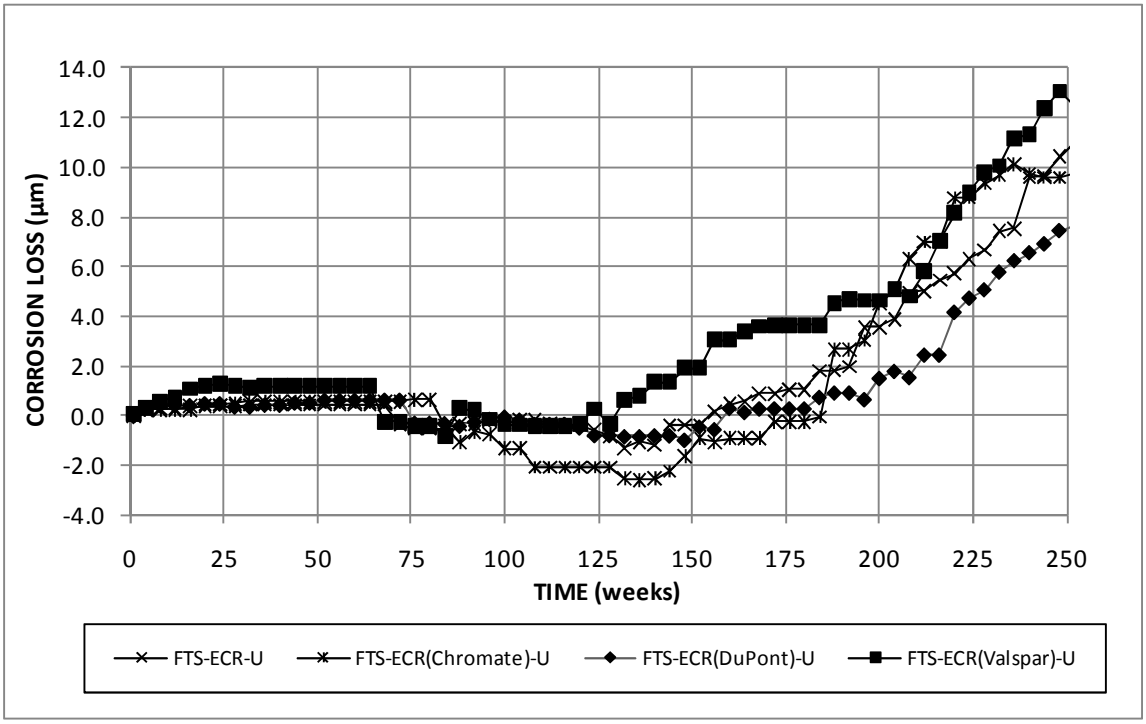

Figure 3.36: Field test specimens, uncracked concrete. Average corrosion losses based on exposed area for specimens with ECR with increased adhesion.

In cracked concrete (Figure 3.37), bars with Valspar epoxy initiate corrosion at the start of testing. The corrosion rate remains approximately constant through 212 weeks, after which the losses increase rapidly through 230 weeks and then level off. The other bars with increased adhesion exhibit behavior similar to conventional ECR. At the end of testing, FTS-ECR(Valspar) exhibits the greatest average corrosion loss at 250 weeks, 36.8 µm. FTS-ECR(DuPont) and FTS-ECR show losses of 25.9 µm and 23.0 µm, respectively. FTS-ECR(Chromate) shows average corrosion losses of 20.3 µm at week 250. Among individual specimens with increased adhesion epoxy in cracked concrete, FTS-ECR(Valspar)-C-1 shows the greatest corrosion losses, 48.5 µm. FTS-ECR(Chromate)-C-1 shows the lowest corrosion loss, 13.5 µm. For specimens with increased adhesion, the corrosion losses in cracked concrete are approximately three times greater than the corrosion losses in uncracked concrete.

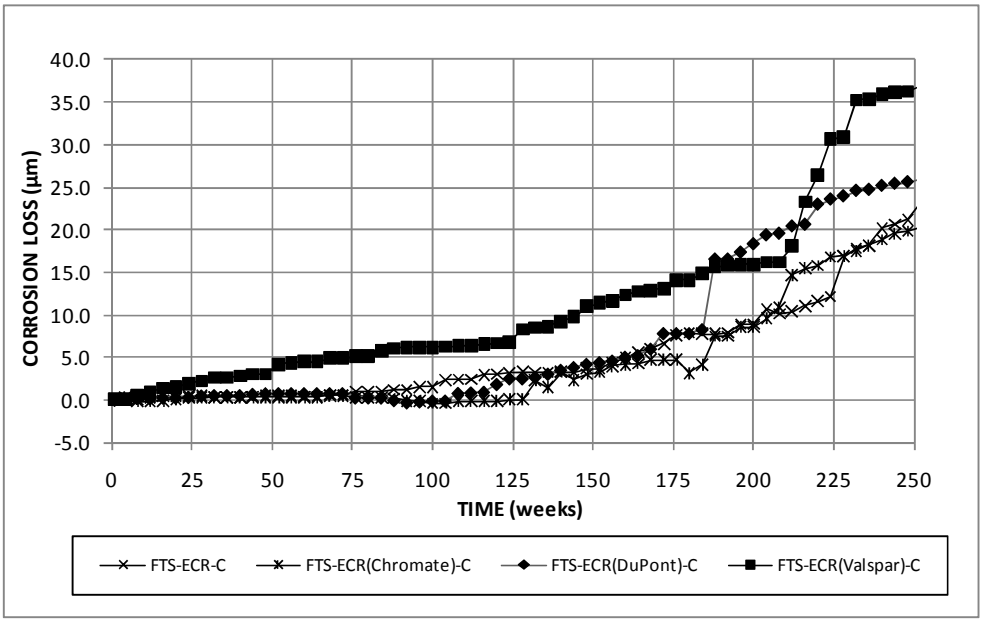

Figure 3.37: Field test specimens, cracked concrete. Average corrosion losses based on exposed area for specimens with ECR with increased adhesion.

Table 3.13: Corrosion Losses (µm) Based on Exposed Area for Field Test Specimens with Epoxy-Coated Reinforcement with Increased Adhesion.

Steel Designation	Exposure time (weeks)	Test Bar 1	2	3	4	Average[a]	Standard Deviation
Uncracked Concrete							
FTS-ECR-U-1	250	9.25	27.0			18.1	12.6
FTS-ECR-U-2	254	6.27	3.29	-2.04	1.62	3.73	2.35
FTS-ECR(Valspar)-U-1	250	3.49	9.18			6.33	4.02
FTS-ECR(Valspar)-U-2	254	9.72	-3.49	38.9	16.0	18.7	10.6
FTS-ECR(DuPont)-U-1	250	11.1	5.57			8.32	3.90
FTS-ECR(DuPont)-U-2	254	6.39	2.87	4.47	14.4	7.03	5.10
FTS-ECR(Chromate)-U-1	250	5.72	5.02			5.37	0.498
FTS-ECR(Chromate)-U-2	254	18.4	-16.5	-2.34	9.93	14.2	5.98
Cracked Concrete							
FTS-ECR-C-1	250	5.72	25.2			15.5	13.8
FTS-ECR-C-2	254	21.9	66.8	17.1	16.4	30.6	24.3
FTS-ECR(Valspar)-C-1	250	27.8	69.2			48.5	29.3
FTS-ECR(Valspar)-C-2	254	8.88	24.9	7.06	59.6	25.1	24.4
FTS-ECR(DuPont)-C-1	250	10.2	19.6			14.9	6.64
FTS-ECR(DuPont)-C-2	254	18.7	11.3	25.6	91.4	36.8	36.9
FTS-ECR(Chromate)-C-1	250	15.3	11.7			13.5	2.52
FTS-ECR(Chromate)-C-2	254	38.7	25.9	19.9	23.7	27.1	8.16

[a] Excludes bars with 0 or negative losses

The average corrosion potentials (versus CSE) for the specimens with ECR with increased adhesion in uncracked concrete are shown in Figure 3.38 (top mat) and Figure 3.39 (bottom mat). Both the top and bottom mats exhibit a general trend of decreasing corrosion potentials during the first 150 weeks of testing, followed by a general trend of increasing corrosion potentials. On the top mat, the corrosion potentials remain between –0.100 V and –0.200 V for the first 25 weeks of testing. The potentials decrease to close to –0.300 V and remain between –0.100V and –0.300 V for much of the test, increasing again after week 200. No significant difference in potentials is observed between conventional ECR and ECR with increased adhesion. Similar behavior is observed on the bottom mat of steel (Figure 3.39).

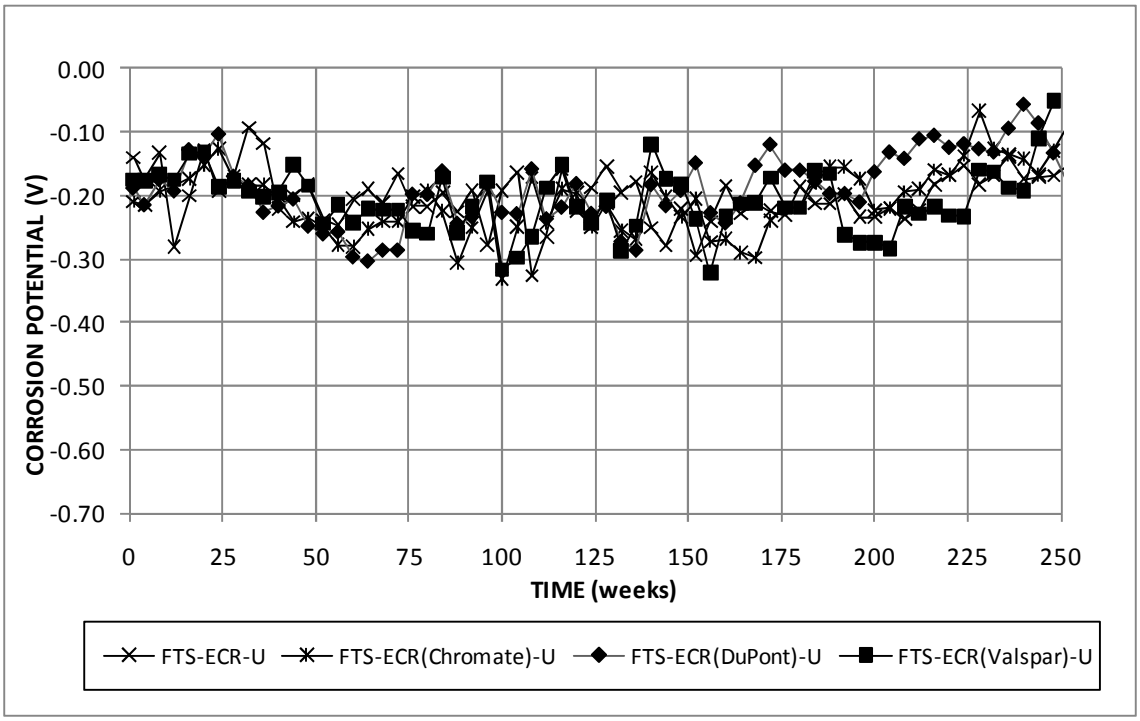

Figure 3.38: Average top mat potential (CSE) for field test specimens with epoxy-coated reinforcement with increased adhesion in uncracked concrete.

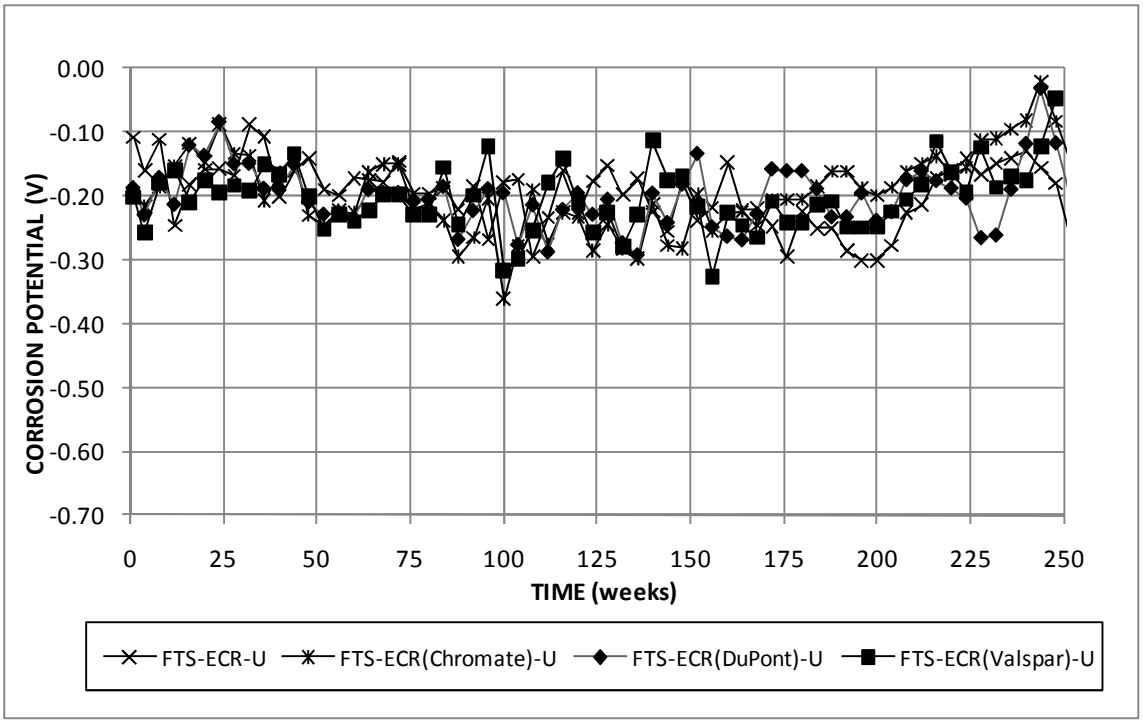

Figure 3.39: Average bottom mat potential (CSE) for field test specimens with epoxy-coated reinforcement with increased adhesion in uncracked concrete.

The average corrosion potentials (versus CSE) for the specimens with ECR with increased adhesion in cracked concrete are shown in Figure 3.40 (top mat) and Figure 3.41 (bottom mat). At the start of testing, top mat corrosion potentials for FTS-ECR(Valspar) are more negative than for the other specimens with ECR with increased adhesion. However, all specimens with ECR with increased adhesion show average potentials of approximately –0.400 V by week 50. The potentials remain between –0.300V and –0.600 V for much of the test, increasing again after week 200. Except for the period between 25 and 75 weeks, no significant difference in potentials is observed between conventional ECR and ECR with increased adhesion. On the bottom mat of steel (Figure 3.41), corrosion potentials start between –0.100 V and –0.200 V and decrease to close to –0.300 V for most of the test, increasing to above –0.200 V over the last 50 weeks.

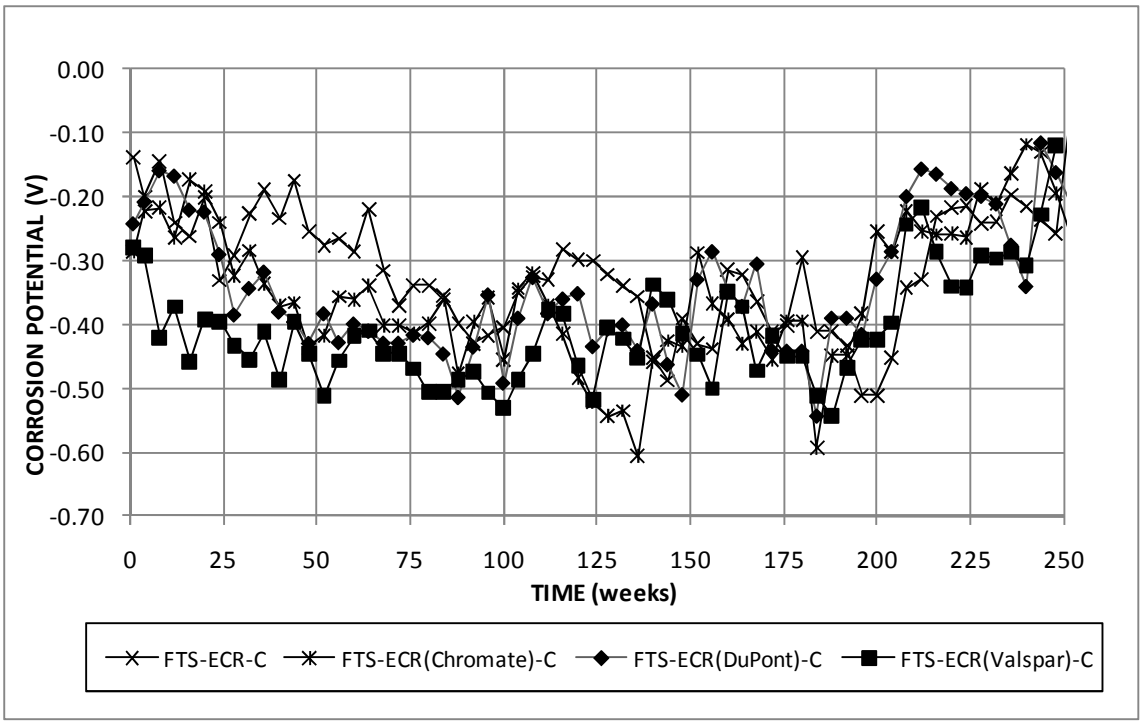

Figure 3.40: Average top mat potential (CSE) for field test specimens with epoxy-coated reinforcement with increased adhesion in cracked concrete.

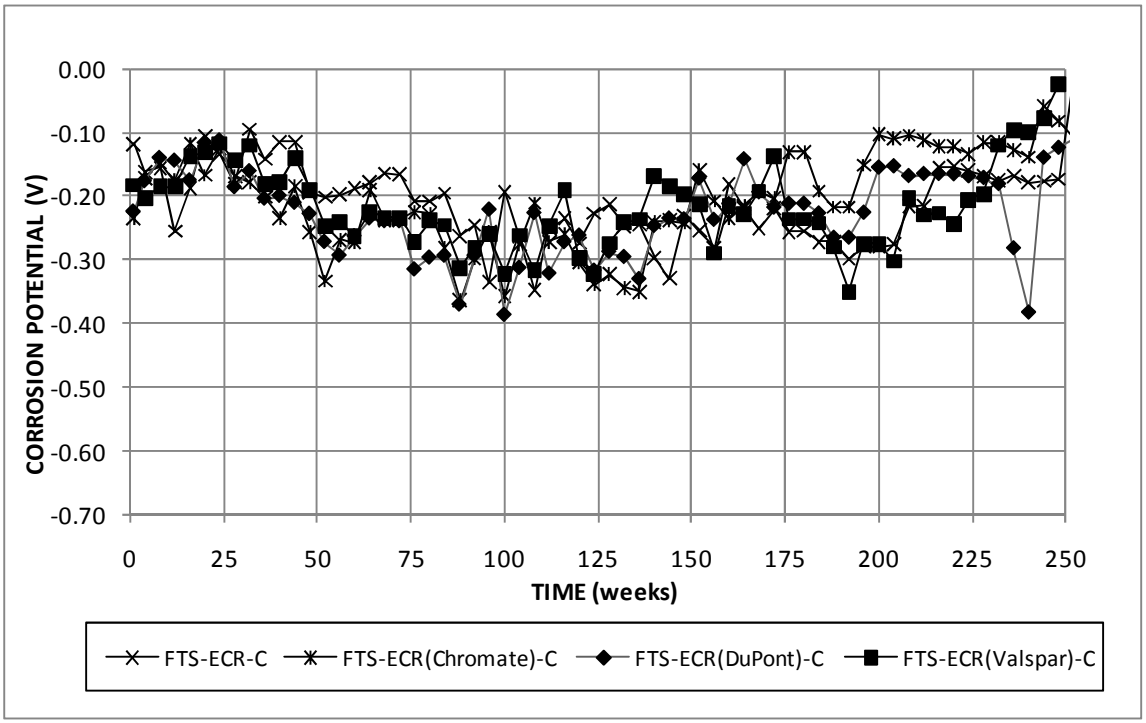

Figure 3.41: Average bottom mat potential (CSE) for field test specimens with epoxy-coated reinforcement with increased adhesion in cracked concrete.

The average mat-to-mat resistances for the specimens with ECR with increased adhesion in uncracked and cracked concrete are shown in Figures 3.42 and 3.43, respectively. For the uncracked concrete specimens, the mat-to-mat resistances increase from approximately 2,000 ohms at the start of testing to around 7,500 ohms at week 150, with some specimens showing mat-to-mat resistances over 10,000 ohms. Mat-to-mat resistance values remain constant or decrease for the remainder of the test. For the cracked concrete specimens (Figure 3.43), the mat-to-mat resistances at the start of testing measure approximately 2,000 ohms and increases throughout the test. In both cracked and uncracked concrete, no significant differences in the mat-to-mat resistances are observed between conventional ECR and ECR with increased adhesion.

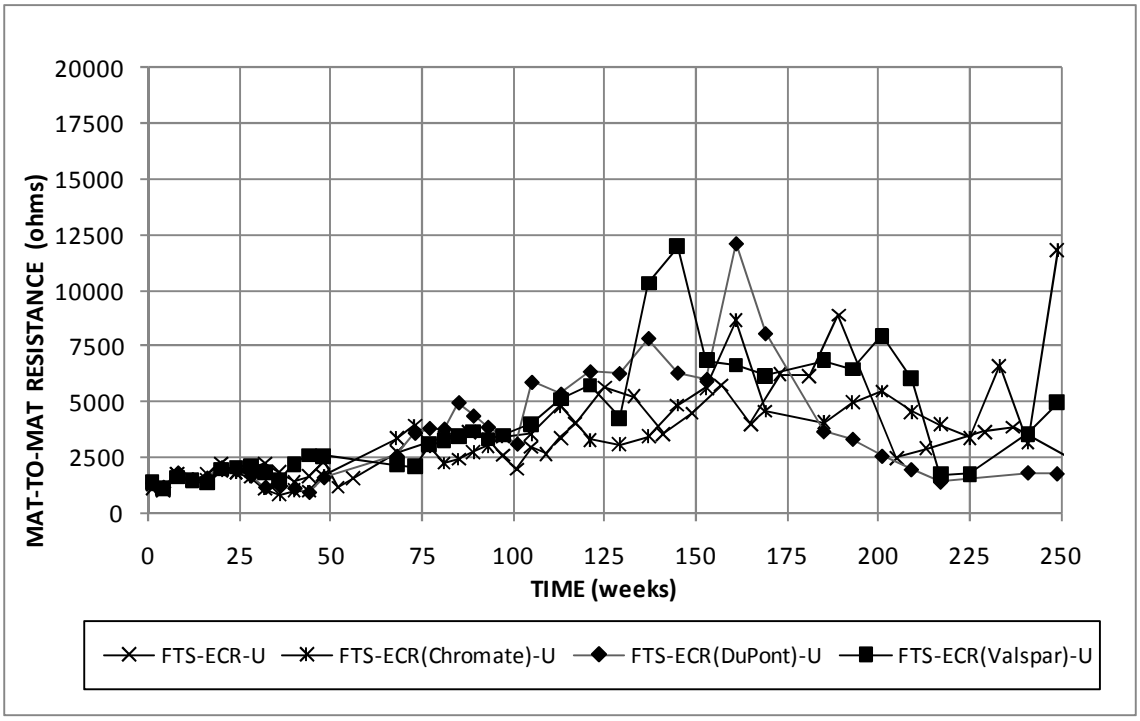

Figure 3.42: Field test specimens. Average mat-to-mat resistance for specimens with epoxy-coated reinforcement with increased adhesion in uncracked concrete.

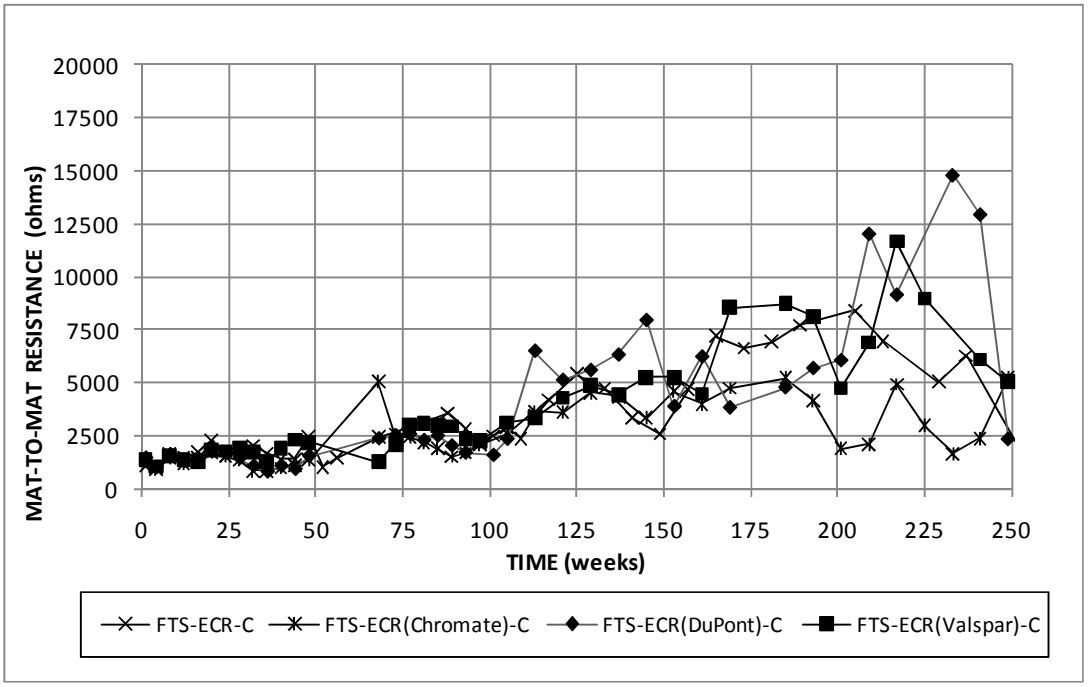

Figure 3.43: Field test specimens. Average mat-to-mat resistance for specimens with epoxy-coated reinforcement with increased adhesion in cracked concrete.

3.3.1.3 Corrosion Inhibitors

Figures 3.44 and 3.45 show the average corrosion rates based on exposed area for ECR with corrosion inhibitors in uncracked and cracked concrete, respectively. In uncracked concrete, FTS-ECR(RH)-U has the highest peak corrosion rate, 20.1 μm/yr at week 205. FTS-ECR(primer/Ca(NO2)2)-U has the next highest peak corrosion rate, 14.7 μm/yr at week 217, followed by conventional ECR with a peak corrosion rate of 13.9 μm/yr at week 237. FTS-ECR(DCI)-U and FTS-ECR(HY)-U have peak corrosion rates of 9.38 μm/yr at week 211 and 7.21 μm/yr at week 169, respectively. In cracked concrete (Figure 3.45), FTS-ECR(RH)-C has the highest peak corrosion rate, 25.8 μm/yr at week 245. The specimens with conventional ECR have a peak corrosion rate of 16.3 μm/yr at week 237, followed by FTS-ECR(DCI)-C and FTS-ECR(primer/Ca(NO2)2)-C with peak corrosion rates of 14.1 μm/yr at week 211 and 14.0 μm/yr at week 161, respectively. FTS-ECR(HY)-C shows the lowest peak corrosion rate, 5.84 μm/yr at week 225.

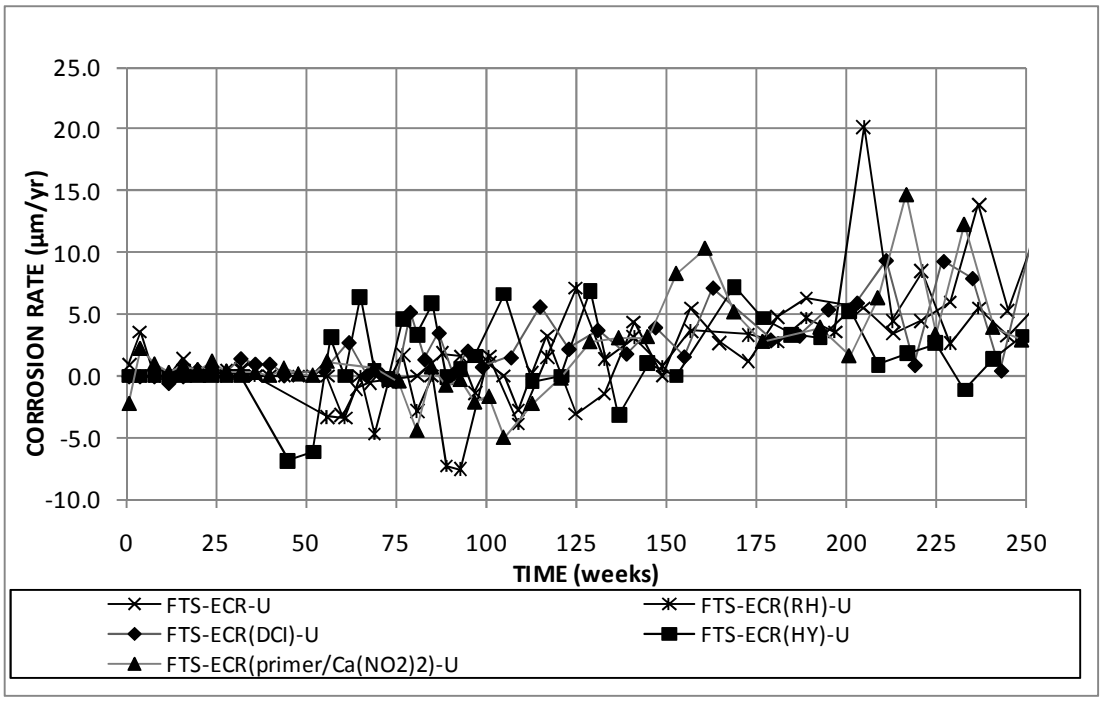

Figure 3.44: Field test specimens, uncracked concrete with corrosion inhibitors. Average corrosion rates based on exposed area for specimens with epoxy-coated reinforcement.

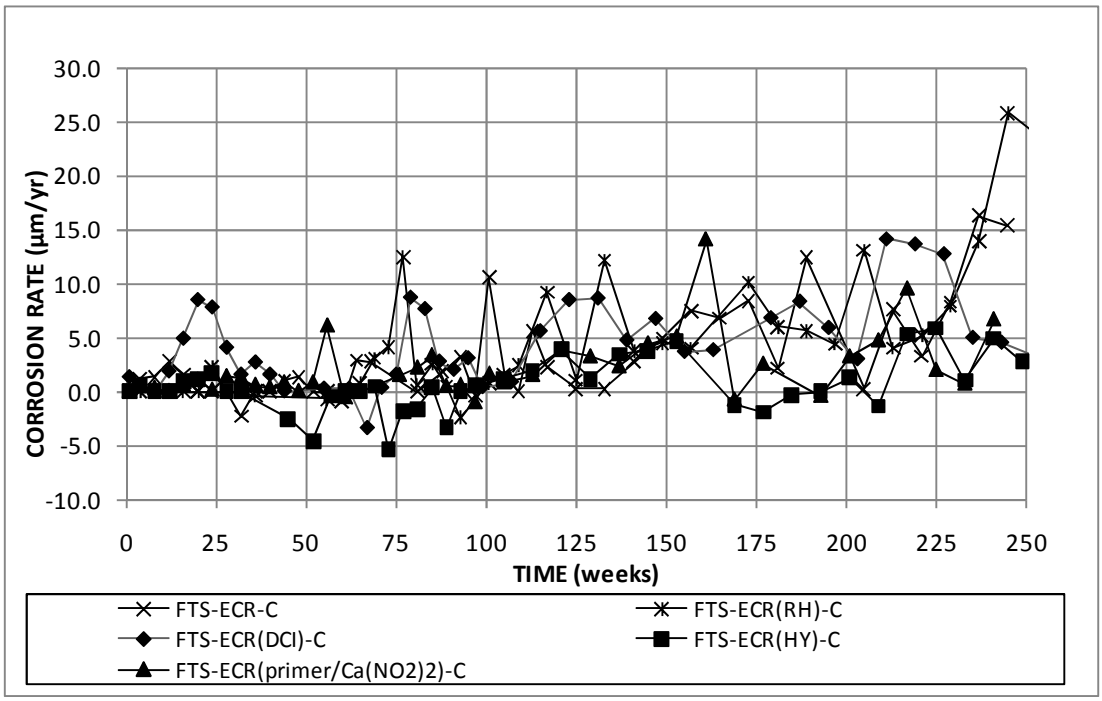

Figure 3.45: Field test specimens, cracked concrete with corrosion inhibitors. Average corrosion rates based on exposed area for specimens with ECR with corrosion inhibitors.

Figure 3.46 shows the average corrosion losses based on exposed area for corrosion inhibitors with epoxy-coated reinforcement in uncracked concrete. ECR in concrete containing DCI and Rheocrete shows increases in corrosion loss starting at approximately 60 weeks, earlier than ECR in concrete with no inhibitor (150 weeks). ECR with the calcium nitrite primer also initiates corrosion at 150 weeks. ECR with Hycrete exhibits negative corrosion losses between weeks 50 and 175, after which corrosion initiates and the corrosion loss increases. After initiation, all systems exhibit similar corrosion rates.

Individual corrosion loss data at the end of testing are summarized in Table 3.14. Negative corrosion losses are observed on test bar 3 from specimen FTS-ECR-U-2, test bar 1 from FTS-ECR(primer/Ca(NO2)2)-U-1, test bars 1, 2, and 3 from specimen FTS-ECR(RH)-U-2, and test bar 1 from specimen FTS-ECR(HY)-U-1 (Figures A37, A45, and A49, Appendix A); these test bars are excluded from the averages. In uncracked concrete, FTS-ECR(RH)-U exhibits the greatest average corrosion loss, 14.3 µm. FTS-ECR(DCI)-U exhibits the next greatest average corrosion loss at 250 weeks, 14.2 µm, followed by FTS-ECR(primer/Ca(NO2)2)-U at 13.5 µm and conventional ECR at 10.9 µm. Specimens containing Hycrete show the least corrosion loss at 250 weeks, averaging 8.75 µm. Among individual specimens containing corrosion inhibitors in uncracked concrete, FTS-ECR(DCI)-U-2 shows the greatest corrosion losses, 21.4 µm, and specimen FTS-ECR(HY)-U-1 shows the lowest corrosion loss, 7.98 µm.

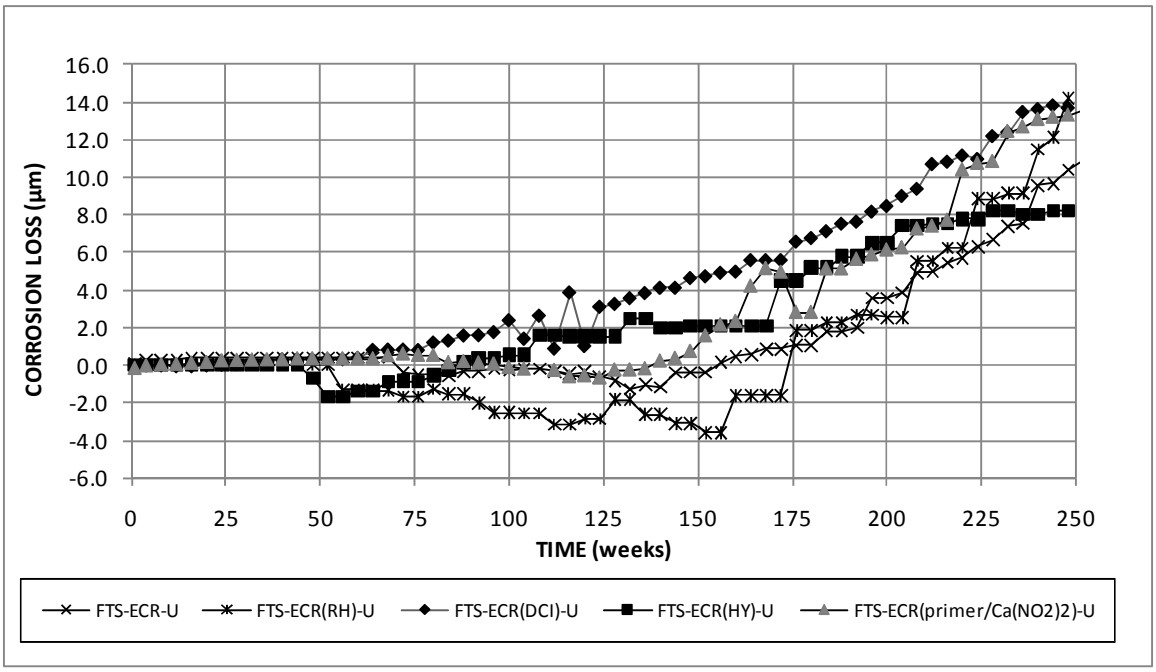

Figure 3.46: Field test specimens, uncracked concrete. Average corrosion losses based on exposed area for specimens with ECR with corrosion inhibitors.

In cracked concrete (Figure 3.47), ECR with DCI begins corroding at 20 weeks. This early initiation is due to variations in the quality of concrete (Tables 2.6, 2.7, and 2.8) rather than a deficiency in the corrosion protection system. ECR with the calcium nitrite primer and ECR with Rheocrete begin corroding around 75 weeks, similar to ECR with no inhibitor. ECR with Hycrete begins corroding after 110 weeks. At first, all systems show similar corrosion rates after initiation. However, ECR with DCI shows an increase in rate after week 125, ECR with Rheocrete shows increases after week 175, and ECR with no inhibitor shows increased corrosion activity after week 225.

At the end of testing, FTS-ECR(RH)-C exhibits the greatest average corrosion loss at 250 weeks, 25.6 µm, followed by FTS-ECR(DCI)-C at 23.2 µm. ECR with no inhibitor shows average losses of 23.0 µm. FTS-ECR(primer/Ca(NO2)2)-C and FTS-ECR(HY)-C show losses of 11.9 µm and 7.09 µm, respectively, and are the only specimens among the field test specimens with inhibitors to show significantly less

corrosion loss than ECR with no inhibitor. Among individual specimens with corrosion inhibitors in cracked concrete, FTS-ECR(RH)-C-2 shows the greatest corrosion losses, 26.4 µm. FTS-ECR(HY)-C-2 shows the least corrosion losses, 4.90 µm. For specimens containing DCI, Rheocrete, and epoxy with a calcium nitrite primer, the corrosion losses in cracked concrete are approximately 1.5 times greater than the corrosion losses in uncracked concrete. The specimens containing Hycrete show corrosion losses in cracked concrete comparable to those observed in uncracked concrete (Table 3.14).

Table 3.14: Corrosion Losses (µm) Based on Exposed Area for Field Test Specimens with Epoxy-Coated Reinforcement with Corrosion Inhibitors

Steel Designation	Exposure time (weeks)	Test Bar 1	2	3	4	Average[a]	Standard Deviation
Uncracked Concrete							
FTS-ECR-U-1	250	9.25	27.0			18.1	12.6
FTS-ECR-U-2	254	6.27	3.29	-2.04	1.62	3.73	2.35
FTS-ECR(primer/Ca(NO2)2)-U-1	250	-0.141	7.73	12.9	11.0	10.5	2.63
FTS-ECR(primer/Ca(NO2)2)-U-2	254	27.1	11.6	9.53	17.9	16.5	7.91
FTS-ECR(DCI)-U-1	250	12.2	14.8	7.57	11.9	11.6	3.00
FTS-ECR(DCI)-U-2	254	24.1	37.7	17.5	6.46	21.4	13.1
FTS-ECR(DCI)-U-3	254	13.8	13.3	2.59	9.00	9.66	5.18
FTS-ECR(RH)-U-1	250	26.6	18.7	6.06	17.6	17.3	8.47
FTS-ECR(RH)-U-2	254	-1.34	-3.12	-1.69	11.2	11.2	-
FTS-ECR(HY)-U-1	250	-0.458	1.25	4.42	18.3	7.98	9.06
FTS-ECR(HY)-U-2	254	8.59	6.69	13.1	9.76	9.52	2.67
Cracked Concrete							
FTS-ECR-C-1	250	5.72	25.2			15.5	13.8
FTS-ECR-C-2	254	21.9	66.8	17.1	16.4	30.6	24.3
FTS-ECR(primer/Ca(NO2)2)-C-1	250	2.27	6.55	18.0	3.59	7.59	7.14
FTS-ECR(primer/Ca(NO2)2)-C-2	254	6.38	16.8	16.0	26.0	16.3	8.00
FTS-ECR(DCI)-C-1	250	16.8	25.3	30.7	28.1	25.2	6.02
FTS-ECR(DCI)-C-2	254	9.00	15.9	28.9	24.9	19.7	8.96
FTS-ECR(DCI)-C-3	254	40.9	48.5	1.48	7.96	24.7	23.4
FTS-ECR(RH)-C-1	250	28.3	32.7	14.8	23.0	24.7	7.70
FTS-ECR(RH)-C-2	254	25.9	22.4	28.4	28.7	26.4	2.92
FTS-ECR(HY)-C-1	250	17.2	7.31	3.31	-2.47	9.27	7.14
FTS-ECR(HY)-C-2	254	1.95	7.85	-2.24	-1.55	4.90	4.17

[a] Excludes bars with 0 or negative losses

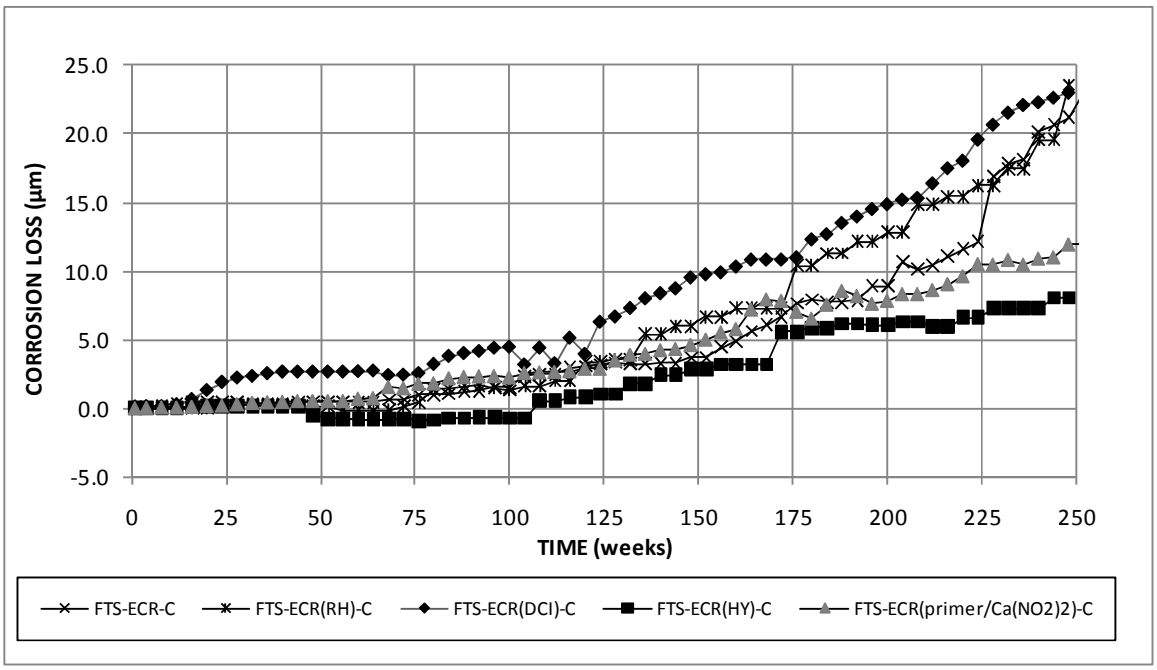

Figure 3.47: Field test specimens, cracked concrete. Average corrosion losses based on exposed area for specimens with ECR with corrosion inhibitors.

The average corrosion potentials (versus CSE) for the specimens with ECR with corrosion inhibitors in uncracked concrete are shown in Figure 3.48 (top mat) and Figure 3.49 (bottom mat). On the top mat, the corrosion potentials remain between –0.100 V and –0.200 V for the first 25 weeks of testing. With the exception of the specimens containing Hycrete, the corrosion potentials for all specimens decrease to close to –0.300 V after week 25 and remain between –0.100V and –0.400 V for the remainder of the test. The average corrosion potential for specimens with Hycrete remains more positive than other specimens, particularly after week 150. On the bottom mat of steel (Figure 3.49), the corrosion potentials for all specimens begin the test between –0.100 V and –0.200 V and decrease to close to and remain near –0.300 V for most of the test, becoming more positive after week 200.

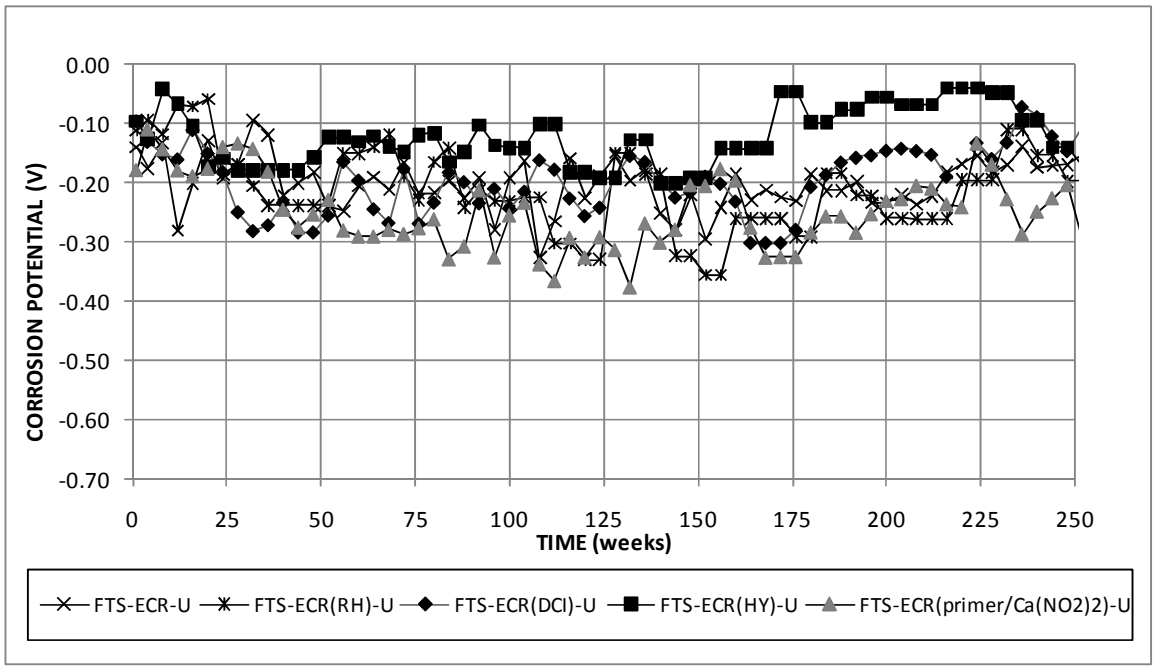

Figure 3.48: Average top mat potential (CSE) for field test specimens with epoxy-coated reinforcement with corrosion inhibitors in uncracked concrete.

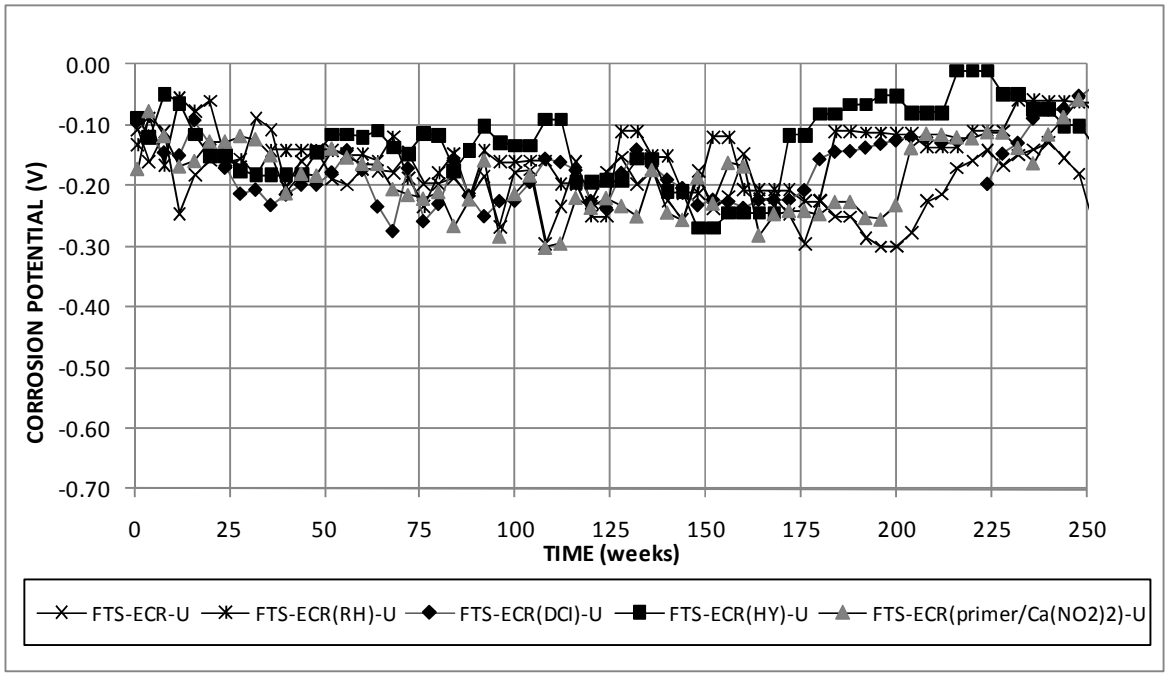

Figure 3.49: Average bottom mat potential (CSE) for field test specimens with epoxy-coated reinforcement with corrosion inhibitors in uncracked concrete.

The average corrosion potentials (versus CSE) for the specimens with ECR in cracked concrete with corrosion inhibitors are shown in Figure 3.50 (top mat) and Figure 3.51 (bottom mat). At the start of testing, the top mat corrosion potentials for all specimens are between –0.100 V and –0.200 V; however, the corrosion potentials for all specimens drop below –0.300 V by week 25. The potentials remain below –0.300V for much of the test, increasing again after week 175. The specimens containing Hycrete show corrosion potentials more positive than –0.225 V after week 200; the other specimens show potentials between –0.200 V and –0.300 V for most of this time. Except for the period between 175 and 255 weeks, no significant difference in potentials is observed between conventional ECR and ECR in concrete with corrosion inhibitors. On the bottom mat of steel (Figure 3.51), the corrosion potentials begin the test between –0.100 V and –0.200 V and decrease to close to –0.300 V for most of the test, becoming more positive after week 175.

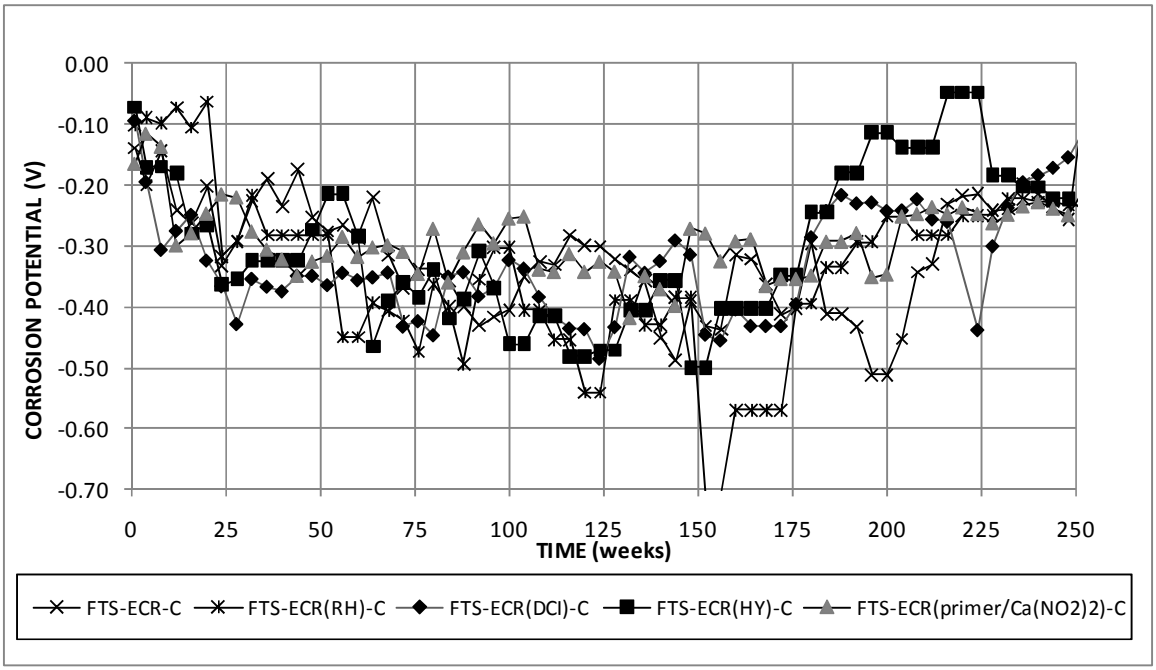

Figure 3.50: Average top mat potential (CSE) for field test specimens with epoxy-coated reinforcement with corrosion inhibitors in cracked concrete.

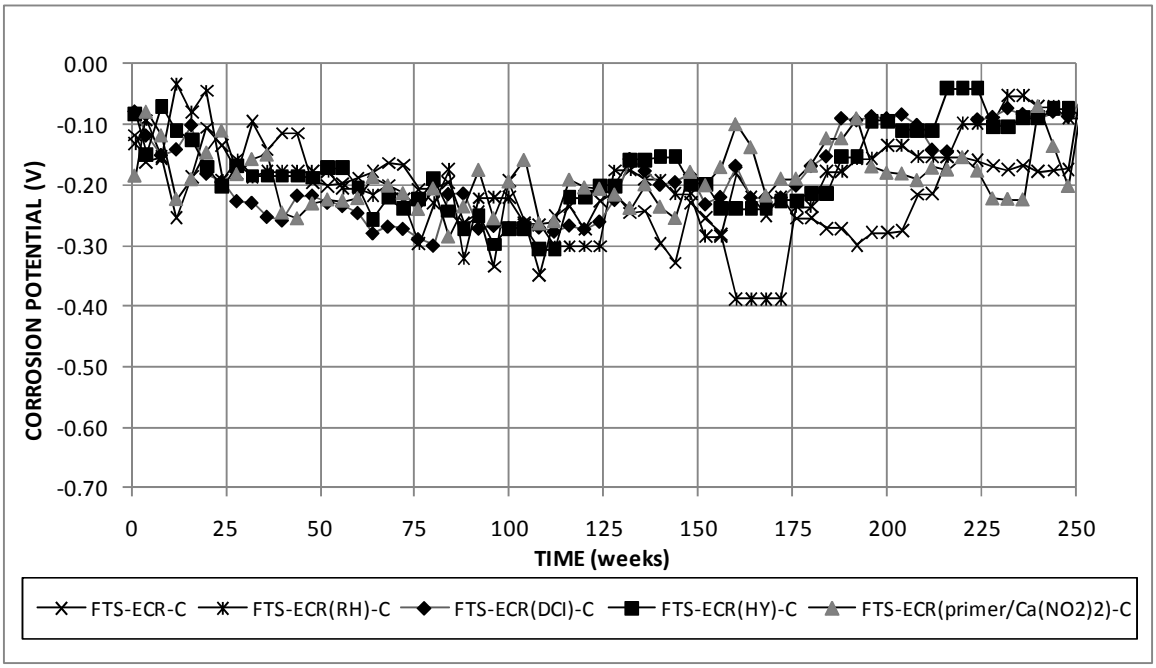

Figure 3.51: Average bottom mat potential (CSE) for field test specimens with epoxy-coated reinforcement with corrosion inhibitors in cracked concrete.

The average mat-to-mat resistances for the specimens with ECR with corrosion inhibitors in uncracked and cracked concrete are shown in Figures 3.52 and 3.53, respectively. For the uncracked concrete specimens, the mat-to-mat resistance of specimens containing Hycrete is significantly higher than for the specimens with the other inhibitors; the specimens with Hycrete show mat-to-mat resistances as high as 16,300 ohms, whereas the mat-to-mat resistances for other specimens increase from approximately 2,000 ohms at the start of testing to around 5,000 ohms at week 150. After week 150, the mat-to-mat resistances for all specimens in uncracked concrete are comparable, with isolated jumps in resistance observed on many specimens. For the cracked concrete specimens (Figure 3.53), the mat-to-mat resistance of all specimens is comparable to values observed in uncracked concrete.

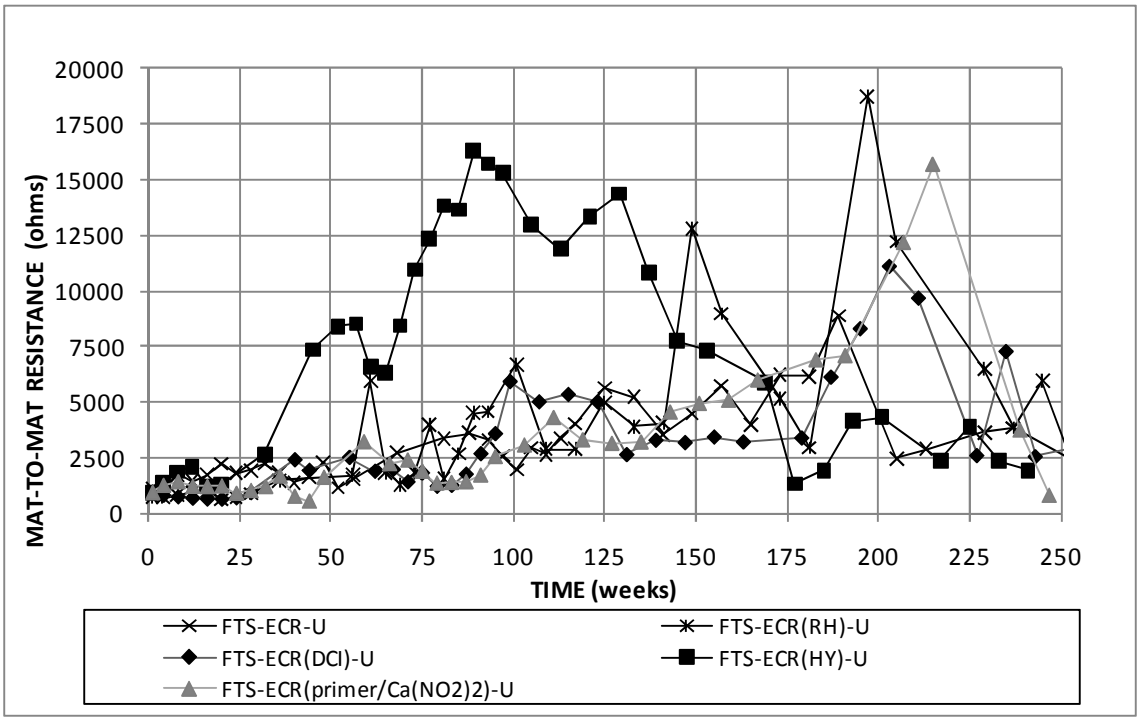

Figure 3.52: Field test specimens. Average mat-to-mat resistance for specimens with epoxy-coated reinforcement in uncracked concrete containing corrosion inhibitors.

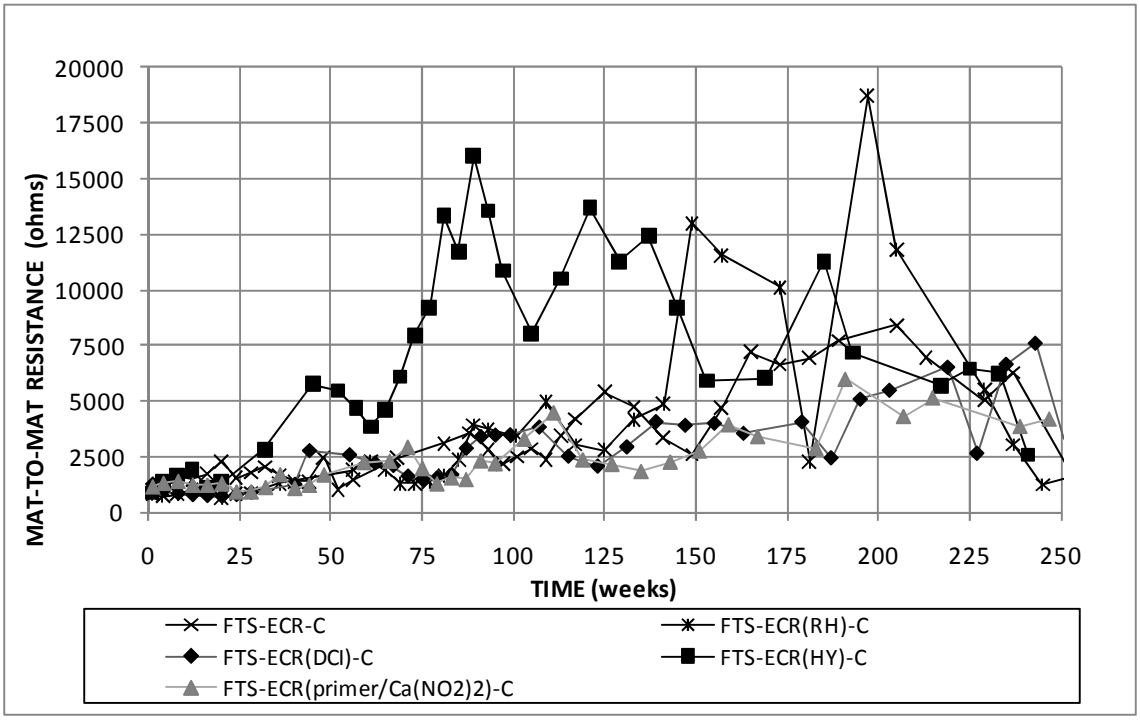

Figure 3.53: Field test specimens. Average mat-to-mat resistance for specimens with epoxy-coated reinforcement in cracked concrete containing corrosion inhibitors.

3.3.1.4 Multiple-Coated Reinforcement

Figures 3.54 and 3.55 show the average corrosion rates based on exposed area for multiple-coated reinforcement in uncracked and cracked concrete, respectively. In uncracked concrete, FTS-MC-U has a lower peak corrosion rate than conventional ECR, 9.17 μm/yr at week 4 compared to 13.9 μm/yr at week 237 for conventional ECR. In cracked concrete (Figure 3.55), FTS-MC-C has the higher peak corrosion rate, 19.4 μm/yr at week 231 compared to specimens with conventional ECR, which has a peak corrosion rate of 16.3 μm/yr at week 237. For the specimens in both uncracked and cracked concrete, the corrosion rate tends to increase with time.

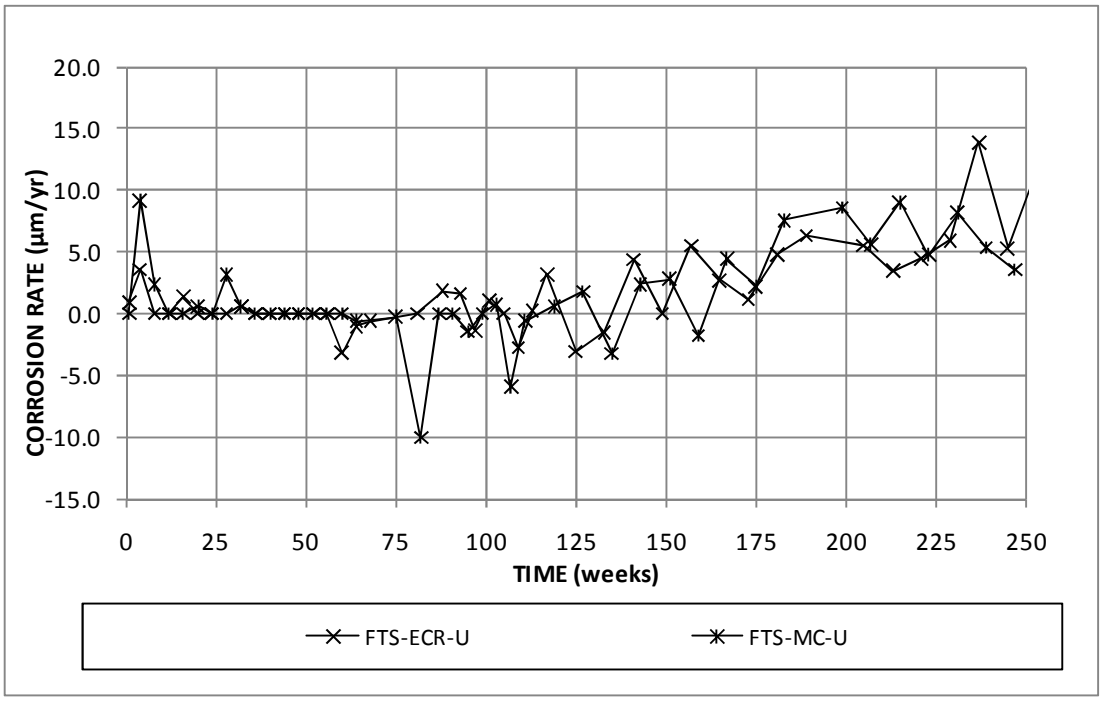

Figure 3.54: Field test specimens, uncracked concrete. Average corrosion rates based on exposed area for specimens with multiple-coated and epoxy-coated reinforcement.

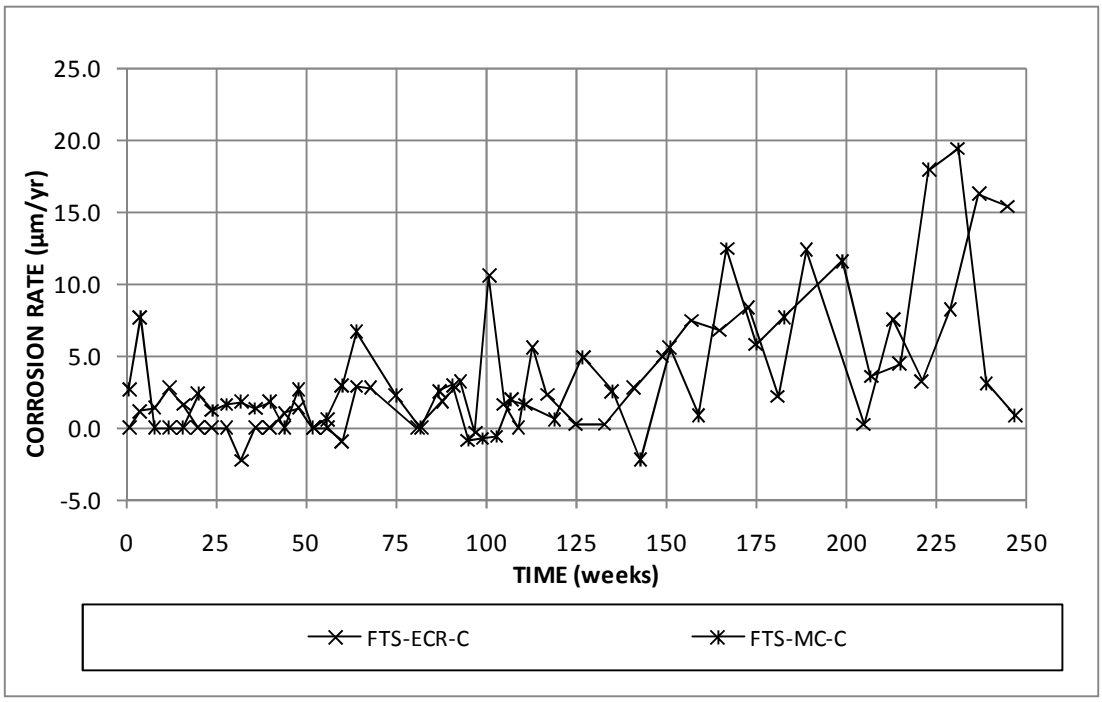

Figure 3.55: Field test specimens, cracked concrete. Average corrosion rates based on exposed area for specimens with multiple-coated and epoxy-coated reinforcement.

Figure 3.56 shows the average corrosion losses based on exposed area for multiple-coated reinforcement and epoxy-coated reinforcement in uncracked concrete. Both ECR and MC bars show corrosion losses increasing after week 150 at a constant rate until the end of testing. Figure 3.57 shows the average corrosion losses based on exposed area for multiple-coated reinforcement and epoxy-coated reinforcement in cracked concrete. The MC bars show an increase in corrosion loss from the start of testing, whereas the corrosion losses for ECR remain at zero until week 75. MC reinforcement shows greater corrosion losses than ECR through week 160, after which the behavior of MC bars is similar to that of ECR.

Individual corrosion loss data at the end of testing are summarized in Table 3.15. In uncracked concrete, the specimens with multiple-coated reinforcement and the specimens with epoxy-coated reinforcement exhibit similar corrosion losses, with FTS-MC-U exhibiting average corrosion losses of 9.99 µm and FTS-ECR-U with average

losses of 10.9 µm. However, individual specimen losses vary greatly, with FTS-ECR-U-1 and FTS ECR-U-2 showing losses of 18.1 and 3.73 µm, respectively, whereas FTS-MC-U-1 and FTS-MC-U-2 show losses of 9.17 and 10.8 µm (Table 3.15). In cracked concrete, the average corrosion losses for conventional ECR and MC reinforcement are again similar, with FTS-MC-C exhibiting average losses of 20.9 µm, whereas FTS-ECR-C exhibits average losses of 23.0 µm. Variation among individual ECR specimens is again greater than variation among individual MC specimens; FTS-ECR-C-1 and FTS-ECR-C-2 show corrosion losses of 15.5 µm and 30.6 µm, whereas FTS-MC-C-1 and FTS-MC-C-2 show corrosion losses of 19.5 µm and 22.4 µm, respectively (Table 3.15).

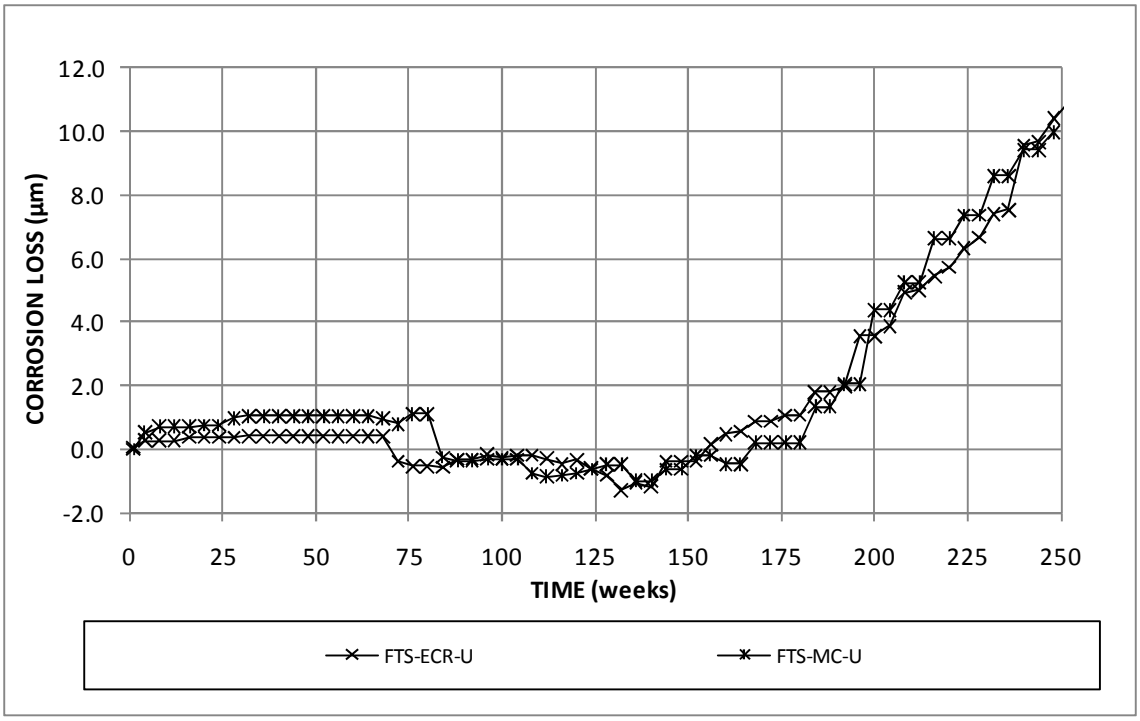

Figure 3.56: Field test specimens, uncracked concrete. Average corrosion losses based on exposed area for specimens with multiple-coated reinforcement and ECR.

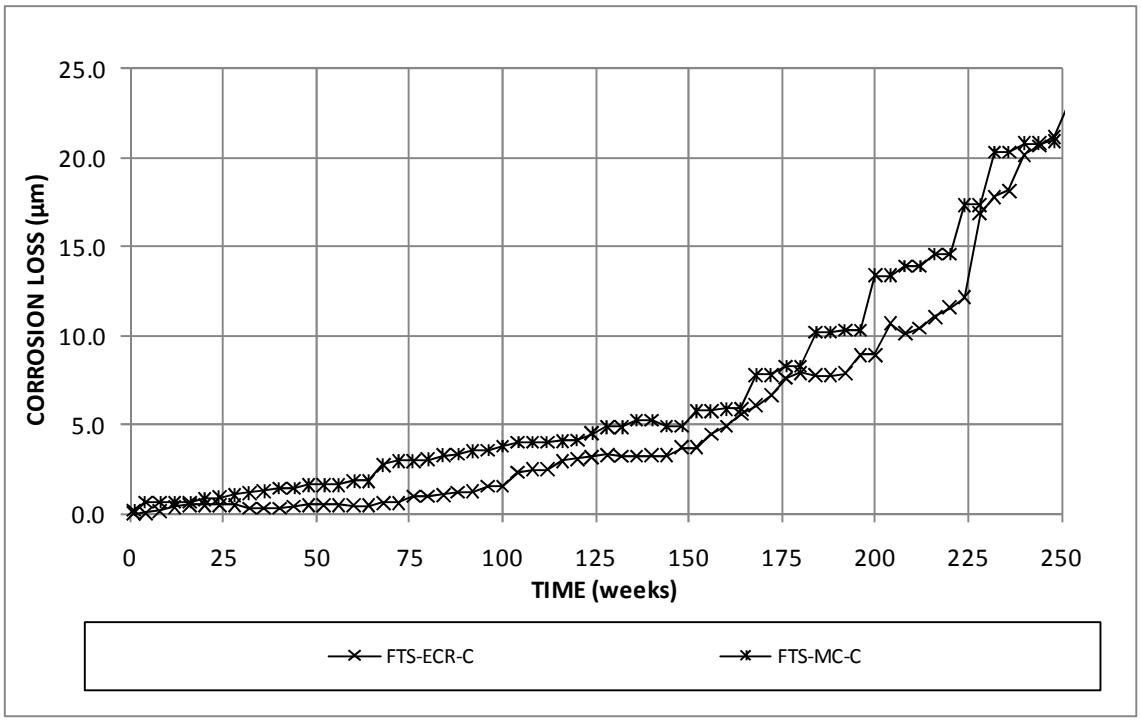

Figure 3.57: Field test specimens, cracked concrete. Average corrosion losses based on exposed area for specimens with multiple-coated reinforcement and ECR.

Table 3.15: Corrosion Losses (µm) Based on Exposed Area for Field Test Specimens with Multiple-Coated Reinforcement

Steel Designation	Exposure time (weeks)	Test Bar 1	2	3	4	Average[a]	Standard Deviation
Uncracked Concrete							
FTS-ECR-U-1	250	9.25	27.0			18.1	12.6
FTS-ECR-U-2	254	6.27	3.29	-2.04	1.62	3.73	2.35
FTS-MC-U-1	250	9.54	8.81			9.17	0.515
FTS-MC-U-2	254	18.4	2.94	2.89	18.9	10.8	9.10
Cracked Concrete							
FTS-ECR-C-1	250	5.72	25.2			15.5	13.8
FTS-ECR-C-2	254	21.9	66.8	17.1	16.4	30.6	24.3
MC (1)	250	17.1	21.8			19.5	3.32
MC (2)	254	28.9	23.8	28.7	8.24	22.4	9.75

[a] Excludes bars with 0 or negative losses

The average corrosion potentials (versus CSE) for the specimens with multiple-coated reinforcement and epoxy-coated reinforcement in uncracked concrete are shown in Figure 3.58 (top mat) and Figure 3.59 (bottom mat). For the specimens with multiple-coated reinforcement, corrosion potentials on the top and bottom mats of steel are significantly more negative than the corrosion potentials for specimens with conventional ECR, with top mat potentials more negative than –0.400 V for much of the test. On the bottom mat, the corrosion potentials for multiple-coated reinforcement in uncracked concrete begin the test around –0.300 V and remain there until week 175, after which the bottom mat potential increases to between –0.100 V and –0.200 V, comparable to conventional ECR (Figure 3.59).

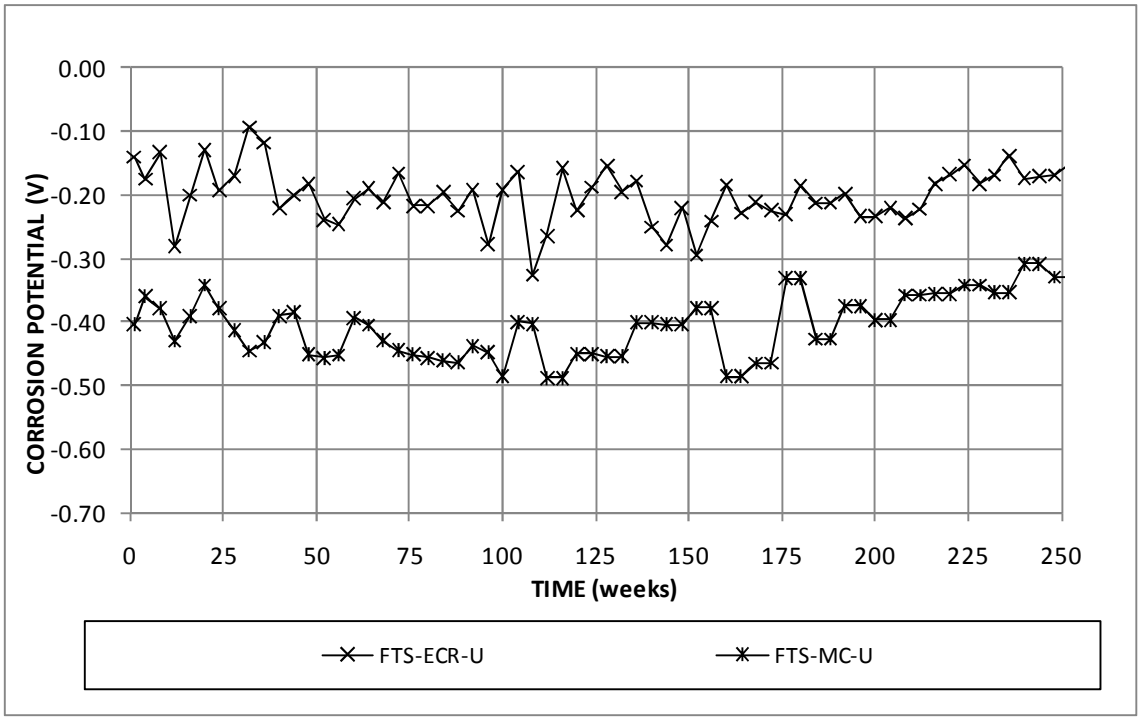

Figure 3.58: Average top mat potential (CSE) for field test specimens with multiple-coated reinforcement in uncracked concrete.

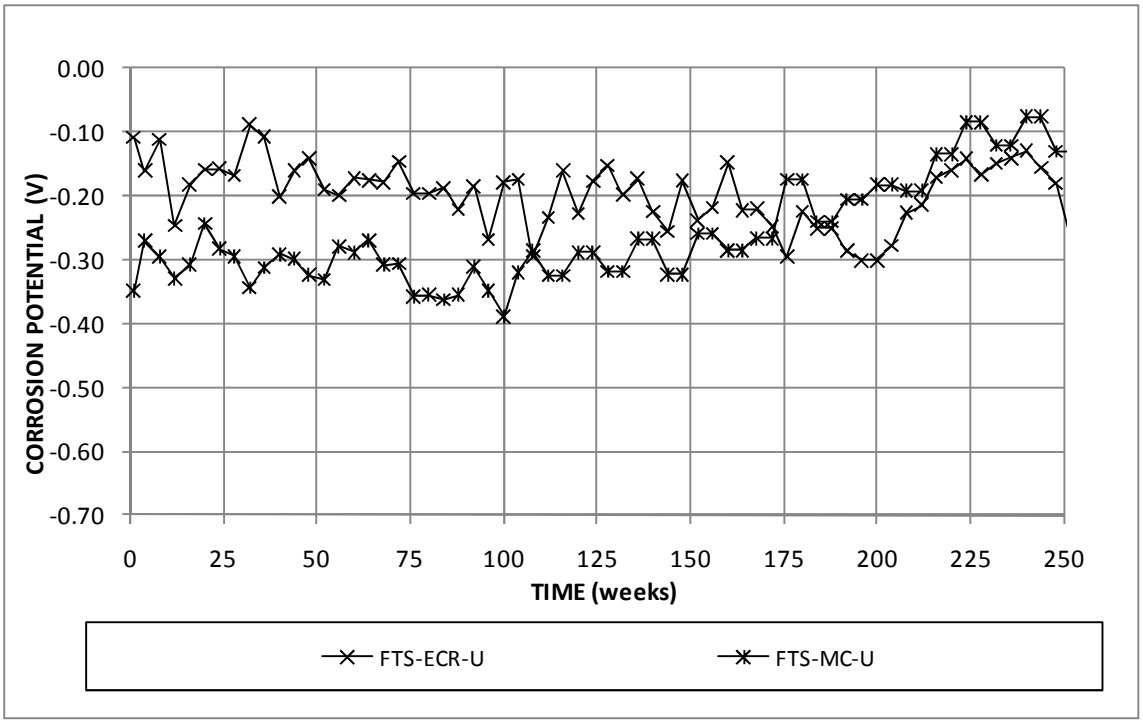

Figure 3.59: Average bottom mat potential (CSE) for field test specimens with multiple-coated reinforcement in uncracked concrete.

The average corrosion potentials (versus CSE) for the specimens with multiple-coated reinforcement and epoxy-coated reinforcement in cracked concrete are shown in Figure 3.60 (top mat) and Figure 3.61 (bottom mat). For the specimens with multiple-coated reinforcement, the corrosion potentials in cracked concrete are more negative than those observed in uncracked concrete, with measured potentials of approximately –0.500 V for much of the test. After 200 weeks, the average top mat potentials of FTS-MC-C increase slightly and are comparable to FTS-ECR-C for the remainder of the test. On the bottom mat (Figure 3.61), the corrosion potentials for multiple-coated reinforcement in cracked concrete are similar to those observed in uncracked concrete; the corrosion potential remains between –0.300 V and –0.400 V for much of the testing, with a slight increase in potential after 150 weeks.

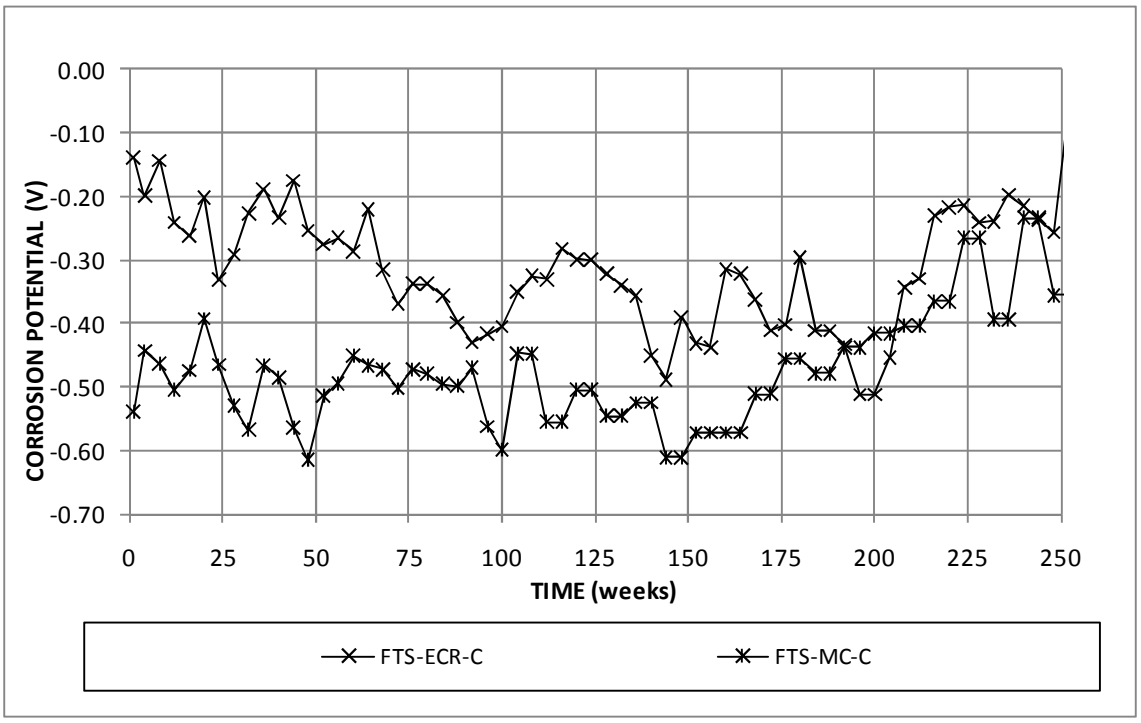

Figure 3.60: Average top mat potential (CSE) for field test specimens with multiple-coated reinforcement in cracked concrete.

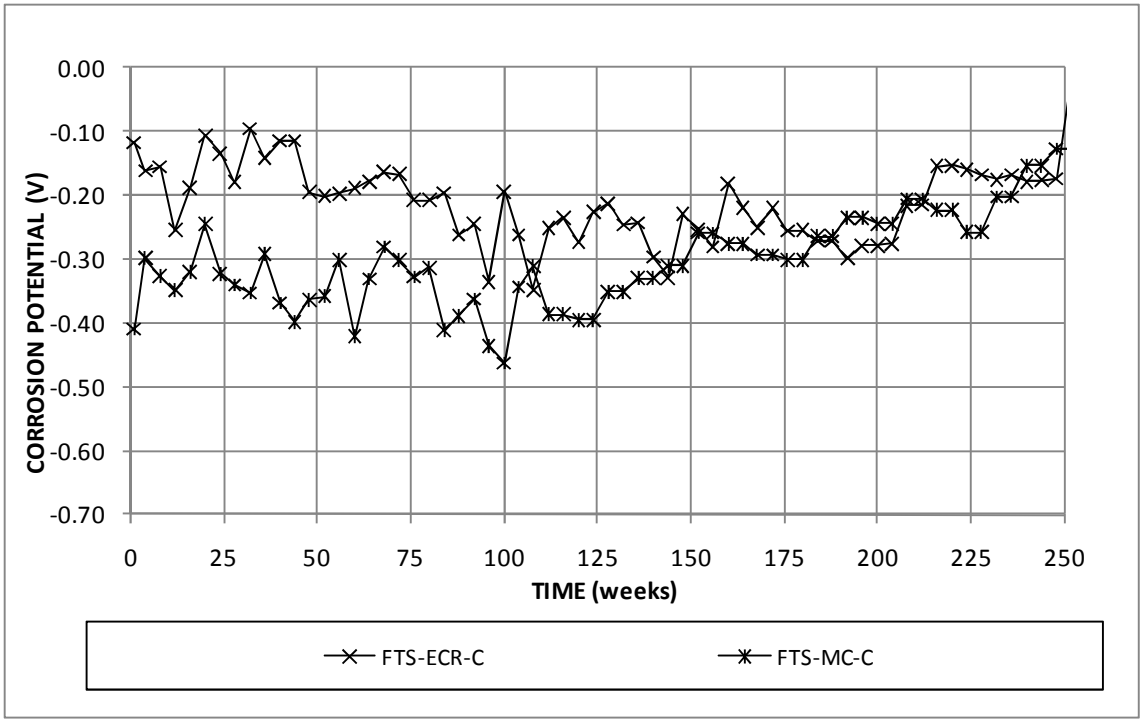

Figure 3.61: Average bottom mat potential (CSE) for field test specimens with multiple-coated reinforcement in cracked concrete.

The average mat-to-mat resistances for the specimens with multiple-coated reinforcement in uncracked and cracked concrete are shown in Figures 3.62 and 3.63, respectively. For the uncracked concrete specimens, the mat-to-mat resistance increases from approximately 2,000 ohms at the start of testing to around 6,000 ohms at week 150. For the cracked concrete specimens (Figure 3.63), the mat-to-mat resistance of all specimens increases throughout the test, approaching 10,000 ohms by the end of testing. No significant difference in mat-to-mat resistance is observed between conventional ECR and MC reinforcement in either cracked or uncracked concrete.

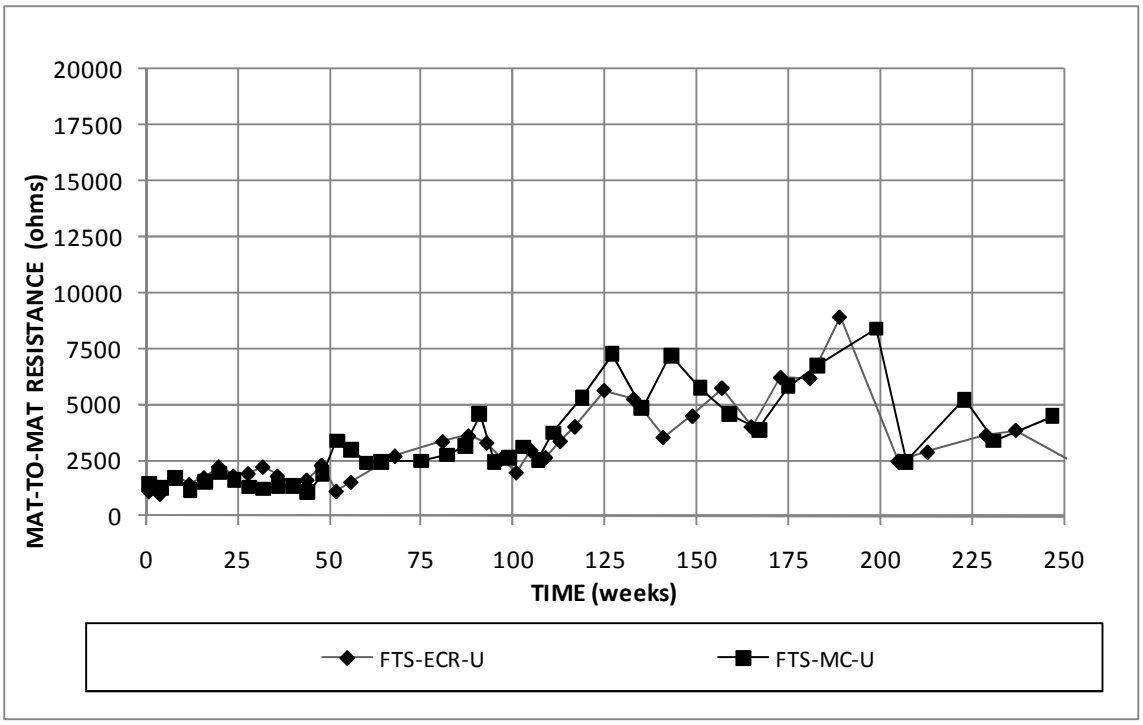

Figure 3.62: Field test specimens. Average mat-to-mat resistance for specimens with multiple-coated reinforcement in uncracked concrete.

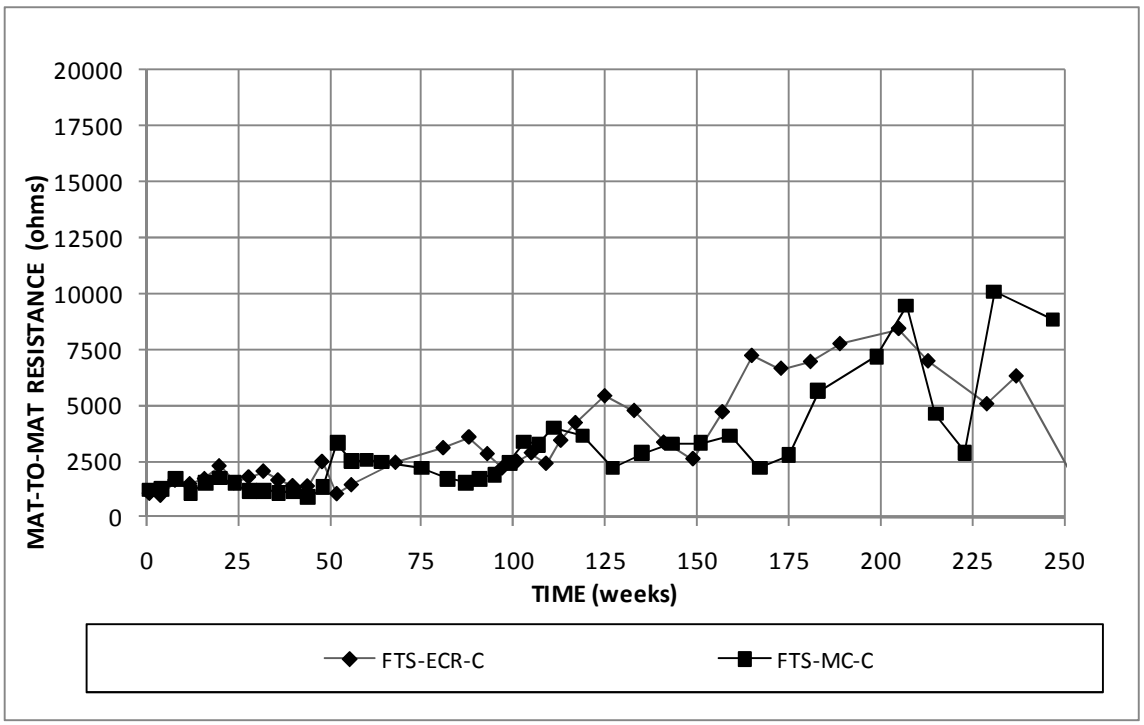

Figure 3.63: Field test specimens. Average mat-to-mat resistance for specimens with multiple-coated reinforcement in cracked concrete.

3.3.2 Field Test Specimen Autopsy Results

3.3.2.1 Visual Observations

After reaching the end of the test, the field test specimens are inspected for signs of staining and cracking prior to autopsy and disbondment. Both specimens with conventional reinforcement in uncracked concrete exhibit moderate staining and cracking at the end of testing, as shown for specimen FTS-Conv.-U-1 in Figure 3.64. Both specimens with conventional reinforcement in cracked concrete exhibit heavy staining, cracking, and spalling at the end of the test, as shown for specimen FTS-Conv.-C-2 in Figure 3.65. No specimens with epoxy-coated reinforcement or multiple-coated reinforcement show signs of staining in either uncracked (Figure 3.66) or cracked (Figure 3.67) concrete. However, specimens with concrete containing Hycrete show signs of scaling in both cracked and uncracked concrete (Figures 3.68 and 3.69). Scaling is not observed on any other specimen.

Figure 3.64: Specimen FTS-Conv.-U-1 at end of test.

Figure 3.65: Specimen FTS-Conv.-C-2 at end of test.

Figure 3.66: Specimen FTS-ECR-U-2 at end of test.

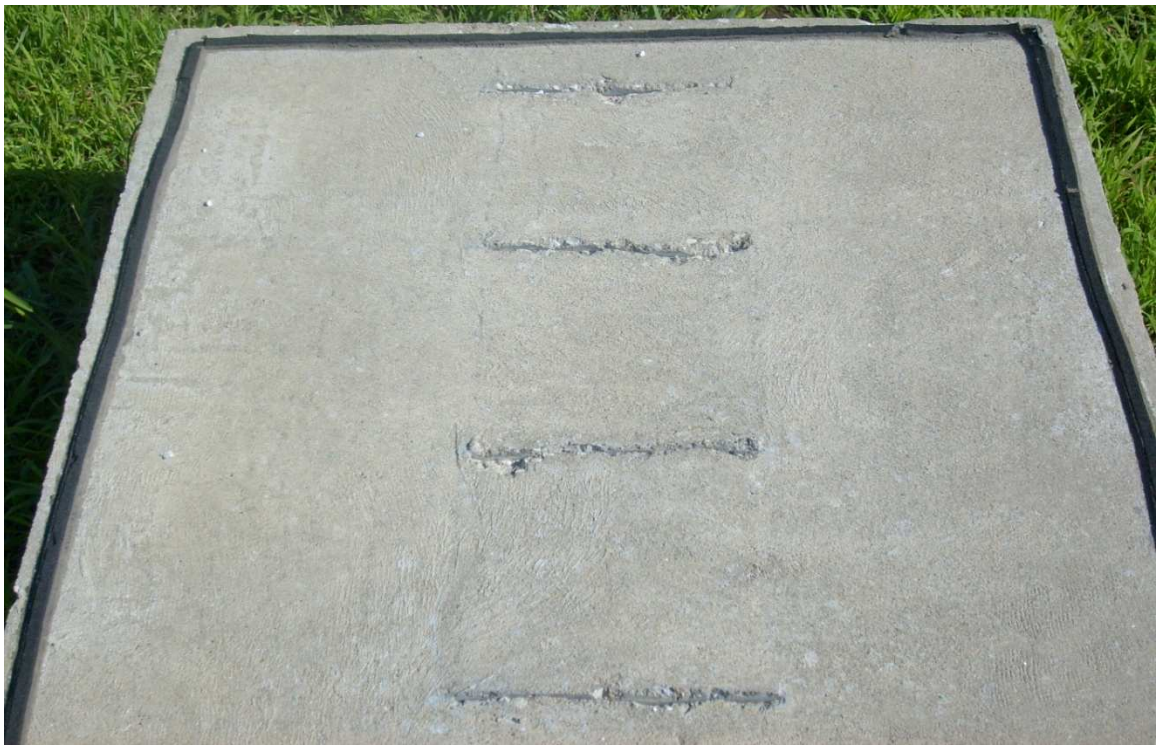

Figure 3.67: Specimen FTS-ECR-C-2 at end of test.

Figure 3.68: Scaling on **s**pecimen FTS-ECR(HY)-C-2 at end of test.

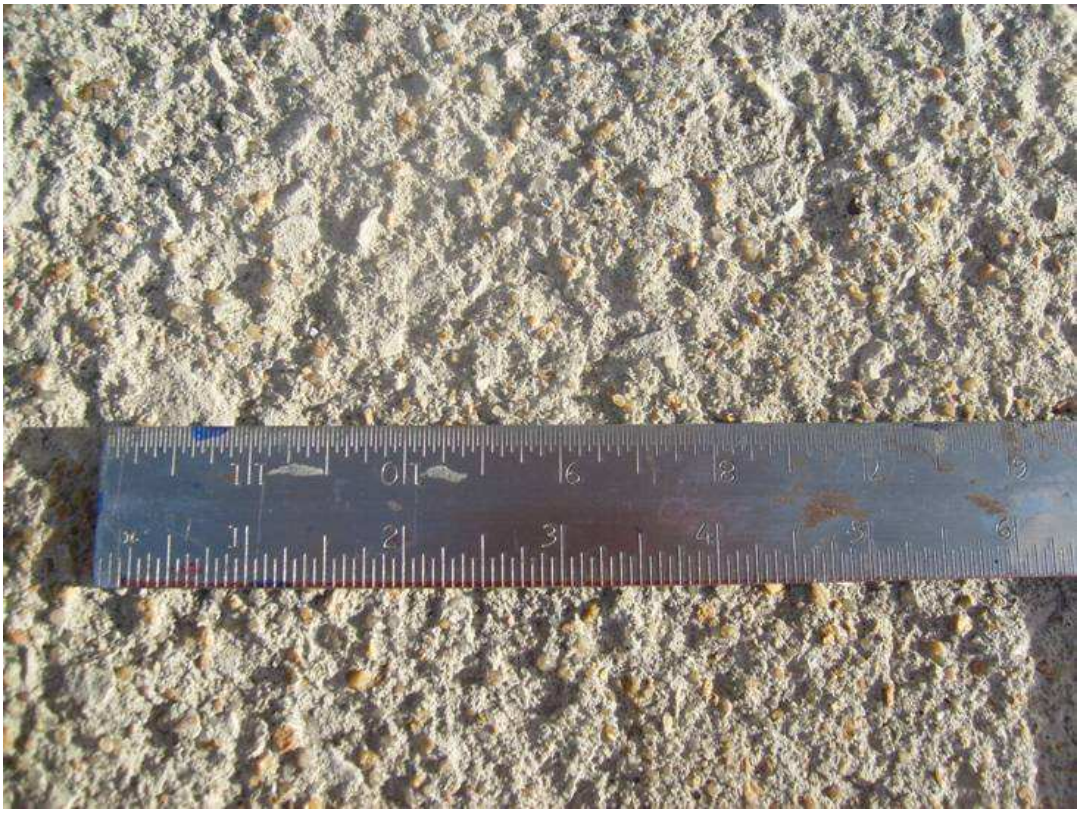

Figure 3.69: Scaling on **s**pecimen FTS-ECR(HY)-C-2 at end of test (detail).

After autopsying the specimens, bars are inspected for corrosion products. For conventional reinforcement in uncracked concrete, moderate to heavy corrosion products are observed on some bars from the top mat of steel, with other bars from the top mat of steel showing light to no corrosion products (Figure 3.70). Bars from the bottom mat of steel show light to no corrosion products (Figure 3.71). In cracked concrete, conventional reinforcement shows moderate to heavy corrosion products on all the bars in the top mat of steel (Figure 3.72), with limited regions of corrosion on the bottom mat of steel (Figure 3.73).

Figure 3.70: Specimen FTS-Conv.-U-2, top mat of steel.

Figure 3.71: Specimen FTS-Conv.-U-2, bottom mat of steel.

Figure 3.72: Specimen FTS-Conv.-C-1, top mat of steel.

Figure 3.73: Specimen FTS-Conv.-C-1, bottom mat of steel.

In uncracked concrete, the epoxy-coated and multiple-coated bars show no signs of corrosion (Figure 3.74). In cracked concrete, several specimens with epoxy-coated reinforcement show signs of staining at the sites of intentional damage (Figure 3.75). Corrosion products at the damage sites are observed on the bars from specimens with conventional ECR in concrete with and without corrosion inhibitors, on ECR with improved adhesion, and on MC reinforcement (Figure 3.76). On several specimens, blistering is also observed (Figure 3.77).

Figure 3.74: FTS-ECR(Chromate)-U-1, showing no visible corrosion products.

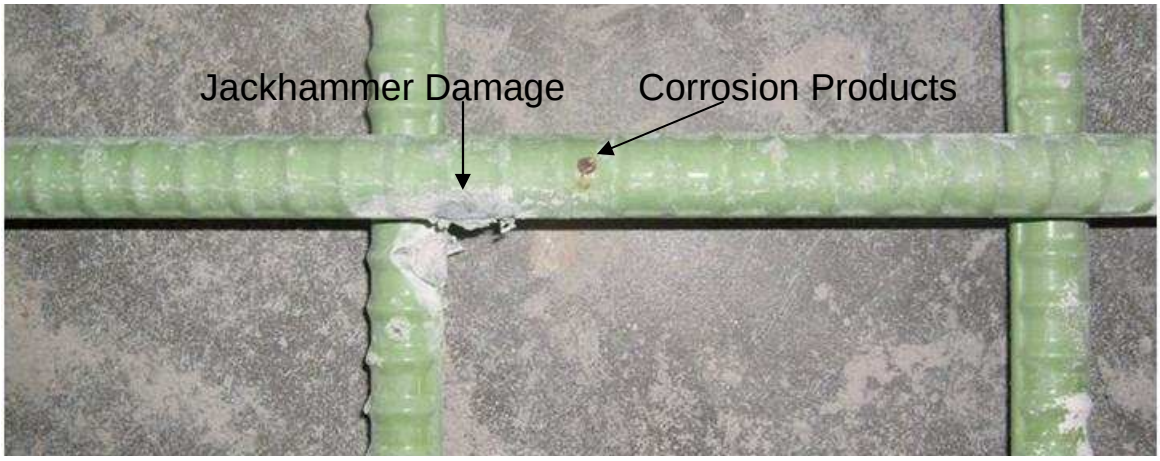

Figure 3.75: FTS-ECR(RH)-C-2, showing staining at an intentional damage site.

Figure 3.76: FTS-MC-C-2, showing staining at an intentional damage site.

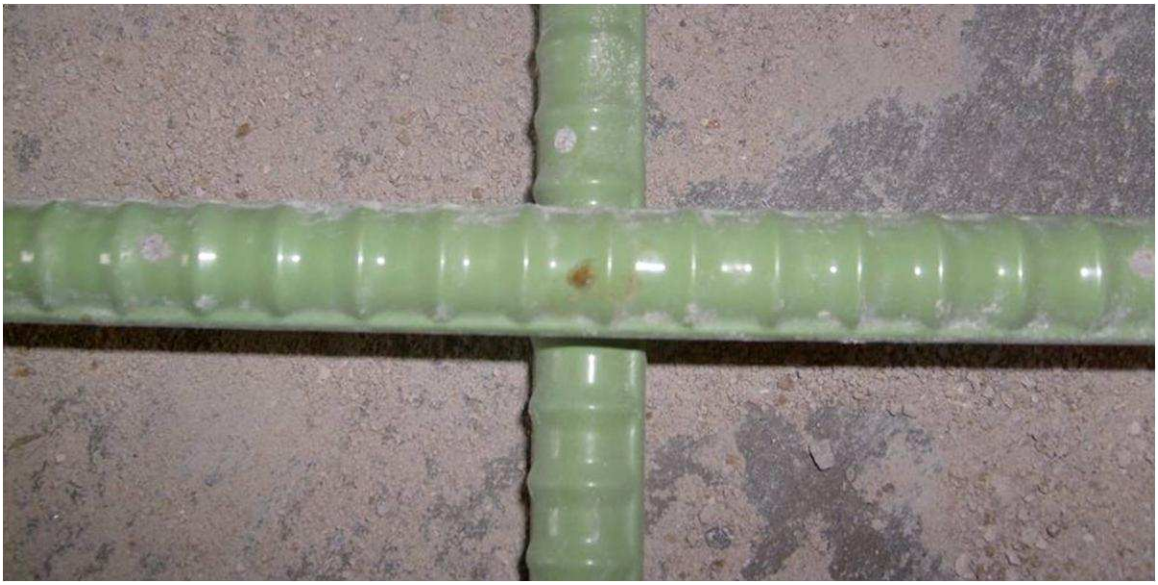

Figure 3.77: FTS-ECR-C-2, showing blistering of the epoxy coating.

3.3.2.2 Disbondment Results

For all test bars, a disbondment test, described in Section 2.3.7.1, is performed. The purpose of the disbondment test is to measure the loss of adhesion between the epoxy and the underlying steel and to examine the bars for signs of underfilm corrosion. Disbondment data in uncracked concrete is summarized in Figure 3.78, with individual disbondment data shown in Appendix D. In uncracked concrete, conventional ECR shows limited disbondment on both top and bottom bars (Figure 3.79), as do all bars with increased adhesion epoxies, ECR in concrete containing Hycrete, and the bars from specimens FTS-ECR(primer/Ca(NO2)2)-U-1 and FTS-MC-U-1 (Figure 3.80). ECR in concrete containing Rheocrete and DCI (Figure 3.81) and bars from specimens FTS-ECR(primer/Ca(NO2)2)-U-2 and FTS-MC-U-2 (Figure 3.82) show moderate amounts of disbondment on the top mat of steel. The variation in disbondment is likely due to variations in the quality of concrete in different batches (Tables 2.6, 2.7, and 2.8) rather than variations in the corrosion protection systems themselves. For the bottom mat of steel, bars show limited to no disbondment from all specimens.

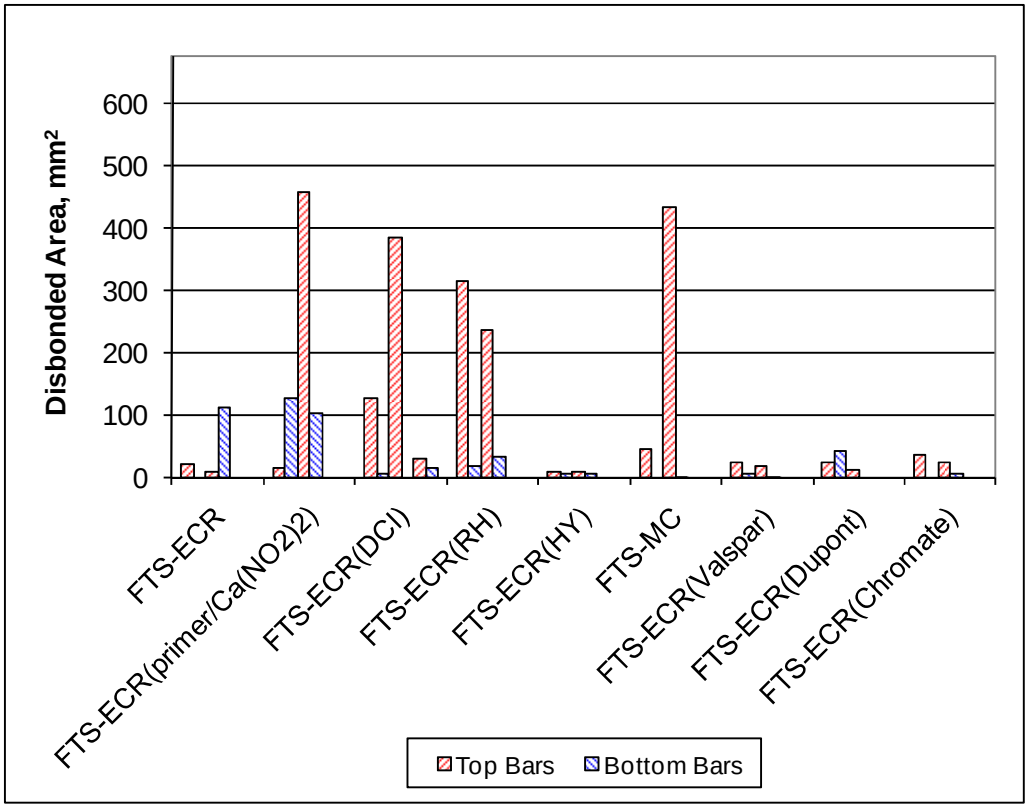

Figure 3.78: Disbonded area for field test specimens in uncracked concrete.

Figure 3.79: FTS-ECR-U-1, showing limited disbondment at an intentional damage site.

Figure 3.80: FTS-MC-U-1, showing limited disbondment at an intentional damage site.

Figure 3.81: FTS-RH-U-2, showing severe disbondment at intentional damage sites.

Figure 3.82: FTS-MC-U-2, showing severe disbondment at an intentional damage site.

Figure 3.83 summarizes disbondment results for field test specimens with cracked concrete. In cracked concrete, test bars from all specimens show significantly increased disbondment compared to bars from specimens in uncracked concrete. The bars from specimens with conventional ECR and ECR with a calcium nitrite primer show moderate amounts of disbondment on the top mat of steel (Figure 3.84). The test bars from specimens containing corrosion inhibitors, such as shown in Figure 3.85, and the test bars from specimens with increased adhesion epoxies, such as shown in Figure 3.86, show significantly greater disbondment compared to control specimens. This is believed to be due to variations in batch quality. MC reinforcement shows less disbondment on the top mat (Figure 3.87) than ECR with increased adhesion and ECR with concrete containing corrosion inhibitors. MC reinforcement also shows the least amount of disbondment on the bottom bars (Figure 3.83).

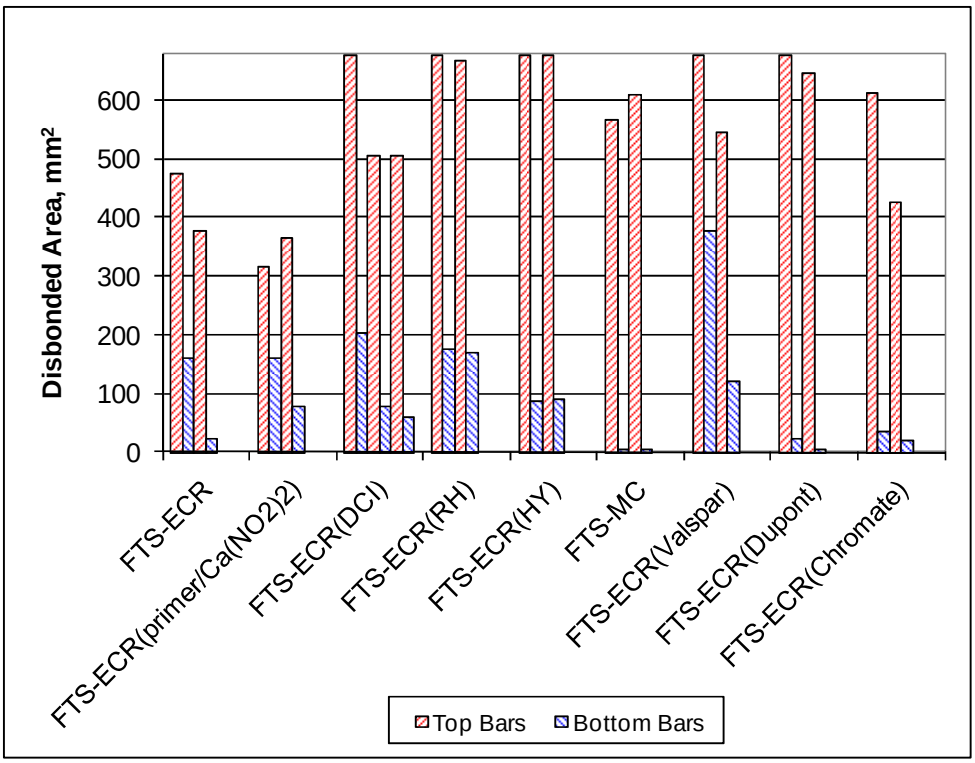

Figure 3.83: Disbonded area for field test specimens in cracked concrete.

Figure 3.84: FTS-ECR-C-2, showing moderate disbondment on a bar from the top mat of steel.

Figure 3.85: FTS-ECR(RH)-C-1, showing total disbondment on a bar from the top mat of steel.

Figure 3.86: FTS-ECR(DuPont)-C-1, showing total disbondment on bars from the top mat of steel.

Figure 3.87: FTS-ECR(RH)-C-1, showing severe disbondment on a bar from the top mat of steel.

In addition to performing disbondment tests on all electrically connected test bars, disbondment tests are also performed on electrically isolated bars from the top mat of steel in uncracked field test specimens. Figure 3.88 summarizes the disbondment results from electrically isolated bars in the top mat of steel and compares the results to those obtained from electrically connected bars. In all specimens, the electrically isolated bars show less disbondment than the electrically connected bars. Electrically isolating the bars eliminates the possibility of macrocell corrosion, resulting in less corrosion loss on electrically isolated bars compared to bars that are electrically connected to other bars. This reduces the disbonded area observed on electrically isolated bars, and in all likelihood, this reduced electrical conductivity applies to most epoxy-coated bars on bridge decks.

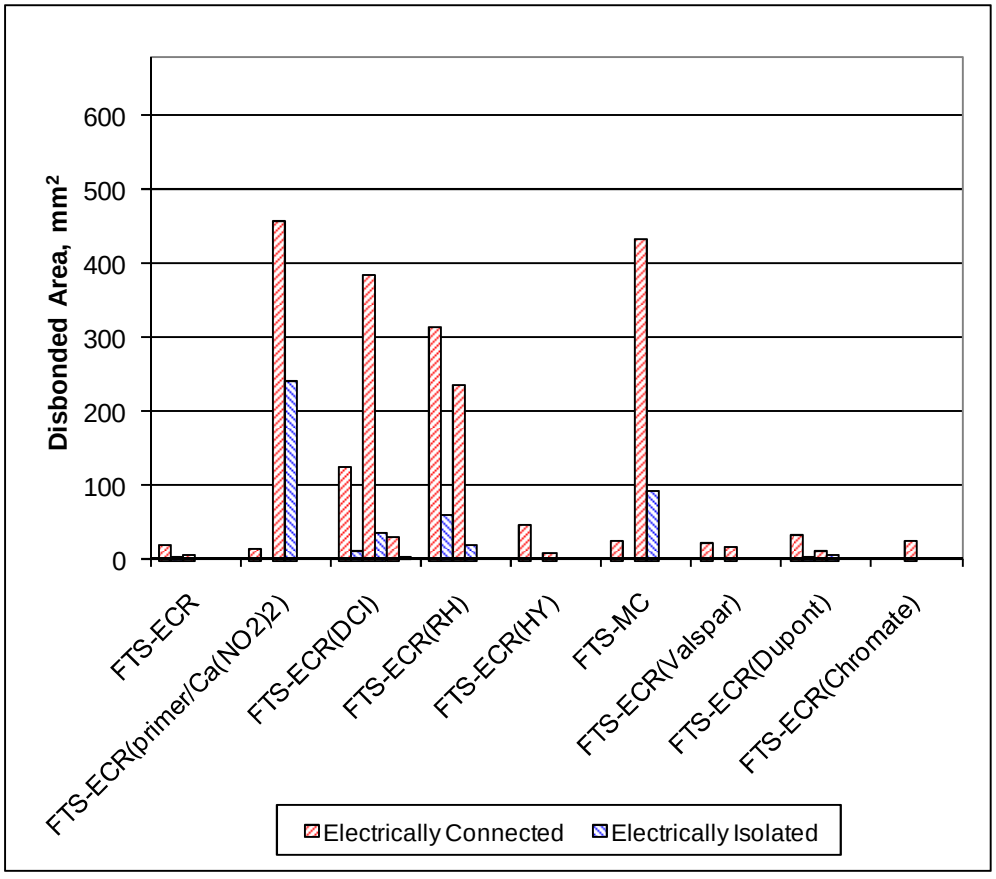

Figure 3.88: Disbonded area for field test specimens in uncracked concrete, top mat of steel, electrically connected and electrically isolated bars.

3.3.2.3 FTS Chloride Concentration Results

Average chloride content at a depth of 25.4 mm (1 in.) for each specimen is presented in Figures 3.89 and 3.90 for uncracked and cracked concrete, respectively. Cores in cracked specimens were taken away from the location of individual cracks; therefore, the chloride concentration obtained does not represent the chloride concentration at the base of a crack. The depth profile data from individual cores are provided in Appendix C. Cores were not taken for cracked or uncracked specimens Conv.-1, ECR-1, ECR(primer/$Ca(NO_2)_2$)-1), MC-1, ECR(Valspar)-1, or ECR(Chromate)-1; however, the chloride concentration at a 25.4-mm (1 in.) depth is estimated for specimens FTS-Conv.-1 and FTS-ECR-1 based on vacuum drill data taken at earlier ages. Specimens FTS-Conv.-2 and FRS-ECR-2 have both vacuum drill chloride samples and core drill chloride samples available – a relationship between vacuum drill chloride samples at 201 weeks and core drill chloride samples at 250 weeks is established using these specimens and applied to the chloride concentration from the vacuum drill samples for specimens FTS-Conv.-1 and FTS-ECR-1 to estimate the chloride content at 250 weeks. The estimated data will be indicated in all subsequent figures and tables.

Figures 3.89 and 3.90 show little difference in chloride concentrations at 25.4-mm (1-in.) depth between uncracked specimens and cracked specimens sampled away from cracks. The control specimens (FTS-Conv., FTS-ECR) show chloride concentrations of 1.97 to 4.40 kg/m^3 (3.31 to 7.40 lb/yd^3). Specimens containing epoxies with increased adhesion show similar chloride concentrations, 3.03 to 4.89 kg/m^3 (5.10 to 8.23 lb/yd^3). Specimens containing Hycrete, however, show significantly less chloride content compared to the control specimens, with values of 0.29 to 1.12 kg/m^3 (0.49 to 1.88 lb/yd^3). The specimens containing Rheocrete, specimens containing DCI, specimens with multiple-coated reinforcement, and specimens with ECR with a calcium nitrite primer all show significantly increased chloride content compared to the control specimens.

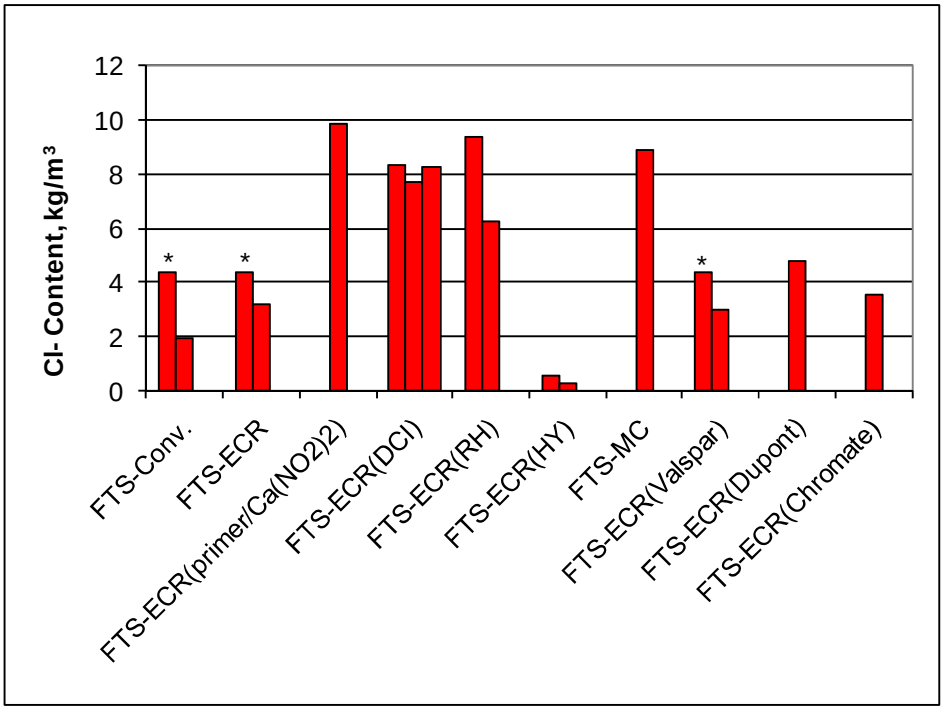

Figure 3.89: Field test specimens, uncracked concrete. Average specimen chloride concentration at a 25.4-mm (1-in.) depth.
*Estimated from vacuum drill chloride data.

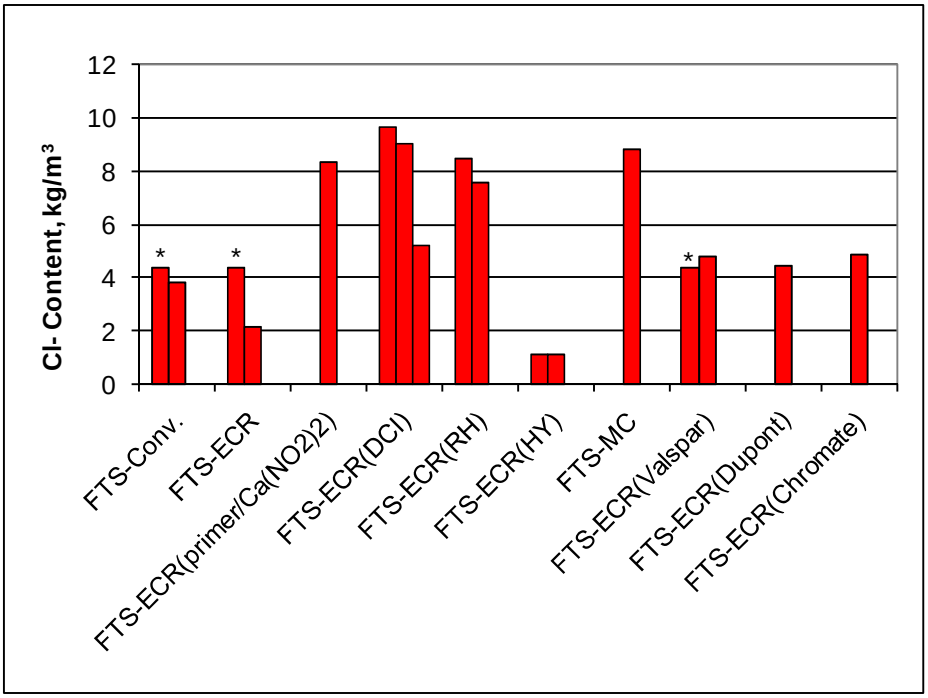

Figure 3.90: Field test specimens, cracked concrete. Average specimen chloride concentration at a 25.4-mm (1-in.) depth, taken away from cracks.
*Estimated from vacuum drill chloride data

An increase in chloride content was not observed in Southern Exposure specimens with inhibitors (Table 3.8); therefore, it is unlikely the increased chloride content in the field test specimens is due to the presence of inhibitors. Variations in concrete quality resulted in lower quality concrete being used for some specimens than for other specimens. The corrosion resistance of these specimens is hindered by the lower quality concrete; specimens containing DCI and Rheocrete performed in a similar manner or worse than control specimens in both cracked and uncracked concrete (Table 3.14). The specimens with multiple-coated reinforcement performed comparably to the specimens containing ECR (Table 3.15), and specimens with the calcium nitrite primer show less corrosion loss than the specimens with ECR in cracked concrete (Table 3.14). All specimens would have performed better in higher quality concrete; the quality of concrete must be considered when comparing corrosion systems.

The average chloride contents at 25.4-mm (1 in.) depth, listed by batch of concrete, are presented in Table 3.16. Batches 1 through 5 consist of concrete with no inhibitor, and batches 6 through 9 consist of concrete with inhibitors. In concrete without inhibitors for which data is available, Batch 3 exhibits the lowest chloride contents at the end of testing, with values ranging from 1.97 to 3.85 kg/m^3 (3.33 to 6.51 lb/yd^3). This batch contains half the control specimens, which may explain the good performance of ECR relative to other systems. Batch 5, used in ECR(primer/Ca(NO2)2)-2 and MC-2, exhibits the highest chloride contents, with values of 8.36 to 9.86 kg/m^3 (14.1 to 16.7 lb/yd^3) at 25.4-mm (1-in.) depth. Among the batches with inhibitors, Batch 9, with concrete containing Hycrete, exhibits the lowest chloride contents, ranging from 0.29 to 1.12 kg/m^3 (0.49 to 1.89 lb/yd^3), due to the decreased permeability of concrete containing Hycrete. Other inhibitors show chloride contents at 25.4-mm (1-in.) depth ranging from 5.20 to 9.67 kg/m^3, (8.79 to 16.3 lb/yd^3), significantly higher than the chloride contents at 25.4-mm (1-in.) depth observed in concrete used to cast control specimens. This increased chloride content is due to lower quality concrete used in these batches and not

an effect of the inhibitors; chloride contents from benchscale specimens (Table 3.8) suggest chloride contents in concrete with DCI should be comparable to or slightly greater than chloride contents in concrete with no inhibitor, and chloride contents in concrete with Rheocrete should be significantly less than chloride contents in concrete with no inhibitor.

Table 3.16: Field Test Specimens – Average Chloride Content by Batch.

	Cl^- Content at 25.4 mm (1 in.)	
	Uncracked	Cracked
Specimen	kg/m^3	kg/m^3
Batch 1[a]		
FTS-Conv.-1	4.40	4.40
FTS-ECR-1	4.40	4.40
FTS(Valspar)-1	4.40	4.40
Batch 2		
FTS-ECR(Chromate)-1	-	-
FTS-ECR(DuPont)-1	-	-
FTS-MC-1	-	-
Batch 3		
FTS-Conv.-2	1.97	3.85
FTS-ECR-2	3.22	2.18
FTS-ECR(primer/Ca(NO2)2)-1	-	-
Batch 4		
FTS-ECR(Chromate)-2	3.53	4.89
FTS-ECR(DuPont)-2	4.78	4.43
FTS(Valspar)-2	3.03	4.82
Batch 5		
FTS-ECR(primer/Ca(NO2)2)-2	9.86	8.36
FTS-MC-2	8.92	8.78
Batch 6		
FTS-ECR(DCI)-1	8.30	9.67
FTS-ECR(DCI)-2	7.73	9.03
Batch 7		
FTS-ECR(DCI)-3	8.26	5.20
Batch 8		
FTS-ECR(RH)-1	9.34	8.49
FTS-ECR(RH)-2	6.23	7.56
Batch 9		
FTS-ECR(HY)-1	0.55	1.12
FTS-ECR(HY)-2	0.29	1.10

[a] Extrapolated from vacuum drill samples taken at 213 weeks

Diffusion coefficients, D_{eff}, and surface chloride concentrations, C_o, were also calculated using Crank's solution to Fick's Second Law [Eq. (2.3)]. The results are summarized in Table 3.17. Diffusion coefficients for control specimens varied from 0.13 to 0.34 mm^2/day (0.00020 to 0.00060 $in.^2$/day). The specimens containing epoxies with increased adhesion have similar diffusion coefficients, 0.23 to 0.50 mm^2/day (0.00036 to 0.00078 $in.^2$/day). The specimens with multiple-coated reinforcement and specimens with a calcium nitrite primer show elevated diffusion coefficients, 0.92 to 1.22 mm^2/day (0.00143 to 0.00189 $in.^2$/day) and 0.93 to 1.17 mm^2/day (0.00144 to 0.00181 $in.^2$/day), respectively. The specimens containing DCI and Rheocrete show the highest values for diffusion coefficients, 0.32 to 2.07 mm^2/day (0.00050 to 0.00321 in^2/day) and 1.28 to 3.48 mm^2/day (0.00198 to 0.00539 $in.^2$/day), respectively. The specimens containing Hycrete show the lowest values for diffusion coefficients, 0.042 to 0.090 mm^2/day (0.000065 to 0.00014 $in.^2$/day).

The apparent surface chloride concentrations for control specimens range from 7.64 to 9.80 kg/m^3 (12.9 to 16.6 lb/yd^3). The specimens with increased adhesion epoxies show slightly elevated surface chloride concentrations, 8.61 to 11.85 kg/m^3 (14.6 to 20.0 lb/yd^3). Among the specimens with corrosion inhibitors, the specimens containing the calcium nitrite primer show the greatest surface chloride contents, 12.40 to 15.38 kg/m^3 (21.0 to 26.0 lb/yd^3). The specimens with Rheocrete and DCI show similar surface chloride concentrations, 9.08 to 13.47 kg/m^3 (15.3 to 22.7 lb/yd^3). The specimens with Hycrete show surface chloride concentrations between 7.49 and 8.90 kg/m^3 (6.29 to 14.6 lb/yd^3), comparable to control specimens. The specimens with multiple-coated reinforcement show surface chloride concentrations between 12.96 and 14.05 kg/m^3 (21.9 to 23.7 lb/yd^3).

Table 3.17: Apparent Surface Chloride Content and Diffusion Coefficients for Field Test Specimens*.

Specimen:	Uncracked		Cracked	
	C_o (kg/m^3)	D_{eff} (mm^2/day)	C_o (kg/m^3)	D_{eff} (mm^2/day)
Controls				
FTS-Conv.-1	-	-	-	-
FTS-Conv.-2	7.67	0.13	7.98	0.34
FTS-ECR-1	-	-	-	-
FTS-ECR-2	9.80	0.19	7.64	0.16
Increased Adhesion				
FTS-ECR(Valspar)-1	-	-	-	-
FTS-ECR(Valspar)-2	8.61	0.23	10.84	0.33
FTS-ECR(DuPont)-1	-	-	-	-
FTS-ECR(DuPont)-2	10.68	0.50	10.86	0.23
FTS-ECR(Chromate)-1	-	-	-	-
FTS-ECR(Chromate)-2	9.51	0.24	11.85	0.29
Inhibitors				
FTS-ECR(DCI)-1	11.05	2.07	13.39	1.48
FTS-ECR(DCI)-2	13.47	1.07	10.11	0.74
FTS-ECR(DCI)-3	11.41	1.22	12.16	0.32
FTS-ECR(RH)-1	11.35	3.48	11.01	2.36
FTS-ECR(RH)-2	9.08	1.28	10.24	1.93
FTS-ECR(HY)-1	8.90	0.058	7.49	0.052
FTS-ECR(HY)-2	8.64	0.042	8.37	0.090
FTS-ECR(primer/Ca(NO2)2)-1	-	-	-	-
FTS-ECR(primer/Ca(NO2)2)-2	15.38	0.93	12.40	1.17
Multiple Coated Bars				
FTS-MC-1	-	-	-	-
FTS-MC-2	12.96	1.22	14.05	0.92

*Note: 1 kg/m^3 = 1.69 lb/yd^3, 1 mm^2/day = 0.00155 in.^{2}/day

3.3.3 Summary-FTS

For both the uncracked and cracked field test specimens, conventional reinforcement shows far greater corrosion losses than epoxy-coated or multiple-coated reinforcement. The epoxies with increased adhesion show no benefit over conventional ECR in terms of corrosion loss or disbondment. Multiple-coated reinforcement performs comparably to conventional ECR in terms of corrosion loss, but exhibits increased disbondment in uncracked concrete, likely due to the higher chloride content and lower quality concrete. ECR in concrete with Rheocrete and DCI performs comparably or worse than ECR with no corrosion inhibitor in terms of corrosion loss and exhibits

greater disbondment; however, this again is likely the result of lower quality concrete and high chloride levels. Epoxy-coated bars with the calcium nitrite primer perform better than conventional ECR in terms of corrosion loss in cracked concrete, but exhibit greater disbondment due to lower quality concrete. ECR in concrete with Hycrete shows less corrosion loss than conventional ECR with no inhibitor in both cracked and uncracked concrete. Disbondment for ECR in concrete with Hycrete is comparable to ECR with no inhibitor in uncracked concrete and is greater than ECR with no inhibitor in cracked concrete. Similar variations in chloride contents and diffusion coefficients are likely the result of the concrete quality variations discussed above.

3.4 RAPID MACROCELL TESTS

The results from the rapid macrocell test program are presented in this section. Macrocell corrosion rate, corrosion loss, corrosion potentials, and mat-to-mat resistance are discussed in Section 3.4.1. The disbondment results are discussed in Section 3.4.2.

A total of 24 specimens with epoxy-coated reinforcement (M-ECR) and 24 specimens with multiple-coated reinforcement (M-MC) were tested under the rapid macrocell test program. The duration of the test ranged from 5 to 40 weeks, with three specimens of each reinforcement type pulled at 5-week intervals. The purpose of this test program is to establish a relationship between corrosion loss, time, and disbondment of the epoxy coating for conventional ECR and multiple-coated reinforcement.

3.4.1 Corrosion Rate, Loss, and Potentials

The average corrosion rates based on total area for macrocell specimens with ECR and MC reinforcement are shown in Figure 3.91. Corrosion rates based on total area for individual specimens are shown in Appendix A. During the first five weeks of testing, the specimens with multiple-coated reinforcement exhibit significantly higher corrosion rates than the specimens with conventional ECR. A slight increase in corrosion

rate is observed for the MC specimens between weeks 15 and 20. Corrosion rates are otherwise comparable to those observed in conventional ECR.

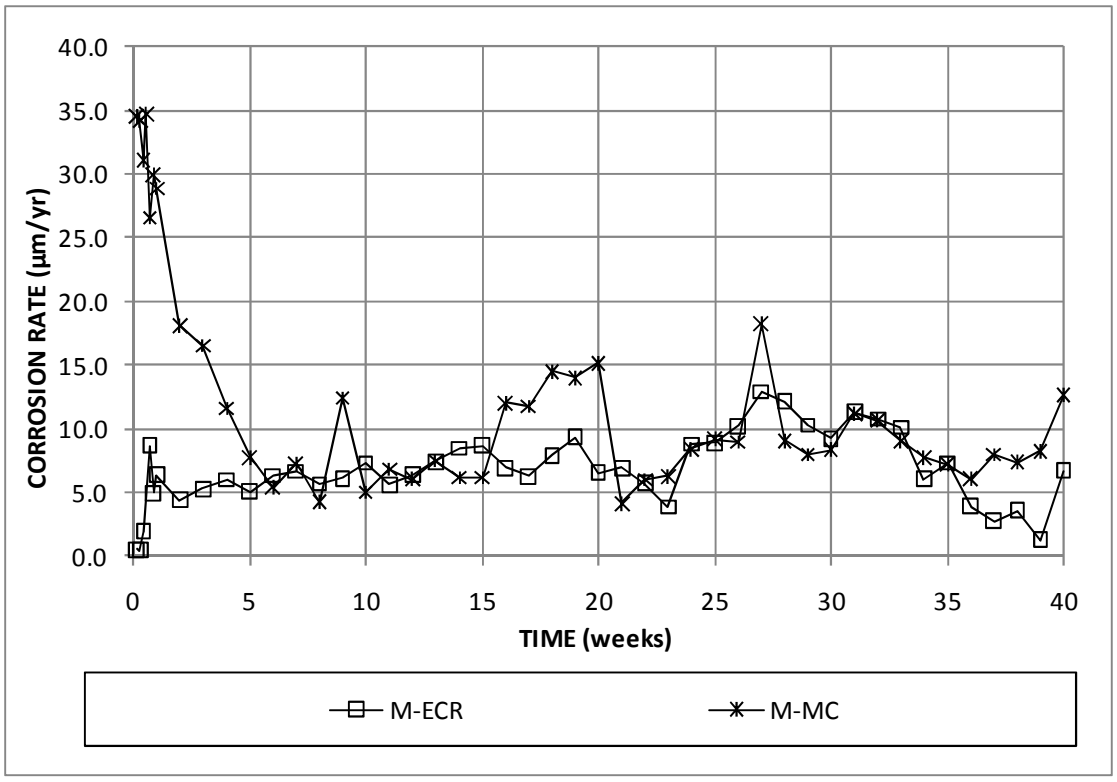

Figure 3.91: Rapid macrocell test. Average corrosion rate based on total area of ECR and MC reinforcement.

The average corrosion losses based on average corrosion rates for the macrocell specimens with ECR and MC reinforcement are shown in Figure 3.92. The corrosion losses for individual specimens are shown in Appendix A. The increased corrosion rate observed for MC reinforcement from weeks 0 to 5 and weeks 15 to 20 results in a greater overall corrosion loss at 40 weeks, 7.55 µm compared to 5.43 µm for ECR. The specimens with MC reinforcement exhibit greater corrosion losses than specimens with ECR throughout the test.

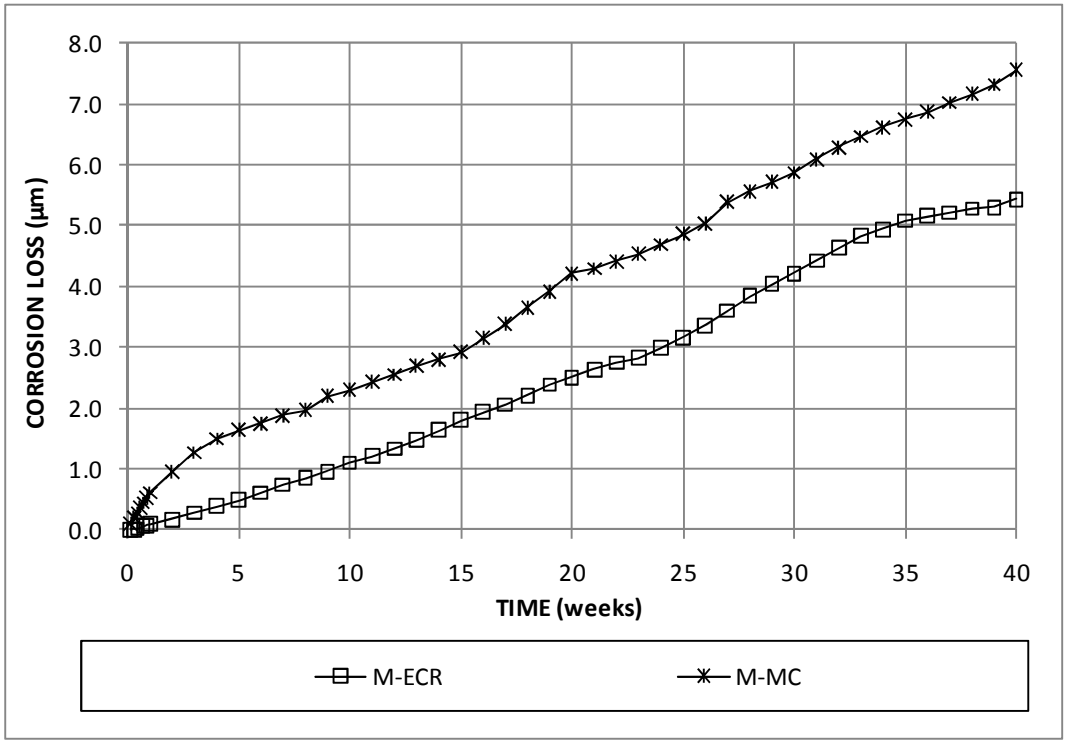

Figure 3.92: Rapid macrocell test. Average corrosion loss based on total area of ECR and MC reinforcement.

The average anode and cathode potentials with respect to a saturated calomel electrode (SCE) are shown in Figures 3.93 and 3.94, respectively, for specimens with conventional ECR and MC reinforcement. At the anode (Figure 3.93), the corrosion potentials of both ECR and MC are more negative than –0.500 V for most of the test. The MC specimens show a more negative anode potential than the ECR specimens for the first 27 weeks of testing. After 27 weeks, the corrosion potentials of the specimens with MC and ECR are comparable.

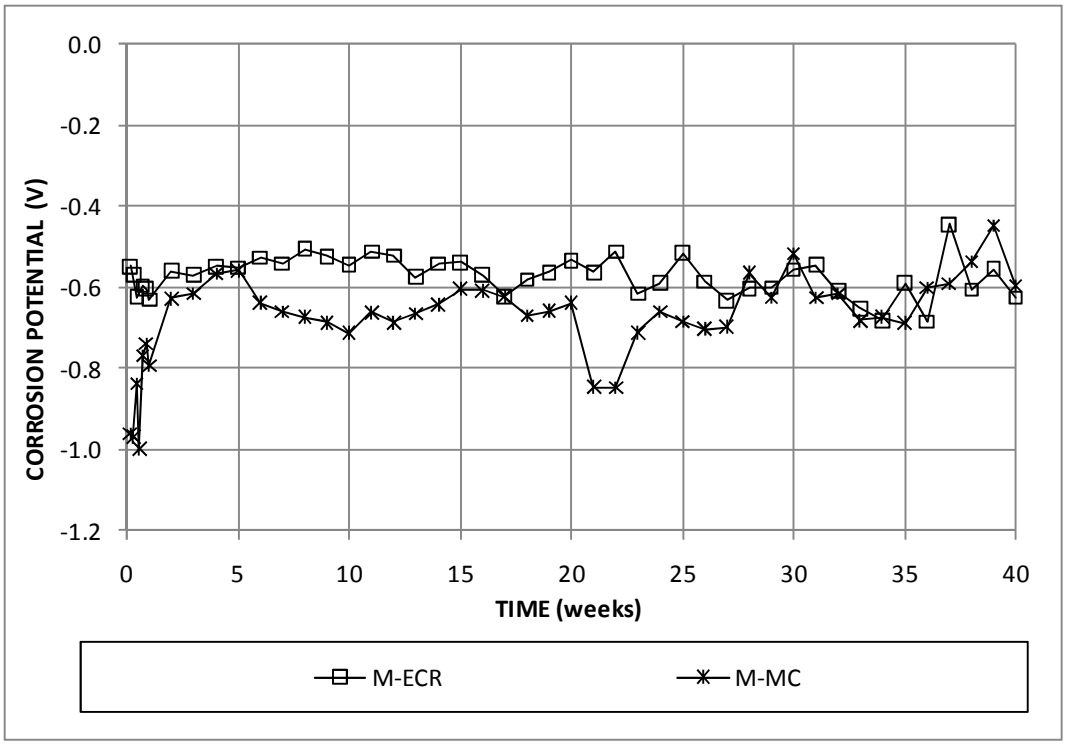

Figure 3.93: Rapid macrocell test. Average anode potential (SCE) of ECR and MC reinforcement.

At the cathode (Figure 3.94), the corrosion potentials of the specimens with both ECR and MC reinforcement are approximately –0.200 V (SCE) at the start of the test. For the ECR specimens, the corrosion potential gradually decreases to approximately –0.350 V by week 40, whereas the corrosion potential of the MC specimens remains approximately –0.200 V until week 36, when it decreases to –0.300 V over a four-week period.

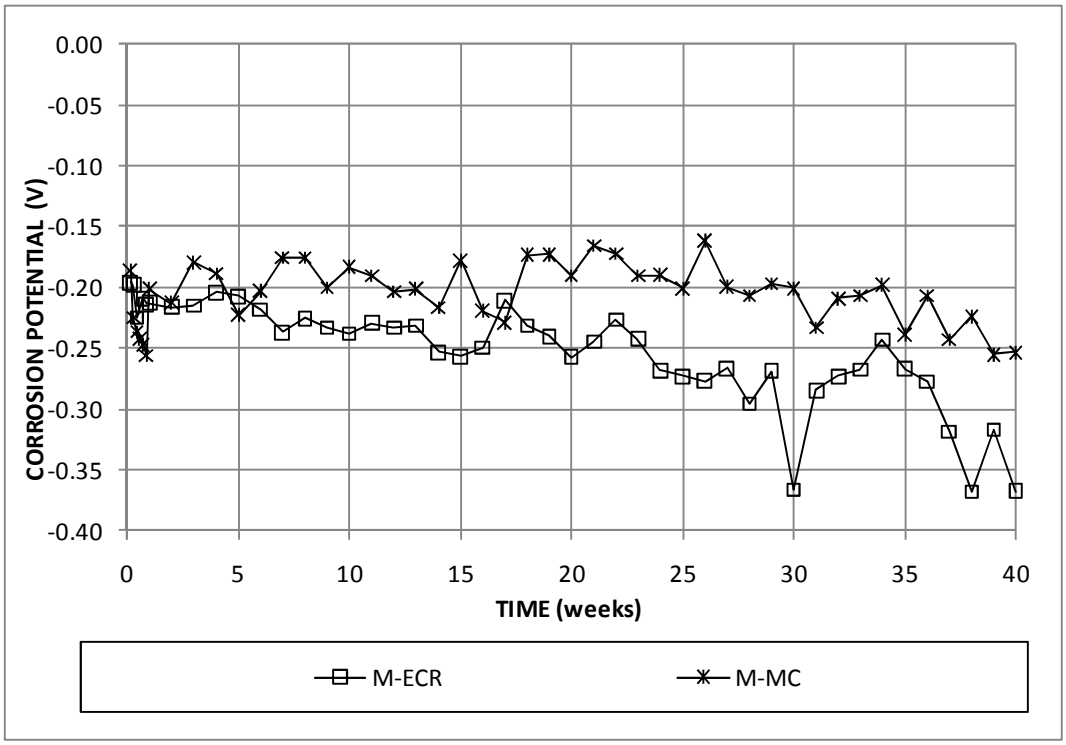

Figure 3.94: Rapid macrocell test. Average cathode potential (SCE) of ECR and MC reinforcement.

Linear polarization resistance (LPR) measurements were performed on selected specimens on a monthly basis. The microcell corrosion losses calculated from the LPR readings are compared to the macrocell corrosion losses in Table 3.18. On average, the microcell corrosion losses are 4.0 times greater than macrocell corrosion losses, with the ratio of microcell to macrocell corrosion loss ranging from 1.45 (M-ECR-7) to 8.41 (M-ECR-13).

Table 3.18: Microcell and Macrocell Corrosion Loss for Selected Rapid Macrocell Specimens.

Specimen	Age (weeks)	Corrosion Loss (µm)	
		Microcell	Macrocell
M-ECR-7	15	2.83	1.95
M-ECR-13	40	55.2	6.56
M-ECR-19	40	19.1	4.95
M-MC-22	40	18.2	7.64
M-MC-23	40	35.4	7.83
M-MC-24	40	31.0	9.04

3.4.2 Visual Observations and Disbonded Area

3.4.2.1 Visual Observations

For specimens with ECR, corrosion products were visible at some damage sites after 5 weeks of testing (Figure 3.95), with moderate amounts of disbondment observed at some damage sites (Figure 3.96). Other damage sites on the ECR bars tested at 5 weeks show no disbondment (Figure 3.96). The ECR bars tested for 10 weeks or longer show disbondment at all damage sites. For the ECR specimens tested for 30 weeks or longer, corrosion products were observed at all damage sites (Figure 3.97), with the disbonded region covering much of the area of the bar (Figure 3.98). The ECR bars removed after 30 to 40 weeks of testing show severe disbondment at all damage sites (Figure 3.98).

Figure 3.95: Rapid macrocell test, M-ECR-1, 5 weeks, before disbondment test.

Figure 3.96: Rapid macrocell test, M-ECR-1, 5 weeks, after disbondment test.

Figure 3.97: Rapid macrocell test, M-ECR-13, 40 weeks, before disbondment test.

Figure 3.98: Rapid macrocell test, M-ECR-21, 35 weeks, after disbondment test.

For the specimens with MC reinforcement, those removed after 5 or 10 weeks of testing show no signs of iron corrosion products (Figure 3.99), in contrast to specimens with ECR, which show visible corrosion products after 5 weeks. Disbondment tests on the MC bars reveal minimal disbondment on specimens removed from testing after 5 or 10 weeks (Figure 3.100). Regions where disbondment does occur on the MC bars show a ring of darkened metal around the damage site, indicating the zinc in this region has been consumed (Figure 3.101). The MC specimens begin to show dark orange iron corrosion products by week 15, with all three of the MC specimens removed at week 40 showing dark iron corrosion products (Figure 3.102). The disbondment tests performed at 40 weeks on the MC bars showed moderate disbondment at all damage sites (Figure 3.103). The corrosion products in the disbonded regions of the MC bars consist of a central circle of dark iron corrosion products around the damage site surrounded by a larger region of light gray corrosion products, most likely from corroding zinc.

Figure 3.99: Rapid macrocell test, M-MC-4, 10 weeks, before disbondment test.

Figure 3.100: Rapid macrocell test, M-MC-4, 10 weeks, after disbondment test.

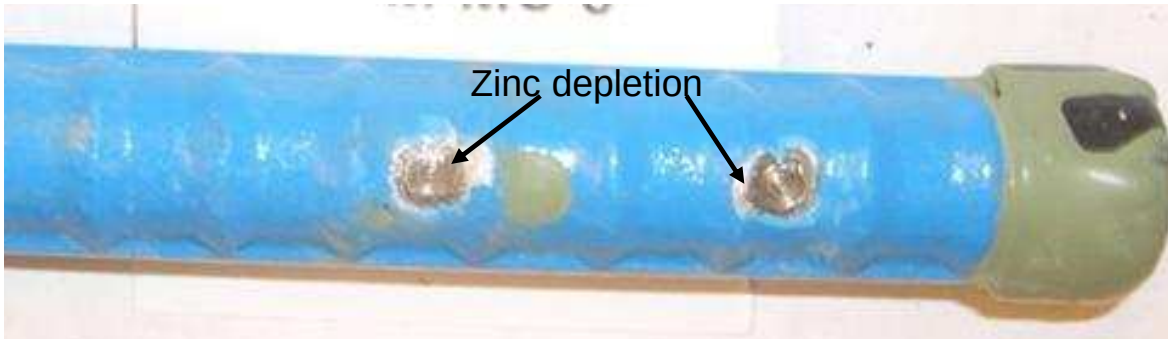

Figure 3.101: Rapid macrocell test, M-MC-5, 10 weeks. Zinc depletion in regions surrounding damage sites.

Figure 3.102: Rapid macrocell test, M-MC-23, 40 weeks, before disbondment test.

Figure 3.103: Rapid macrocell test, M-MC-23, 40 weeks, after disbondment test.

In general, damage sites with visible corrosion products tend to exhibit greater disbondment than damage sites with no visible corrosion products for both ECR (Figure 3.96) and MC (Figure 3.103). Both disbonded area and visible corrosion increase with time. The corrosion products at the damage sites are dark orange or brown in color.

Corrosion products underneath disbonded epoxy are initially black (Figure 3.96), but turn dark orange with exposure to air as the corrosion products oxidize.

3.4.2.2 Disbondment Results

Disbonded area and corrosion loss for the ECR and MC bars are summarized in Tables 3.19 and 3.20, respectively. Figures 3.104 and 3.105 show average disbonded area at a damage site versus time for ECR and MC reinforcement, respectively. A best fit line is plotted for each set of data. Based on the best fit lines, disbondment of epoxy-coated reinforcement progresses at twice the rate of disbondment of multiple-coated reinforcement, with ECR showing increases in disbonded area averaging 10.8 mm^2/week compared to 5.32 mm^2/week for MC reinforcement. It should be noted that disbondment at a given age varies widely for both M-ECR and M-MC specimens, especially at later ages (Tables 3.19 and 3.20).

Figures 3.106 and 3.107 show disbonded area vs. macrocell corrosion loss for ECR and MC reinforcement, respectively. The epoxy-coated reinforcement shows greater disbondment at a given corrosion loss than the multiple-coated reinforcement; on average, the disbondment of the ECR increases by 56.3 mm^2 for every 1 µm of corrosion loss, compared to an average increase of 26.5 mm^2 for every 1 µm of corrosion loss for the MC bars. The difference in disbondment rate between ECR and MC reinforcement is more pronounced in specimens with low corrosion losses. For the epoxy-coated reinforcement with less than 2.0 µm of corrosion loss, the disbondment rate ranges from 50.7 to 308.1 mm^2 per µm of loss, with an average rate of 159.9 mm^2/µm. For the multiple-coated reinforcement with less than 2.0 µm of corrosion loss, the disbondment rate ranges from 2.80 to 27.6 mm^2 per µm of loss, with an average rate of 15.3 mm^2/µm.

Table 3.19: Disbonded Area and Corrosion Loss for Rapid Macrocell Specimens with ECR.

Specimen	Week	Average Disbonded Area (mm^2)	Corrosion Loss (µm)	Disbondment Rate (mm^2/µm)
M-ECR-1	5	35.5	0.359	98.8
M-ECR-2	5	16.1	0.318	50.7
M-ECR-3	5	37.1	0.233	159.2
M-ECR-4	10	74.2	0.638	116.3
M-ECR-5	10	158.1	0.513	308.1
M-ECR-6	10	133.9	1.29	103.8
M-ECR-7	15	116.1	1.92	60.5
M-ECR-8	15	154.8	0.428	361.8
M-ECR-9	15	187.1	3.35	55.8
M-ECR-10	20	175.8	4.99	35.2
M-ECR-11	20	338.7	4.59	73.8
M-ECR-12	20	140.3	4.71	29.8
M-ECR-13	40	456.5	4.94	92.4
M-ECR-14	25	567.7	3.73	152.2
M-ECR-15	25	187.1	1.04	179.9
M-ECR-16	25	408.1	2.16	188.9
M-ECR-17	30	232.3	3.35	69.3
M-ECR-18	30	162.9	2.37	68.7
M-ECR-19	40	261.3	4.64	56.3
M-ECR-20	30	198.4	5.75	34.5
M-ECR-21	35	874.2	6.24	140.1
M-ECR-22	35	222.6	5.41	41.1
M-ECR-23	35	598.4	3.27	183.0
M-ECR-24	40	241.9	5.38	45.0

Table 3.20: Disbonded Area and Corrosion Loss for Rapid Macrocell Specimens with MC reinforcement.

Specimen	Week	Average Disbonded Area (mm^2)	Corrosion Loss (µm)	Disbondment Rate (mm^2/µm)
M-MC-1	5	9.7	1.11	8.71
M-MC-2	5	4.8	1.73	2.80
M-MC-3	5	21.0	1.3	16.1
M-MC-4	10	41.9	1.97	21.3
M-MC-5	10	43.5	3.42	12.7
M-MC-6	10	50.0	3.17	15.8
M-MC-7	15	77.4	4.97	15.6
M-MC-8	15	54.8	1.99	27.6
M-MC-9	15	74.2	2.98	24.9
M-MC-10	20	133.9	6.12	21.9
M-MC-11	20	125.8	4.19	30.0
M-MC-12	20	69.4	3.03	22.9
M-MC-13	25	162.9	3.58	45.5
M-MC-14	25	137.1	2.86	47.9
M-MC-15	25	146.8	6.61	22.2
M-MC-16	30	116.1	5.48	21.2
M-MC-17	30	98.4	3.13	31.4
M-MC-18	30	156.5	3.93	39.8
M-MC-19	35	117.7	6.89	17.1
M-MC-20	35	129.0	6.73	19.2
M-MC-21	35	308.1	8.64	35.7
M-MC-22	40	127.4	7.64	16.7
M-MC-23	40	177.4	7.83	22.7
M-MC-24	40	301.6	9.04	33.4

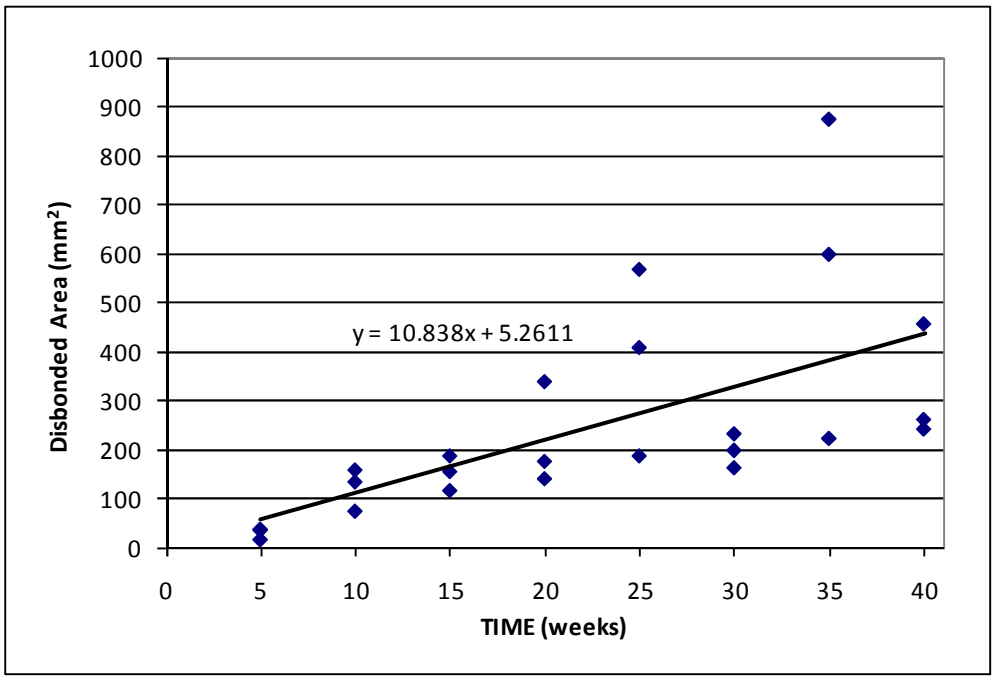

Figure 3.104: Rapid Macrocell Test, specimens with ECR. Disbonded area versus time. y = disbonded area (mm^2), x = time (weeks)

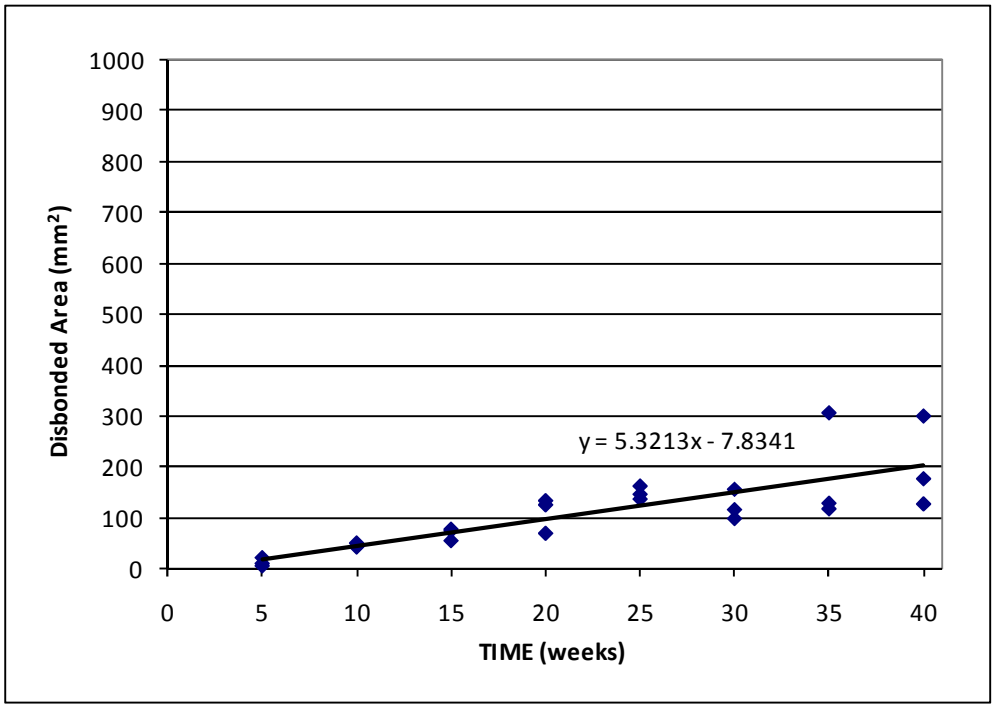

Figure 3.105: Rapid Macrocell Test, specimens with MC reinforcement. Disbonded area versus time. y = disbonded area (mm^2), x = time (weeks)

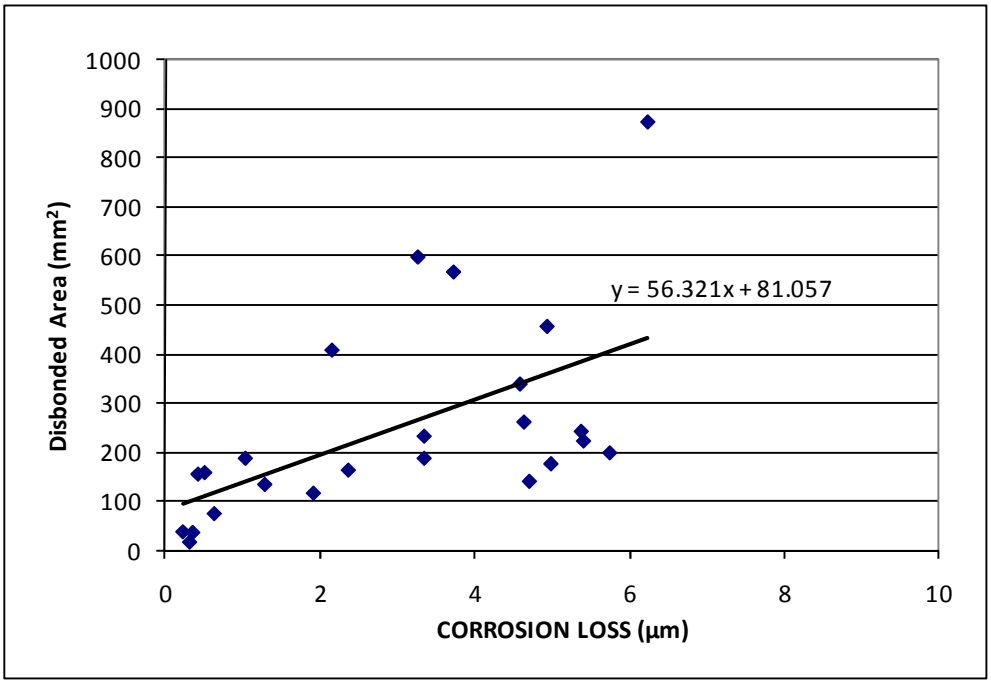

Figure 3.106: Rapid Macrocell Test, specimens with ECR. Disbonded area versus corrosion loss. y = disbonded area (mm^2), x = corrosion loss (µm)

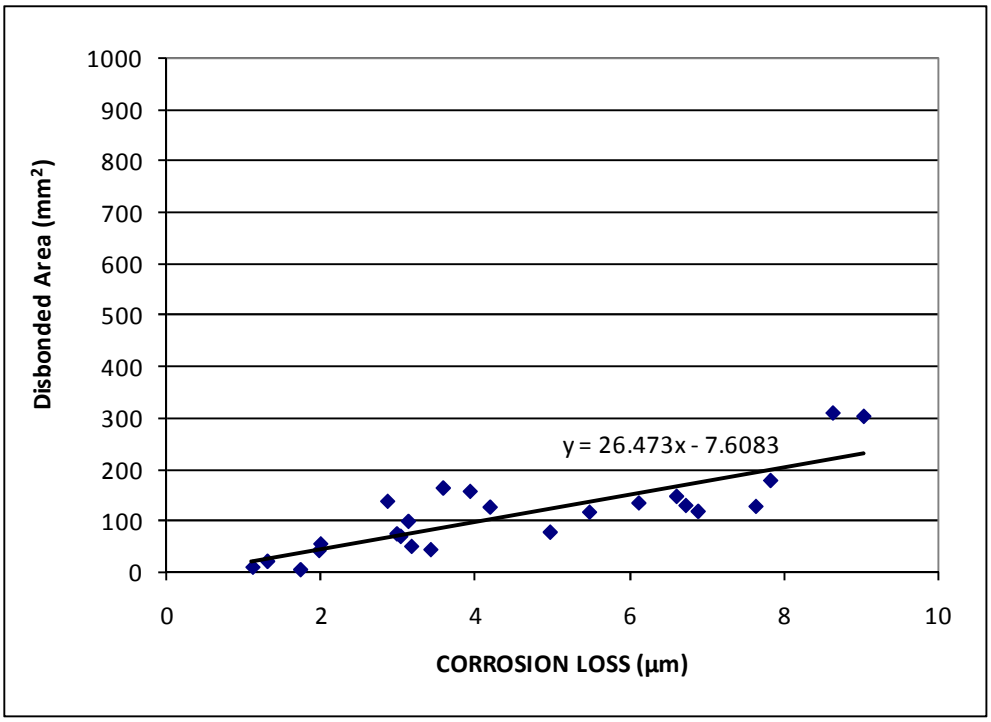

Figure 3.107: Rapid Macrocell Test, specimens with MC reinforcement. Disbonded area versus corrosion loss. y = disbonded area (mm^2), x = corrosion loss (µm)

In addition to the rapid macrocell specimens, five epoxy-coated bars and five multiple-coated bars with damaged regions identical to those used in the rapid macrocell test were exposed to a simulated pore solution without salt to determine the disbondment of the coatings with time in the absence of chlorides and chloride-induced corrosion. The results are shown in Figure 3.108. At 10 weeks, the multiple-coated bars show a disbonded area of 25.8 mm^2, whereas ECR shows no disbondment. However, at 20 weeks, the epoxy-coated and multiple-coated reinforcement exhibit the same degree of disbondment in the absence of corrosion, and at later ages, specimens with epoxy-coated reinforcement exhibit greater disbonded areas than specimens with multiple-coated reinforcement (Figure 3.108). For both ECR and MC bars, disbondment at 40 weeks in the absence of chlorides is 20 to 25 percent of the values observed at 40 weeks in bars subjected to chloride-induced corrosion.

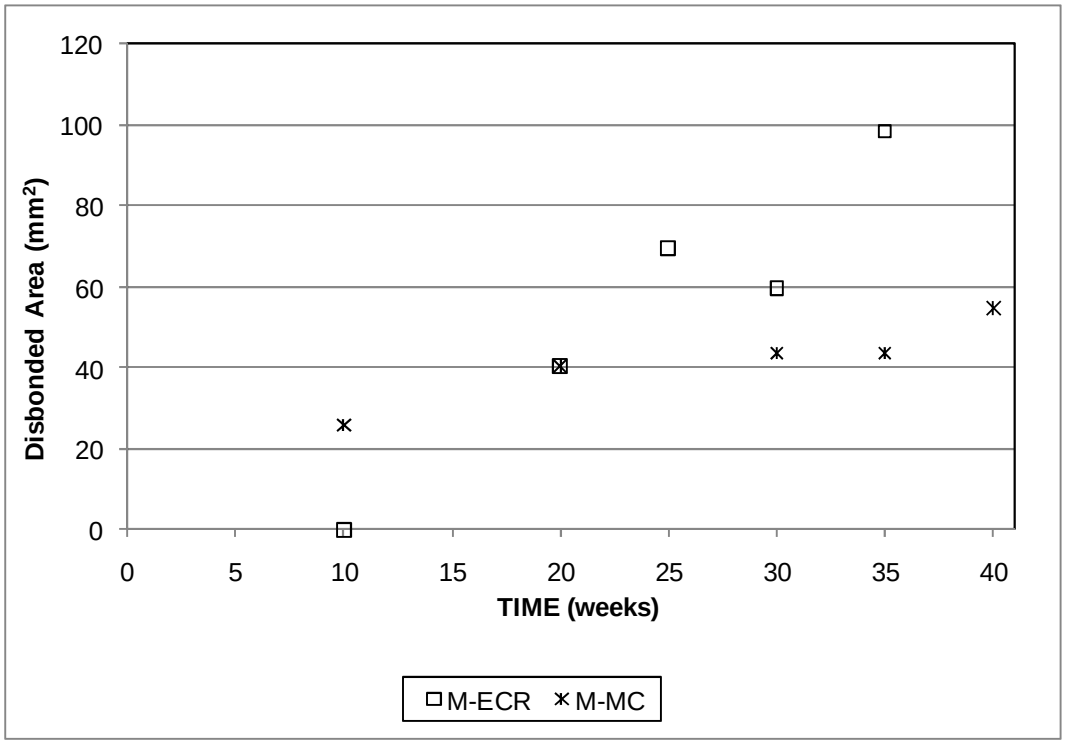

Figure 3.108: Disbonded area vs. time for ECR and MC reinforcement in simulated pore solution without salt.

3.4.3 Summary

For the rapid macrocell test, the specimens with multiple-coated reinforcement show greater corrosion losses than the specimens with conventional ECR. However, the multiple-coated reinforcement shows significantly less disbondment than ECR, both as a function of corrosion loss and as a function of time.

3.5 KDOT BRIDGE PROJECTS

This section presents results from testing on two bridge decks in Kansas cast with pickled 2205 stainless steel reinforcement (2205p), the Doniphan County (DCB) and Mission Creek (MCB) bridges, first reported by Gou et al. (2006). Benchscale and field test specimens, also containing 2205p reinforcement, were cast using trial batch concrete from each bridge, as were field test specimens containing conventional and epoxy-coated reinforcement. The benchscale results are discussed in Section 3.5.1. The field test specimen results are discussed in Section 3.5.2, and the bridge potential mappings are described in Section 3.5.3.

3.5.1 Southern Exposure and Cracked Beam Tests

A total of 11 Southern Exposure and 9 cracked beam specimens were cast using pickled 2205 stainless steel (2205p) and trial batch concrete for the Doniphan County (DCB) and Mission Creek (MCB) bridges. Six Southern Exposure and four cracked beam specimens were removed from testing at 240 weeks to evaluate the condition of the stainless steel. An additional cracked beam specimen was removed at 306 weeks due to damage to the wiring. As of August 31, 2010, the remaining DCB specimens have reached 341 weeks and the remaining MCB specimens have reached 315 weeks. Testing continues on these specimens.

3.5.1.1 Corrosion Rates, Losses, and Potentials

The average corrosion rates for the DCB and MCB Southern Exposure specimens are shown in Figure 3.109. Individual corrosion rates appear in Appendix A. Corrosion

rates to date have remained low, with neither series of specimens exhibiting a corrosion rate greater than 0.305 µm/yr. The DCB specimens exhibit corrosion rates less than 0.01 µm/yr for the first 175 weeks of testing. Between weeks 175 and 250, the average corrosion rate occasionally increases from zero for periods of one to two weeks, never exceeding 0.05 µm/yr. The corrosion rate increases from zero at week 331, reaching a peak of 0.122 µm/yr at week 336. The corrosion rate remains slightly positive as of August 31, 2010. The MCB specimens exhibit a slightly negative corrosion rate during the first 175 weeks of testing. A negative corrosion rate indicates electrons are flowing from the bottom bars to the top bars, either due to corrosion on the bottom mat of steel or, more likely, due to low levels of oxidation on all bars and the greater number of bars in the bottom mat of steel. After 175 weeks, the corrosion rate becomes positive after week 175, reaching a peak of 0.305 µm/yr at week 295. The corrosion rate remains positive as of week 295.

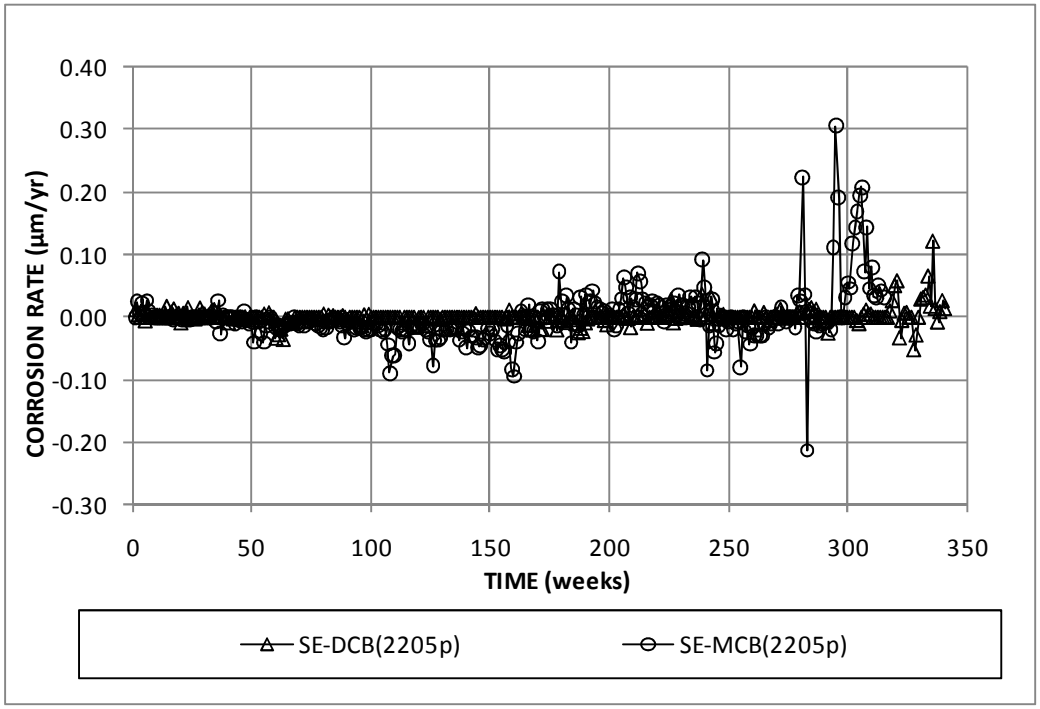

Figure 3.109: Southern Exposure test. Average corrosion rate for DCB and MCB specimens.

The average corrosion losses for the DCB and MCB Southern Exposure specimens are shown in Figure 3.110. Individual corrosion losses are presented in Appendix A, with losses as of August 31, 2010 summarized in Table 3.21. The corrosion losses for both DCB and MCB specimens remain low, with the DCB specimens exhibiting average losses of 0.011 µm at week 341 and the MCB specimens exhibiting no significant losses at week 315; however, the negative corrosion rates observed at early ages in the MCB specimens cause the corrosion loss to become negative (Figure 3.110), decreasing the apparent corrosion loss at later ages. Considering only specimens exhibiting positive corrosion losses, the DCB specimens show average losses of 0.039 µm at week 341. No currently running MCB specimen shows significant losses at week 315. On an individual basis, specimen SE-DCB(2205p)-2 exhibits the highest positive corrosion loss, 0.039 µm at week 341. Specimen SE-MCB(2205p)-5 exhibits a corrosion loss of 0.167 µm prior to being removed from testing at week 240. The other specimens exhibit corrosion losses less than 0.01 µm.

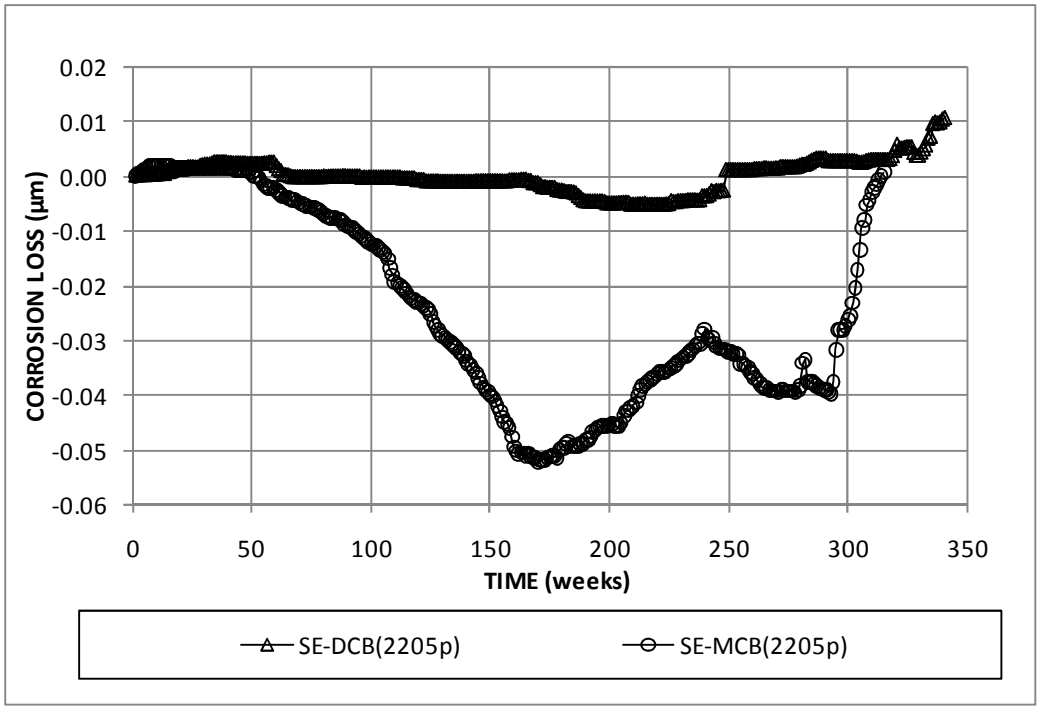

Figure 3.110: Southern Exposure test. Average corrosion loss for DCB and MCB specimens.

Table 3.21: Individual Corrosion Loss for KDOT Bridge Project Southern Exposure Specimens.

Specimen	Age (weeks)	Corrosion Loss (µm)
SE-DCB(2205p)-1	341	-0.005
SE-DCB(2205p)-2	341	0.039
SE-DCB(2205p)-3	341	-0.002
SE-DCB(2205p)-4[a]	240	0.003
SE-DCB(2205p)-5[a]	240	-0.013
SE-DCB(2205p)-6[a]	240	-0.008
SE-MCB(2205p)-1	315	-0.156
SE-MCB(2205p)-2	315	-0.051
SE-MCB(2205p)-3[a]	240	-0.001
SE-MCB(2205p)-4[a]	240	-0.042
SE-MCB(2205p)-5[a]	240	0.167

[a] Removed from testing

The average top mat and bottom mat corrosion potentials (versus CSE) for the DCB and MCB Southern Exposure specimens are shown in Figures 3.111 and 3.112, respectively. Individual specimen potentials are shown in Appendix A. For the top mat (Figure 3.111), the initial potentials are approximately –0.200 V (CSE) and, with the exception of isolated readings more negative than –0.300 V, remain between –0.100 V and –0.300 V throughout the test. The corrosion potentials for the bottom mat of steel are similar to those measured on the top mat of steel for both the MCB and the DCB specimens (Figure 3.112).

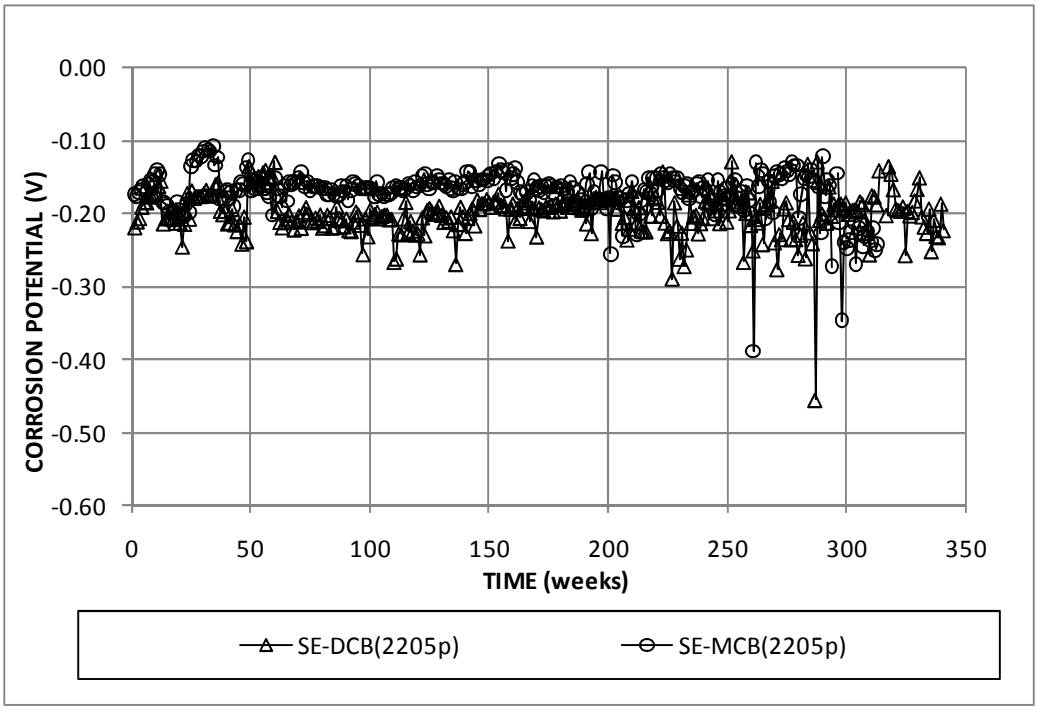

Figure 3.111: Average top mat corrosion potentials for DCB and MCB Southern Exposure specimens.

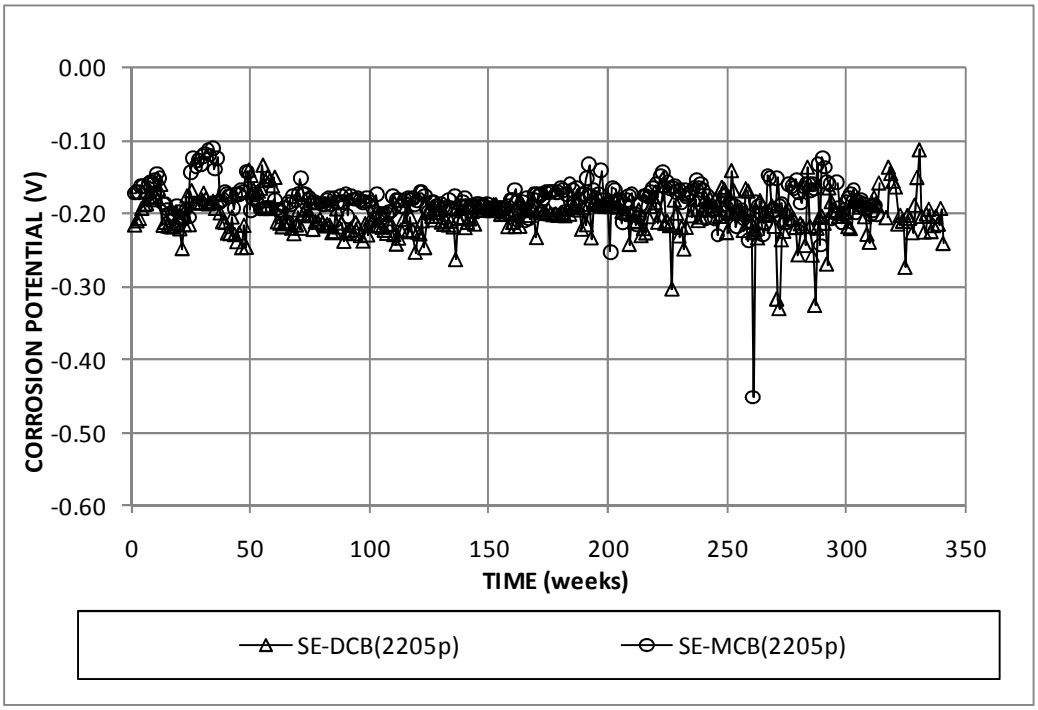

Figure 3.112: Average bottom mat corrosion potentials for DCB and MCB Southern Exposure specimens.

The average mat-to-mat resistances for DCB and MCB Southern Exposure specimens are shown in Figure 3.113. Individual specimen resistances are shown in Appendix B. The SE-DCB and SE-MCB specimens each begin the test with an average mat-to-mat resistance of approximately 200 ohms. The average mat-to-mat resistance of the SE-DCB specimens increases to around 8,000 ohms by week 200, after which the readings vary greatly. The average resistance remains around 8,000 ohms. The average mat-to-mat resistance of the SE-MCB specimens remains lower, approaching 1000 ohms by week 250 and remaining between 600 and 1,000 ohms through week 315 (Figure 3.113).

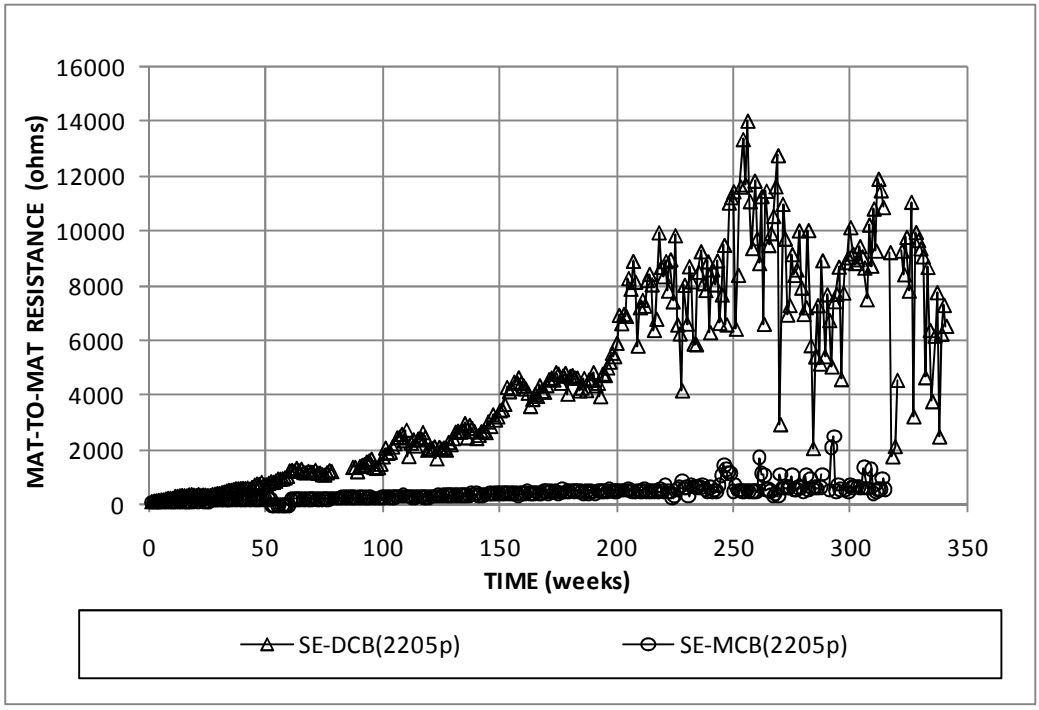

Figure 3.113: Average mat-to-mat resistances for DCB and MCB Southern Exposure specimens.

The average corrosion rates for the DCB and MCB cracked beam specimens are shown in Figure 3.114. While the corrosion rates to date have remained low, the corrosion rates for both DCB and MCB cracked beam specimens are greater than

observed for the Southern Exposure specimens. Like the SE specimens, the CB specimens also at times exhibit significant "negative" corrosion rates. The DCB specimens remain passive for the first 100 weeks of testing. Between weeks 100 and 150, the average corrosion rate increases above zero for periods of several weeks, never exceeding 0.1 µm/yr. The peak corrosion rate of 0.084 µm/yr occurs at week 128. After week 150, the corrosion rate returns to zero, with infrequent jumps in rate occurring through week 341. The MCB specimens exhibit a slightly negative corrosion rate through much of the testing. The corrosion rate increases after 175 weeks and alternates between "negative" (bottom bar) and positive corrosion through week 315, reaching its peak of 0.445 µm/yr at week 291 as part of a series of spikes occurring between week 275 and 300. After week 300, the corrosion rate drops to zero and remains low through week 315.

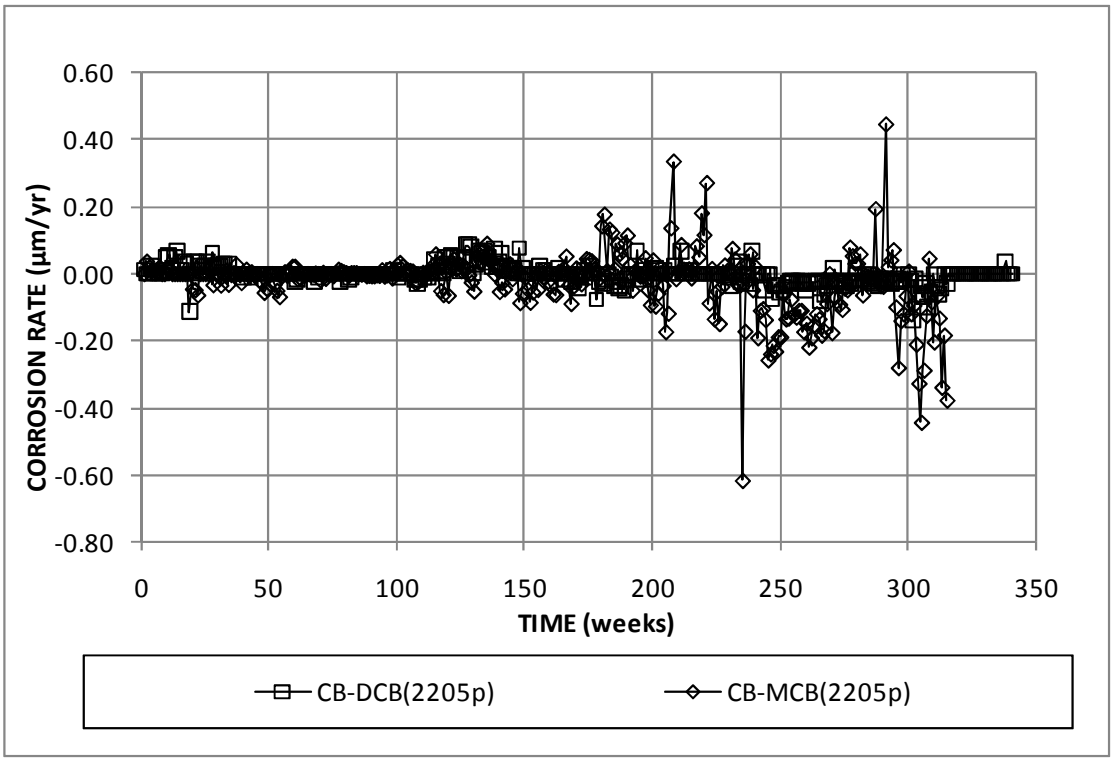

Figure 3.114: Cracked beam test. Average corrosion rate for DCB and MCB specimens.

The average corrosion losses for DCB and MCB cracked beam specimens (based on average corrosion rates) are shown in Figure 3.115. Individual corrosion losses as of August 31, 2010 are summarized in Table 3.22. The average corrosion losses for the DCB and MCB specimens remain low; the DCB specimens show average losses of –0.012 µm at week 341 and the MCB specimens show average losses of –0.147 µm at week 315. Excluding specimens with negative corrosion, no currently running DCB or MCB specimen exhibits corrosion. On an individual basis, specimen CB-DCB(2205p)-2 exhibits a significant positive corrosion loss, 0.104 µm, at the time of its removal from testing at week 240. The only remaining cracked beam DCB specimen exhibits losses of –0.099 µm at week 341. CB-MCB(2205p)-4 exhibits corrosion losses of 0.949 µm at 240 weeks, and specimen CB-MCB(2205p)-6 exhibits corrosion losses of 0.039 µm at its removal from testing at 240 weeks. All other CB-MCB specimens exhibit negative corrosion losses.

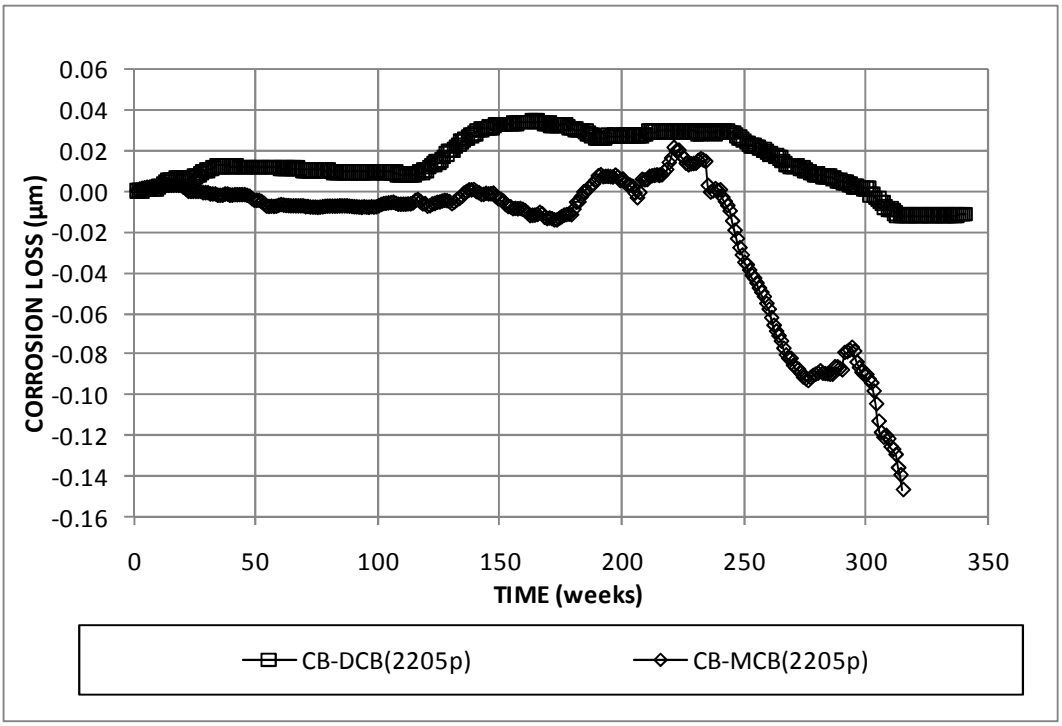

Figure 3.115: Cracked beam test. Average corrosion loss for DCB and MCB specimens.

Table 3.22: Individual Corrosion Loss for KDOT Bridge Project Cracked Beam Specimens.

Specimen	Age (weeks)	Corrosion Loss (µm)
CB-DCB(2205p)-1	341	-0.099
CB-DCB(2205p)-2[a]	240	0.104
CB-DCB(2205p)-3[a]	308	0.007
CB-MCB(2205p)-1	315	-0.268
CB-MCB(2205p)-2	315	-0.112
CB-MCB(2205p)-3	315	-0.634
CB-MCB(2205p)-4[a]	240	0.949
CB-MCB(2205p)-5[a]	240	-0.413
CB-MCB(2205p)-6[a]	240	0.039

[a] Removed from testing

The average top mat and bottom mat corrosion potentials (versus CSE) for the DCB and MCB cracked beam specimens are shown in Figures 3.116 and 3.117, respectively. For the top mat (Figure 3.116), the initial average potentials are approximately –0.200 V (CSE) and, with the exception of isolated readings more negative than –0.300 V, remain between –0.100 V and –0.300 V throughout the test. The corrosion potentials for the bottom mat of steel are similar to those measured for the top mat of steel for both the MCB and the DCB specimens (Figure 3.117).

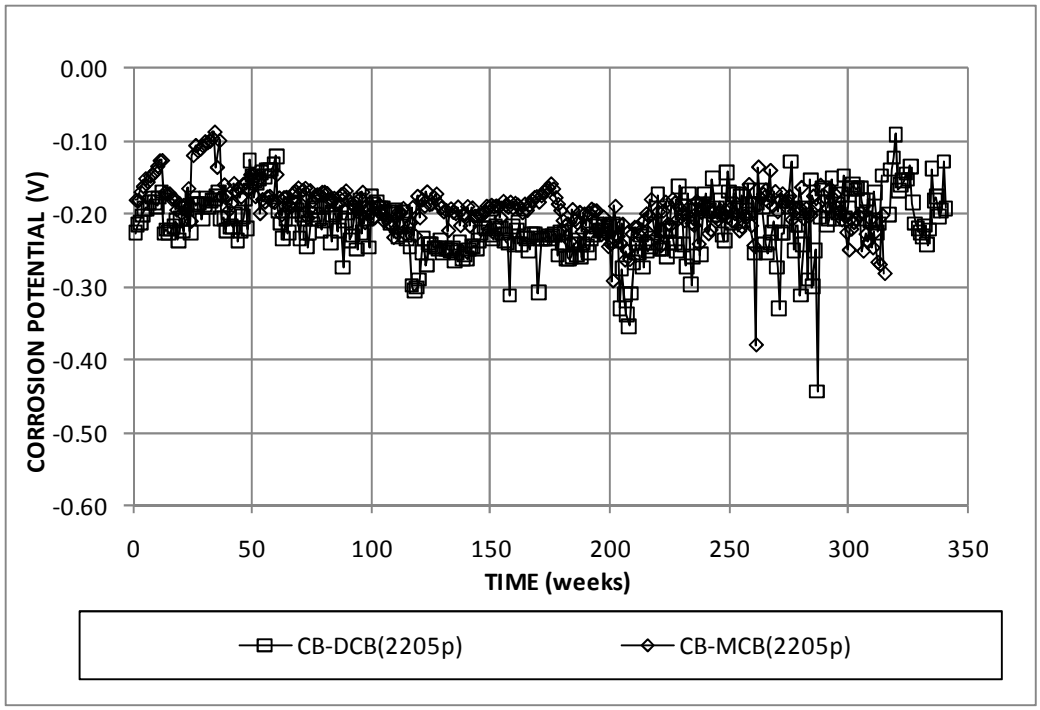

Figure 3.116: Average top mat corrosion potentials for DCB and MCB cracked beam specimens.

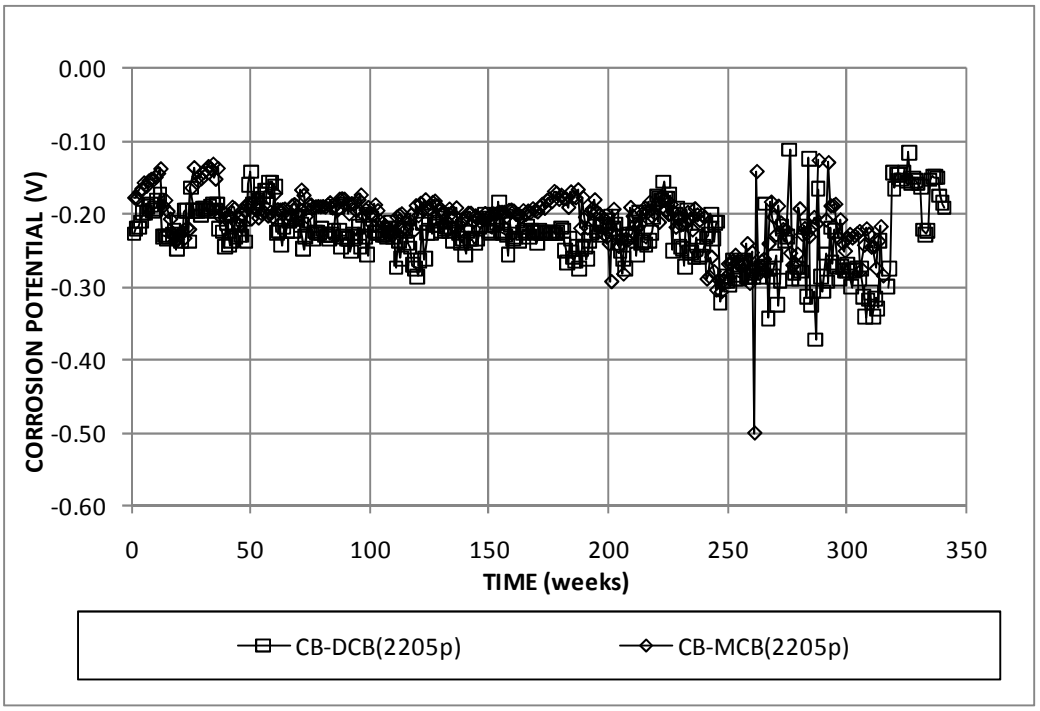

Figure 3.117: Average bottom mat corrosion potentials for DCB and MCB cracked beam specimens.

The average mat-to-mat resistances for the DCB and the MCB cracked beam specimens are shown in Figure 3.118. The CB-DCB specimens begin the test with an average mat-to-mat resistance of approximately 250 ohms. The average mat-to-mat resistance of the CB-DCB specimens increases to around 12,000 ohms by week 150, after which the readings vary greatly. The average resistance remains around 12,000 ohms until week 300, after which the average resistance decreases. The average mat-to-mat resistance of the CB-MCB specimens remains lower than that of the CB-DCB specimens, approaching 2,000 ohms by week 150 and remaining approximately constant through week 315 (Figure 3.118), likely due to the less permeable concrete in DCB specimens. The average mat-to-mat resistances for cracked beam specimens are approximately twice those observed in Southern Exposure specimens because the specimens are one-half the width.

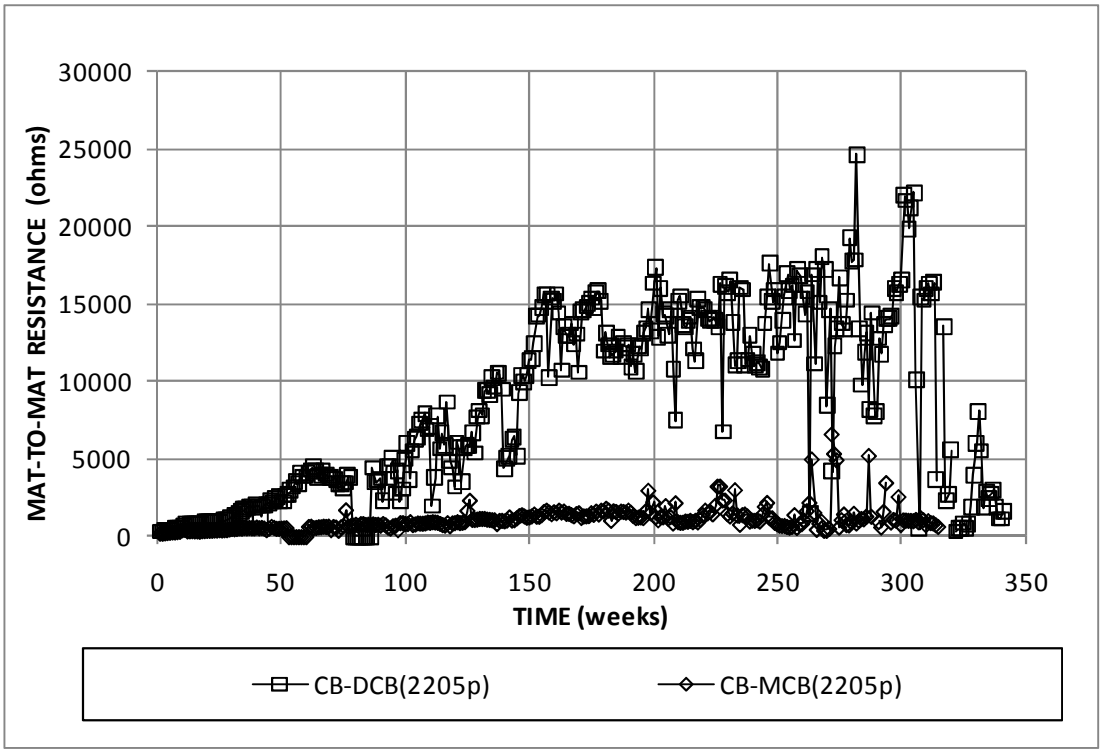

Figure 3.118: Average mat-to-mat resistances for DCB and MCB cracked beam specimens.

3.5.1.2 Visual Observations

Periodic inspections of the Southern Exposure and cracked beam specimens in the KDOT bridge project program have uncovered staining near the ends of the bar on many specimens (Figure 3.119). This is believed to be the result of corrosion of the components of the electrical connection. No staining has been observed on the surface of any specimen.

For the Southern Exposure specimens removed from testing, limited corrosion products have been observed on two specimens. In one case, the corrosion products are observed at the base of a rib on specimen SE-MCB(2205p)-5 (Figure 3.120). Corrosion products are also observed at the ends of the top mat of steel on specimen SE-MCB(2205p)-5 (Figure 3.121). The latter may be due to crevice corrosion. Other Southern Exposure specimens show no signs of corrosion (Figure 3.122).

For the cracked beam specimens removed from testing, corrosion products are observed near the end of the top bar of specimen CE-DCB(2205p)-2 (Figure 3.123). Corrosion products are also observed at the ends of the top bar on specimen CB-MCB(2205p)-4 (Figure 3.124). Corrosion in these cases may also be due to crevice corrosion or galvanic effects between the copper wire and bar. Other cracked beam specimens show no signs of corrosion (Figure 3.125).

Figure 3.119: CB-MCB(2205p)-5, 240 weeks. Staining at bar ends.

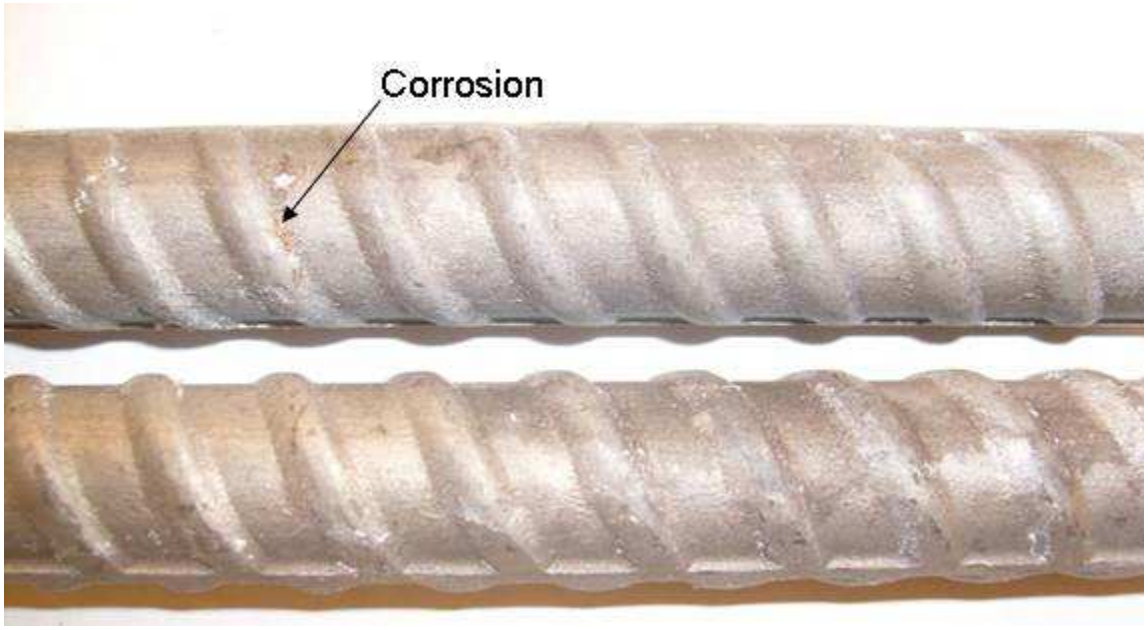

Figure 3.120: SE-MCB(2205p)-3, 240 weeks. Limited corrosion on top bar.

Figure 3.121: SE-MCB(2205p)-5, 240 weeks. Corrosion at ends of top bar.

Figure 3.122: SE-DCB(2205p)-5, 240 weeks. Top mat above label, bottom mat below label. No visible corrosion.

Figure 3.123: CB-DCB(2205p)-2, 240 weeks. Corrosion near bar end.

Figure 3.124: CB-MCB(2205p)-2, 240 weeks. Corrosion at bar end.

Figure 3.125: CB-MCB(2205p)-4, 240 weeks. No visible corrosion.

3.5.1.3 KDOT Benchscale Chloride Concentration Results

3.5.1.3.1 Chloride Content at Corrosion Initiation

During the course of testing, four Southern Exposure specimens initiated corrosion, at ages of 180 to 281 weeks. Since stainless steel reinforcement is expected to have a lower corrosion rate than conventional steel, the threshold corrosion rate for corrosion of conventional steel reinforcement, 0.3 µm/yr, is not used. Instead, corrosion initiation for specimens containing 2205p reinforcement is defined as an increase in the corrosion rate accompanied by a drop in the corrosion potential for the top mat of steel (Figures A65, A66, A69, and A70, Appendix A). Chloride content at corrosion initiation is summarized in Table 3.23. The specimens exhibit an average chloride content at corrosion initiation ranging from 11.14 to 19.13 kg/m^3 (18.73 to 32.18 lb/yd^3), with an overall average of 15.60 kg/m^3 (26.24 lb/yd^3). It is uncertain, however, that these specimens initiated corrosion at these times. Of the four specimens sampled, only SE-MCB(2205p)-5 exhibits a sustained positive corrosion rate after initiation, which upon autopsy was found to be due to crevice corrosion at the bar end (Figure 3.121). After initiation, the remaining specimens exhibit isolated spikes in corrosion rates, ranging from 0.70 to –0.41 µm/yr; however, the rates return to zero shortly thereafter (Figures A65, A66, A69, and A70, Appendix A). The chloride threshold presented in this section should therefore be taken as a conservative estimate of the true critical chloride corrosion threshold for 2205p reinforcement.

Table 3.23: Chloride Content at Corrosion Initiation for Specimens Containing Pickled 2205 Stainless Steel.

Specimen	Initiation Age (weeks)	Corrosion Rate (μm/yr)	Corrosion Potential (V)	Water Soluble Cl^- Content (kg/m^3) at Sample Sites						Average	Std. Dev.	COV
				# 1	# 2	# 3	# 4	# 5	# 6			
DCB(2205p)-1										[a]		
DCB(2205p)-2										[a]		
DCB(2205p)-3										[a]		
DCB(2205p)-4	229	0.061	-0.302	11.25	10.50	9.51	13.50	9.16	12.91	11.14	1.77	0.16
DCB(2205p)-5										[a]		
DCB(2205p)-6										[a]		
MCB(2205p)-1										[a]		
MCB(2205p)-2	281	0.446	-0.249	17.10	15.86	19.73	24.57	19.58	19.13	19.33	2.99	0.15
MCB(2205p)-3	206	0.16	-0.292	18.86	18.75	13.84	13.95	17.96	18.64	17.00	2.43	0.14
MCB(2205p)-4										[a]		
MCB(2205p)-5	180	0.335	-0.233	14.85	14.48	17.03	16.35	11.10		14.76	2.30	0.16

[a] No corrosion initiation

3.5.1.3.2 Chloride content at End of Life

All Southern Exposure specimens removed from testing at 240 weeks were sampled to determine the chloride concentration at the depth of the top mat of steel, as described in Section 2.3.6. In addition, the three SE-MCB specimens removed from testing were sampled for chlorides with a 6.4-mm (0.25-in.) drill bit centered at depths of 15.9, 28.6, 54.0, 79.4, and 136.5 mm (0.625, 1.125, 2.125, 3.125, and 5.375 in.) from the top surface. Chloride concentration vs. depth for each specimen is plotted in Figure 3.126, with individual chloride content data presented in Appendix C. The chloride depth profile for the SE-MCB specimens reveals little variation among the specimens, with chloride contents adjacent to the top mat of steel ranging from 17.46 to 20.12 kg/m^3 (29.37 to 33.84 lb/yd^3) and chloride contents adjacent to the bottom mat of steel ranging from 1.61 to 3.13 kg/m^3 (2.71 to 5.26 lb/yd^3).

Table 3.24 shows that the SE-DCB specimens appear to have been made with less permeable concrete than the SE-MCB specimens; the average chloride content at 240 weeks for the DCB specimens is 10.29 kg/m^3 (17.31 lb/yd^3), compared with 18.83 kg/m^3 (31.67 lb/yd^3) for the MCB specimens. The increased chloride content in the MCB

specimens compared to the DCB specimens may explain why three of the four specimens that initiated corrosion are SE-MCB specimens (Table 3.23).

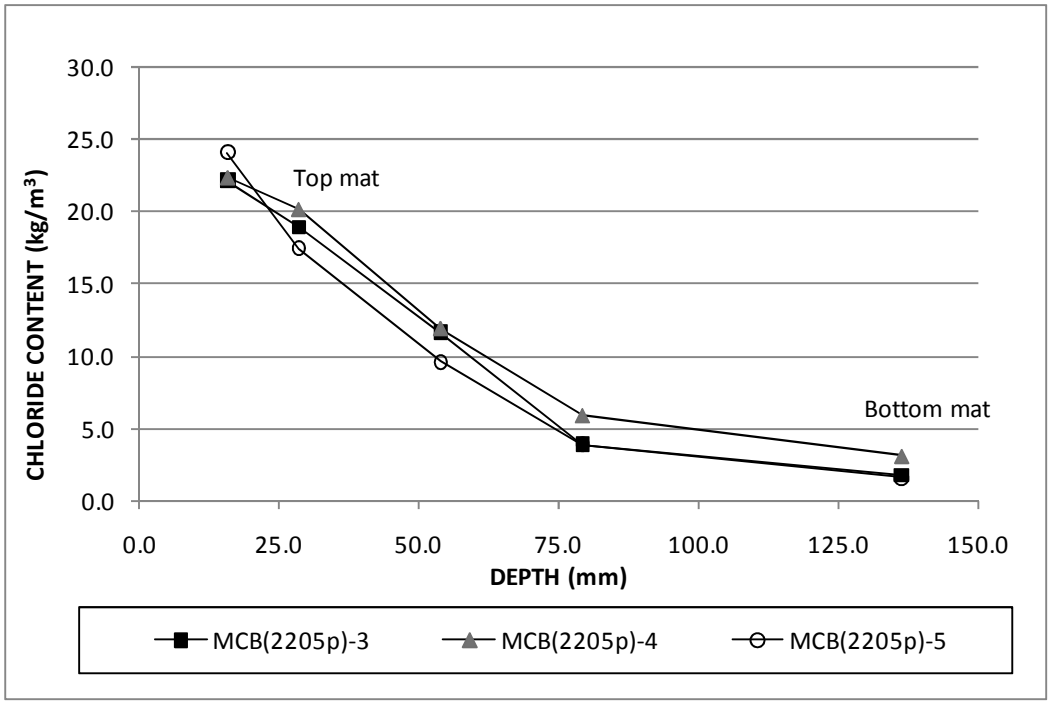

Figure 3.126: Chloride depth profile at 240 weeks for SE-MCB specimens.

Table 3.24: Chloride Content at End of Life for Specimens Containing Pickled 2205 Stainless Steel.

Specimen	Age (weeks)	Water Soluble Cl^- Content (kg/m^3) at Sample Sites						Average	Std. Dev.	COV
		# 1	# 2	# 3	# 4	# 5	# 6			
DCB(2205p)-4	240	10.20	10.69	10.73	12.60	14.36	10.35	11.49	1.65	0.14
DCB(2205p)-5	240	9.90	9.08	10.09	11.78	14.29	6.53	10.28	2.61	0.25
DCB(2205p)-6	240	9.53	8.74	10.39	8.10	9.08	8.79	9.10	0.78	0.09
MCB(2205p)-3	240	19.16	18.11	18.71	18.99	21.53	16.88	18.90	1.53	0.08
MCB(2205p)-4	240	17.81	15.90	19.46	22.99	24.45		20.12	3.56	0.18
MCB(2205p)-5	240	16.58	15.71	17.14	21.50	16.37		17.46	2.31	0.13

3.5.2 Field Test Specimens

A total of 12 field test specimens were cast using trial batch concrete for the Doniphan County (DCB) and Mission Creek (MCB) bridges. For the Doniphan County Bridge, all reinforcement was cast in uncracked concrete, with two specimens containing conventional reinforcement (FTS-DCB(Conv.)), two specimens containing undamaged ECR (FTS-DCB(ECR)), and two specimens containing pickled 2205 stainless steel (FTS-DCB(2205p)). For the Mission Creek Bridge, two specimens contain conventional reinforcement (FTS-MCB(Conv.)), two specimens contain ECR damaged with 16 3-mm (0.125-in.) diameter holes (FTS-MCB(ECR)), and two specimens contain pickled 2205 stainless steel (FTS-MCB(2205p)). For each type of reinforcement, one MCB specimen has uncracked concrete and one MCB specimen has cracked concrete.

At 240 weeks, one DCB specimen containing each type of reinforcement was autopsied to allow for examination of the reinforcement. Chloride data were not obtained from these specimens. Data for the remaining specimens is presented through week 327 for the DCB specimens and through week 301 for the MCB specimens.

3.5.2.1 Corrosion Rates, Losses, and Potentials

Average corrosion rates for FTS-MCB and FTS-DCB specimens are presented in Figures 3.127 and 3.128, respectively. All corrosion rates are based on total area. Corrosion rates for individual specimens are presented in Appendix A. For the DCB specimens (uncracked concrete), specimens with conventional reinforcement exhibit the greatest corrosion rates, with a peak corrosion rate of 1.35 µm/yr at week 115 (Figure 3.127a). The specimens with ECR and 2205p reinforcement show much lower corrosion rates. The specimens with ECR initiate corrosion at week 135. After week 159, the corrosion rate remains above zero with the exception of week 191, with periodic spikes in corrosion rates and a peak corrosion rate of 0.10 µm/yr at week 319. The specimens with 2205p reinforcement show a peak corrosion rate of 0.0018 µm/yr at week 91 (Figure 3.127b); however, no sustained positive corrosion rate is observed.

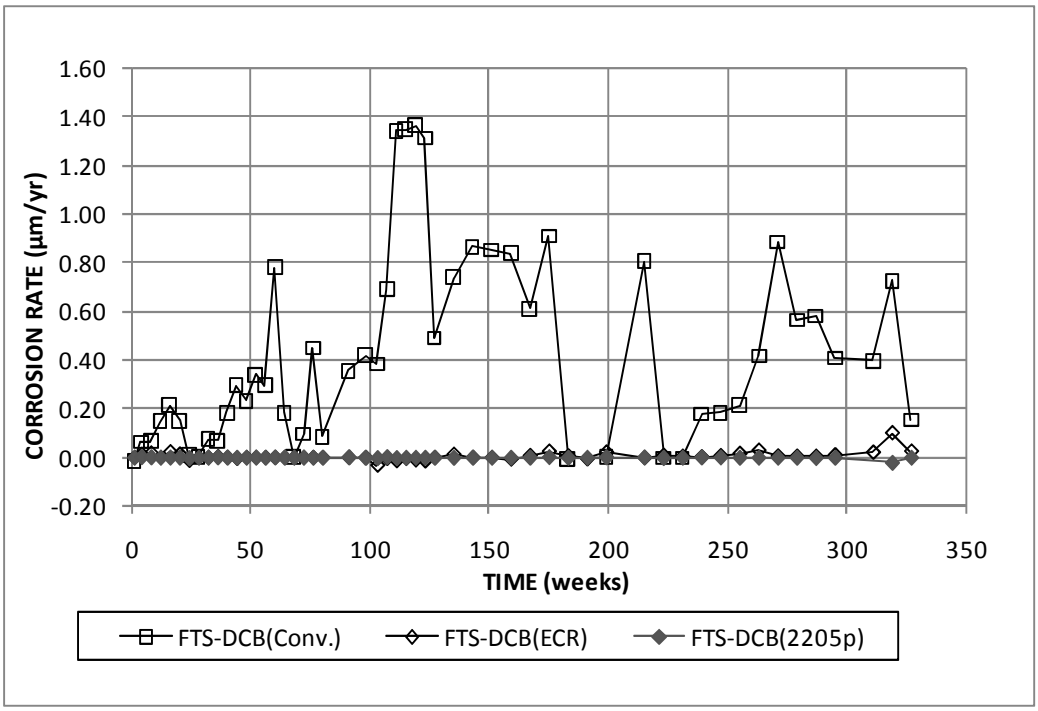

Figure 3.127a: Field test specimens, uncracked concrete. Average corrosion rates based on total area for DCB specimens.

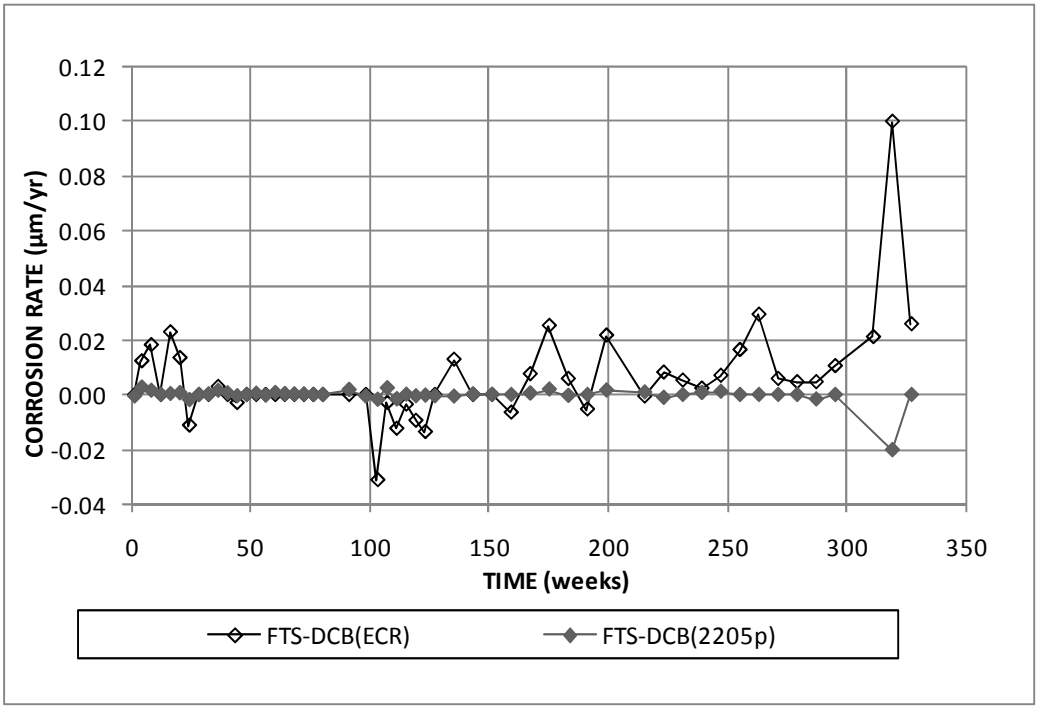

Figure 3.127b: Field test specimens, uncracked concrete. Average corrosion rates based on total area for DCB specimens (different scale).

For the MCB specimens in uncracked concrete, the specimen with conventional reinforcement shows the greatest corrosion rate, with a peak corrosion rate of 3.64 µm/yr at week 157 (Figure 3.128a). The specimens with ECR and 2205p reinforcement show lower corrosion rates. The specimen with ECR shows a peak corrosion rate of 0.046 µm/yr at week 191 and the specimen with 2205p reinforcement shows a peak corrosion rate of 0.0092 µm/yr at week 91 (Figure 3.128b). Neither specimen exhibits sustained positive corrosion rates. For the MCB specimens in cracked concrete, the specimen with conventional reinforcement exhibits a peak corrosion rate of 9.37 µm/yr at week 93, nearly three times greater than the peak corrosion rate observed in uncracked concrete (Figure 3.128a). The specimen with ECR shows a peak corrosion rate of 0.084 µm/yr at week 189, with a positive corrosion rates observed between week 175 and 263. The specimen with 2205p reinforcement shows a peak corrosion rate of 0.319 µm/yr at week 165 (Figure 3.128b); however, variations in corrosion rate between –0.82 and 0.31 µm/yr are observed after week 141.

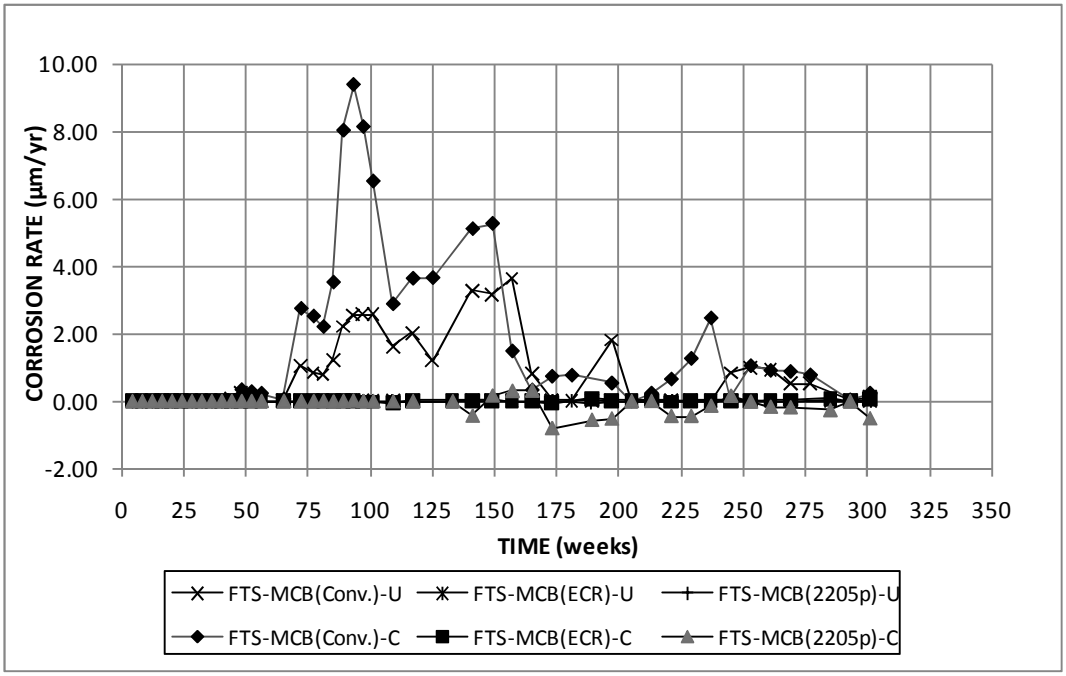

Figure 3.128a: Field test specimens, cracked and uncracked concrete. Average corrosion rates based on total area for MCB specimens.

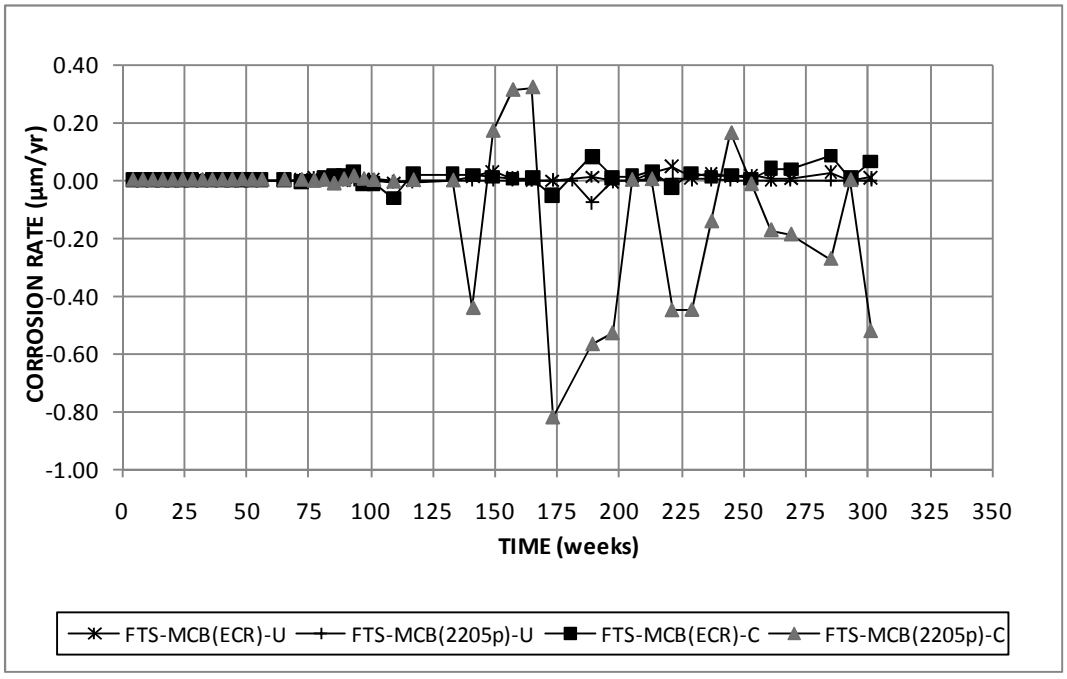

Figure 3.128b: Field test specimens, cracked and uncracked concrete. Average corrosion rates based on total area for MCB specimens (different scale).

The average corrosion losses for the DCB specimens are presented in Figure 3.129, with corrosion losses for individual specimens at 327 weeks summarized in Table 3.25. The specimens with the conventional reinforcement show the greatest average loss, 2.66 µm at week 327. The average rate (the slope of the corrosion loss plot) for conventional reinforcement increases between weeks 100 and 175 before returning to a rate similar to that observed between weeks 50 and 100. The specimens with ECR have an average losses of 0.044 µm; however, the corrosion losses are observed primarily on specimen FTS-DCB(ECR)-2. Specimen FTS-DCB(ECR)-1 was autopsied at 240 weeks and exhibits a loss of only 0.005 µm at 240 weeks. The specimens with 2205p reinforcement show negligible losses as of week 327.

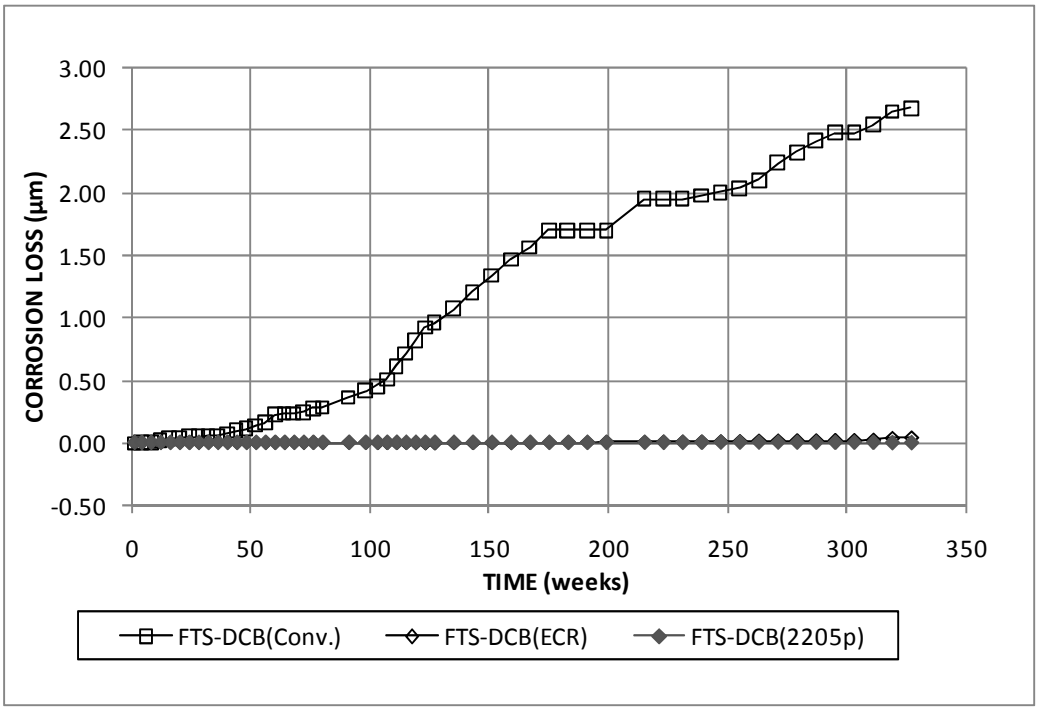

Figure 3.129a: Field test specimens, uncracked concrete. Average corrosion losses based on total area for DCB specimens.

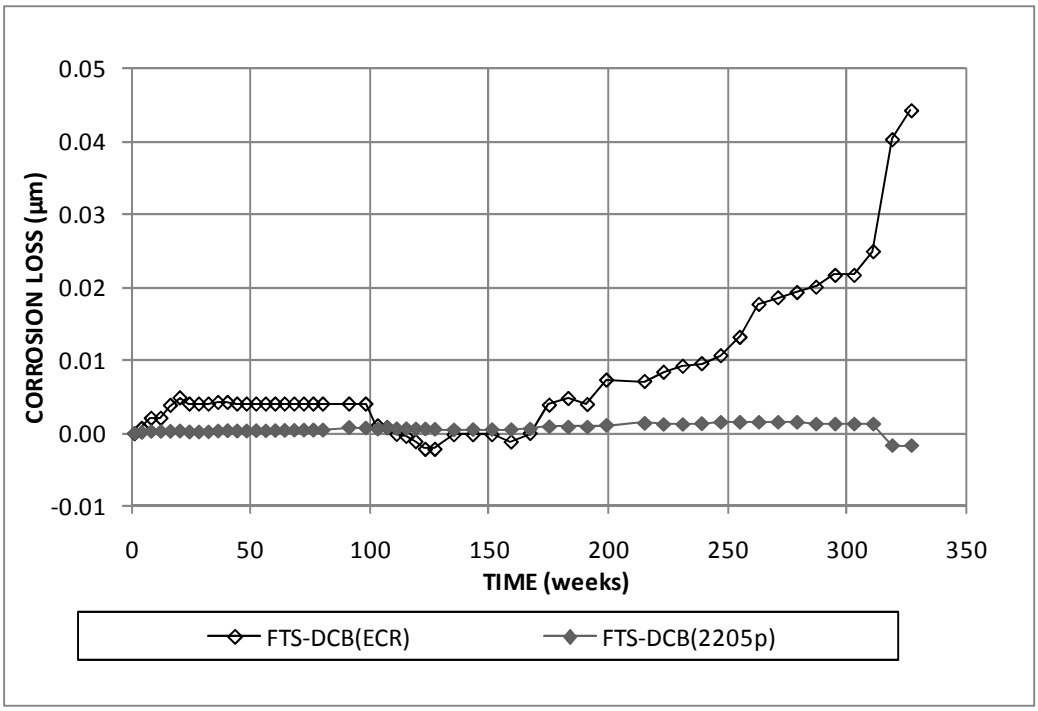

Figure 3.129b: Field test specimens, uncracked concrete. Average corrosion losses based on total area for DCB specimens (different scale).

Table 3.25: Individual Corrosion Losses for DCB and MCB Field Test Specimens

Specimen	Exposure Time (weeks)	Average Corrosion Loss (µm)	
		Total Area	Exposed Area
Doniphan County Bridge (Uncracked)			
FTS-DCB(Conv.)-1	240	2.66	-
FTS-DCB(Conv.)-2	327	2.05	
FTS-DCB(ECR)-1	240	0.005	-
FTS-DCB(ECR)-2	327	0.044	
FTS-DCB(2205p.)-1	240	0.002	
FTS-DCB(2205p.)-2	327	0.000	-
Mission Creek Bridge			
Cracked			
FTS-MCB(Conv.)	301	9.47	-
FTS-MCB(2205p)	301	-0.547	-
FTS-MCB(ECR)	301	0.076	29.7
Uncracked			
FTS-MCB(Conv.)	301	5.24	-
FTS-MCB(2205p)	301	-0.024	-
FTS-MCB(ECR)	301	0.039	15.1

The corrosion losses for the MCB specimens are presented in Figure 3.130 and in Table 3.25. In both cracked and uncracked concrete, specimens with conventional reinforcement initiate corrosion at week 75. Conventional reinforcement in cracked concrete shows greater losses than the values observed for conventional reinforcement in uncracked concrete throughout the test. In uncracked concrete, the specimen with conventional reinforcement shows the greatest loss, 5.24 µm at week 301. The specimen with ECR has a loss of 0.039 µm at 301 weeks. The specimen with 2205p reinforcement has negligible losses as of week 301. In cracked concrete, the specimen with conventional reinforcement has a loss of 9.47 µm at week 301, approximately two times greater than the losses observed in uncracked concrete. The specimen with ECR has a loss of 0.076 µm at 301 weeks. The specimen with 2205p reinforcement shows

negligible losses as of week 301; the negative corrosion loss is not assumed to be corrosion of the bottom mat, as visual inspections show no signs of corrosion.

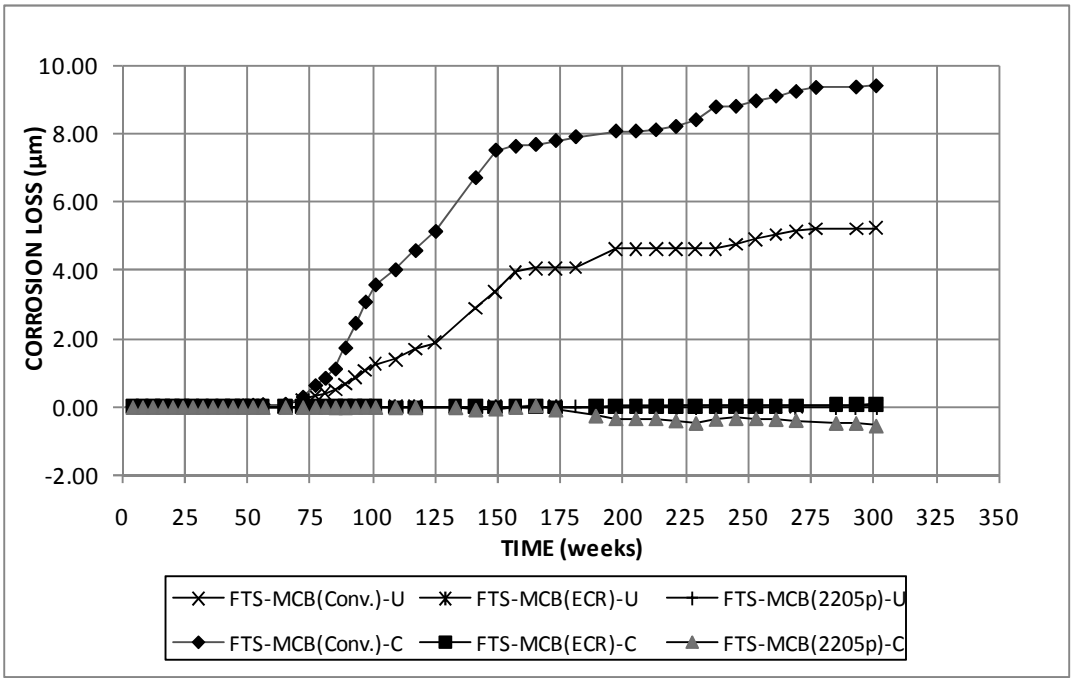

Figure 3.130a: Field test specimens, cracked and uncracked concrete. Average corrosion losses based on total area for MCB specimens.

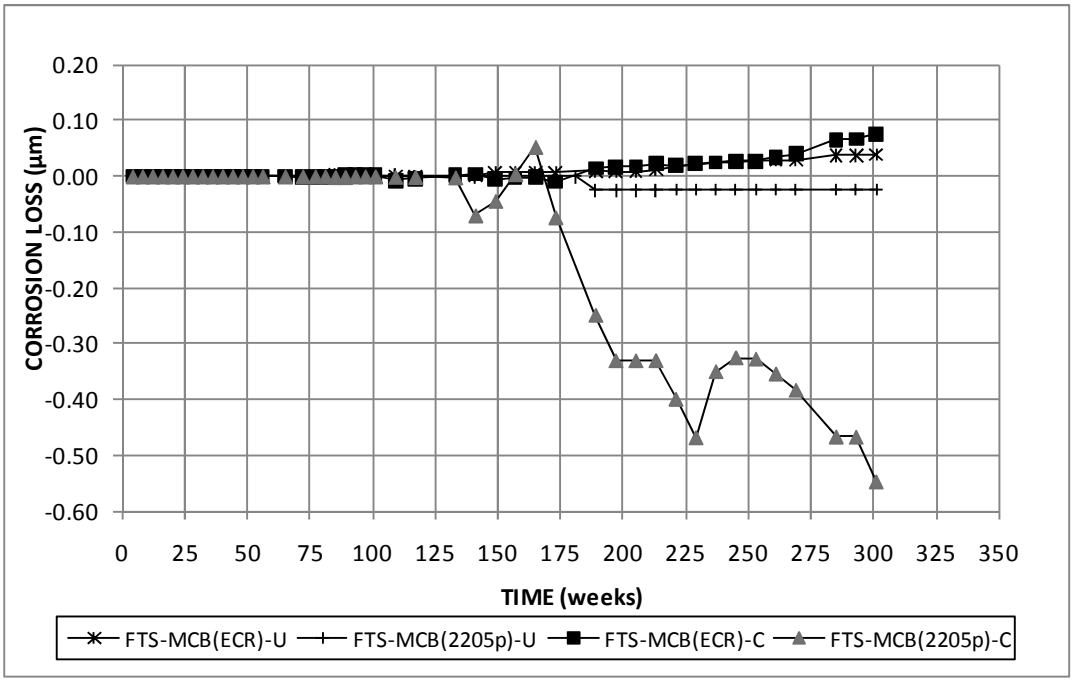

Figure 3.130b: Field test specimens, cracked and uncracked concrete. Average corrosion losses based on total area for MCB specimens (different scale).

Figures 3.131 and 3.132 show the average corrosion potentials (versus CSE) for the top and bottom mats, respectively, of the DCB specimens. Through 50 weeks, all specimens exhibit a corrosion potential between –0.100 V and –0.200 V. After week 50, the potential of the specimens with conventional reinforcement drops below –0.500 V by week 100, returning to between –0.300 V and –0.400 V after week 150. The specimens with ECR and 2205p reinforcement show similar potentials through week 150, both between –0.200 V and –0.300V. After week 150, the corrosion potential of the specimens with 2205p reinforcement becomes more positive than –0.200 V, while the corrosion potential of the specimens with ECR remains between –0.200 V and –0.300 V (Figure 3.131). For the bottom mat of steel, the potential of specimens with conventional reinforcement drops below –0.400 V by week 100, returning to between –0.200 V and –0.300 V after week 150. Aside from an isolated reading at week 117, the corrosion potentials for the bottom mat for the specimens with 2205p and ECR remain more positive than –0.300 V throughout the test (Figure 3.132).

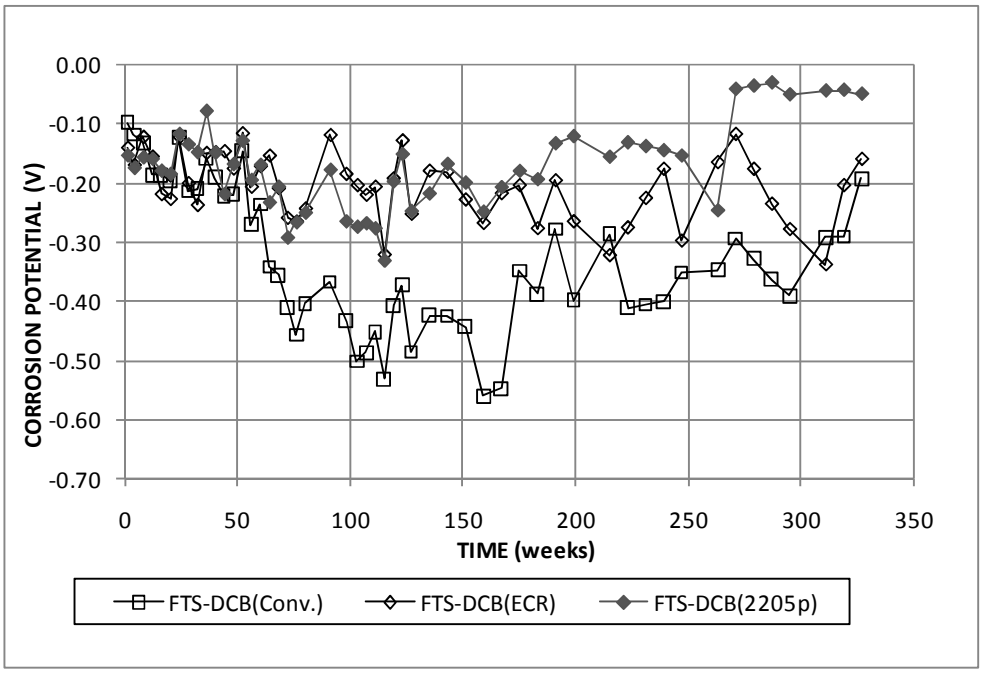

Figure 3.131: Field test specimens, uncracked concrete. Average top mat corrosion potential (CSE) for DCB specimens.

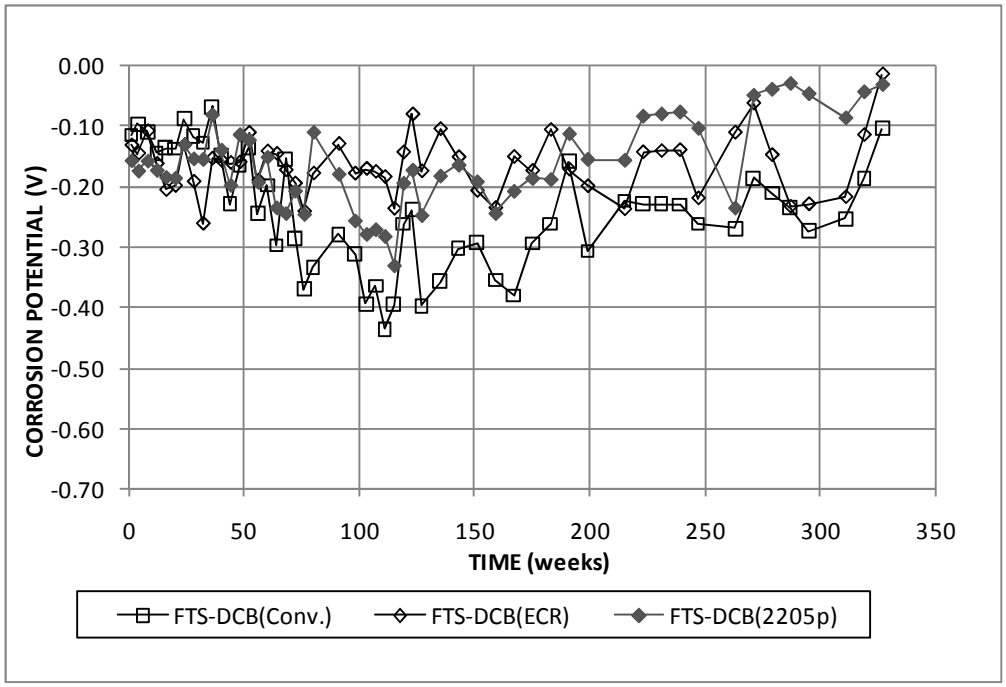

Figure 3.132: Field test specimens, uncracked concrete. Average bottom mat corrosion potential (CSE) for DCB specimens.

Figures 3.133 and 3.134 show the average corrosion potentials (versus CSE) for the top and bottom mats, respectively, of the MCB specimens with and without cracks. In the specimens without cracks, the corrosion potential varies between –0.100 V and –0.200 V through week 25. After week 25, the potential of the top mat for specimens with conventional reinforcement drops below –0.500 V by week 75, remaining there through week 175. After week 175, the top mat potential of the specimens with conventional reinforcement in uncracked concrete gradually increases, returning to between –0.300 V and –0.400 V after week 250. The specimens with ECR and 2205p reinforcement show similar top mat potentials through week 250, between –0.200 V and –0.300V. After week 250, the corrosion potential of specimens with 2205p reinforcement begins to increase towards –0.050 V (Figure 3.133). In cracked concrete, the initial top mat potential for the specimen with conventional reinforcement is measured at –0.400 V. The potential drops to –0.600 V by week 175, after which it gradually increases to –0.300 V by week 293. After week 100, the top mat corrosion

potential of specimen FTS-MCB(Conv.)-U drops to the level of the corrosion potential of specimen FTS-MCB(Conv.)-C. The potentials of the two specimens remain similar for the balance of the test (Figure 3.133). The corrosion potential of the specimen with ECR in cracked concrete also drops to around –0.500 V at week 75, only to return to approximately –0.300 V by week 141, after which it does not drop significantly. The top mat corrosion potentials of the specimens with 2205p reinforcement in cracked and uncracked concrete are similar through week 301, and do not drop below –0.300 V.

For the bottom mat of steel (Figure 3.134), the specimens with 2205p reinforcement exhibit a slightly more positive corrosion potential than the other specimens. No other significant differences in bottom mat corrosion potential are observed, and no specimen exhibits a corrosion potential more negative than –0.400 V through week 301. All specimens exhibit decreasing bottom mat corrosion potentials through week 125, after which the corrosion potentials tend to increase.

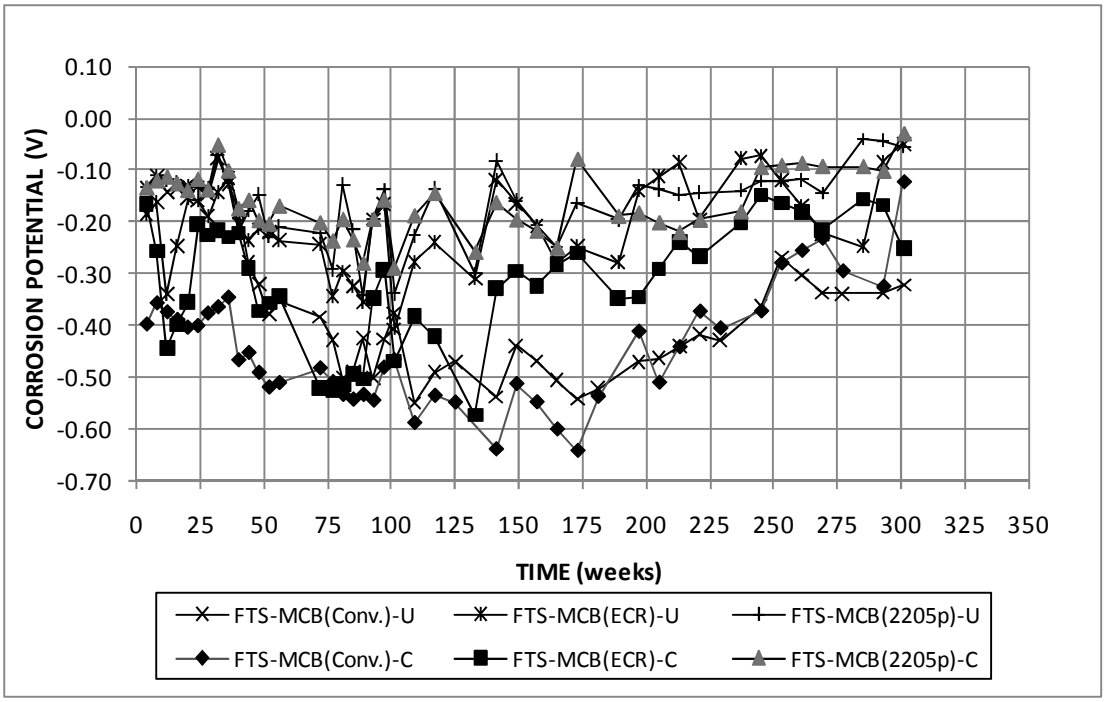

Figure 3.133: Field test specimens, cracked and uncracked concrete. Top mat corrosion potential (CSE) for MCB specimens.

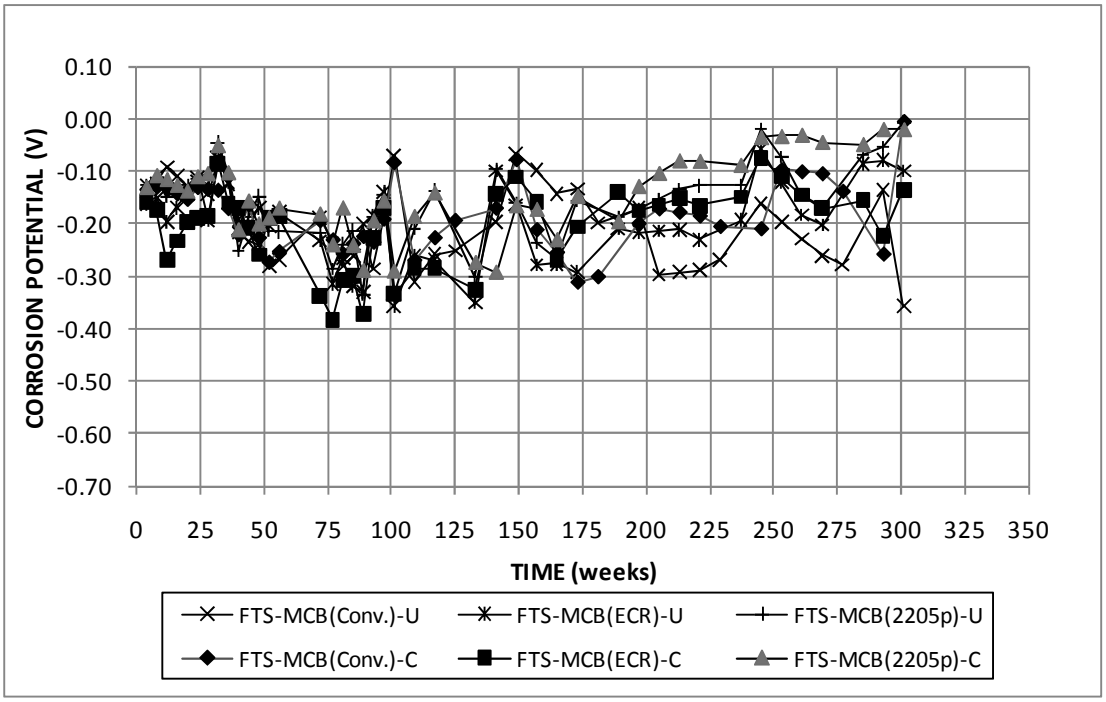

Figure 3.134: Field test specimens, cracked and uncracked concrete. Bottom mat corrosion potential (CSE) for MCB specimens.

The mat-to-mat resistances for the DCB and MCB specimens are shown in Figures 3.135 and 3.136, respectively. For the DCB specimens, the specimens with ECR show initial resistances of approximately 6,000 ohms. The resistance quickly increases to over 12,000 ohms before beginning a decreasing trend that lasts through week 327. The specimens with conventional and 2205p reinforcement exhibit initial mat-to-mat resistances of approximately 10 ohms. The resistance for both sets of specimens tends to increase through week 327, approaching 500 ohms. For the MCB specimens (Figure 3.136), the specimens with ECR exhibit initial resistances of approximately 1,000 ohms. The resistance increases to approximately 10,000 ohms around week 150 before decreasing through week 301. Like the DCB specimens, the MCB specimens with conventional and 2205p reinforcement exhibit initial mat-to-mat resistances of approximately 10 ohms, which increase to approximately 500 ohms through week 327.

No significant difference is observed between the mat-to-mat resistances of the cracked and uncracked specimens.

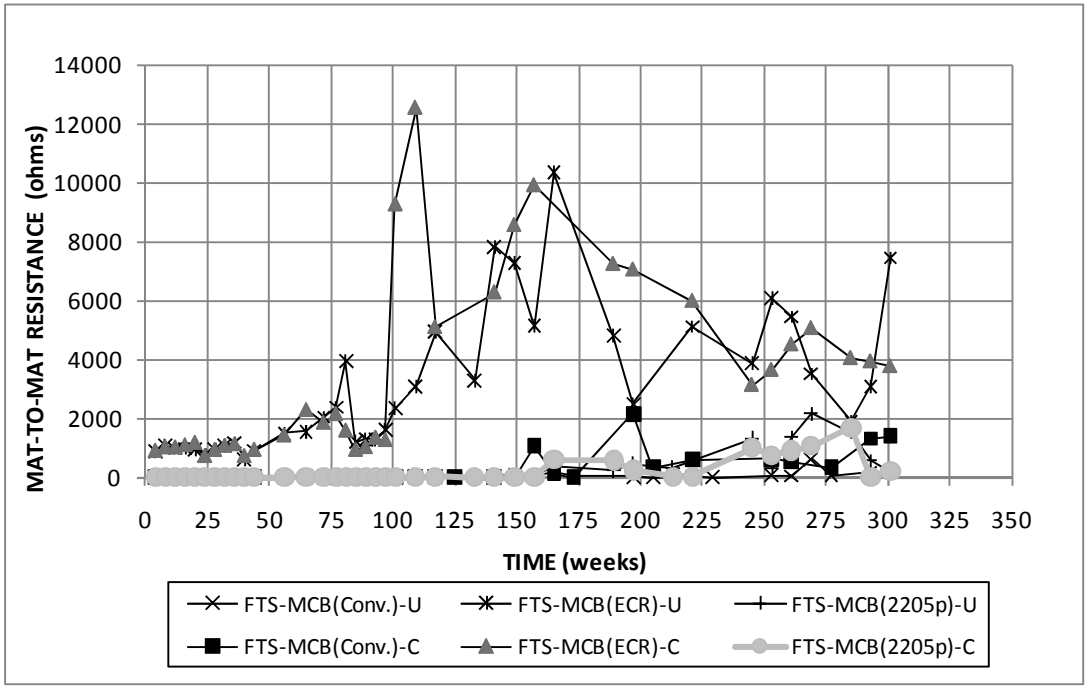

Figure 3.135: Field test specimens, cracked and uncracked concrete. Average mat-to-mat resistance for DCB specimens.

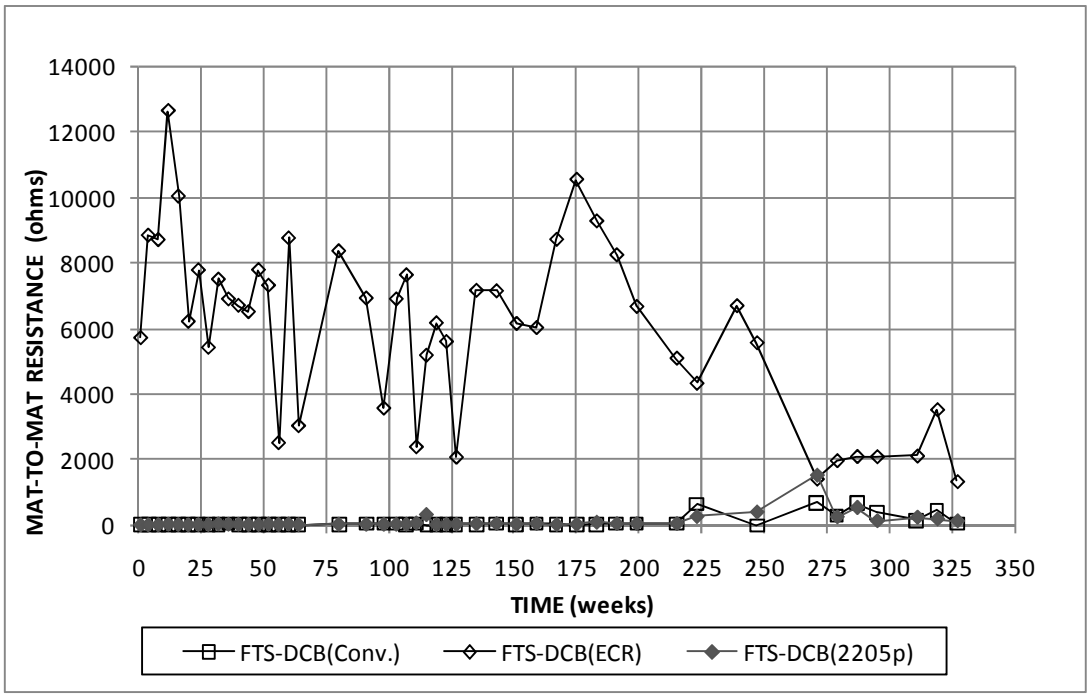

Figure 3.136: Field test specimens, cracked and uncracked concrete. Average mat-to-mat resistance for MCB specimens.

3.5.2.2 Visual Observations

All specimens are periodically inspected for signs of staining and cracking during testing. For the DCB specimens, the specimens with conventional reinforcement show moderate staining and signs of cracking (Figure 3.137). The specimens with epoxy-coated reinforcement (Figure 3.138) and 2205p reinforcement (Figure 3.139) show no signs of staining. For the MCB specimens, the specimens with conventional reinforcement show heavy staining and cracking in both uncracked concrete (Figure 3.140) and cracked concrete (Figure 3.141), while the specimens with ECR (Figure 3.142) and 2205p reinforcement (Figure 3.143) show no staining in either cracked or uncracked concrete.

Figure 3.137: Specimen FTS-DCB(Conv.)-1, 240 weeks.

Figure 3.138: Specimen FTS-DCB(ECR)-1, 240 weeks.

Figure 3.139: Specimen FTS-DCB(2205p)-1, 240 weeks.

Figure 3.140: Specimen FTS-MCB(Conv.)-U-1, 301 weeks.

Figure 3.141: Specimen FTS-MCB(Conv.)-C-1, 301 weeks.

Figure 3.142: Specimen FTS-MCB(ECR)-U-1, 301 weeks.

Figure 3.143: Specimen FTS-MCB(2205p)-C-1, 301 weeks.

The three DCB specimens that were terminated at 240 weeks were autopsied. The autopsy of specimen FTS-DCB(Conv.)-1 reveals moderate to heavy corrosion on all bars in the top mat (Figure 3.144) and light to moderate corrosion on some bars in the bottom mat (Figure 3.145). Specimen FTS-DCB(ECR)-1 shows no visible corrosion (Figure 3.146). No disbondment of the epoxy coating was noted. Specimen FTS-DCB(2205p)-1 also shows no signs of corrosion (Figure 3.147).

Figure 3.144: Specimen FTS-DCB(Conv.)-1, selected bars from top mat of steel showing heavy corrosion.

Figure 3.145: Specimen FTS-DCB(Conv.)-1, selected bars from bottom mat of steel showing moderate corrosion.

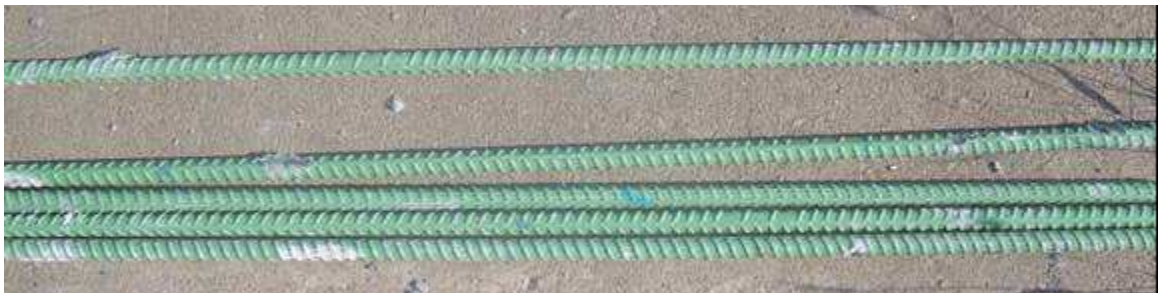

Figure 3.146: Specimen FTS-DCB(ECR)-1, selected bars from top mat of steel showing no corrosion. (White marks are jackhammer damage)

Figure 3.147: Specimen FTS-DCB(2205p)-1, selected bars from top mat of steel showing no corrosion.

3.5.3 Bridge Potential Mappings

Corrosion potential mappings are performed biannually on the Doniphan County and Mission creek bridges, two bridges cast with pickled 2205 stainless steel reinforcement in 2004. The bridges are fully described in Section 2.7. Selected corrosion potential mappings are presented in this section; all corrosion potential mappings performed to date are shown in Appendix E.

3.5.3.1 Mission Creek Bridge

Figure 3.148 shows the second corrosion potential mapping for the Mission Creek Bridge, taken on April 1, 2005. The corrosion potential with respect to a copper/copper sulfate electrode (CSE) over most of the bridge deck (3 to 26 m (9.28 to 85.3 ft) from the west end of the bridge) is more positive than –0.150 V, indicating a passive condition according to ASTM C876. The regions by the abutments show potentials more negative than –0.200 V, with locations at the east abutment more negative than –0.350 V. According to ASTM C876, this indicates a state of active corrosion. However, the limited oxygen access to the abutments will cause the potentials to be more negative than they would be in the presence of oxygen; the decreased potential in this case does not indicate active corrosion. It is also possible that the decreased potentials in the abutments are due to the use of conventional steel form ties (Figure 3.149).

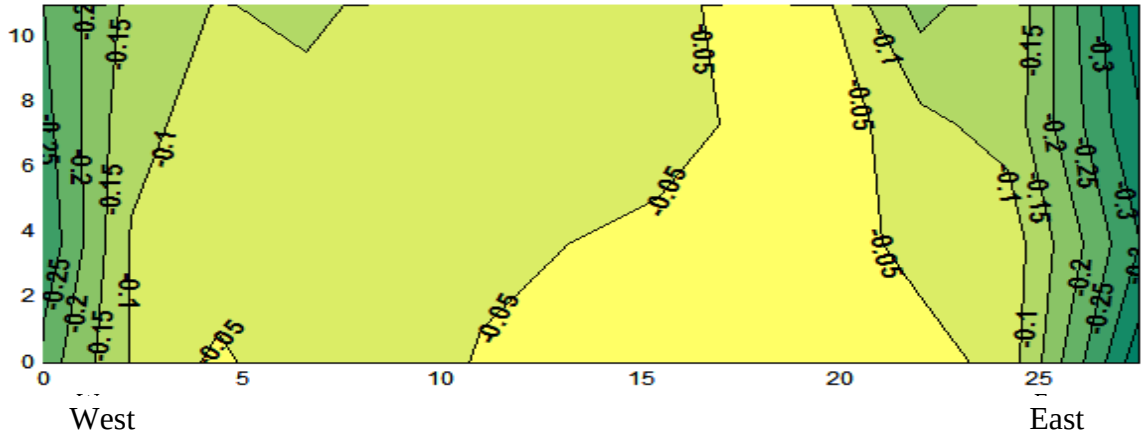

Figure 3.148: Bridge potential mapping for Mission Creek Bridge, April 1st, 2005.

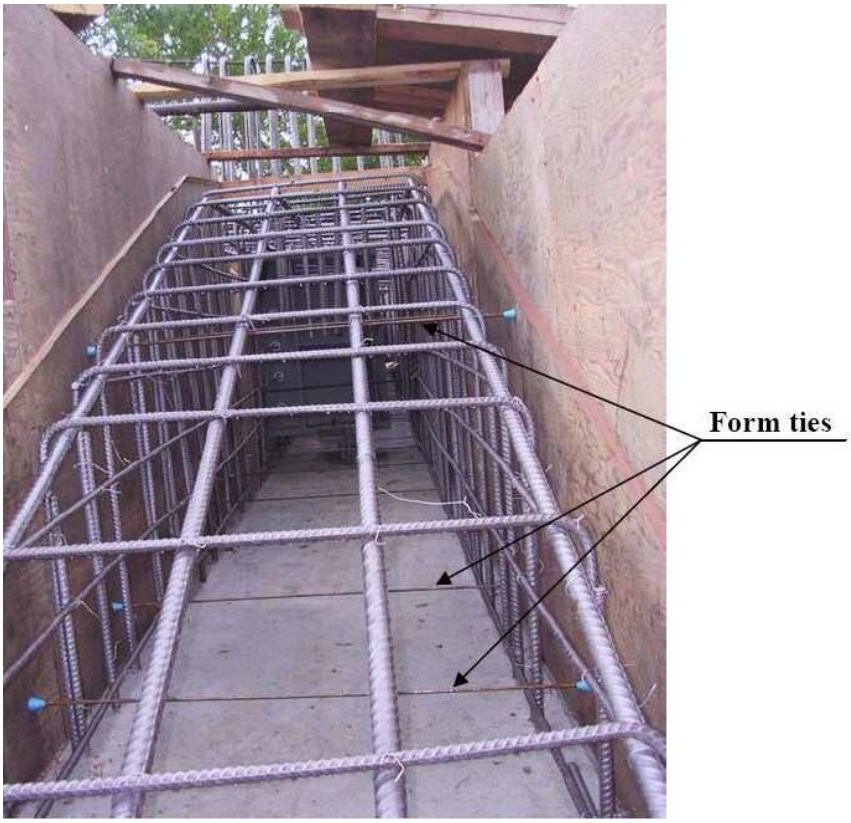

Figure 3.149: Conventional steel form ties in Mission Creek Bridge abutment.

Figure 3.150 shows the twelfth corrosion potential mapping for the Mission Creek Bridge, taken on April 27, 2010. The corrosion potential with respect to a copper/copper sulfate electrode (CSE) over most of the bridge deck (3 to 26 m (9.28 to 85.3 ft) from the west end of the bridge) is more positive than –0.150 V, indicating a passive condition

according to ASTM C876. The abutments show potentials approaching –0.350 V due to either the lack of oxygen to the abutment or the use of conventional steel form ties. Overall, the reinforcement in the bridge remains in a passive condition based on ASTM C876.

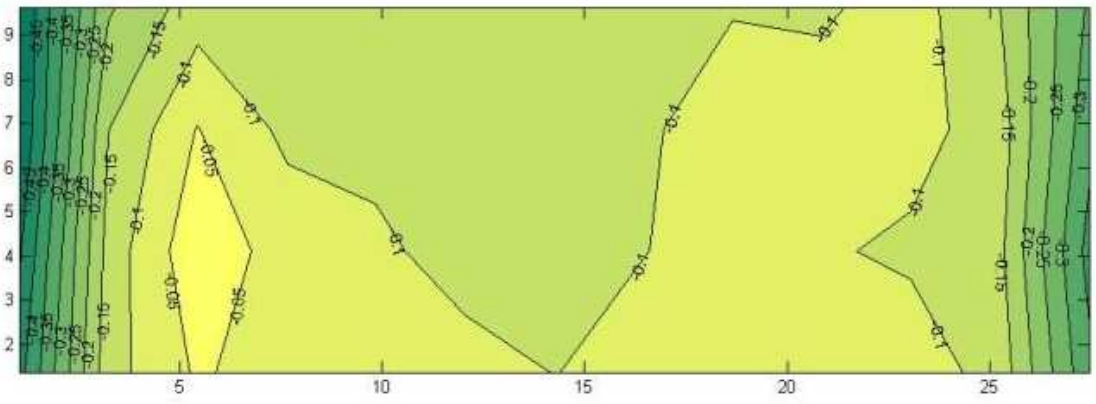

West East

Figure 3.150: Bridge potential mapping for Mission Creek Bridge, April 27th, 2010.

3.5.3.2 Doniphan County Bridge

Figure 3.151 shows the first corrosion potential mapping for the Doniphan County Bridge, taken on September 17, 2004. Over most of the bridge deck, the corrosion potential remains more positive than –0.150 V (CSE), indicating a passive condition. Decreases in potential are observed near the abutments, again likely due to decreased oxygen penetration at the abutments or the use of conventional steel form ties in the abutments. The twelfth bridge potential mapping was performed on April 29, 2010 and is shown in Figure 3.152. Corrosion potentials over much of the bridge remain more positive than –0.200 V. Near the north side of the bridge, isolated regions show potentials approaching –0.250 V, falling in the range of uncertain corrosion activity according to ASTM C876. The corrosion potentials at the abutments remain more

negative than –0.300 V. Overall the reinforcement in the bridge remains in a passive condition based on ASTM C876.

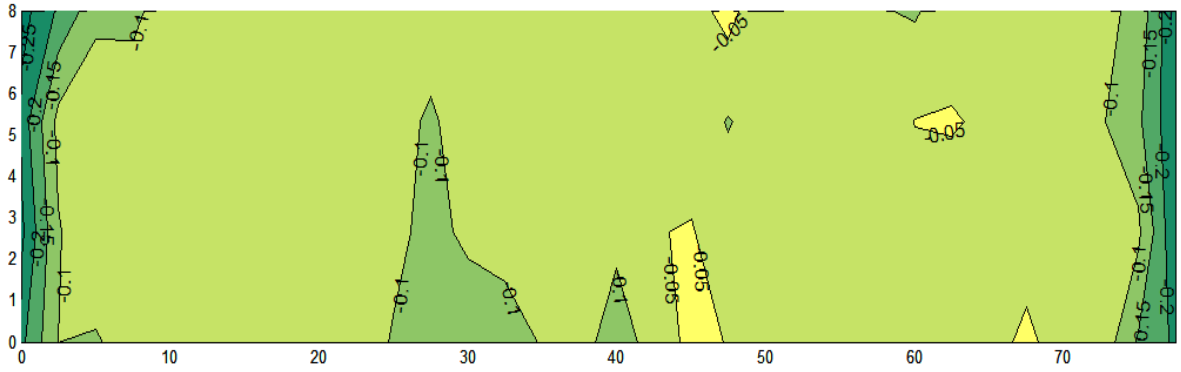

West East

Figure 3.151: Bridge potential mapping for Doniphan County Bridge, September 17th 2004.

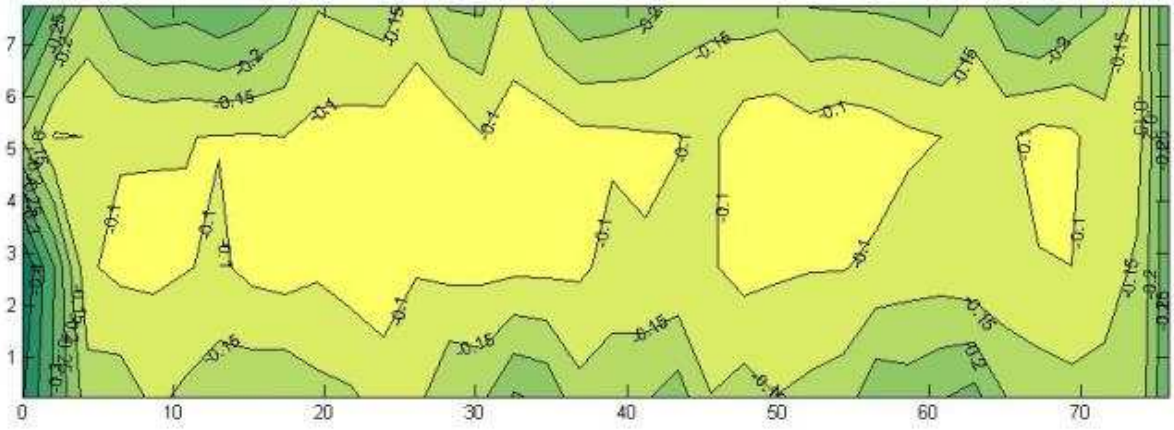

West East

Figure 3.152: Bridge potential mapping for Doniphan County Bridge, April 29th 2010.

3.5.4 KDOT Bridge Projects Summary

For the benchscale specimens with 2205p reinforcement, limited corrosion has been observed in some specimens. Other specimens remain passive after over six years of testing. For the field test specimens, the 2205p reinforcement shows negligible corrosion losses in both cracked and uncracked concrete. ECR shows limited corrosion

losses in both cracked and uncracked concrete, with no visible corrosion products on the autopsied specimen. The specimens with conventional reinforcement show significant corrosion losses with cracking and spalling in both cracked and uncracked concrete. The bridge potential mappings of two bridges cast with 2205p reinforcement indicate that the steel remains in a passive state after six years of service.

CHAPTER 4

CORROSION LOSS REQUIRED TO CRACK CONCRETE CONTAINING CONVENTIONAL, EPOXY-COATED, AND GALVANIZED REINFORCEMENT

4.1 INTRODUCTION

The corrosion of steel reinforcement in concrete is a destructive process for both the steel and the concrete. The corrosion products of steel occupy several times the volume of solid steel, resulting in cracking and spalling of the concrete cover once a sufficient amount of corrosion loss has occurred. Several studies have worked to establish a relationship between corrosion loss and cracking of concrete cover for uncoated conventional reinforcement (Rasheeduzzafar et al. 1992a, Alonso et al. 1997, Maaddawy and Soudki 2003, Torres-Acosta and Sagues 2004). In addition, Torres-Acosta and Sagues (2004) examined the effects of localized corrosion, although the corroding areas examined by Torres-Acosta were much larger than the area typically exposed due to damage to epoxy-coated reinforcement.

Limited research has been performed on the amount of corrosion loss required to crack concrete for galvanized reinforcement. Sergi, Short, and Page (1985) found the corrosion product of zinc is often zinc oxide (ZnO). The volume of zinc oxide is only 1.5 times that of solid zinc (Hime and Machin 1993), whereas the volume of ferric oxide is 3 times that of solid steel (Suda et al. 1993), indicating that the corrosion loss required to crack concrete for specimens with galvanized reinforcement should be greater than the corrosion loss required to crack concrete with conventional reinforcement. However, under certain conditions zinc can also form zinc hydroxychloride II ($Zn_5(OH)_8Cl_2$-H_2O) (Sergi et al. 1985), which has 3.6 times the volume of solid zinc (Hime and Machin 1993). The formation of zinc hydroxychloride II will result in corrosion losses for galvanized reinforcement at the onset of cracking similar to those observed for conventional reinforcement. Rasheeduzzafar et al. (1992b) studied conventional and

galvanized reinforcement cast in concrete with chloride contents at casting ranging from 2.4 to 19.2 kg/m^3 (4 to 32 lb/yd^3). Rasheeduzzafar et al. found specimens containing galvanized reinforcement took longer to crack concrete than specimens containing conventional reinforcement; however, the corrosion loss at crack initiation was not determined.

The research presented in this chapter examines the corrosion losses required to crack concrete cover for conventional, galvanized, and damaged epoxy-coated reinforcement. Specimens with conventional and galvanized reinforcement are tested at varying covers to establish a relationship between corrosion loss and cracking for conventional and galvanized reinforcement. Epoxy-coated reinforcement is also tested at 25-mm (1 in.) cover with varying damage patterns to determine the effect of damaged area on corrosion loss required to crack concrete. Experimental specimens are described in more detail in Section 4.2.3. Two-dimensional and three-dimensional finite element models, described in Section 4.2.8, are created to test the corrosion loss to crack concrete for multiple combinations of cover and damaged area. The results from the finite element models are compared with experimental results from this study and other studies, and an expression is developed relating damaged area, concrete cover, and corrosion loss to cause cracking.

4.2 EXPERIMNENTAL PROCEDURE

4.2.1 Mixture Proportions

The mixture proportions used in the concrete for all specimens are shown in Table 4.1. The materials used are listed below. The mixture includes salt equivalent to 2% chlorides by weight of cement to destabilize the passive layer of the reinforcement and increase the ionic conductivity of the concrete. The salt is dissolved in the mix water prior to casting.

Cement – Type I/II portland cement.

Water – Municipal tap water.

Fine Aggregate – Kansas River sand. Bulk specific gravity (SSD) = 2.62, absorption 0.8%, fineness modulus 2.51.

Coarse Aggregate – Crushed limestone from Fogle quarry. Nominal maximum size 19 mm (0.75 in.), bulk specific gravity (SSD) = 2.58, absorption 2.3%, unit weight 1536 kg/m^3 (95.9 lb/ft^3).

Salt – Sodium chloride, added to mix water as specified in Table 4.1.

Air Entraining Agent – Daravair 1400, manufactured by W.R. Grace.

Table 4.1: Mix proportions for cracking specimens

Cement, kg/m^3 (lb/yd^3)	**Water, kg/m^3 (lb/yd^3)**	**Fine Aggregate, kg/m^3 (lb/yd^3)**	**Coarse Aggregate, kg/m^3 (lb/yd^3)**	**NaCl, kg/m^3 (lb/yd^3)**	**AEA, L/m^3 (oz/yd^3)**
356 (598)	160 (269)	854 (1435)	883 (1484)	11.7 (19.8)	2.66 (68.9)

4.2.2 Materials

The following materials are used in the cracking tests described in this chapter.

Wire – External specimen connections from the reinforcing steel to the terminal box are made with 16-gauge multi-strand copper wire.

Multimeter – The multimeter is used to measure current flow to each specimen.

Power Supply – The power supply is used to drive the corrosion of the test bar. An Intertech PGS 151 galvanostat is used for conventional and galvanized reinforcement. A BK Precision 1710 30V power supply is used for epoxy-coated reinforcement. The change in equipment is necessitated by the higher resistance of specimens with epoxy-coated reinforcement.

Stainless Steel Screws/Washers – Used to hold reinforcement in place in formwork and to connect wires to specimens during testing.

4.2.3 Specimens

A schematic of the cracking specimens is shown in Figure 4.1. The cracking specimens are beam specimens, 152 mm (6 in.) wide by 305 mm (12 in.) long. The height of the specimens is dependent on the concrete cover. The top bar is the test bar and consists of conventional, galvanized, or epoxy-coated reinforcement. The bottom bars are pickled 2205 duplex stainless steel. All bars are No. 16 (No. 5) reinforcing steel. Specimens are connected to a power supply to drive corrosion on the test bar and are kept ponded with deionized water.

A total of 34 specimens are tested in five series. Series 1 consists of beams with conventional and galvanized reinforcement with 25.4-mm (1-in.) concrete cover. Series 2 consists of beams with conventional and galvanized reinforcement with 12.7-mm (0.5-in.) concrete cover. Series 3 tests conventional and galvanized reinforcement with 51-mm (2-in.) cover. Series 4 tests damaged epoxy-coated reinforcement with 25.4-mm (1-in.) concrete cover. Series 5 tests two specimens with galvanized reinforcement and 25.4-mm (1-in.) cover, with specimens removed from testing at crack initiation. Testing continues on Series 1, 2, and 3 until the crack reaches a width of 0.508 mm (0.02 in.). Testing continues on Series 4 until the crack spans the full length of the specimen, as the lower corrosion rate for specimens containing ECR makes continuing the test until the crack reaches a width of 0.508 mm (0.02 in.) impractical.

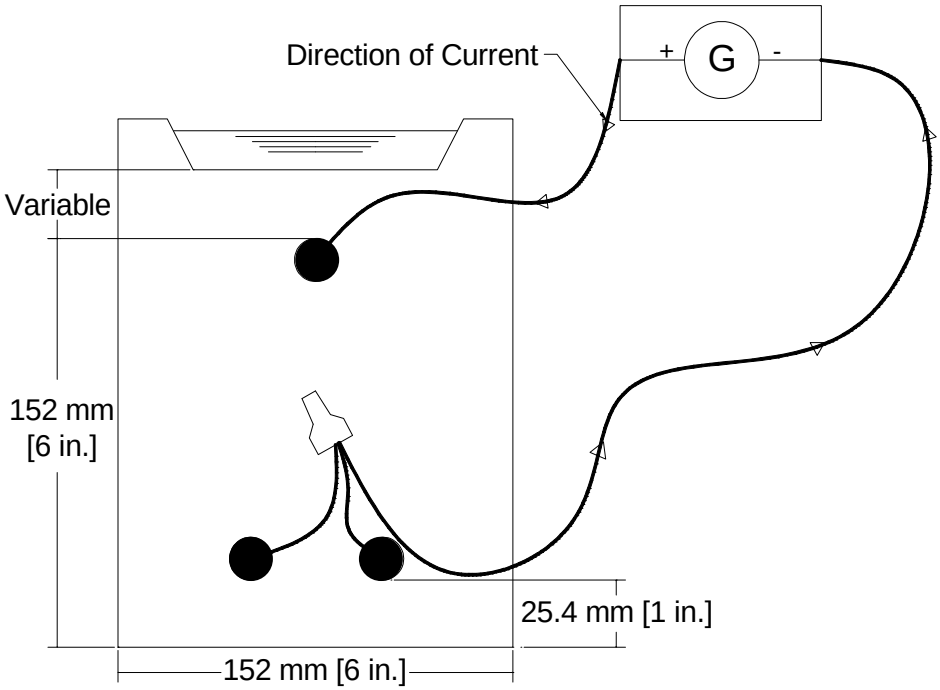

Figure 4.1: Cracking Specimen

4.2.4 Test Procedure

The test begins 14 days after the specimens are cast. During the test, the current to each specimen is measured daily. Dividing the measured current by the surface area of the test bar (or the damaged area for epoxy-coated reinforcement) gives the corrosion current density, which is used to determine corrosion rate using Faraday's equation [Eq. (1.13)]. Specimens are visually monitored daily for staining and cracking using a crack comparator. The corrosion loss at staining, crack initiation, and propagation of the crack to the full specimen length is recorded. In addition, the crack width as a function of corrosion loss is tracked for specimens with conventional and galvanized reinforcement.

4.2.5 Formwork

Formwork for cracking specimens is constructed from 19-mm (0.75-in.) thick plywood treated with polyurethane and consists of four face pieces and a base. Specimens are cast upside-down. A tapered 114 × 267 × 19 mm (4.5 × 10.5 × 0.75 in.) plywood insert is affixed to the formwork base to create a concrete dam used to hold water on the specimen (Figure 4.1). Holes are drilled on two opposing faces to allow the

reinforcement to be held in place during casting. The faces and base are held together with 32-mm (1.25-in.) long 10-24 stainless steel machine screws. The interior surfaces of the form are coated with mineral oil prior to placement of the reinforcement.

4.2.6 Fabrication

Specimen fabrication for cracking specimens proceeds as follows:

1. Reinforcing bars are cut to 305 mm (12 in.) with a band saw. Cut ends are ground to remove sharp edges.
2. Both ends of the bars are drilled and tapped to a depth of 19 mm (0.75 in.) with 10-24 threads.
3. Epoxy-coated reinforcement is intentionally damaged. Four specimens are damaged using a 3-mm (0.125-in.) diameter four-flute drill bit and a milling machine to create two holes spaced 102-mm (4-in.) on center in the epoxy on one side of the bar (Figure 4.2). Four specimens are damaged with a high-speed sanding tool to create two 3-mm (0.125-in.) wide half rings extending between the two longitudinal ribs on one side of the bar, spaced 102-mm (4-in.) on center (Figure 4.2).

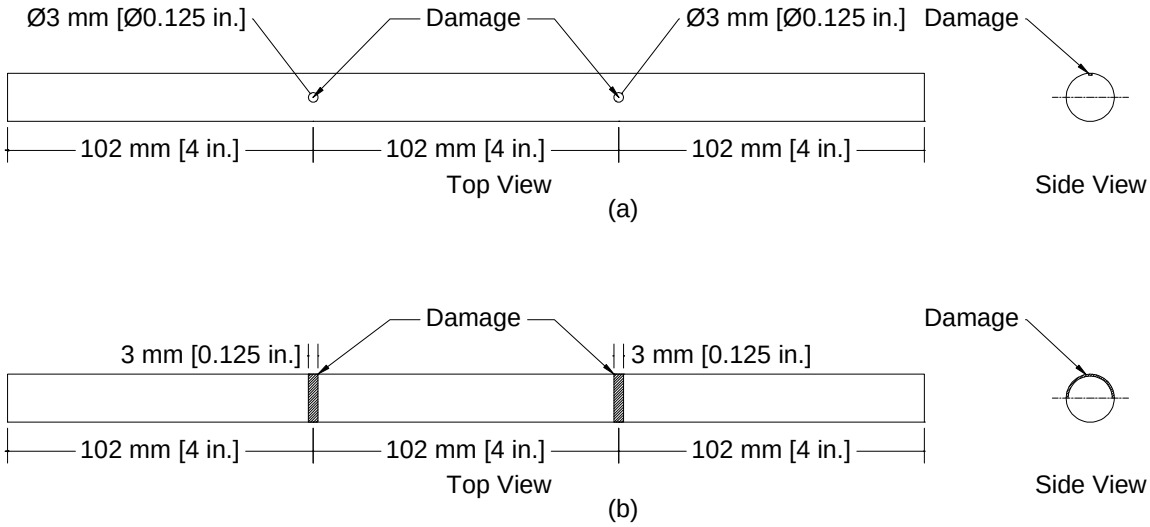

Figure 4.2: Damage patterns for epoxy-coated reinforcement. (a) Two holes (2h), (b) Two half-rings (2r).

4. Epoxy-coated bars are cleaned with warm soapy water, rinsed and allowed to dry. Conventional steel and galvanized bars are soaked in acetone for a minimum of two hours and scrubbed to remove any oil.
5. The reinforcement is placed in the assembled formwork described in Section 4.2.4 and held in place with 32-mm (1.25-in.) long 10-24 threaded stainless steel machine screws. For epoxy-coated reinforcement, two specimens of each damage type are aligned so that the damaged region faces the top surface (vertical alignment). The two remaining specimens are aligned with the damaged area facing the side of the specimen (horizontal alignment).
6. Specimens are cast with concrete using the mixture proportions in Table 4.1. Specimens are filled in two layers. After each layer, the concrete is consolidated on a 60-Hz, 0.15-mm (6-mil) amplitude vibrating table for 30 seconds. The free surface of the concrete (the bottom of the specimen) is finished with a float.
7. Specimens are cured for 14 days in the forms at room temperature. Wet burlap and plastic are used to minimize evaporation.
8. Prior to testing, wire leads are connected to the top and bottom bars using 10-24 × 13 mm (0.5 in.) stainless steel screws and a No. 10 stainless steel washer.
9. Top and bottom bars are connected to the power supply. Specimens are placed on 2 × 2 wooden studs to allow air flow under the specimens.

4.2.7 Test Program

The test program is summarized in Table 4.2. The conventional and galvanized reinforcement are tested with 12.7-mm (0.5-in.), 25.4-mm (1-in.), and 51-mm (2-in.) concrete cover. The galvanized reinforcement has a nominal coating thickness of 0.150 mm (0.006 in.). The epoxy-coated reinforcement is tested using a 25.4-mm (1-in.) cover with two damage patterns as described in Section 4.2.6.

Table 4.2: Corrosion Loss to Cause Cracking: Number of Specimens in Test Program

	Cover		
System	**12.7 mm (0.5 in.)**	**25.4 mm (1 in.)**	**51 mm (2 in.)**
Uncoated bars (Conv.)	4	4	4
Galvanized bars (Zn)	4	6[a]	4
ECR-2 hole damage pattern			
Horizontal alignment (ECR-2h-H)		2	
Vertical alignment (ECR-2h-V)		2	
ECR-2 ring damage pattern			
Horizontal alignment (ECR-2r-H)		2	
Vertical alignment (ECR-2r-V)		2	

[a] Two specimens removed from testing at crack initiation

4.2.8 Finite Element Modeling of Corrosion Loss and Cracking

To further study the relationship between corrosion loss and cracking, two and three-dimensional finite element models are created using ABAQUS 6.9. The two-dimensional models are used to model uniform corrosion of a reinforcing bar. The three dimensional models are tested with uniform corrosion over the entire bar, as well as with areas of localized corrosion. The model represents a slab with mirror symmetry about the axis of the reinforcement (Figure 4.3). The crack is assumed to propagate along the vertical boundary of the model centered on the reinforcing bar. A series of nonlinear springs are used to provide horizontal restraint along the plane of the crack to represent the nonlinear behavior of the concrete as it cracks.

The properties of the springs are based on measurements of fracture energy of concrete (Darwin et al. 2001). Darwin et al. tested notched beams in center-point loading. Fracture energy was calculated by determining the area under the load-deflection curves for each specimen. Darwin et al. found that for concretes older than five days, fracture energy is governed by coarse aggregate properties and is independent of *w/c* ratio, compressive strength, and age of concrete. The spring properties are adjusted to provide a fracture energy of 61 N/m (0.35 lb/in.), comparable to the value

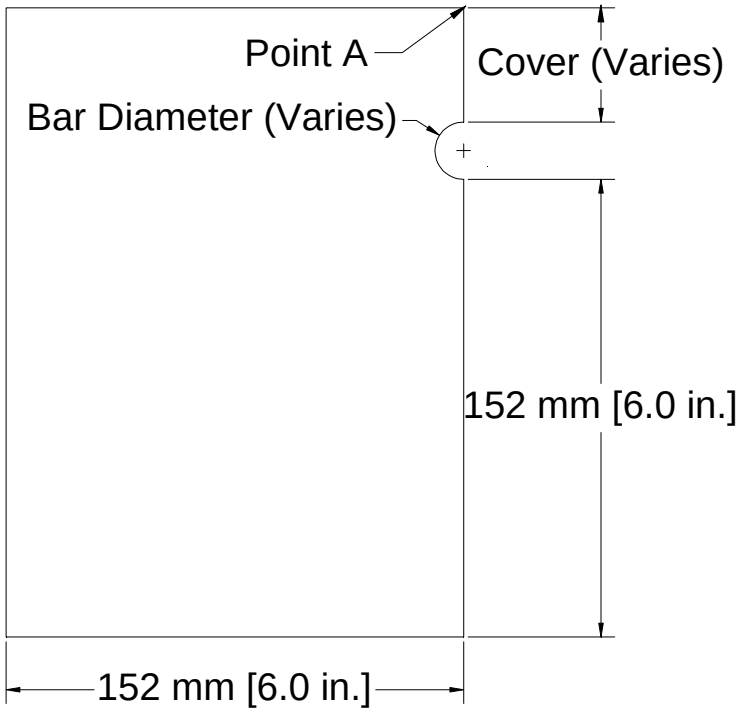

Figure 4.3: Two dimensional finite element model of concrete cracking behavior.

reported by Darwin et al. (2001). The initial stiffness of the springs provides an elastic modulus of 27.6 GPa (4,000 ksi) and a peak tensile stress of 2.76 MPa (400 psi). The spring behavior for a spring density of 6200 springs/m^2 (4 springs/in.^{2}) is shown in Figure 4.4. Material away from the plane of the crack is assumed to be linear and elastic, with an elastic modulus of 27.6 GPa (4,000 ksi) and a Poisson's ratio of 0.2. Corrosion is assumed to occur uniformly over the entire surface of the conventional and galvanized bars and over the localized damaged regions of epoxy-coated bars. The buildup of corrosion products is represented by applying a uniform deflection normal to the reinforcing bar surface. The volume ratio of corrosion products to corrosion loss *n* is assumed to be 3.0 based on work by Suda et al (1993). A visible crack is assumed to have formed when the horizontal deflection at the top surface of the model (point A in Figure 4.3) reaches 25 µm (0.001 in.). With the model symmetry, this corresponds to a 50-µm (0.002-in.) wide crack. The displacement at the surface of the concrete at the location of the reinforcing bar required to cause the formation of the crack, Δ_{crit}, is

converted to a corrosion loss (x_{crit}) using Eq. (4.1). The term (n-1) in the denominator accounts for the volume of the reinforcing bar that is converted to corrosion product.

$$x_{crit} = \frac{\Delta_{crit}}{n-1} \tag{4.1}$$

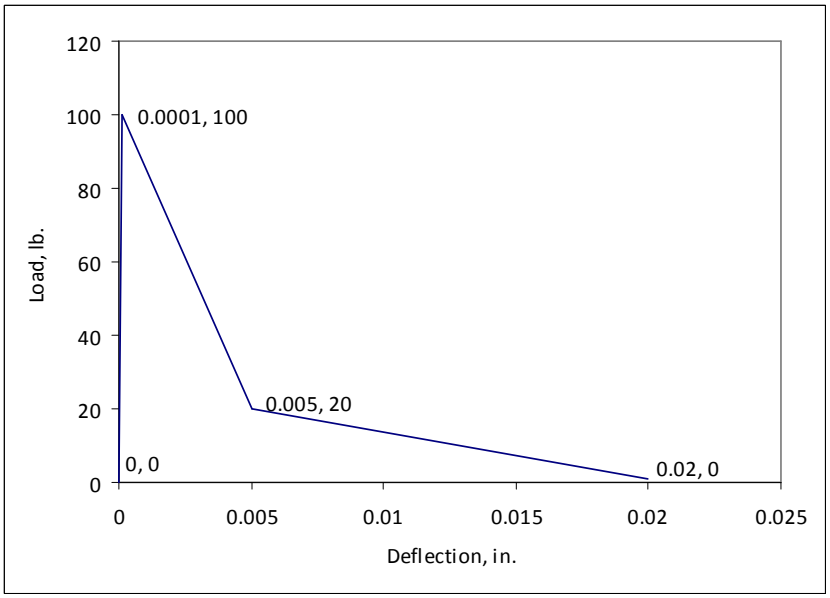

Figure 4.4: Load-deflection behavior for nonlinear spring model. Spring density 6200 springs/m^2 (4 springs/in.^{2})

Figures 4.5 and 4.6 show typical finite element model meshes used for the two and three-dimensional models. The model dimensions are shown in Figure 4.3. For the two-dimensional finite element models, concrete covers of 6.4 mm (0.25 in.), 12.7 mm (0.5 in.), 19 mm (0.75 in.), 25.4 mm (1 in.), 38 mm (1.5 in.), 51 mm (2 in.), 76 mm (3 in.), and 102 mm (4 in.) and bar diameters of 12.7 mm (0.5 in.), 19 mm (0.75 in.), and 25.4 mm (1 in.) are evaluated. For the three-dimensional finite element models, concrete covers of 51 mm (2 in.) and 76 mm (3 in.) and bar diameters of 12.7 mm (0.5 in.), 19 mm (0.75 in.), and 25.4 mm (1 in.) are used. The 2D model has a unit length and the 3D model has a length of 508 mm (20 in.).

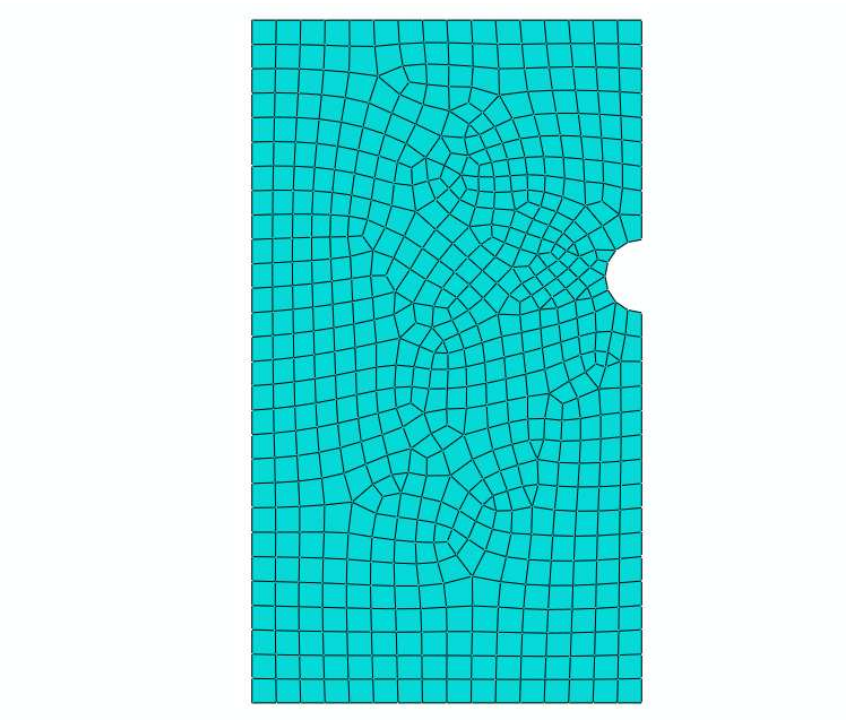

Figure 4.5: Two-dimensional FEA model.

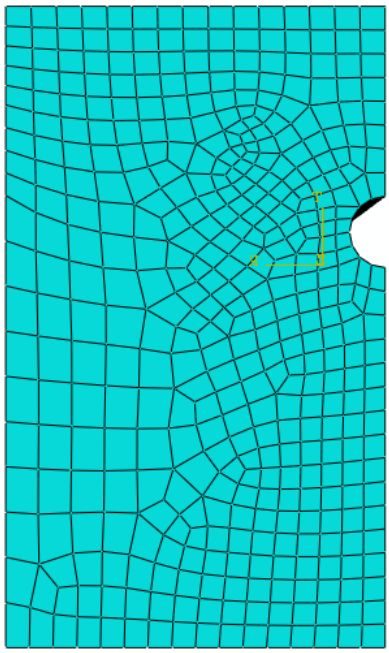

Figure 4.6: End view for three-dimensional FEA model.

To select the element type for the 2D model, a sample model is analyzed using each of the three element options provided by ABAQUS – quad, quad-dominated, and tri. The quad mesh contains only quadrilateral elements. The quad-dominated mesh uses

predominantly quadrilateral elements, but also uses triangular elements as the program deems necessary. The tri mesh uses only triangular elements. The mesh seed size for these models is 12.7 mm (0.5 in.). The corrosion loss required to produce a 50-µm (0.002-in.) wide crack for each element type is listed in Table 4.3. The values range from 38.48 to 38.99 µm. Since no significant difference in element types is observed, the default option (quad-dominated) is used.

Table 4.3: Effect of 2D Element Type on Corrosion Loss.

Mesh Type	Corrosion Loss to Produce a 50-µm Crack, µm[a]
Quad	38.99
Quad-dominated	38.48
Tri	38.74

[a] 1 µm = 0.0000394 in.

To determine the mesh seed size, a sample model is analyzed using quad-dominated elements with mesh seed sizes ranging from 1.55 to 25.4 mm (0.06125 to 1 in.). The results are presented in Figure 4.7. Since no significant difference in results is observed for mesh seed sizes smaller than 6.4 mm (0.25 in.), a 6.4-mm (0.25-in.) mesh seed size is used for all 2D models.

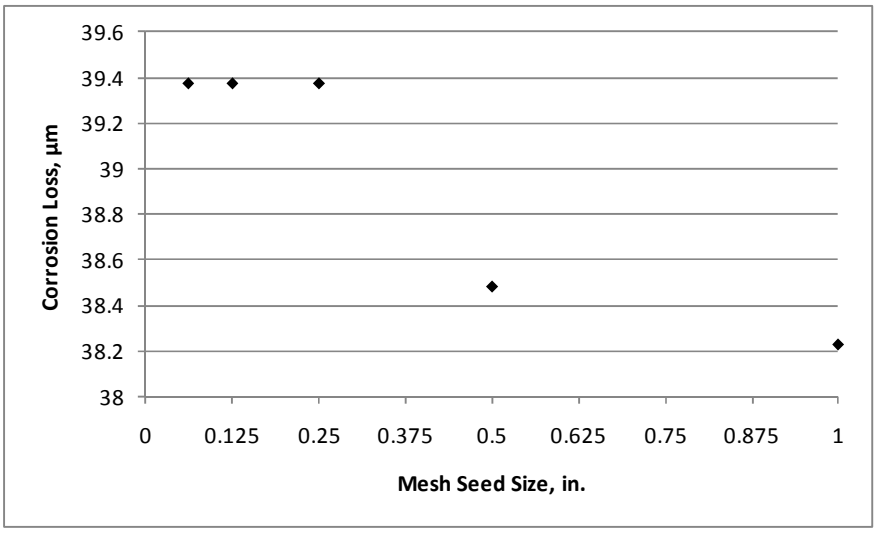

Figure 4.7: Effect of mesh seed size on corrosion loss required to produce a 50-µm crack.

To select the element type for the 3D model, a 3D sample model is analyzed using each for the four element choices provided by ABAQUS – hex, hex-dominated, tet, and wedge. The hex contains only hexagonal elements, the tet mesh uses only tetrahedral elements, and the wedge mesh uses only wedge (five-sided) elements. The hex-dominated mesh uses predominantly hexagonal elements, but will also use other elements as the program deems necessary. The mesh seed size for these models is 6.4 mm (0.25 in.). The corrosion loss required to produce a 50-µm (0.002-in.) wide crack for each element type is listed in Table 4.4. The values range from 64.2 to 65.4 µm. Since no significant difference in element types is observed, the default option (hex) is used. For most of the model, a 6.4-mm (0.25-in.) mesh seed size is used. However, in the central 51-mm (2-in.) region of the model, a 1.55-mm (0.06125-in.) mesh seed size is used to accommodate damage patterns with a 1.55-mm (0.06125-in.) width.

Table 4.4: Effect of 3D Element Type on Corrosion Loss.

Mesh Type	Corrosion Loss to Produce a 50-µm Crack, µm[a]
Hex	64.5
Hex-dominated	64.2
Wedge	64.8
Tet	65.4

[a] 1 µm = 0.0000394 in.

The 2D model is used to analyze uniform corrosion over the entire bar surface. For the 3D model, three damage patterns are analyzed for each combination of cover and bar diameter, as shown in Figure 4.8. The first damage pattern simulates corrosion along the entire circumference of the bar. Models with this damage pattern are designated FR (full ring corrosion pattern). The second damage pattern simulates corrosion along half the bar circumference and is designated HR. The third damage pattern simulates corrosion along one quarter of the bar circumference and is designated QR. The length

of the FR damage pattern along the bar ranges from 3.2 mm (0.125 in.) to 508 mm (20 in.). The length of the HR damage pattern along the bar ranges from 3.2 mm (0.125 in.) to 203 mm (8 in.), and the length of the QR damage pattern along the bar ranges from 1.6 mm (0.0625 in.) to 203 mm (8 in.).

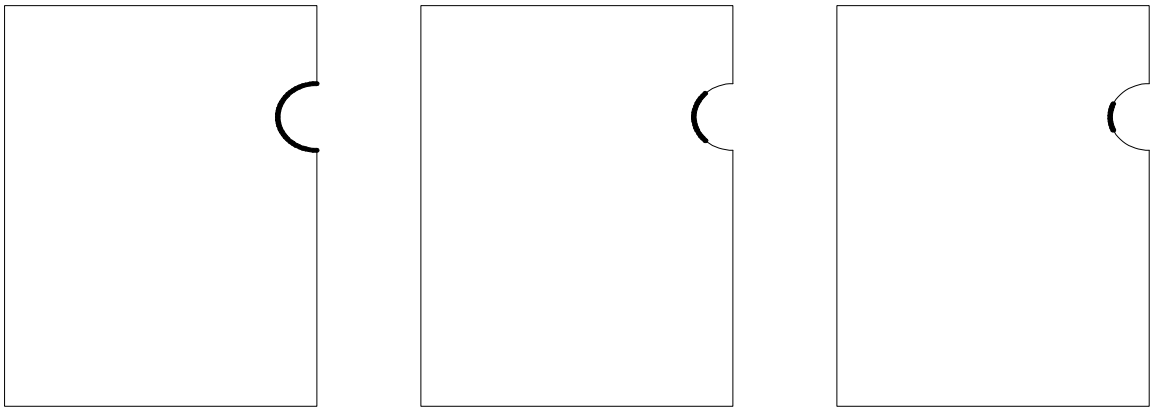

Figure 4.8: Bar damage patterns for three dimensional finite element models (cross section view). (a) Full ring (FR), (b) Half ring (HR), (c) Quarter ring (QR).

4.3 EXPERIMENTAL RESULTS

4.3.1 Conventional and Galvanized Reinforcement

The values of corrosion loss to initiate cracking for conventional and galvanized reinforcement are summarized in Table 4.5 and shown in Figure 4.9, with the standard deviation represented by error bars. The corrosion losses for individual specimens are presented in Tables F.1 through F.3 of Appendix F. For all concrete covers, galvanized reinforcement requires significantly greater corrosion losses to crack the concrete cover than conventional reinforcement. For 12.7-mm (0.5-in.) cover, conventional reinforcement requires an average corrosion loss of 10.6 µm to crack the concrete cover, compared to 45.9 µm for galvanized reinforcement. For 25.4-mm (1-in.) cover, conventional reinforcement requires an average corrosion loss of 22.4 µm to crack the

concrete cover, compared to 49.7 µm for galvanized reinforcement, and for 51-mm (2-in.) cover, conventional reinforcement requires an average corrosion loss of 29.7 µm to crack the concrete cover, compared to 68.0 µm for galvanized reinforcement. For conventional reinforcement, increasing the cover from 12.7 mm (0.5 in.) to 51 mm (2 in.) nearly triples the corrosion loss required to crack concrete from 10.6 µm to 29.7 µm, an increase of 19.1 µm. For galvanized reinforcement, the loss increases by 48 percent from 45.9 µm to 68.0 µm, an increase of 22.1 µm.

Table 4.5: Corrosion Loss Results for Specimens with Conventional and Galvanized Reinforcement

Corrosion Loss (µm) at:	Specimen					
	13 mm (0.5 in.) Cover		25 mm (1 in.) Cover		51 mm (2 in.) Cover	
	Conv.	Zn	Conv.	Zn	Conv.	Zn
Staining						
Average	6.73	35.44	18.91	42.11	28.83	87.11
SD[a]	2.63	15.63	9.54	9.07	2.84	-[b]
COV[c]	0.39	0.44	0.50	0.22	0.10	-[b]
Crack Initiation						
Average	10.55	45.92	22.44	49.70	29.72	62.00
SD	2.79	17.03	5.54	9.63	4.64	18.28
COV	0.26	0.37	0.25	0.19	0.16	0.29
0.25 mm (0.01 in.) Crack Width						
Average	23.22	64.48	38.75	66.01	36.91	68.66
SD	4.08	24.22	5.89	18.40	5.02	17.78
COV	0.18	0.38	0.15	0.28	0.14	0.26
0.33 mm (0.013 in.) Crack Width						
Average	34.14	81.63	46.09	91.02	48.90	81.80
SD	8.08	23.30	0.78	29.02	8.33	21.74
COV	0.24	0.29	0.02	0.32	0.17	0.27
0.41 mm (0.016 in.) Crack Width						
Average	53.68	99.40	53.75	117.86	60.75	105.72
SD	8.96	24.82	7.11	24.25	9.79	34.75
COV	0.17	0.25	0.13	0.21	0.16	0.33
0.51 mm (0.02 in.) Crack Width						
Average	73.00	120.35	75.66	153.11	74.67	132.68
SD	19.68	32.69	11.98	32.27	14.85	53.42
COV	0.27	0.27	0.16	0.21	0.20	0.40

[a] Standard deviation

[b] Only one specimen exhibited surface staining

[c] Coefficient of Variation

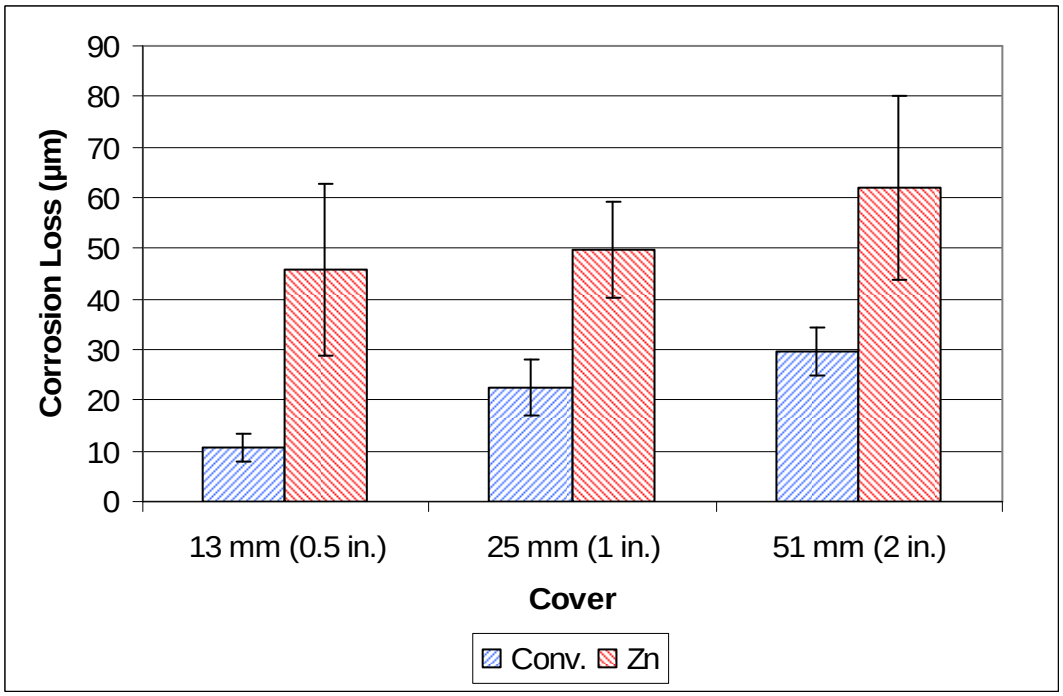

Figure 4.9: Average corrosion loss required to crack concrete (first visible surface crack) for specimens with conventional (Conv.) and galvanized (Zn) reinforcement.

Table 4.5 and Figure 4.10 show the corrosion losses at staining, crack initiation, and various stages of crack growth for the specimens. Figure 4.10 shows that along with the losses corresponding to crack initiation, the losses required to produce a given crack width are considerably higher for galvanized reinforcement than for conventional reinforcement. The slope of the corrosion loss vs. crack width line in Figure 4.10 is greater for galvanized reinforcement than for conventional reinforcement. For 25.4-mm (1-in.) cover, conventional reinforcement requires an additional average corrosion loss of 36.7 µm to increase the crack width from 0.25 mm (0.01 in.) (losses of 38.8 µm) to 0.51 mm (0.02 in.) (losses of 75.5 µm). For galvanized reinforcement, the additional corrosion loss is 87.1 µm to increase the crack width from 0.25 mm (0.01 in.) (losses of 66.0 µm) to 0.51 mm (0.02 in.) (losses of 153.1 µm).

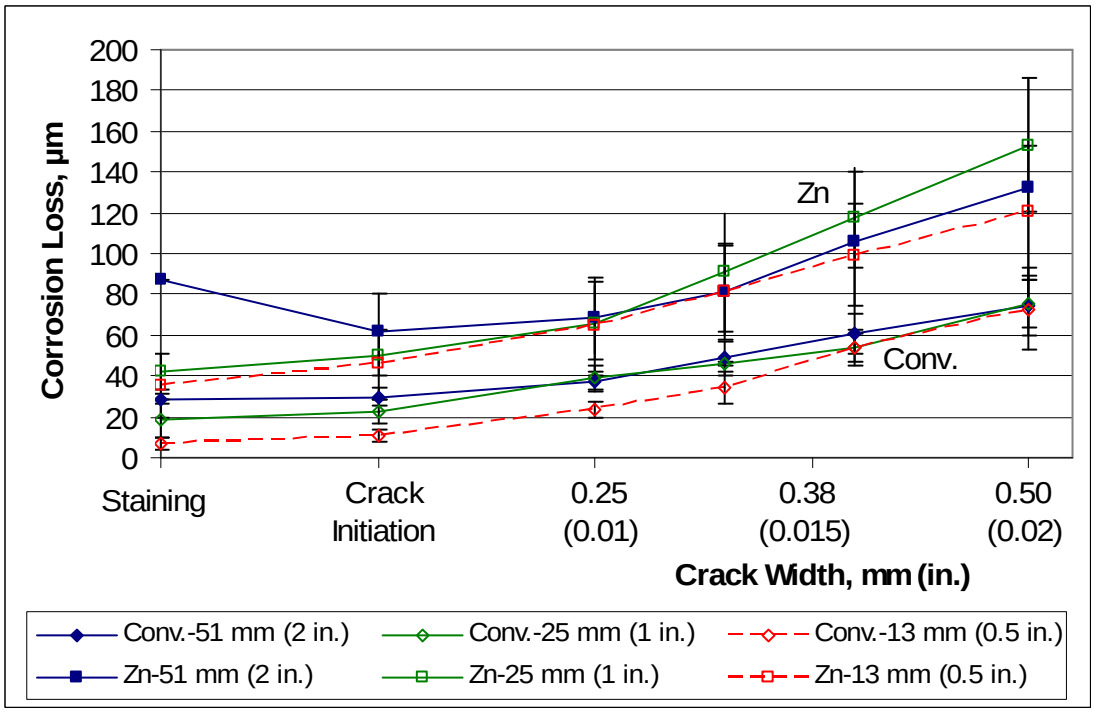

Figure 4.10: Average corrosion loss at staining, crack initiation, and at stages of crack growth. Standard deviation of all values given by error bars.

With the exception of three of the four specimens containing galvanized reinforcement with 51-mm (2-in.) cover, all specimens showed signs of staining on the upper surface of the concrete. Most specimens showed surface staining shortly before a visible crack was detected. The three specimens with galvanized reinforcement and 51-mm (2-in.) cover that did not show signs of surface staining did show staining in the concrete surrounding the bar when the specimens were autopsied. Stains on the upper surface of specimens containing either conventional (Figure 4.11) or galvanized reinforcement (Figure 4.12) were an orange-brown color, often with green or black near the center (Figure 4.11). The green-black staining turned orange with time. The similarities in corrosion products, coupled with the absence of zinc corrosion products on the surface, suggests that the staining and cracking observed for the galvanized reinforcement was ultimately due to corrosion of the underlying steel. This conclusion is also supported by observations of the bars (described next).

Figure 4.11: Specimen Conv.-1, 25-mm (1-in.) cover. Surface cracking and staining.

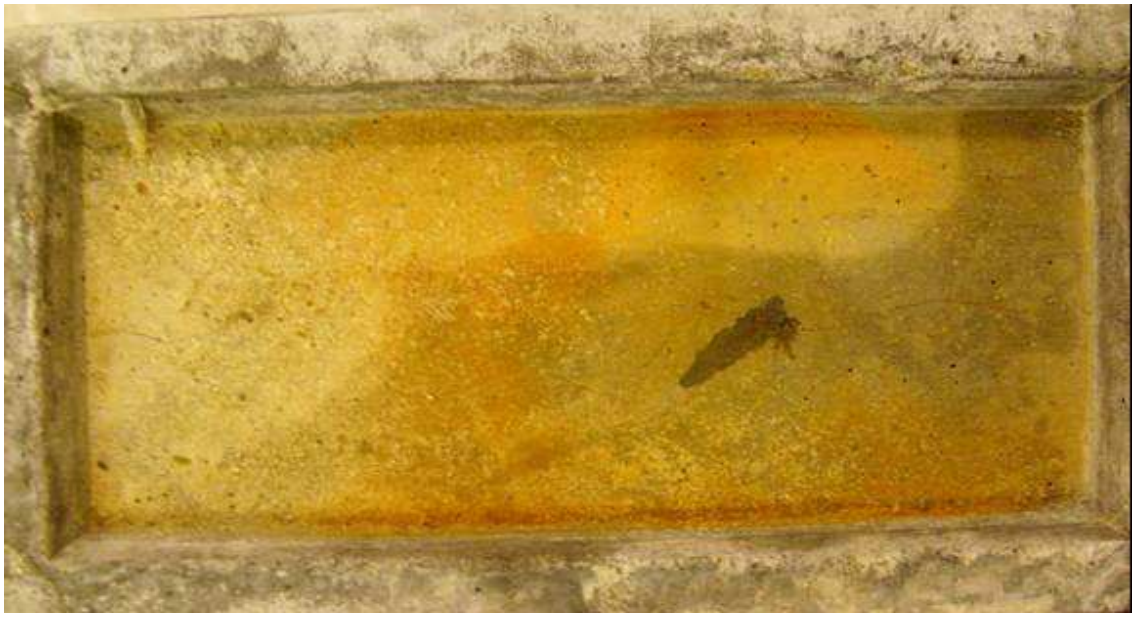

Figure 4.12: Specimen Zn-4, 25-mm (1-in.) cover. Surface cracking and staining.

Autopsy results from all specimens with conventional reinforcement show heavy corrosion losses over the entire bar surface (Figure 4.13). Staining is apparent in the concrete surrounding the reinforcement (Figure 4.14). Figure 4.14 shows a side view of the concrete around the reinforcement, split along the plane of the crack. Orange

corrosion products are visible in regions where the staining reached the surface. Greenish-black corrosion products are visible in regions isolated from the atmosphere (Figure 4.15). All photos were taken immediately after autopsy.

(a)

(b)

Figure 4.13: Specimen Conv.-3, 51-mm (2-in.) cover. Test bar after autopsy. (a) Top side. (b) Bottom side. Photos taken immediately after autopsy.

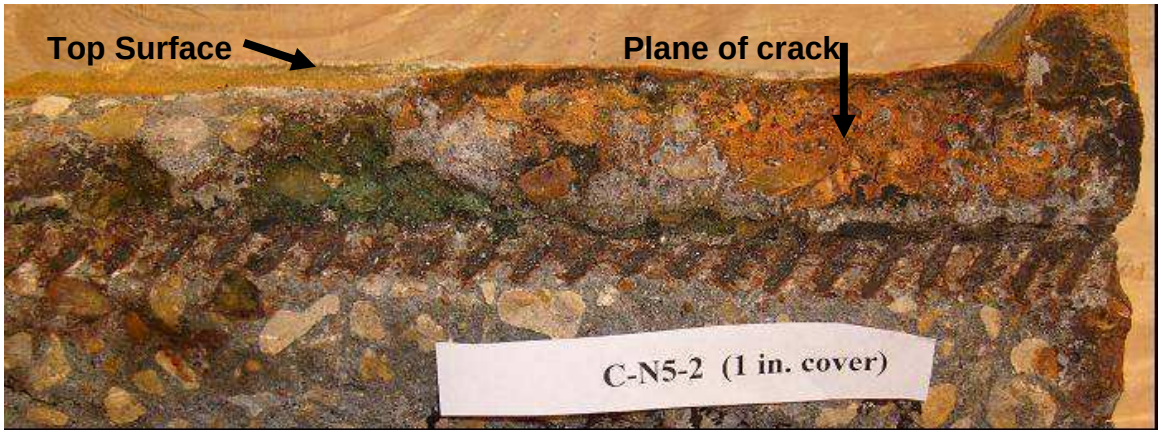

Figure 4.14: Specimen Conv.-2, 25-mm (1-in.) cover. Side view; plane of crack visible above reinforcement. Photos taken immediately after autopsy.

Figure 4.15: Specimen Conv.-2, 25-mm (1-in.) cover. Top view; concrete at the depth of reinforcement. Photos taken immediately after autopsy.

The autopsy found that galvanized reinforcement exhibits signs of pitting corrosion. Some regions of the test bar exhibit heavy corrosion products, while in other sections, the galvanized coating is untouched (Figure 4.16). Most of the uncorroded regions are located on the top face of the bar, a result of the bottom side of the bar having more even exposure to the ions migrating from the bottom bars. Measurements with a coating thickness gauge show no significant loss in the areas that appear uncorroded. Visual estimations of uncorroded surface areas were performed on all bars after autopsy – results appear in Table 4.6. The bars with 12.7-mm (0.5-in.) cover show the greatest average uncorroded area, 29 percent, likely due to the decreased cover interfering with ion transport to the top side of the bar. The bars with 25.4-mm (1-in.) and 51-mm (2-in.) cover show average uncorroded areas of 6 and 13 percent, respectively. The corrosion products on the concrete surrounding the galvanized reinforcement resemble those seen in specimens with conventional reinforcement (Figure 4.17, Figure 4.18), indicating that the bulk of corrosion products applying pressure to the surrounding concrete are corrosion products of iron and not those of zinc.

(a)

(b)

Figure 4.16: Specimen Zn-2, 25 mm (1 in.) cover. Test bar after autopsy. (a) Top side. (b) Bottom side. Photos taken immediately after autopsy.

Table 4.6: Estimated Uncorroded Surface Area of Galvanized Reinforcement

Specimen	Estimated Uncorroded Area		
	Cover		
	12.7 mm (0.5 in.)	25 mm (1 in.)	51 mm (2 in.)
Zn-1	30%	8%	5%
Zn-2	30%	5%	10%
Zn-3	40%	5%	50%
Zn-4	15%	5%	30%
Average:	**29%**	**6%**	**13%**

Figure 4.17: Specimen Zn-4, 25 mm (1 in.) cover. Side view; plane of crack visible above reinforcement. Photos taken immediately after autopsy.

Figure 4.18: Specimen Zn-4, 25 mm (1 in.) cover. Top view; specimen split at depth of reinforcement. Photos taken immediately after autopsy.

To determine if the pitting observed on galvanized reinforcement is also present at crack initiation, two additional specimens with galvanized reinforcement and 25.4-mm (1-in.) cover were cast and autopsied at the onset of cracking. Greenish-black corrosion products were visible along the crack at the upper surface of the specimens (Figure 4.19); the corrosion products turned orange about 2 hours after exposure to air. The autopsy reveals pitting (Figure 4.20a) and localized corrosion (Figure 4.20b) on the bars similar to that observed in the specimens autopsied after the crack had propagated and widened. As discussed earlier, uncorroded regions were more common on the top (Figure 4.20a) than the bottom side of the test bar (Figure 4.20c). These results suggest that cracking of the concrete due to corrosion of the galvanized reinforcement did not result due to the buildup of zinc corrosion products but rather due to the formation of corrosion products from the intermetallic steel-zinc layers or from the underlying steel.

Figure 4.19: Galvanized reinforcement, 25 mm (1 in.) cover. Staining on surface at crack initiation.

(a)

(b)

(c)

Figure 4.20: Galvanized reinforcement, 25 mm (1 in.) cover. Test bar after autopsy at crack initiation. (a) Top side. (b) Detail of top side. (c) Bottom side. Photos taken immediately after autopsy.

4.3.2 Epoxy-Coated Reinforcement

The corrosion losses required to crack concrete cover for specimens containing damaged epoxy-coated reinforcement are shown in Table 4.7. The losses are presented based on both the total area of the bar and the damaged (exposed) area in the epoxy. The bars with two half-rings have a nominal exposed area ten times greater than do the bars

with two holes in the epoxy; however, autopsy results reveal significant blistering on bars with holes in the epoxy (Figure 4.21). Blistering is also present on the bars with the half-rings, but is less severe and exposes less than the area exposed by the rings. Table 4.6 reflects an estimate of the increased exposed area from the blistered regions for all specimens. Ignoring the blistered regions, specimens with two half-rings have an exposed area of 150.8 mm^2 (0.234 $in.^2$) and specimens with two holes have an exposed area of 15.8 mm^2 (0.024 $in.^2$).

Table 4.7 shows no significant difference in the corrosion loss required to crack the concrete cover between the specimens with the damage pattern oriented horizontally or vertically. The corrosion losses on both the total and exposed areas indicate that the corrosion loss required to crack the concrete cover increases as exposed area decreases. Based on total and exposed area including blisters, the specimens with two holes in the epoxy require somewhat less than twice the corrosion loss to crack the concrete cover as the specimens with two half-rings in the epoxy.

Table 4.7: Average Corrosion Loss to Crack Concrete Cover for Specimens with Epoxy-Coated Reinforcement

Specimen	Exposed Area (Including Blisters), mm^2 ($in.^2$)	Corrosion Loss Based on Total Area (µm)	Corrosion Loss Based on Exposed Area (µm)
ECR-2 hole damage pattern			
ECR-2h-H-1	188.3 (0.292)	10.14	730
ECR-2h-H-2	233.5 (0.362)	10.10	587
	ECR-2h-H Avg.	**10.12**	**659**
ECR-2h-V-1	181.8 (0.282)	11.67	874
ECR-2h-V-2	201.1 (0.312)	7.58	510
	ECR-2h-V Avg.	**9.70**	**692**
ECR-2 ring damage pattern			
ECR-2r-H-1	208.9 (0.324)	6.07	421
ECR-2r-H-2	234 (0.363)	5.87	363
	ECR-2r-H Avg.	**5.97**	**392**
ECR-2r-V-1	254 (0.394)	6.22	354
ECR-2r-V-2	208.9 (0.324)	6.15	426
	ECR-2r-V Avg.	**6.18**	**390**

Figure 4.21: Test bar from specimen ECR-2h-V-2

Figure 4.22 shows a specimen at crack initiation. Figure 4.23 shows a specimen with the crack spanning the length of the specimen. No specimens containing epoxy-coated reinforcement showed signs of surface staining during the test. After testing, however, staining is observed on the concrete surrounding the damaged regions in the epoxy when the specimens are autopsied (Figures 4.24 and 4.25).

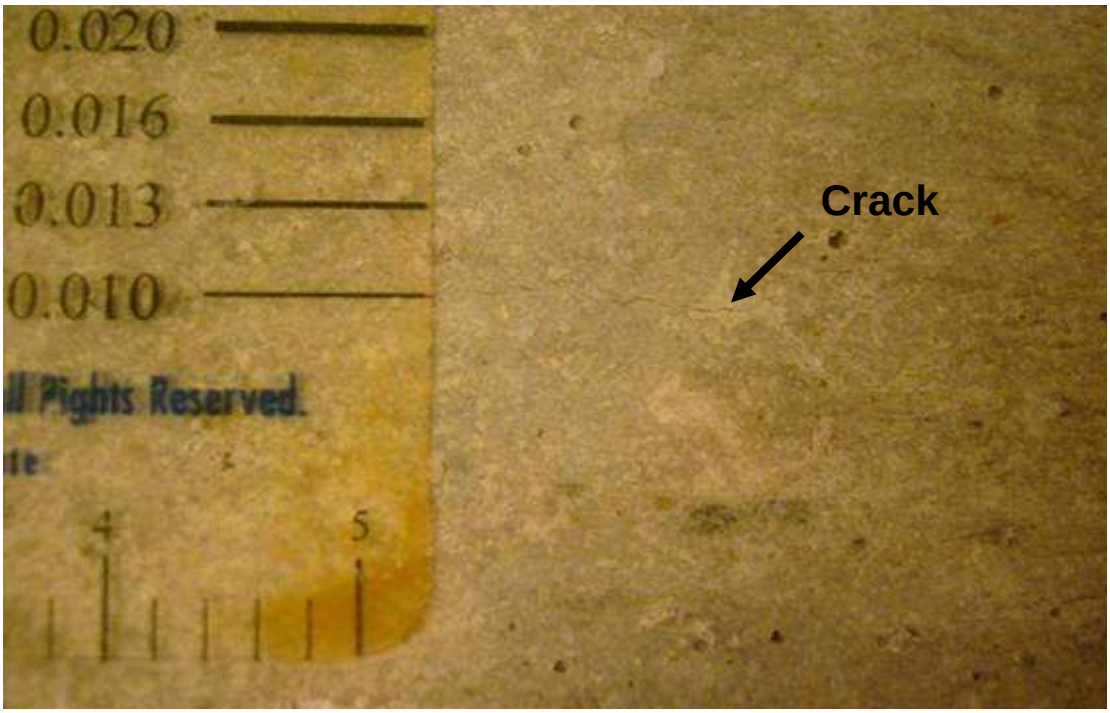

Figure 4.22: Crack initiation. Specimen ECR-2r-H-2.

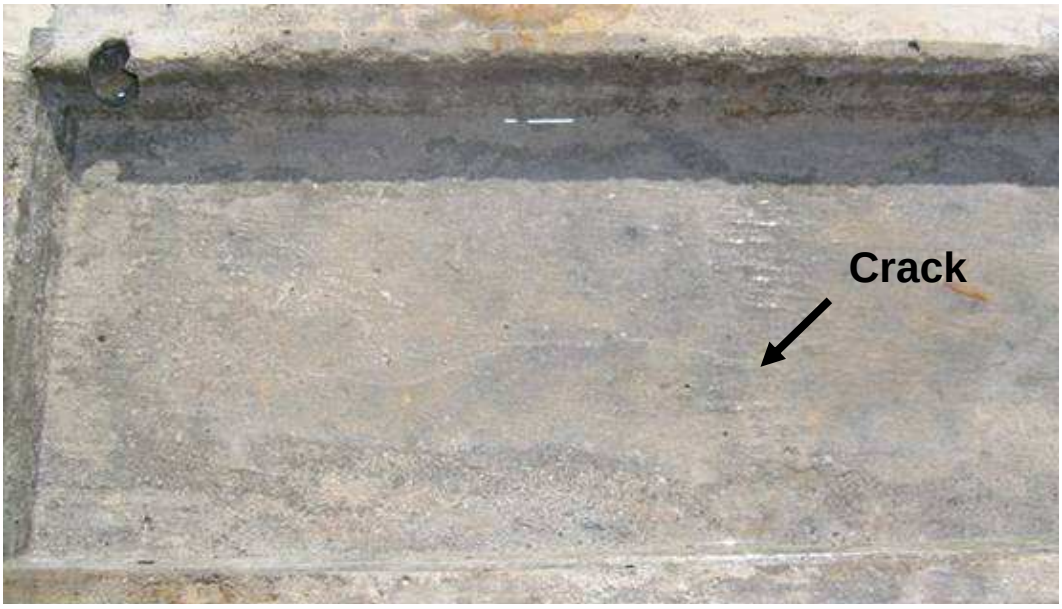

Figure 4.23: Crack propagation. Specimen ECR-2H-V-1.

Figure 4.24: Concrete surrounding test bar from specimen 2h-V-1.

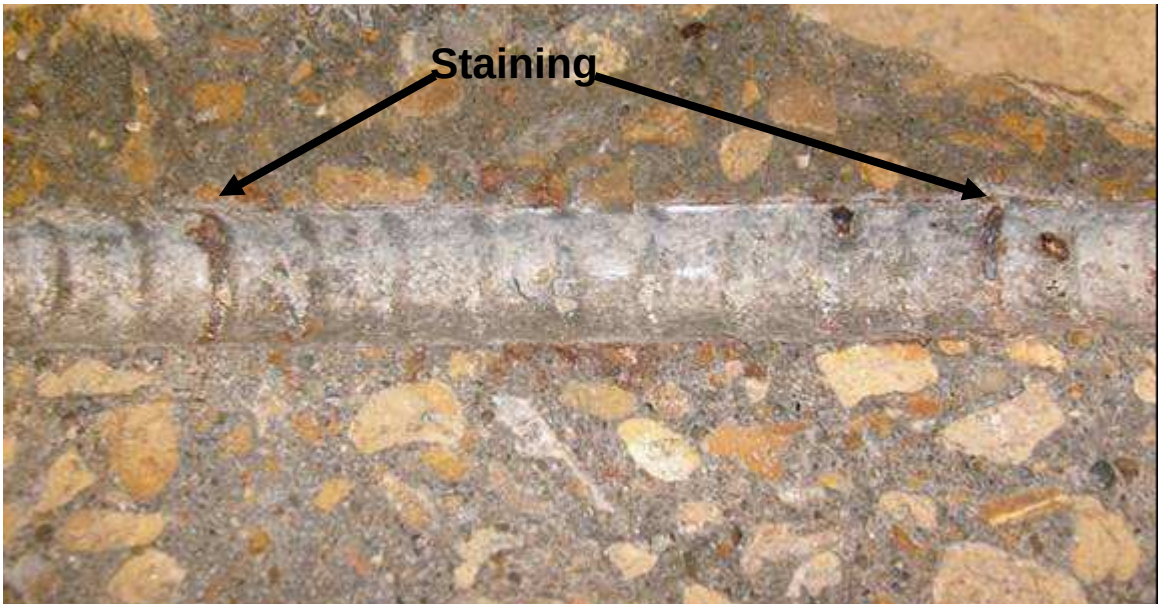

Figure 4.25: Concrete surrounding test bar from specimen 2r-H-2.

4.4 FINITE ELEMENT RESULTS

The corrosion losses that cause a 50-µm (0.002-in.) wide crack to form at the surface of the specimen based on the two-dimensional (2D) finite element analyses are shown in Table 4.8. The corrosion losses are plotted as a function of concrete cover in Figure 4.26. The results suggest a linear relationship [for covers between 6 and 102 mm (0.25 and 4 in.)] between concrete cover and corrosion loss required to cause cracking. A slight dependence on bar diameter is also noted; Figure 4.27 shows best-fit lines for each of the three bar diameters over the range of covers from 19 to 76 mm (0.75 to 3 in.). Figure 4.27 shows that as cover increases, bars with smaller diameters require greater corrosion losses to crack concrete than bars with larger diameters. An analysis of the data suggests Equation (4.2a) as a best fit expression. The metric equivalent is presented as Equation (4.2b).

$$x_{crit} = 0.53\left(\frac{C}{D^{0.38}} + 1\right) \tag{4.2a}$$

where

x_{crit} = corrosion loss at crack initiation, mil

C = cover, in.

D = bar diameter, in.

$$x_{crit} = 1.8\left(\frac{C}{D^{0.38}} + 7.5\right) \tag{4.2b}$$

where

x_{crit} = corrosion loss at crack initiation, μm

C = cover, mm.

D = bar diameter, mm.

Table 4.8: Finite Element Results-2D model

Cover, mm (in.)	Bar Diameter, mm (in.)	Corrosion Loss to Crack Concrete*, μm
6.4 (0.25)	12.7 (0.5)	19.7
13 (0.5)	12.7 (0.5)	20.3
25 (1)	12.7 (0.5)	26.0
38 (1.5)	12.7 (0.5)	35.6
51 (2)	12.7 (0.5)	45.1
76 (3)	12.7 (0.5)	56.5
9.5 (0.375)	19 (0.75)	19.7
19 (0.75)	19 (0.75)	25.4
38 (1.5)	19 (0.75)	33.7
57 (2.25)	19 (0.75)	45.1
76 (3)	19 (0.75)	56.5
13 (0.5)	25.4 (1)	20.3
25 (1)	25.4 (1)	26.7
51 (2)	25.4 (1)	40.6
76 (3)	25.4 (1)	51.1
102 (4)	25.4 (1)	76.2

*50-μm (0.002-in.) crack width

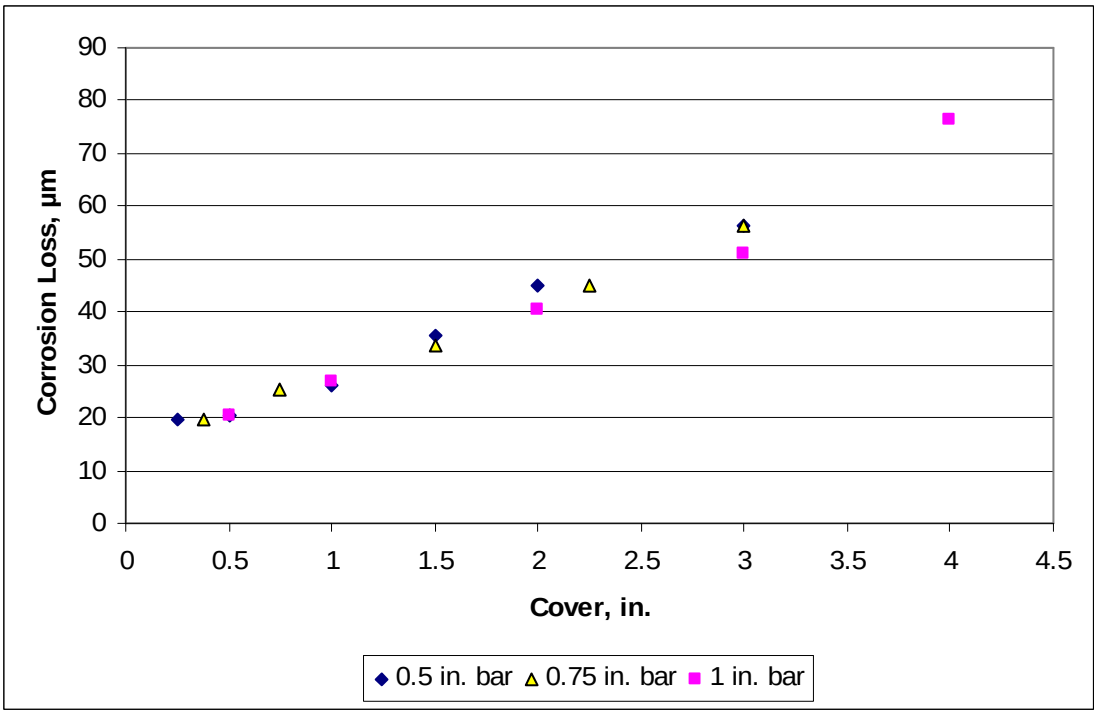

Figure 4.26: Corrosion loss to crack concrete versus cover. 2D FEA model.

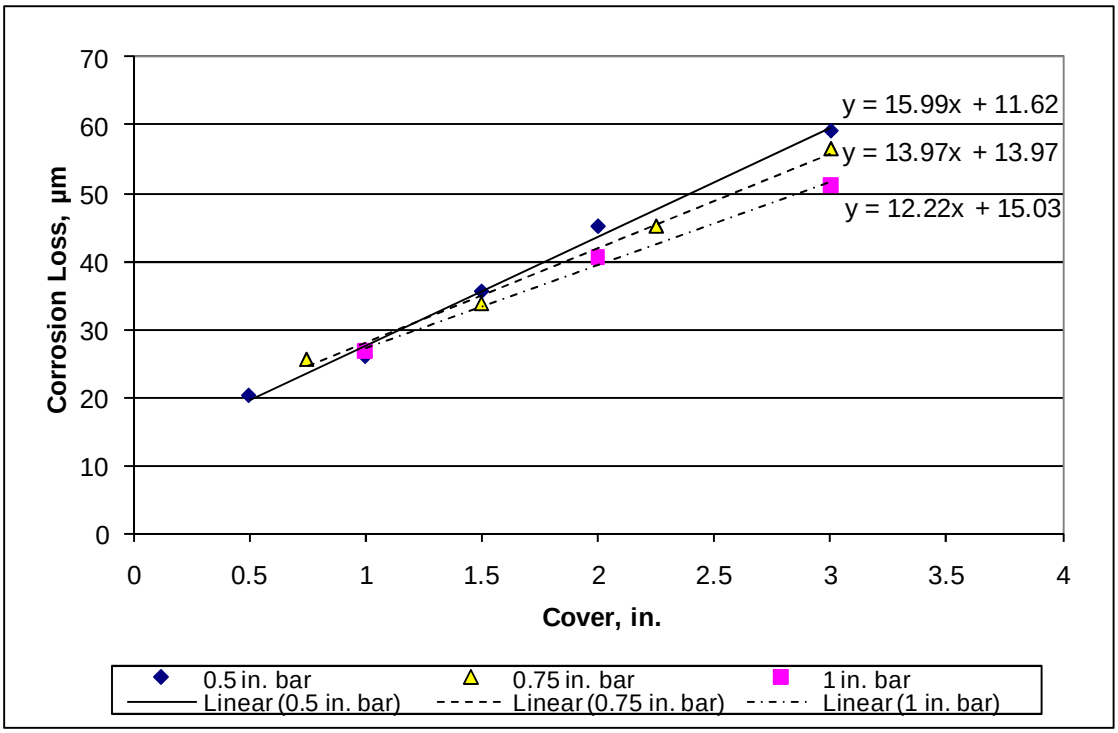

Figure 4.27: Corrosion loss to crack concrete versus cover showing effect of bar diameter. 2D FEA model.

To verify the accuracy of the 2D finite element model, the results obtained from the model are compared with the experimental results presented in Section 4.3.1 along with experimental results obtained by Saeki et al. (1988), Rasheeduzzafar et al. (1992), Alonso et al. (1998), and Torres-Acosta and Sagues (2004) for corrosion along the full length of conventional reinforcement. The data from these sources are shown in Table 4.9. The experimental data are plotted along with the finite element results in Figure 4.28. Data presented in Section 4.3.1 are labeled "KU"; other data are identified by the first author. A best-fit line for the results from the finite element model is also shown. While there is much scatter in the experimental data, the corrosion loss required to crack concrete, as predicted by the finite element model, provides an excellent representation of the bulk of the experimental data.

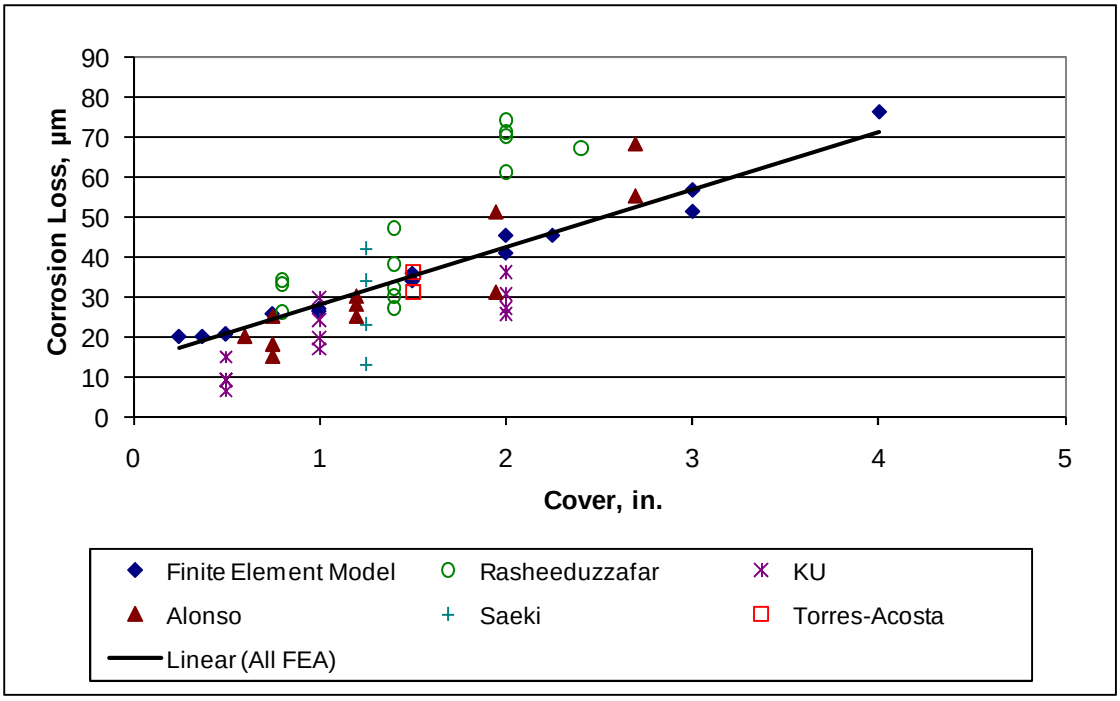

Figure 4.28: Corrosion loss to crack concrete versus cover. 2D finite element model (FEM) with experimental data.

Table 4.9: Corrosion Loss to Crack Concrete-Results from Other Research. Corrosion along Entire Bar Length.

	Cover, mm (in.)	Diameter, mm (in.)	Corrosion Loss, µm
Torres-Acosta and Sagues (2004)	39 (1.5)	13 (0.5)	35.9
	39 (1.5)	13 (0.5)	31.1
Alonso et al. (1998)	20 (0.75)	16 (0.63))	15
	15 (0.6)	8 (0.31)	20
	30 (1.2)	16 (0.63)	25
	30 (1.2)	16 (0.63)	28
	30 (1.2)	16 (0.63)	30
	50 (2)	16 (0.63)	31
	50 (2)	12 (0.47)	51
	70 (2.7)	16 (0.63)	55
	70 (2.7)	10 (0.39)	68
	20 (0.75)	16 (0.63)	25
	20 (0.75)	16 (0.63)	18
Rasheeduzzafar et al. (1992)	19 (0.75)	13 (0.5)	33
	19 (0.75)	13 (0.5)	26
	19 (0.75)	13 (0.5)	34
	38 (1.5)	13 (0.5)	32
	38 (1.5)	13 (0.5)	30
	38 (1.5)	13 (0.5)	47
	38 (1.5)	13 (0.5)	38
	38 (1.5)	13 (0.5)	27
	38 (1.5)	13 (0.5)	27
	50 (2)	13 (0.5)	70
	50 (2)	13 (0.5)	71
	50 (2)	13 (0.5)	74
	50 (2)	13 (0.5)	61
	60 (2.4)	13 (0.5)	67
Saeki et al. (1988)	31.75 (1.25)	9.5 (0.375)	42
	31.75 (1.25)	12.7 (0.5)	34
	31.75 (1.25)	19 (0.75)	23
	31.75 (1.25)	25 (1)	13

To determine the accuracy of Eq. (4.2), the results predicted by Eq. (4.2) are compared with experimental results and finite element model results in Figure 4.29. The proposed equation [Eq. (4.2)] overestimates the corrosion loss required to crack concrete for most cases in which the actual corrosion loss required to crack the concrete is less than 45 µm. An alternate equation is proposed [Eq.(4.3)] that provides a somewhat more conservative estimate of the corrosion loss required to crack concrete (Figure 4.30).

$$x_{crit} = 0.53\left(\frac{C}{D^{0.38}} + 0.6\right) \tag{4.3a}$$

where

x_{crit} = corrosion loss at crack initiation, mil

C = cover, in.

D = bar diameter, in.

$$x_{crit} = 1.8\left(\frac{C}{D^{0.38}} + 4.5\right) \tag{4.3b}$$

where

x_{crit} = corrosion loss at crack initiation, μm

C = cover, mm.

D = bar diameter, mm.

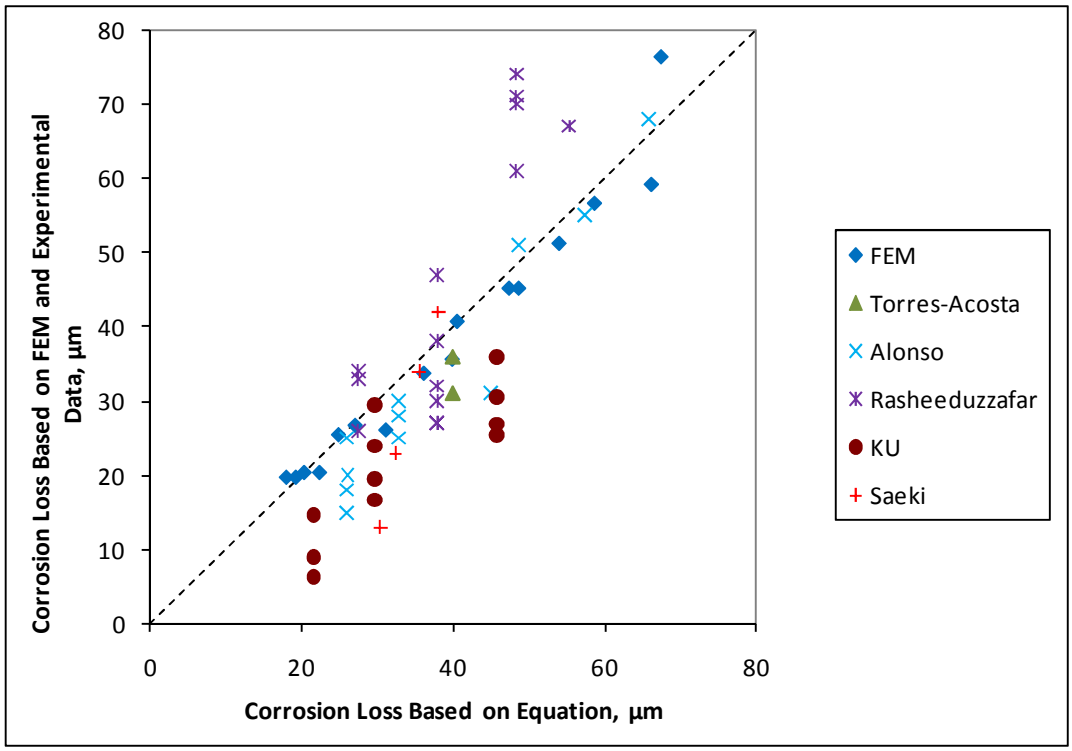

Figure 4.29: Corrosion loss to crack concrete for uniform general corrosion based on experimental and FEM results versus corrosion losses predicted by Eq. (4.2).

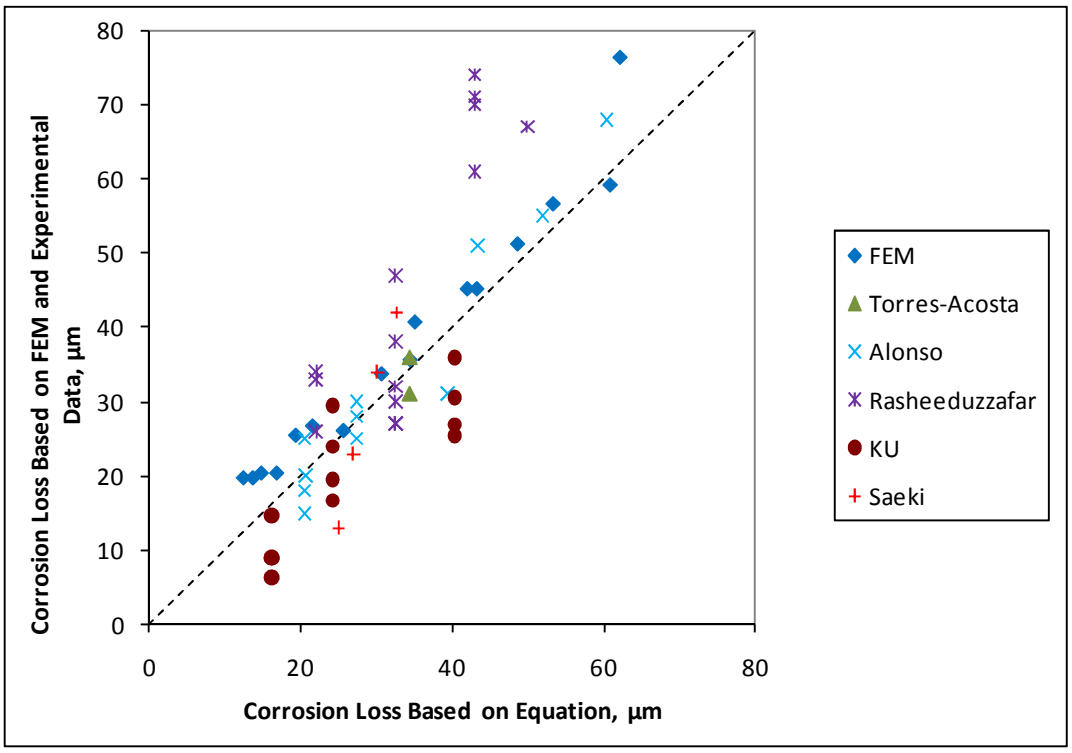

Figure 4.30: Corrosion loss to crack concrete for uniform general corrosion based on experimental and FEM results versus corrosion losses predicted by Eq. (4.3).

The corrosion losses to cause cracking based on the three-dimensional (3D) finite element model are shown in Tables 4.10 and 4.11. The models with 51-mm (2-in.) cover and a 203-mm (8-in.) and 508-mm (20-in.) length of bar corroding show similar corrosion losses at crack initiation. The behavior of the 3D FEM under full bar length [508-mm (20-in.)] corrosion is compared to the 2D FEM in Figure 4.31. The corrosion losses to cause cracking obtained from these models are similar. All models show a difference in corrosion loss to crack concrete between 2D and 3D models of less than 1 µm, with the exception of models with a 25.4-mm (1-in.) diameter bar and 76-mm (3-in.) cover, which shows a 2.9 µm difference in corrosion loss to cause cracking between the 2D and 3D models, a 5.7 percent difference.

Table 4.10: Finite Element Results-3D model, 51 mm (2 in.) cover

Corrosion Pattern	12.7 mm (0.5 in.) Bar Diameter		19 mm (0.75 in.) Bar Diameter		25 mm (1 in.) Bar Diameter	
	Exposed Area, mm^2 ($in.^2$)	Corrosion Loss at Cracking, µm	Exposed Area, mm^2 ($in.^2$)	Corrosion Loss at Cracking, µm	Exposed Area, mm^2 ($in.^2$)	Corrosion Loss at Cracking, µm
Full Ring						
508 mm (20 in.) Length	10134 (15.7)	46	15201 (23.6)	43	20268 (31.4)	40
203 mm (8 in.) Length	4054 (6.28)	57	6080 (9.42)	44	8107 (12.6)	41
102 mm (4 in.) Length	2027 (3.14)	79	3040 (4.71)	57	4054 (6.28)	56
51 mm (2 in.) Length	1013 (1.57)	159	1520 (2.36)	133	2027 (3.14)	80
25 mm (1 in.) Length	507 (0.785)	330	760 (1.18)	254	1013 (1.57)	144
12.7 mm (0.5 in.) Length	253 (0.392)	483	380 (0.589)	381	507 (0.785)	281
6.4 mm (0.25 in.) Length	127 (0.196)	659	190 (0.295)	508	253 (0.392)	361
3.2 mm (0.125 in.) Length	63.3 (0.098)	851	95 (0.147)	658	127 (0.196)	502
Half Ring						
102 mm (4 in.) Length	1013 (1.57)	178	1520 (2.36)	152	2027 (3.14)	88
51 mm (2 in.) Length	507 (0.785)	273	760 (1.18)	229	1013 (1.57)	150
25 mm (1 in.) Length	253 (0.392)	425	380 (0.589)	347	507 (0.785)	279
12.7 mm (0.5 in.) Length	127 (0.196)	635	190 (0.295)	502	253 (0.392)	418
6.4 mm (0.25 in.) Length	63.3 (0.098)	904	95.0 (0.147)	704	127 (0.196)	572
3.2 mm (0.125 in.) Length	31.7 (0.049)	1228	47.5 (0.074)	973	63.3 (0.098)	784
Quarter Ring						
102 mm (4 in.) Length	507 (0.785)	216	760 (1.18)	191	1013 (1.57)	170
51 mm (2 in.) Length	253 (0.392)	337	380 (0.589)	292	507 (0.785)	259
25 mm (1 in.) Length	127 (0.196)	546	190 (0.295)	470	253 (0.392)	404
12.7 mm (0.5 in.) Length	63.3 (0.098)	861	95.0 (0.147)	737	127 (0.196)	622
6.4 mm (0.25 in.) Length	31.7 (0.049)	1293	47.5 (0.074)	1090	63.3 (0.098)	890
3.2 mm (0.125 in.) Length	15.8 (0.025)	1969	23.8 (0.037)	1562	31.7 (0.049)	1226
1.6 mm (0.0625 in.) Length	7.9 (0.012)	2654	11.8 (0.018)	2223	15.8 (0.025)	1930

Table 4.11: Finite Element Results-3D model, 76 mm (3 in.) cover

Corrosion Pattern	12.7 mm (0.5 in.) Bar Diameter		19 mm (0.75 in.) Bar Diameter		25 mm (1 in.) Bar Diameter	
	Exposed Area, mm^2 ($in.^2$)	Corrosion Loss at Cracking, µm	Exposed Area, mm^2 ($in.^2$)	Corrosion Loss at Cracking, µm	Exposed Area, mm^2 ($in.^2$)	Corrosion Loss at Cracking, µm
Full Ring						
508 mm (20 in.) Length	10134 (15.7)	57	15201 (23.6)	56	20268 (31.4)	54
203 mm (8 in.) Length	4054 (6.28)	102	6080 (9.42)	152	8107 (12.6)	83
102 mm (4 in.) Length	2027 (3.14)	216	3040 (4.71)	267	4054 (6.28)	108
51 mm (2 in.) Length	1013 (1.57)	445	1520 (2.36)	406	2027 (3.14)	267
25 mm (1 in.) Length	507 (0.785)	660	760 (1.18)	584	1013 (1.57)	446
12.7 mm (0.5 in.) Length	253 (0.392)	927	380 (0.589)	813	507 (0.785)	611
6.4 mm (0.25 in.) Length	127 (0.196)	1295	190 (0.295)	1067	253 (0.392)	853
3.2 mm (0.125 in.) Length	63.3 (0.098)	1689	95 (0.147)	1321	127 (0.196)	1116
Half Ring						
102 mm (4 in.) Length	1013 (1.57)	368	1520 (2.36)	356	2027 (3.14)	328
51 mm (2 in.) Length	507 (0.785)	559	760 (1.18)	521	1013 (1.57)	483
25 mm (1 in.) Length	253 (0.392)	838	380 (0.589)	762	507 (0.785)	693
12.7 mm (0.5 in.) Length	127 (0.196)	1219	190 (0.295)	1118	253 (0.392)	968
6.4 mm (0.25 in.) Length	63.3 (0.098)	1676	95.0 (0.147)	1461	127 (0.196)	1283
3.2 mm (0.125 in.) Length	31.7 (0.049)	2261	47.5 (0.074)	1842	63.3 (0.098)	1689
Quarter Ring						
102 mm (4 in.) Length	507 (0.785)	508	760 (1.18)	445	1013 (1.57)	394
51 mm (2 in.) Length	253 (0.392)	737	380 (0.589)	622	507 (0.785)	610
25 mm (1 in.) Length	127 (0.196)	1067	190 (0.295)	927	253 (0.392)	902
12.7 mm (0.5 in.) Length	63.3 (0.098)	1626	95.0 (0.147)	1308	127 (0.196)	1270
6.4 mm (0.25 in.) Length	31.7 (0.049)	2350	47.5 (0.074)	1791	63.3 (0.098)	1702
3.2 mm (0.125 in.) Length	15.8 (0.025)	3226	23.8 (0.037)	2502	31.7 (0.049)	2273
1.6 mm (0.0625 in.) Length	7.9 (0.012)	4343	11.8 (0.018)	3543	15.8 (0.025)	3226

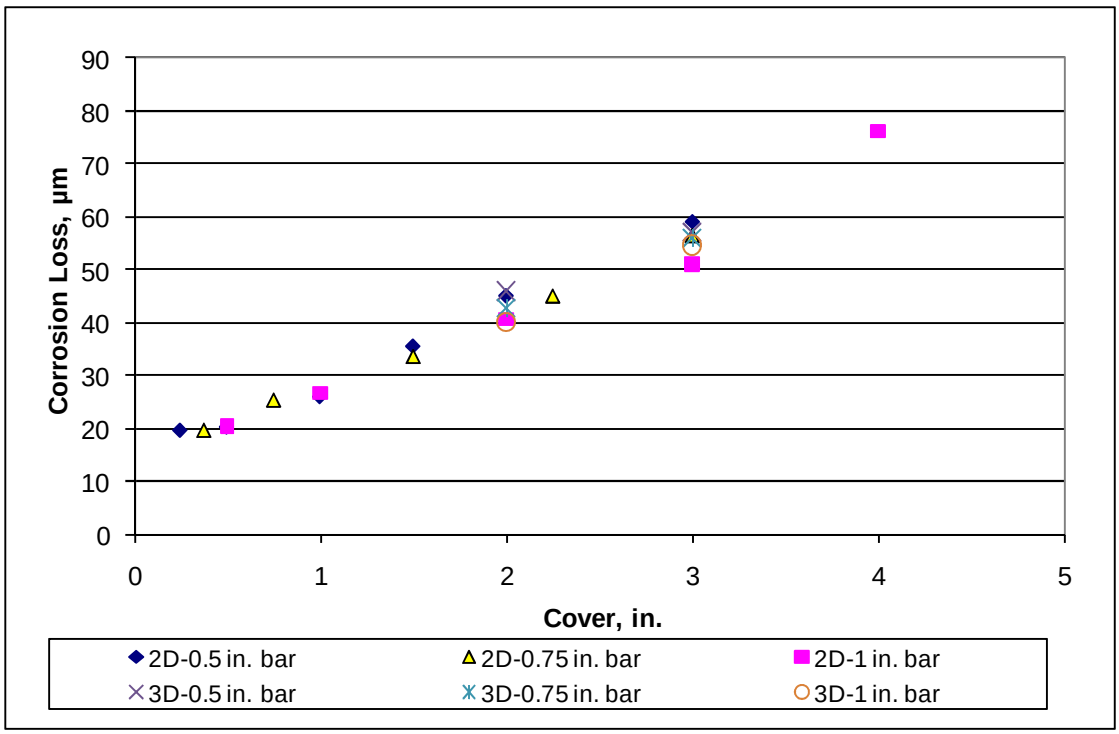

Figure 4.31: Corrosion loss to crack concrete for uniform general corrosion versus cover. 2D and 3D FEM.

The number of variables studied in the 3D FEM make plotting all data points on a single plot impractical. Instead, data subsets holding as many variables constant as possible are analyzed to determine the effect of a variable on the corrosion loss required to crack concrete. Furthermore, corroding area, bar diameter, length of corroding region, and damage pattern are not independent variables – specifying any three variables restricts the fourth to a single value. For this analysis, the effect of cover, bar diameter, corroding area, and corroding length are analyzed with the goal of creating an equation that reduces to Eq. (4.3) in the case of general corrosion. Corroding area will be expressed as a fraction of the total area of the bar, A_f ($A_f = A_{corroding}/A_{bar}$).

The corrosion loss to crack concrete is plotted versus exposed area for a 12.7-mm (0.5-in.) diameter bar with 51-mm (2-in.) cover in Figure 4.32. A line of the form Ax^b is fit to the data. Table 4.12 summarizes the values of A and b for all 3D finite element

models. Based on Table 4.12, it may be reasonably assumed the constant *b* is equal to –0.6, while the constant *A* is dependent on other variables.

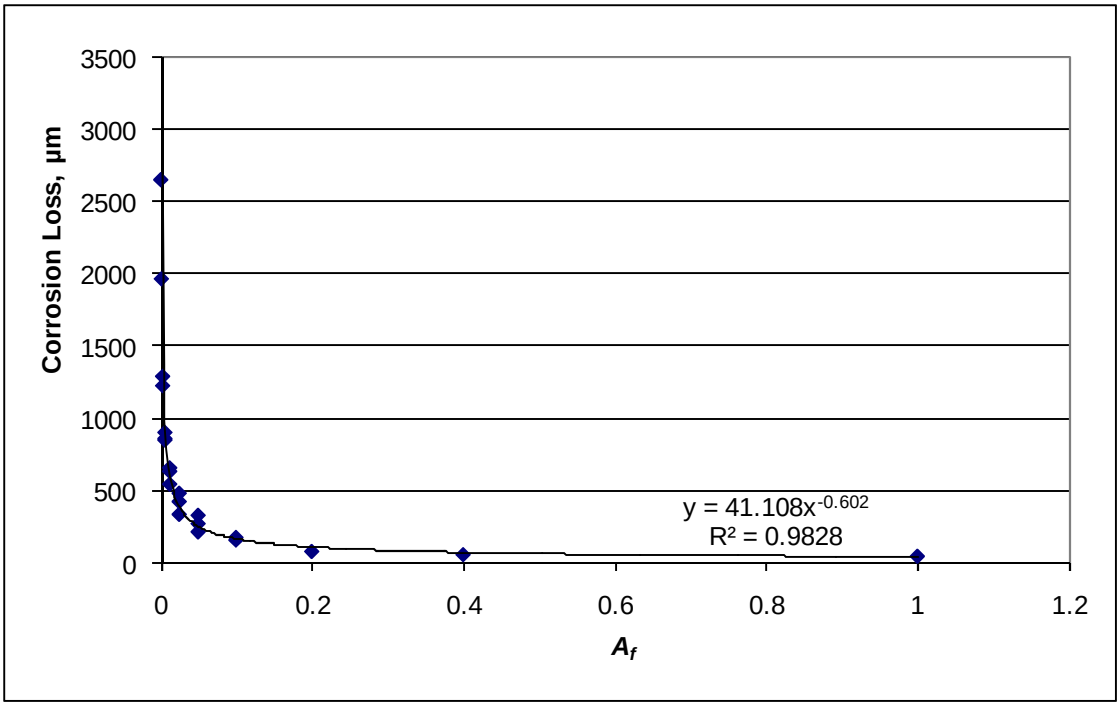

Figure 4.32: Corrosion loss to crack concrete versus fraction of exposed area A_f with best-fit line. 12.7-mm (0.5-in.) diameter bar, 51-mm (2-in.) cover.

Table 4.12: Constants *A* and *b* for best-fit line Ax^b to Corrosion Loss versus A_f plots.

Bar Diameter, mm (in.)	Cover, mm (in.)	*A*	*b*
12.7 (0.5)	51 (2)	41.11	-0.602
19 (0.75)	51 (2)	34.20	-0.597
25.4 (1)	51 (2)	26.60	-0.600
12.7 (0.5)	76 (3)	85.11	-0.587
19 (0.75)	76 (3)	78.97	-0.592
25.4 (1)	76 (3)	60.65	-0.589

Figure 4.33 shows the relationship between corrosion loss and cover for all bars with a corroding area of 1013 mm^2 (1.57 in.^{2}). Similar plots are analyzed for other exposed areas. For bars with a fixed damage pattern and diameter, increasing the cover from 51 to 76 mm (2 to 3 in.) approximately doubles the corrosion loss required to crack concrete. This suggests that for localized corrosion, the corrosion loss required to crack

concrete is proportional to cover squared. For larger corroding areas, the relationship between corrosion loss and cover becomes linear, as shown in Eqs. (4.2) and (4.3).

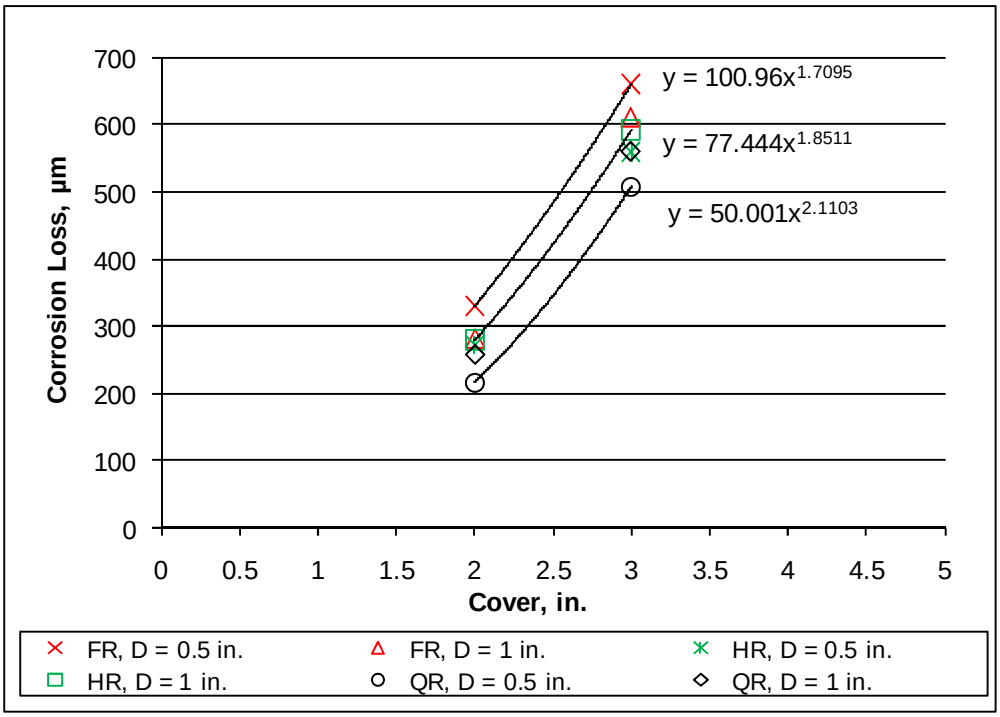

Figure 4.33: Corrosion loss to crack concrete versus cover. 1013-mm^2 (1.57-in.^{2}) corroding area. Corrosion loss = y, cover = x.

Figure 4.34 shows the relationship between corrosion loss and fractional corroding length L_f ($L_f = L_{corroding}/L_{bar}$) for all bars with a corroding area of 1013 mm^2 (1.57 in.^{2}). Similar plots are analyzed for other lengths. A best-fit power line to the data suggests a relationship between corrosion loss and fractional corroding length to the –0.1 power.

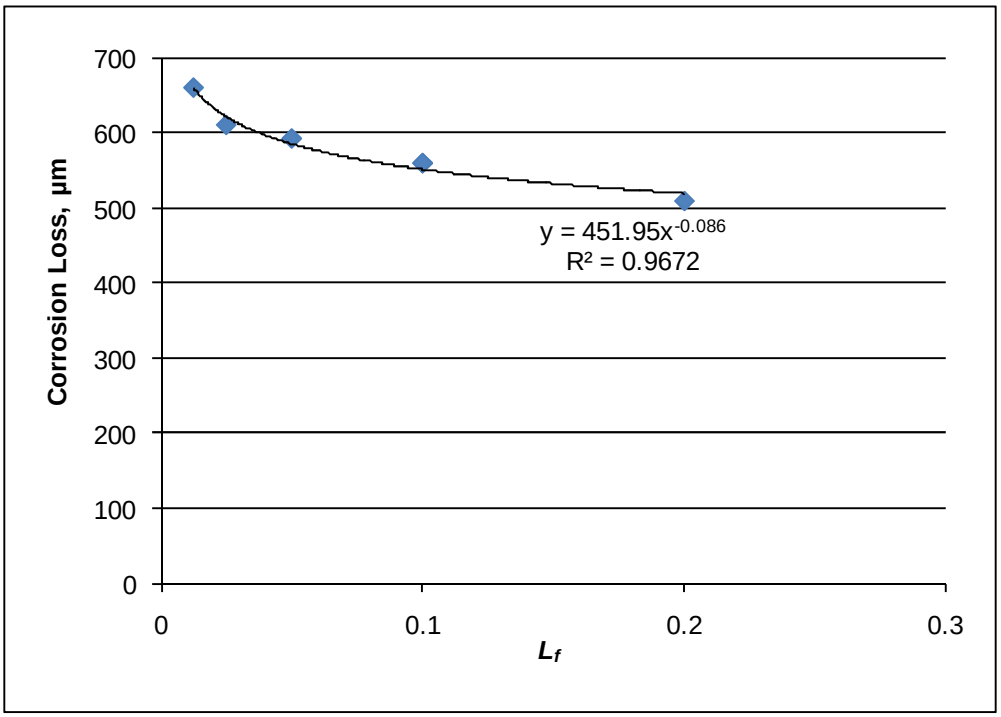

Figure 4.34: Corrosion loss to crack concrete versus L_f with best fit line. 1013-mm^2 (1.57-in.^{2}) corroding area. Corrosion loss = y, $L_f = x$.

Based on the data presented above, Eq. (4.4a) (English units) and Eq. (4.4b) (metric units) represent a potential relationship between corrosion loss and the variables in this study. The term 3^{A_f-1} is required for localized corrosion and reduces to 1 for general corrosion.

$$x_{crit} = 0.53\left(\frac{C^{2-A_f}}{D^{0.38}L_f{}^{0.1}A_f{}^{0.6}} + 0.6\right)\times 3^{A_f-1} \qquad (4.4a)$$

where

x_{crit} = corrosion loss at crack initiation, mil

C = cover, in.

D = bar diameter, in.

L_f = fractional length of bar corroding, $L_{corroding}/L_{bar}$

A_f = fractional area of bar corroding, $A_{corroding}/A_{bar}$

$$x_{crit} = 45\left(\frac{\left[C/25.4\right]^{2-A_f}}{D^{0.38}L_f{}^{0.1}A_f{}^{0.6}} + 0.2\right)\times 3^{A_f-1} \qquad (4.4b)$$

where

x_{crit} = corrosion loss at crack initiation, μm

C = cover, mm

D = bar diameter, mm

L_f = fractional length of bar corroding, $L_{corroding}/L_{bar}$

A_f = fractional area of bar corroding, $A_{corroding}/A_{bar}$

Figure 4.35 compares the corrosion losses for the finite element models with the corrosion losses predicted by Eq. (4.4). There is some scatter, but Eq. (4.4) provides a reasonable match with the results obtained from the finite element model.

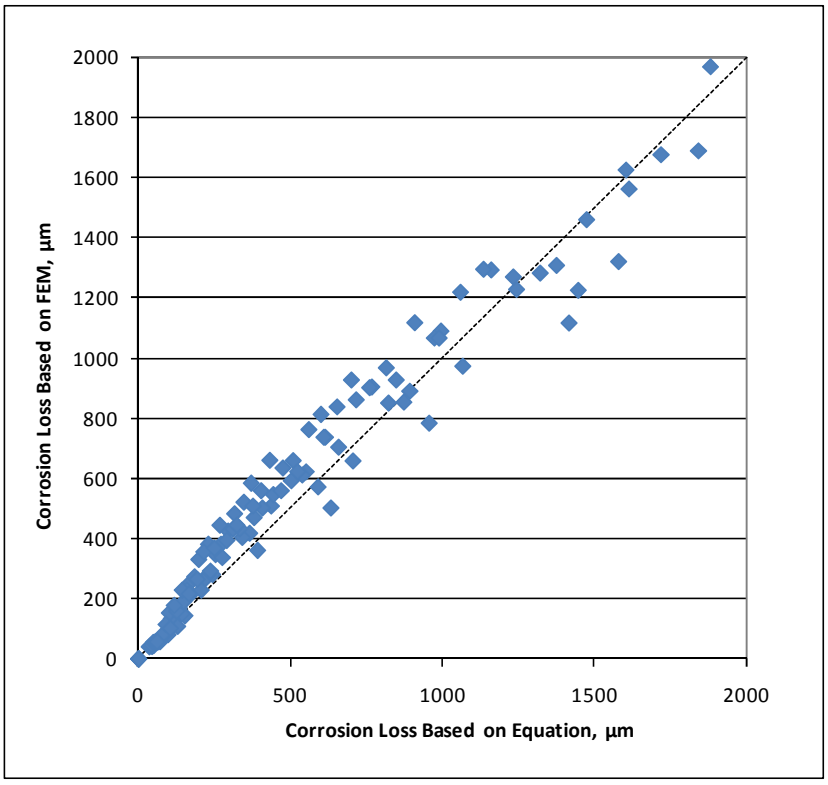

Figure 4.35: Corrosion loss to crack concrete for localized corrosion based on the finite element model (FEM) results versus corrosion losses calculated by Eq. (4.4).

To verify the accuracy of Eq. (4.4), the corrosion loss predicted by the equation is compared to the experimental data for localized corrosion of ECR presented in Table 4.5 as well as experimental results presented by Rasheeduzzafar et al. (1992), Alonso et al. (1998), and Torres-Acosta and Sagues (2004), which are summarized in Table 4.13. Data for generalized corrosion of steel (corrosion of a full length bar, see Table 4.9) are also included in the analysis to check the accuracy of the equation for bars with large corroding areas. The comparison is presented in Figure 4.36, along with the comparison for the 3D finite element model results shown in Figure 4.35.

Table 4.13: Corrosion Loss to Crack Concrete-Results from Other Research (Localized Corrosion)

	Cover, mm	**Diameter, mm**	**Exposed Area, mm^2**	**Bar Area, mm^2**	**Exposed Length, mm**	**Bar Length, mm**	**Corrosion Loss, µm**
Alonso et al. (1998)	19	14.6	17448	17448	381	381	15
	15.2	8.0	9550	9550	381	381	20
	30.4	16.0	19101	19101	381	381	25
	30.4	16.0	19101	19101	381	381	28
	30.4	16.0	19101	19101	381	381	30
	49.4	15.9	19024	19024	381	381	31
	49.4	11.8	14041	14041	381	381	51
	68.4	15.5	18558	18558	381	381	55
	68.4	9.8	11665	11665	381	381	68
	19	14.6	17448	17448	381	381	25
	19	14.6	17448	17448	381	381	18
	29	38.1	91207	91207	381	381	3
Rasheeduzzafar et al. (1992)	20	13	22462	22462	550	550	33
	20	13	22462	22462	550	550	26
	20	13	22462	22462	550	550	34
	35	13	22462	22462	550	550	32
	35	13	22462	22462	550	550	30
	35	13	22462	22462	550	550	47
	35	13	22462	22462	550	550	38
	35	13	22462	22462	550	550	27
	35	13	22462	22462	550	550	27
	50	13	22462	22462	550	550	70
	50	13	22462	22462	550	550	71
	50	13	22462	22462	550	550	74
	50	13	22462	22462	550	550	61
	60	13	22462	22462	550	550	67

Table 4.13 (continued): Corrosion Loss to Crack Concrete-Results from Other Research (Localized Corrosion)

	Cover, mm	Diameter, mm	Exposed Area, mm^2	Bar Area, mm^2	Exposed Length, mm	Bar Length, mm	Corrosion Loss, µm
Torres-Acosta and Sagues (2004)	27.6	21	2105	16757	32	254	48.3
	27.6	21	2105	16757	32	254	66.4
	40.3	21	2738	20122	42	305	88.2
	40.3	21	2738	20122	42	305	69.6
	65.7	21	4486	26785	68	406	76.5
	65.7	21	4486	26785	68	406	121.8
	40.3	21	2764	20122	42	305	55.2
	40.3	21	2764	20122	42	305	68.9
	40.3	21	1260	13393	19	203	141.2
	40.3	21	1260	13393	19	203	70.6
	40.3	21	2738	20122	42	305	60.3
	40.3	21	2738	20122	42	305	65.0
	40.3	21	22827	26785	346	406	28.4
	40.3	21	22827	26785	346	406	7.2
	27.5	21	1649	26785	25	406	30.8
	40.3	21	1649	26785	25	406	61.6
	45	13	4084	16581	100	406	84.0
	45	13	1021	16581	25	406	336.0
	38	13	4084	16581	100	406	49.8
	38	13	4084	16581	100	406	49.8
	13	13	4084	16581	100	406	31.1
	13	13	1021	16581	25	406	37.3
	13	13	1021	16581	25	406	49.8
	13	13	4084	16581	100	406	34.2
	28.8	13	796	16581	20	406	207.4
	30.3	13	796	16581	20	406	111.7
	39	13	15928	16581	390	406	35.9
	39	13	15928	16581	390	406	31.1
	39	13	1593	16581	39	406	151.6
	39	13	1593	16581	39	406	159.6
	39	13	327	16581	8	406	233.3
	39	13	327	16581	8	406	272.2
	27.5	6.4	603	8163	30	406	63.2
	26.5	6.4	603	8163	30	406	84.3
	39	13	1593	16581	39	406	271.2
	39	13	1593	16581	39	406	191.5
	39	13	1593	16581	39	406	159.6
	39	13	1593	16581	39	406	151.6

Figure 4.36a covers the range of the experimental data in Table 4.13. There is a moderate degree of scatter for both the FEM and experimental results, but the finite element model generally agrees with the experimental data. Equation (4.4) provides a generally conservative estimate of the corrosion loss required to crack concrete based on both the experimental and finite element results; that is, in most cases Eq. (4.4) underestimates the loss required to cause a crack to form.

The finite element models extend well beyond the range of experimental data (Figure 4.36b); additional testing will be needed to verify the accuracy of the finite element model in this range. The KU specimens with actual corrosion losses between 350 and 900 µm (Figure 4.36b) represent the epoxy-coated bars with half-rings and holes in the epoxy. Equation (4.4) is very conservative for these specimens, predicting losses of approximately 200 µm, compared to the 350 to 900 µm range in actual losses. Equation (4.4) is most conservative for the epoxy-coated specimens with two holes in the epoxy; these specimens are shown as open circles in Figure 4.36b, as the uncertainty in the exposed area due to blistering of the epoxy calls the accuracy of these data points into question.

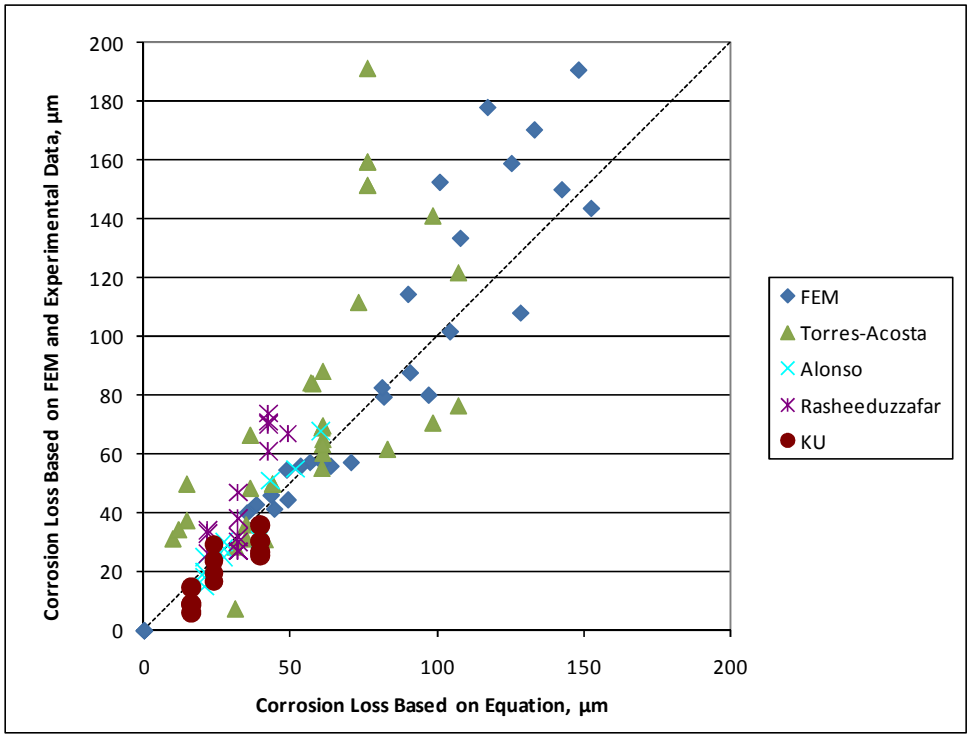

Figure 4.36a: Corrosion loss in localized corrosion specimens versus corrosion loss predicted by Eq. (4.4). 3D FE model with experimental data.

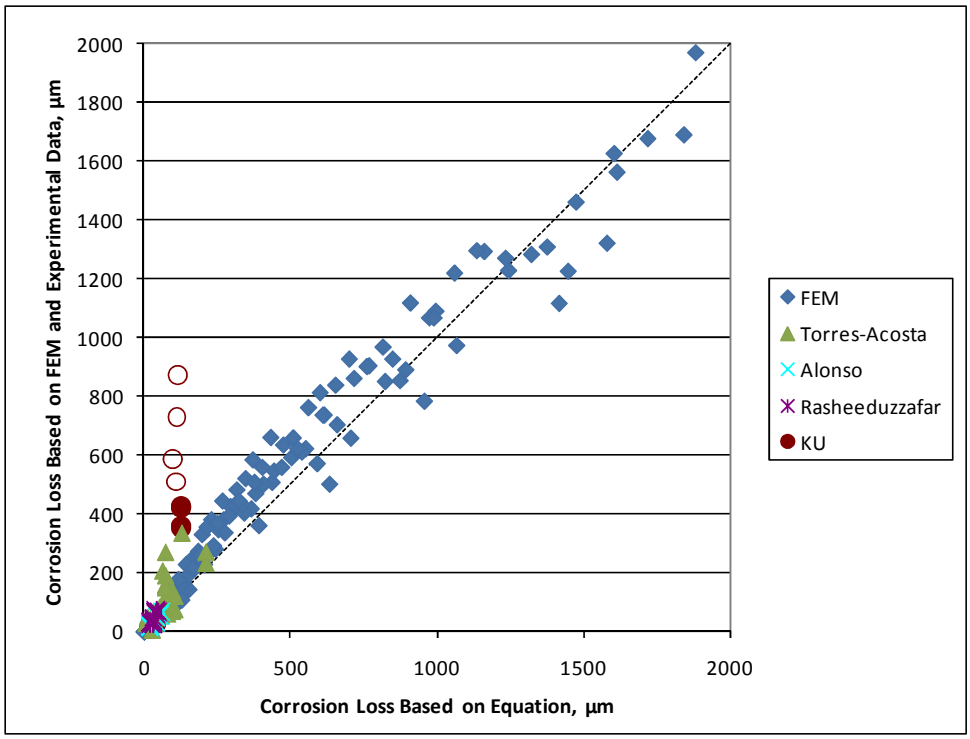

Figure 4.36b: Corrosion loss in localized corrosion specimens versus corrosion loss predicted by Eq. (4.4). 3D FE model with experimental data (Different scale).

4.5 DISCUSSION

As discussed in Section 1.4, Torres-Acosta and Sagues (2004) derived an expression [Eq. (1.11)] relating bar cover, bar diameter, and localized corrosion length with the corrosion loss required for crack initiation based on experimental results.

$$x_{crit} = 11.0\frac{C}{D}\left(\frac{C}{L}+1\right)^2 \tag{1.11}$$

where

x_{crit} = corrosion loss at crack initiation, μm

C = cover, mm

D = bar diameter, mm

L= length of exposed steel, mm

Figures 4.37a and b compare the corrosion losses predicted by the equation with the experimental data for localized corrosion of ECR presented in Table 4.5, as well as the finite element results and the experimental results presented by Rasheeduzzafar et al. (1992), Alonso et al. (1998), and Torres-Acosta and Sagues (2004) (Table 4.13), as done for Eq. (4.4) in Figures 4.36a and 4.36b.

Comparing Figures 4.36a and 4.37a shows that for bars that require less than 50 μm of loss to crack concrete, Eq. (1.11) and Eq. (4.4) perform comparably. However, the equation developed by Torres-Acosta [Eq. (1.11)] is less conservative than Eq. (4.4) based on both experimental and finite element model results for bars that require greater than 50 μm of loss to crack concrete (compare Figures 4.37a and 4.36a); that is, the corrosion loss required to crack concrete predicted by Eq. (1.11) is greater than the corrosion loss required to crack concrete in the test specimens and for many of the finite element results. Equation (4.4), in contrast, is more conservative with respect to many of the experimental specimens (Figure 4.36a). Equation (1.11) overestimates a significant portion of the experimental results obtained by Torres-Acosta and Sagues, in one case

predicting a corrosion loss of 173 µm for a specimen that only required 63 µm of loss to crack concrete. For all experimental specimens with actual losses greater than 60 µm, Eq. (1.11) overestimates the corrosion loss requited to crack concrete for over 75 percent of the specimens. In comparison, Eq. (4.4) overestimates the corrosion loss to crack concrete for only 14 percent of the specimens with actual losses greater than 60 µm.

Comparing Eq. (1.11) and Eq. (4.4) based on results from the finite element model (Figure 4.37b) suggests that Eq. (1.11) becomes increasingly inaccurate and unconservative for bars that require very large corrosion losses to crack concrete (Figure 4.37b). Furthermore, results from the finite element models where greater than 1200 µm of loss is required to crack concrete do not appear in Figure 4.37b, as Eq. (1.11) predicts that greater than 2000 µm of loss is required to crack the concrete.

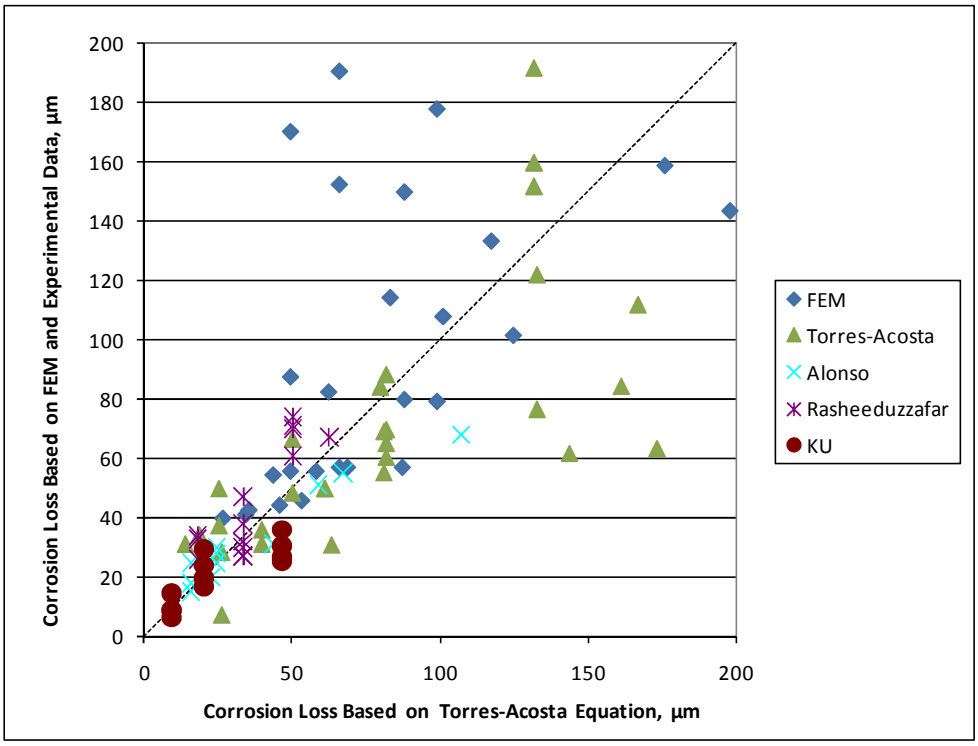

Figure 4.37a: Corrosion loss in localized corrosion specimens versus corrosion loss predicted by Eq. (1.11). 3D FE model with experimental data.

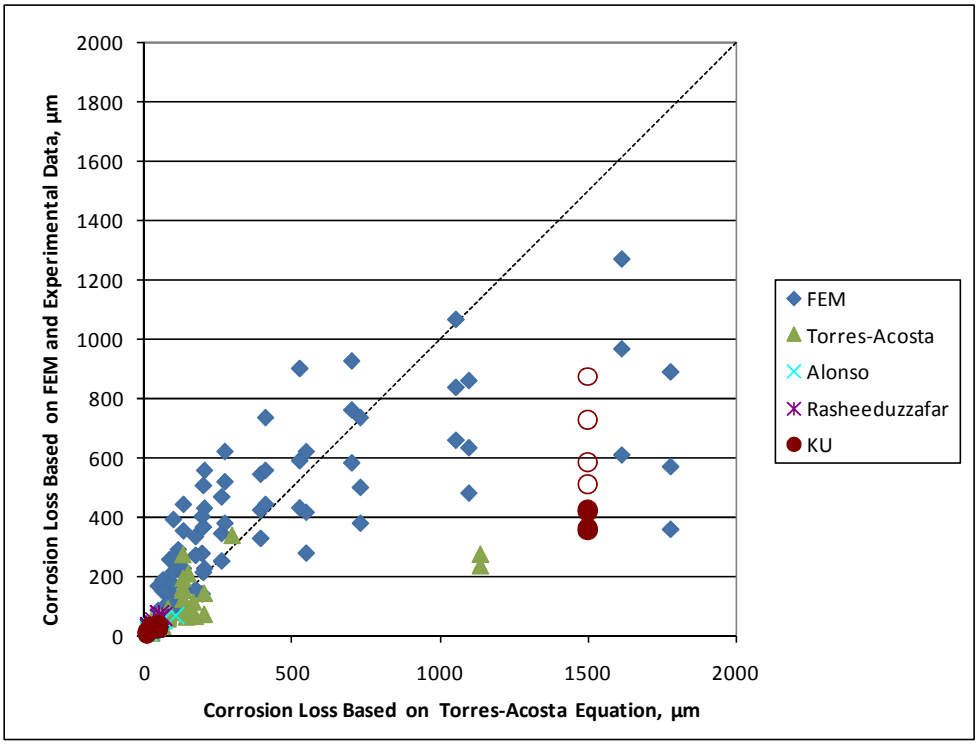

Figure 4.37b: Corrosion loss in localized corrosion specimens versus corrosion loss predicted by Eq. (1.11). 3D FE model with experimental data (Different scale).

The ratio of experimentally obtained corrosion losses required to crack concrete to the corrosion losses obtained by Eqs. (4.4) and (1.11) is also used to judge the degree of conservatism in each equation. A ratio less than 1.0 indicates an unconservative estimate for that specimen. Figures 4.38a and 4.38b compare this ratio for each equation based on corrosion losses obtained from experimental and finite element model results, respectively. Over the range of available experimental data (Figure 4.38a), Eqs. (4.4) and (1.11) perform comparably, with Eq. (4.4) being more conservative for systems where actual losses exceeded 50 µm. As discussed in Section 1.4, the available experimental data involves exposed areas far larger than those typically observed on damaged ECR. The specimens with damaged ECR tested as part of this study developed blisters that greatly increased the exposed area; therefore, only finite element model results are available for small exposed areas. Over the range of finite element model data, Eq.

(1.11) rapidly becomes unconservative, as noted by the large percentage of ratios of FEM predicted corrosion losses to Eq. (1.11) predicted losses that are much less than 1.0 for models with expected corrosion losses greater than 500 µm. In contrast, Eq. (4.4) does not exhibit this behavior. Therefore, Eq. (4.4) is used to determine the corrosion loss required to crack concrete for damaged ECR.

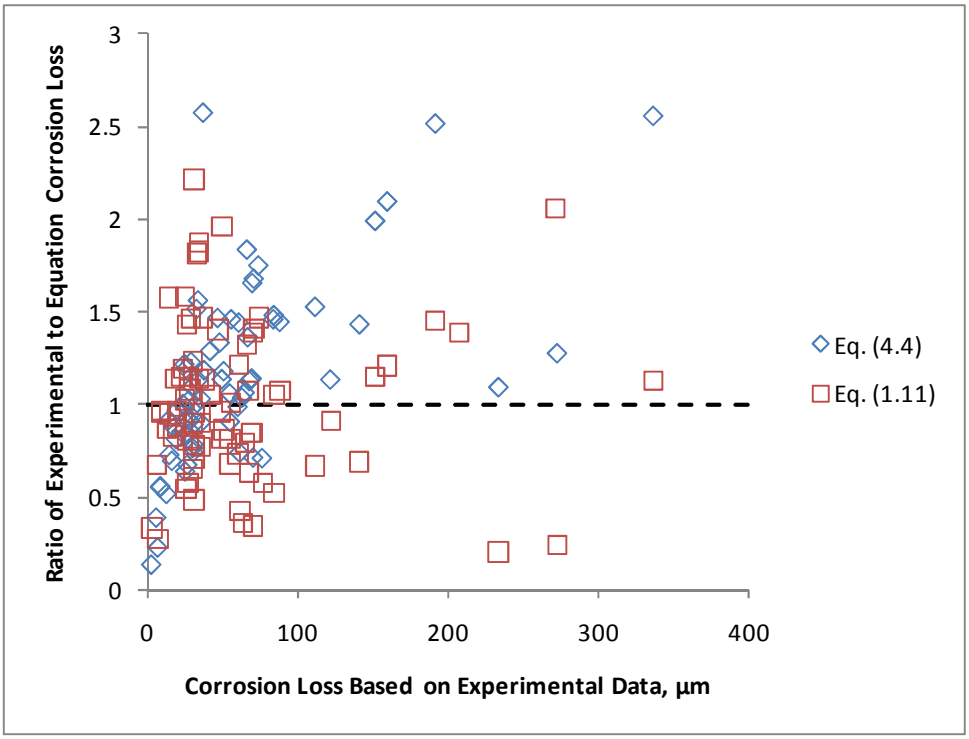

Figure 4.38a: Ratio of experimentally derived corrosion loss to predicted corrosion loss versus corrosion loss to crack concrete based on experimental data.

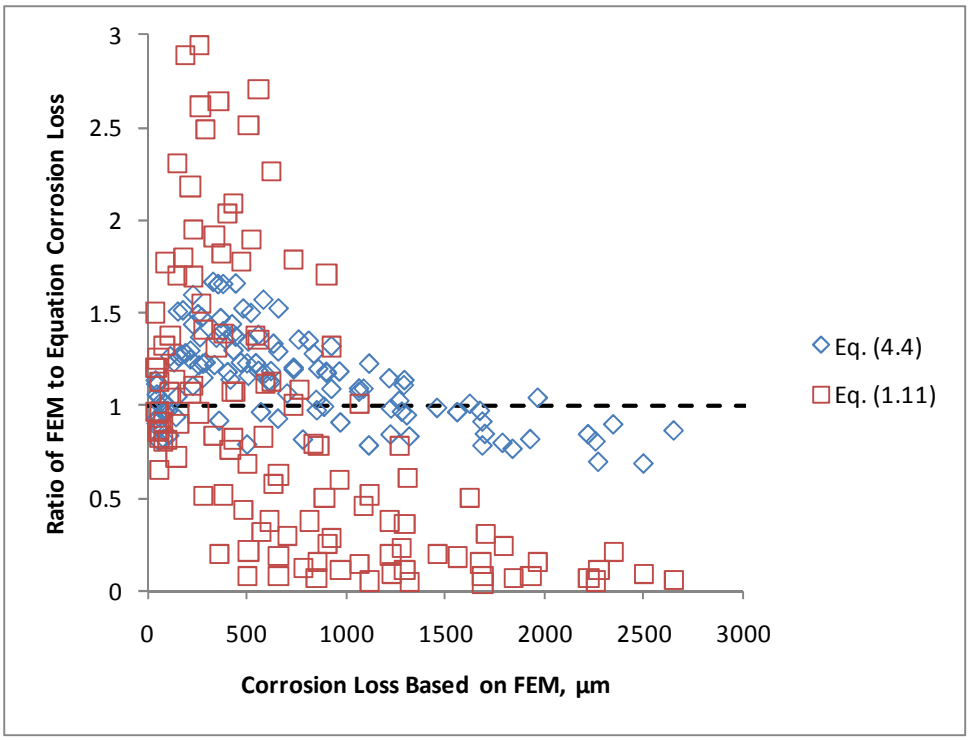

Figure 4.38b: Ratio of FEM derived corrosion loss to predicted corrosion loss versus corrosion loss to crack concrete based on FEM.

Equation (4.4) may be used to estimate the corrosion loss to cause cracking in reinforced concrete bridge decks. Cover and bar diameter are both well-defined parameters for a given bridge deck. The fraction of damaged area, A_f, for epoxy-coated reinforcement requires some estimation; the bench-scale and field test specimens tested in this study have values of A_f between 0.002 and 0.005. For bare steel, A_f may be taken as 1.

The corroding length, L_f, is more difficult to estimate. The bench-scale and field test specimens with epoxy-coated bars in this study have values of L_f between 0.021 and 0.052. Figure 4.37 shows the calculated corrosion loss from Equation 4.4 with L_f allowed to vary and all other parameters held fixed (cover = 76.4 mm (3 in.), bar diameter = 16 mm (0.63 in.), A_f = 0.005). Figure 4.39 shows Eq. (4.4) does not vary strongly with L_f, and, since the calculated corrosion loss needed to crack concrete decreases as L_f increases, L_f may be conservatively taken as 1 if a better estimate is not available. To

gauge the degree of conservatism implicit in taking $L_f = 1$, the corrosion loss predicted by Eq. (4.4) with $L_f = 1$ is compared to the experimental data listed in Table 4.13 in Figure 4.40. Figure 4.40 shows that taking $L_f = 1$ results in Eq. (4.4) underestimating the corrosion loss required to crack concrete, especially at smaller exposed lengths; with data points above the dashed line indicating Eq. 4.4 is underestimating the corrosion loss required to crack concrete for the corresponding specimens. The data points in the upper right corner of Figures 4.36b and 4.39b correspond to specimens with $L_f < 1$. Comparing Figures 4.40 and 4.36 (for which the actual value of L_f is used) shows that for specimens with small exposed lengths, taking $L_f = 1$ results in a modestly conservative underestimation of the corrosion loss required to crack concrete.

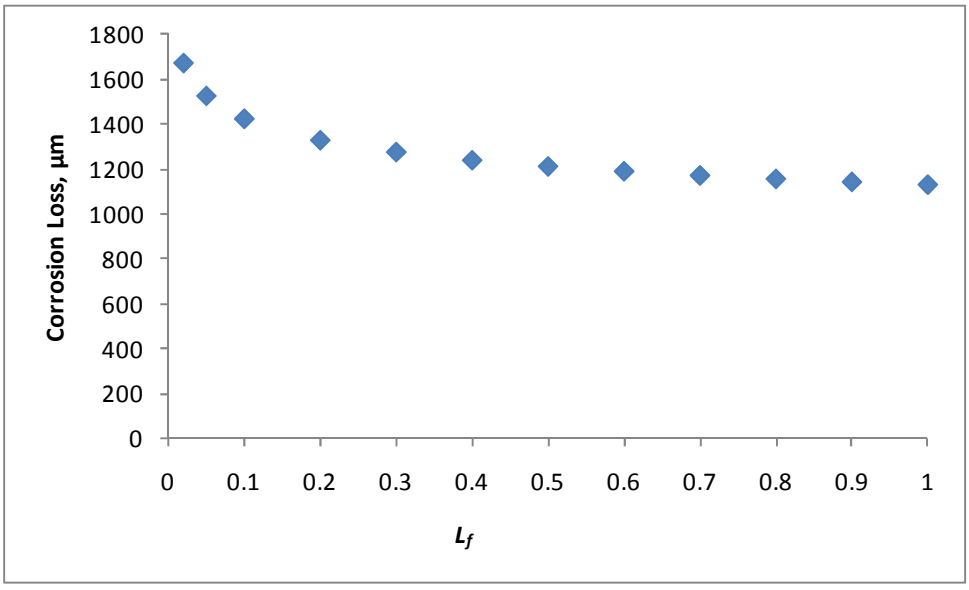

Figure 4.39: Corrosion loss predicted by Eq. (4.4) versus L_f with all other variables held fixed.

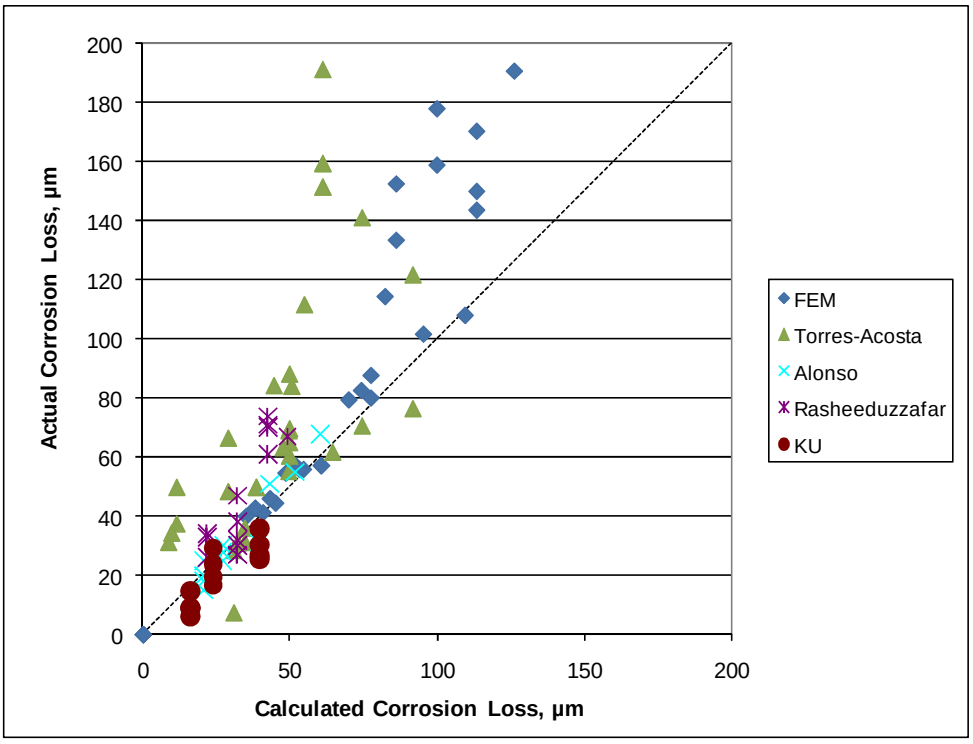

Figure 4.40a: Corrosion loss in localized corrosion specimens versus corrosion loss predicted by Eq. (4.4) with $L_f = 1$. 3D FE model with experimental data.

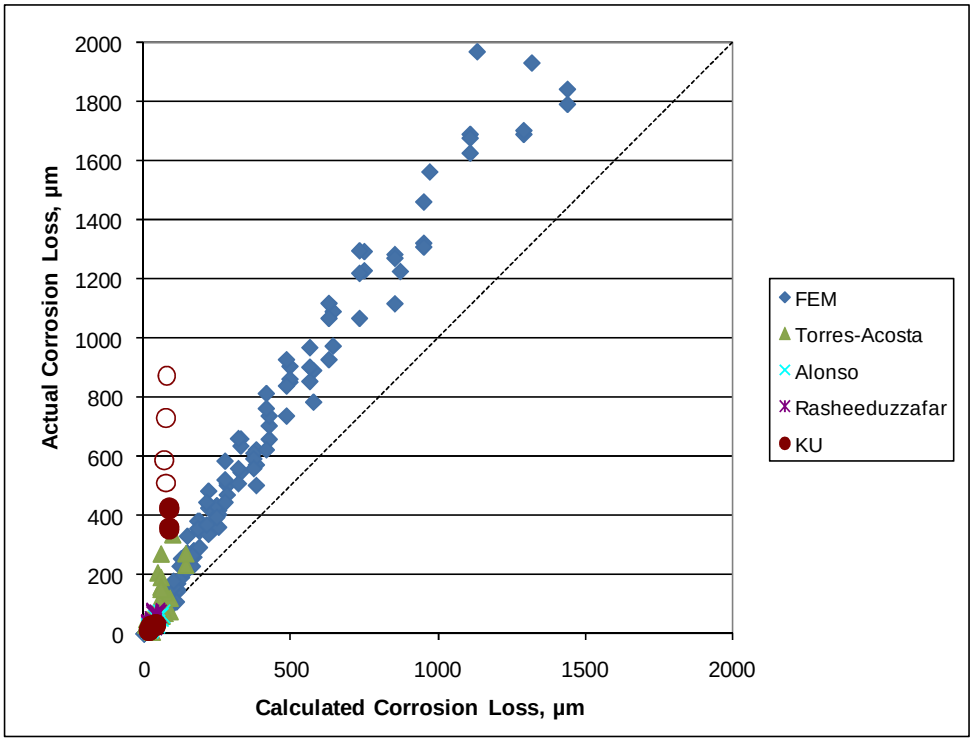

Figure 4.40b: Corrosion loss in localized corrosion specimens versus corrosion loss predicted by Eq. (4.4) with $L_f = 1$. 3D FE model with experimental data (Different scale).

4.6 CONCLUSIONS

The following conclusions are drawn based on the data and analysis presented in this chapter.

1. Galvanized reinforcement requires greater corrosion losses to crack concrete cover than conventional reinforcement.
2. For general corrosion, the corrosion loss required to crack concrete is directly proportional to the concrete cover. For localized corrosion, the corrosion loss required to crack concrete cover is proportional on the cover squared.
3. For localized corrosion, decreasing the corroding area of the bar increases the corrosion loss on the exposed area needed to crack concrete.
4. The finite element model developed for this study provides reasonably accurate predictions of the corrosion losses required to crack concrete when compared to experimental results from this and other studies.
5. The corrosion loss required to crack concrete may be predicted using the following equation

$$x_{crit} = 45\left(\frac{\left[C/25.4\right]^{2-A_f}}{D^{0.38}L_f^{\,0.1}A_f^{\,0.6}} + 0.2\right)\times 3^{A_f-1} \qquad (4.4b)$$

where

x_{crit} = corrosion loss at crack initiation, μm

C = cover, mm

D = bar diameter, mm

L_f = fractional length of bar corroding, $L_{corroding}/L_{bar}$

A_f = fractional area of bar corroding, $A_{corroding}/A_{bar}$

CHAPTER 5

PORE SOLUTION ANALYSIS OF CEMENT PASTES CONTAINING CORROSION INHIBITORS

5.1 INTRODUCTION

The reaction of portland cement with water involves a series of chemical reactions known as hydration. Hydrated portland cement forms a complex microstructure that consists of, among other components, calcium silicate hydrate (C–S–H), calcium hydroxide, and fluid-filled capillary pores (Mindess, Young, and Darwin 2003). The fluid in these pores is termed pore solution. Pore solution is an ionic solution whose composition depends on the nature of the cement paste surrounding it (Mindess et al. 2003). Extracting the pore solution and analyzing its composition can provide insight into the composition of the cement paste.

Pore solution is readily extracted from cement paste prior to set; however, the pore solution composition is not representative of that in hydrated cement paste. Barneyback and Diamond (1981) and Farzammehr (1985) used a cylindrical pressure vessel capable of applying pressures up to 550 MPa (80,000 psi) to extract pore solution from hardened cement pastes. A similar pressure vessel was used for this study and will be described in Section 5.2.3.

In this study, pore solutions are analyzed from cement pastes containing three corrosion inhibitors, calcium nitrite (DCI-S), Rheocrete 222+, and Hycrete. Cement paste with no inhibitor is analyzed as a control. Of specific interest are the concentrations of hydroxide, fluoride, chloride, sulfate, phosphate, nitrate, and nitrite ions. The pore solutions are collected at ages of 1 and 7 days.

Li, Sagues, and Poor (1999) compared pore solution pH of concrete containing a calcium nitrite corrosion inhibitor to the pH of concrete that did not contain a corrosion inhibitor. Specimens were cured at 100% relative humidity for 9 days, after which holes were drilled into the specimens, 0.4 mL deionized water injected into the holes, and the

holes stoppered. Pore solution leached into the water, allowing the pH to be monitored over time. The pore solution of specimens with no calcium nitrite had an average pH of 13.0 after curing for nine days, with a peak pH of 13.5 at day 25 of the test. The pore solution of specimens containing calcium nitrite had a pH of 12.8 after curing with a peak pH of 13.2 at 25 days. The effect of Rheocrete and Hycrete on pore solution pH, as well as the effect of calcium nitrite, Rheocrete, and Hycrete on ionic concentrations in pore solution, has not been established.

5.2 EXPERIMENTAL PROCEDURE

5.2.1 Mixture Proportions

The mixture proportions used for the specimens are shown in Table 5.1. The water-cement ratio for all mixes is 0.45. The materials used are listed below. The quantity of inhibitor used is selected so that the ratio of inhibitor to cement content is equivalent to that recommended by the manufacturer for a concrete mixture containing 355 kg/m^3 (598 lb/yd^3) of cement. The equivalent dosage per cubic meter (cubic yard) of concrete is also shown in Table 5.1 and is the same as listed in Section 2.2.2.

Water – Reverse osmosis filtered water with a minimum resistivity of 18 Mohm-cm.

Cement – Type I/II portland cement, lot number 2307, produced by Ash Grove Cement Company in Chanute, KS. The chemical composition, specific gravity, and fineness of the cement are shown in Table 5.2.

DCI – Darex Corrosion Inhibitor (DCI-S), a calcium nitrite inhibitor manufactured by W.R. Grace. A set retarder in added to limit the effects of calcium nitrite as an accelerator. Designation DCI.

Rheocrete – Rheocrete 222+, a water-based solution of esters and amines manufactured by BASF, Inc. Designation RH.

Hycrete – Hycrete DSS (disodium tetrapropenyl succinate), manufactured by Hycrete, Inc. Designation HY.

Table 5.1: Mix Proportions for Cement Paste

Mix Designation	Water, kg (lb.)	Cement, kg (lb.)	Inhibitor, mL (oz.)	Inhibitor*, L/m^3 (gal/yd^3)
Control	0.409 (0.90)	0.909 (2.0)	-	-
RH	0.395 (0.87)	0.909 (2.0)	12.8 (0.43)	5 (1.01)
DCI	0.373 (0.82)	0.909 (2.0)	38.4 (1.30)	15 (3.03)
HY	0.386 (0.85)	0.909 (2.0)	21.6 (0.73)	7.6 (1.54)

*Equivalent dosage for concrete with a cement content of 355 kg/m^3 (598 lb/yd^3) and *w/c* = 0.45

Table 5.2: Portland Cement Chemical Composition

Item	% by Weight
SiO_2	20.39
Al_2O_3	4.50
Fe_2O_3	3.50
CaO	63.59
MgO	1.90
SO_2	2.51
Na_2O	0.17
K_2O	0.50
Loss on Ignition	2.12
C_3S	54
C_2S	18
C_3A	6
C_4AF	11
Specific Gravity	3.15
Fineness (m^3/kg)	339

5.2.2 Formwork

Forms consist of a 95-mm (3.75-in.) long section of 1.5-in. Schedule 40 PVC pipe. One end of the pipe was attached with silicone caulk to a 19-mm (0.75-in.) thick plywood base. No oil or other release agent is used with the formwork. The specimens are 95-mm (3.75-in.) long with a diameter of 41 mm (1.61 in.).

5.2.3 Pore Press Pressure Vessel

The pore press pressure vessel used in this study is based on the design by Barneyback and Diamond (1981) and is shown in Figure 5.1. A description of apparatus

fabrication is provided by Farzammehr (1985). A description of each part follows. All steel is SAE 4340 alloy steel

Piston Assembly – An assembly consisting of a piston shaft and piston head. The shaft is 55-mm (1.75-in.) in diameter and 152-mm (6-in.) long. The head is 102 mm (4 in.) in diameter and 44 mm (1.75 in.) thick. The two pieces are connected with a threaded machine screw.

Teflon Disc – A 44-mm (1.75-in.) diameter, 6-mm (0.25-in.) thick Teflon disc used as a seal.

Die body – A steel cylinder with inner diameter 44 mm (1.75 in.), outer diameter 184 mm (7.25 in.), and height 127 mm (5 in.).

Platen – A 51-mm (2-in.) thick base with a 3 mm (0.125 in.) circular groove cut in the upper face in line with the fluid drain to allow for drainage of pore solution. The bottom face is machined to fit snugly on the base.

Fluid Drain – An angled hole cut through the base of the platen to allow for pore solution collection. A 114-mm (4.5-in.) long plastic tube with an inner diameter of 3 mm (0.125 in.) and an outer diameter of 9 mm (0.375 in.) is pressed snugly into the drain to aid in solution collection.

Base – A steel cylinder with an inner diameter of 48 mm (1.875 in.) and an outer diameter of 98 mm (3.875 in.).

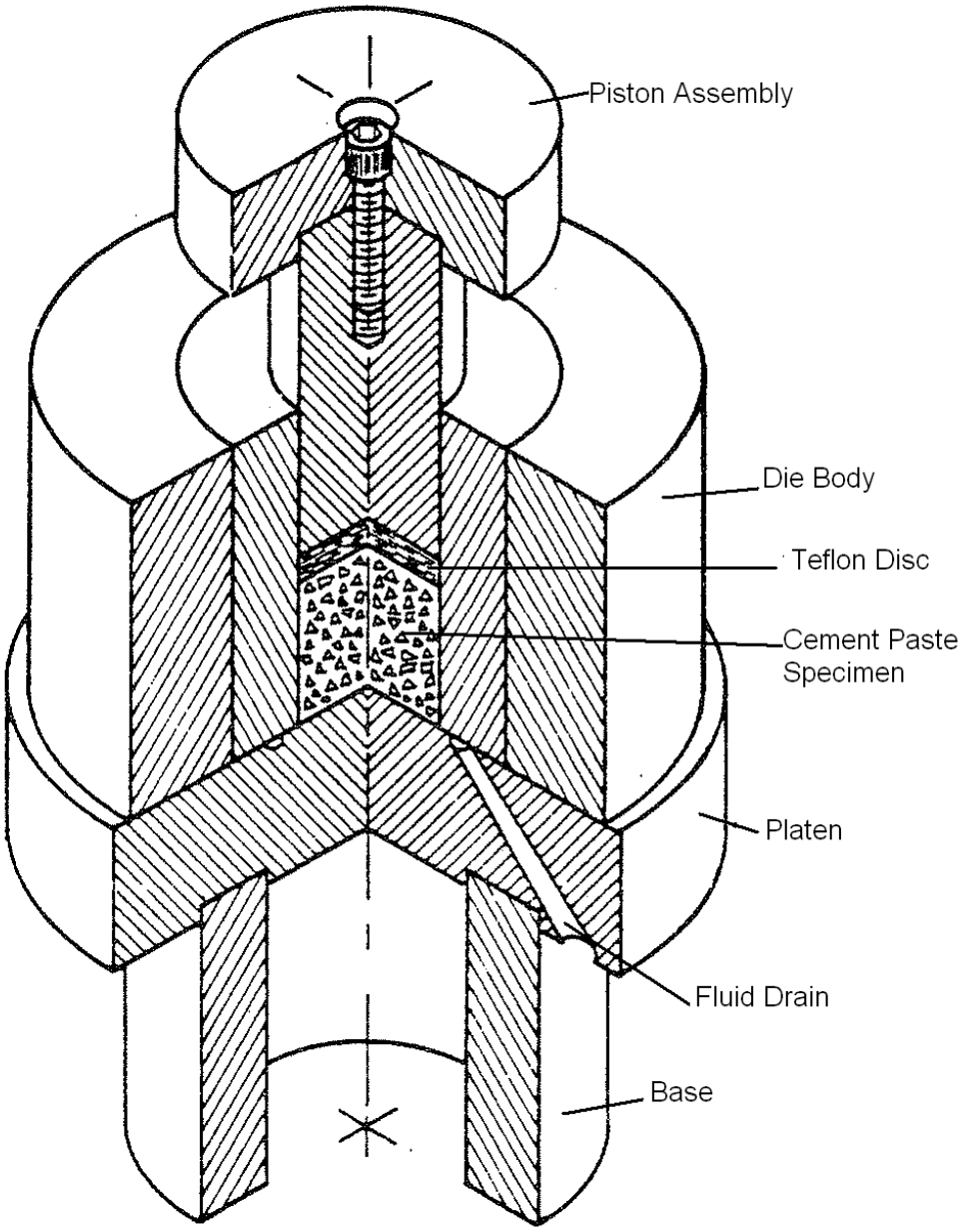

Figure 5.1: Pore Press Pressure Vessel (Barneyback and Diamond 1981)

5.2.4 Specimen Casting and Sample Collection

The procedure for casting and collecting pore solution samples is described below.

1. Cement paste is mixed using a Hobart Model N-50 mortar mixer using the proportions listed in Table 5.1.
2. Specimens are cast in the formwork described in Section 5.2.2. Specimens are filled in two equal layers. A 3-mm (0.125-in.) diameter rod is used to consolidate the paste, and the outside of the mold is tapped lightly with the palm of the hand to remove air voids. The proportions in Table 5.1 provide enough cement paste for three specimens.
3. Specimens are tightly covered with plastic bags and cured at room temperature in the molds until testing.
4. Specimens are removed from forms approximately one hour prior to testing using a high-speed cutting tool. Debris is removed using compressed air and specimens are immediately sealed in plastic bags and labeled.
5. Specimens are placed in the pressure vessel described in Section 5.2.3. Load is applied to the piston assembly with a computer-controlled testing machine with a capacity of 2,670 kN (600,000 lbf). A glass container with a capacity of 50 mL is placed under the fluid drain tubing to collect pore solution.
6. Pressure within the vessel is increased to 550 MPa (80,000 psi) over a three minute period and held at 550 MPa (80,000 psi) for an additional three minutes.
7. The pressure vessel is unloaded and the specimen extracted. The glass container with pore solution is immediately sealed and labeled for analysis. All interior surfaces of the pressure vessel are cleaned with reverse osmosis filtered water and allowed to dry prior to testing the next sample.
8. The volume of pore solution collected is recorded to the nearest 0.1 mL.

5.2.5 Analysis Methods

Hydroxyl ion concentration is determined by titration with dilute hydrochloric acid. All other ionic concentrations are determined using ion chromatography. Pore solutions are diluted by a factor of 10 to both provide enough solution for analysis and minimize interference from the hydroxyl ions in the chromatography analysis. Results are presented in terms of concentration in undiluted pore solution. Three series of cement paste specimens are analyzed. Series 1 is tested for pH (HCl titration) only, while Series 2 and 3 are tested using both HCl titration and ion chromatography. The HCl titration and chromatography procedures are described in Sections 5.2.5.1 and 5.2.5.2, respectively.

5.2.5.1 Hydrochloric Acid Titration to Determine pH

The process for determining the pH of expressed pore solution is detailed below.

1. 2.0 mL of diluted pore solution is added to 18.0 mL of reverse-osmosis filtered water in a 100 mL beaker.
2. 5 drops of bromothymol blue indicator dye is added to solution.
3. The beaker is placed on a magnetic stirrer and a stir rod is used to keep the solution mixed.
4. The solution is titrated with 0.050 N HCl until the bromothymol blue dye turns a pale green, indicating the endpoint of the titration. The volume of HCl required to reach the endpoint is recorded to the nearest 0.1 mL.

With the volume of HCl required to reach a neutral pH known, the initial hydroxyl ion concentration may be determined.

$$V_{\mathrm{HCl}} \times [H^+] = V_S \times [OH^-]_S \tag{5.1}$$

where:

V_{HCl} = Volume of HCl added to reach endpoint, mL

$[H^+]$ = Concentration of H^+ ions in acid

V_S = Initial volume of solution, mL

$[OH^-]_S$ = Concentration of OH^- ions in sample

With $[H^+]$ = 0.05 N, V_S = 2.0 mL, and V_{HCl} known, Eq. (5.1) reduces to

$$[OH^-]_S = 0.025 \times V_{HCl} \tag{5.2}$$

The resulting hydroxyl ion concentration is multiplied by 10 to obtain the concentration in the undiluted pore solution. The pH of the pore solution may then be calculated using Eq. (5.3).

$$pH = 14 + \log[OH^-] \tag{5.3}$$

5.2.5.2 Ion Chromatography Analysis

Ion chromatography is an analytical method that separates ions from solution based on their charge and size. The sample to be analyzed is loaded into an absorptive matrix known as a column. Ions in the sample are bound to the column by coulombic forces. An ion extraction liquid (eluent) is used to strip ions in the sample from the column. As the eluent concentration increases, it displaces ions from the solution being analyzed, with each species being displaced at a specific concentration of eluent (Small 1989). The concentration of eluent increases with time; therefore, a given species will be released from the column at a specific point in time during the analysis. The concentration of ions in the solution being analyzed is determined by measuring the conductivity of the fluid leaving the column; an increase in conductivity at a point in time indicates the presence of the ion known to be extracted at that time (Small 1989). Plotting conductivity versus time results in several ‘peaks’ at times when ions are extracted. By comparing the area under these peaks to the area under peaks from a standard solution, the concentration of ions in a sample may be determined. A sample chromatograph plot is shown in Figure 5.2.

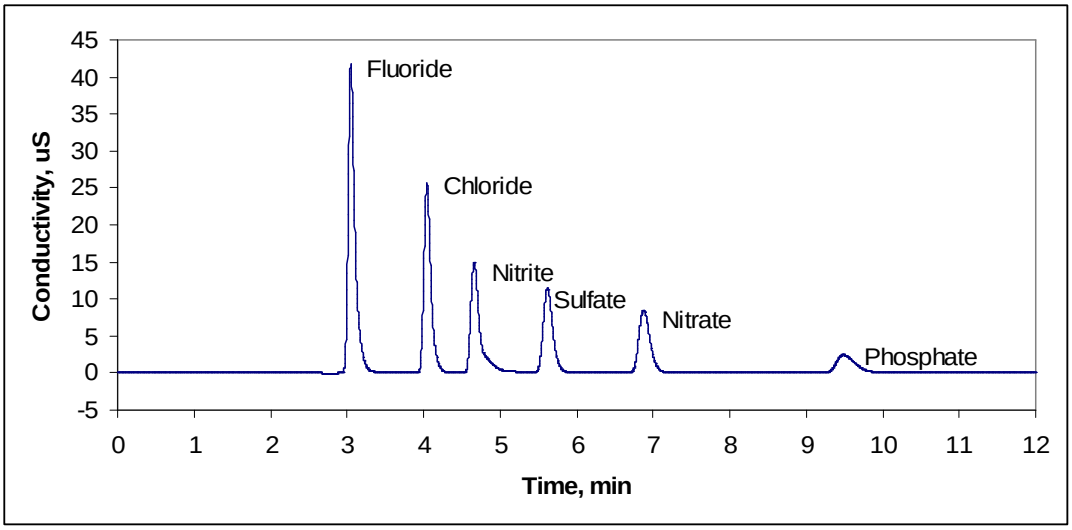

Figure 5.2: Sample Chromatograph Plot (10 ppm standard solution)

For this study, a Dionex ICS-2000 chromatograph with an AS40 autosampler is used. Chromatograph settings are given below.

Cell Temperature – 30° C (86° F)

Column Temperature – 35° C (95° F)

Suppressor Current – 75 mA

Eluent – 30 mM Hydroxide

Sample Rate – 5 Hz

The procedure for analyzing pore solution samples is as follows.

1. 5.0 mL of diluted solution is placed in a labeled beaker and capped. The beaker cap has a connection to allow the extraction of solution through the cap and contains a 0.45 µm (0.018 mil) filter to prevent any suspended solids from entering the chromatograph.
2. 1 L of standard solution is prepared with a concentration of 1000 ppm of sodium fluoride, sodium chloride, sodium nitrite, sodium phosphate, sodium sulfate, and potassium nitrate as ionic standards. The standard is diluted to 100 ppm, 10 ppm, and 1 ppm to serve as calibration points for the chromatograph. Reverse osmosis filtered water is used as a blank.

3. The standards are analyzed by the chromatograph, followed by the pore solution samples. After the pore solution samples are analyzed, an additional set of standards are analyzed to ensure no significant drift in the calibration occurred during testing.
4. The peak area data from the standards are plotted versus concentration and a best-fit line to the data is established to obtain a relation between peak area and concentration for each ion.
5. The peak area data for each ion from each diluted pore solution sample is converted to concentration using the relations found in step 4. Concentrations in the diluted pore solution are multiplied by 10 to convert to the concentrations found in undiluted pore solution.

5.3 RESULTS

5.3.1 Volume of Pore Solution Collected

The volume of pore solution collected from the Series 2 and 3 specimens is presented in Table 5.3. No volume data was recorded for Series 1. Specimens with no inhibitor (control), tested one day after casting, produced slightly more pore solution than those containing a corrosion inhibitor. For specimens tested seven days after casting, there is no significant difference between conventional cement paste and cement paste with corrosion inhibitors in terms of average volume of pore solution collected. All specimens exhibited a reduction in pore solution volume of about 80 percent between day 1 and day 7.

Table 5.3: Collected Pore Solution Volumes at Day 1 and Day 7

Specimen	Volume Collected, mL				Average Volume, mL	
	Series 2		Series 3			
	1 day	7 day	1 day	7 day	1 day	7 day
Control	11.4	2.4	10.8	1.6	11.1	2.0
RH	9.7	1.7	8.8	2.4	9.25	2.05
DCI	7.4	2.1	11.7	1.9	9.55	2.0
HY	9.8	1.8	9.3	1.8	9.55	1.8

5.3.2 pH of Pore Solutions from Cement Pastes Containing Inhibitors

The average pH from the three series of cement pastes tested is shown in Figure 5.3, with error bars indicating the range of values obtained. Individual pH data appear in Appendix G. Specimens containing DCI exhibit pH values significantly lower than the control specimens, with average values of pore solution pH of 13.2 and 13.4 for solutions extracted day and seven days after casting, respectively, compared to average values of pore solution pH of 13.6 and 13.7 in pore solutions extracted from the control specimens at the same ages. Specimens containing Rheocrete exhibit somewhat higher values of pore solution pH than cement pastes with no inhibitor, with average values of pH of 13.7 and 13.8 in pore solutions extracted one day and seven days after casting. No significant difference in pH is observed for specimens containing Hycrete compared to specimens with no inhibitor.

For all specimens, the pH values increase between one and seven days. Similar results were observed by Li et al. (1999); pore solutions collected from concrete containing a calcium nitrite inhibitor and concrete without an inhibitor show increases in pH between one and seven days. The pH values remain constant until day 25, after which the pH values decrease slightly.

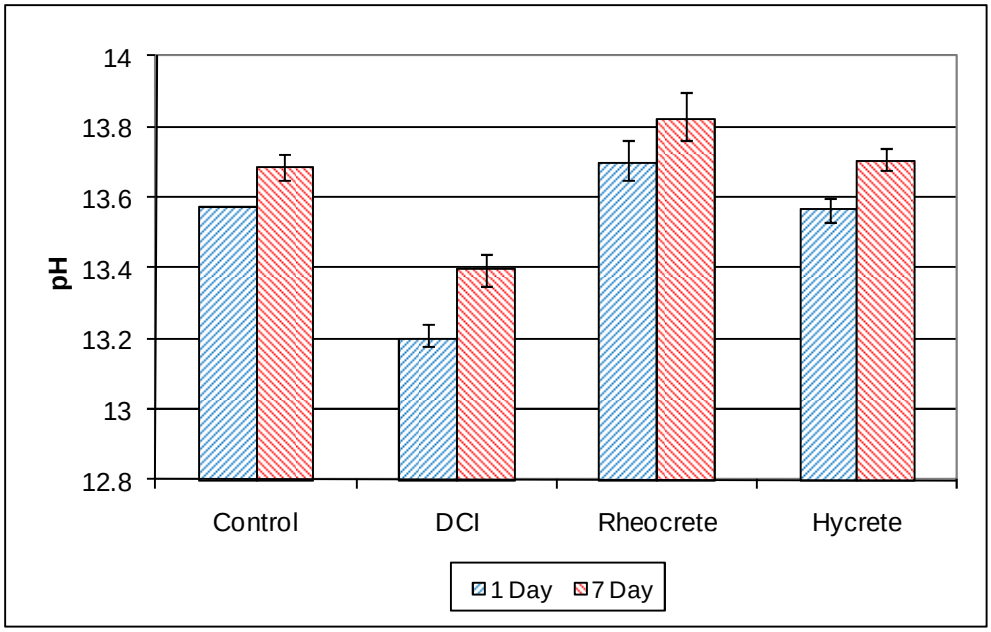

Figure 5.3: Average pore solution pH for cement pastes.

Table 5.4: Average Ion Concentration for Pore Solution from Cement Pastes

Specimen		Ion Concentration (ppm)					
		Fluoride	**Chloride**	**Nitrite**	**Sulfate**	**Nitrate**	**Phosphate**
1 day	Conv.	58	102	109	501	8	0
	Rheocrete	27	37	204	771	8	3
	DCI	23	69	9352	167	756	3
	Hycrete	59	57	255	2318	5	3
7 day	Conv.	70	25	352	607	17	3
	Rheocrete	109	36	312	1752	17	6
	DCI	38	57	10762	674	828	0
	Hycrete	34	22	245	1499	25	3

5.3.3 Ion Concentration of Pore Solutions

The average ion concentrations from the pore solutions are presented in Table 5.4. The ion concentrations from Series 2 and Series 3 are presented individually in Appendix G. Concentrations of less than 10 ppm correspond to a concentration of less than 1 ppm in the diluted test sample. These concentrations are below the range of the standards used and are not considered significant.

Fluoride and chloride levels are low in all specimens. No significant difference in fluoride or chloride ion concentration is observed between the specimens with inhibitors in pore solutions collected one day or seven days after casting.

Moderate levels of nitrite are observed in the control specimens, as well as specimens containing Rheocrete and Hycrete. As expected, the pore solutions from specimens with DCI (calcium nitrite) show high levels of nitrite for specimens tested both one and seven days after casting. It should be noted that the concentration of nitrites in the samples containing DCI exceeds the range of concentrations in the standards; the values presented are extrapolated from the calibration and are approximate.

For pore solutions collected one day after casting, specimens containing DCI show decreased sulfate ion concentration compared to conventional specimens. Specimens containing Hycrete show increased sulfate ion concentration, with average concentrations nearly five times that of the control specimens. Sulfate levels in specimens containing Hycrete decrease somewhat in specimens tested seven days after casting but remain significantly higher than the control specimens. An analysis of the Hycrete inhibitor indicated low levels of sulfate (5 ppm), not enough to explain the high sulfate concentration in the pore solution. Specimens containing Rheocrete also show increased sulfate levels at seven days, however, sulfate levels at one day are only slightly higher than control specimens. An analysis of Rheocrete also shows low sulfate levels (3 ppm). Full results of the inhibitor analysis are presented in Table G.4 of Appendix G.

Nitrate levels in all specimens are low with the exception of specimens containing DCI, which show levels of approximately 800 ppm both one and seven days after casting. This is likely due to the oxidation of some of the added nitrite.

No significant phosphate levels are detected in any pore solutions.

5.4 DISCUSSION

The decrease in pH noted in specimens with DCI was also noted in research by Li et al. (1999). A decrease in alkalinity typically reduces the corrosion resistance of reinforcing steel (Verbeck 1975); the corrosion resistance provided by DCI appears to occur in spite of this reduction in pH. Similarly, the corrosion resisting properties of Rheocrete may be due in part to the increase in alkalinity of the pore solution; however, the primary mechanism of corrosion resistance is likely the decreased permeability caused by Rheocrete (Soylev and Richardson 2008).

The increased sulfate content at early ages observed for specimens with Hycrete may explain the adverse effects Hycrete has on hardened concrete. Xing et al. (2010) noted that corrosion specimens with Hycrete had a significantly reduced critical chloride corrosion threshold; 0.37 kg/m^3 (0.63 lb/yd^3) compared to 0.96 kg/m^3 (1.62 lb/yd^3) for specimens with no inhibitor. However, the time to corrosion initiation was approximately twice that of concrete without an inhibitor. Research by Somuah et al. (1991) showed that sulfate ions act to destabilize the passive layer on steel reinforcement in a manner similar to chlorides. It is possible that the presence of a second destabilizing species (sulfate ions) reduces the quantity of chlorides needed to initiate corrosion. Many studies have noted a significant decrease in strength for concrete with Hycrete (Goodwin et al. 2000, Civjan et al. 2003, Gong et al. 2006, Wojakowski and Distlehorst 2009, Xing et al. 2010). Concrete is subject to deterioration by external sulfate attack (Kumar and Rao 1995, Mindess et al. 2003); it is possible that elevated internal sulfate levels, especially at early ages, may explain the strength reduction.

Nmai et al. (1992) and Xing et al. (2010) noted a reduction in strength of approximately 10 percent for concrete containing Rheocrete compared to concrete with no inhibitor. It is possible that the elevated sulfate levels (observed here at seven days) affects the strength of concrete containing Rheocrete; the low sulfate levels observed at one day may explain why the decrease in strength observed for concrete containing

Rheocrete is not as severe as the reduction in strength observed for concrete containing Hycrete.

5.5 CONCLUSIONS

Based on the analysis of pore solution from cement pastes with corrosion inhibitors, the following conclusions may be drawn.

1. The pH of concrete pore solution increases between one and seven days.
2. The addition of calcium nitrite lowers the pH of pore solution.
3. The addition of Rheocrete 222+ raises the pH of pore solution.
4. The addition of calcium nitrite significantly increases the quantity of nitrites and nitrates in pore solution while decreasing the sulfate concentrations one day after casting.
5. The addition of Rheocrete 222+ increases the sulfate concentration in pore solution at seven days. No effect is observed on the concentration of sulfates at one day.
6. The addition of Hycrete increases sulfate concentrations both one and seven days after casting. More research is needed to determine if the elevated sulfate concentrations explain the decreased strength and critical chloride corrosion observed in specimens containing Hycrete.

CHAPTER 6

EVALUATION AND ECONOMIC ANALYSIS

This chapter presents an evaluation of the results reported in Chapters 3, 4, and 5. A comparison between Southern Exposure, cracked beam, and field test specimen performance is made using data presented in this report and in research performed by Draper et al. (2009) and Xing et al. (2010). An average corrosion rate is calculated for each corrosion protection system and used in conjunction with the corrosion loss required to crack concrete (Chapter 4) and the time to corrosion initiation (Chapter 3) to determine the service life for each corrosion protection system.

6.1 AVERAGE CORROSION RATES BASED ON CORROSION LOSSES

6.1.1 Procedure

The method for determining the average corrosion rate after initiation for a corrosion protection system proceeds as follows: The corrosion loss plots for individual specimens for each corrosion protection system are analyzed. The corrosion loss plots for FTS-ECR(RH)-U are shown in Figure 6.1 and will be used to demonstrate the method for determining the average corrosion rate. Other corrosion loss plots for field test specimens and for Southern Exposure and cracked beam specimens with conventional reinforcement and corrosion inhibitors are presented in Appendix A. Corrosion loss plots for Southern Exposure and cracked beam specimens with epoxy-coated reinforcement, ECR with increased adhesion, ECR with corrosion inhibitors, and multiple-coated reinforcement are presented in Appendix A of the report by Draper et al. (2009).

To determine the average corrosion rate from the corrosion loss plot (Figure 6.1a), the location at which the corrosion loss of each individual specimen or bar begins to increase steadily is determined and marked (Figure 6.1b). A line connecting the corrosion loss at corrosion initiation to the corrosion loss at the end of testing is drawn for each specimen (Figure 6.1c). The slope of this line is the average corrosion rate for each

specimen. The average of the individual corrosion rates is taken as the average corrosion rate for the corrosion protection system. Specimens or bars that show no increase in corrosion loss, such as FTS-ECR(RH)-U-2 (3) in Figure 6.1, are excluded from the average. The corrosion rates for systems with coated bars are based on the exposed (damaged) area of the bar. Epoxy-coated bars in the bench-scale tests have four or ten holes in the epoxy coating, while field test specimens have 16 holes in the epoxy. Corrosion rates for each system are combined to produce a single average corrosion rate.

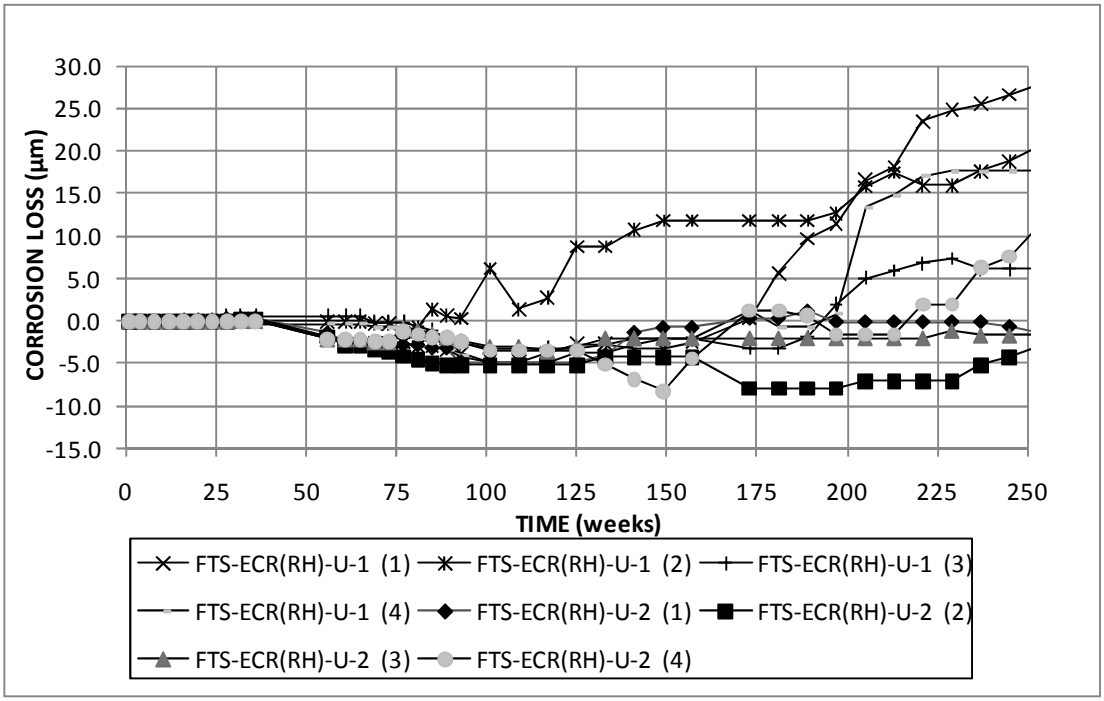

Figure 6.1a: Individual corrosion losses based on exposed area for field test specimens containing Rheocrete in uncracked concrete.

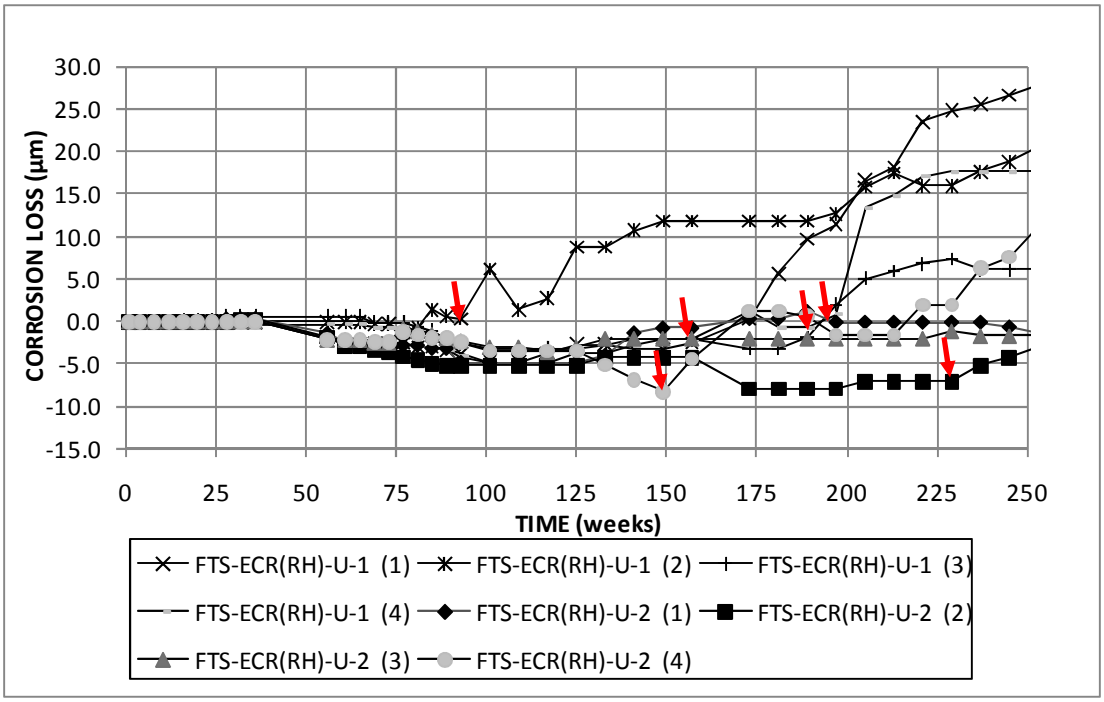

Figure 6.1b: Individual corrosion losses based on exposed area for field test specimens containing Rheocrete in uncracked concrete with corrosion initiation marked.

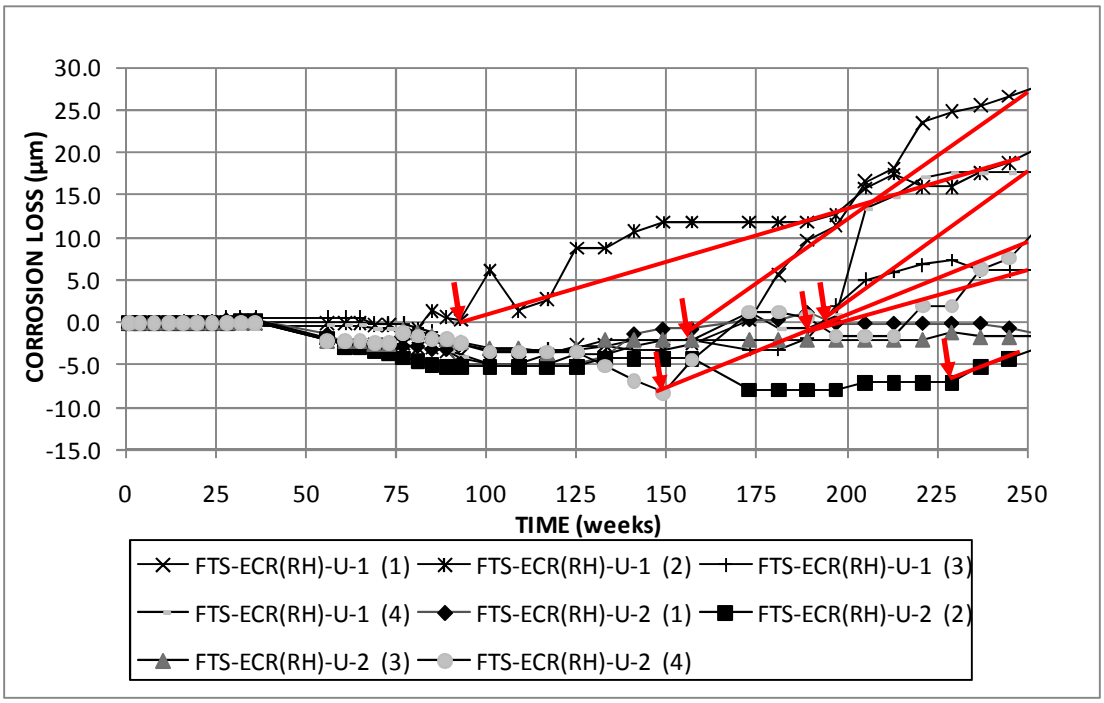

Figure 6.1c: Individual corrosion losses based on exposed area for field test specimens containing Rheocrete in uncracked concrete with lines connecting corrosion loss at initiation to corrosion loss at end of life.

6.1.2 Southern Exposure and Cracked Beam Specimen Results

Table 6.1 shows the individual and average corrosion rates after corrosion initiation, along with the standard deviation and coefficient of variation, for the Southern Exposure specimens. The corrosion rates for specimens with conventional and stainless steel are based on total area; all other corrosion rates are based on exposed area. Based on total area, the specimens with conventional reinforcement (Conv.) tested by Draper et al. (2009) have lower average corrosion rates (5.69 µm/yr) than the specimens with a different heat of conventional reinforcement (Conv.2) presented in Chapter 3 (10.2 µm/yr). The specimens containing conventional reinforcement (Conv.2) and corrosion inhibitors were cast at the same time with the same cement. The specimens containing Conv.2 reinforcement and DCI have an average corrosion rate approximately two-thirds that of specimens without an inhibitor, 6.67 µm/yr compared to 10.2 µm/yr. The specimens containing Conv.2 reinforcement and Rheocrete have an average corrosion rate of 2.91 µm/yr, 28 percent of that observed in the control specimens. The specimens containing Conv.2 reinforcement and Hycrete have the lowest average corrosion rate, 1.25 µm/yr, 12 percent of that observed in the control specimens. The specimens with 2205 pickled stainless steel have an average corrosion rate of 0.074 µm/yr. All specimens with epoxy-coated reinforcement have corrosion rates of less than 0.05 µm/yr based on total area.

Based on exposed area, the specimens with multiple-coated reinforcement have the greatest average corrosion rate, 31.6 µm/yr. This is due to the more active nature of zinc, which will sacrificially corrode to protect the underlying steel. The specimens with conventional ECR have an average corrosion rate of 10.4 µm/yr. For the specimens containing ECR and corrosion inhibitors, the specimens containing DCI and Rheocrete have average corrosion rates slightly less than that of the specimens containing no inhibitor, 7.81 and 8.63 µm/yr, respectively. The specimens containing ECR with a calcium nitrite primer have an average corrosion rate of 12.6 µm/yr, greater than

conventional ECR. The specimens containing ECR with Hycrete have an average corrosion rate of 0.674 µm/yr. Among the specimens with the increased adhesion epoxies, corrosion rates are between 12.4 and 16.9 µm/yr, all greater than that of conventional ECR.

Table 6.1: Average Corrosion Rate (µm/yr) after Corrosion Initiation for Southern Exposure Specimens.

	System	Specimen 1	2	3	4	5	6	Average	Standard Deviation	COV
Total Area	**Control**									
	Conv.[a]	5.35	4.41	5.10	6.04	5.82	7.40	5.69	1.01	0.18
	Conv.2	10.7	9.74	10.0				10.1	0.49	0.05
	Corrosion Inhibitors									
	Conv.2(DCI)	7.81	5.11	7.09				6.67	1.40	0.21
	Conv.2(RH)	2.57	2.60	3.56				2.91	0.56	0.19
	Conv.2(HY)	0.791	1.03	1.92				1.25	0.60	0.48
	Stainless Steel									
	DCB-2205p	[b]	0.080	[b]	[b]	[b]	[b]	0.074	0.05	0.69
	MCB-2205p	[b]	0.026	[b]	[b]	0.116	[b]			
Exposed Area	**Control**									
	ECR[a]	13.6	[b]	[b]	5.98	18.4	12.7	10.43	5.32	0.51
		6.74	5.09	[b]						
	Corrosion Inhibitors									
	ECR(DCI)[a]	[b]	9.36	[b]	[b]	11.8	2.33	7.81	4.90	0.63
	ECR(RH)[a]	[b]	[b]	5.94	[b]	11.3	[b]	8.63	3.80	0.44
	ECR(HY)[a]	[b]	[b]	[b]	[b]	[b]	0.674	0.674	-	-
	ECR(primer/$Ca(NO_2)_2$)[a]	[b]	3.66	22.0	6.56	24.4	6.39	12.6	9.79	0.78
	Multiple Coated Bars									
	MC[a]	5.55	22.7	36.9	6.57	23.1	7.52	31.6	26.2	0.83
		19.6	29.2	13.1	65.9	80.7	68.8			
	Increased Adhesion									
	ECR(Chromate)[a]	[b]	13.0	18.1	1.18	11.6	20.5	12.9	7.48	0.58
	ECR(DuPont)[a]	13.8	24.3	[b]	4.72	7.79	11.2	12.4	7.51	0.61
	ECR(Valspar)[a]	15.5	5.91	44.0	12.3	6.52	17.4	16.9	14.0	0.83

[a] Corrosion loss data from Draper et al. (2009)

[b] No corrosion observed

Table 6.2 shows the individual and average corrosion rates for the cracked beam specimens. As seen for the Southern Exposure specimens (Table 6.1), the CB-Conv.

specimens reported by Draper et al. (2009) show lower average corrosion rates than the CB-Conv.2 specimens presented in Chapter 3, 7.00 µm/yr compared to 16.3 µm/yr (Table 6.2). The average corrosion rate of all specimens with conventional reinforcement is 48 percent greater for the cracked beam specimens than for the Southern Exposure specimens. The specimens containing DCI and conventional reinforcement have the greatest average corrosion rate of the specimens containing conventional reinforcement and inhibitors, 14.5 µm/yr, or approximately 89 percent of the average corrosion rate observed for control specimens. The specimens containing Rheocrete have an average corrosion rate of 11.9 µm/yr, which is 73 percent of that observed in control specimens, and the specimens containing Conv.2 reinforcement and Hycrete have the lowest average corrosion rate, 4.17 µm/yr, or 26 percent of that observed in control specimens. The corrosion rates in the cracked beam specimens with conventional reinforcement and corrosion inhibitors are two to four times higher than the corrosion rates observed in the matching Southern Exposure specimens. The specimens with 2205 pickled stainless steel have an average corrosion rate of 0.218 µm/yr.

Based on exposed area, the specimens with multiple-coated reinforcement exhibit the greatest average corrosion rate, 68.6 µm/yr, more than twice the rate observed in Southern Exposure specimens. At 8.07 µm/yr, the specimens with conventional ECR have an average corrosion rate that is slightly less than that observed in Southern Exposure specimens. The specimens with corrosion inhibitors and ECR have greater corrosion rates than the specimens without inhibitors, ranging from 8.73 to 17.0 µm/yr. Among the specimens with the increased adhesion epoxies, the corrosion rates are between 16.4 and 25.9 µm/yr, all greater than the rates observed for the specimens with conventional ECR.

Table 6.2: Average Corrosion Rate (µm/yr) after Corrosion Initiation for Cracked Beam Specimens.

	System	Specimen 1	2	3	4	5	6	Average	Standard Deviation	COV
Total Area	**Control**									
	Conv.[a]	9.42	4.50	3.82	8.32	8.18	7.74	7.00	2.27	0.32
	Conv.2	24.6	12.2	12.1				16.3	7.16	0.44
	Corrosion Inhibitors									
	Conv.2(DCI)	17.5	14.4	11.6				14.5	2.96	0.20
	Conv.2(RH)	13.6	9.80	12.4				11.9	1.96	0.16
	Conv.2(HY)	4.91	3.44	4.16				4.17	0.74	0.18
	Stainless Steel									
	DCB-2205p	[b]	0.036	[b]				0.218	0.159	0.73
	MCB-2205p	[b]	0.328	[b]	[b]	0.29	[b]			
Exposed Area	**Control**									
	ECR[a]	8.57	18.3	2.63	2.29	9.20	3.69	8.07	5.86	0.73
		13.8	12.2	1.99						
	Corrosion Inhibitors									
	ECR(DCI)[a]	6.19	18.9	16.6	4.58	16.7	4.10	11.2	6.90	0.62
	ECR(RH)[a]	12.7	15.3	17.8	27.1	14.2	15.1	17.0	5.21	0.31
	ECR(HY)[a]	1.87	6.98	25.5	[b]	13.3	6.37	10.8	9.18	0.85
	ECR(primer/$Ca(NO_2)_2$)[a]	2.38	13.5	5.74	15.6	6.02	9.19	8.73	5.03	0.58
	Multiple Coated Bars									
	MC[a]	36.8	44.7	169	16.2	10.5	39.7	68.6	51.9	0.76
		129	68.7	98.7	21.8	132	55.5			
	Increased Adhesion									
	ECR(Chromate)[a]	14.1	11.9	29.1	2.37	14.3	50.4	20.4	17.0	0.84
	ECR(DuPont)[a]	33.5	48.5	14.5	13.2	14.7	31.1	25.9	14.2	0.55
	ECR(Valspar)[a]	41.1	16.9	0.770	8.28	4.62	26.6	16.4	15.3	0.93

[a] Corrosion loss data from Draper et al. (2009)

[b] No corrosion observed

The specimens containing corrosion inhibitors and conventional reinforcement all show significant reductions in the average corrosion rate compared to specimens without inhibitors in both cracked and uncracked concrete, although the reductions in the corrosion rate in cracked concrete are somewhat less than those observed in uncracked concrete. However, three of the four systems combining corrosion inhibitors with ECR exhibit corrosion rates in Southern Exposure specimens that are comparable to that observed in concrete without corrosion inhibitors. All cracked beam specimens

containing corrosion inhibitors and ECR also have average corrosion rates greater than that observed for the specimens with conventional ECR alone. Because the corrosion rates for specimens with ECR are very low even in the absence of inhibitors, small variations (in absolute terms) in the voltage drop across the 10-ohm resistor for specimens with ECR are large compared to the magnitude of the voltage drop and will be reflected as large changes in corrosion rate. As a result, the coefficients of variation in corrosion rate observed in most of the specimens containing coated bars are large. Given the large variations in performance among specimens, the performance of specimens containing DCI and Rheocrete with epoxy-coated reinforcement is comparable to specimens containing ECR in concrete without corrosion inhibitors in both cracked and uncracked concrete. Likewise, the performance of ECR with the calcium nitrite primer in cracked beam specimens is comparable to the performance of conventional ECR. The specimens containing Hycrete and ECR show some improvement compared to the control specimens in uncracked concrete, but no improvement is observed in cracked concrete. Overall, specimens containing any form of ECR exhibit low corrosion rates compared to specimens with conventional reinforcement. The Student's T-test is used to determine the significance of these differences in corrosion rate in Section 6.5.2.1.

6.1.3 Field Test Specimen Results

Tables 6.3 shows the individual and average corrosion rates after corrosion initiation for the field test specimens with uncracked concrete. Based on total area, the specimens with conventional reinforcement show the greatest average corrosion rate, 0.882 µm/yr. No corrosion is observed in the specimens with pickled 2205 reinforcement.

Based on exposed area, the specimens with ECR exhibit an average corrosion rate of 5.68 µm/yr. The specimens with the increased adhesion Valspar epoxy and the specimens with multiple-coated reinforcement have average corrosion rates greater than

Table 6.3: Average Corrosion Rate (µm/yr) after Corrosion Initiation for Field Test Specimens with Uncracked Concrete.

	System	Specimen	Bar				Average	Standard Deviation	COV
			1	2	3	4			
Total Area	**Control**								
	Conv.	1	1.55	0.77			0.882	0.62	0.71
		2	[a]	0.322					
	Stainless Steel								
	2205p	1	[a]	[a]			-	-	-
		2	[a]	[a]					
Exposed Area	**Control**								
	ECR	1	9.86	10.1			5.68	4.21	0.74
		2	0.587	4.90	[a]	2.97			
	Corrosion Inhibitors								
	ECR(DCI)	1	3.58	3.69	1.64	2.73	4.26	2.81	0.66
		2	6.62	10.3	4.95	1.41			
		3	4.47	7.86	0.904	2.96			
	ECR(RH)	1	10.2	5.24	6.49	3.97	5.43	3.68	0.68
		2	1.49	0.856	[a]	9.72			
	ECR(HY)	1	1.82	[a]	1.75	6.09	2.89	1.62	0.56
		2	1.52	3.74	3.11	2.18			
	ECR(primer/$Ca(NO_2)_2$)	1	[a]	1.89	4.25	2.60	4.49	2.95	0.66
		2	10.3	3.78	2.36	6.22			
	Multiple Coated Bars								
	MC	1	5.54	6.58			6.31	3.39	0.54
		2	11.9	6.35	1.29	6.68			
	Increased Adhesion								
	ECR(Chromate)	1	4.86	2.50			4.83	3.35	0.69
		2	10.4	[a]	1.97	4.40			
	ECR(DuPont)	1	5.35	2.95			5.14	5.99	1.17
		2	0.710	5.35	1.41	17.0			
	ECR(Valspar)	1	2.38	9.77			9.11	4.90	0.54
		2	15.0	[a]	12.0	6.39			

[a] No corrosion observed

those observed in specimens with conventional ECR, with average rates of 9.11 and 6.31 µm/yr, respectively. All specimens containing corrosion inhibitors and ECR have average corrosion rates comparable to or less than those observed in specimens with conventional ECR only. The specimens containing Rheocrete and ECR have the greatest average corrosion rate among specimens containing inhibitors, 5.43 µm/yr. The specimens containing DCI and ECR and those containing ECR with the calcium nitrite

primer exhibit similar corrosion rates of 4.26 and 4.49 µm/yr, respectively. The specimens containing Hycrete and ECR have the lowest average corrosion rate, 2.89 µm/yr. Specimens containing increased adhesion Chromate and DuPont ECR have average corrosion rates of 4.83 and 5.14 µm/yr, respectively, that are comparable to the corrosion rate observed in specimens with conventional ECR.

Table 6.4 shows the individual and average corrosion rates for field test specimens with cracks in the concrete above the top reinforcing bar. Based on total area, the specimens with conventional reinforcement show an average corrosion rate based on total area, 0.939 µm/yr. No corrosion is observed in the specimens with pickled 2205 reinforcement.

Based on exposed area, the specimens with ECR show an average corrosion rate of 8.13 µm/yr, which is greater than the other specimens, except for the specimens containing Rheocrete (8.38 µm/yr) and the specimens containing ECR with a chromate pretreatment (8.94 µm/yr). Among the specimens containing corrosion inhibitors, the specimens containing Rheocrete have the greatest average corrosion rate, 8.38 µm/yr. The specimens containing DCI and the specimens containing ECR with the calcium nitrite primer have corrosion rates of 5.79 and 4.65 µm/yr, respectively. The specimens containing Hycrete have the lowest average corrosion rate, 4.32 µm/yr. The specimens containing the increased adhesion DuPont and Valspar ECR show average corrosion rates of 6.50 and 7.64 µm/yr, respectively. It is important to note that, as discussed in Section 3.3.2, the concrete in specimens containing conventional ECR is of higher quality than the concrete in specimens containing DCI, Rheocrete, MC bars, and the bars with the calcium nitrite primer, which might explain the superior performance of ECR relative to these corrosion protection systems, both in cracked and uncracked concrete (Tables 6.3 and 6.4).

Table 6.4: Average Corrosion Rate (µm/yr) after Corrosion Initiation for Field Test Specimens with Cracked Concrete.

	System	Specimen	Bar				Average	Standard Deviation	COV
			1	2	3	4			
Total Area	**Control**								
	Conv.	1	0.482	1.65			0.939	0.61	0.65
		2	0.897	0.731					
	Stainless Steel								
	2205p	1	[a]	[a]			-	-	-
		2	[a]	[a]					
Exposed Area	**Control**								
	ECR	1	2.91	10.3			8.13	7.82	0.96
		2	5.76	22.6	4.58	5.72			
	Corrosion Inhibitors								
	ECR(DCI)	1	3.20	4.97	8.67	8.22	5.79	3.60	0.62
		2	1.62	10.1	7.52	5.51			
		3	0.634	0.500	7.95	10.6			
	ECR(RH)	1	9.92	8.34	6.07	7.74	8.38	1.64	0.20
		2	11.2	8.38	7.68	7.78			
	ECR(HY)	1	6.12	2.06	12.0	[a]	4.32	4.31	1.00
		2	2.12	2.28	[a]	1.36			
	ECR(primer/$Ca(NO_2)_2$)	1	9.28	2.22	4.75	[a]	4.65	2.13	0.46
		2	1.78	4.25	3.90	6.40			
	Multiple Coated Bars								
	MC	1	5.64	10.9			8.11	5.29	0.65
		2	1.47	5.89	6.40	14.2			
	Increased Adhesion								
	ECR(Chromate)	1	5.06	5.79			8.94	8.65	0.97
		2	25.6	6.43	6.31	11.4			
	ECR(DuPont)	1	3.79	5.72			6.50	4.05	0.62
		2	10.8	2.30	12.8	7.10			
	ECR(Valspar)	1	3.76	11.6			7.64	4.93	0.65
		2	7.19	16.5	8.46	1.99			

[a] No corrosion observed

6.1.4 Bench-scale Linear Polarization Resistance (LPR) Results

The average corrosion rates based on total corrosion loss after corrosion initiation as measured by LPR are also calculated for the bench-scale specimens. LPR data for the Southern Exposure and cracked beam specimens with epoxy-coated reinforcement, ECR

with increased adhesion, ECR with corrosion inhibitors, and multiple-coated reinforcement appear in reports by Draper et al. (2009) and Xing et al. (2010).

Table 6.5 shows the average total corrosion rates for Southern Exposure specimens based on LPR. As before, the corrosion rates for specimens with conventional reinforcement are based on total area, and the corrosion rates for specimens with epoxy-coated reinforcement are based on exposed area. Among specimens with conventional reinforcement, the specimens with Conv. and Conv.2 reinforcement show similar corrosion rates, at 20.5 and 17.0 µm/yr, respectively. It should be noted that although Conv. reinforcement exhibits lower macrocell corrosion rates in the Southern Exposure test program than Conv.2 reinforcement (Table 6.1), it exhibits greater total corrosion rates based on LPR than Conv.2 reinforcement. The total corrosion rate of Conv.2(DCI) is 9.79 µm/yr, 58 percent of the rate measured for Conv.2 with no inhibitor. Conv.2(RH) and Conv.2(HY) have corrosion rates equal to 22 and 11 percent of that measured for Conv.2 with no inhibitor.

Among the specimens with epoxy coatings, the specimens with multiple-coated reinforcement exhibit the highest total corrosion rate, 219 µm/yr. The specimens with bars with increased adhesion epoxies exhibit corrosion rates between 24.3 and 84.6 µm/yr, all greater than conventional ECR (21.2 µm/yr). The specimen with ECR in concrete containing DCI exhibits a corrosion rate of 32.6 µm/yr, greater than the rate of the specimen with conventional ECR alone. These corrosion rates are greater than the rates measured for the specimen with conventional ECR in all likelihood due to variations among specimens (LPR is only performed on a single specimen for each corrosion protection system) and not deficiencies in the corrosion protection system. The specimens with ECR in concrete containing Rheocrete and Hycrete show very low corrosion rates, at 1.72 and 1.64 µm/yr, respectively.

Table 6.5: Total Corrosion Rate (µm/yr) after Corrosion Initiation from LPR Corrosion Loss for SE Specimens.

	Specimen	Corrosion Rate
Total Area	**Control**	
	Conv.[a]	20.5
	Conv.2	17.0
	Corrosion Inhibitors	
	Conv.2(DCI)	9.79
	Conv.2(RH)	3.82
	Conv.2(HY)	1.82
Exposed Area	**Control**	
	ECR[a]	21.2
	Corrosion Inhibitors	
	ECR(DCI)[a]	32.6
	ECR(RH)[a]	1.72
	ECR(HY)[a]	1.64
	ECR(primer/$Ca(NO_2)_2$)[a]	10.2
	Multiple Coated Bars	
	MC[a]	219
	Increased Adhesion	
	ECR(Chromate)[a]	24.3
	ECR(DuPont)[a]	50.2
	ECR(Valspar)[a]	84.6

[a] Corrosion loss data from Draper et al. (2009)

Table 6.6 shows the average total corrosion rates after corrosion initiation based on LPR for the cracked beam specimens. The corrosion rates for specimens with conventional reinforcement are based on total area, and the corrosion rates for specimens with epoxy-coated reinforcement are based on exposed area. Among the specimens with conventional reinforcement, the specimens with Conv. and Conv.2 reinforcement have total corrosion rates of 90.3 and 30.6 µm/yr, respectively. Again, Conv. reinforcement exhibits lower macrocell corrosion rates in the cracked beam test program than Conv.2 reinforcement (Table 6.2), but greater total corrosion rates based on LPR compared to Conv.2 reinforcement. The total corrosion rates of specimens with Conv.2(DCI) and Conv.2(RH) are 107 and 48.3 µm/yr, respectively, which are both greater than the rate of

the specimen with Conv.2 and no inhibitor. As discussed earlier, these corrosion rates are greater than control specimen corrosion rates in all likelihood due to variations among specimens and not deficiencies in the corrosion protection system. The Conv.2(HY) specimen has a corrosion rate equal to 60 percent of the rate exhibited by the control specimen.

Table 6.6: Total Corrosion Rate (µm/yr) after Corrosion Initiation from LPR Corrosion Loss for CB Specimens

	Specimen	Corrosion Rate
Total Area	**Control**	
	Conv.[a]	90.3
	Conv.2	30.6
	Corrosion Inhibitors	
	Conv.2(DCI)	107
	Conv.2(RH)	48.3
	Conv.2(HY)	18.2
Exposed Area	**Control**	
	ECR[a]	169
	Corrosion Inhibitors	
	ECR(DCI)[a]	174
	ECR(RH)[a]	364
	ECR(HY)[a]	96.4
	ECR(primer/$Ca(NO_2)_2$)[a]	181
	Multiple Coated Bars	
	MC[a]	562
	Increased Adhesion	
	ECR(Chromate)[a]	277
	ECR(DuPont)[a]	195
	ECR(Valspar)[a]	399

[a] Corrosion loss data from Draper et al. (2009)

Among the specimens with epoxy coatings, the specimen with the multiple-coated reinforcement exhibits the greatest total corrosion rate of 562 µm/yr. The specimens with epoxy-coated bars with increased adhesion exhibit corrosion rates between 195 and 399 µm/yr – all greater than the rate observed for the specimen with conventional ECR (169

µm/yr). The specimens with ECR in concrete containing Rheocrete and DCI exhibit corrosion rates of 364 and 174 µm/yr, respectively, values that are greater than the corrosion rate for the specimen with conventional ECR alone. The specimen with ECR in concrete containing Hycrete has the lowest corrosion rate among specimens with bars with epoxy coatings, at 96.4 µm/yr.

A comparison is made between total corrosion rate and macrocell corrosion rate for bench-scale specimens in Section 6.4. The relationship between total and macrocell corrosion rate for bench-scale specimens is used to estimate the total corrosion rate for field test specimens based on the macrocell FTS rates presented in Tables 6.3 and 6.4. This estimated total FTS corrosion rate is used to estimate the service life of each corrosion protection system.

6.2 COMPARISONS BETWEEN TEST METHODS

All the corrosion protection systems in this study are tested with multiple test programs, including Southern Exposure, cracked beam, and field test specimens with cracked and uncracked concrete. To establish relationships between the test programs, the average corrosion rates presented in Section 6.1 are compared across the test programs.

6.2.1 Comparison between Southern Exposure and Cracked Beam Tests

6.2.1.1 Conventional Reinforcement and ECR

Figure 6.2 compares the average corrosion rates based on total area for Southern Exposure and cracked beam specimens containing conventional reinforcement with and without corrosion inhibitors and the specimens with ECR. The x-axis shows the average corrosion rates from the Southern Exposure test program, and the y-axis shows the average corrosion rates from the cracked beam test program. The error bars parallel to the x-axis indicate the minimum and maximum corrosion rates observed in an individual Southern Exposure specimen of a given type, and the error bars parallel to the y-axis

show minimum and maximum corrosion rates for cracked beam specimens of a given type. A best fit line passing through the origin is fit to the data.

As shown in Figure 6.2, the specimens with conventional ECR show negligible corrosion losses based on total area compared to the specimens with conventional reinforcement with and without inhibitors. A general trend is observed in the data, with the best-fit line passing near the range for all data points with the exception of specimens containing Rheocrete. The slope of the best-fit line indicates that the cracked beam specimens with conventional reinforcement exhibit an average corrosion rate 1.8 times greater than those observed in the Southern Exposure specimens (Figure 6.2).

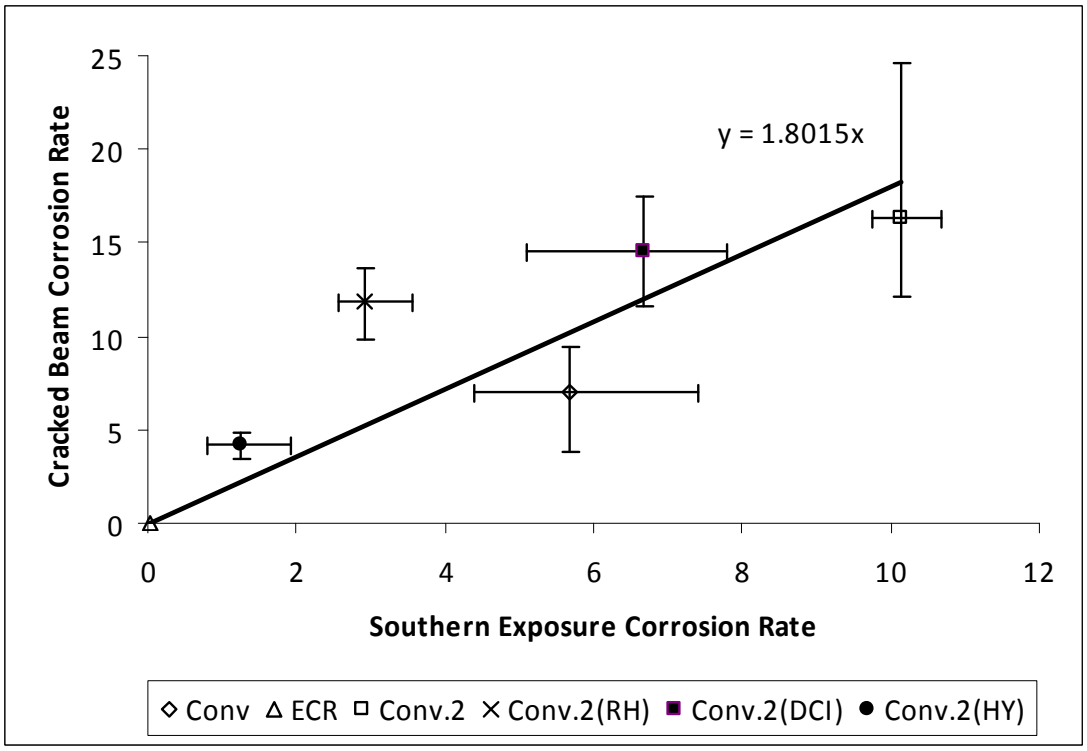

Figure 6.2: Comparison between average corrosion rates after corrosion initiation (µm/yr) based on total area for Southern Exposure and cracked beam specimens with conventional reinforcement with and without inhibitors.

6.2.1.2 ECR with Increased Adhesion

Figure 6.3 compares the average corrosion rates based on exposed area for Southern Exposure and cracked beam specimens containing ECR and ECR with increased adhesion. The specimens with increased adhesion show greater average corrosion rates than specimens with conventional ECR in both the Southern Exposure and cracked beam tests. A best-fit line indicates that cracked beam specimens containing ECR with increased adhesion exhibit average corrosion rates 1.60 times greater than the Southern Exposure specimens. Conventional ECR is included in the figure for comparison, but is not used in determining the best-fit line.

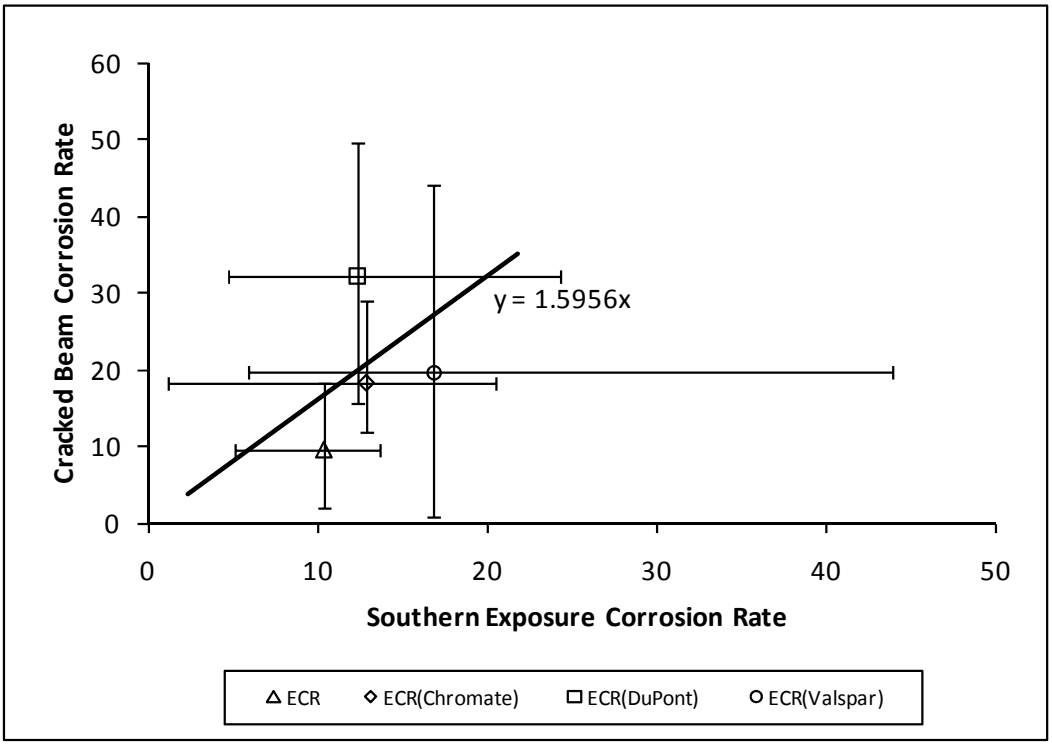

Figure 6.3: Comparison between average corrosion rates after corrosion initiation (µm/yr) based on exposed area for Southern Exposure and cracked beam specimens containing ECR and ECR with increased adhesion (ECR excluded from best-fit line).

6.2.1.3 ECR with Corrosion Inhibitors

Figure 6.4 compares the average corrosion rates based on exposed area for the Southern Exposure and cracked beam specimens containing ECR in concrete containing corrosion inhibitors and the specimens containing ECR with the calcium nitrite primer. The specimens containing Hycrete show significantly greater corrosion rates in the cracked beam test than those in the Southern Exposure test. The other specimens containing corrosion inhibitors show similar average rates between the Southern Exposure and cracked beam tests. A best fit line shows that cracked beam specimens containing corrosion inhibitors exhibit average corrosion rates 1.16 times greater than the Southern Exposure specimens.

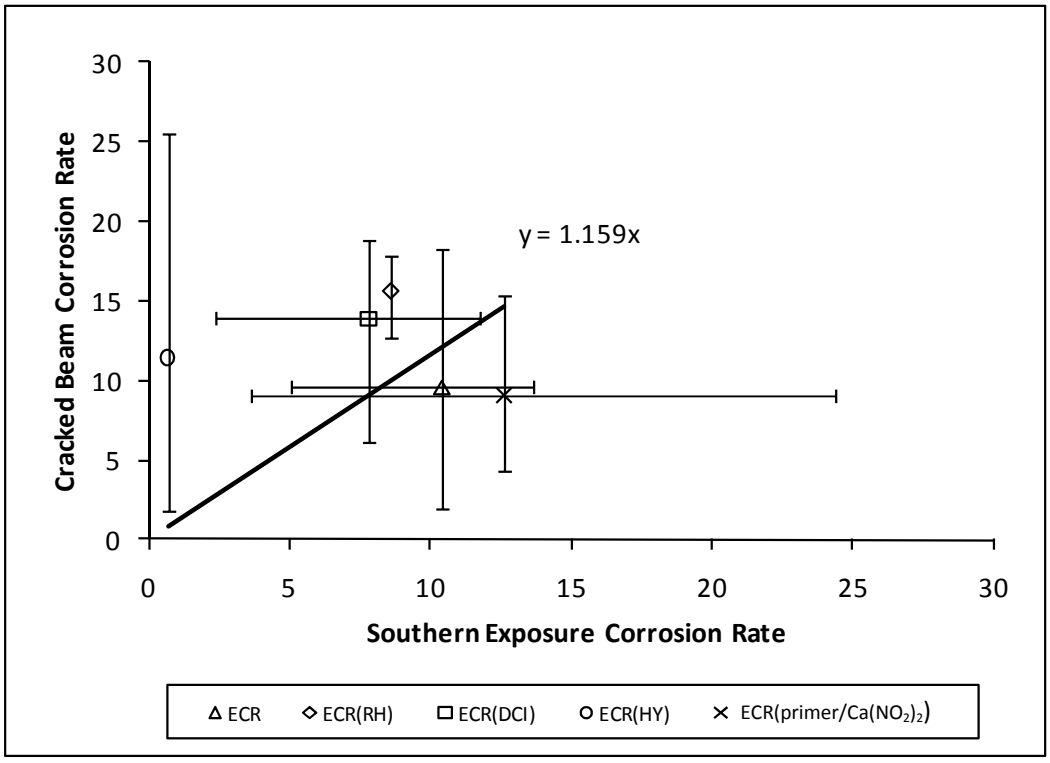

Figure 6.4: Comparison between average corrosion rates after corrosion initiation (µm/yr) based on exposed area for Southern Exposure and cracked beam specimens containing ECR in concrete with corrosion inhibitors and ECR with the calcium nitrite primer (ECR and ECR(HY) excluded from best-fit line).

6.2.1.4 Multiple-Coated Reinforcement

Figure 6.5 compares the average corrosion rates based on exposed area for Southern Exposure and cracked beam specimens containing multiple-coated reinforcement. The specimens containing multiple-coated reinforcement show significantly greater average corrosion rates than the specimens with conventional ECR in both the Southern Exposure and cracked beam tests. In the cracked beam test, specimens with multiple-coated reinforcement exhibit average corrosion rates that are over twice as high as those observed in the Southern Exposure test. Specimens with MC reinforcement also exhibit a much greater variation in corrosion rates than specimens with ECR.

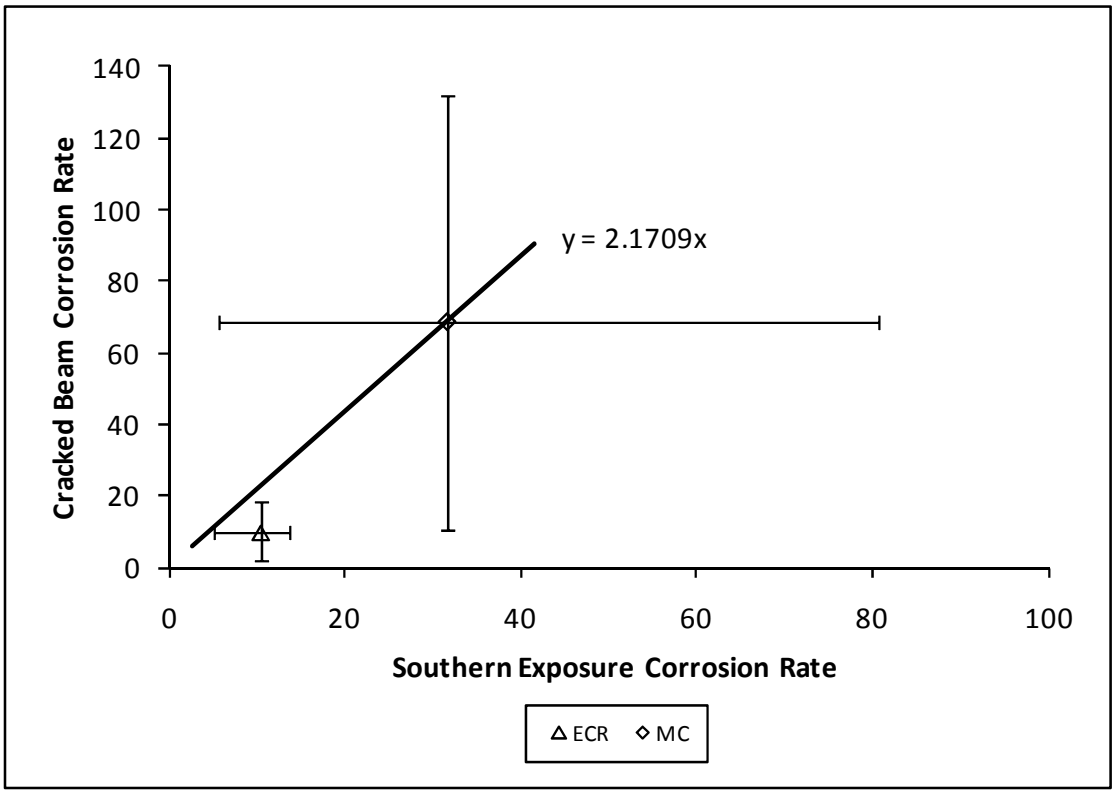

Figure 6.5: Comparison between average corrosion rates after corrosion initiation (µm/yr) based on exposed area for Southern Exposure and cracked beam specimens containing MC reinforcement.

6.2.1.5 Summary

Figure 6.6 compares the average corrosion rates based on exposed area for all Southern Exposure and cracked beam specimens with coated reinforcement. A best-fit line through all the data points shows that the cracked beam specimens exhibit a corrosion rate approximately 1.78 times greater than that of the Southern Exposure specimens, with an R^2 value of 0.72. (R^2 values were not calculated for Figures 6.2 through 6.5 due to the low number of data points in those figures).

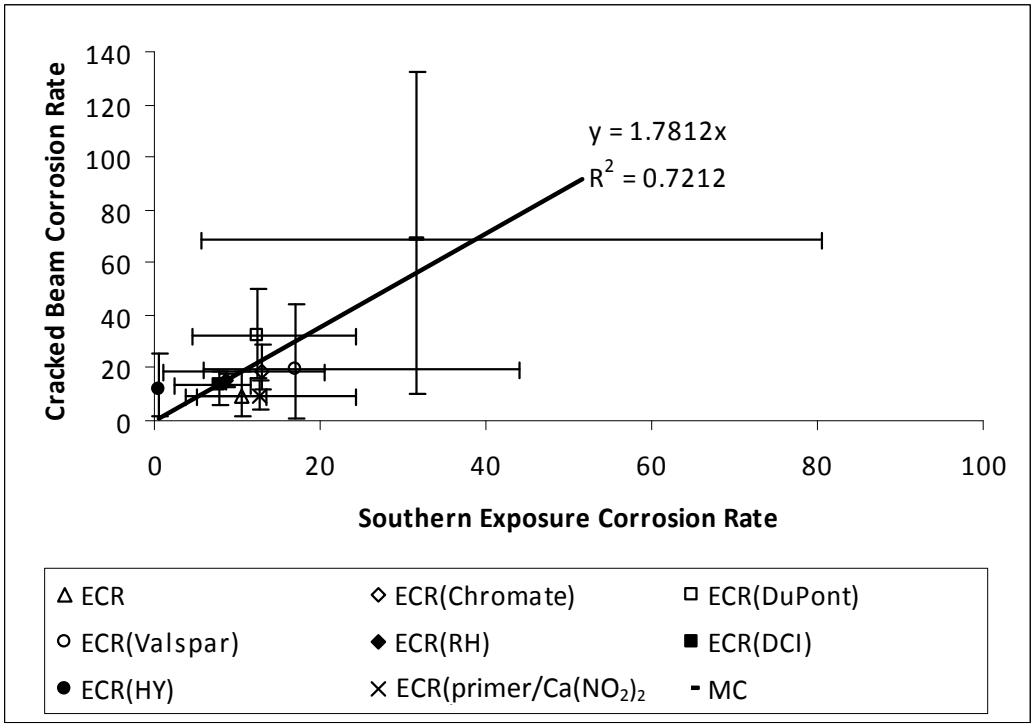

Figure 6.6a: Comparison between average corrosion rates after corrosion initiation (µm/yr) based on exposed area for all Southern Exposure and cracked beam specimens.

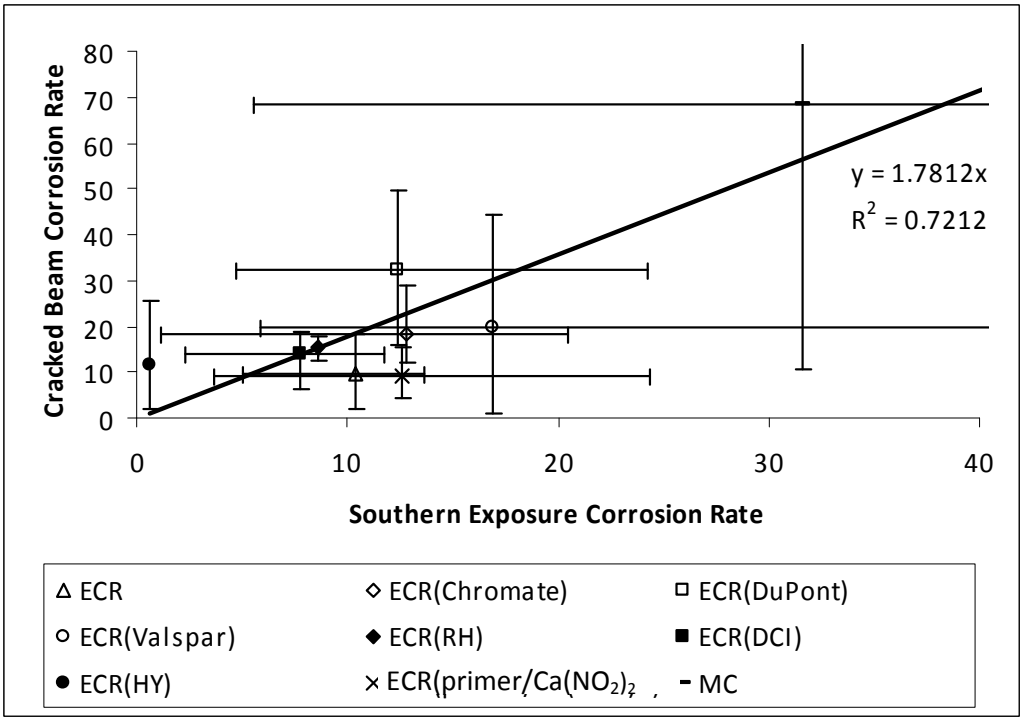

Figure 6.6b: Comparison between average corrosion rates after corrosion initiation (µm/yr) based on exposed area for all Southern Exposure and cracked beam specimens (different scale).

6.2.2 Comparison between Uncracked and Cracked Field Test Specimens

6.2.2.1 Conventional Reinforcement and ECR

Figure 6.7 compares the average corrosion rates based on total area for uncracked and cracked field test specimens containing conventional reinforcement and specimens with ECR. The x-axis shows the average corrosion rates from the field test specimens with uncracked concrete, and the y-axis shows the average corrosion rates from the field test specimens with simulated cracks placed above four reinforcing bars in the top mat of reinforcement.

Figure 6.7 shows that the specimens with ECR have negligible corrosion losses based on total area when compared to the specimens with conventional reinforcement. The specimens with conventional reinforcement show similar corrosion rates in cracked

and uncracked concrete, with a large variation in corrosion rate among specimens in uncracked concrete. (Figure 6.7).

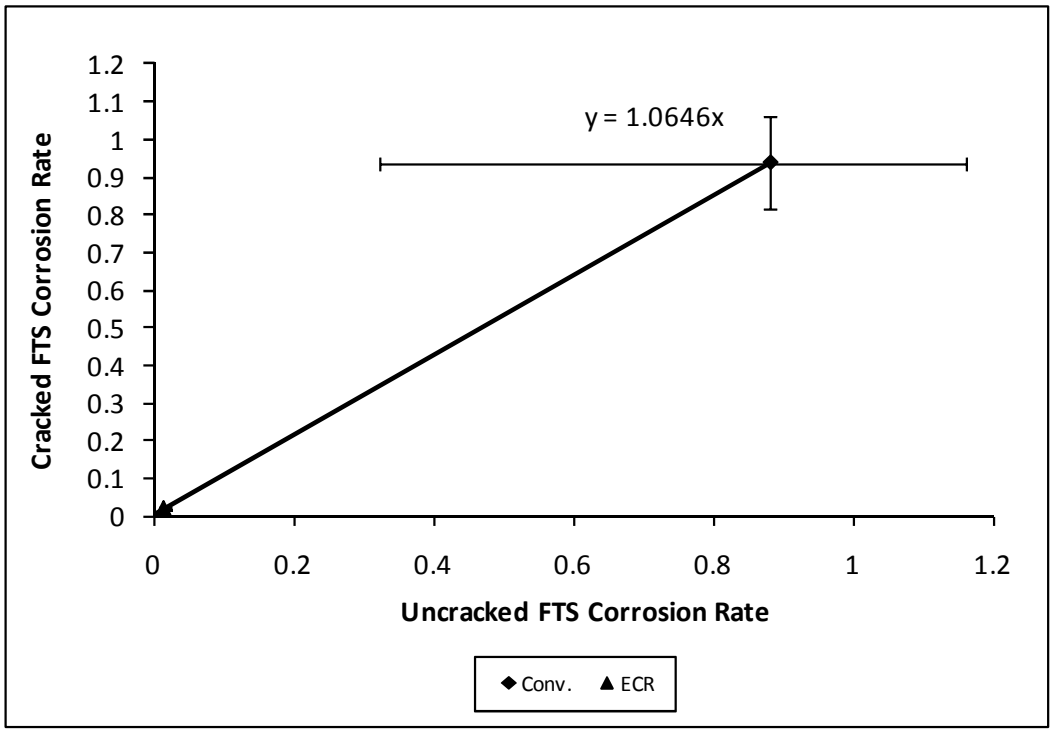

Figure 6.7: Comparison between average corrosion rates after corrosion initiation (µm/yr) based on total area for uncracked and cracked field test specimens with conventional and epoxy-coated reinforcement.

6.2.2.2 ECR with Increased Adhesion

Figure 6.8 compares the average corrosion rates based on exposed area for uncracked and cracked field test specimens containing ECR and ECR with increased adhesion. The specimens with increased adhesion show average corrosion rates comparable to the specimens with conventional ECR in cracked field test specimens; however, in uncracked concrete, the specimens with increased adhesion epoxy from Valspar show significantly higher corrosion rates than the specimens with conventional ECR. A best-fit line indicates that the cracked field test specimens containing ECR with increased adhesion exhibit average corrosion rates that are approximately 1.10 times that in the uncracked FTS.

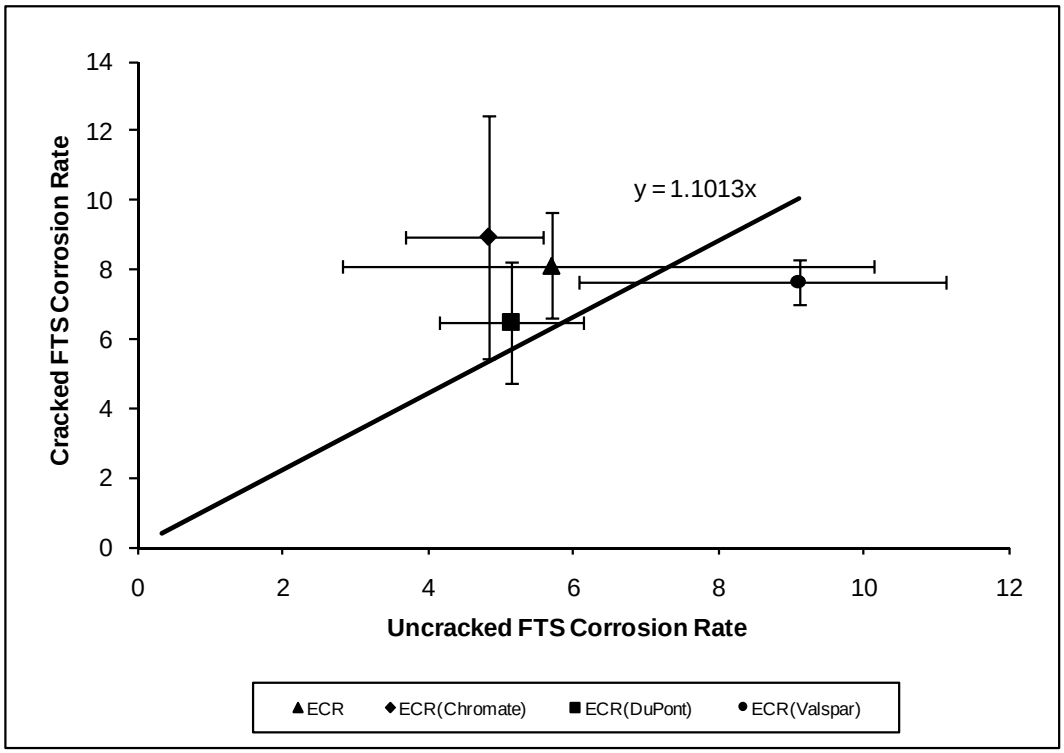

Figure 6.8: Comparison between average corrosion rates after corrosion initiation (µm/yr) based on exposed area for uncracked and cracked field test specimens containing ECR and ECR with increased adhesion (ECR excluded from best-fit line).

6.2.2.3 ECR with Corrosion Inhibitors

Figure 6.9 compares the average corrosion rates based on exposed area for uncracked and cracked field test specimens containing ECR in concrete containing corrosion inhibitors. The specimens containing Rheocrete show average corrosion rates comparable to the rates observed in specimens with conventional ECR; however, the quality of concrete for specimens containing Rheocrete is lower than the quality of concrete for specimens containing conventional ECR, as discussed in Section 3.3.2. The other specimens containing corrosion inhibitors show lower average rates than the specimens without inhibitors in both cracked and uncracked concrete. A best fit line shows the specimens containing corrosion inhibitors exhibit corrosion rates in cracked

field test specimens that are approximately 1.36 times those observed in uncracked field test specimens.

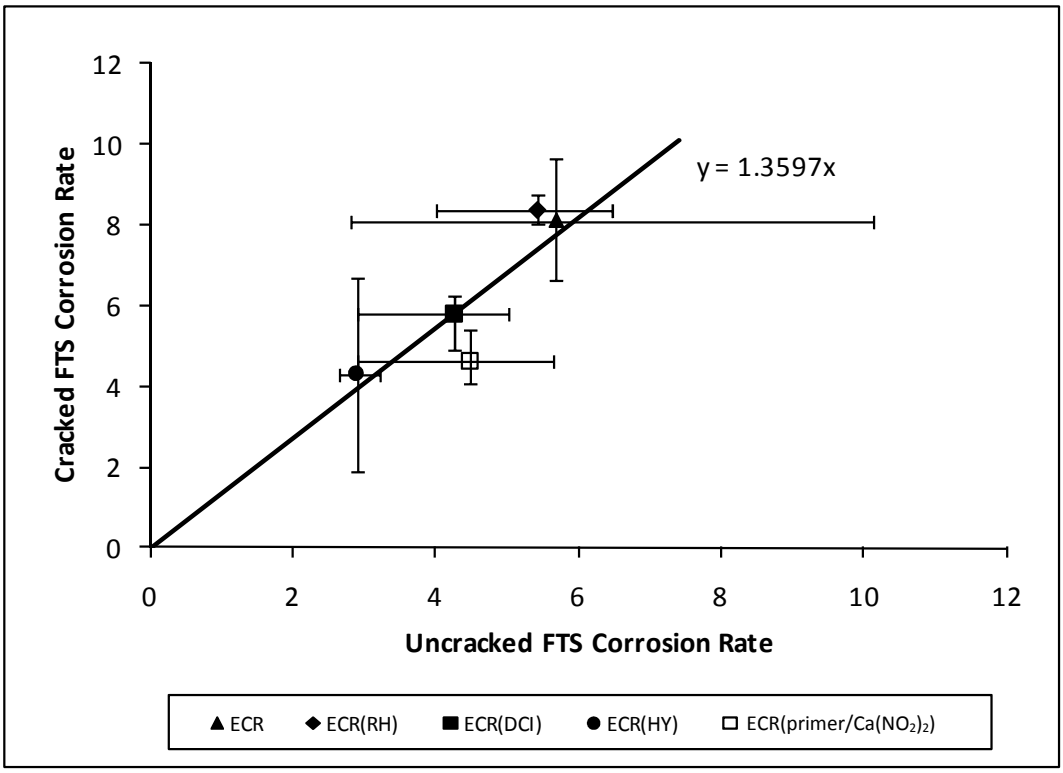

Figure 6.9: Comparison between average corrosion rates after corrosion initiation (µm/yr) based on exposed area for uncracked and cracked field test specimens containing ECR in concrete with corrosion inhibitors (ECR excluded from best-fit line).

.2.2.4 Multiple-Coated Reinforcement

Figure 6.10 compares the average corrosion rates based on exposed area for uncracked and cracked field test specimens containing multiple-coated reinforcement. In field test specimens, multiple-coated reinforcement exhibits average corrosion rates comparable to the specimens with conventional ECR in both cracked and uncracked concrete, as opposed to the bench-scale specimens where MC reinforcement exhibits corrosion rates over five times that of conventional ECR. The cracked field test specimens with multiple-coated reinforcement have an average corrosion rate approximately 1.29 times that of the uncracked field test specimens.

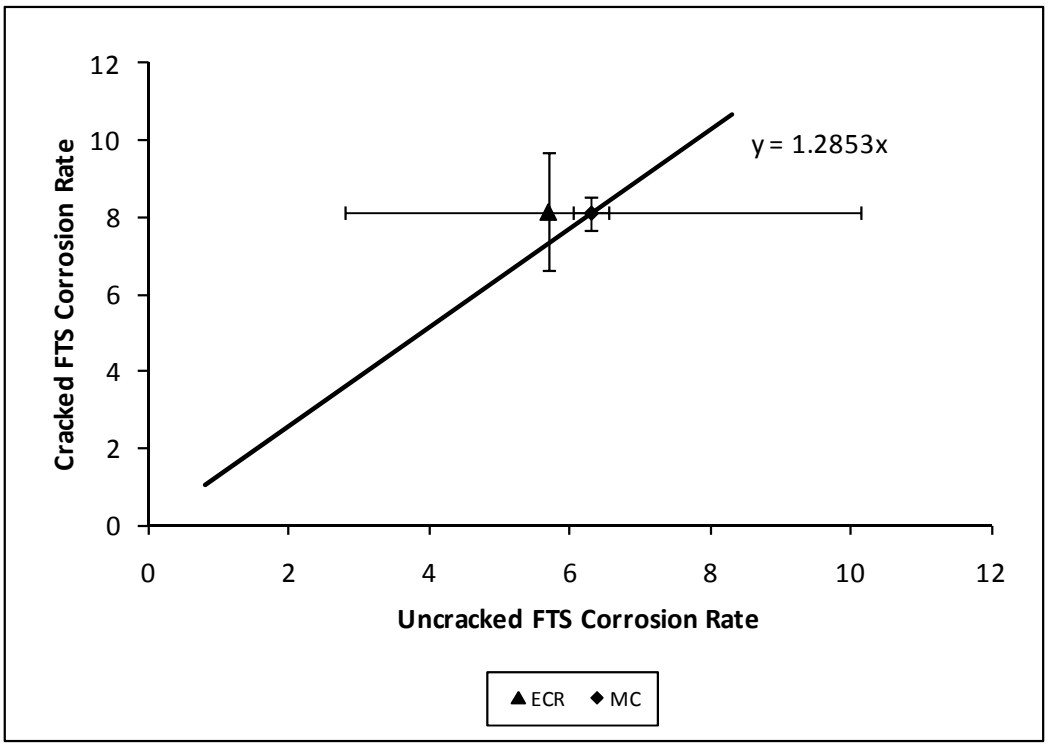

Figure 6.10: Comparison between average corrosion rates after corrosion initiation (µm/yr) based on exposed area for uncracked and cracked field test specimens containing ECR and MC reinforcement (ECR excluded from best-fit line).

6.2.2.5 Summary

Figure 6.11 compares the average corrosion rates based on exposed area for all uncracked and cracked field test with ECR or MC reinforcement. A best-fit line through all of the data points shows that the field test specimens with cracked concrete exhibit a corrosion rate that is about 23 percent greater than that of the field test specimens with uncracked concrete. By comparison, the cracked beam specimens exhibit a corrosion rate that is 78 percent greater than the Southern Exposure specimens (Figure 6.6). One possible explanation for this discrepancy is that in the cracked beam specimens, the crack exposes a proportionally greater percentage of the bar length than it does in the cracked field test specimens. The top mat of the cracked beam specimens consists of a 304.8-mm (12-in.) long bar with a 152.4-mm (6-in.) long crack, exposing 50 percent of the bar length. The test bar for the field test specimens has a test length of 991 mm (39 in.) with a 304.8-mm (12-in.) long crack, exposing 30 percent of the bar length. Furthermore, the

CB specimens are subjected to more frequent and more severe salt exposure than the field test specimens.

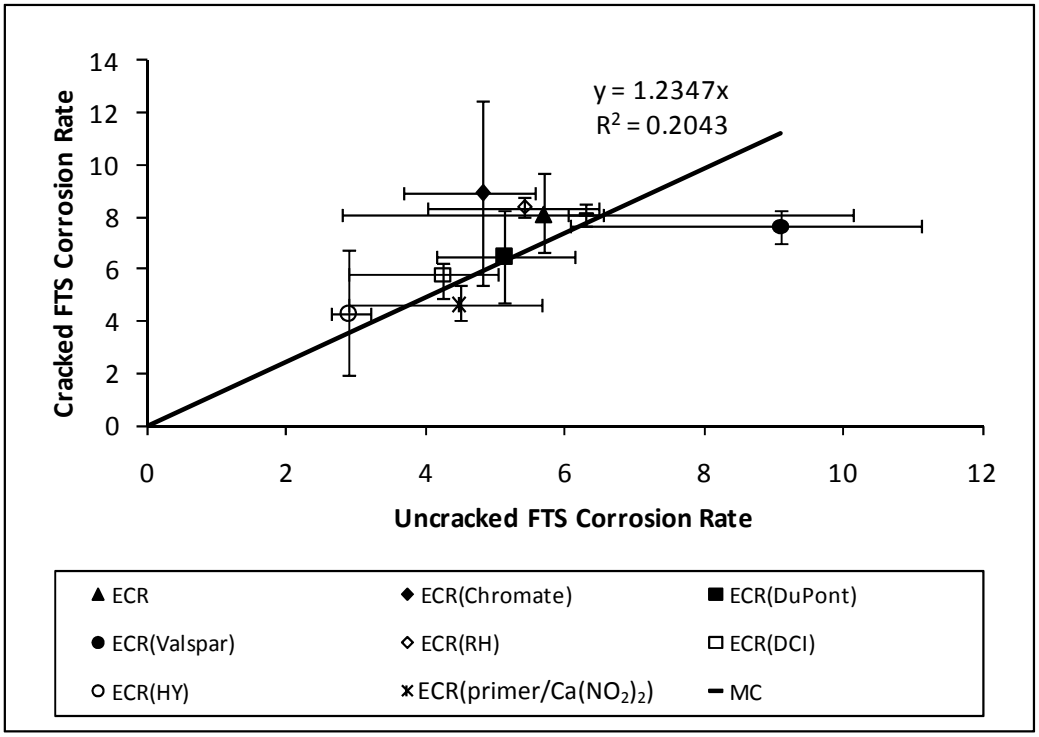

Figure 6.11: Comparison between average corrosion rates after corrosion initiation (µm/yr) based on exposed area for all uncracked and cracked field test specimens.

6.2.3 Comparison between Bench-scale and Field Test Specimens

6.2.3.1 Conventional Reinforcement and ECR

Figures 6.12a and 6.12b compare the average corrosion rates based on total area for the bench-scale and field test specimens containing conventional reinforcement and the specimens with ECR in uncracked and cracked concrete, respectively. The x-axis shows the average corrosion rates for the bench-scale specimens, and the y-axis shows the average corrosion rates for the field test specimens. Comparisons are made between the Southern Exposure and the uncracked field test specimens (indicated with a U) and between the cracked beam and the cracked field test specimens (indicated with a C).

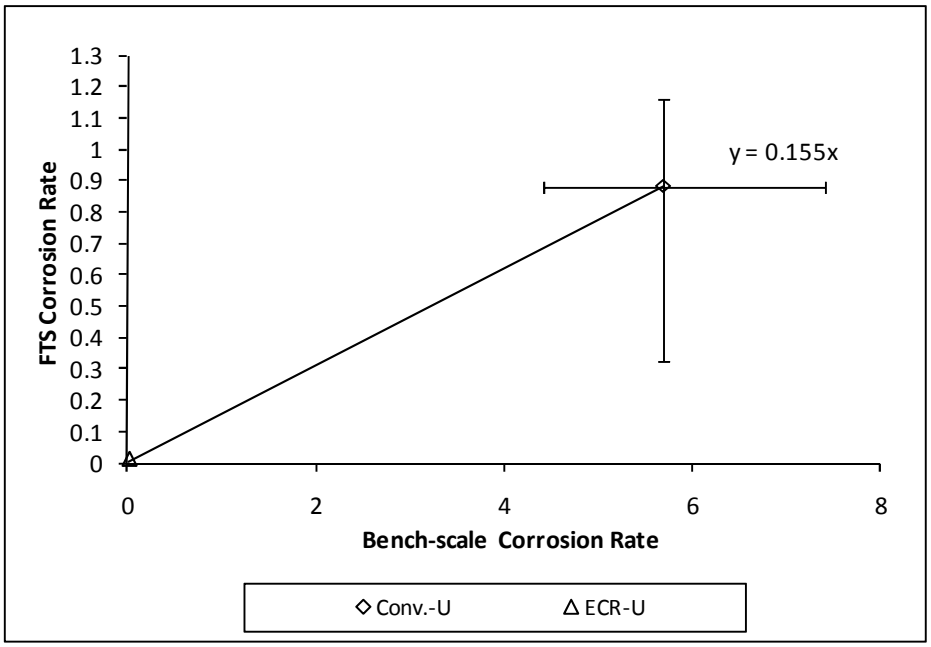

Figure 6.12a: Comparison between average corrosion rates after corrosion initiation (µm/yr) based on total area for bench-scale and field test specimens with conventional and epoxy-coated reinforcement in uncracked concrete.

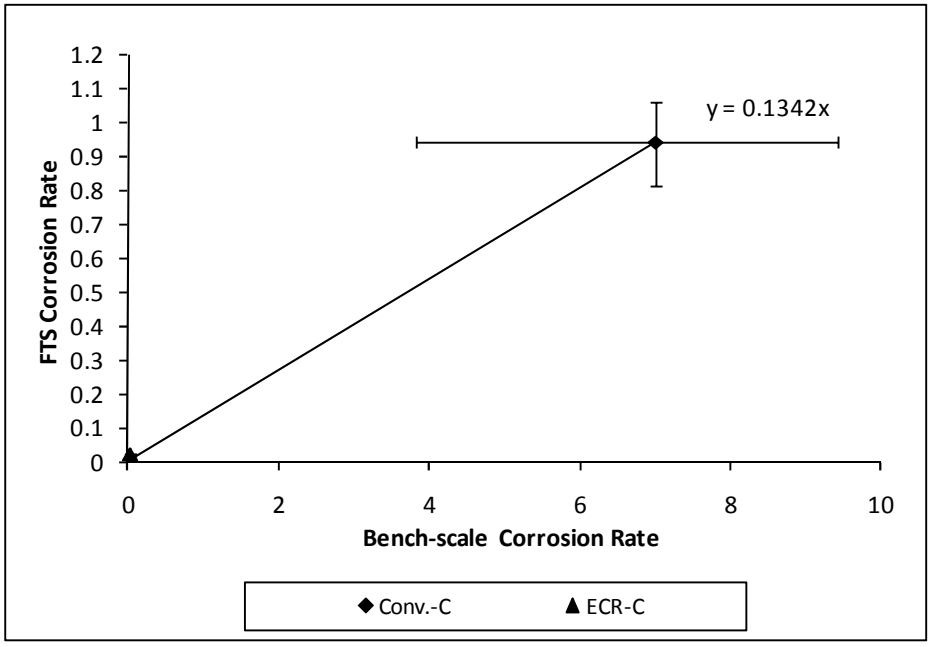

Figure 6.12b: Comparison between average corrosion rates after corrosion initiation (µm/yr) based on total area for bench-scale and field test specimens with conventional and epoxy-coated reinforcement in cracked concrete.

As shown before, Figures 6.12a and 6.12b demonstrate that the specimens with ECR have negligible corrosion losses based on total area when compared to specimens with conventional reinforcement. In uncracked and cracked concrete, the average corrosion rates for conventional reinforcement in the field test are on average 15.5 and 13.4 percent of the rates observed in the bench-scale tests.

6.2.3.2 ECR with Increased Adhesion

Figures 6.13a and 6.13b compare the average corrosion rates based on exposed area for the bench-scale and field test specimens containing ECR and ECR with increased adhesion in uncracked and cracked concrete, respectively. All of the specimens containing ECR with increased adhesion have greater corrosion rates in the cracked beam specimens than in the Southern Exposure specimens. With the exception of specimens containing Valspar increased adhesion epoxy, specimens containing reinforcement with increased adhesion epoxies have greater corrosion rates in cracked field test specimens than in uncracked field test specimens. ECR-DuPont-C exhibits behavior significantly different from other systems and is not included in the best-fit line. A best-fit line to the corrosion rates for ECR with increased adhesion shows that the specimens containing ECR with increased adhesion exhibit average corrosion rates in the field test specimens that are 46 and 44 percent of those observed in the bench-scale specimens in uncracked and cracked concrete, respectively.

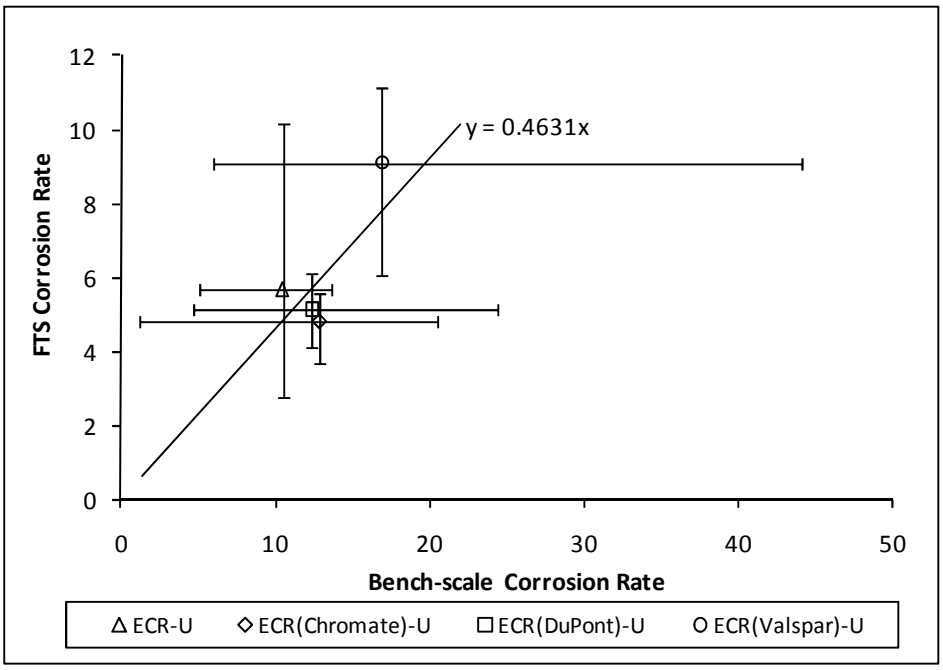

Figure 6.13a: Comparison between average corrosion rates after corrosion initiation (µm/yr) based on exposed area for bench-scale and field test specimens containing ECR and ECR with increased adhesion in uncracked concrete (ECR excluded from best-fit line).

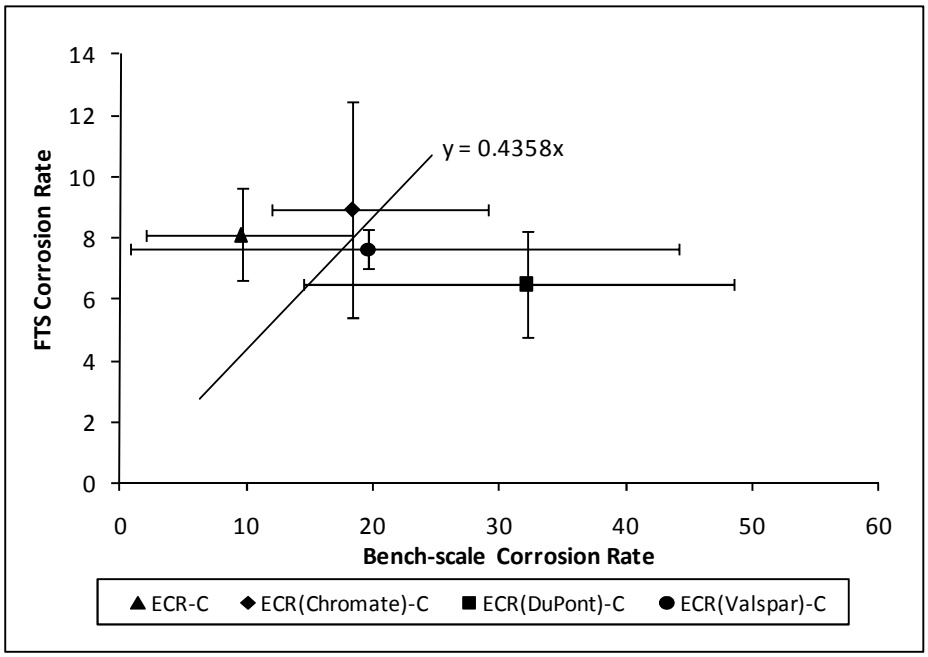

Figure 6.13b: Comparison between average corrosion rates after corrosion initiation (µm/yr) based on exposed area for bench-scale and field test specimens containing ECR and ECR with increased adhesion in cracked concrete (ECR excluded from best-fit line).

6.2.3.3 ECR with Corrosion Inhibitors

Figures 6.14a and 6.14b compare the average corrosion rates based on exposed area for the bench-scale and field test specimens containing ECR in concrete containing corrosion inhibitors in uncracked and cracked concrete, respectively. Many of the specimens show large variations in the range of corrosion rates, particularly the specimens containing ECR with the calcium nitrite primer. ECR-HY-U exhibits behavior significantly different from other systems and is not included in the best-fit line. Again, the comparison between corrosion rates in the bench-scale and field tests are similar in uncracked and cracked concrete; a best-fit line for the corrosion rates for ECR with inhibitors shows the average corrosion rate for specimens containing corrosion inhibitors in field test specimens is about 47 percent of the rate observed in the bench-scale specimens in both uncracked and cracked concrete.

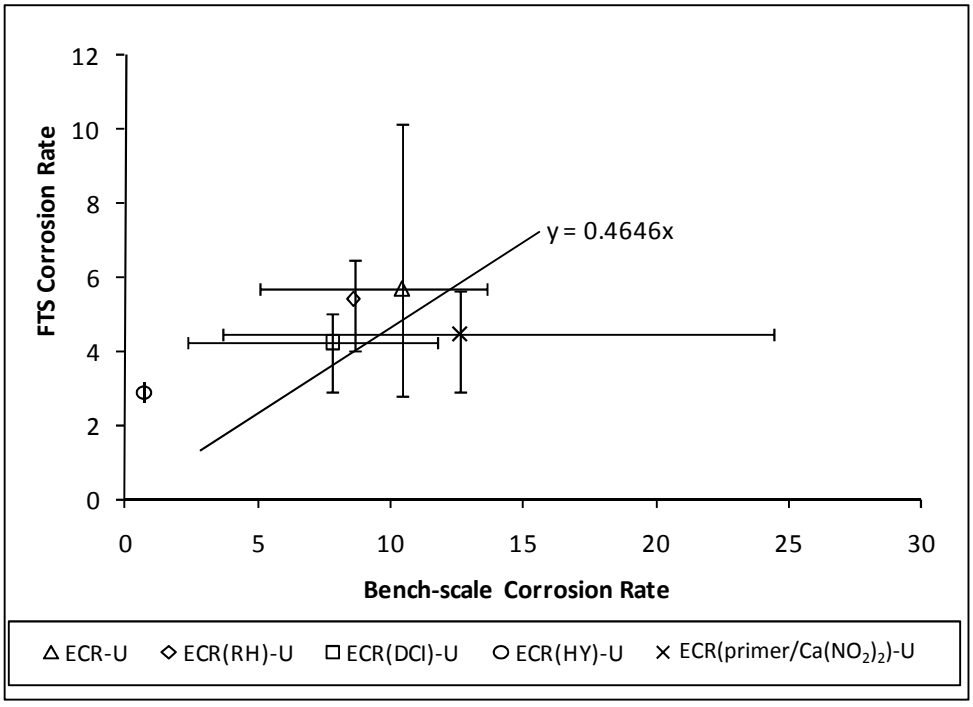

Figure 6.14a: Comparison between average corrosion rates after corrosion initiation (µm/yr) based on exposed area for bench-scale and field test specimens containing ECR in concrete with corrosion inhibitors in uncracked concrete (ECR excluded from best-fit line).

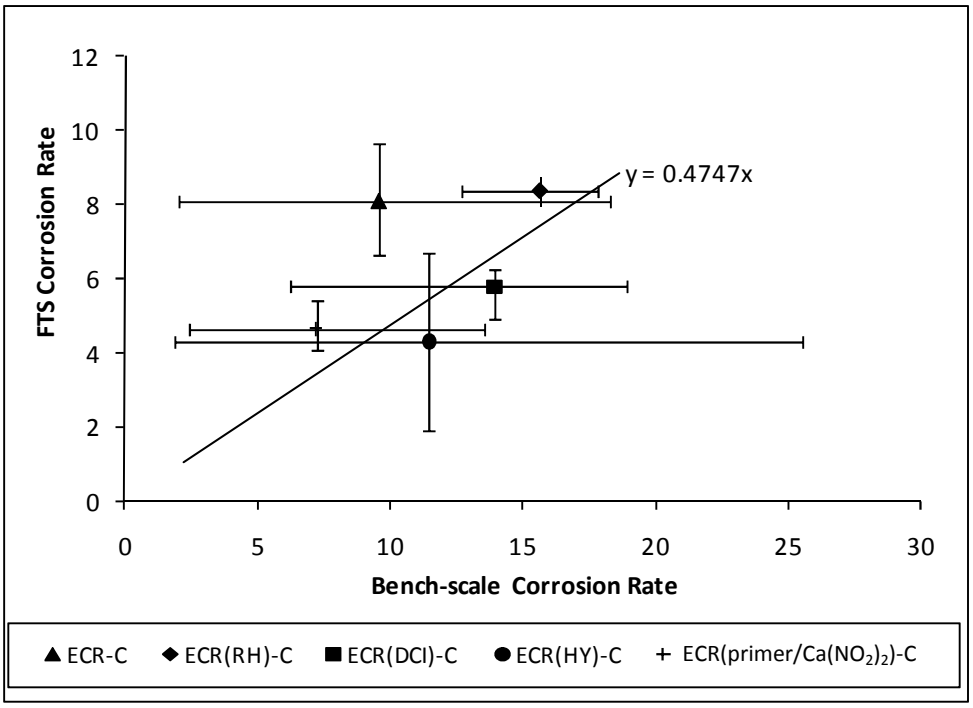

Figure 6.14b: Comparison between average corrosion rates after corrosion initiation (µm/yr) based on exposed area for bench-scale and field test specimens containing ECR in concrete with corrosion inhibitors in uncracked concrete (ECR excluded from best-fit line).

6.2.3.4 Multiple-Coated Reinforcement

Figures 6.15a and 6.15b compare the average corrosion rates based on exposed area for the bench-scale and field test specimens containing ECR and multiple-coated reinforcement in uncracked and cracked concrete, respectively. In the field test specimens, the specimens containing multiple-coated reinforcement have average corrosion rates that are comparable to specimens with conventional ECR; however, the corrosion rates for the bench-scale specimens containing MC reinforcement are several times greater than the corrosion rates for bench-scale specimens containing ECR. As a result, field test specimens containing MC reinforcement exhibit average corrosion rates in uncracked and cracked concrete that are only about 20 and 12 percent, respectively, of those observed in bench-scale specimens; ratios that are comparable to that observed for conventional reinforcement but are far lower than observed in any other specimens

containing bars with an epoxy coating. This difference in performance is likely due to the difference in the moisture content of concrete between the bench-scale and field tests – while concrete in the bench-scale tests is saturated for over three quarters of the test, concrete in the field test remains dry for most of the test. Because of its greater reactivity, zinc would be expected to be more sensitive to moisture content than iron. This suggests multiple-coated reinforcement in a bridge deck will show corrosion rates comparable to conventional ECR; however, MC reinforcement in continuously saturated concrete, such as a bridge pier in a marine environment, would exhibit very high corrosion rates.

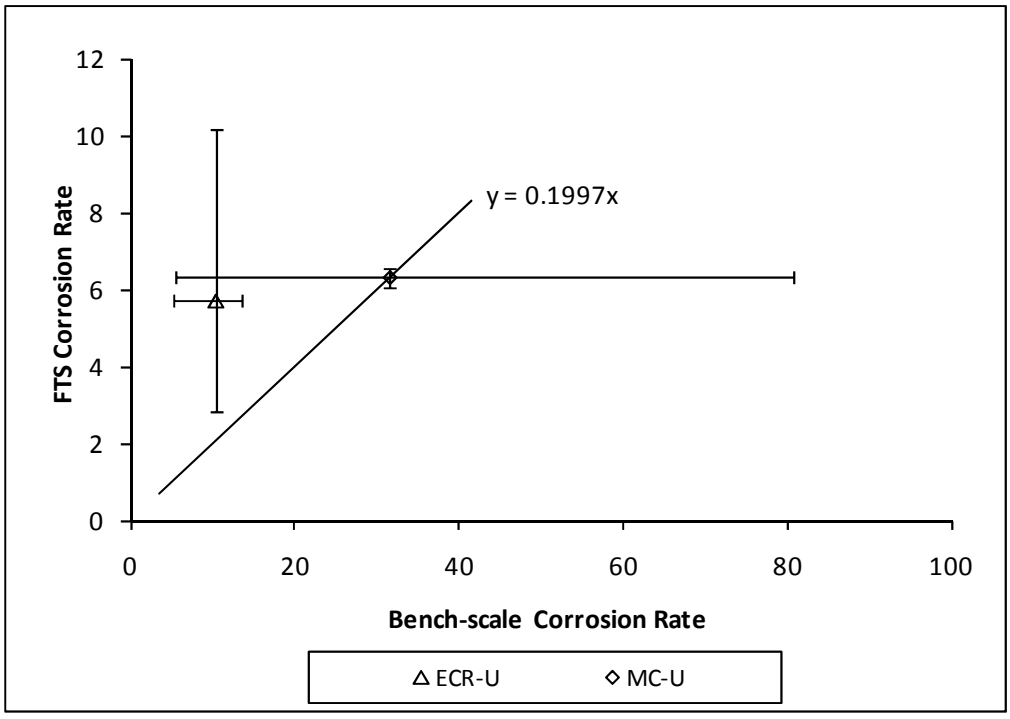

Figure 6.15a: Comparison between average corrosion rates after corrosion initiation (µm/yr) based on exposed area for bench-scale and field test specimens containing ECR and MC reinforcement in uncracked concrete (ECR excluded from best-fit line).

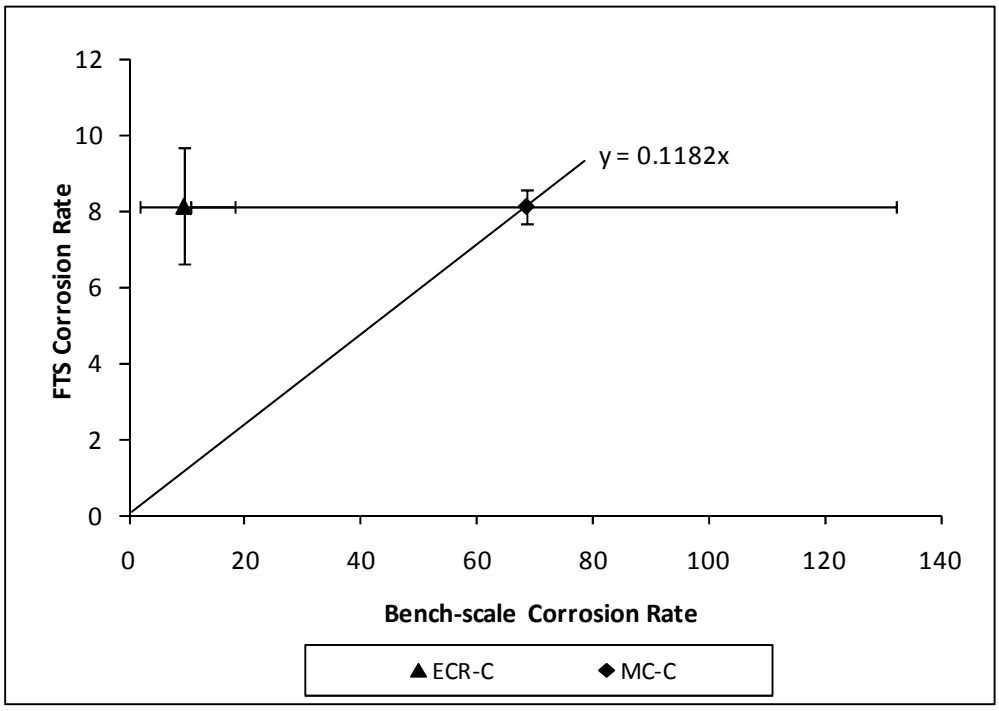

Figure 6.15b: Comparison between average corrosion rates after corrosion initiation (µm/yr) based on exposed area for bench-scale and field test specimens containing ECR and MC reinforcement in cracked concrete (ECR excluded from best-fit line).

6.2.3.5 Summary

Figure 6.16a compares the average corrosion rates based on exposed area for all bench-scale and field test specimens with ECR or MC reinforcement. A best-fit line through all of the data points shows that the average corrosion rate in field test specimens is about 23 percent of that observed in bench-scale specimens. However, this percentage is lowered somewhat by the behavior exhibited by the field test specimens with multiple-coated reinforcement (Figure 6.15). Furthermore, ECR(DuPont)-C and ECR(HY)-U appear to be outliers, as described above. Removing the specimens with the multiple-coated bars (Figure 6.16b) and the two outliers shows that for the specimens with ECR, corrosion rates in the field test specimens are about 47 percent of those observed in bench-scale specimens. The higher corrosion rates exhibited by the bench-scale tests are due to the harsher exposure conditions in the Southern Exposure and cracked beam test programs.

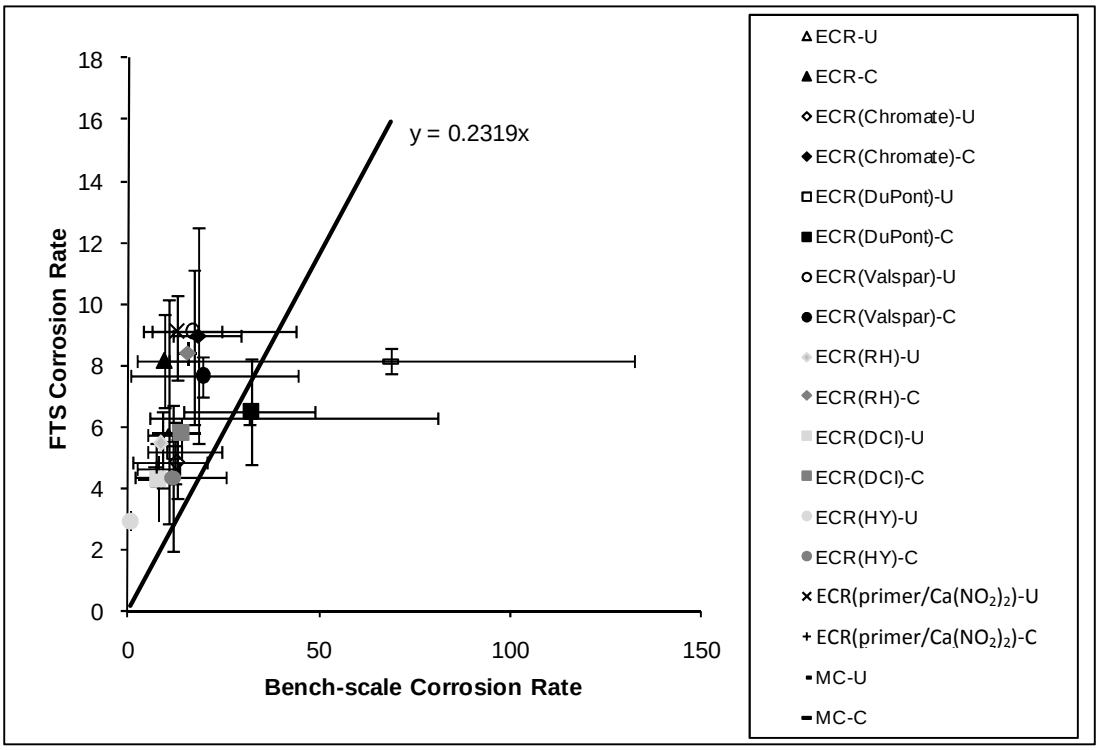

Figure 6.16a: Comparison between average corrosion rates after corrosion initiation (µm/yr) based on exposed area for all bench-scale and field test specimens.

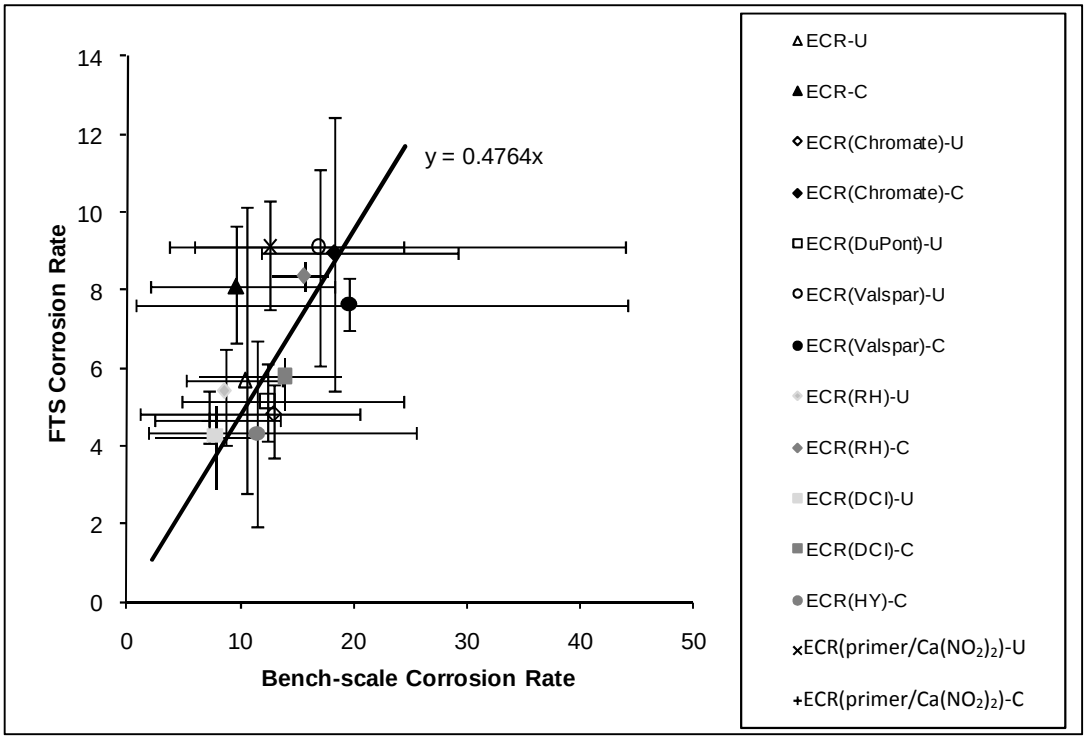

Figure 6.16b: Comparison between average corrosion rates after corrosion initiation (µm/yr) based on exposed area for all bench-scale and field test specimens (MC bars and outliers excluded).

6.3 CORROSION LOSS AND DISBONDMENT

To obtain a broader understanding of the performance of the different corrosion protection systems, the corrosion loss for each specimen is plotted against the measured disbondment of the epoxy coating. After establishing relationships between corrosion loss and disbondment for the individual corrosion protection systems, the relationship between corrosion loss and disbondment is compared across test programs. The relationship between corrosion loss and disbondment for Southern Exposure and cracked beam specimens containing epoxy-coated bars with and without inhibitors, ECR with increased adhesion, and MC bars was originally discussed by Draper et al. (2009).

6.3.1 Corrosion Loss Versus Disbondment – All Test Programs

6.3.1.1 ECR

Average corrosion loss is compared with disbonded area for specimens containing conventional ECR in Figure 6.17. The x-axis shows the macrocell corrosion loss based on exposed area at the end of testing, while the y-axis indicates the disbonded area measured after autopsy. The data points indicate average values for each test program, with the error bars indicating minimum and maximum values. The dashed horizontal line at 677 mm^2 (1.05 $in.^2$) indicates the value corresponding to total disbondment, as discussed in Section 2.3.7. A best-fit line to the data is used to establish a relationship between corrosion loss and disbonded area. For conventional ECR, the best-fit line indicates that, on average, a 1-µm increase in corrosion loss will result in a 22.8 mm^2 (0.035 $in.^2$) increase in disbonded area, with 29.7 µm of corrosion loss being required for total disbondment to occur (Figure 6.17). For comparison, conventional ECR shows a disbondment rate of 56.1 mm^2 per µm of loss in the rapid macrocell test (Section 3.4).

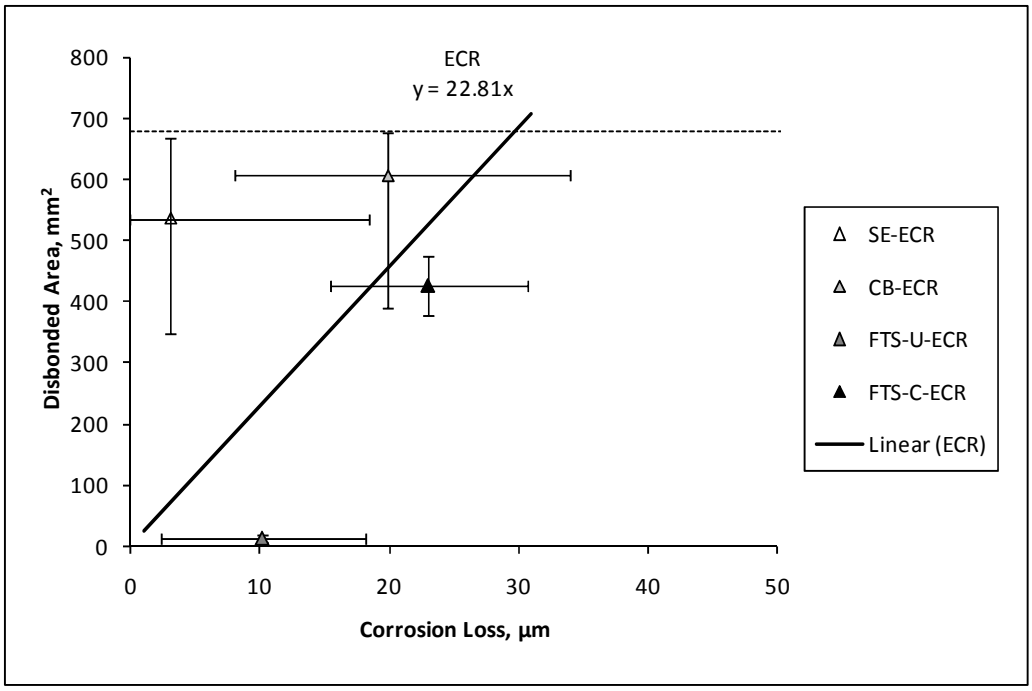

Figure 6.17: Corrosion loss versus disbondment for test specimens containing ECR.

6.3.1.2 Increased Adhesion Epoxies

Average corrosion loss is compared with disbonded area for specimens containing ECR with increased adhesion in Figure 6.18. Specimens with conventional ECR are also shown in the figure for comparison. The specimens containing epoxies with increased adhesion exhibit slightly less disbondment at a specific corrosion loss when compared to specimens with conventional ECR, with a 1-µm increase in loss resulting in an additional 18.1 mm^2 (0.028 $in.^2$) of disbonded area for specimens with increased adhesion. Epoxies with increased adhesion should exhibit total disbondment after 36.8 µm of loss, compared to 29.7 µm for specimens with conventional ECR. However, given the degree of scatter in the data, this difference is not significant.

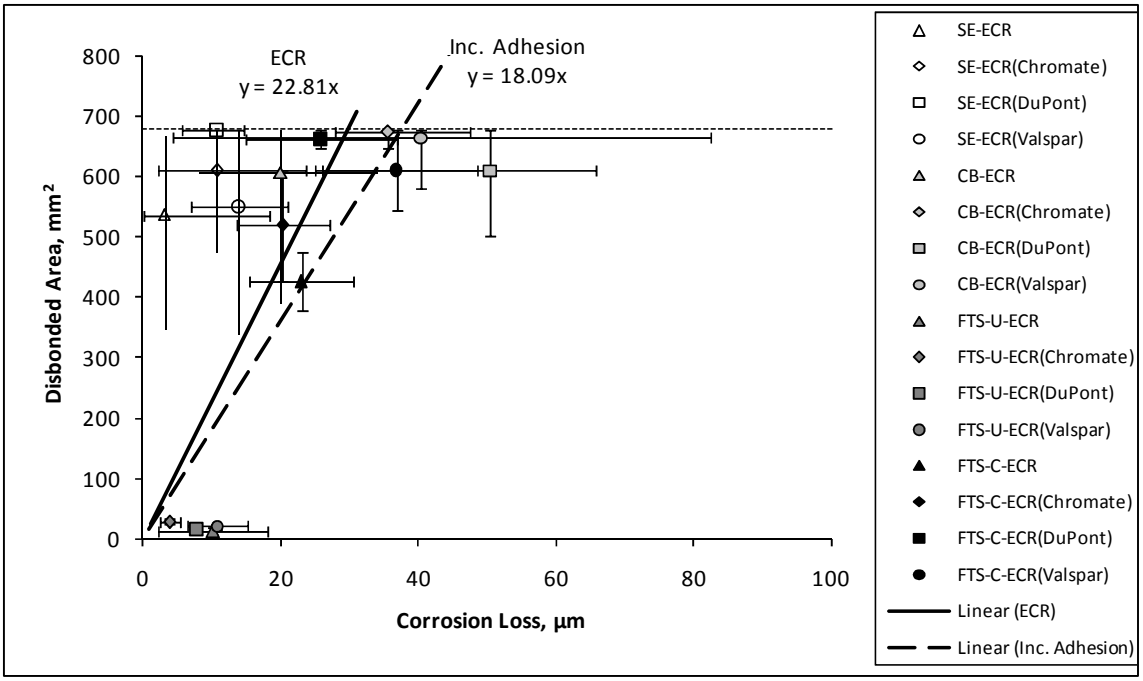

Figure 6.18: Corrosion loss versus disbondment for test specimens containing ECR with increased adhesion.

6.3.1.3 ECR with Corrosion Inhibitors

Average corrosion loss is compared with disbonded area for specimens containing ECR in concrete containing corrosion inhibitors in Figure 6.19. The specimens containing corrosion inhibitors exhibit slightly more disbondment at a specific corrosion loss compared to specimens containing conventional ECR without inhibitors, with 1 µm of loss resulting in an additional 30.7 mm^2 (0.048 $in.^2$) of disbonded area for specimens containing corrosion inhibitors. Specimens containing corrosion inhibitors should exhibit total disbondment after 22.1 µm of loss, compared to 29.7 µm for specimens with conventional ECR. However, as for the epoxies with increased adhesion, given the degree of scatter in the data, this difference is not significant.

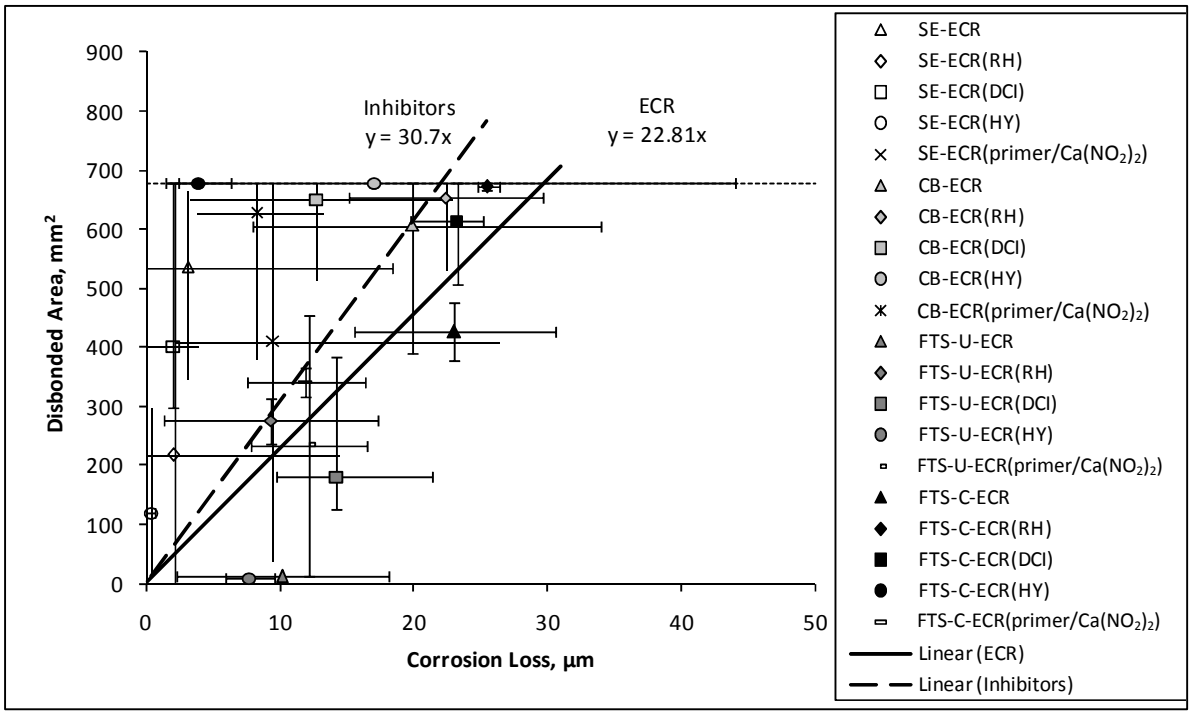

Figure 6.19: Corrosion loss versus disbondment for test specimens containing ECR with increased adhesion.

6.3.1.4 MC Reinforcement

Average corrosion loss is compared with disbonded area for specimens containing multiple-coated reinforcement in Figure 6.20. Specimens containing multiple-coated reinforcement exhibit significantly less disbondment at a specific corrosion loss as compared to specimens containing ECR, with a 1-µm increase in loss causing an additional 4.34 mm^2 (0.007 $in.^2$) of disbonded area for specimens containing MC reinforcement. MC reinforcement should exhibit total disbondment after 156 µm of loss, compared to 29.7 µm for specimens with conventional ECR. In contrast to the other specimens, this result is statistically significant. For comparison, MC bars in the rapid macrocell test exhibit a disbondment rate of 26.5 mm^2 per µm of loss, about half the rate of conventional ECR specimens in the rapid macrocell test and over six times the average disbondment rate observed in for MC reinforcement in bench-scale and field specimens.

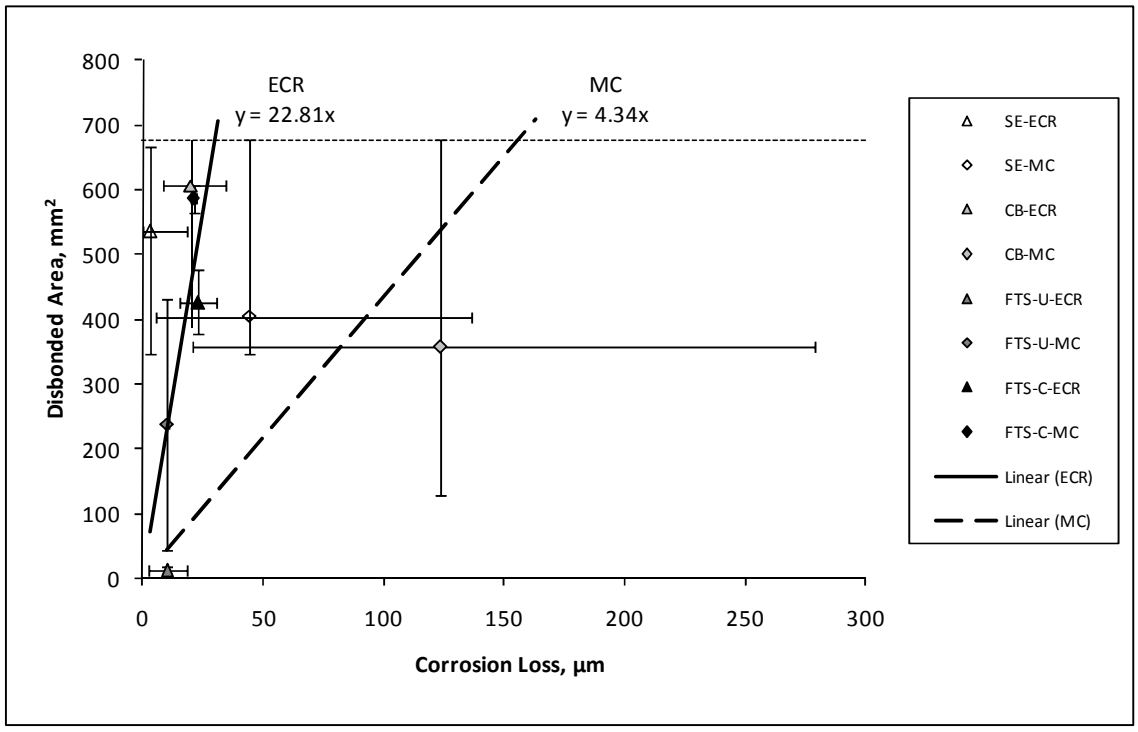

Figure 6.20: Corrosion loss versus disbondment for test specimens containing MC reinforcement.

6.3.2 Corrosion Loss Versus Disbondment – Comparison Between Test Programs

To compare test programs based on disbondment of epoxy coatings, the relationship between corrosion loss and disbondment is now compared across the programs. As described in Section 6.3.1.4, multiple-coated reinforcement exhibits significantly different behavior compared with other epoxy-coated bars in terms of corrosion loss and disbondment; therefore, specimens with multiple-coated reinforcement are excluded from the corrosion loss versus disbondment plots for each test program. The other protection systems are analyzed together to provide enough data points for a meaningful analysis.

6.3.2.1 Southern Exposure Test

Average corrosion loss is compared with disbondment for all of the Southern Exposure specimens (excluding those with MC reinforcement) in Figure 6.21. Across the Southern Exposure specimens, a 1-µm increase in loss results in a 53.5-mm^2 (0.083-in.^{2})

increase in disbonded area, close to the value of 56.1 mm^2 (0.087 $in.^2$) for the rapid macrocell test. On average, the Southern Exposure specimens should exhibit total disbondment after a corrosion loss of 12.7 µm.

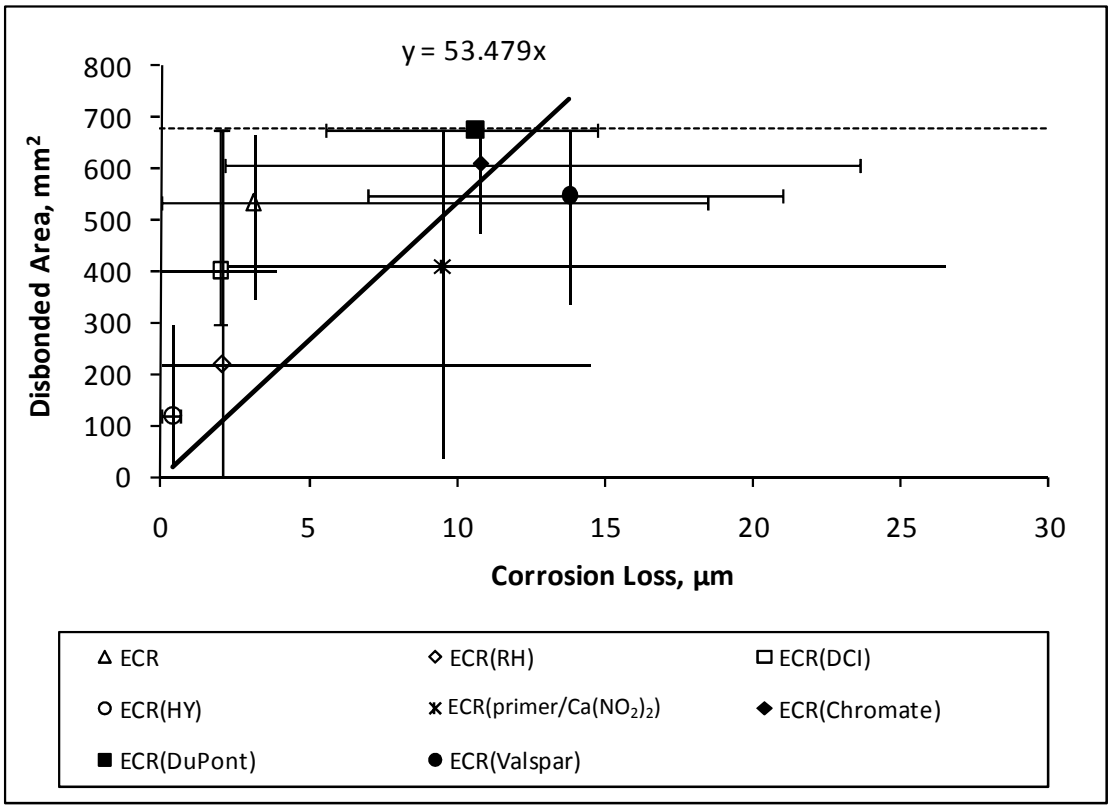

Figure 6.21: Corrosion loss versus disbondment for Southern Exposure specimens.

6.3.2.2 Cracked Beam Test

Average corrosion loss is compared with disbondment for all of the cracked beam specimens (excluding those with MC reinforcement) in Figure 6.22. Nearly all of the cracked beam specimens exhibit total disbondment; therefore, a best-fit line is not established. It should be noted, however, that the average corrosion loss for most cracked beam specimens is well above the 12.7-µm corrosion loss corresponding to total disbondment predicted from the Southern Exposure test. As such, the observation of total disbondment on most cracked beam specimens is not unexpected.

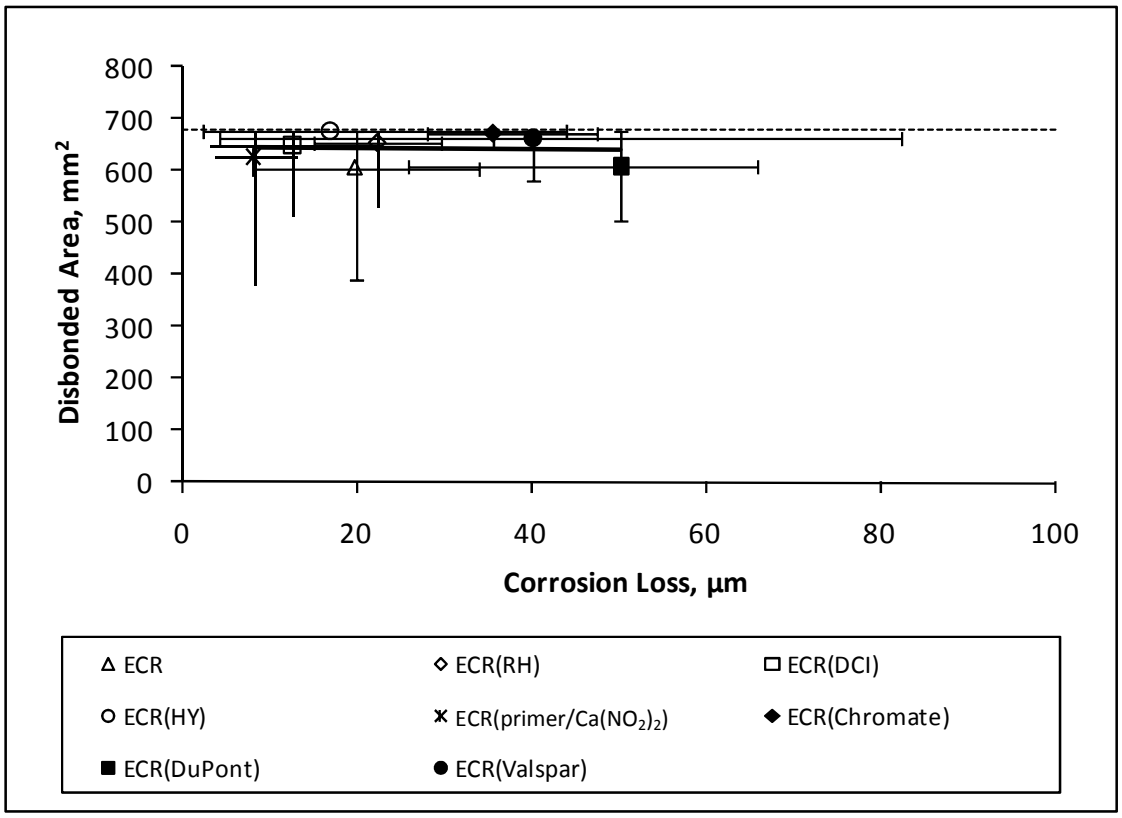

Figure 6.22: Corrosion loss versus disbondment for cracked beam specimens.

6.3.2.3 Field Test Specimens-Uncracked

Average corrosion loss is compared with disbondment for all of the uncracked field test specimens (excluding those with MC reinforcement) in Figure 6.23. For the uncracked field test specimens, a 1-µm increase in corrosion loss results in a 10.9-mm^2 (0.017-in.^{2}) increase in disbonded area, about one-fifth the rate for the Southern Exposure and rapid macrocell tests. The individual average values, however, vary greatly. Although no specimen exhibits total disbondment, the best-fit line predicts a specimen with an epoxy coating will exhibit total disbondment after 62.1 µm of loss. This value is nearly five times the corrosion loss required for total disbondment in the Southern Exposure test. It is possible that the degree of saturation and chloride content obtained in the Southern Exposure specimens [chloride contents measured for Southern Exposure specimens at 96 weeks (Draper et al. 2009) are often greater than chloride contents

measured for field test specimens at 250 weeks] results in more disbondment at a given corrosion loss. However, disbondment tests performed on bars in simulated pore solution in the absence of chlorides (Section 3.4) exhibit a time-dependency. Clearly, time alone is not enough to account for the observed difference in disbondment.

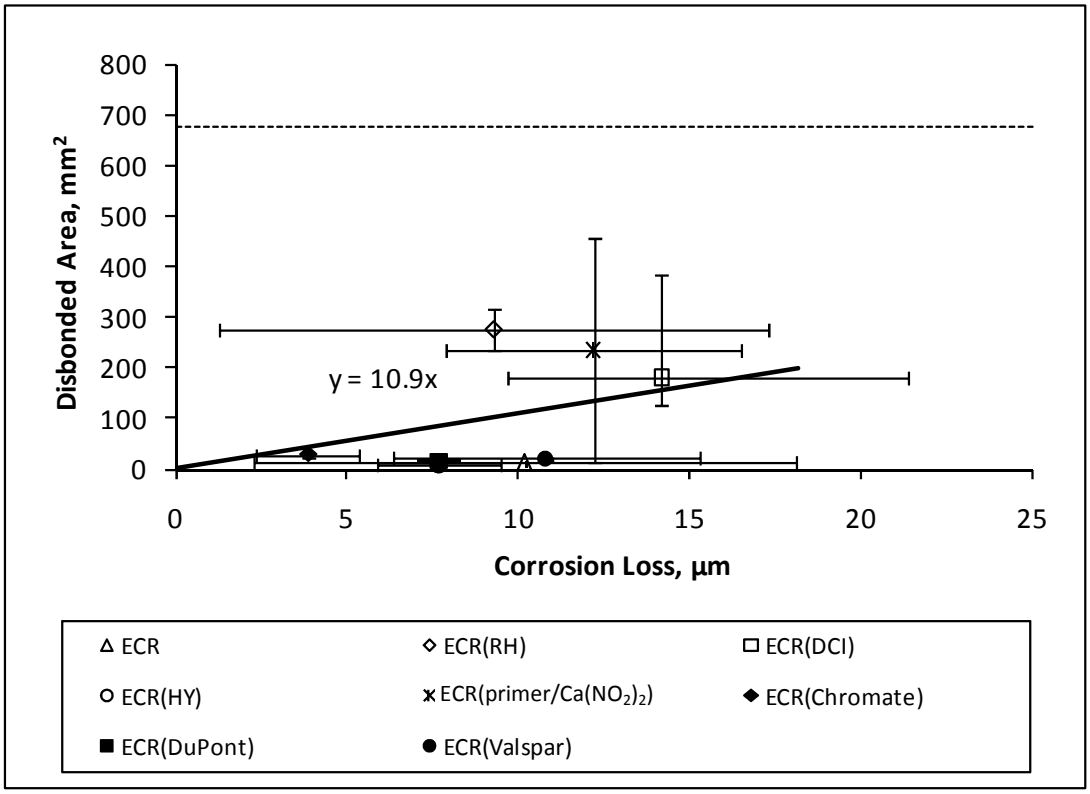

Figure 6.23: Corrosion loss versus disbondment for uncracked field test specimens.

6.3.2.4 Field Test Specimens-Cracked

Average corrosion loss is compared with disbondment for all of the cracked field test specimens (excluding those with MC reinforcement) in Figure 6.24. For the cracked field test specimens, a 1-µm increase in corrosion loss results in a 22.8-mm^2 increase in disbonded area, which is about twice that observed in the uncracked field test specimens. Estimates using a best-fit line show that a specimen with an epoxy coating would exhibit total disbondment after 29.8 µm of loss. As before, the bars in the field test specimens require significantly greater corrosion losses to exhibit total disbondment than the bars in

the bench-scale specimens. It should be noted, however, that the specimens containing Hycrete exhibit total disbondment at a corrosion loss of just 3.9 µm, approximately one-eighth the overall average.

A comparison between the SE and uncracked FTS specimens indicates that approximately five times the corrosion loss is needed to cause total disbondment in FTS when compared to the bench-scale specimens. If the relationship holds true between cracked beam and cracked FTS, the cracked beam specimens should exhibit total disbondment after a corrosion loss of just 6 µm. Additional testing is needed to determine if this prediction is accurate, because all existing cracked beam specimens exhibit corrosion losses far greater than that predicted to cause total disbondment using the relationship established above.

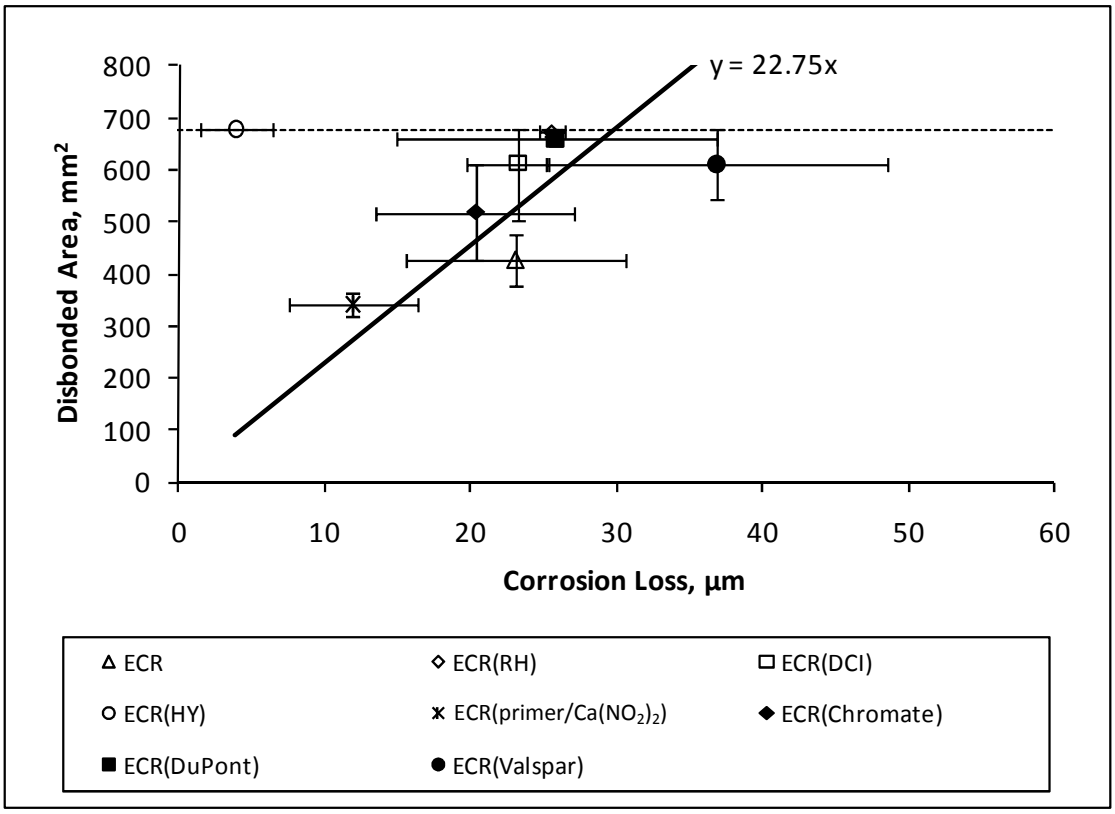

Figure 6.24: Corrosion loss versus disbondment for cracked field test specimens.

6.3.2.5 Summary

Table 6.7 summarizes the average increase in disbonded area associated with a 1-µm increase in corrosion loss for bench-scale, field test, and rapid macrocell (Chapter 3) specimens. Table 6.7 shows that there is a direct relation between the severity of the exposure conditions and the amount of disbondment observed as a function of corrosion loss. A 1-µm increase in corrosion loss causes the greatest increase in disbonded area for rapid macrocell specimens, 56.3 mm^2, with the Southern Exposure specimens exhibiting similar behavior with 53.5 mm^2 of disbondment per µm of corrosion loss. Both the uncracked and cracked FTS show significantly lower increases in disbonded area for a given increase in corrosion loss, 10.9 and 22.8 mm^2 per µm of loss, respectively. The salt exposure for field test specimens is less severe than for Southern Exposure and macrocell specimens, indicating the rate of disbondment is dependent on environment.

Table 6.7: Disbondment as a Function of Corrosion Loss

Test Program	Increase in Disbonded Area per Unit Corrosion Loss[a], mm^2
Southern Exposure	53.5
Cracked Beam	-
FTS-Uncracked	10.9
FTS-Cracked	22.8
Macrocell	56.3

[a] Increase in disbonded area associated with a 1-µm increase in corrosion loss

6.4 RELATIONSHIP BETWEEN TOTAL AND MACROCELL CORROSION RATE

Figure 6.25 compares the average macrocell and total corrosion rates after corrosion initiation for the Southern Exposure specimens with conventional reinforcement with and without inhibitors. The total corrosion rate, as measured by LPR,

is plotted on the y-axis, and macrocell corrosion rate is plotted on the x-axis. Each data point in Figure 6.25 (and the other figures in Section 6.4) represents a single specimen. Among the Southern Exposure specimens with conventional reinforcement, the total corrosion rates are on average 1.79 times the macrocell corrosion rates.

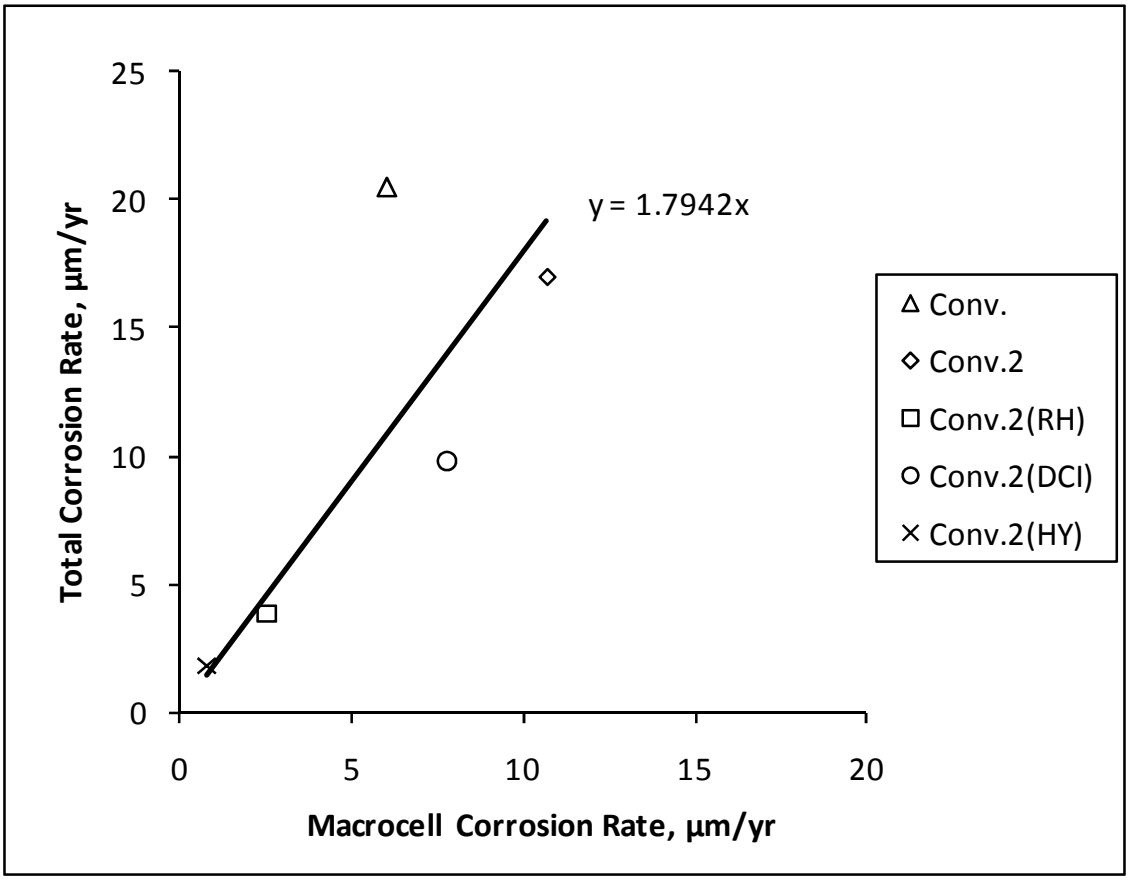

Figure 6.25: Total versus macrocell corrosion rate after corrosion initiation. SE specimens with conventional reinforcement.

Figure 6.26 compares the average macrocell and total corrosion rates after corrosion initiation based on exposed area for the SE specimens with epoxy-coated bars. Among the Southern Exposure specimens with bars having epoxy coatings, the total corrosion rates are on average 3.15 times the macrocell corrosion rates. The results exhibit far more scatter than do those for conventional steel.

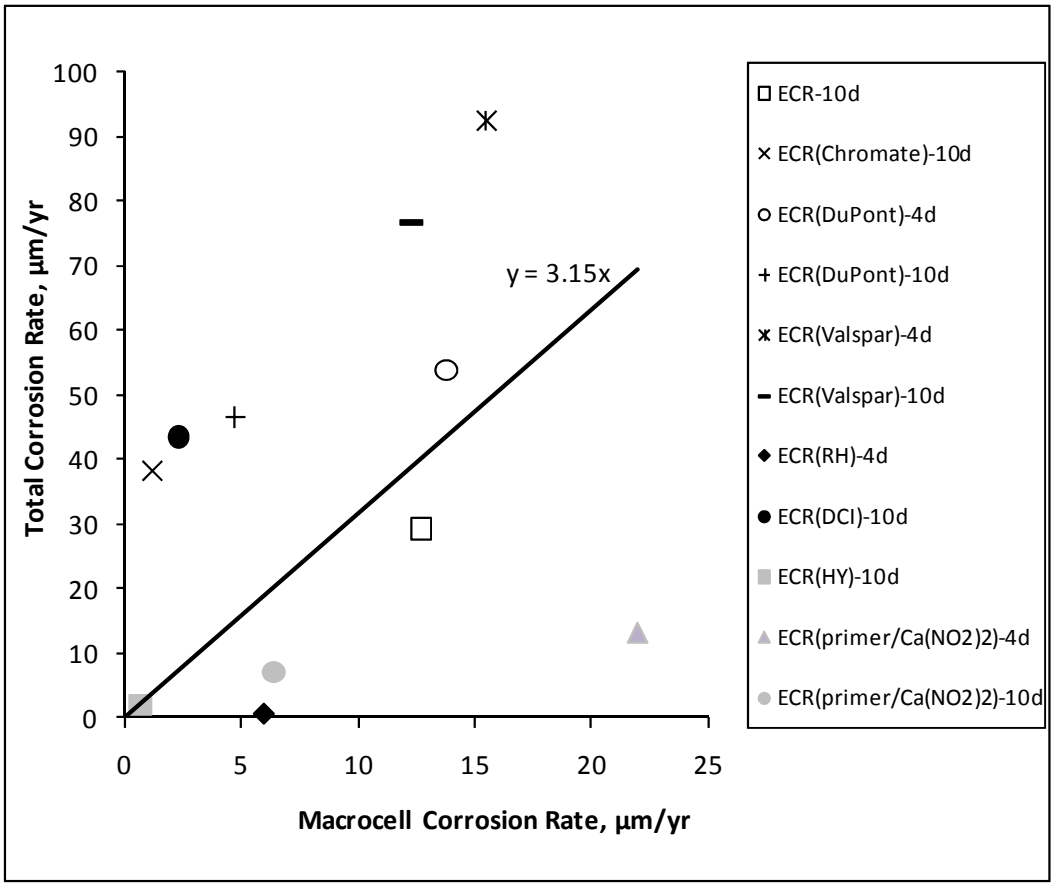

Figure 6.26: Total versus macrocell corrosion rate after corrosion initiation. SE specimens with ECR.

Figure 6.27 compares the average macrocell and total corrosion rates after corrosion initiation based on exposed area for the SE specimens with multiple-coated bars. For this corrosion protection system, the total corrosion rates are on average 6.93 times the macrocell corrosion rates.

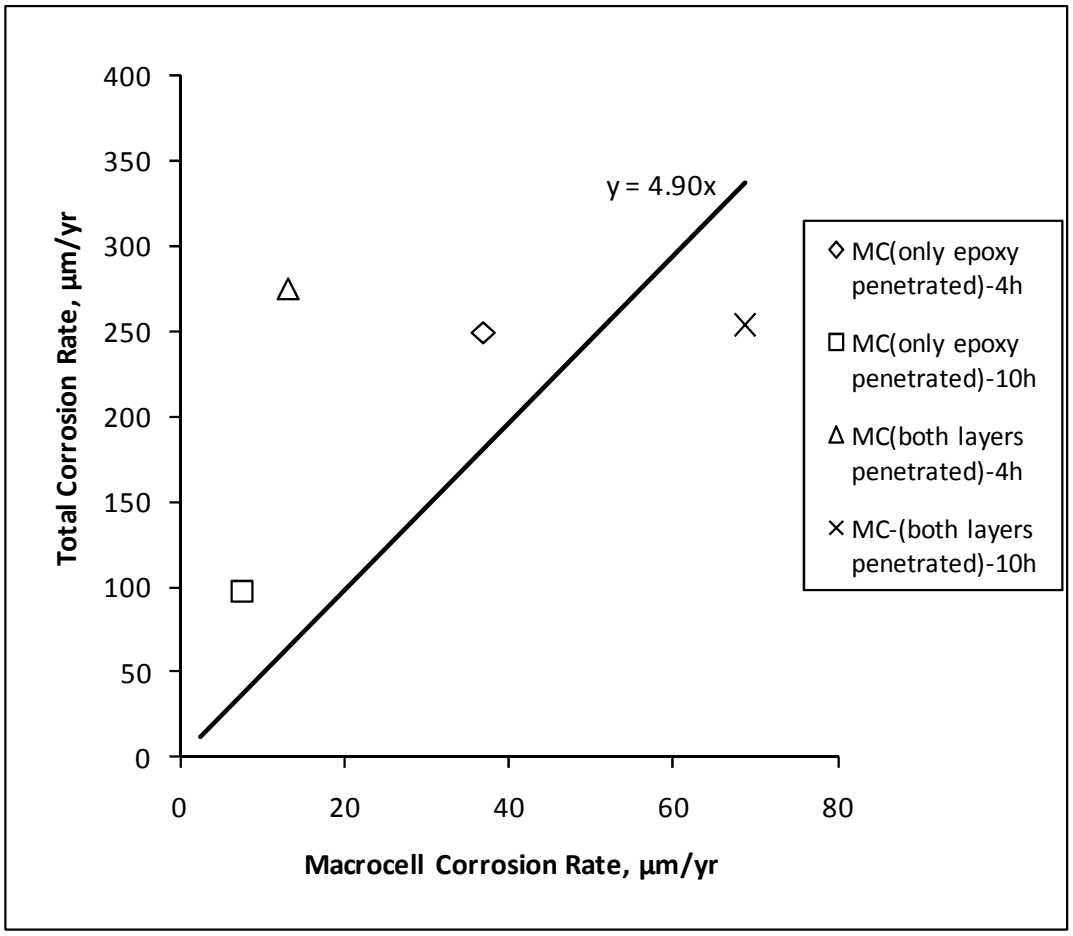

Figure 6.27: Total versus macrocell corrosion rate after corrosion initiation. SE specimen with MC reinforcement.

Figure 6.28 compares the average macrocell and total corrosion rates after corrosion initiation for CB specimens with conventional reinforcement. Among the cracked beam specimens with conventional reinforcement, the total corrosion rates are on average 3.49 times the macrocell corrosion rates. There is, however, a large degree of scatter in the data.

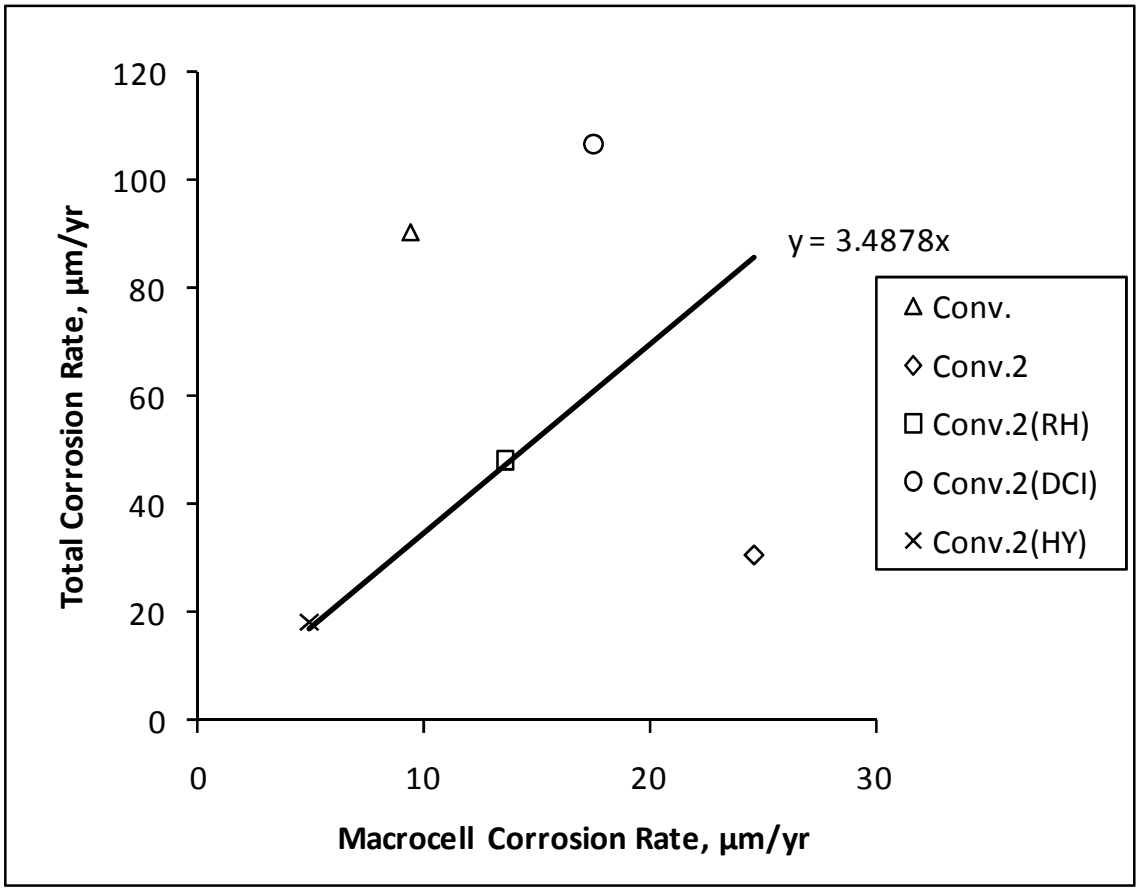

Figure 6.28: Total versus macrocell corrosion rate after corrosion initiation. CB specimens with conventional reinforcement.

Figure 6.29 compares the average macrocell and total corrosion rates after corrosion initiation based on exposed area for CB specimens with epoxy-coated bars. Among the cracked beam specimens with bars having epoxy coatings, the total corrosion rates are on average 12.36 times greater than the macrocell corrosion rates.

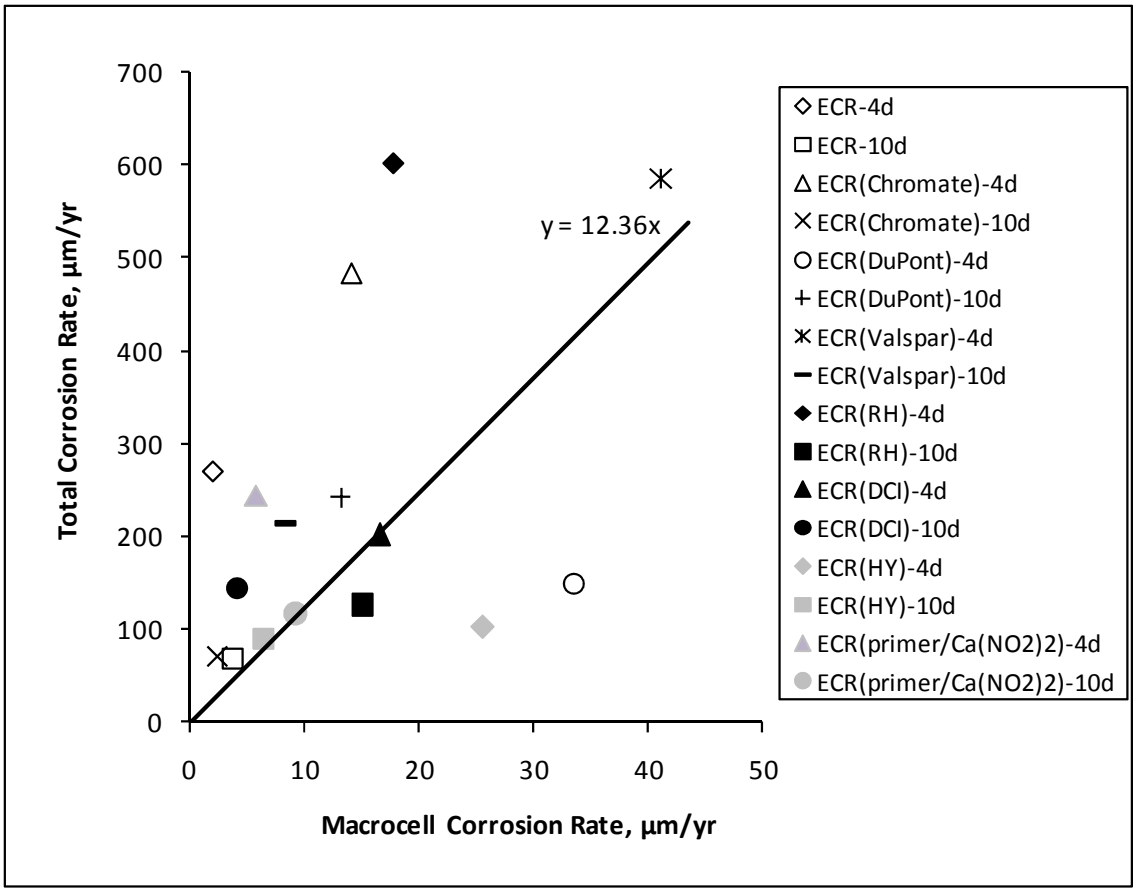

Figure 6.29: Total versus macrocell corrosion rate after corrosion initiation. CB specimens with ECR.

Figure 6.30 compares the average macrocell and total corrosion rates after corrosion initiation based on exposed area for the CB specimens with multiple-coated bars. For this corrosion protection system, the total corrosion rates are 5.82 times the macrocell corrosion rates.

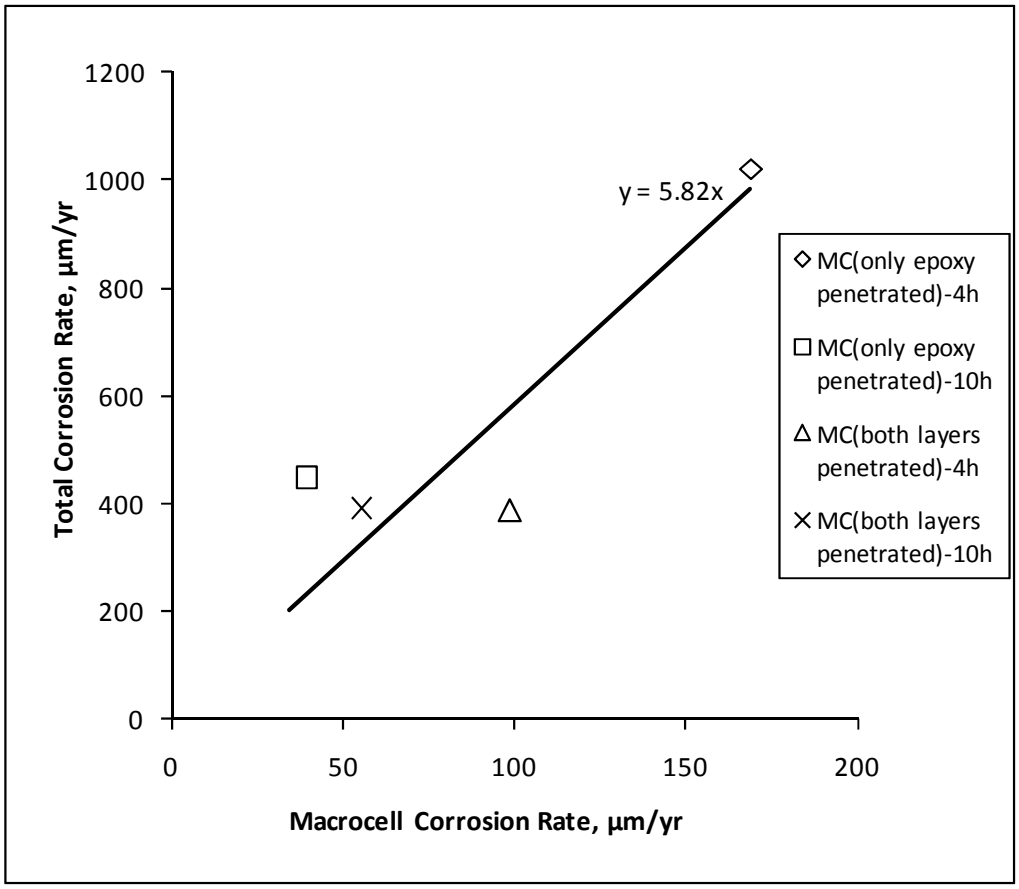

Figure 6.30: Total versus macrocell corrosion rate after corrosion initiation. SE specimens with MC reinforcement.

6.5 ESTIMATING TIME TO FIRST REPAIR

The time to first repair for a reinforced concrete bridge deck may be divided into two phases – the time to reach the critical chloride corrosion threshold and the time from the onset of corrosion to cracking of the concrete cover. The procedures for estimating time to corrosion initiation and time to cracking of concrete cover are discussed in Sections 6.5.1 and 6.5.2, respectively. KDOT and SDDOT maintenance engineers

estimate times to first repair of 10 to 25 years for bridges with conventional reinforcement and 35 to 40 years for bridges containing ECR (Darwin et al. 2002). These estimates are used to verify the accuracy of the method described below.

6.5.1 Time to Corrosion Initiation

To determine the time to corrosion initiation, the critical chloride corrosion threshold for conventional reinforcement is compared with the chloride content in bridge decks as a function of time. Lindquist et al. (2006) obtained chloride samples at 19-mm (0.75-in.) increments to a depth of 95 mm (3.75 in.) from 57 bridge decks at locations both on cracks and away from cracks. The chloride contents interpolated to 76.2-mm (3 in.), corresponding to the cover of the top mat of reinforcing steel, taken at crack locations on bridges with an average annual daily traffic (AADT) greater than 7500 are shown in Figure 6.31.

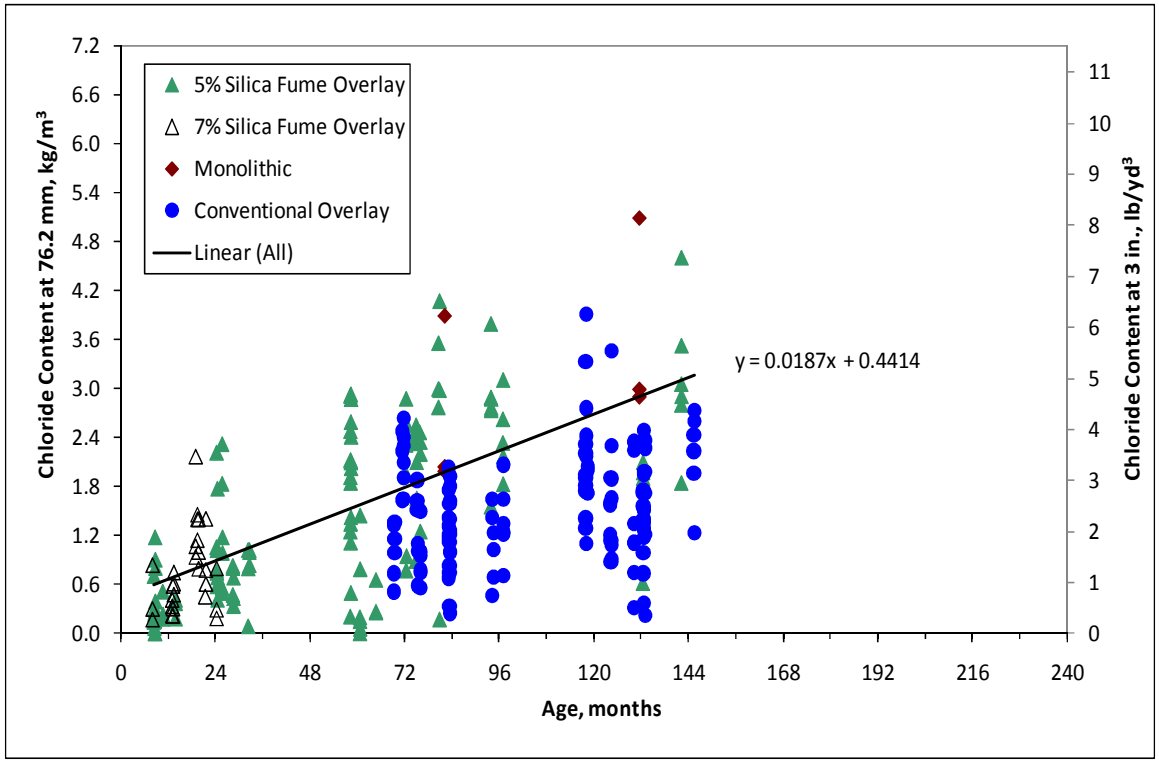

Figure 6.31: Chloride contents at 76.2-mm (3-in.) depth taken at crack locations on bridges with AADT > 7500 (Lindquist et al. 2006). x = age (months), y = chloride content (kg/m^3)

Tables 6.8a and b list the critical chloride corrosion thresholds for each corrosion protection system in this study and from prior research (Draper et al. 2009, Xing et al. 2010). The average chloride threshold values are weighted by the number of samples collected in each study. Conv. reinforcement exhibits an average critical chloride corrosion threshold (CCCT) of 0.90 kg/m^3 (1.52 lb/yd^3), close to the value for Conv.2, which exhibits an average CCCT of 0.98 kg/m^3 (1.66 lb/yd^3). Given the similar values of CCCT in Conv. and Conv.2 reinforcement, the two values are averaged to obtain a single weighted CCCT value (weighted by the number of chloride samples) for conventional reinforcement, 0.94 kg/m^3 (1.58 lb/yd^3). Similarly, CCCT values for Conv. and Conv.2 reinforcement in concrete containing Rheocrete, DCI, and Hycrete are averaged to obtain weighted CCCT values of 1.35, 1.81, and 0.49 kg/m^3 (2.28, 3.05, and 0.83 lb/yd^3), respectively.

Conventional ECR exhibits an average CCCT of 4.31 kg/m^3 (7.28 lb/yd^3), whereas systems with ECR with increased adhesion have CCCT values ranging from 4.97 to 6.08 kg/m^3 (8.40 to 10.3 lb/yd^3) (Draper et al. 2009). The values for ECR are significantly greater than that of conventional reinforcement. To initiate corrosion on a coated bar, the chloride threshold must be reached at a damage site, as opposed to uncoated bars, which initiate corrosion once the chloride threshold is reached anywhere on the bar surface. This results in an increase in average chloride content at the depth of the reinforcement for coated bars at corrosion initiation. Increased adhesion of the epoxy should not affect the chloride threshold of the steel; therefore, the CCCT values for conventional ECR and ECR with increased adhesion are averaged to produce a single CCCT of 5.00 kg/m^3 (8.45 lb/yd^3) (not shown in Table 6.8). This value is used in the current study to calculate the time to corrosion initiation for both ECR and ECR with increased adhesion.

Table 6.8a: Critical Chloride Corrosion Threshold (CCCT) for Corrosion Protection Systems (kg/m^3).

System	Southern Exposure CCCT[a]	Initiation Beam CCCT[b]	Weighted Average CCCT
Controls			
Conv.	0.77	0.94	0.90
Conv.2	0.88[c]	1.00[d]	0.98
		Conv. Avg.	**0.94**
ECR	4.31[e]	-	4.31[e]
Inhibitors			
Conv.(RH)	-	1.23	1.23
Conv.2(RH)	2.16[c]	-	2.16
		Conv.(RH) Avg.	**1.35**
Conv.(DCI)	-	1.49	1.49
Conv.2(DCI)	3.72[c]	-	3.72
		Conv.(DCI) Avg.	**1.81**
Conv.(HY)	-	0.37	0.37
Conv.2(HY)	1.19[c]	0.51[d]	0.61
		Conv.(HY) Avg.	**0.49**
ECR(RH)	4.10	-	4.10
ECR(DCI)	5.83	-	5.83
ECR(HY)	1.00	-	1.00
ECR(primer/Ca(NO2)2)	7.11	-	7.11
Multiple Coatings			
MC	2.00	-	2.00
Increased Adhesion			
ECR(Chromate)	5.69	-	5.69
ECR(DuPont)	4.97	-	4.97
ECR(Valspar)	6.08	-	6.08
Stainless Steel			
2205p[f]	15.6	-	15.6[f]

[a] Average of 36 samples from Draper et al. (2009) unless otherwise noted

[b] Average of 120 samples from Xing et al. (2010) unless otherwise noted

[c] Average of 18 samples from current study

[d] Average of 100 samples from current study

[e] Based on 90 samples

[f] Lower bound estimate of CCCT for 2205p (based on 24 samples)

Table 6.8b: Critical Chloride Corrosion Threshold (CCCT) for Corrosion Protection Systems (lb/yd^3).

System	Southern Exposure CCCT[a]	Initiation Beam CCCT[b]	Weighted Average CCCT
Controls			
Conv.	1.30	1.59	1.52
Conv.2	1.49[c]	1.69[d]	1.66
		Conv. Avg.	**1.58**
ECR	7.28[e]	-	7.28[e]
Inhibitors			
Conv.(RH)	-	2.08	2.08
Conv.2(RH)	3.65[c]	-	3.65
		Conv.(RH) Avg.	**2.28**
Conv.(DCI)	-	2.52	2.52
Conv.2(DCI)	6.29[c]	-	6.29
		Conv.(DCI) Avg.	**3.05**
Conv.(HY)	-	0.63	0.63
Conv.2(HY)	2.01[c]	0.86[d]	1.04
		Conv.(HY) Avg.	**0.83**
ECR(RH)	6.93	-	6.93
ECR(DCI)	9.85	-	9.85
ECR(HY)	1.69	-	1.69
ECR(primer/Ca(NO2)2)	12.0	-	12.0
Multiple Coatings			
MC	3.38	-	3.38
Increased Adhesion			
ECR(Chromate)	9.62	-	9.62
ECR(DuPont)	8.40	-	8.40
ECR(Valspar)	10.28	-	10.3
Stainless Steel			
2205p[f]	26.4	-	26.4[f]

[a] Average of 36 samples from Draper et al. (2009) unless otherwise noted

[b] Average of 120 samples from Xing et al. (2010) unless otherwise noted

[c] Average of 18 samples from current study

[d] Average of 100 samples from current study

[e] Based on 90 samples

[f] Lower bound estimate of CCCT for 2205p (based on 24 samples)

Among specimens with ECR and inhibitors, ECR in concrete with DCI exhibits a CCCT value of 5.83 kg/m^3 (9.85 lb/yd^3), greater than the CCCT for ECR alone. However, ECR in concrete with Rheocrete exhibits a CCCT of 4.10 kg/m^3 (6.93 lb/yd^3), lower than the CCCT for ECR in concrete with no inhibitor. Concrete with Rheocrete raises the CCCT of conventional reinforcement relative to conventional reinforcement without an inhibitor, and there is no reason to expect different behavior when Rheocrete is used in conjunction with ECR. Therefore, ECR with Rheocrete is assumed to have a CCCT equal to that of conventional ECR alone, 5.00 kg/m^3 (8.45 lb/yd^3). ECR in concrete with Hycrete exhibits a lower CCCT relative to ECR in concrete with no inhibitor at just 1.08 kg/m^3 (1.82 lb/yd^3), compared to 5.00 kg/m^3 (8.45 lb/yd^3) for ECR in concrete with no inhibitors. Relatively speaking, this is similar to conventional reinforcement, which exhibits a CCCT of 0.49 kg/m^3 (0.83 lb/yd^3) in concrete with Hycrete, compared to 0.94 kg/m^3 (1.59 lb/yd^3) in concrete with no inhibitors.

In the Southern Exposure test, MC reinforcement exhibits a lower CCCT than ECR, 2.00 kg/m^3 (3.38 lb/yd^3). A study (Darwin et al. 2009) examining the critical chloride corrosion threshold of galvanized reinforcement, however, found that galvanized steel had an average critical chloride corrosion threshold of 1.52 kg/m^3 (2.57 lb/yd^3) compared to 0.97 kg/m^3 (1.63 lb/yd^3) for conventional reinforcement. Based on this study, there is no reason to expect MC reinforcement to have a lower CCCT than ECR; therefore, MC reinforcement is assigned the same CCCT as ECR, 5.00 kg/m^3 (8.45 lb/yd^3). 2205p reinforcement exhibits a CCCT of 15.6 kg/m^3 (26.4 lb/yd^3), which, as discussed in Section 3.5.1.3, is a lower bound estimate for the CCCT of 2205p stainless steel.

The CCCT values listed in Table 6.8 are used with the best-fit line for the chloride contents on crack locations in bridge decks (Figure 6.31) to determine the time to corrosion initiation for each corrosion protection system. The results are listed in Table 6.9.

Table 6.9: Estimated Time to Corrosion Initiation for Corrosion Protection Systems in a Bridge Deck with 76.2-mm (3-in.) Cover on Top Reinforcing Steel.

System	Chloride Threshold (kg/m^3)	Age at Cl- Initiation in Bridge Decks (years)
Controls		
Conv.	0.94	2.2
ECR	5.00	20.3
Inhibitors		
Conv.(RH)	1.35	4.1
Conv.(DCI)	1.81	6.1
Conv.(HY)	0.49	(0.2) 1.0[a]
ECR(RH)	5.00	20.3
ECR(DCI)	5.83	24.0
ECR(HY)	1.08	2.8
ECR(primer/Ca(NO2)2)	7.11	29.7
Multiple Coatings		
MC	5.00	20.3
Increased Adhesion		
ECR(Chromate)	5.00	20.3
ECR(DuPont)	5.00	20.3
ECR(Valspar)	5.00	20.3
Stainless Steel		
2205p	15.6[b]	67.6[b]

[a] Rounded up from 0.2 years
[b] Lower-bound estimate of critical chloride corrosion threshold and time to corrosion initiation

For the systems with bare bars, Conv.(HY) has the lowest time to initiation of corrosion, 0.2 years. Since salt is not applied to bridge decks until the first winter, this value is rounded up to one year. Conventional reinforcement with no inhibitor initiates corrosion after 2.2 years. Rheocrete and DCI extend the initiation time of conventional reinforcement to 4.1 and 6.1 years, respectively. The lower-bound estimate for initiation for 2205p reinforcement is 67.6 years, the longest time to initiation among the systems in this study. As discussed in Section 3.5.1.3, most 2205p specimens did not exhibit sustained corrosion after initiation in the Southern Exposure test; therefore, the chloride

threshold for 2205p stainless steel, on which the time to initiation is based, should be taken as a lower-bound estimate.

For the systems with coated bars, ECR and ECR with increased adhesion initiate corrosion after 20.3 years. The addition of calcium nitrite (DCI) to the concrete slightly increases the time to corrosion initiation to 24 years, and the addition of a calcium nitrite primer under the epoxy increases the time to corrosion initiation to 29.7 years. ECR in cracked concrete with Hycrete initiates corrosion after 2.5 years, and MC reinforcement initiates corrosion after 20.3 years.

6.5.2 Propagation Time to Cracking of Concrete Cover

6.5.2.1 Estimation of Total Corrosion Rate in Bridge Decks

To determine the time required to crack the concrete cover, the average corrosion rate for each system and the corrosion loss to cause cracking are determined. Field test corrosion rates are chosen as the basis for the economic analysis because the field test specimens most closely resemble a bridge deck in terms of reinforcement layout and exposure conditions. As described in Section 2.5.5, the rate of salt application to the field test specimens matches the average rate for bridge decks in Kansas. For systems where field test specimen results are not available, the average macrocell corrosion rates from the bench-scale tests (Tables 6.1 and 6.2) are converted to an equivalent field test corrosion rate using the relationships established in Section 6.2.3. Since both microcell and macrocell corrosion contributes to the corrosion loss required to crack concrete, the macrocell corrosion rate is converted into a total corrosion rate using the relationships established in Section 6.4. The corrosion loss to crack concrete is calculated using Eq. (4.4), which, when divided by the total corrosion rate, gives the time from corrosion initiation to cracking of the concrete cover.

Table 6.10 lists bench-scale macrocell corrosion rates for Conv. reinforcement without inhibitors and Conv.2 reinforcement with and without inhibitors. The bench-scale

Table 6.10: Equivalent Corrosion Rates for Conventional Reinforcement with Inhibitors (µm/yr).

System	Concrete[a]	Macrocell Corrosion Rate	Ratio of Conv.2 to Conv. Rate	Modified Corrosion Rate (Conv.*)[b]
Corrosion Rate (Total Area)				
Conv.	U	5.69		-
	C	7.00		-
Conv.2	U	10.1	1.77	5.69
	C	16.3	2.32	7.00
Conv.2(RH)	U	2.91	1.77	1.64
	C	11.90	2.32	5.13
Conv.2(DCI)	U	6.67	1.77	3.77
	C	14.50	2.32	6.24
Conv.2(HY)	U	1.25	1.77	0.706
	C	4.17	2.32	1.80

[a] U = uncracked concrete (SE), C = cracked concrete (CB)

[b] Estimated corrosion rate in conjunction with Conv. reinforcement

macrocell corrosion rates for Conv.2 reinforcement are 10.1 and 16.3 µm/yr in uncracked and cracked concrete (Southern Exposure and cracked beam specimens), respectively, about twice the average corrosion rates for Conv. reinforcement (5.69 and 7.00 µm/yr in uncracked and cracked concrete, respectively). All inhibitors reduce the corrosion rate of Conv.2 reinforcement compared to Conv.2 reinforcement with no inhibitor, but in cracked concrete Conv.2(RH) and Conv.2(DCI) show corrosion rates greater than those observed for Conv. reinforcement. It is assumed that if the inhibitors were used in conjunction with Conv. reinforcement, the resulting corrosion rates would be less than the corrosion rate measured for Conv. reinforcement with no inhibitor. Since all other protection systems used the same heat of steel as Conv. reinforcement, the only way to achieve a fair comparison between systems is to reduce the corrosion rates for the systems with Conv.2 reinforcement with inhibitors by the ratio of the Conv.2 corrosion rate to the Conv. corrosion rate. When referring to these modified corrosion rate data for conventional reinforcement in concrete with corrosion inhibitors, the designation Conv.* is used. The modified corrosion rates for these systems are also presented in Table 6.10. Based on the modified corrosion rate, the estimated rates for Conv.*(RH) are 1.64 and

5.13 µm/yr in uncracked and cracked concrete, respectively. Conv.*(DCI) has corrosion rates of 3.77 and 6.24 µm/yr in uncracked and cracked concrete, respectively, and Conv.*(HY) has corrosion rates of 0.706 and 1.80 µm/yr in uncracked and cracked concrete, respectively.

To determine the statistical significance of the differences in corrosion rates between corrosion protection systems, a two-tailed Student's T-test is used. The student's T-test is a method of statistical analysis that compares the means and variances of two data sets to determine the probability, α, that any differences between the two data sets could have arisen by chance; that is, differences in the mean values are due to the natural variability of the test program, not differences in the effectiveness of the corrosion protection systems. For this analysis, a value of α of 0.20 is used as the threshold for statistical significance; a single combined average corrosion rate is used between systems when $\alpha > 0.20$. Bare bars, for which corrosion rates are presented based on total area, are examined separately from coated bars, for which corrosion rates are based on exposed area.

Tables 6.11a and 6.11b list α values for corrosion protection systems with bare bars in Southern Exposure and cracked beam specimens, respectively. The corrosion rates for conventional reinforcement with inhibitors are scaled by the ratio of Conv.2 corrosion rate to Conv. corrosion rate prior to analysis, as shown in Table 6.10. The comparison between rates from the Southern Exposure test (Table 6.11a) shows that all differences between protection systems are statistically significant, with all α values less than 0.05. The results from the analysis of corrosion rates from the cracked beam test (Table 6.11b), however, show that differences in corrosion rates between Conv., Conv.*(RH) and Conv.*(DCI) are not statistically significant in cracked concrete ($\alpha > 0.20$). Therefore, the three systems are treated as representative of the same population, the corrosion rates from these systems are averaged, and a single rate of 6.34 µm/yr is used as the macrocell corrosion rate in cracked concrete for these specimens.

Table 6.11a: Student's T-Test Results (α Values) for Corrosion Rates Based on Total Area of Corrosion Protection Systems from Southern Exposure Tests.

	Corrosion Rate (µm/yr)	Conv.	Conv.*(RH)	Conv.*(DCI)	Conv.*(HY)	2205p
Corrosion Rate (µm/yr)		**5.69**	**1.64**	**3.77**	**0.706**	**0.074**
Conv.	**5.69**	1	9.4E-06	5.0E-03	1.5E-06	4.0E-07
Conv.*(RH)	**1.64**	9.4E-06	1	1.2E-02	2.5E-02	1.1E-03
Conv.*(DCI)	**3.77**	5.0E-03	1.2E-02	1	3.5E-03	1.3E-03
Conv.*(HY)	**0.706**	1.5E-06	2.5E-02	3.5E-03	1	3.2E-02
2205p	**0.074**	4.0E-07	1.1E-03	1.3E-03	3.2E-02	1

Table 6.11b: Student's T-Test Results (α Values) for Corrosion Rates based on Total Area of Corrosion Protection Systems from Cracked Beam Tests.

	Corrosion Rate (µm/yr)	Conv.	Conv.*(RH)	Conv.*(DCI)	Conv.*(HY)	2205p
Corrosion Rate (µm/yr)		**7.00**	**5.15**	**6.24**	**1.80**	**0.214**
Conv.	**7.00**	1	0.22	0.31	0.004	0.004
Conv.*(RH)	**5.15**	0.22	1	0.28	0.003	0.004
Conv.*(DCI)	**6.24**	0.31	0.28	1	0.004	0.008
Conv.*(HY)	**1.80**	0.004	0.003	0.004	1	0.008
2205p	**0.214**	0.004	0.004	0.008	0.008	1

Tables 6.12a and 6.12b list α values for corrosion protection systems with coated bars under the Southern Exposure and cracked beam test programs, respectively. Since only one Southern Exposure specimen with Hycrete initiated corrosion, a statistical analysis cannot be performed for that system. The comparison between rates for the Southern Exposure test (Table 6.12a) shows that only MC reinforcement has a statistically significant difference in corrosion rate compared to the other systems, with all α values less than 0.20, with the exception of comparisons between MC and ECR(RH) and ECR(Valspar). ECR(HY) is also assumed to have a statistically significant difference in corrosion rate compared to other systems due to the order of magnitude

difference in corrosion rate between ECR(HY) and the other corrosion protection systems. Therefore, the corrosion rates from the Southern Exposure test for all systems except MC and ECR(HY) are averaged to obtain a single rate of 11.51 µm/yr.

The results from the analysis of corrosion rates from the cracked beam tests (Table 6.12b) show no statistically significant differences between ECR, ECR(DCI), ECR(HY), and ECR(primer/$Ca(NO_2)_2$) ($\alpha > 0.20$). Therefore, the corrosion rates for these systems are averaged, and a single equivalent rate of 9.52 µm/yr is used as the bench-scale macrocell corrosion rate in cracked concrete for these systems. Although ECR(RH), ECR(Chromate), ECR(DuPont), and ECR(Valspar) do show significant differences in performance relative to ECR, the corrosion rates exhibited by these systems are significantly greater than that for ECR (Table 6.13). There is no reason to expect the use of a corrosion inhibitor or an epoxy with increased adhesion will accelerate the corrosion rate; the greater corrosion rates observed are likely due to variations in the test or in concrete quality. Therefore, the averaged corrosion rate for ECR, 9.52 µm/yr, is also used to represent the cracked beam corrosion rate for these systems.

Table 6.12a: Student's T-Test Results (α Values) for Corrosion Rates Based on Exposed Area of Corrosion Protection Systems from Southern Exposure Tests.

	Corrosion Rate (µm/yr)	ECR	ECR(DCI)	ECR(RH)	ECR(HY)	ECR(primer/$Ca(NO_2)_2$)	ECR(Chromate)	ECR(DuPont)	ECR(Valspar)	MC
Corrosion Rate (µm/yr)		**10.43**	**7.81**	**8.63**	**0.674**	**12.61**	**12.86**	**12.37**	**16.93**	**31.63**
ECR	**10.43**	1	0.500	0.274	-	0.649	0.544	0.628	0.313	0.071
ECR(DCI)	**7.81**	0.500	1	0.291	-	0.468	0.344	0.391	0.324	0.150
ECR(RH)	**8.63**	0.274	0.291	1	-	0.613	0.569	0.529	0.977	0.471
ECR(HY)	**0.674**	-	-	-	-	-	-	-	-	-
ECR(primer/$Ca(NO_2)_2$)	**12.61**	0.621	0.468	0.613	-	1	0.964	0.966	0.577	0.140
ECR(Chromate)	**12.86**	0.544	0.344	0.569	-	0.964	1	0.919	0.576	0.142
ECR(DuPont)	**12.37**	0.628	0.391	0.529	-	0.966	0.919	1	0.532	0.132
ECR(Valspar)	**16.93**	0.313	0.324	0.977	-	0.577	0.576	0.532	1	0.220
MC	**31.63**	0.071	0.150	0.471	-	0.140	0.142	0.132	0.220	1

Table 6.12b: Student's T-Test Results (α Values) for Corrosion Rates Based on Exposed Area of Corrosion Protection Systems from Cracked Beam Tests.

	Corrosion Rate (μm/yr)	ECR	ECR(DCI)	ECR(RH)	ECR(HY)	ECR(primer/Ca(NO$_2$)$_2$)	ECR(Chromate)	ECR(DuPont)	ECR(Valspar)	MC
Corrosion Rate (μm/yr)		**8.07**	**11.2**	**17.0**	**10.8**	**8.73**	**20.4**	**25.9**	**16.4**	**68.6**
ECR	**8.07**	1	0.364	0.014	0.506	0.826	0.064	0.005	0.158	0.005
ECR(DCI)	**11.2**	0.364	1	0.145	0.938	0.497	0.250	0.046	0.465	0.027
ECR(RH)	**17.0**	0.014	0.145	1	0.211	0.026	0.720	0.243	0.893	0.067
ECR(HY)	**10.8**	0.506	0.938	0.211	1	0.645	0.292	0.072	0.494	0.041
ECR(primer/Ca(NO$_2$)$_2$)	**8.73**	0.826	0.497	0.026	0.645	1	0.140	0.019	0.270	0.021
ECR(Chromate)	**20.4**	0.064	0.250	0.720	0.292	0.140	1	0.554	0.680	0.064
ECR(DuPont)	**25.9**	0.005	0.046	0.243	0.072	0.019	0.554	1	0.290	0.097
ECR(Valspar)	**16.4**	0.158	0.465	0.893	0.494	0.270	0.680	0.290	1	0.045
MC	**68.6**	0.005	0.027	0.067	0.041	0.021	0.064	0.097	0.045	1

The Student's T-test described above is also applied the corrosion rates observed in field test specimens (Tables 6.3 and 6.4). The analysis is not performed on bare bar systems in field specimens as only two such systems were tested in the field, Conv. and 2205p, and the specimens containing 2205p did not initiate corrosion. Tables 6.13a and 6.13b list α values for corrosion protection systems with coated bars in the field test specimens with uncracked and cracked concrete, respectively. The comparison between rates from the field test with uncracked concrete (Table 6.13a) shows no statistically significant differences between ECR, ECR(RH), ECR(DCI), ECR(primer/Ca(NO2)2), and ECR(Chromate), and ECR(DuPont) ($\alpha > 0.20$). Although ECR(Valspar) and MC are statistically different from other corrosion protection systems, they are not statistically different from conventional ECR, and these differences are believed due to variations in concrete quality. At 2.89 μm/yr, the corrosion rate for ECR(HY) is 68 percent of the next closest corrosion rate and is statistically different from the rates for ECR, ECR(RH), ECR(Valspar), and MC. The corrosion rates for uncracked field test specimens for all systems, except ECR(HY), are averaged to obtain a single rate of 5.66 μm/yr.

Table 6.13a: Student's T-Test Results (α Values) for Corrosion Rates Based on Exposed Area of Corrosion Protection Systems from Field Test Specimens with Uncracked Concrete.

	Corrosion Rate (μm/yr)	ECR	ECR(DCI)	ECR(RH)	ECR(HY)	ECR(primer/$Ca(NO_2)_2$)	ECR(Chromate)	ECR(DuPont)	ECR(Valspar)	MC
Corrosion Rate (μm/yr)		**5.68**	**4.26**	**5.43**	**2.89**	**4.49**	**4.83**	**5.14**	**9.11**	**6.31**
ECR	**5.68**	1	0.425	0.915	0.136	0.574	0.732	0.949	0.269	0.763
ECR(DCI)	**4.26**	0.425	1	0.446	0.256	0.871	0.726	0.563	0.020	0.176
ECR(RH)	**5.43**	0.915	0.446	1	0.120	0.606	0.778	0.989	0.166	0.636
ECR(HY)	**2.89**	0.136	0.256	0.120	1	0.233	0.209	0.295	0.010	0.033
ECR(primer/$Ca(NO_2)_2$)	**4.49**	0.574	0.871	0.606	0.233	1	0.856	0.708	0.067	0.301
ECR(Chromate)	**4.83**	0.732	0.726	0.778	0.209	0.856	1	0.836	0.145	0.463
ECR(DuPont)	**5.14**	0.949	0.563	0.989	0.295	0.708	0.836	1	0.305	0.750
ECR(Valspar)	**9.11**	0.269	0.020	0.166	0.010	0.067	0.145	0.305	1	0.305
MC	**6.31**	0.763	0.176	0.636	0.033	0.301	0.463	0.750	0.305	1

Table 6.13b: Student's T-Test Results (α Values) for Corrosion Rates Based on Exposed Area of Corrosion Protection Systems from Field Test Specimens with Cracked Concrete.

	Corrosion Rate (μm/yr)	ECR	ECR(DCI)	ECR(RH)	ECR(HY)	ECR(primer/$Ca(NO_2)_2$)	ECR(Chromate)	ECR(DuPont)	ECR(Valspar)	MC
Corrosion Rate (μm/yr)		**8.13**	**5.79**	**8.38**	**4.32**	**4.65**	**8.94**	**6.5**	**7.64**	**8.11**
ECR	**8.13**	1	0.275	0.923	0.234	0.200	0.745	0.656	0.733	0.918
ECR(DCI)	**5.79**	0.275	1	0.072	0.448	0.475	0.126	0.501	0.415	0.258
ECR(RH)	**8.38**	0.923	0.072	1	0.024	0.004	0.554	0.416	0.577	0.947
ECR(HY)	**4.32**	0.234	0.448	0.024	1	0.862	0.144	0.269	0.241	0.181
ECR(primer/$Ca(NO_2)_2$)	**4.65**	0.200	0.475	0.004	0.862	1	0.112	0.216	0.190	0.137
ECR(Chromate)	**8.94**	0.745	0.126	0.554	0.144	0.112	1	0.424	0.486	0.643
ECR(DuPont)	**6.5**	0.656	0.501	0.416	0.269	0.216	0.424	1	0.893	0.675
ECR(Valspar)	**7.64**	0.733	0.415	0.577	0.241	0.190	0.486	0.893	1	0.774
MC	**8.11**	0.918	0.258	0.947	0.181	0.137	0.643	0.675	0.774	1

The results from the analysis of corrosion rates from the cracked field test specimens (Table 6.13b) show no statistically significant differences between ECR, ECR(Chromate), ECR(DuPont), ECR(Valspar), ECR(RH), and MC ($\alpha > 0.20$). Although the corrosion rates for ECR in conjunction with inhibitors in the concrete are not significantly different from the rates for ECR alone, the rate for ECR(DCI) and ECR(HY)

are significantly different from the rates observed for ECR(RH) and ECR(Chromate). Furthermore, the systems with inhibitors were in lower-quality concrete than ECR with no inhibitors. Had the concrete quality been equal, it is believed the differences in corrosion rate between ECR and ECR with inhibitors would be significant. Therefore, only ECR, ECR(Chromate), ECR(DuPont), ECR(Valspar), ECR(RH), and MC are averaged; a single rate of 7.95 µm/yr is used as the macrocell corrosion rate in cracked concrete for these systems. ECR(primer/$Ca(NO_2)_2$) exhibits corrosion rates somewhat lower than ECR in cracked field test specimens. However, as observed in bench-scale tests, this protection only lasts until the primer coating is consumed, after which the bar behaves similarly to conventional ECR. The field test did not last long enough for this to occur; therefore, epoxy-coated bars with the calcium nitrite primer are conservatively assigned the same corrosion rate as ECR in cracked concrete for purposes of determining propagation time to cracking.

Tables 6.12 and 6.13 show that all systems except ECR(HY) and MC show similar performance relative to conventional ECR in the bench-scale and field tests. MC bars show significantly worse performance relative to ECR in the bench-scale tests, but performance comparable to ECR in the field test specimens. The concrete in field test specimens is dry during most of the testing period, whereas bench-scale specimens are kept saturated for over three quarters of the time. The poor performance of MC bars in the Southern Exposure test is likely due to the concrete remaining saturated for extended periods of time. Since this not representative of the conditions in bridge decks, only the field test corrosion rates accurately reflect the behavior of MC bars in bridge decks. It is important to note, however, that the bench-scale test results indicate MC bars may be a poor choice in a marine or other environment where the concrete remains saturated for extended periods of time. ECR(HY) exhibits lower corrosion rates relative to ECR in the Southern Exposure tests than in the field test; however, the corrosion rate for ECR(HY) in the Southern Exposure test is based on only a single specimen. Again, the field test

specimen corrosion rates should provide a more accurate representation of the corrosion rate for ECR(HY) in bridge decks.

The corrosion rates from field test specimens are used to determine the propagation time to cracking of the concrete. For conventional reinforcement with inhibitors, no field test specimens were cast, so an equivalent FTS corrosion rate is determined based on the bench-scale corrosion rates determined from the statistical analysis above and the relationships derived in Section 6.2.3. An equivalent corrosion rate is also calculated for 2205p reinforcement, as no corrosion has been observed to date in the field test specimens. The equivalent field test corrosion rates for these systems are listed in Table 6.14. The rates for FTS(Conv.) are included for comparison. In cracked concrete, there is no significant difference between the performance of Conv.*(RH), Conv.*(DCI), and conventional reinforcement with no inhibitor (Table 6.11b); these systems are assigned the same corrosion rate as conventional reinforcement in cracked concrete in the field tests, 0.939 µm/yr. For all other cases, the Southern Exposure macrocell corrosion rates of bare bars are multiplied by 0.155 to obtain the equivalent FTS corrosion rate in uncracked concrete (Figure 6.12a), and the cracked beam macrocell corrosion rates of bare bars are multiplied by 0.134 to obtain the equivalent FTS corrosion rate in cracked concrete (Figure 6.12b). Among the systems with bare bars, conventional reinforcement has the highest FTS corrosion rates in both uncracked and cracked concrete, 0.882 and 0.939 µm/yr, respectively. Conv.*(RH) and Conv.*(DCI) also have equivalent FTS corrosion rates of 0.939 µm/yr in cracked concrete, but have rates lower than conventional reinforcement with no inhibitor in uncracked concrete, at 0.255 and 0.584 µm/yr, respectively. Conv.*(HY) has the lowest equivalent FTS corrosion rates among specimens with conventional reinforcement, 0.109 and 0.241 µm/yr in uncracked and cracked concrete, respectively. 2205p has the lowest equivalent rates of all the systems, 0.0115 and 0.0287 µm/yr in uncracked and cracked concrete, respectively.

Table 6.14: Equivalent FTS Corrosion Rates (µm/yr) for Bare Bar Corrosion Protection Systems.

System	Concrete[a]	Benchscale Corrosion Rate	Equivalent FTS Corrosion Rate[b]
FTS(Conv.)	U	-	0.882
	C	-	0.939
Conv.*(RH)	U	1.64	0.255
	C	6.34	0.939
Conv.*(DCI)	U	3.77	0.584
	C	6.34	0.939
Conv.*(HY)	U	0.706	0.109
	C	1.80	0.241
2205p	U	0.074	0.0115
	C	0.214	0.0287

[a] U = uncracked concrete, C = cracked concrete

[b] Estimated using a ratio of FTS to bench-scale rate of 0.155 in uncracked concrete and 0.134 in cracked concrete.

The corrosion rates for bare bar systems assume the entire area of steel is corroding; however, autopsy results from field test specimens indicate corrosion occurs in localized regions on the bars (Figures 3.70 and 3.72). A visual inspection of conventional reinforcement from field test specimens at the end of testing indicates that corrosion covers only about one-third the total area of bars in uncracked concrete and about 40 percent of the total area of bars in cracked concrete. Since corrosion is only occurring on limited regions of the bar, the corrosion rates for bare bars in uncracked and cracked concrete are multiplied by 3 and 2.5, respectively, to obtain a macrocell corrosion rate based on effective area for these systems. The results are listed in Table 6.15. As before, conventional reinforcement in concrete with no inhibitor has the greatest corrosion rates based on effective area in both uncracked and cracked concrete, 2.65 and 2.35 µm/yr, respectively. 2205p has the lowest corrosion rates based on effective area in uncracked and cracked concrete, 0.034 and 0.072 µm/yr, respectively. These adjustments appear to be appropriate, not only based on the observed area undergoing corrosion but

also based on the time to cracking observed for the Conv. field test specimens, as will be discussed in Section 6.5.2.2.

Table 6.15: Equivalent FTS Corrosion Rates (µm/yr) for Bare Bar Corrosion Protection Systems based on Effective Area.

System	Concrete[a]	FTS Corrosion Rate (Total Area)[b]	FTS Corrosion Rate (Effective Area)[c]
Conv.	U	0.882	2.65
	C	0.939	2.35
Conv.*(RH)	U	0.25	0.765
	C	0.939	2.35
Conv.*(DCI)	U	0.58	1.75
	C	0.939	2.35
Conv.*(HY)	U	0.109	0.328
	C	0.24	0.602
2205p	U	0.0115	0.034
	C	0.0287	0.072

[a] U = uncracked concrete, C = cracked concrete

[b] See Table 6.14

[c] Estimated using a ratio of 3 in uncracked concrete and 2.5 in cracked concrete.

The corrosion rates presented in Tables 6.3, 6.4, and 6.15 are based on macrocell corrosion losses. However, both macrocell and microcell corrosion losses contribute to cracking and spalling of the concrete. To estimate the total (macrocell plus microcell) corrosion rate, the ratios of total to macrocell corrosion rate for bench-scale specimens (Figures 6.25 through 6.30) are applied to the macrocell field test corrosion rates calculated above. The corrosion rates for bare bars are multiplied by 1.79 (Figure 6.25) and 3.49 (Figure 6.28) to obtain the estimated total corrosion rate in uncracked and cracked concrete, respectively. Similarly, to obtain the estimated total corrosion rates for epoxy-coated bars in uncracked concrete, cracked concrete, and MC bars in uncracked and cracked concrete, the macrocell corrosion rates for each system are multiplied by 3.15, 12.36, 4.90, and 5.82, respectively. The estimated total corrosion rates are presented in Table 6.16. Standard deviations for each system are based on the standard

deviations in Tables 6.1 through 6.4 and are multiplied by the same ratios as the corrosion rates.

Table 6.16: Estimated Total Corrosion Rates in Bridge Decks (µm/yr) for Corrosion Protection Systems.

System	Concrete[a]	Macrocell Corrosion Rate[b]	Estimated Total Corrosion Rate[c]	Standard Deviation[d]
Corrosion Rate (Total Area)				
Conv.	U	2.65	4.74	0.845
	C	2.35	8.19	2.54
Conv.*(RH)	U	0.765	1.37	0.265
	C	2.35	8.19	2.54
Conv.*(DCI)	U	1.75	3.14	0.657
	C	2.35	8.19	2.54
Conv.*(HY)	U	0.328	0.588	0.280
	C	0.602	2.10	0.37
2205p	U	0.034	0.062	0.042
	C	0.072	0.250	0.23
Corrosion Rate (Exposed Area)				
ECR	U	5.66	17.8	12.8
	C	7.95	98.3	59.0
ECR(Chromate)	U	5.66	17.8	12.8
	C	7.95	98.3	59.0
ECR(DuPont)	U	5.66	17.8	12.8
	C	7.95	98.3	59.0
ECR(Valspar)	U	5.66	17.8	12.8
	C	7.95	98.3	59.0
ECR(RH)	U	5.66	17.8	12.8
	C	7.95	98.3	59.0
ECR(DCI)	U	5.66	17.8	12.8
	C	5.79	71.6	44.4
ECR(HY)	U	2.89	9.1	5.10
	C	4.32	53.4	53.4
ECR(primer/Ca(NO2)2)	U	5.66	17.8	12.8
	C	7.95	98.3	59.0
MC	U	5.66	27.7	19.9
	C	7.95	46.3	27.8

[a] U = uncracked concrete, C = cracked concrete

[b] See Tables 6.3, 6.4, and 6.15

[c] Macrocell corrosion rate multiplied by a ratio of 1.79, 3.15, and 4.90 for bare, coated and MC bars in uncracked concrete. Macrocell corrosion rate multiplied by 3.49, 12.36, and 5.82 for bare, coated, and MC bars in cracked concrete.

[d] Based on Tables 6.1 through 6.4 with same multipliers as applied to corrosion rate.

For systems with bare bars in uncracked concrete, Conv. has the highest total corrosion rate, 4.74 µm/yr, while 2205p has the lowest estimated total corrosion rate, 0.062 µm/yr. For systems with bare bars in cracked concrete, Conv. has the greatest total corrosion rate, 8.10 µm/yr, and 2205p has the lowest estimated total corrosion rate, 0.250 µm/yr.

For systems with coated bars in uncracked concrete, conventional ECR, ECR with increased adhesion, ECR in concrete with Rheocrete, and ECR with the calcium nitrite primer are all assigned total corrosion rates of 17.8 and 98.3 µm/yr in uncracked and cracked concrete, respectively. MC has a higher corrosion rate than ECR in uncracked concrete, 27.7 µm/yr, but a lower corrosion rate than ECR in cracked concrete, 46.3 µm/yr. This is due to the different behavior of zinc with respect to the ratio of total to macrocell corrosion rate (Figures 6.27 and 6.30). This behavior will only govern until the 50-µm zinc layer is consumed, after which the bar will corrode as conventional ECR. ECR(HY) has the lowest estimated total corrosion rates in both uncracked and cracked concrete, 9.1 and 53.4 µm/yr, respectively.

6.5.2.2 Comparison of Estimated Total Corrosion Rates in Bridge Decks with Field Test Observations

In the field test specimens with conventional reinforcement, cracking was observed above seven of the eight instrumented test bars. Therefore, it is possible to compare the corrosion rate for conventional reinforcement predicted in Table 6.16 to the actual corrosion rate that is required to crack the concrete during the time from corrosion initiation to cracking of concrete in the field test specimens. The age at crack initiation for each bar is estimated from photographs of each specimen taken approximately annually beginning at year three of testing, with the age at cracking assumed to be the average of the specimen age in the last photograph where no cracking is observed above the test bar and the specimen age in the first photograph where cracking is observed. The

age at corrosion initiation is determined from the macrocell corrosion rate and corrosion potential for each bar. The corrosion loss required to crack concrete in field test specimens is estimated using Eq. (4.4).

$$x_{crit} = 45\left(\frac{\left[C/25.4\right]^{2-A_f}}{D^{0.38} \times L_f^{\,0.1} \times A_f^{\,0.6}} + 0.2\right) \times 3^{A_f - 1} \tag{4.4}$$

where

x_{crit} = corrosion loss at crack initiation, μm

C = cover, mm. (25.4 mm)

D = bar diameter, mm. (16 mm)

L_f = fractional length of bar corroding, $L_{\text{corroding}}/L_{\text{bar}}$ (1 for uncoated bars)

A_f = fractional area of bar corroding, $A_{\text{corroding}}/A_{\text{bar}}$ (1 for uncoated bars)

$$x_{crit} = 45\left(\frac{\left[25.4/25.4\right]^{2-1}}{16^{0.38} \times 1^{0.1} \times 1^{0.6}} + 0.2\right) \times 3^{1-1}$$

$$x_{crit} = 24.7\,\mu\text{m}$$

Using this estimate for the corrosion loss required to crack concrete and the time from corrosion initiation to cracking, the average total corrosion rate for each bar is calculated. The results are shown in Table 6.17. On average, specimens show a total corrosion rate of 8.75 μm/yr, comparable to the 8.19 μm/yr estimated corrosion rate in cracked concrete (Table 6.16), but significantly higher than the corrosion rate for uncracked concrete predicted in Table 6.16. The field test specimens show high variation in concrete quality, as discussed earlier, and the exact age at crack initiation is unknown. It should be noted that the field test specimens show similar estimated total corrosion rates in uncracked and cracked concrete, and that the average rate agrees with the predicted corrosion rate for cracked concrete. This suggests that the corrosion rates in cracked concrete from Table 6.16 will give the best estimate of the total corrosion rate in bridge decks.

Table 6.17: Estimated Total Corrosion Rates for FTS Test Bars

Bar	Age at Corrosion Initiation (weeks)	Estimated Age at Cracking (weeks)	Estimated Time from Initiation to Cracking (weeks)	Estimated Corrosion Loss at Cracking (µm)	Estimated Total Corrosion Rate (µm/yr)
FTS-U-1-1	81	227	146	24.7	8.8
FTS-U-1-2	68	183	115	24.7	11.17
FTS-U-2-1[a]					
FTS-U-2-2	69	222	153	24.7	8.39
FTS-C-1-1	40	227	187	24.7	6.87
FTS-C-1-2[b]					
FTS-C-2-1	24	171	147	24.7	8.74
FTS-C-2-2	20	171	151	24.7	8.51
				Average:	**8.75**

[a] No cracking observed

[b] Cracking occurred prior to first photo

6.5.2.3 Calculation of Propagation Time to Crack Concrete Cover

The corrosion loss required to crack concrete cover for each system is determined from Eq. (4.4). The calculations consider a bridge deck containing No. 16 (No. 5) reinforcing steel with 76.2-mm (3-in.) clear concrete cover over the top mat of the steel. Stainless steel reinforcement is assumed to behave similarly to conventional reinforcement in terms of the corrosion losses required to crack concrete. For conventional reinforcement, the entire bar is exposed and able to corrode. Using Eq. (4.4),

$$x_{crit} = 45\left(\frac{\left[{}^{76.2}\!/_{25.4}\right]^{2-1}}{16^{0.38}\times 1^{0.1}\times 1^{0.6}} + 0.2\right)\times 3^{1-1}$$

$$x_{crit} = 56\,\mu\text{m}$$

This compares to 53 µm that would be obtained with the Torres-Acosta equation [Eq. (1.11)].

For epoxy-coated reinforcement, a damage pattern equal to that used for the field test is assumed, 3-mm (0.125-in.) diameter holes spaced at 0.124 m (4.9 in.) on each side of the bar. First, the fractional area of exposed bar, A_f, is calculated.

$$A_f = \frac{2 \times \pi \left({}^{d_h}\!/_{2} \right)^2}{\pi d_b l} = \frac{2 \times \pi \left({}^{3\text{mm}}\!/_{2} \right)^2}{\pi \times 16\,\text{mm} \times 124\,\text{mm}} = 0.0023$$

Then, the fractional length of exposed bar, L_f, is calculated.

$$L_f = \frac{d_h}{l} = \frac{3\,\text{mm}}{124\,\text{mm}} = 0.024$$

The values for A_f and L_f calculated above are used in Eq. (4.4) to calculate the corrosion loss required to crack concrete for epoxy-coated bars.

$$x_{crit} = 45\left(\frac{\left[{}^{76.2}\!/_{25.4} \right]^{2-0.0023}}{16^{0.38} \times 0.024^{0.1} \times 0.0023^{0.6}} + 0.2 \right) \times 3^{0.0023-1}$$

$$x_{crit} = 2434\,\mu\text{m}$$

The comparisons of the corrosion loss required to crack concrete for conventional and galvanized reinforcement suggest galvanized reinforcement requires twice as much corrosion loss to crack the concrete as iron (Figure 4.9). The MC bars in this study have a 50-µm (2-mil) thick zinc coating underneath the epoxy; the loss of 50 µm of zinc is equivalent to the loss of 25 µm of iron when calculating the corrosion loss to crack concrete. Once this zinc layer is consumed, iron will begin to corrode; to account for this, it is assumed that MC reinforcement requires an additional 25 µm of corrosion loss compared to ECR to crack concrete. Thus, for the first 50 µm of loss, the zinc corrosion rate is used, with the corrosion products having half the effect as conventional iron. After 50 µm of loss, the corrosion rate for conventional ECR is used and the corrosion products are assumed to be iron.

The time from corrosion initiation to cracking of the concrete cover (propagation time) for each system is found by taking the corrosion losses required to crack concrete, calculated above, and dividing by the estimated average corrosion rates in Table 6.16. This is done using both the average of the cracked and uncracked corrosion rates and the corrosion rates from cracked concrete only. Because bridge decks inevitably develop

cracks over the reinforcement, the comparisons using the corrosion rates in cracked concrete likely provide the more accurate representation of corrosion in bridge decks. The results using the average of the corrosion rates in cracked and uncracked concrete are presented as a less severe alternative.

The estimated times to first cracking after corrosion initiation are presented in Table 6.18. Based on the corrosion rate in cracked concrete, stainless steel exhibits the longest time to first cracking of the concrete, 224 years. Specimens with conventional reinforcement exhibit a time to cracking of 6.8 years after corrosion initiation. Specimens with epoxy coatings exhibit average times to cracking between 24.8 and 45.6 years.

Table 6.18: Estimated Times to First Cracking After Corrosion Initiation

System	Time to Damage-Cracked (years)[a]	Time to Damage-Average (Cracked and Uncracked) (years)[b]
Conv.	6.8	8.7
Conv.*(RH)	6.8	11.7
Conv.*(DCI)	6.8	9.9
Conv.*(HY)	26.6	41.6
2205p	223.8	359.2
ECR	24.8	49.2
ECR(Chromate)	24.8	49.2
ECR(DuPont)	24.8	49.2
ECR(Valspar)	24.8	49.2
ECR(RH)	24.8	49.2
ECR(DCI)	34.0	61.7
ECR(HY)	45.6	91.9
ECR(primer/$Ca(NO_2)_2$)	24.8	49.2
MC	25.5	49.8

[a] Time to cracking after corrosion initiation based on corrosion rate in cracked concrete

[b] Time to cracking after corrosion initiation based on average corrosion rate in uncracked and cracked concrete

6.5.3 Time to First Repair

The time to first repair for each corrosion protection system is found by combining the time to corrosion initiation (Table 6.9), the time to cracking of the concrete after initiation (Table 6.18), and the time from the first crack to the repair of the deck. The latter period is based on the observation that a bridge deck is not fully repaired at the development of the first crack. Rather, the bridge typically undergoes a series of short-term temporary repairs. To account for the period of temporary repairs, a five year delay between first cracking and repair is assumed for all corrosion protection systems.

Tables 6.19a and 6.19b compare expected times to first repair for all corrosion protection systems based on the corrosion rate in cracked concrete and the average of the corrosion rates in cracked and uncracked concrete, respectively. Based on the corrosion rate in cracked concrete (Table 6.19a), conventional reinforcement has an expected time to first repair of 14 years, which is within the range of 10 to 25 years predicted by KDOT and SDDOT maintenance engineers (Darwin et al. 2002). Among systems with conventional reinforcement with inhibitors, conventional reinforcement used in conjunction with concrete containing Rheocrete and DCI have expected times to first repair slightly greater than those observed for conventional reinforcement without inhibitors, 16 and 18 years. At 33 years, conventional reinforcement used in conjunction with concrete containing Hycrete has more than twice the age to first repair as does conventional reinforcement with no inhibitor. Pickled 2205 stainless steel has an expected time to first repair of 297 years, which is the longest among all systems tested. ECR and ECR with increased adhesion have expected times to first repair of 50 years, compared to the 35 to 40 years estimated by KDOT and SDDOT (Darwin et al. 2002). It should be noted that most bridges containing ECR have not yet reached this age. Systems containing ECR used in concrete containing corrosion inhibitors have times to first repair ranging from 50 to 63 years. Systems with MC reinforcement have an expected time to first repair of 51 years.

Table 6.19a: Time to First Repair for Corrosion Protection Systems Based on Corrosion Rate in Cracked Concrete.

System	Time to Initiation (years)[a]	Time from Initiation to Cracking (years)[b]	Time from Cracking to Repair (Years)[c]	Expected Time to First Repair (Years)
Conv.	2.2	6.8	5	14
Conv.*(RH)	4.1	6.8	5	16
Conv.*(DCI)	6.1	6.8	5	18
Conv.*(HY)	1.0	26.6	5	33
2205p	67.6	224	5	297
ECR	20.3	24.8	5	50
ECR(Chromate)	20.3	24.8	5	50
ECR(DuPont)	20.3	24.8	5	50
ECR(Valspar)	20.3	24.8	5	50
ECR(RH)	20.3	24.8	5	50
ECR(DCI)	24.0	34.0	5	63
ECR(HY)	2.5	45.6	5	53
ECR(primer/$Ca(NO_2)_2$)	29.7	24.8	5	59
MC	20.3	25.5	5	51

[a] See Table 6.9

[b] See Table 6.18 (Cracked Rate)

[c] Assumed 5 years for all systems

Based on the average corrosion rate in uncracked and cracked concrete (Table 6.19b), conventional reinforcement has an expected time to first repair of 16 years. Conventional reinforcement used in conjunction with concrete containing Rheocrete and DCI have expected times to first repair of 21 years, and conventional reinforcement used in conjunction with concrete containing Hycrete has a time to first repair of 48 years. Pickled 2205 stainless steel has an expected time to first repair of 432 years. ECR and ECR with increased adhesion have expected times to first repair of 67 years. Systems containing ECR used with concrete containing corrosion inhibitors have times to first repair ranging from 67 to 85 years. Systems with MC reinforcement have an expected time to first repair of 68 years.

Table 6.19b: Time to First Repair for Corrosion Protection Systems Based on Average Corrosion Rate in Uncracked and Cracked Concrete.

System	Time to Initiation (years)[a]	Time from Initiation to Cracking (years)[b]	Time from Cracking to Repair (Years)[c]	Expected Time to First Repair (Years)
Conv.	2.2	8.7	5	16
Conv.*(RH)	4.1	11.7	5	21
Conv.*(DCI)	6.1	9.9	5	21
Conv.*(HY)	1.0	41.6	5	48
2205p	67.6	359	5	432
ECR	20.3	42	5	67
ECR(Chromate)	20.3	42	5	67
ECR(DuPont)	20.3	42	5	67
ECR(Valspar)	20.3	42	5	67
ECR(RH)	20.3	42	5	67
ECR(DCI)	24.0	54	5	83
ECR(HY)	2.5	78	5	85
ECR(primer/Ca(NO2)2)	29.7	42	5	77
MC	20.3	43	5	68

[a] See Table 6.9

[b] See Table 6.18 (Average of Uncracked and Cracked Rate)

[c] Assumed 5 years for all systems

6.6 COST EFFECTIVENESS

6.6.1 Initial Cost

The material costs for reinforcement and inhibitors used in this analysis are provided by the material suppliers. For conventional reinforcement, a base cost of $0.77/kg ($0.35/lb) is used. ECR and ECR with increased adhesion from DuPont and Valspar have a base cost of $0.99/kg ($0.45/lb). ECR with chromate pretreatment and ECR with the calcium nitrite primer have a base cost of $1.10/kg ($0.50/lb). MC reinforcement has a base cost of $1.65/kg ($0.75/lb). Pickled 2205 stainless steel is assumed to have a base cost of $5.19/kg ($2.35/lb) (Balma et al. 2005). A placement cost of $1.14/kg ($0.52/lb) is used for all reinforcement. A steel reinforcement density of 163 kg/m^3 (275 lb/yd^3) is used, based on the average quantity of steel used in 12 bridge decks constructed in Kansas between 2004 and 2007 (Xing et al. 2010). Assuming a 216-mm

(8.5-in.) thick bridge deck, 35.2 kg/m^2 (64.9 lb/yd^2) of steel is required per unit surface area of deck. The reinforcement costs for all systems are shown in Table 6.20.

Table 6.20: Total In-Place Cost for Reinforcement per Unit Area of Bridge Deck

Reinforcement	Reinforcement Cost		Reinforcement Use		Total Cost	
	$/kg	$/lb	kg/m^2	lb/yd^2	$/m^2	$yd^2
Conv.	$1.91	$0.87	35.2	64.9	$67.23	$56.35
2205p	$6.33	$2.88	35.2	64.9	$222.82	$186.74
ECR	$2.13	$0.97	35.2	64.9	$74.98	$62.84
ECR(Chromate)	$2.24	$1.02	35.2	64.9	$78.85	$66.08
ECR(DuPont)	$2.13	$0.97	35.2	64.9	$74.98	$62.84
ECR(Valspar)	$2.13	$0.97	35.2	64.9	$74.98	$62.84
ECR(primer/Ca(NO_2)$_2$)	$2.24	$1.02	35.2	64.9	$78.85	$66.08
MC	$2.79	$1.27	35.2	64.9	$98.21	$82.31

The base in-place cost of concrete with no inhibitors used in this study is $735.74/m^3 ($562.51/yd^3) (Xing et al. 2010). For corrosion inhibitors, the dosage rates are the rates used in this study and are based on manufacturer recommendations. Rheocrete costs $6.08/L ($23.00/gal) and has dosage rate of 5 L/m^3 (1 gal/yd^3), equal to $30.40/m^3 ($23.00/yd^3) over the base cost of the concrete. DCI costs $1.32/L ($5.00/gal) and has a dosage rate of 15 L/m^3 (3 gal/yd^3), equal to $19.80/m^3 ($15/yd^3). Hycrete costs $4.95/L ($18.75/gal) and has a dosage rate of 7.6 L/m^3 (1.54 gal/yd^3). To counteract the reduction in strength and low freeze-thaw resistance observed in concrete containing Hycrete (Section 1.7.3.3), an additional 35.6 kg/m^3 (60 lb/yd^3) of portland cement at $0.138/kg ($0.0625/lb) is added, for a cost of $42.53/m^3 ($32.63/yd^3) for Hycrete over the in-place cost of conventional concrete. While the extra cement should counteract the negative impact of Hycrete on strength and freeze-thaw resistance, it will increase the tendency of the concrete to crack (Darwin et al. 2004, 2010). This increased cracking potential, however, is not included in the analysis that follows.

Assuming a 216-mm (8.5-in.) thick bridge deck, 0.215 m^3 of concrete are required for a 1 m^2 surface area of deck (0.236 yd^3 per yd^2 of deck). Concrete costs for all corrosion protection systems per unit surface area are shown in Table 6.21.

Table 6.21: Total In-Place Cost for Concrete per Unit Area of Bridge Deck

System	Concrete Cost		Inhibitor Cost		Concrete Use		Total Cost	
	$/$m^3$	$/$yd^3$	$/$m^3$	$/$yd^3$	m^3/m^2	yd^3/yd^2	$/$m^2$	$yd^2
Conv.	$735.75	$562.51	-	-	0.216	0.236	158.92	132.75
RH	$735.75	$562.51	$30.40	$23.00	0.216	0.236	165.49	138.18
DCI	$735.75	$562.51	$19.80	$15.00	0.216	0.236	163.20	136.29
HY[a]	$740.66	$566.29	$37.62	$28.88	0.216	0.236	168.11	140.46

[a] Additional 35.9 kg/m^3 (60 lb/yd^3) cement added to counteract strength reduction

The total initial cost, equal to the sum of reinforcement and concrete costs, for each system is shown in Table 6.22. A deck with conventional reinforcement has the lowest initial in-place cost, $226.15/$m^2$ ($189.10/$yd^2$). This increases to $233.90/$m^2$ ($195.59/$yd^2$) for ECR, which is more than the cost of a deck with conventional steel and DCI or Rheocrete, $230.43/$m^2$ ($192.64/$yd^2$) or $232.72/$m^2$ ($194.53/$yd^2$), respectively, but less than the cost of a deck with conventional steel and Hycrete, $235.34/$m^2$ ($196.81/$yd^2$). At $257.13/$m^2$ ($215.06/$yd^2$), a deck with MC reinforcement has the highest in-place cost of all systems with an epoxy coating. A deck with pickled 2205 stainless steel has the highest overall initial cost, $381.74/$m^2$ ($319.49/$yd^2$).

Table 6.22: Total In-Place Cost for Corrosion Protection Systems

System	Reinforcement Cost		Concrete Cost		Total Cost	
	$/m^2	$yd^2	$/m^2	$yd^2	$/m^2	$yd^2
Conv.	$67.23	$56.35	$158.92	$132.75	$226.15	$189.10
Conv.(RH)	$67.23	$56.35	$165.49	$138.18	$232.72	$194.53
Conv.(DCI)	$67.23	$56.35	$163.20	$136.29	$230.43	$192.64
Conv.(HY)	$67.23	$56.35	$168.11	$140.46	$235.34	$196.81
2205p	$222.82	$186.74	$158.92	$132.75	$381.74	$319.49
ECR	$74.98	$62.84	$158.92	$132.75	$233.90	$195.59
ECR(Chromate)	$78.85	$66.08	$158.92	$132.75	$237.77	$198.83
ECR(DuPont)	$74.98	$62.84	$158.92	$132.75	$233.90	$195.59
ECR(Valspar)	$74.98	$62.84	$158.92	$132.75	$233.90	$195.59
ECR(RH)	$74.98	$62.84	$165.49	$138.18	$240.46	$201.02
ECR(DCI)	$74.98	$62.84	$163.20	$136.29	$238.17	$199.13
ECR(HY)	$74.98	$62.84	$168.11	$140.46	$243.08	$203.30
ECR(primer/Ca(NO2)2)	$78.85	$66.08	$158.92	$132.75	$237.77	$198.83
MC	$98.21	$82.31	$158.92	$132.75	$257.13	$215.06

6.6.2 Repair Costs

The current analysis assumes a 75-year design life. For corrosion systems that will require repair before 75 years, the costs of repairs to the deck are included in the analysis. A repair cost of $349/m^2 ($292/yd^2) is used for all corrosion protection systems, based on an analysis by Darwin et al. (2007b). The repair cost is based on bridges with conventional reinforcement because most bridge decks cast with ECR have not required repairs to date. Because most of the repair costs are independent of the type of reinforcement used in the deck, it is not expected that the cost of repairing a bridge deck containing ECR will be significantly different from the cost of repairing a bridge deck containing conventional reinforcement. Repairs are assumed to last for 25 years (Darwin et al. 2007b).

6.6.3 Present Value

The total lifecycle cost of each corrosion protection system is calculated using the times to first repair listed in Table 6.19. Cost effectiveness is based on the initial cost of the deck and the present value of future repair costs. The present value is calculated as:

$$P = F(1+i)^{-n} \tag{6.1}$$

where

P = Present value

F = Future cost of repair ($\$349/m^2$)

i = Discount rate

n = Time to repair

For this study, discount rates of 2%, 4%, and 6% are assumed. A value of 2% is most realistic and is used for most of the discussion that follows.

Tables 6.23a and b list the estimated costs over a 75-year design life using the time to first repair based on the corrosion rate in cracked concrete. Under this scenario, all of the corrosion protection systems, with the exception of pickled 2205 stainless steel, require repair during a 75-year design life. ECR in concrete with DCI is the most cost-effective protection system, with a present cost of $\$338/m^2$ ($\$283/yd^2$) at a discount rate of 2%. ECR with the calcium nitrite primer and ECR(HY) have present costs of \$345 and $\$365/m^2$ (\$289 and $\$305/yd^2$) at a discount rate of 2%. Conventional ECR, as well as increased adhesion epoxies from DuPont and Valspar, have present costs of $\$363/m^2$ ($\$304/yd^2$) at a discount rate of 2%, making these systems are more cost-effective than ECR(HY). MC reinforcement and 2205p stainless steel have present costs of $\$385/m^2$ and $\$382/m^2$ (\$322 and $\$319/yd^2$), respectively, at a 2% discount rate. The differences in present cost between the coated bar systems and 2205p stainless steel are small and are not significant. Conventional reinforcement has the highest present cost, $\$750/m^2$ ($\$627/yd^2$) at a 2% discount rate. Conventional reinforcement used in conjunction with concrete containing Rheocrete and DCI has present costs of $\$737/m^2$ and $\$717/m^2$ (\$617

and \$598/yd^2), respectively. Conventional reinforcement used in conjunction with concrete containing Hycrete has the lowest present cost among systems with conventional reinforcement, \$530/m^2 (\$443/yd^2), but is less cost-effective than any of the coated bar systems or 2205p.

Table 6.23a: Total Costs Over 75-Year Design Life (\$/m^2) for Corrosion Protection Systems Using Time to First Repair Based on Corrosion Rates in Cracked Concrete.

System	Initial Cost (\$/m^2)	Time to Repair (years)			Repair Cost (\$/m^2)	Present Cost (\$/m^2)		
		1	2	3		i=2%	i=4%	i=6%
Conv.	226	14	39	64	\$349	\$750	\$531	\$424
Conv.*(RH)	233	16	41	66	\$349	\$737	\$516	\$411
Conv.*(DCI)	230	18	43	68	\$349	\$715	\$492	\$389
Conv.*(HY)	235	33	58	-	\$349	\$530	\$369	\$300
2205p	382	>75	-	-	\$349	\$382	\$382	\$382
ECR	234	50	-	-	\$349	\$363	\$283	\$253
ECR(Chromate)	238	50	-	-	\$349	\$367	\$287	\$257
ECR(DuPont)	234	50	-	-	\$349	\$363	\$283	\$253
ECR(Valspar)	234	50	-	-	\$349	\$363	\$283	\$253
ECR(RH)	240	50	-	-	\$349	\$370	\$289	\$259
ECR(DCI)	238	63	-	-	\$349	\$338	\$268	\$247
ECR(HY)	243	53	-	-	\$349	\$365	\$287	\$259
ECR(primer/Ca$(NO_2)_2$)	238	59	-	-	\$349	\$345	\$272	\$249
MC	257	51	-	-	\$349	\$385	\$305	\$275

Table 6.23b: Total Costs Over 75-Year Design Life (\$/yd^2) for Corrosion Protection Systems Using Time to First Repair Based on Corrosion Rates in Cracked Concrete.

System	Initial Cost (\$/yd^2)	Time to Repair (years)			Repair Cost (\$/yd^2)	Present Cost (\$/yd^2)		
		1	2	3		i=2%	i=4%	i=6%
Conv.	189	14	39	64	\$292	\$627	\$444	\$355
Conv.*(RH)	195	16	41	66	\$292	\$617	\$432	\$343
Conv.*(DCI)	193	18	43	68	\$292	\$598	\$412	\$325
Conv.*(HY)	197	33	58	-	\$292	\$443	\$308	\$251
2205p	319	>75	-	-	\$292	\$319	\$319	\$319
ECR	196	50	-	-	\$292	\$304	\$237	\$211
ECR(Chromate)	199	50	-	-	\$292	\$307	\$240	\$215
ECR(DuPont)	196	50	-	-	\$292	\$304	\$236	\$211
ECR(Valspar)	196	50	-	-	\$292	\$304	\$236	\$211
ECR(RH)	201	50	-	-	\$292	\$309	\$242	\$217
ECR(DCI)	199	63	-	-	\$292	\$283	\$224	\$207
ECR(HY)	203	53	-	-	\$292	\$305	\$240	\$216
ECR(primer/Ca$(NO_2)_2$)	199	59	-	-	\$292	\$289	\$227	\$208
MC	215	51	-	-	\$292	\$322	\$255	\$230

Tables 6.24a and b list the estimated design life costs using the time to first repair based on the average of corrosion rates in cracked and uncracked concrete. Under this scenario, ECR(DCI), ECR(HY), and ECR(primer/$Ca(NO_2)_2$) do not require repair during a 75-year design life. In this scenario, ECR with the calcium nitrite primer and ECR in concrete with DCI are the most cost-effective protection systems, with a present cost of $\$238/m^2$ ($\$199/yd^2$) at a discount rate of 2%. ECR(HY) has a present cost of $\$243/m^2$ ($\$203/yd^2$) at a discount rate of 2%, lower than the present cost of conventional ECR, ECR(DuPont), and ECR(Valspar), $\$326/m^2$ ($\$273/yd^2$). MC is the most expensive of the coated bar systems, with a present cost of $\$348/m^2$ ($\$291/yd^2$).

It should be noted that ECR, ECR(Chromate), ECR(DuPont), ECR(Valspar), and ECR(RH) have a 67-year time to first repair, and given the large standard deviations of the corrosion rates (Table 6.16), it is possible they could achieve a 75-year design life under this scenario. Assuming a 75-year design life for these systems makes ECR, ECR(DuPont), and ECR(Valspar) the most cost-effective systems, at $\$234/m^2$ ($\$196/yd^2$).

Conventional reinforcement has the highest present cost, $\$731/m^2$ ($\$611/yd^2$) at a 2% discount rate. Conventional reinforcement used in conjunction with concrete containing Rheocrete and DCI has present costs of $\$691/m^2$ and $\$687/m^2$ ($578 and $\$574/yd^2$), respectively. Conventional reinforcement used in conjunction with concrete containing Hycrete has the lowest present cost among systems with conventional reinforcement, $\$454/m^2$ ($\$380/yd^2$), but is less cost-effective than any of the coated bar systems or 2205p, the latter with a cost of $\$382/m^2$ ($\$319/yd^2$).

Table 6.24a: Total Costs Over 75-Year Design Life ($/m^2) for Corrosion Protection Systems Using Time to First Repair Based on Average Corrosion Rates in Uncracked and Cracked Concrete.

System	Initial Cost ($/m^2)	Time to Repair (years)			Repair Cost ($/m^2)	Present Cost ($/m^2)		
		1	2	3		i=2%	i=4%	i=6%
Conv.	226	16	41	66	$349	$731	$510	$404
Conv.*(RH)	233	21	46	71	$349	$691	$467	$367
Conv.*(DCI)	230	21	46	71	$349	$687	$463	$363
Conv.*(HY)	235	48	73	-	$349	$454	$309	$262
2205p	382	>75	-	-	$349	$382	$382	$382
ECR	234	67	-	-	$349	$326	$259	$241
ECR(Chromate)	238	67	-	-	$349	$330	$263	$245
ECR(DuPont)	234	67	-	-	$349	$326	$259	$241
ECR(Valspar)	234	67	-	-	$349	$326	$259	$241
ECR(RH)	240	67	-	-	$349	$333	$265	$247
ECR(DCI)	238	>75	-	-	$349	$238	$238	$238
ECR(HY)	243	>75	-	-	$349	$243	$243	$243
ECR(primer/Ca(NO2)2)	238	>75	-	-	$349	$238	$238	$238
MC	257	68	-	-	$349	$348	$281	$264

Table 6.24b: Total Costs Over 75-Year Design Life ($/yd^2) for Corrosion Protection Systems Using Time to First Repair Based on Average Corrosion Rates in Uncracked and Cracked Concrete.

System	Initial Cost ($/yd^2)	Time to Repair (years)			Repair Cost ($/yd^2)	Present Cost ($/yd^2)		
		1	2	3		i=2%	i=4%	i=6%
Conv.	189	16	41	66	$292	$611	$427	$338
Conv.*(RH)	195	21	46	71	$292	$578	$390	$307
Conv.*(DCI)	193	21	46	71	$292	$574	$387	$303
Conv.*(HY)	197	48	73	-	$292	$380	$259	$219
2205p	319	>75	-	-	$292	$319	$319	$319
ECR	196	67	-	-	$292	$273	$216	$201
ECR(Chromate)	199	67	-	-	$292	$276	$220	$205
ECR(DuPont)	196	67	-	-	$292	$273	$216	$201
ECR(Valspar)	196	67	-	-	$292	$273	$216	$201
ECR(RH)	201	67	-	-	$292	$278	$222	$207
ECR(DCI)	199	>75	-	-	$292	$199	$199	$199
ECR(HY)	203	>75	-	-	$292	$203	$203	$203
ECR(primer/Ca(NO2)2)	199	>75	-	-	$292	$199	$199	$199
MC	215	68	-	-	$292	$291	$235	$221

CHAPTER 7

CONCLUSIONS AND RECOMMENDATIONS

7.1 SUMMARY

The performance of corrosion protection systems for reinforcing steel in concrete is evaluated. In addition to conventional and conventional epoxy-coated reinforcement, the corrosion protection systems include:

- Conventional reinforcement and conventional reinforcement used in conjunction with one of three corrosion inhibitors: DCI-S, Rheocrete 222+, or Hycrete DSS;
- Conventional epoxy-coated reinforcement (ECR), ECR in conjunction with DCI-S, Rheocrete 222+, or Hycrete DSS, and ECR with a microencapsulated calcium nitrite primer;
- ECR with a chromate pretreatment and two epoxies from DuPont and Valspar, all designed to have improved adhesion to the underlying steel;
- Multiple-coated reinforcement – ECR with a 50-µm (2-mil) thick zinc coating underneath the epoxy;
- Pickled 2205 stainless steel;
- Galvanized reinforcement.

Conventional steel with and without corrosion inhibitors and pickled 2205 stainless steel are evaluated using Southern Exposure and cracked beam tests. All systems except galvanized reinforcement and conventional reinforcement with corrosion inhibitors are evaluated using field test specimens in both cracked and uncracked concrete. Epoxy-coated reinforcement and multiple-coated reinforcement are evaluated using rapid macrocell tests to determine the effect of corrosion loss and time on the disbondment of the epoxy coating. Selected bench-scale (Southern Exposure and cracked beam) specimens are monitored with linear polarization resistance to determine total corrosion losses.

Two bridge decks in Kansas, cast with 2205 stainless steel, are monitored using corrosion potential mapping. Bench-scale and field test specimens containing conventional, epoxy-coated, and 2205 stainless steel, cast using trial-batch concrete from each bridge, are tested to determine relative corrosion performance.

Conventional, galvanized, and epoxy-coated bars are evaluated using impressed current to determine the corrosion loss required to crack concrete for each system. A finite element model is developed to represent general and localized corrosion, and the results are used to develop a relationship between concrete cover, bar diameter, and area of bar corroding, and the corrosion loss required to crack concrete. An analysis of pore solutions expressed from cement pastes containing corrosion inhibitors is performed, with pH and selected ion concentrations measured from solutions collected one and seven days after casting.

Results obtained from bench-scale and field test specimens are used to estimate cost effectiveness for each system under a 75-year service life.

7.2 CONCLUSIONS

Based on the analysis and results presented in this report, the following conclusions may be drawn.

1. Conventional reinforcement exhibits the highest corrosion rates among all systems studied.
2. While corrosion inhibitors reduce the corrosion rates observed for conventional reinforcement, the combination of conventional reinforcement and corrosion inhibitors is not as cost-effective as epoxy-coated reinforcement.
3. Epoxy coatings significantly reduce corrosion rates compared to conventional reinforcement.
4. Corrosion inhibitors, in conjunction with both ECR and conventional reinforcement, reduce corrosion rates in uncracked concrete; however, corrosion

inhibitors are significantly less effective in cracked concrete. Corrosion inhibitors also show relatively less effect when used with ECR than when used with conventional reinforcement.

5. Of the corrosion inhibitors tested, Hycrete is the most effective at reducing corrosion rates. However, more testing is needed to establish the resistance of concrete containing Hycrete to scaling when subjected to freezing and thawing in the presence of deicing chemicals and the reduction in concrete compressive strength caused by Hycrete.
6. An analysis of pore solution extracted from cement pastes containing inhibitors shows increased sulfate levels in samples collected from cement pastes containing Hycrete one and seven days after casting and in samples collected from cement pastes containing Rheocrete seven days after casting. Increased sulfate levels may explain some of the adverse effects on scaling resistance and compressive strength observed in concrete containing Hycrete and a slightly reduced compressive strength for concrete containing Rheocrete.
7. Epoxy coatings with improved adhesion to the underlying steel perform comparably to, but no better than, conventional ECR in terms of corrosion loss and disbondment of the coating.
8. Multiple-coated reinforcement exhibits greater corrosion losses than conventional ECR in bench-scale specimens, but comparable performance in field test specimens. Multiple-coated reinforcement exhibits less disbondment than ECR.
9. Disbondment of epoxy coatings increases with corrosion loss and the severity of the exposure conditions.
10. Laboratory and field measurements show that pickled 2205 stainless steel reinforcement has excellent corrosion resistance in chloride-contaminated concrete.

11. The corrosion losses required to crack concrete for galvanized reinforcement are at least two times greater than the losses required to crack concrete for conventional reinforcement.
12. For bare conventional steel reinforcing bars, the corrosion losses required to crack concrete are directly proportional to the clear concrete cover. For isolated regions of corrosion, such as occurs at damage sites on ECR, the relationship changes to one that is directly proportional to square of the concrete cover as the exposed region on the bar decreases. An equation is developed to predict the corrosion losses required to crack concrete for both bare reinforcement and damaged epoxy-coated reinforcement.
13. A bridge deck containing pickled 2205 stainless steel has the longest design life among all corrosion protection systems tested. The high critical chloride threshold and low corrosion rate of pickled 2205 reinforcing steel may make it cost-effective in environments with severe chloride exposure; however, for the exposure conditions seen on a typical bridge deck in Kansas, stainless steel reinforcement has a present cost over a 75-year design life that is 10 to 20 percent more expensive than epoxy-coated reinforcement.
14. A bridge deck containing conventional reinforcement has the shortest design life of all corrosion protection systems tested. The use of corrosion inhibitors in conjunction with conventional reinforcement increases the design life of the bridge deck; however, the design life remains less than that of conventional ECR.
15. Based on an economic analysis, corrosion protection systems using either coated or stainless steel reinforcement are significantly more cost-effective than any of the systems evaluated containing conventional reinforcing steel. The differences in cost-effectiveness between the different coated bar systems and stainless steel are not significant.

7.3 RECOMMENDATIONS

1. Although epoxy-coated reinforcement shows significant disbondment in bench-scale and field test specimens, the effect of disbondment of epoxy coatings on long-term corrosion resistance is not known and should be investigated further.
2. Multiple-coated reinforcement exhibits significantly less disbondment than conventional ECR and may be cost-effective if testing reveals disbondment to have a significant negative impact on long-term corrosion resistance. Bench-scale test results, however, suggest that MC reinforcement would perform poorly in marine environments or other locations where the concrete remains continuously saturated; further study of both MC and galvanized bars is needed to verify this result.
3. Additional research into the effect of the sulfate content in concrete on the critical chloride corrosion threshold of reinforcement is needed to determine if the elevated sulfate content observed in pore solution from cement pastes containing Hycrete is the cause of the low chloride threshold in concrete containing Hycrete.
4. The corrosion loss required to crack concrete cover for MC and stainless steel reinforcement is not known and should be determined in a future study.

REFERENCES

AASHTO T 260-94 (1997). "Standard Method of Test for Sampling and Testing for Chloride Ion in concrete and Concrete Raw Materials," *Standard Specifications for Transportation Materials and Methods of Sampling and Testing,* AASHTO. pp. 925-931.

ACI Committee 222 (2001). *Protection of Metals in Concrete Against Corrosion* (222R-01), American Concrete Institute, Farmington Hills, MI, 41 pp.

Alonso, C., Andrade, C., Rodriguez, J., and Diaz, J.M. (1998). "Factors Controlling Cracking of Concrete Affected by Reinforcement Corrosion," *Materials and Structures*, Vol. 31, No. 211, Aug.-Sept., pp. 435-441.

Ann, K. and Song, H. (2007). "Chloride Threshold Level for Corrosion of Steel in Concrete," *Corrosion Science*, Vol. 49, No. 11, Nov., pp. 4113-4133.

ASTM A775/A775M (2007). (ASTM A755-07). "Standard Specification for Epoxy Coated Steel Reinforcing Bars," ASTM International, West Conshohocken, PA. 11 pp.

ASTM A955/A955M (2009). (ASTM A955-09). "Standard Specification for Deformed and Plain Stainless-Steel Reinforcing Bars for Concrete Reinforcement," ASTM International, West Conshohocken, PA. 11 pp.

ASTM C876 (2009) (ASTM C876-09). "Standard Test Method for Corrosion Potentials of Uncoated Reinforcing Steel in Concrete," ASTM International, West Conshohocken, PA. 7 pp.

ASTM G109 (2007). (ASTM G109-07). "Standard Test Method for Determining Effects of Chemical Admixtures on Corrosion of Embedded Steel Reinforcement in Concrete Exposed to Chloride Environments," ASTM International, West Conshohocken, PA. 6 pp.

Balabanic, B., Bicanic, N, and Durekovic, A. (1996). "The Influence of W/C Ratio, Concrete Cover Thickness and Degree of Water Saturation on the Corrosion Rate of Reinforcing Steel in Concrete," *Cement and Concrete Research,* Vol. 26, No. 5, Jul., pp. 761-769.

Balma, J., Darwin, D., Browning, J., and Locke, C. (2005). "Evaluation of Corrosion Protection Systems and Corrosion Testing Methods for Reinforcing Steel in Concrete," *SM Report* 76, University of Kansas Center for Research, Lawrence, KS, 517 pp.

Barneyback, R. and Diamond, S. (1981). "Expression and Analysis of Pore Fluids from Hardened Cement Pastes and Mortars," *Cement and Concrete Research*, Vol. 11, No. 2, Mar., pp. 279-285.

Batis, G., Pantazopoulou, P., and Routoulas A. (2003). "Corrosion Protection Investigation of Reinforcement by Inorganic Coating in the Presence of Alkanolamine-based Inhibitor," *Cement and Concrete Research,* Vol. 25, No. 3, Apr., pp. 371-377.

Bola, M. and Newtson, C. (2005). "Field Evaluation of Marine Structures Containing Calcium Nitrite," *Journal of Performance of Constructed Facilities*, Vol. 19, No. 1, Feb., pp. 28-35.

Cady, P and Weyers, R. (1992). "Predicting Service Life of Concrete Bridge Decks Subject to Corrosion," *Corrosion Forms and Control for Infrastructure.* ASTM STP 1137, ASTM, Philadelphia, pp. 328-338.

Civjan, S., LaFave, J., Lovett, D., Sund, D., and Trybulski, J. (2003). "Performance Evaluation and Economic Analysis of Combinations of durability Enhancing Admixtures (Mineral and Chemical) in Structural Concrete for the Northeast U.S.A.," *New England Transportation Consortium,* Report NETCR-36. 165 pp.

Clifton, J., Beeghly, H., and Mathey, R. (1975). "Protecting Reinforcing Bars from Corrosion With Epoxy Coatings," C*orrosion of Metals in Concrete* (SP-49), American Concrete Institute, Farmington Hills, MI, pp. 115-132.

Darwin, D., Locke, C., Balma, J., and Kahrs, J. (1999). "Evaluation of Stainless Steel Clad Reinforcing Bars," *SL Report* 99-3, University of Kansas Center for Research, Lawrence, KS, 45 pp.

Darwin, D., Barham, S., Kozul, R., and Luan, S. (2001). "Fracture Energy of High-Strength Concrete," *ACI Materials Journal*, Vol. 98, No. 5, Sept.-Oct., pp. 410-417.

Darwin, D., Browning, J., Nguyen, T., and Locke, C. (2002). "Mechanical and Corrosion Properties of a High-Strength, High Chromium Reinforcing Steel for Concrete," *SM Report 66*, University of Kansas Center for Research, Lawrence, KS, 142 pp.

Darwin, D., Browning, J., and Lindquist, W. D. (2004). "Control of Cracking in Bridge Decks: Observations from the Field," Cement, Concrete and Aggregates, ASTM International, Vol. 26, No. 2, Dec., pp. 148-154.

Darwin, D., Browning, J., Nguyen, T., and Locke, C. (2007a). "Evaluation of Metallized Stainless Steel Clad Reinforcement," *SM Report* 90, University of Kansas Center for Research, Lawrence, KS, 156 pp.

Darwin, D., Browning, J., Locke, C., and Nguyen, T. (2007b). "Multiple Corrosion Protection Systems for Reinforced Concrete Bridge Components," *SM Report* 84, University of Kansas Center for Research, Lawrence, KS, 116 pp.

Darwin, D., Browning, J., O'Reilly, M., Xing, L., and Ji, J. (2009). "Critical Chloride Corrosion Threshold of Galvanized Reinforcing Bars," *ACI Materials Journal*, Vol. 106, No. 2, Mar.-Apr., pp. 176-183.

Darwin, D., Browning, J., Lindquist, W., McLeod, H. A. K., Yuan, J., Toledo, M., and Reynolds, D. (2010). "Low-Cracking, High-Performance Concrete Bridge Decks – Case Studies Over the First 6 Years," Transportation Research Record: Journal of the Transportation Research Board, No. 2202, pp. 61-69.

Draper, J., Darwin, D., Browning, J., and Locke, C. (2009). "Evaluation of Multiple Corrosion Protection Systems for Reinforced Concrete Bridge Decks," *SM Report* 96, University of Kansas Center for Research, Lawrence, KS. 431 pp.

Fanous, P., and Wu, H. (2005). "Performance of Coated Reinforcing Bars in Cracked Bridge Decks," *Journal of Bridge Engineering*, Vol. 10, No. 3, May-Jun., pp. 255-261.

Farzammehr, H. (1985). "Pore Solution Analysis of Sodium Chloride and Calcium Chloride Containing Cement Pastes," *MS Thesis*, University of Oklahoma, Norman, OK. 101 pp.

FHWA (2007). "Deficient Bridges by State and Highway Systems" http://www.fhwa.dot.gov/bridge/defbr07.cfm. Accessed 05/17/2010.

Gong, L., Darwin, D., and Browning, J. (2006). "Evaluation of Multiple Corrosion Protection Systems and Stainless Steel Clad Reinforcement for Reinforced Concrete," *SM Report* 82, University of Kansas Center for Research, Lawrence, KS, 621 pp.

Goodwin, P., Frantz, G., and Stephens, J. (2000). "Protection of Reinforcement with Corrosion Inhibitors, Phase II," *CDOT Report* No. JHR 00-279. 137 pp.

Guo, G., Darwin, D., and Browning, J. (2006). "Laboratory and Field Tests of Multiple Corrosion Protection Systems for Reinforced Concrete Bridge Components," *SM Report* 85, University of Kansas Center for Research, Lawrence, KS, 865 pp.

Haran, B., Popov, B., Petrou, M., and White, R. (2000). "Studies on Galvanized Carbon steel in $Ca(OH)_2$ Solutions," *ACI Materials Journal*, Vol. 97, No. 4, July-Aug., pp. 425-431.

Hartt, W. and Nam, J. (2008). "Effect on Cement Alkalinity on Chloride Threshold and Time-to-Corrosion of Reinforcing Steel in Concrete," *Corrosion*, Vol. 64, No 8, Aug., pp. 671-680.

Hartt, W., Powers, R., Marino, F., Paredes, M., Simmons, R., Yu, H., Himiob, R., and Virmani, P. (2009). "Corrosion Resistant Alloys for Reinforced Concrete," FHWA Publication FHWA-HRT-09-020. 146 pp.

Hasan, H., Ramirez, J., and Cleary, D. (1995). "Indiana Evaluates Epoxy-Coated Steel Reinforcement," *Better Roads*, Vol. 65, No. 5, May, pp. 21, 25.

Hausmann, D. (1967). "Steel Corrosion in Concrete," *Materials Protection*, Vol. 6, No. 11, Nov., pp. 19-22.

Hime, W. and Machin, M. (1993). "Performance Variations of Galvanized Steel in Mortar and Concrete," *Corrosion*, Vol. 49, No. 10, Oct., pp. 858-860.

Hope, B. and Ip, A. (1987). "Chloride Corrosion Threshold in Concrete," *ACI Materials Journal*, Vol. 84, No. 4, Jul-Aug, pp. 306-314.

Hope, B. and Ip, A. (1989). "Corrosion Inhibitors for Use in Concrete," *ACI Materials Journal*, Vol. 86, No. 6, Nov.-Dec., pp. 602-608.

Hussain, S., Al-Gahtani, A., and Rasheeduzzafar (1996). "Chloride Threshold for Corrosion of Reinforcement in Concrete," *ACI Materials Journal*, Vol. 93, No. 6, Nov.-Dec., 5 pp.

Ji, J., Darwin, D., and Browning, J. (2005). "Corrosion Resistance of Microcomposite and Duplex Stainless Steels for Reinforced Concrete Bridge Decks," *SM Report* 80, University of Kansas Center for Research, Lawrence, KS, 508 pp.

Jones, D. (1996). *Principles and Prevention of Corrosion*. Upper Saddle River, NJ, Prentice Hall, 572 pp.

Kepler, J., Darwin, D., and Locke, C. (2000). "Evaluation of Corrosion Protection Methods for Reinforced Concrete Highway Structures," *SM Report* 58, University of Kansas Center for Research, Lawrence, KS, 231 pp.

Koch, G., Broongers, H., Thompson, N., Virmani, Y., and Payer, J. (2002). "Corrosion Cost and Preventive Strategies in the United States," Report No. FHWA-RD-01-156, FHWA, McLean, VA, 773 pp.

Kranc, S., Sagues, A., and Presuel-Moreno, F. (2002). "Decreased Corrosion Initiation Time of Steel in Concrete due to Reinforcing Bar Obstruction of Diffusional Flow," *ACI Materials Journal*, Vol. 99, No. 1, Jan.-Feb., pp. 51-53.

Kumar, S. and Rao, K. (1995). "Strength Loss in Concrete Due to Varying Sulfate Exposures". *Cement and Concrete Research*, Vol. 25, No. 1, pp. 57-62.

Lau, K. and Sagues, A. (2009). "Corrosion of Epoxy- and Polymer/Zinc-Coated Rebar in Simulated Concrete Pore Solution," *Corrosion*, Vol. 65, No. 10, Oct., pp. 681-694.

Li, L., Sagues, A. and Poor, N. (1999). "In Situ Leaching Investigation of pH and Nitrite Concentration in Concrete Pore Solution," *Cement and Concrete Research*, Vol. 29, pp. 315-321.

Lindquist, W., Darwin, D., Browning, J., and Miller, G. (2006). "Effect of Cracking on Chloride Content in Concrete Bridge Decks," *ACI Materials Journal,* Vol. 103, No. 6, Nov.-Dec., pp. 467-473.

Maaddawy, T. and Soudki, K. (2003). "Effectiveness of Impressed Current Technique to Simulate Corrosion of Steel Reinforcement in Concrete," *Journal of Materials in Civil Engineering*, Vol. 15, No. 1, Jan.-Feb., pp. 41-47.

Macias, A. and Andrade, C. (1987). "Corrosion of Galvanized Steel Reinforcements in Alkaline Solutions Part 2: SEM Study and Identification of Corrosion Products," *British Corrosion Journal*, Vol. 22, No. 2, pp. 119-129.

Manning, D. (1996). "Corrosion Performance of Epoxy-Coated Reinforcing Steel: North American Experience," *Construction & Building Materials*, Vol. 10, No. 5, July, pp. 349-365

McDonald, D., Pfiefer, D., Sherman, M., and Blake, G. (1996). "Slowing Corrosion Damage in Concrete: The Use of Organic-Coated, Ceramic-Clad, Metallic-Clad and Solid Metallic Reinforcing Bars," *Materials for the New Millennium: Proceedings of the Materials Engineering Conference*, Vol. 2, pp. 1266-1275

McLeod, H., Darwin, D., and Browning, J. (2009). "Development and Construction of Low-Cracking High-Performance Concrete (LC-HPC) Bridge Decks: Construction Methods, Specifications, and Resistance to Chloride Ion Penetration," *SM Report* 94, University of Kansas Center for Research, Lawrence, KS, 848 pp.

Mindess, S., Young, J., and Darwin, D. (2003). *Concrete*, 2nd Ed., Pearson Education, Inc., Upper Saddle River, NJ, 644 pp.

Miura, T., Itabashi, H., and Iwaki, I. (1997). "Study on Allowable Coating Damage of Epoxy-Coated Reinforcing Bars," *ACI Materials Journal,* Vol. 94, No. 4, July-Aug., pp. 267-272.

Nmai, C., Farrington, S., and Bobrowski, G. (1992). "Organic-Based Corrosion-Inhibiting Admixture for Reinforced Concrete," *Concrete International*, Vol. 14, No. 4, Apr., pp. 45-51.

Oh, B., Yang, S., and Shin, Y. (2003). "Experimental Investigation of the Threshold Chloride Concentration for Corrosion Initiation in Reinforced Concrete Structures," *Magazine of Concrete Research,* Vol. 55, No. 2, Apr., pp. 117-124.

Pyc, W., Zemajtis, J., Weyers, R., and Sprinkel, M. (1999). "Evaluating Corrosion-Inhibiting Admixtures," *Concrete International*, Vol. 21, No. 4, Apr., pp. 39-44.

Ramniceanu, A., Weyers, R., Riffle, J., and Sprinkel, M. (2008). "Parameters Governing Corrosion Protection Efficacy of Fusion-Bonded Epoxy Coatings on Reinforcing Bar," *ACI Materials Journal*, Vol.105, No. 5, Sept.-Oct., pp. 459-467.

Rasheeduzzafar, Al-Saadoun, S., and Al-Gahtani, A. (1992a). "Corrosion Cracking in Relation to Bar Diameter, Cover, and Concrete Quality", *Journal of Materials in Civil Engineering*, Vol. 4, No. 4, Nov., pp. 327-342.

Rasheeduzzafar, Dakhil, F., Bader, M., and Khan, M. (1992b). "Performance of Corrosion Resisting Steels in Chloride-Bearing Concrete", *ACI Materials Journal*, Vol. 89, No. 5, Sept.-Oct., pp. 439-448.

Reed, R., Krauss, P., Sherman, M., and McDonald, D. (2003). "Coating Repaired Rebar," *Concrete Construction*, Vol. 48, No. 3, Mar., pp. 55-59.

Roberge, P. (2008). *Corrosion Engineering: Principles and Practice.* Chicago, McGraw Hill, 754 pp.

Rodriguez, O. and Hooton, D. (2003). "Influence of Cracks on Chloride Ingress into Concrete," *ACI Materials Journal*, Vol. 100, No. 2, Mar.-Apr., pp. 120-126.

Ryou, J. and Ann, K. (2008). "Variation in the Chloride Threshold Level for Steel in Concrete Arising from Different Chloride Sources," *Magazine of Concrete Research*, Vol. 60, No. 3, Apr., pp. 177-187.

Samples, L. (1998). "Durability of Concrete Bridge Decks with Emphasis on Epoxy-Coated Bars," Ph.D. dissertation, Purdue University, 226 pp.

Saeki, N., Fujita, Y., Takada, N., and Ohta, T. (1988). "Control of Rust Damage of Reinforced Concrete in a Corrosive Environment," *Concrete in Marine Environment*, Proceedings of the Second International Conference, SP-109, American Concrete Institute, Farmington Hills, Mich., pp. 163-177.

Saraswathy, V., and Song, H. (2005). "Performance of Galvanized and Stainless Steel Rebars in Concrete Under Macrocell Corrosion Conditions," *Materials and Corrosion* Vol. 56, No. 10, Oct., pp. 685-691.

Schiegg, Y., Buchler, M., and Brem, M. (2009). "Potential Mapping Technique for the Detection of Corrosion in Reinforced Concrete Structures: Investigation of Parameters Influencing the Measurement and Determination of the Reliability of the Method," *Materials and Corrosion*, Vol. 60, No. 2, Feb., pp. 79-86.

Schiessl, P and Breit, W. (1996). "Local Repair Measures at Concrete Structures Damaged by Reinforcement Corrosion," *Corrosion of Reinforcement in Concrete Construction.* Ed. Page, C., Bamforth, B., and Figg, J., SCI, London, pp. 525-534.

Scott, A., and Alexander, M.G. (2007). "The Influence of Binder Type, Cracking and Cover on Corrosion Rates of Steel in Chloride-Contaminated Concrete," *Magazine of Concrete Research*, Vol. 59, No. 7, Sep., pp 495-505.

Sergi, G., Short, N., and Page, C. (1985). "Corrosion of Galvanized and Galvanannealed Steel in Solutions of pH 9.0-14.0," *Corrosion/85: international Corrosion Forum Devoted Exclusively to the Protection and Performance of Materials*. Boston, MA; March 25-29, 1985.

Small, H. (1989). *Ion Chromatography*. New York, Plenum Press, 276 pp.

Somuah, S., Boah, J., Leblanc, P., Al-Tayyib, A., and Al-Mana, A. (1991). "Effect of Sulfate and Carbonate Ions on Reinforcing Steel Corrosion as Evaluated Using AC Impedance Spectroscopy," *ACI Materials Journal*, Vol. 88, No. 1, Jan.-Feb., pp. 49-55.

Soylev, T.A. and Richardson, M.G. (2008). "Corrosion Inhibitors for Steel in Concrete: State-of-the-Art Report," *Construction and Building Materials*, Vol. 22, No. 4, Apr., pp.609-622.

Suda, K., Misra, S., and Motohashi, K. (1993). "Corrosion Products of Reinforcing Bars Embedded in Concrete," *Corrosion Science*, Vol. 35, No. 7, July, pp. 1543-1549.

Treadaway, K. and Davies, H. (1989). "Performance of Fusion-Bonded Epoxy Coated Steel Reinforcement," *The Structural Engineer*, Vol. 67, No. 6, Mar., pp. 99-108.

Treadaway, K., Cox, R., and Brown, B. (1989). "Durability of Corrosion Resisting Steels in Concrete," *Proceedings: Institution of Civil Engineers*, Vol. 86, No. 1, Apr., pp. 305-331.

Torres-Acosta, A. and Sagues, A. (2004). "Concrete Cracking by Localized Steel Corrosion-Geometric Effects," *ACI Materials Journal*, Vol. 101, No. 6, Nov.-Dec., pp. 501-507.

Vassie, P. (1996). "A Discussion of Methods for Preventing Reinforcement Corrosion in Bridges," *Corrosion of Reinforcement in Concrete Construction.* Ed. Page, C., Bamforth, B., and Figg, J., SCI, London, pp. 654-661.

Verbeck, G. (1975) "Mechanisms of Corrosion of Steel in Concrete," C*orrosion of Metals in Concrete* (SP 49), American Concrete Institute, Farmington Hills, MI, pp. 21-38.

Wenzlick, J. and Yin, X. (2003). "Evaluation of Stainless Steel Reinforcement, Construction Report," Missouri Department of Transportation, *Report* RDT03-003, 52 pp.

Weyers, R., Pyc, W., and Sprinkel, M. (1998). "Estimating the Service Life of Epoxy-Coated Reinforcing Steel," *ACI Materials Journal*, Vol. 95, No. 5, Sept.-Oct., pp. 546-557.

Weyers, R., Ramniceanu, A., and Weyers, S. (2009). "Failure of a Deck Closure Pour on Interstate 81," PowerPoint Presentation, American Concrete Institute Convention, New Orleans, LA, Nov. 9, 2009.

Wojakowski, J. and Distlehorst, J. (2009). "Laboratory and Field Testing of Hycrete Corrosion-Inhibiting Admixture for Concrete," *Proceedings of the 2009 Mid-Continent Transportation Research Symposium*. Ames, Iowa; August 2009.

Xing, L., Darwin, D., and Browning, J. (2010). "Evaluation of Multiple Corrosion Protection Systems and Corrosion Inhibitors for Reinforced Concrete Bridge Decks," *SM Report* 99, University of Kansas Center for Research, Lawrence, KS, 507 pp.

Yu, H. and Hartt, W. (2007a). "Effects of Reinforcements and Coarse Aggregates on Chloride Ingress into Concrete and Time-to-Corrosion: Part 1-Spatial Chloride Distribution and Implications," *Corrosion*, Vol. 63, No. 9, Sept., pp.843-849.

Yu, H. and Hartt, W. (2007b). "Effects of Reinforcements and Coarse Aggregates on Chloride Ingress into Concrete and Time-to-Corrosion: Part 2-Spatial Distribution of Coarse Aggregates," *Corrosion*, Vol. 63, No. 10, Oct., pp.924-931.

APPENDIX A

CORROSION RATE, LOSS, AND POTENTIALS OF LABORATORY AND FIELD SPECIMENS

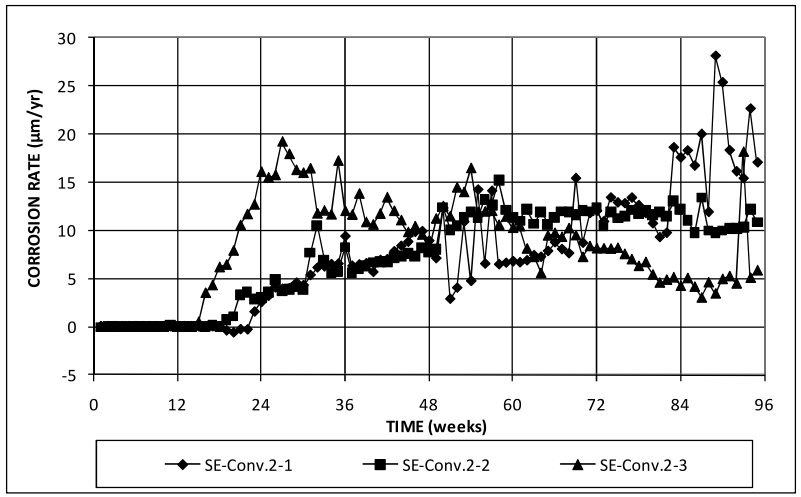

(a)

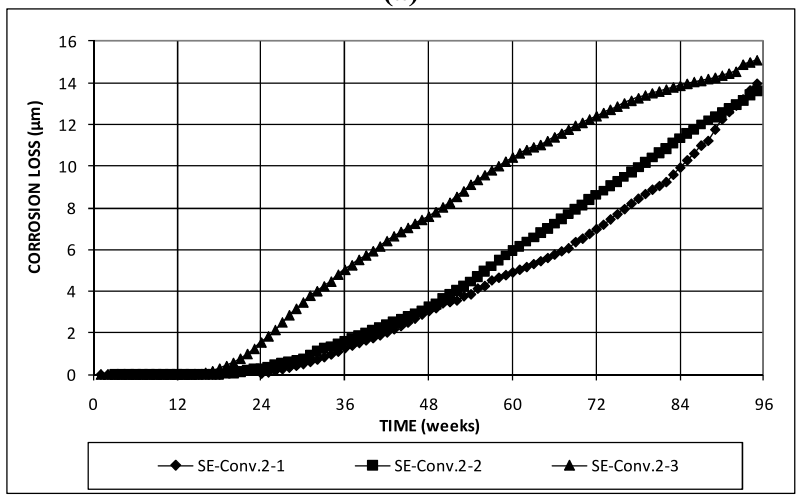

(b)

Figure A.1: (a) Corrosion rate and (b) total corrosion losses for Southern Exposure specimens with no corrosion inhibitor.

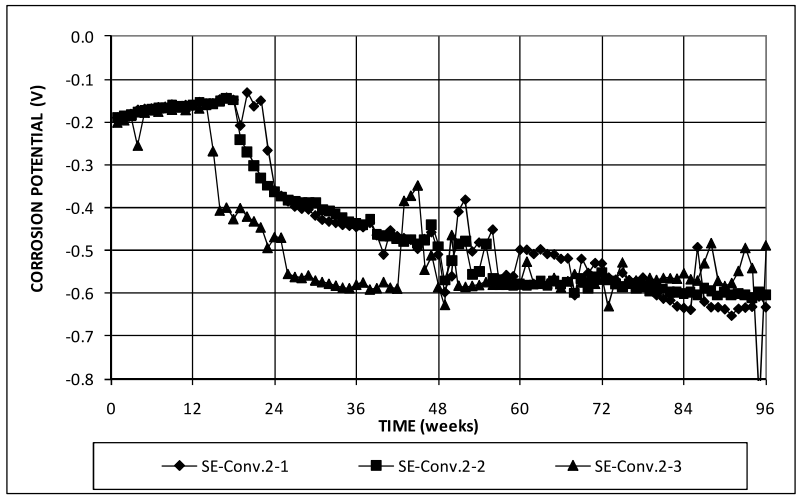

(a)

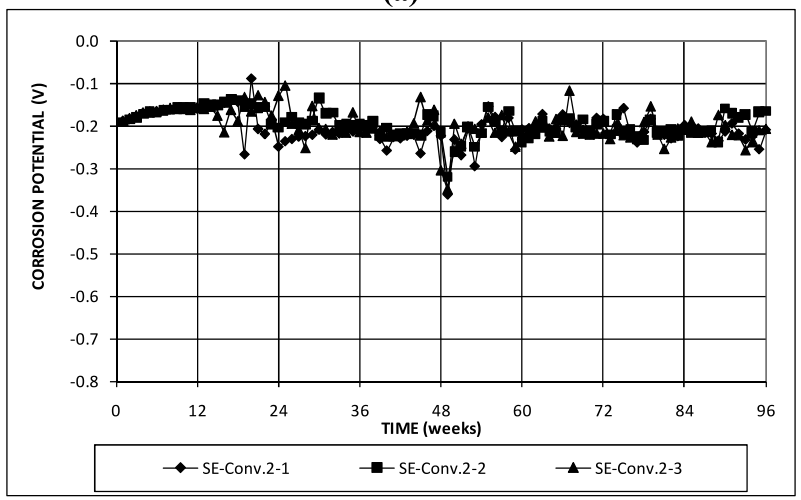

(b)

Figure A.2: (a) Top mat corrosion potentials and (b) bottom mat corrosion potentials for Southern Exposure specimens with no corrosion inhibitor.

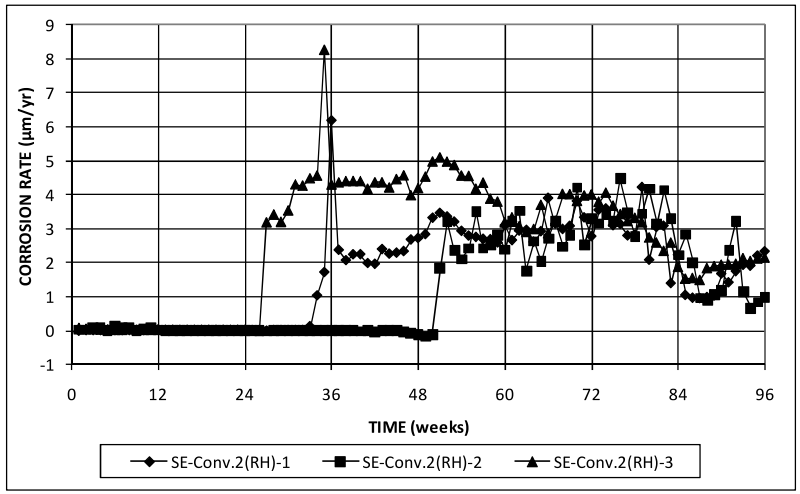

(a)

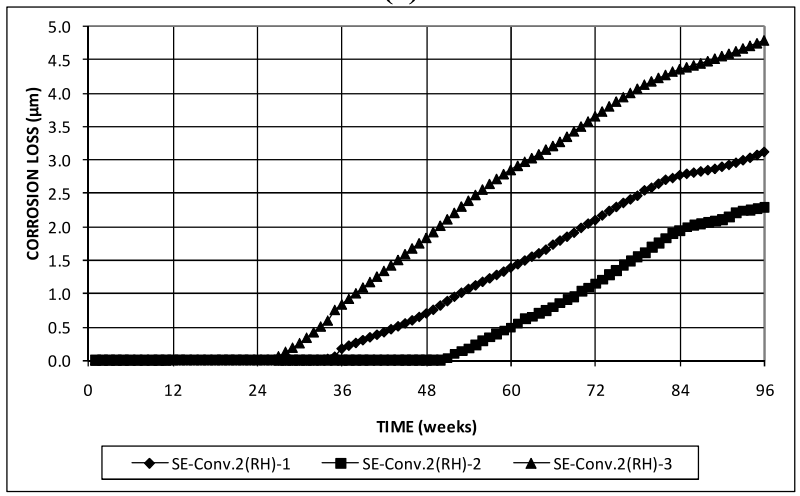

(b)

Figure A.3: (a) Corrosion rate and (b) total corrosion losses for Southern Exposure specimens with Rheocrete.

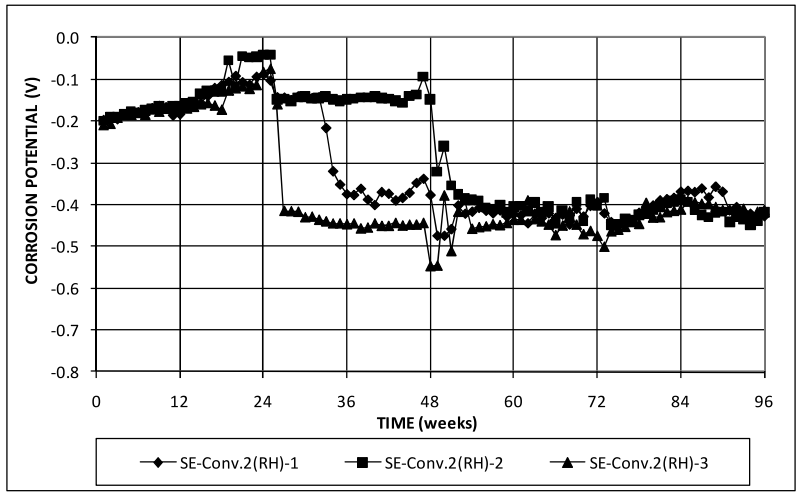

(a)

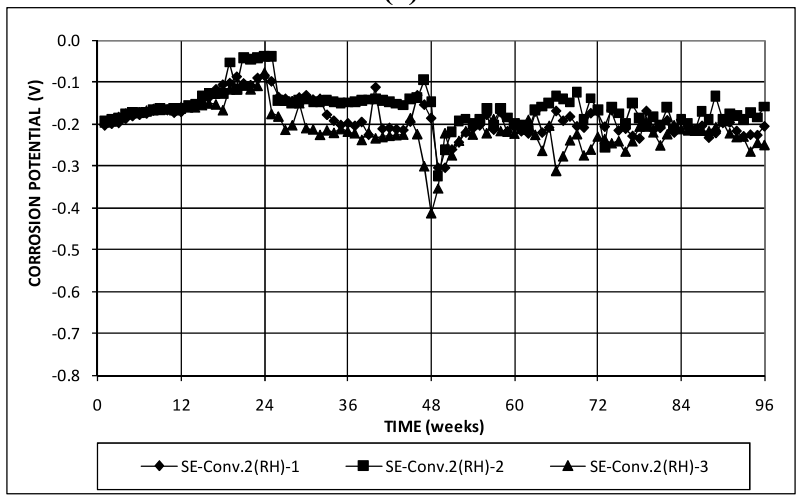

(b)

Figure A.4: (a) Top mat corrosion potentials and (b) bottom mat corrosion potentials for Southern Exposure specimens with Rheocrete.

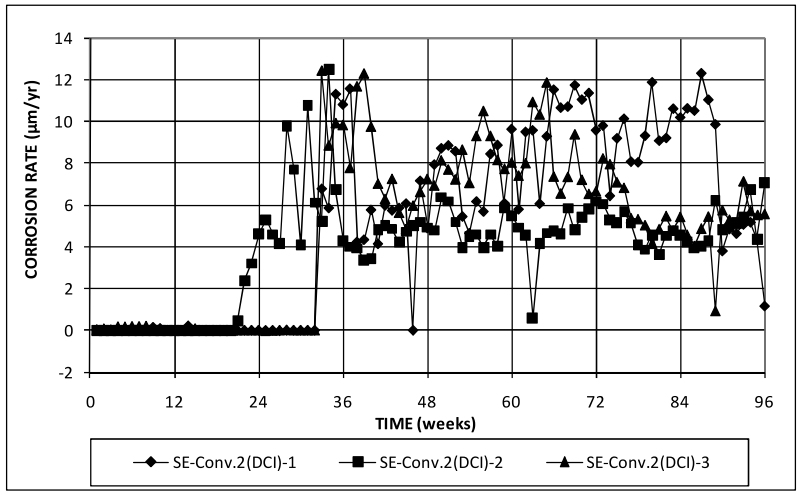

(a)

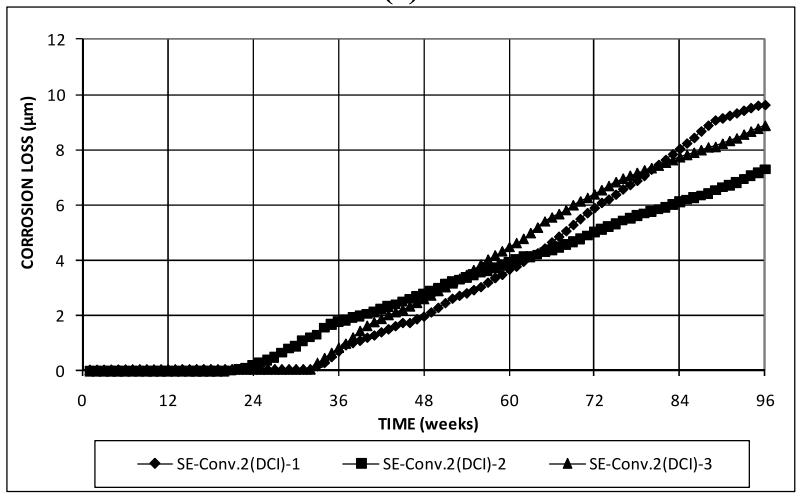

(b)

Figure A.5: (a) Corrosion rate and (b) total corrosion losses for Southern Exposure specimens with DCI.

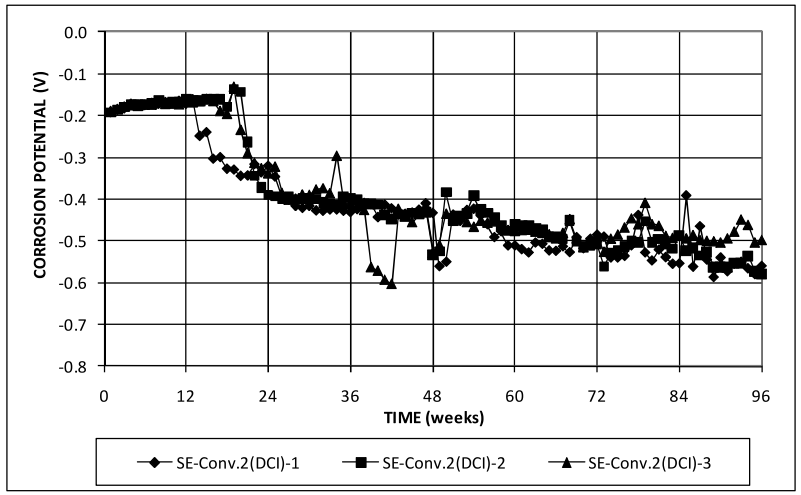

(a)

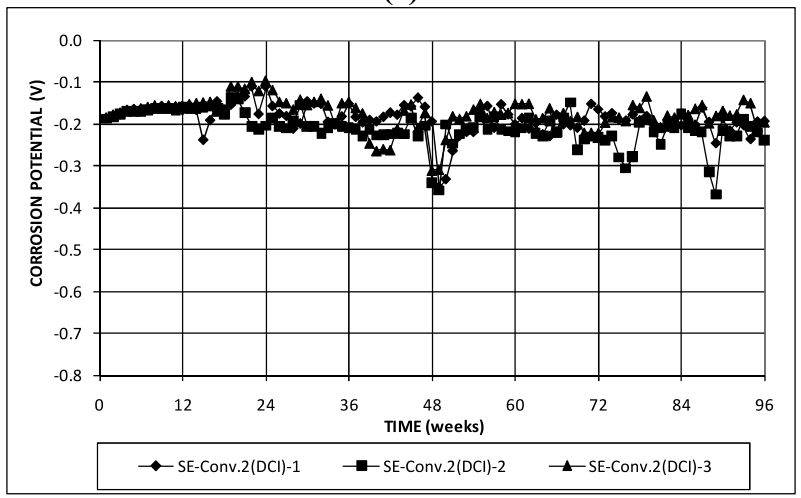

(b)

Figure A.6: (a) Top mat corrosion potentials and (b) bottom mat corrosion potentials for Southern Exposure specimens with DCI.

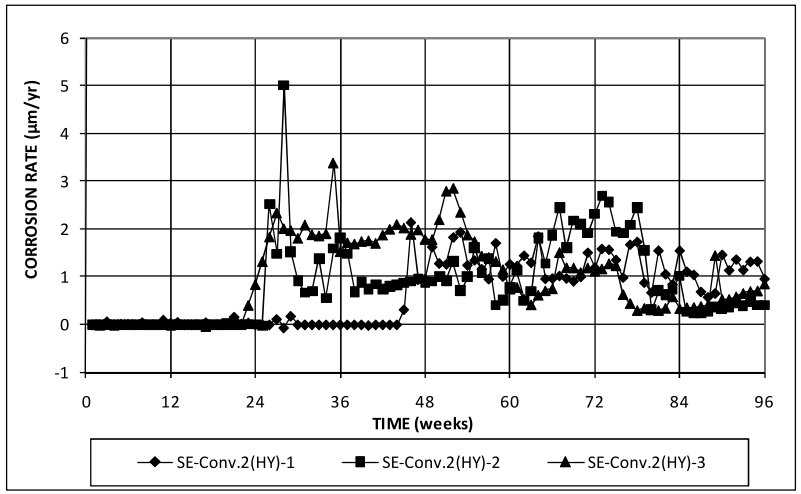

(a)

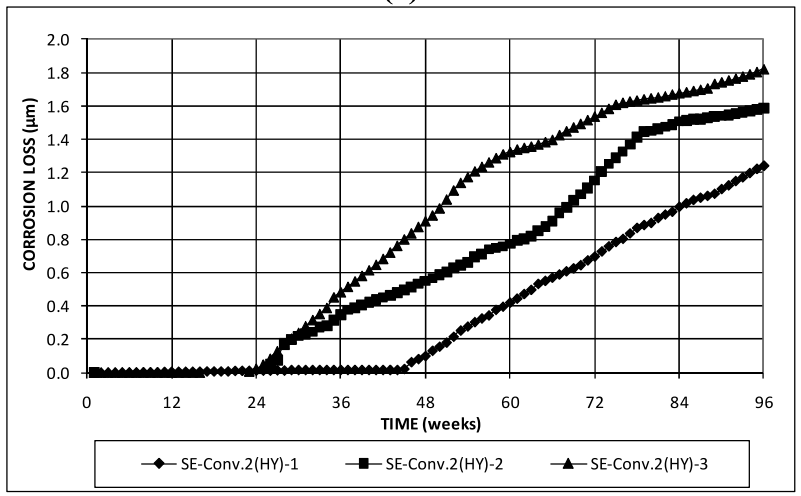

(b)

Figure A.7: (a) Corrosion rate and (b) total corrosion losses for Southern Exposure specimens with Hycrete.

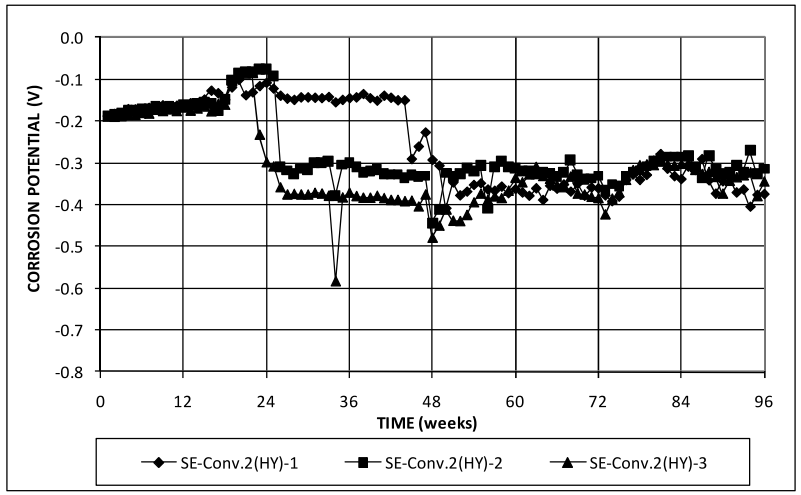

(a)

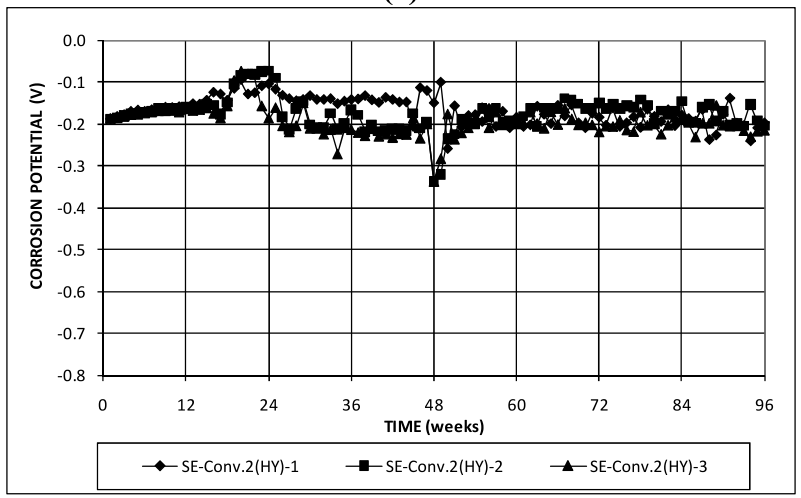

(b)

Figure A.8: (a) Top mat corrosion potentials and (b) bottom mat corrosion potentials for Southern Exposure specimens with Hycrete.

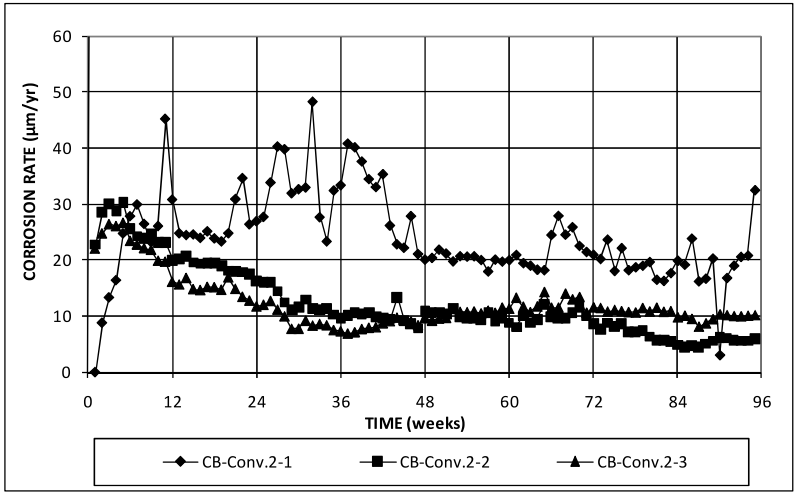

(a)

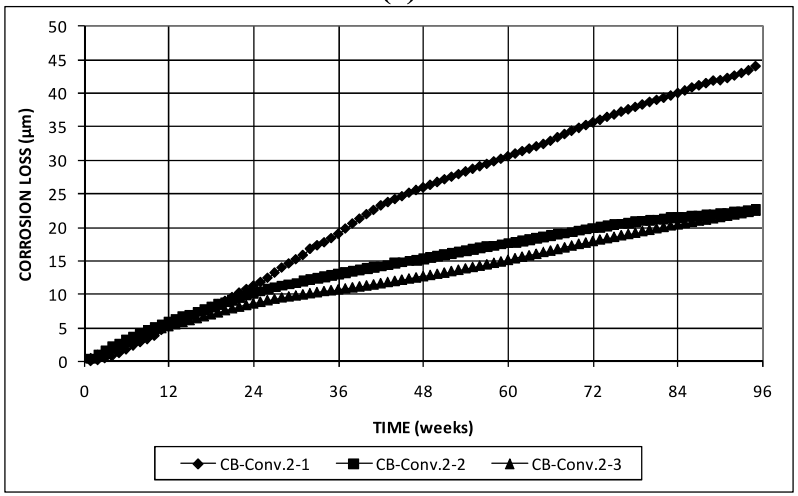

(b)

Figure A.9: (a) Corrosion rate and (b) total corrosion losses for cracked beam specimens with no corrosion inhibitor.

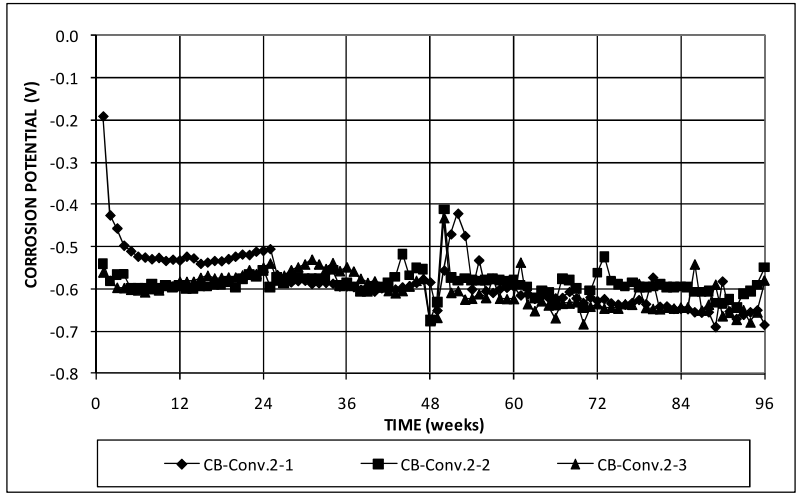

(a)

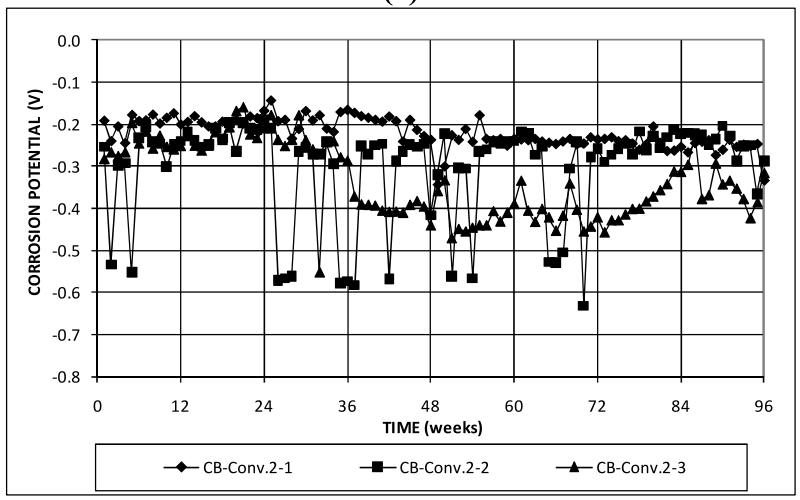

(b)

Figure A.10: (a) Top mat corrosion potentials and (b) bottom mat corrosion potentials for cracked beam specimens with no corrosion inhibitor.

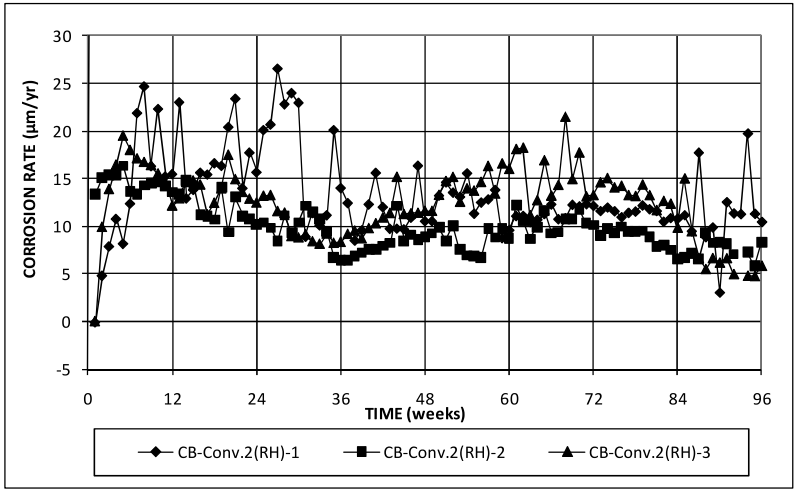

(a)

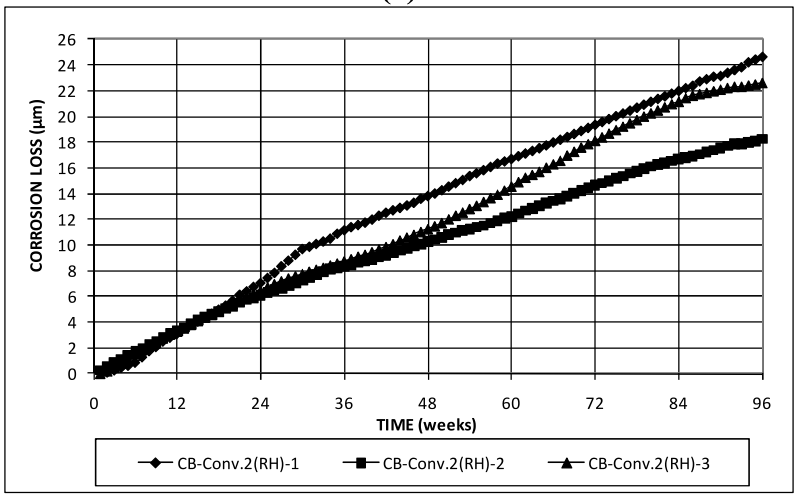

(b)

Figure A.11: (a) Corrosion rate and (b) total corrosion losses for cracked beam specimens with Rheocrete.

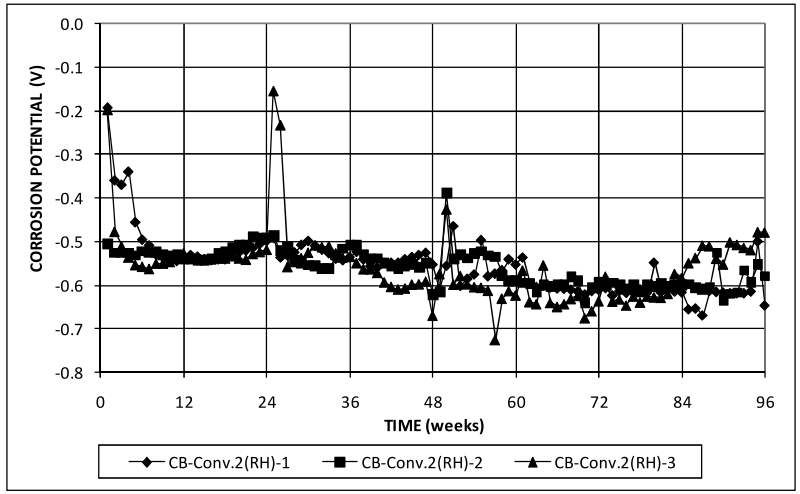

(a)

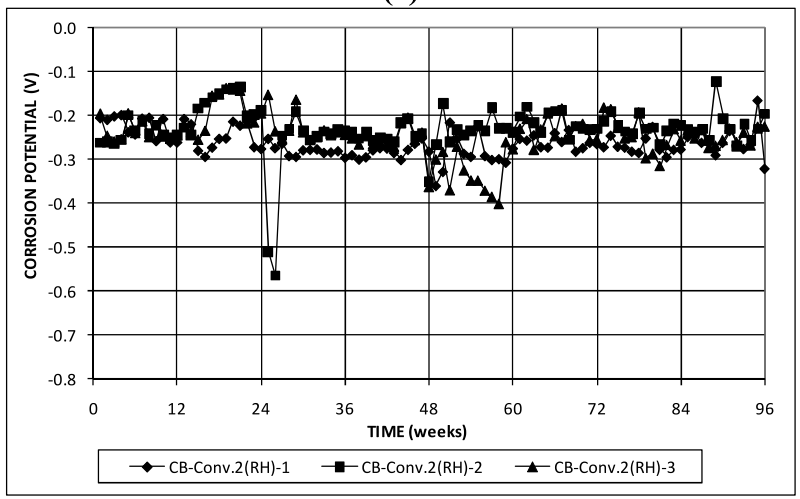

(b)

Figure A.12: (a) Top mat corrosion potentials and (b) bottom mat corrosion potentials for cracked beam specimens with Rheocrete.

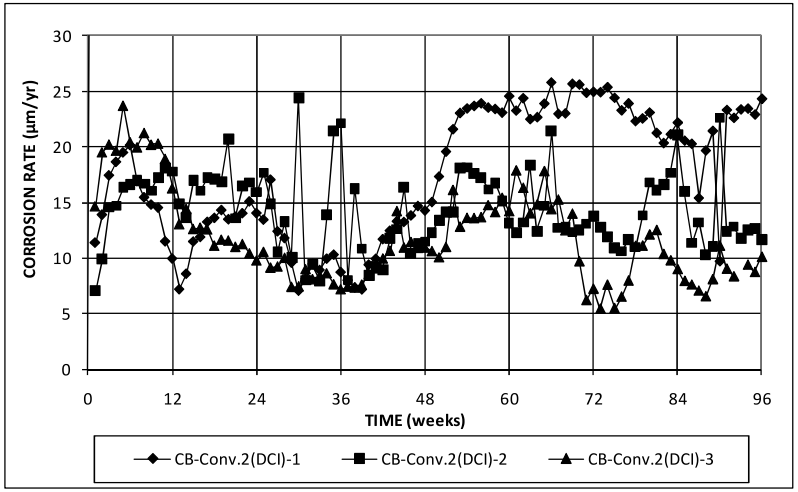

(a)

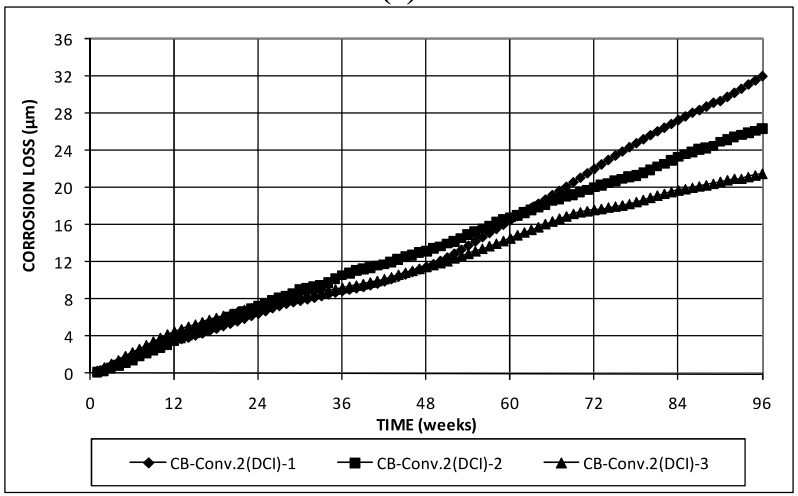

(b)

Figure A.13: (a) Corrosion rate and (b) total corrosion losses for cracked beam specimens with DCI.

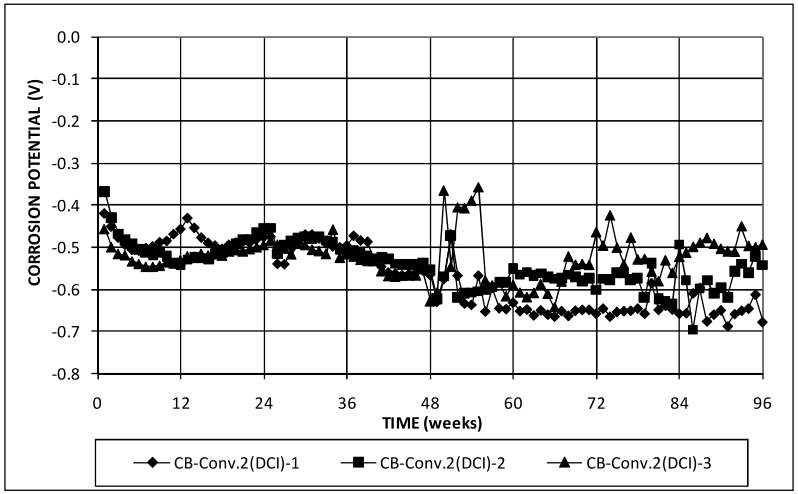

(a)

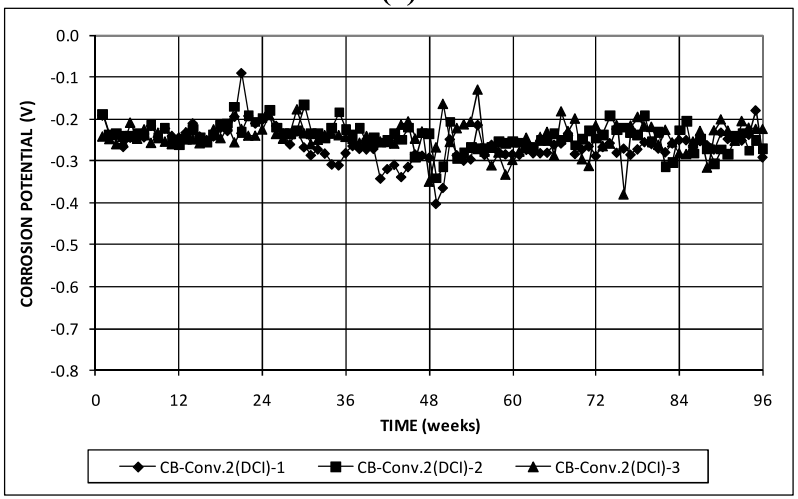

(b)

Figure A.14: (a) Top mat corrosion potentials and (b) bottom mat corrosion potentials for cracked beam specimens with DCI.

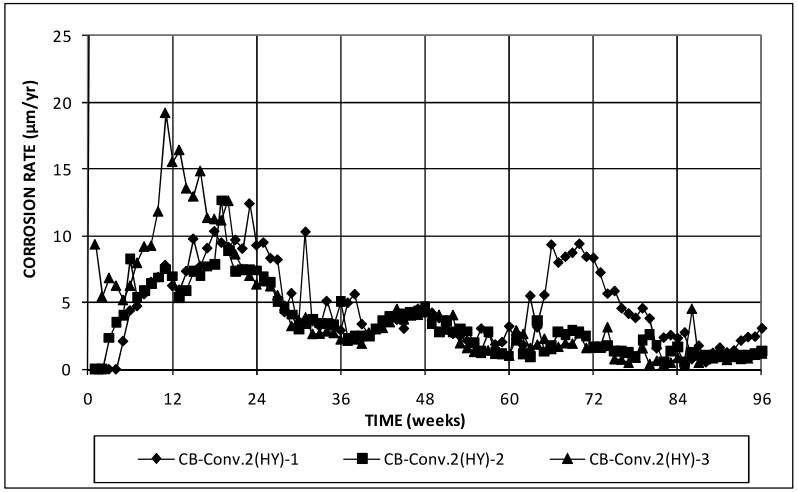

(a)

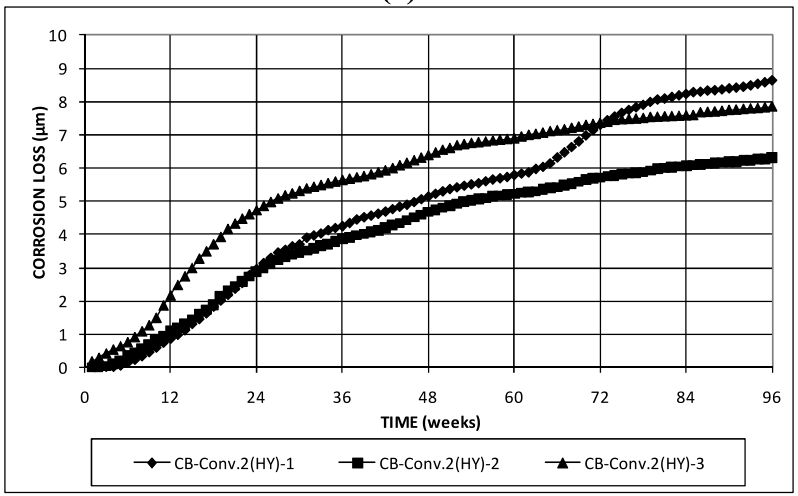

(b)

Figure A.15: (a) Corrosion rate and (b) total corrosion losses for cracked beam specimens with Hycrete.

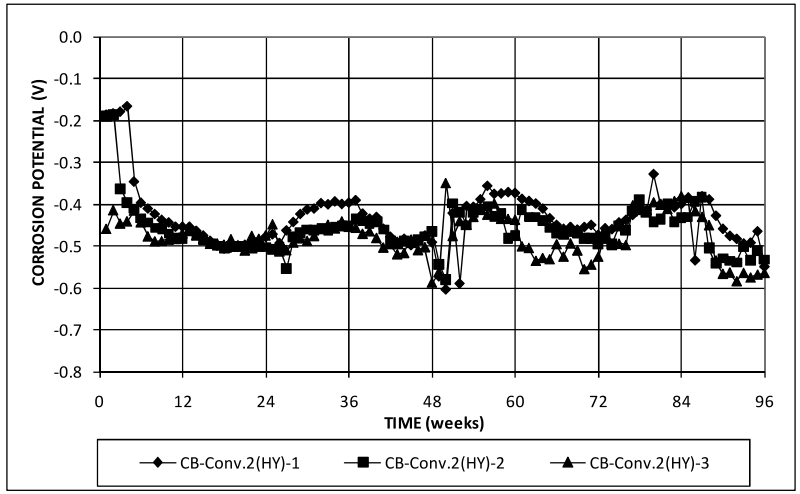

(a)

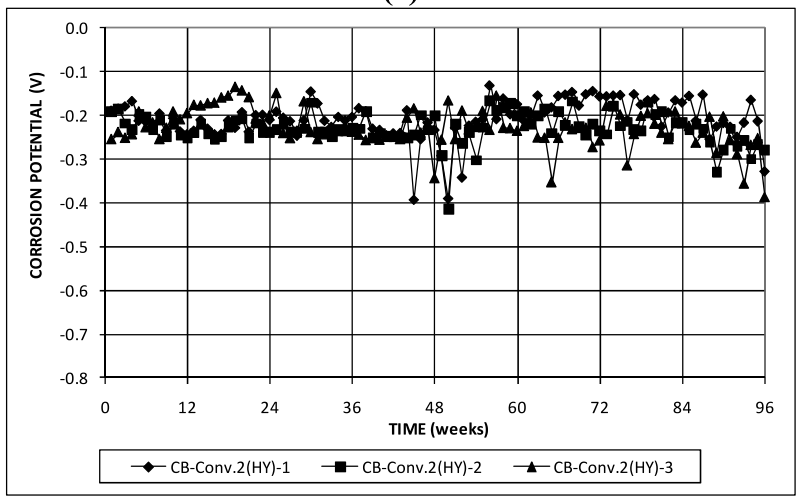

(b)

Figure A.16: (a) Top mat corrosion potentials and (b) bottom mat corrosion potentials for cracked beam specimens with Hycrete.

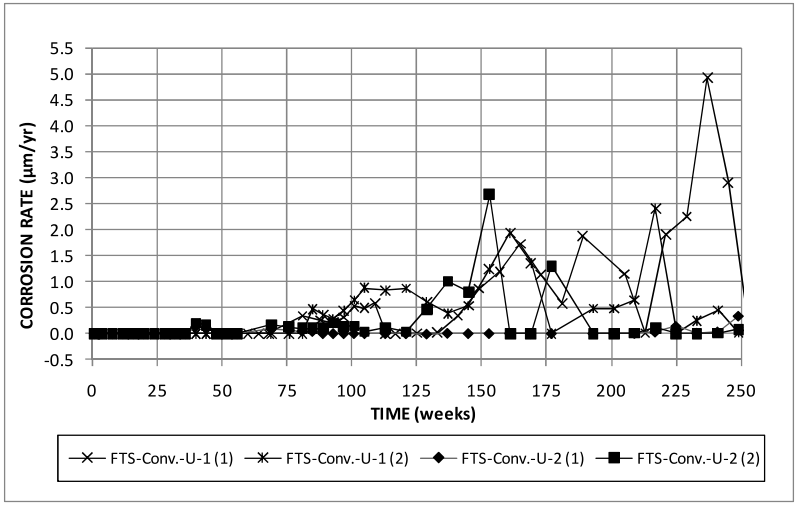

(a)

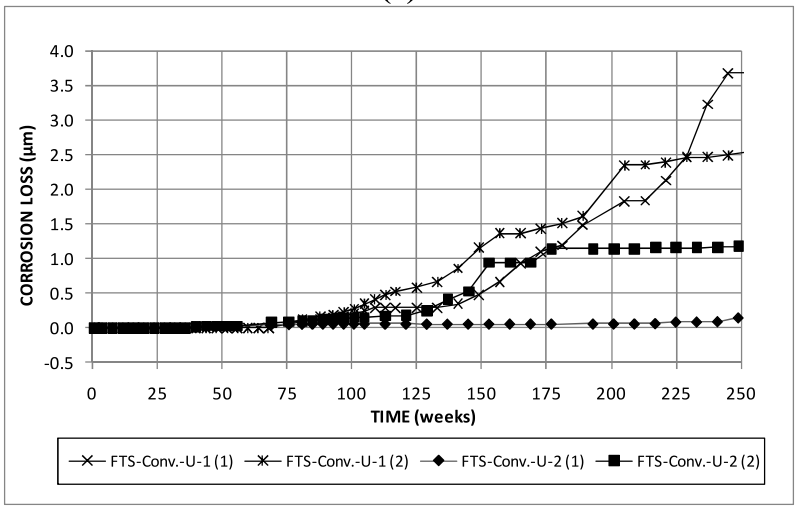

(b)

Figure A.17: (a) Corrosion rate and (b) corrosion losses based on total area for field test specimens with conventional reinforcement in uncracked concrete.

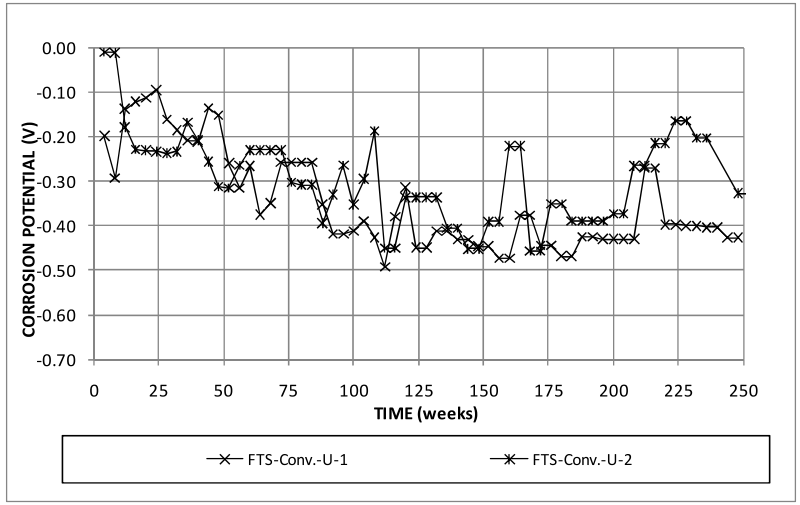

(a)

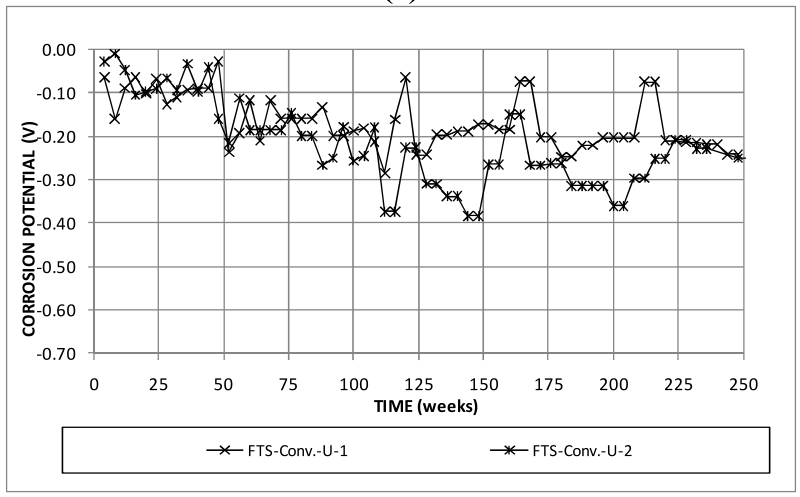

(b)

Figure A.18: (a) Top mat corrosion potentials and (b) bottom mat corrosion potentials for field test specimens with conventional reinforcement in uncracked concrete.

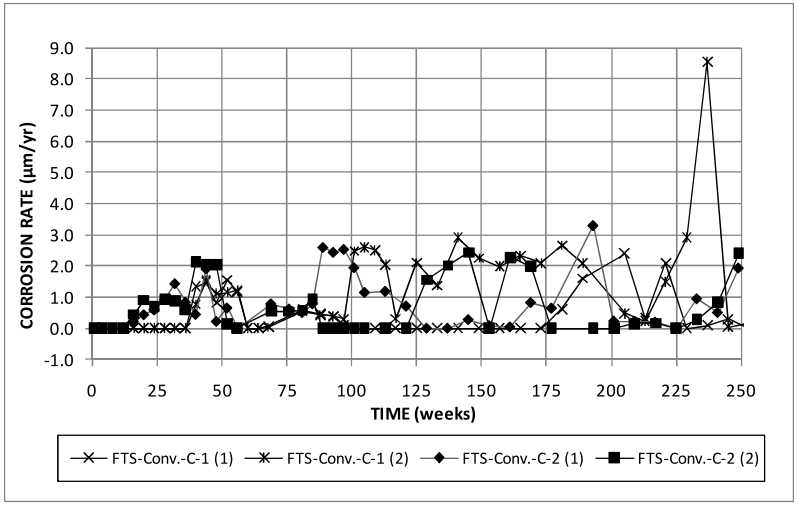

(a)

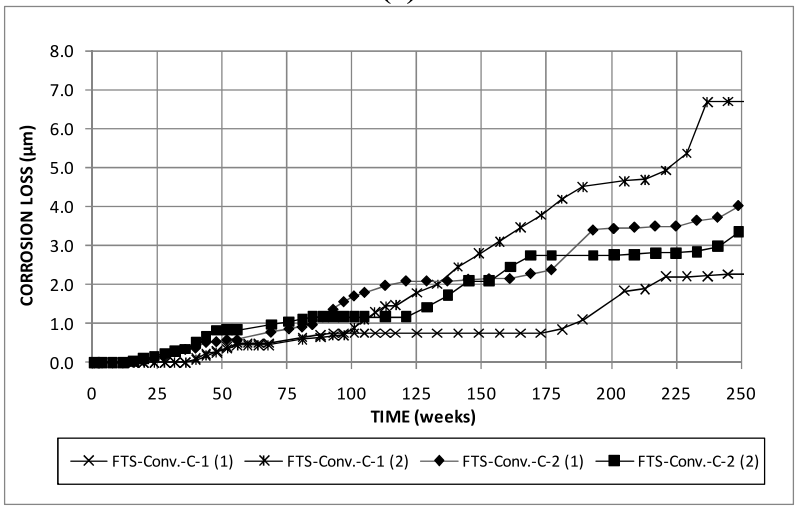

(b)

Figure A.19: (a) Corrosion rate and (b) corrosion losses based on total area for field test specimens with conventional reinforcement in cracked concrete.

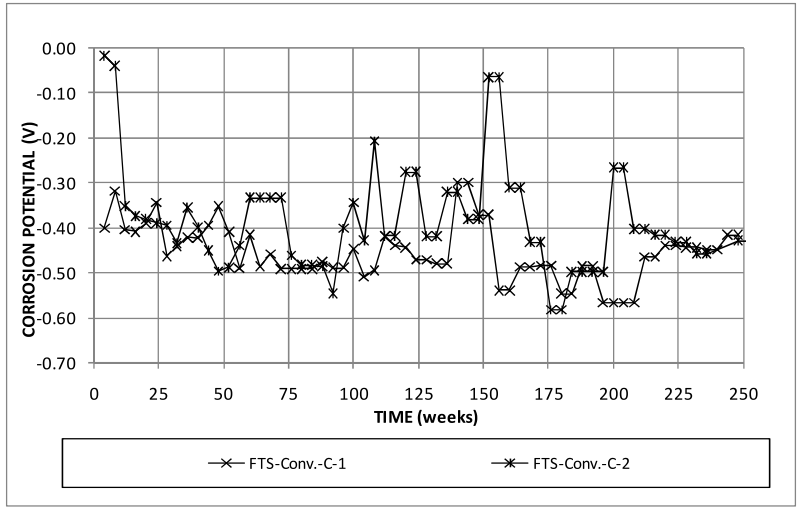

(a)

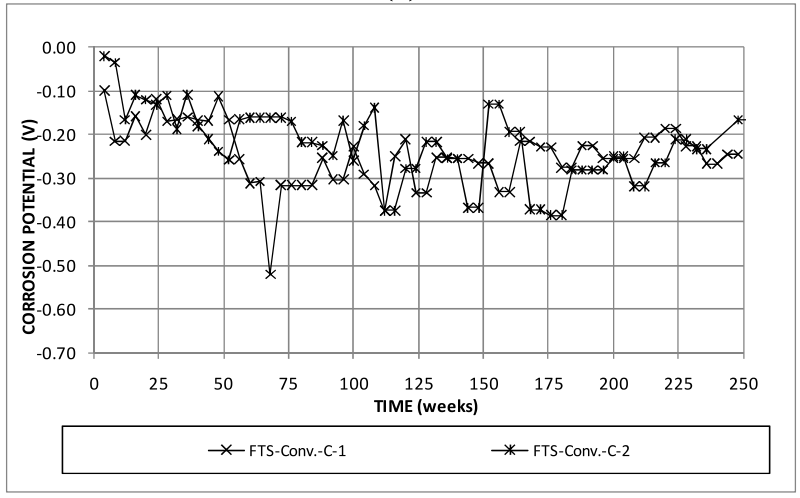

(b)

Figure A.20: (a) Top mat corrosion potentials and (b) bottom mat corrosion potentials for field test specimens with conventional reinforcement in cracked concrete.

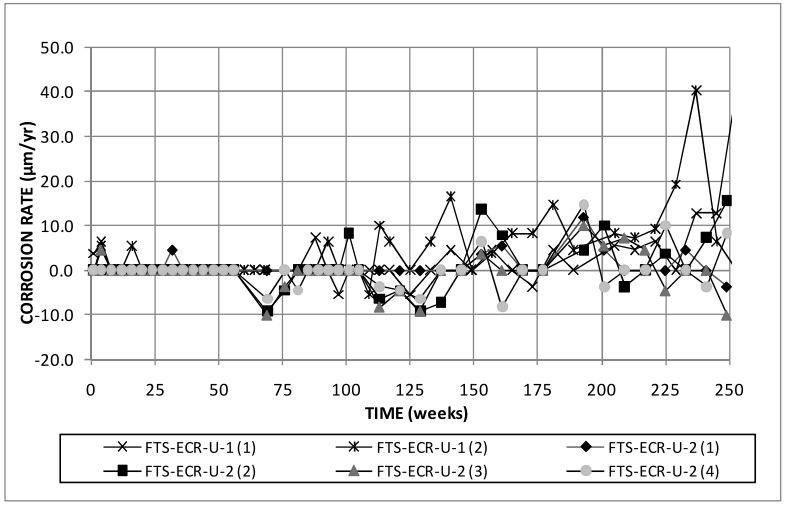

(a)

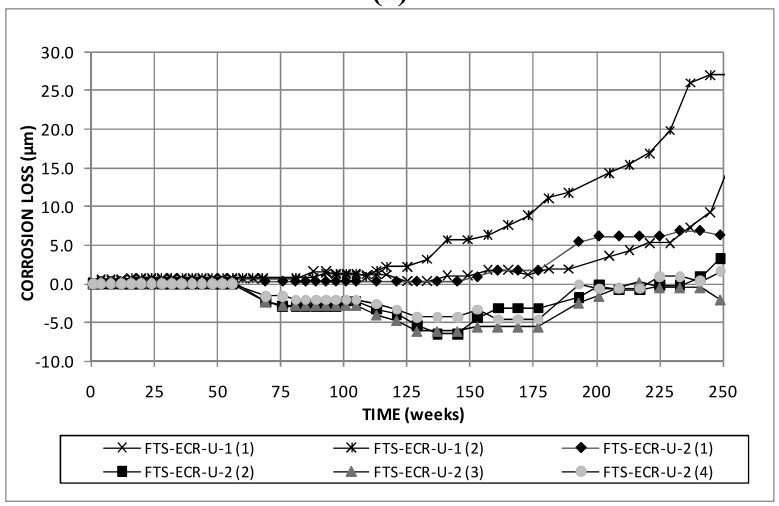

(b)

Figure A.21: (a) Corrosion rate and (b) corrosion losses based on exposed area for field test specimens with ECR in uncracked concrete.

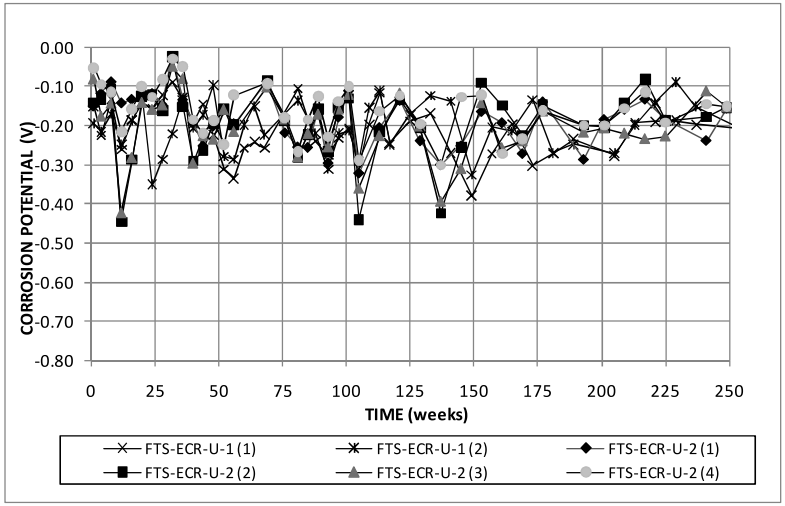

(a)

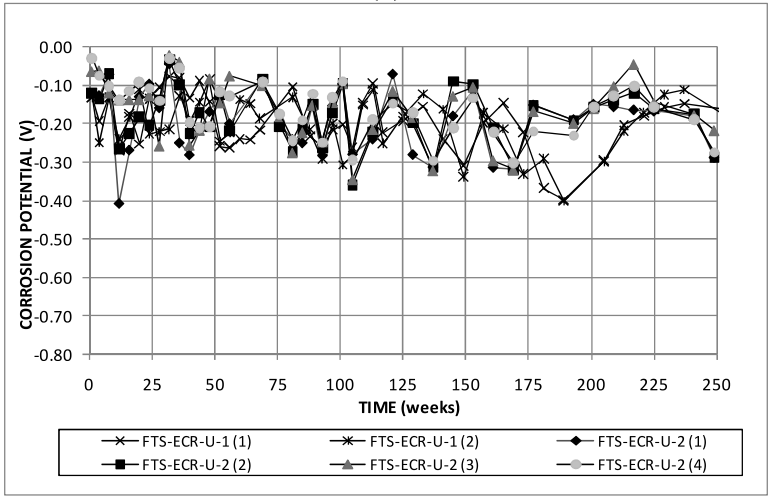

(b)

Figure A.22: (a) Top mat corrosion potentials and (b) bottom mat corrosion potentials for field test specimens with ECR in uncracked concrete.

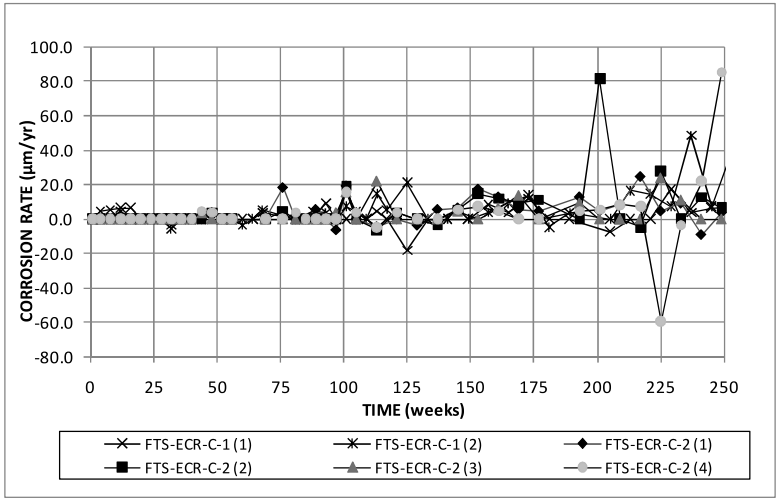

(a)

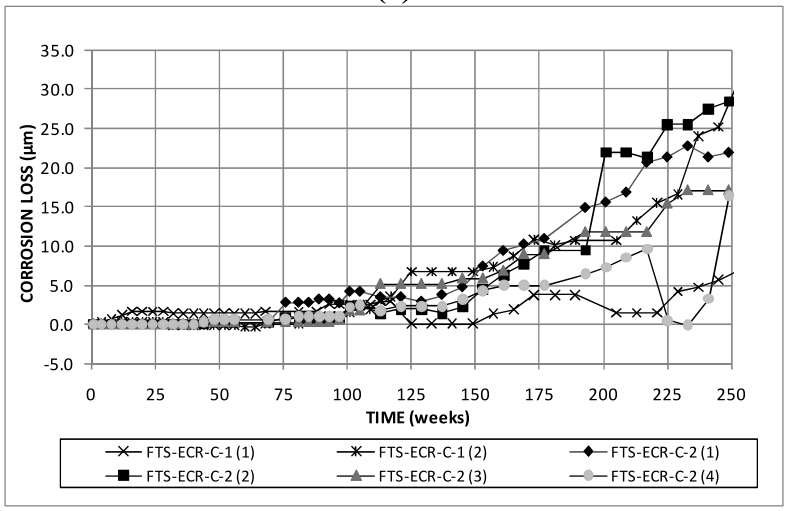

(b)

Figure A.23: (a) Corrosion rate and (b) corrosion losses based on exposed area for field test specimens with ECR in cracked concrete.

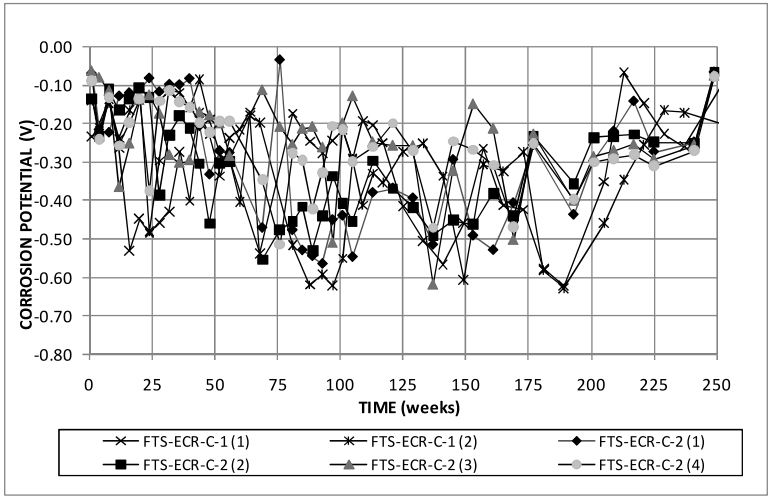

(a)

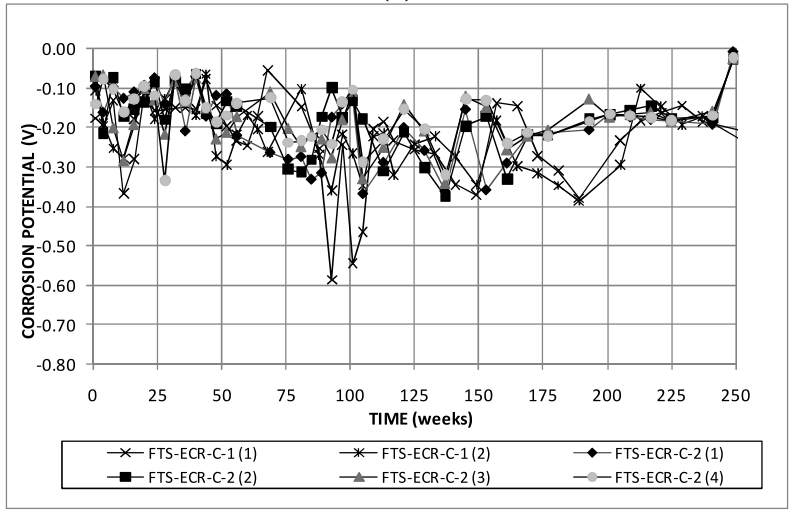

(b)

Figure A.24: (a) Top mat corrosion potentials and (b) bottom mat corrosion potentials for field test specimens with ECR in uncracked concrete.

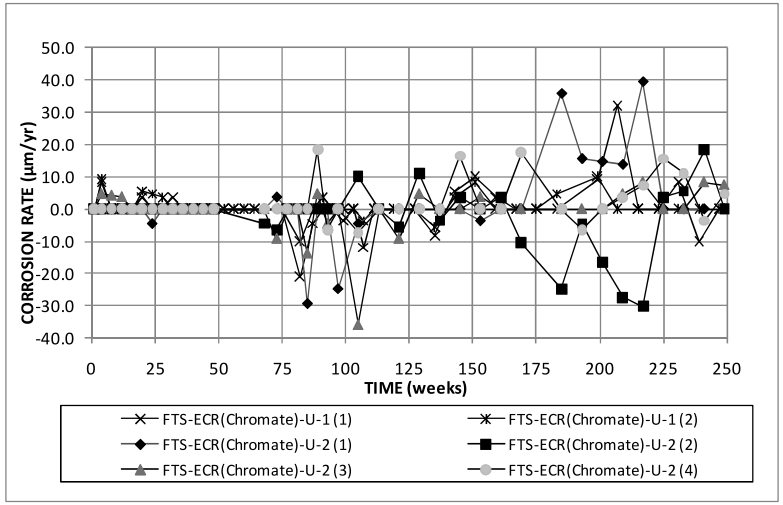

(a)

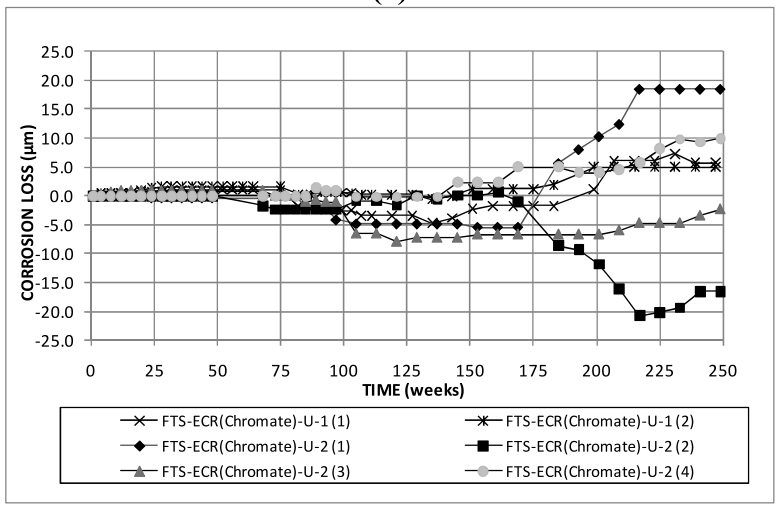

(b)

Figure A.25: (a) Corrosion rate and (b) corrosion losses based on exposed area for field test specimens with ECR with chromate pretreatment in uncracked concrete.

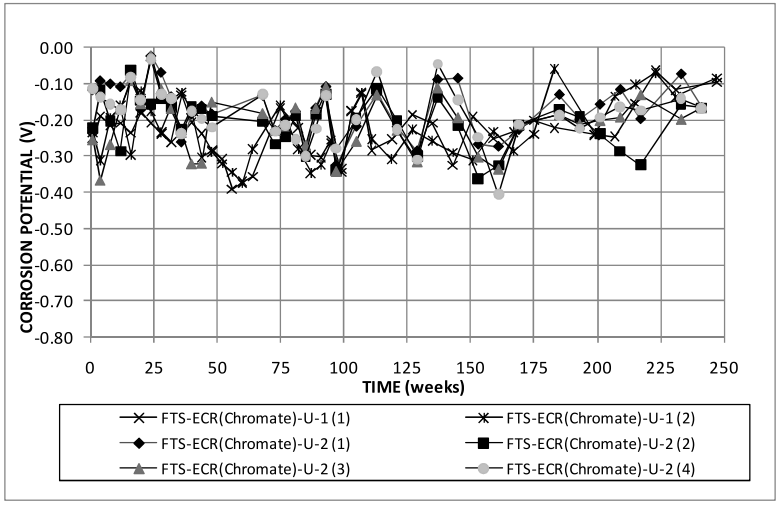

(a)

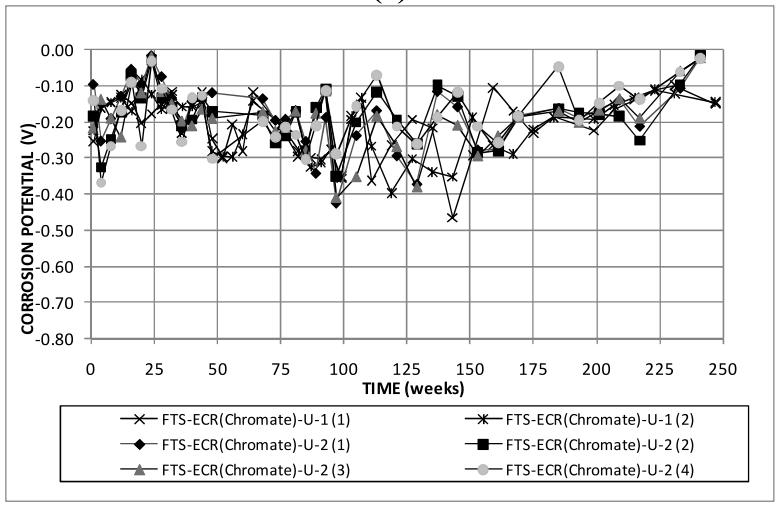

(b)

Figure A.26: (a) Top mat corrosion potentials and (b) bottom mat corrosion potentials for field test specimens with ECR with chromate pretreatment in uncracked concrete.

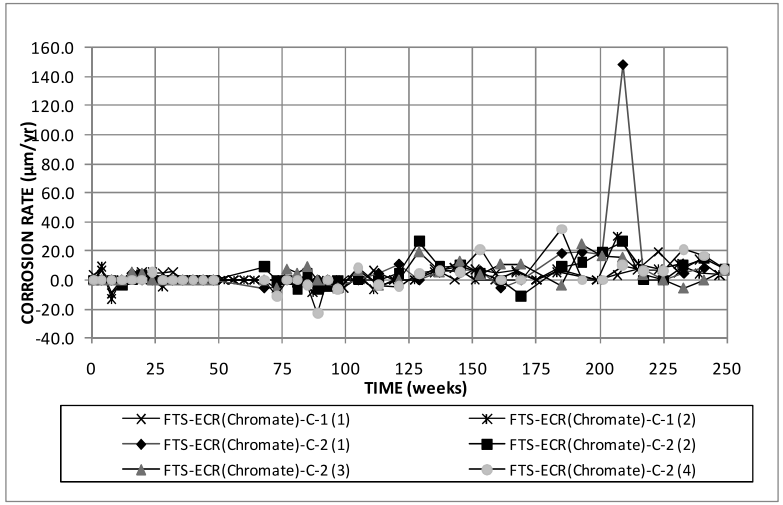

(a)

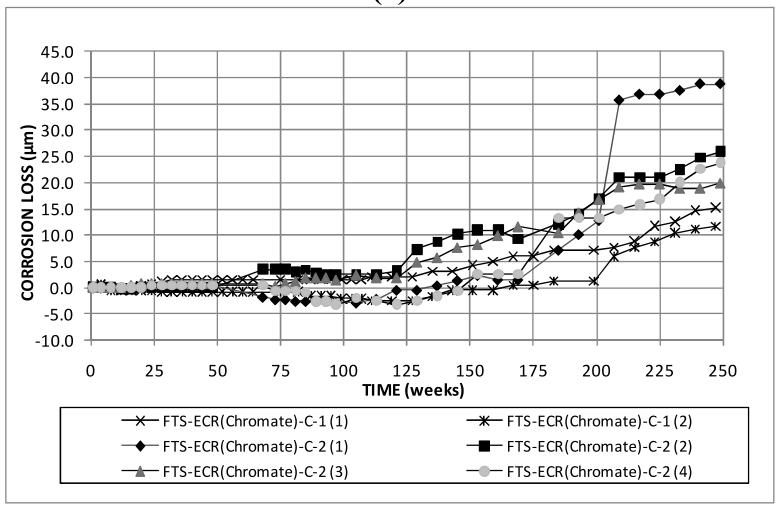

(b)

Figure A.27: (a) Corrosion rate and (b) corrosion losses based on exposed area for field test specimens with ECR with chromate pretreatment in cracked concrete.

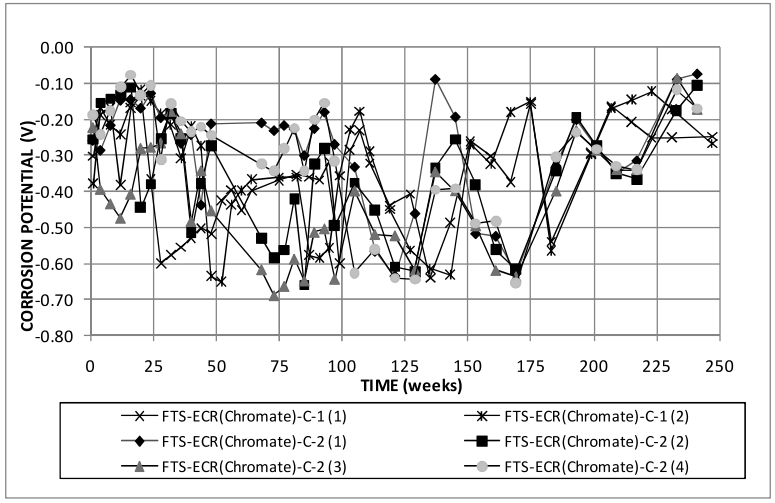

(a)

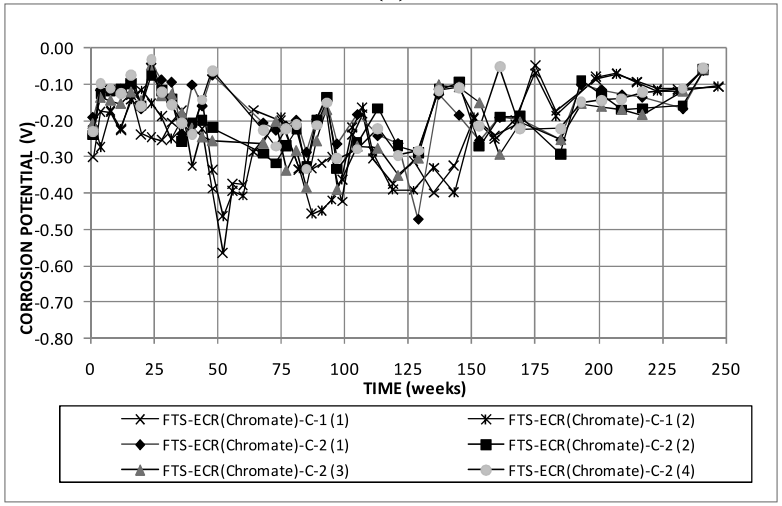

(b)

Figure A.28: (a) Top mat corrosion potentials and (b) bottom mat corrosion potentials for field test specimens with ECR with chromate pretreatment in cracked concrete.

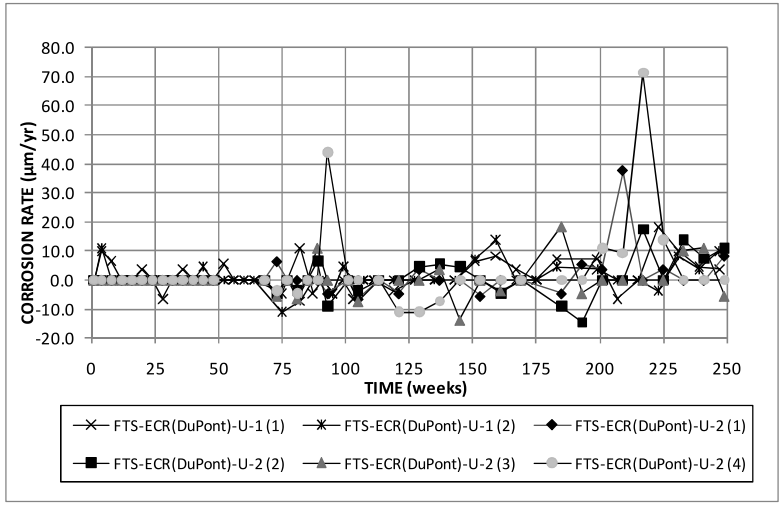

(a)

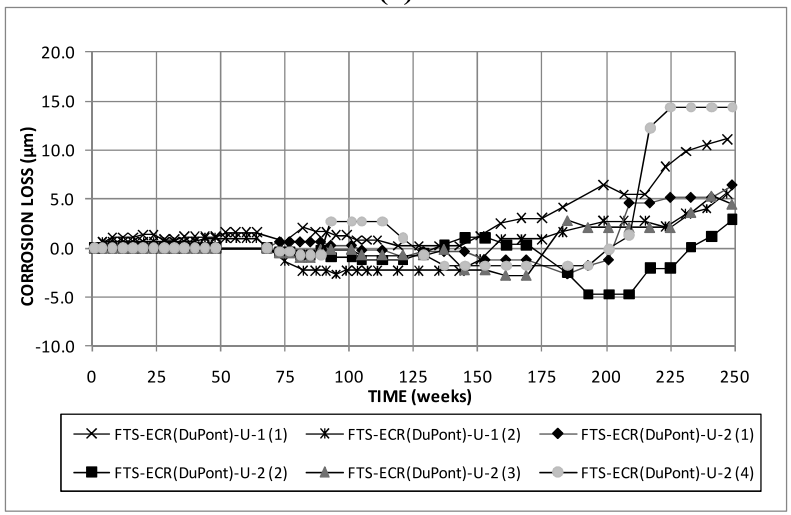

(b)

Figure A.29: (a) Corrosion rate and (b) corrosion losses based on exposed area for field test specimens with ECR from DuPont in uncracked concrete.

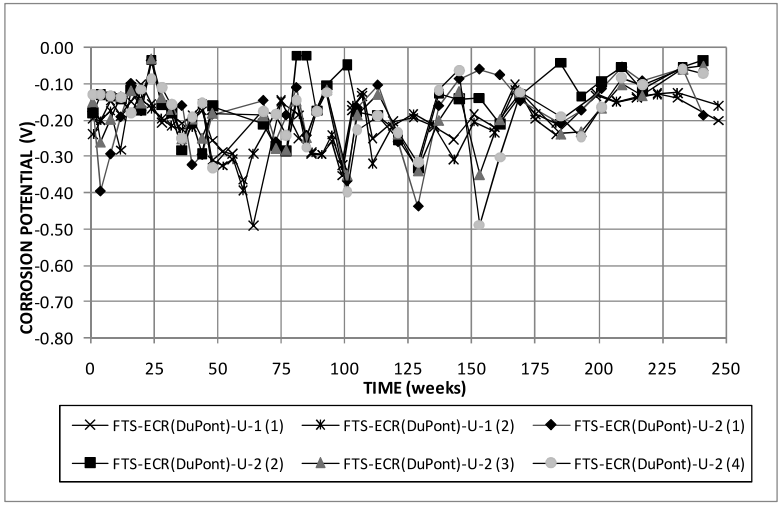

(a)

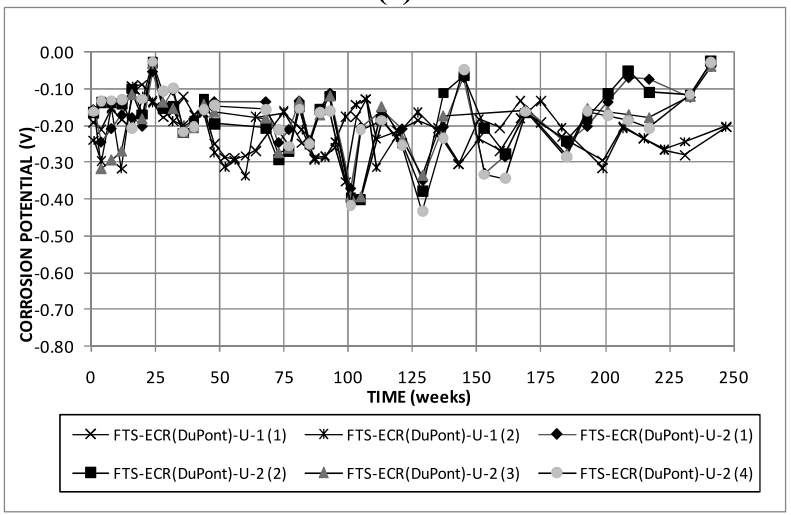

(b)

Figure A.30: (a) Top mat corrosion potentials and (b) bottom mat corrosion potentials for field test specimens with ECR from DuPont in uncracked concrete.

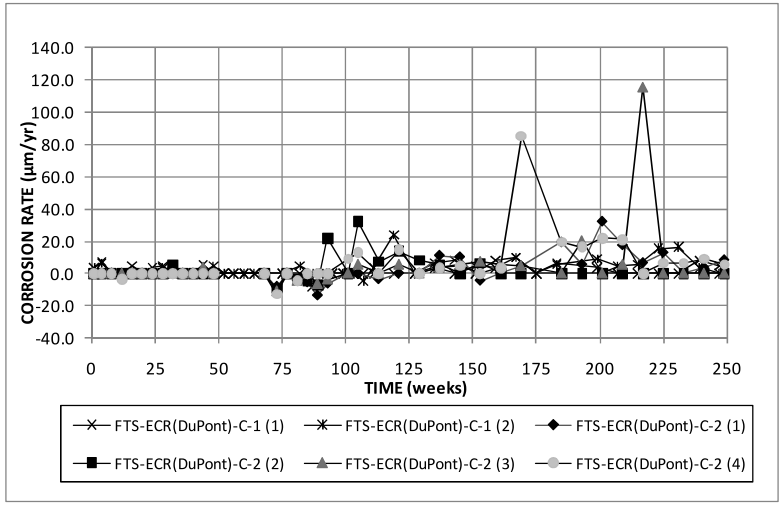

(a)

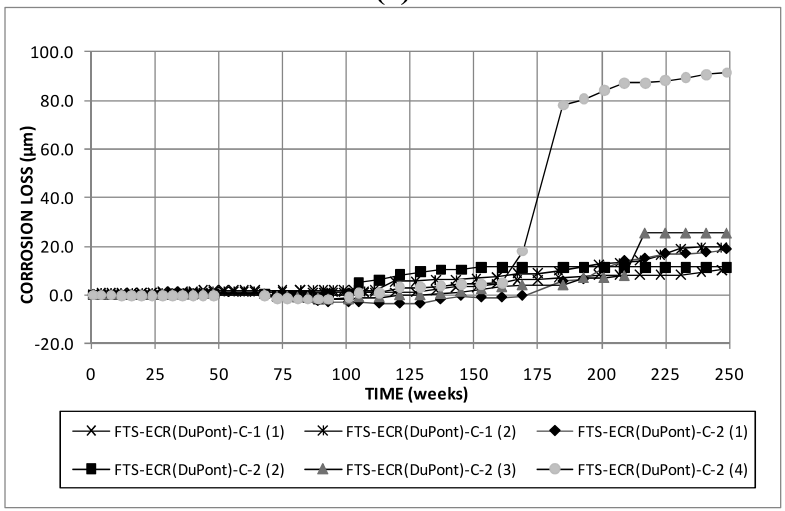

(b)

Figure A.31: (a) Corrosion rate and (b) corrosion losses based on exposed area for field test specimens with ECR from DuPont in cracked concrete.

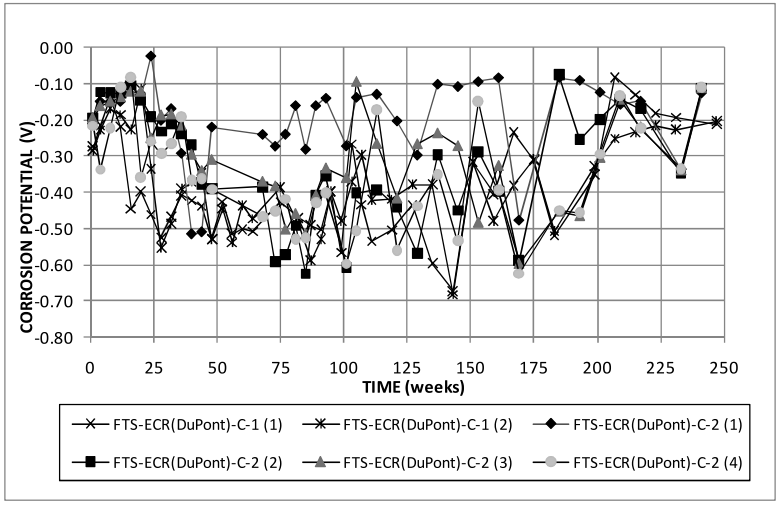

(a)

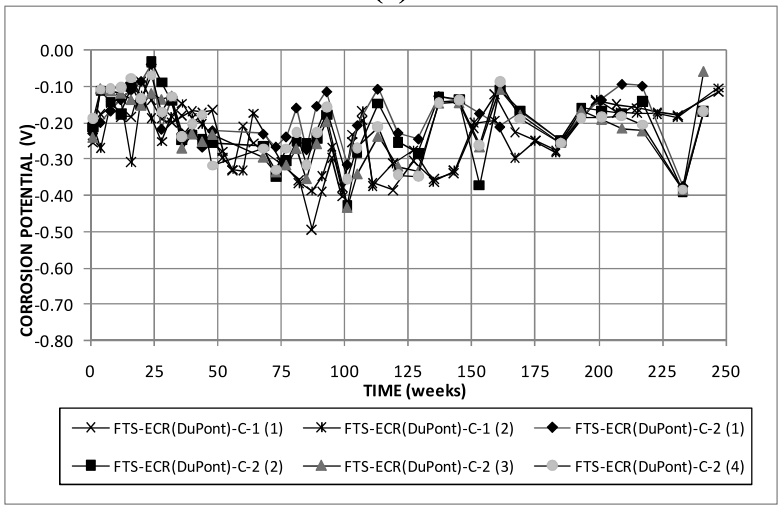

(b)

Figure A.32: (a) Top mat corrosion potentials and (b) bottom mat corrosion potentials for field test specimens with ECR from DuPont in cracked concrete.

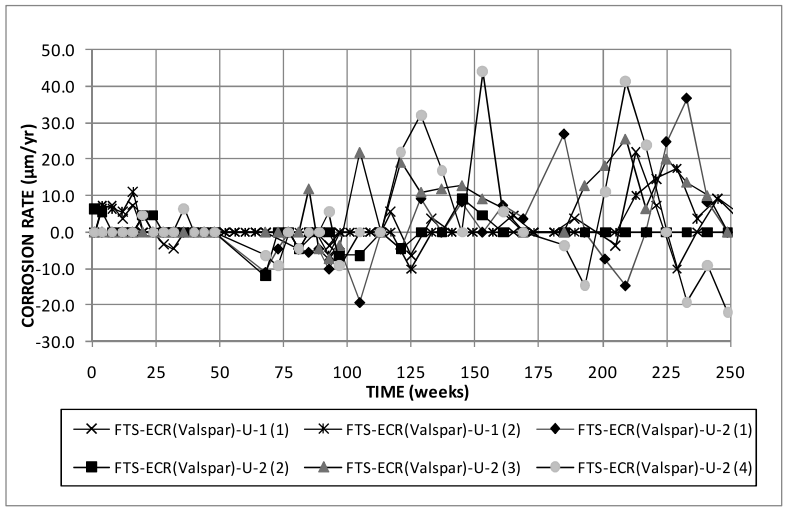

(a)

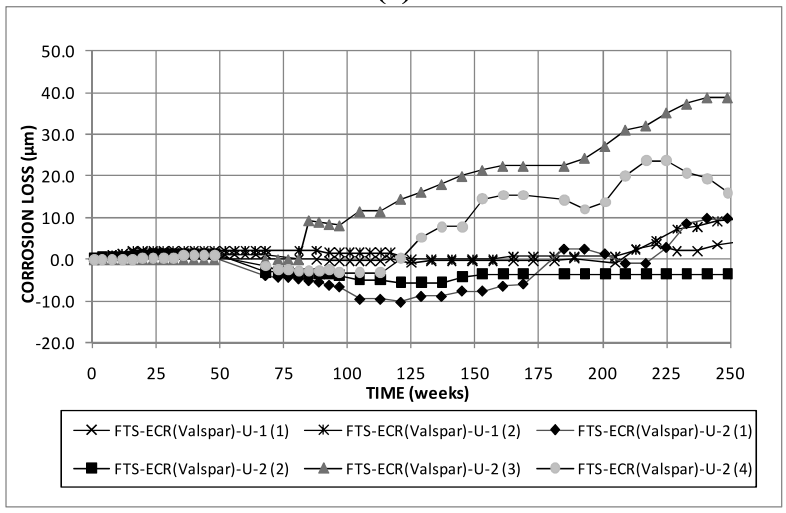

(b)

Figure A.33: (a) Corrosion rate and (b) corrosion losses based on exposed area for field test specimens with ECR from Valspar in uncracked concrete.

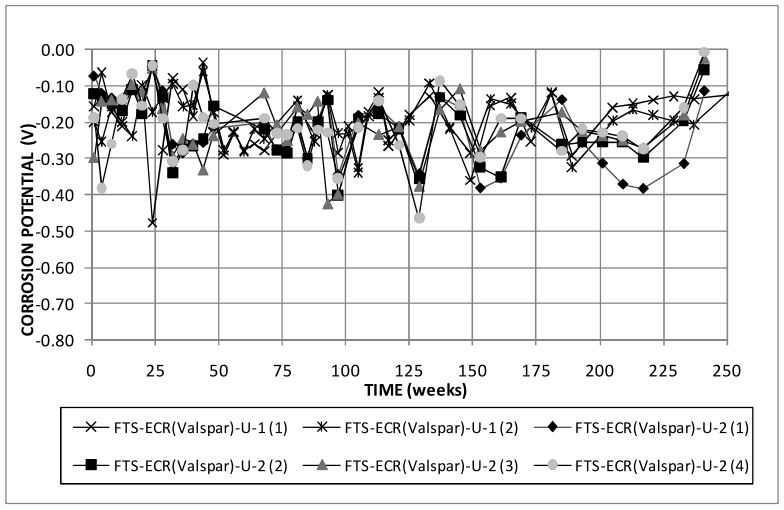

(a)

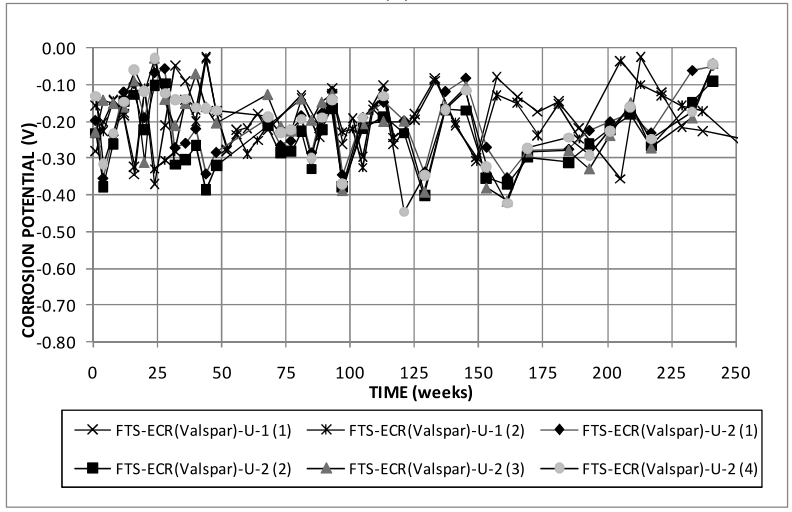

(b)

Figure A.34: (a) Top mat corrosion potentials and (b) bottom mat corrosion potentials for field test specimens with ECR from Valspar in uncracked concrete.

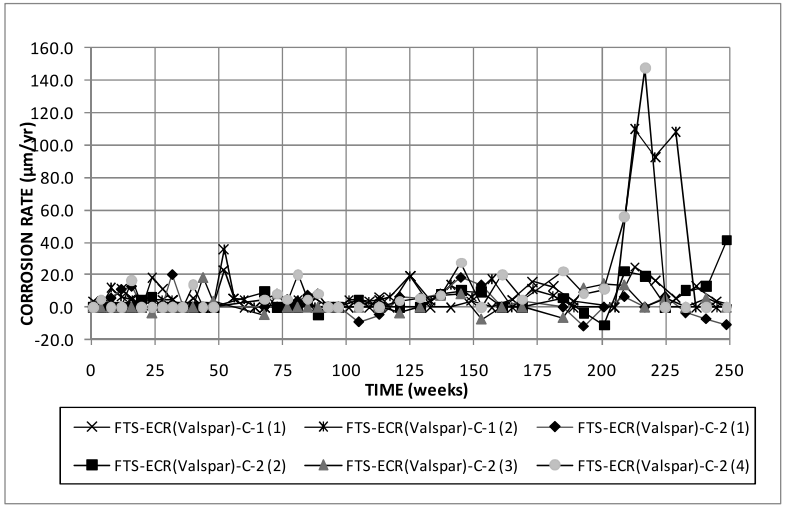

(a)

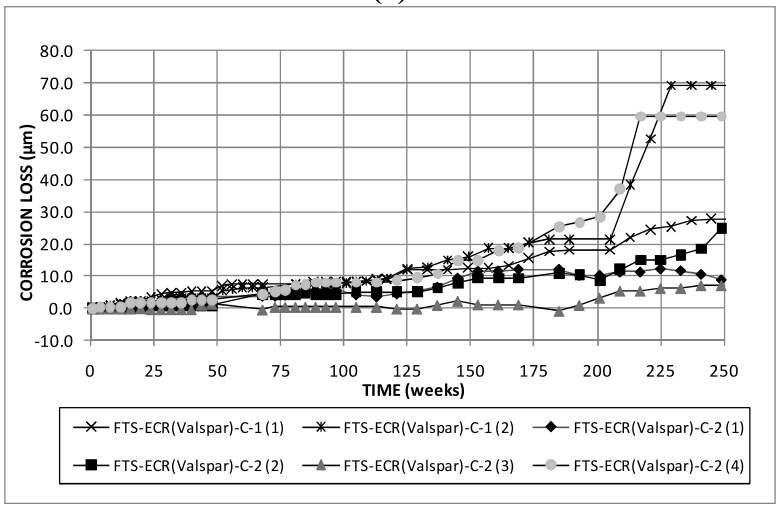

(b)

Figure A.35: (a) Corrosion rate and (b) corrosion losses based on exposed area for field test specimens with ECR from Valspar in cracked concrete.

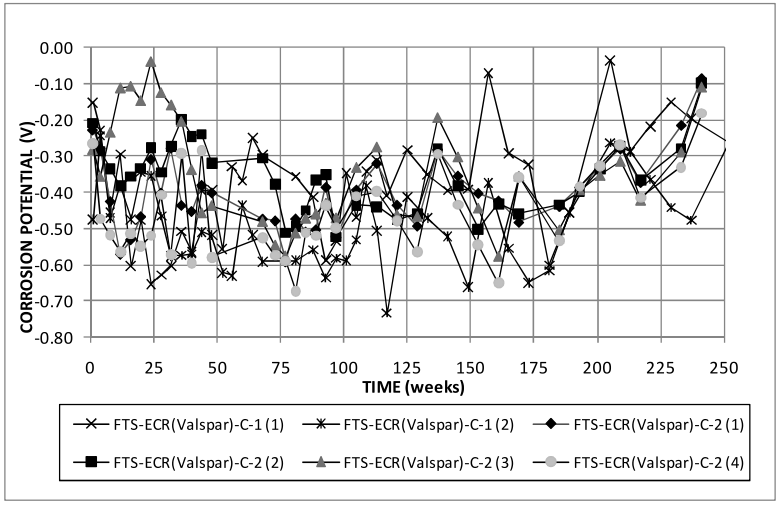

(a)

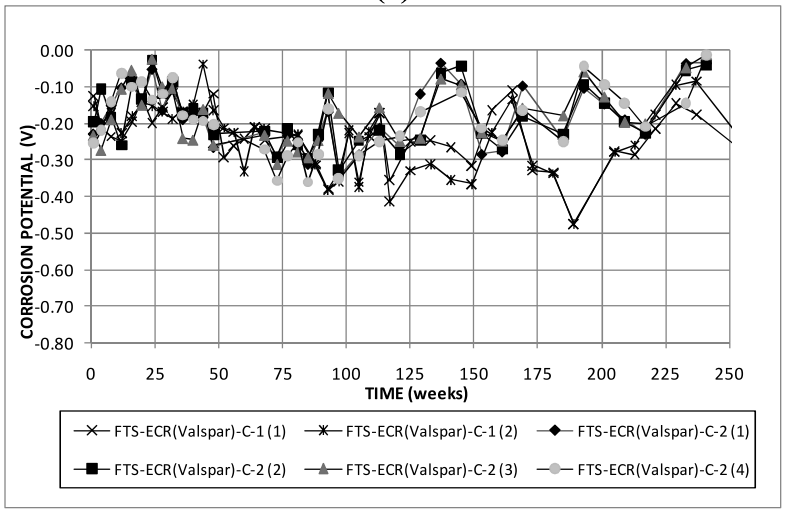

(b)

Figure A.36: (a) Top mat corrosion potentials and (b) bottom mat corrosion potentials for field test specimens with ECR from Valspar in cracked concrete.

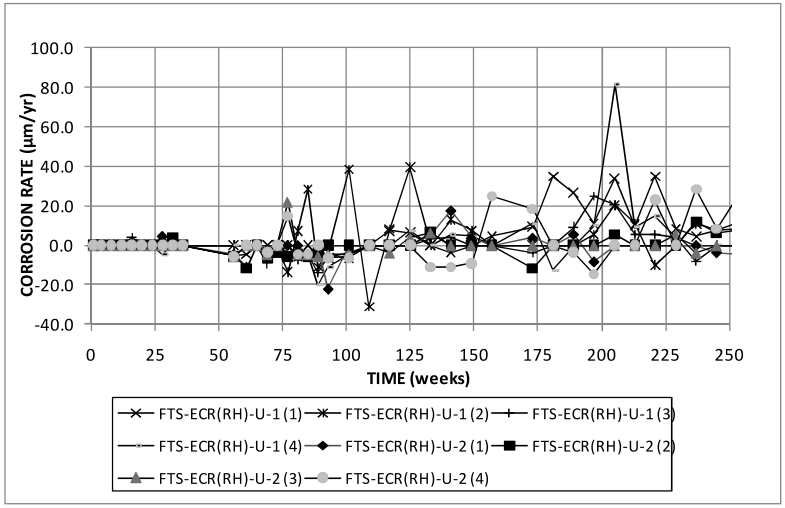

(a)

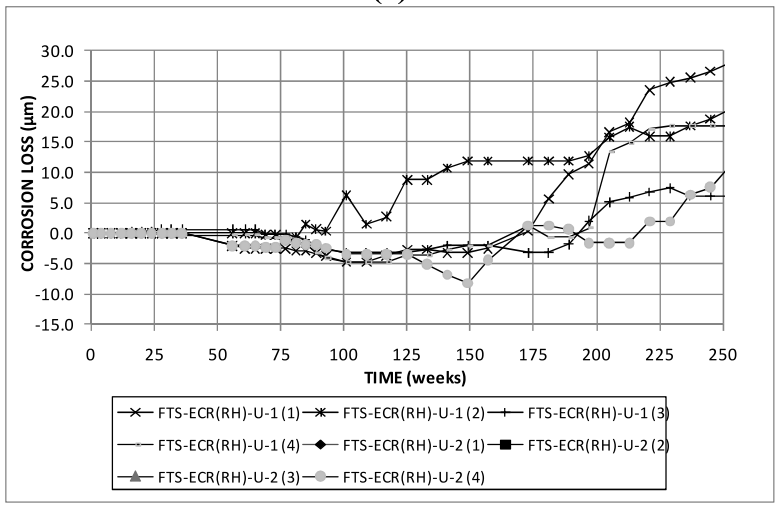

(b)

Figure A.37: (a) Corrosion rate and (b) corrosion losses based on exposed area for field test specimens with ECR in uncracked concrete containing Rheocrete.

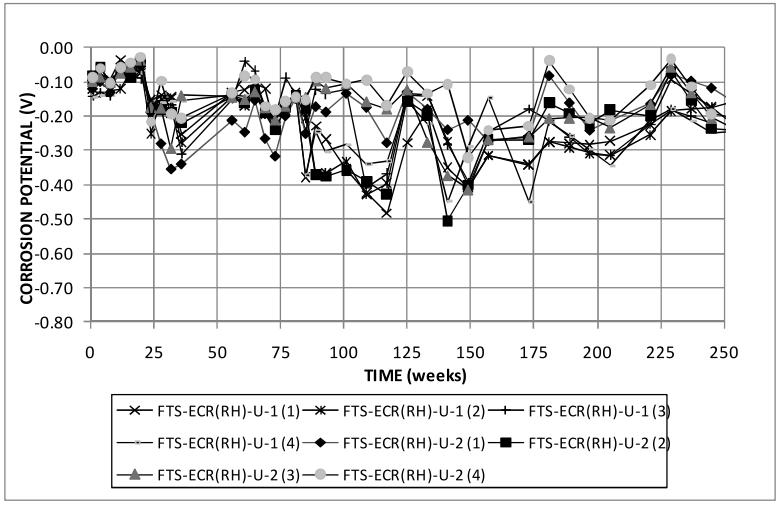

(a)

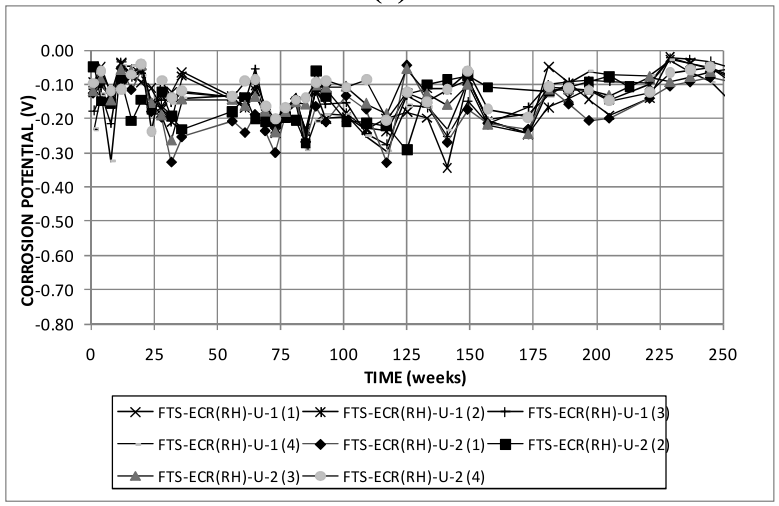

(b)

Figure A.38: (a) Top mat corrosion potentials and (b) bottom mat corrosion potentials for field test specimens with ECR in uncracked concrete containing Rheocrete.

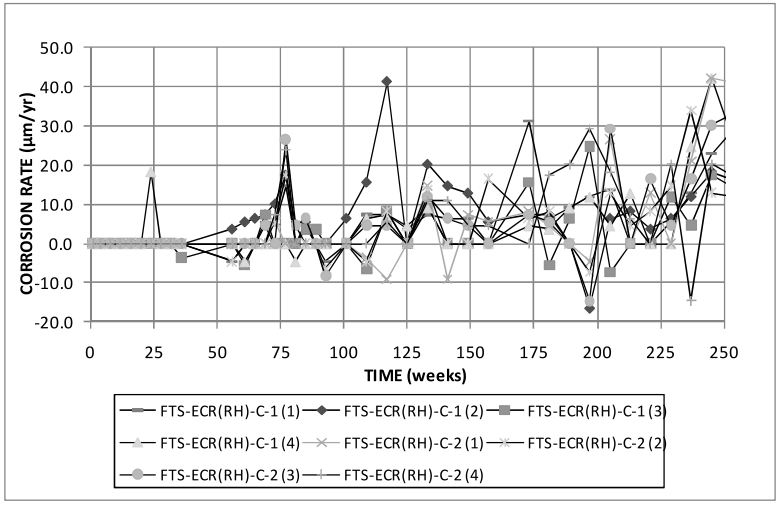

(a)

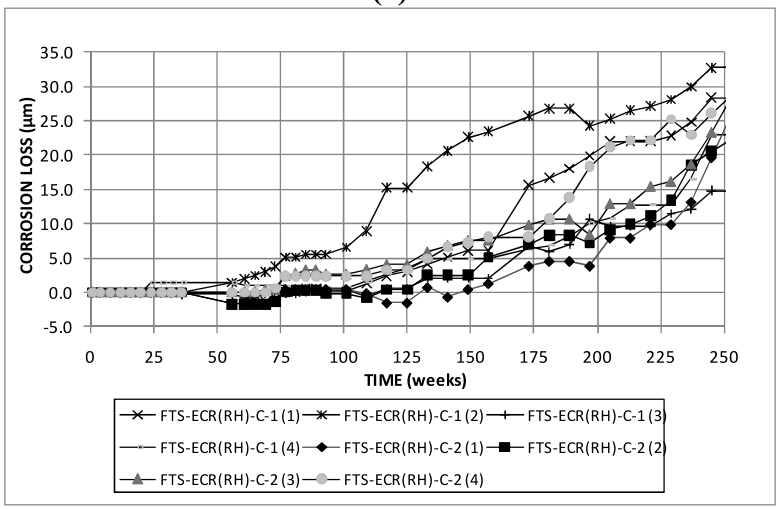

(b)

Figure A.39: (a) Corrosion rate and (b) corrosion losses based on exposed area for field test specimens with ECR in cracked concrete containing Rheocrete.

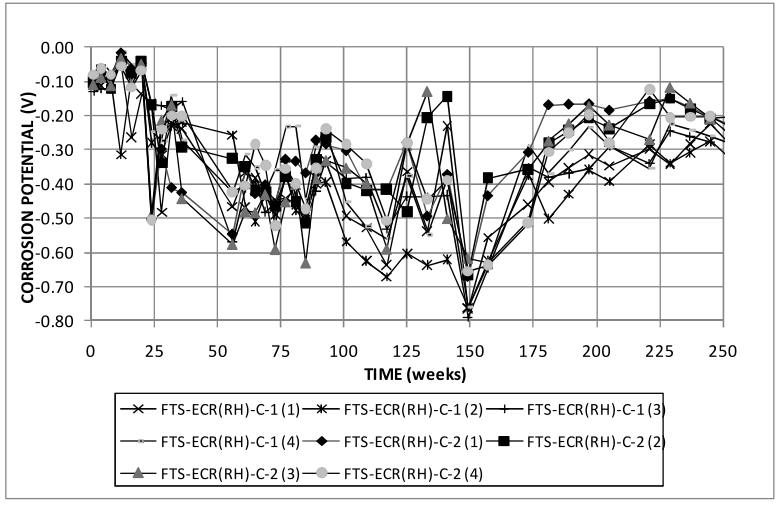

(a)

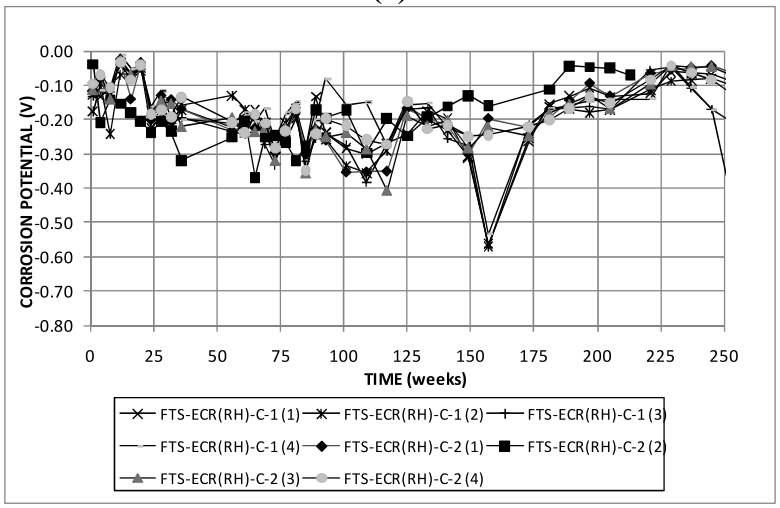

(b)

Figure A.40: (a) Top mat corrosion potentials and (b) bottom mat corrosion potentials for field test specimens with ECR in cracked concrete containing Rheocrete.

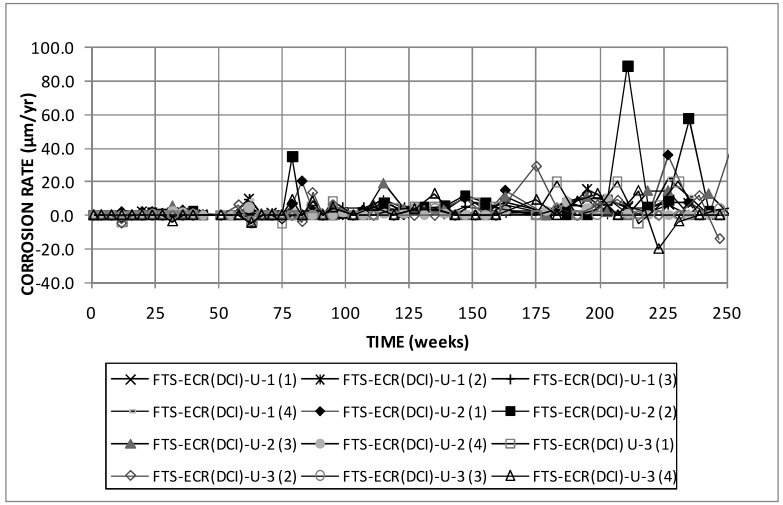

(a)

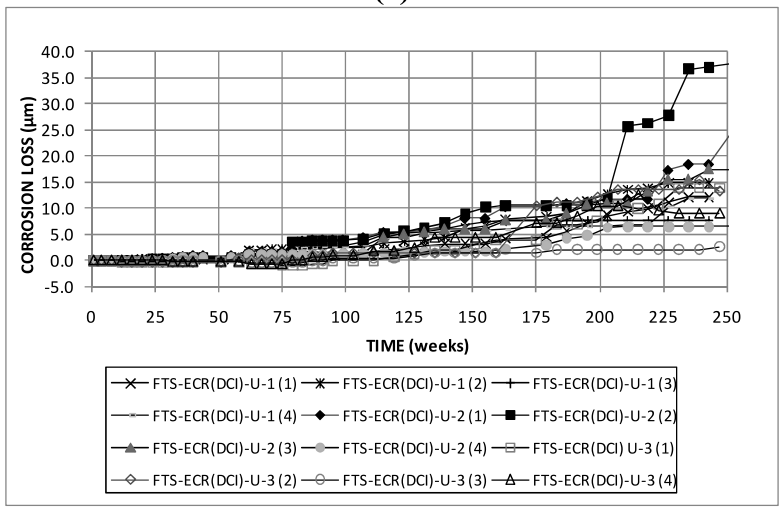

(b)

Figure A.41: (a) Corrosion rate and (b) corrosion losses based on exposed area for field test specimens with ECR in uncracked concrete containing DCI.

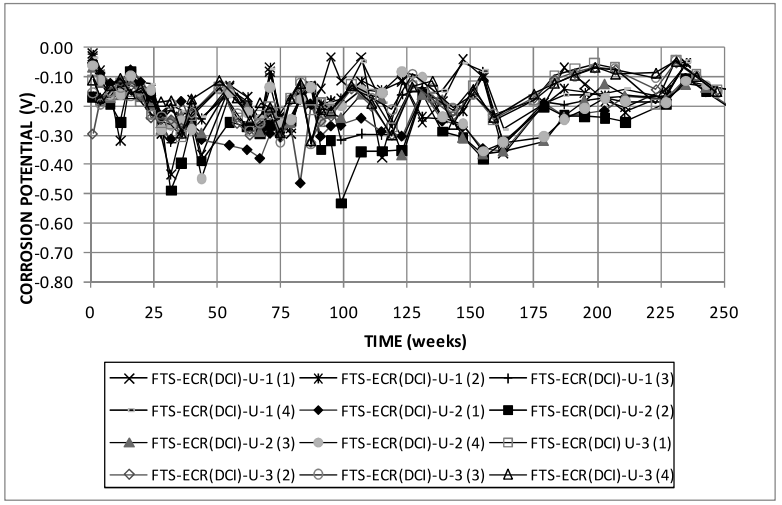

(a)

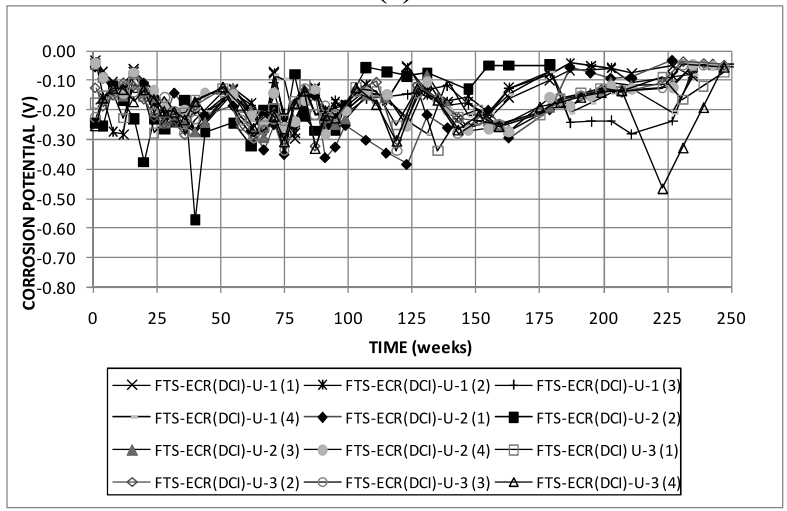

(b)

Figure A.42: (a) Top mat corrosion potentials and (b) bottom mat corrosion potentials for field test specimens with ECR in uncracked concrete containing DCI.

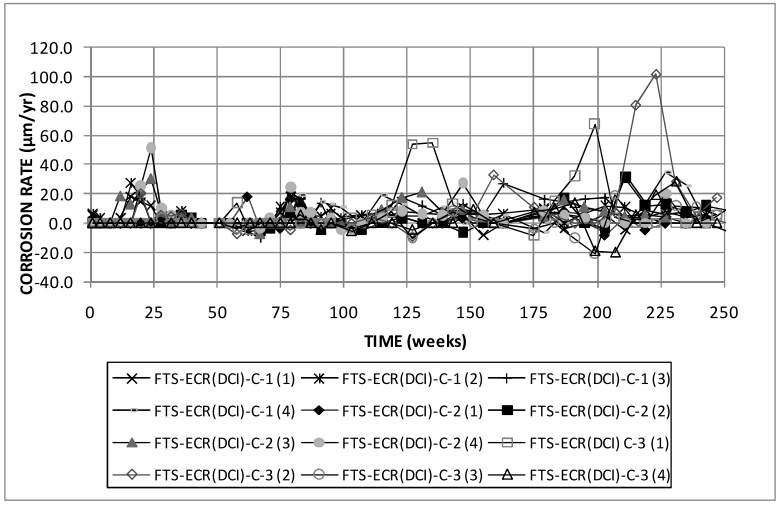

(a)

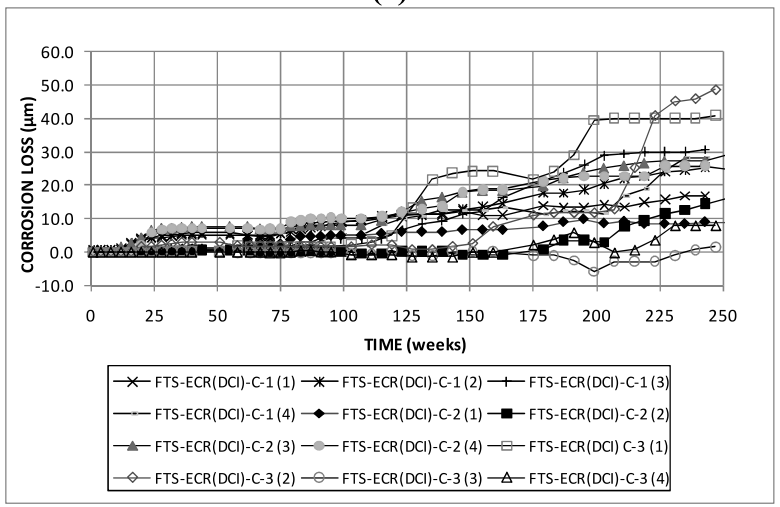

(b)

Figure A.43: (a) Corrosion rate and (b) corrosion losses based on exposed area for field test specimens with ECR in cracked concrete containing DCI.

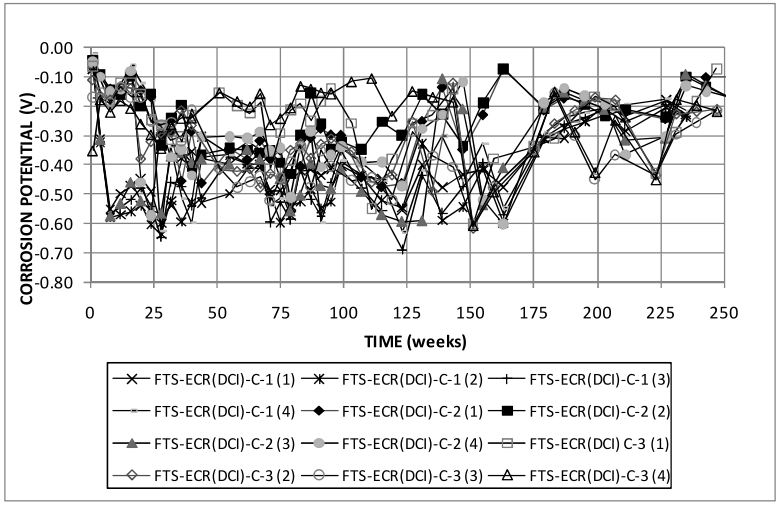

(a)

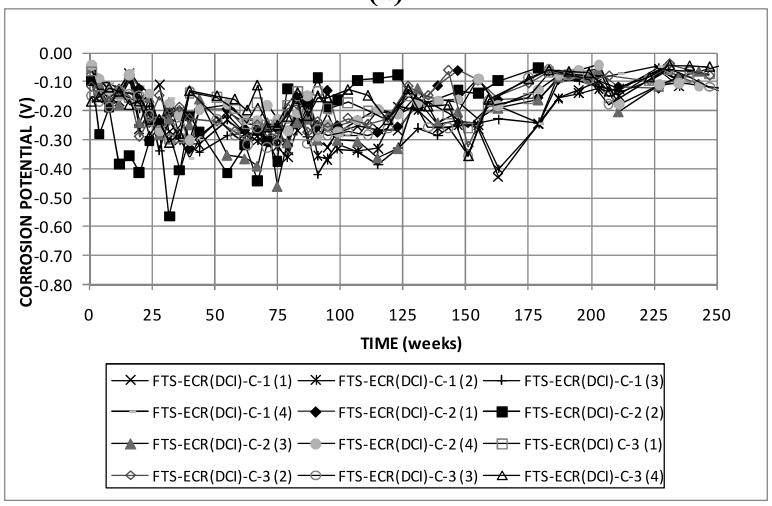

(b)

Figure A.44: (a) Top mat corrosion potentials and (b) bottom mat corrosion potentials for field test specimens with ECR in cracked concrete containing DCI.

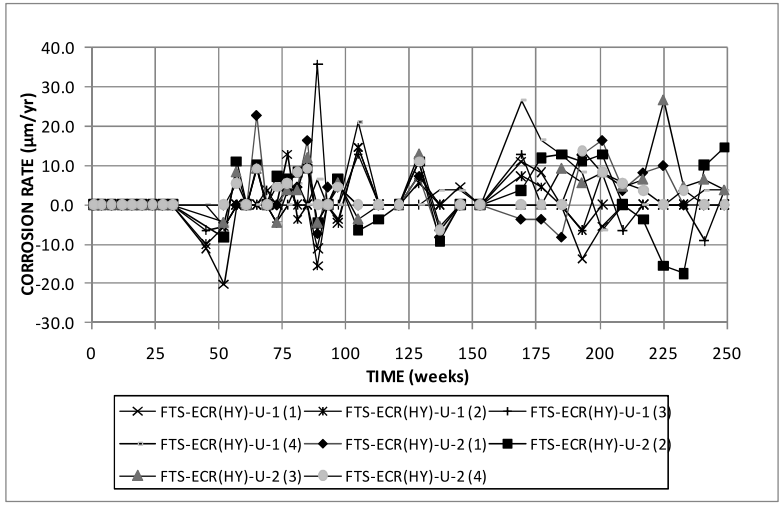

(a)

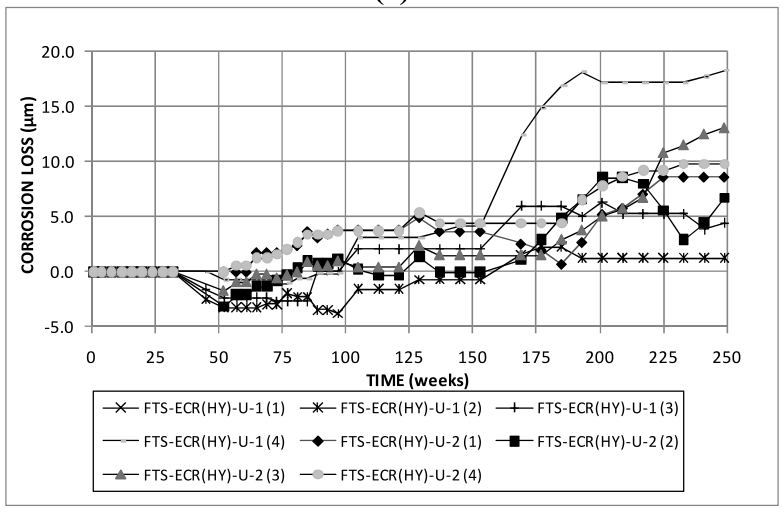

(b)

Figure A.45: (a) Corrosion rate and (b) corrosion losses based on exposed area for field test specimens with ECR in uncracked concrete containing Hycrete.

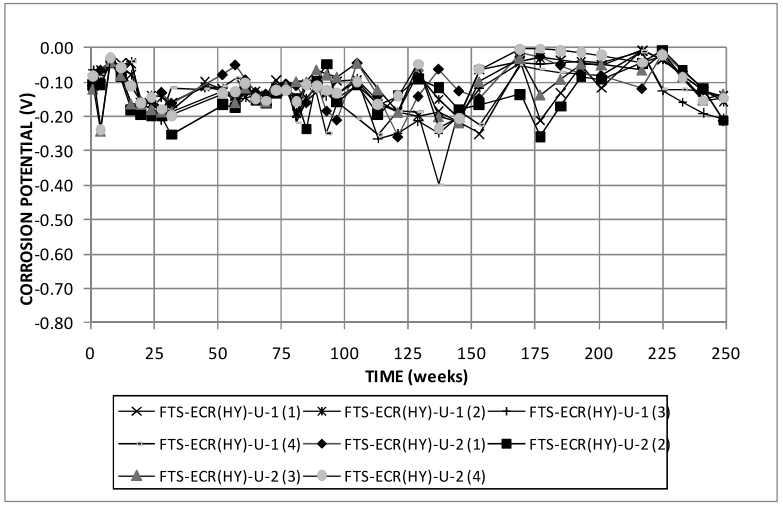

(a)

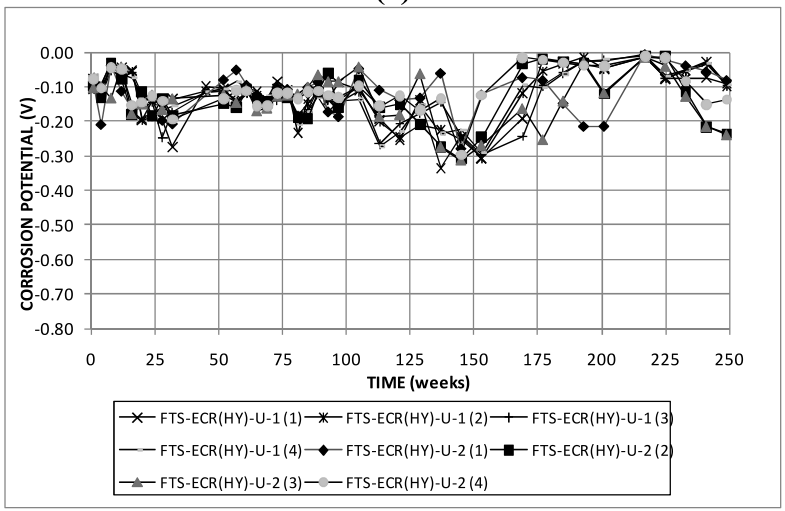

(b)

Figure A.46: (a) Top mat corrosion potentials and (b) bottom mat corrosion potentials for field test specimens with ECR in uncracked concrete containing Hycrete.

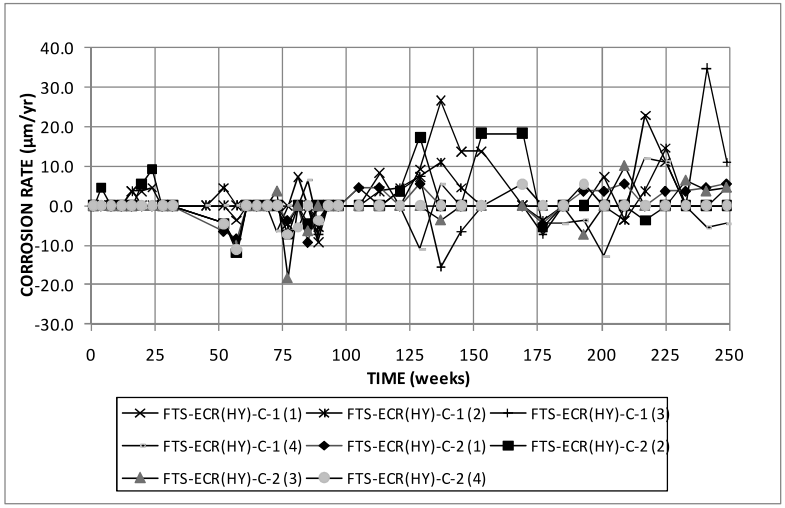

(a)

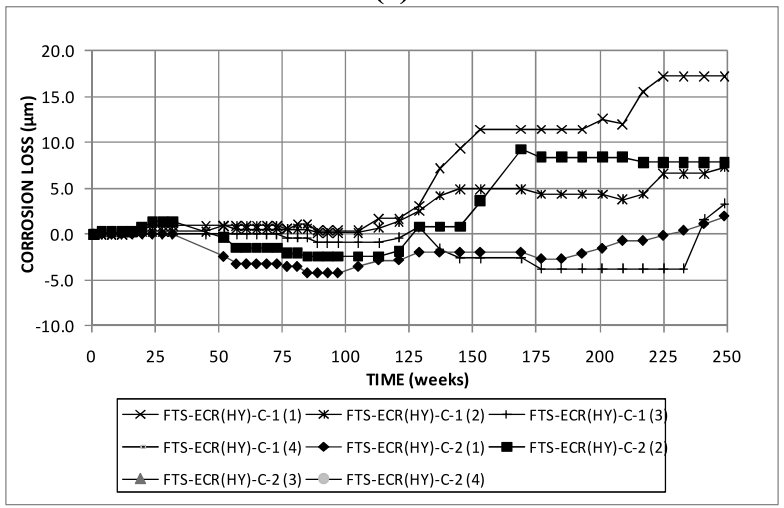

(b)

Figure A.47: (a) Corrosion rate and (b) corrosion losses based on exposed area for field test specimens with ECR in uncracked concrete containing Hycrete.

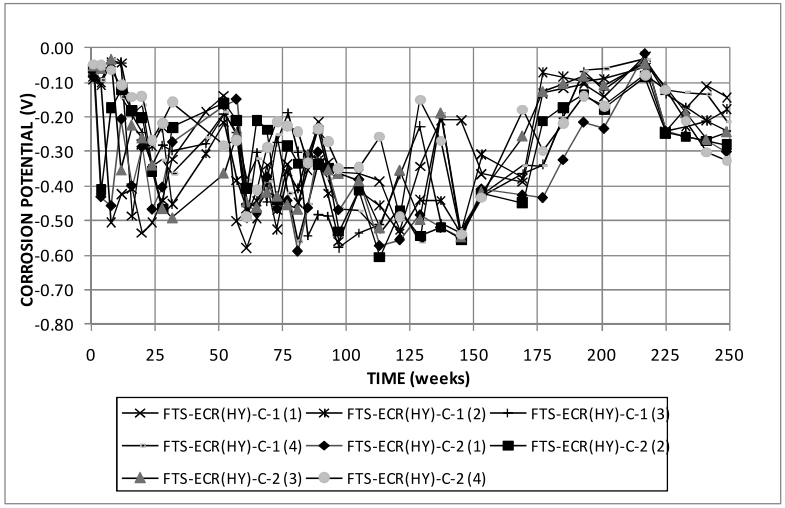

(a)

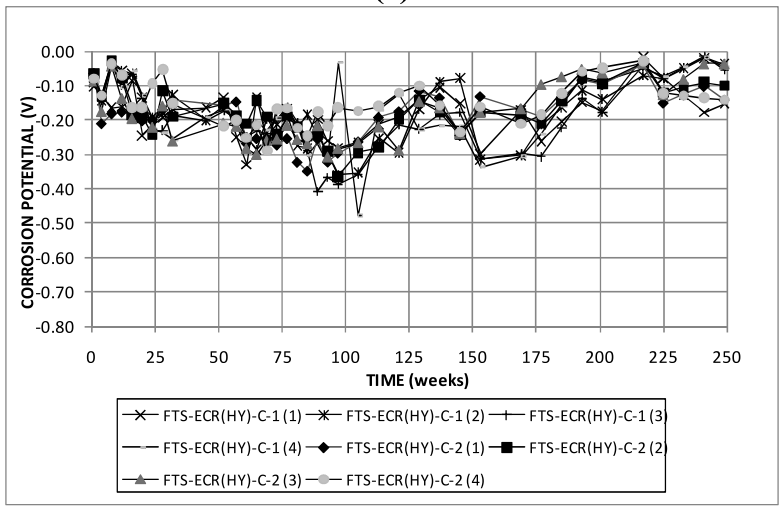

(b)

Figure A.48: (a) Top mat corrosion potentials and (b) bottom mat corrosion potentials for field test specimens with ECR in uncracked concrete containing Hycrete.

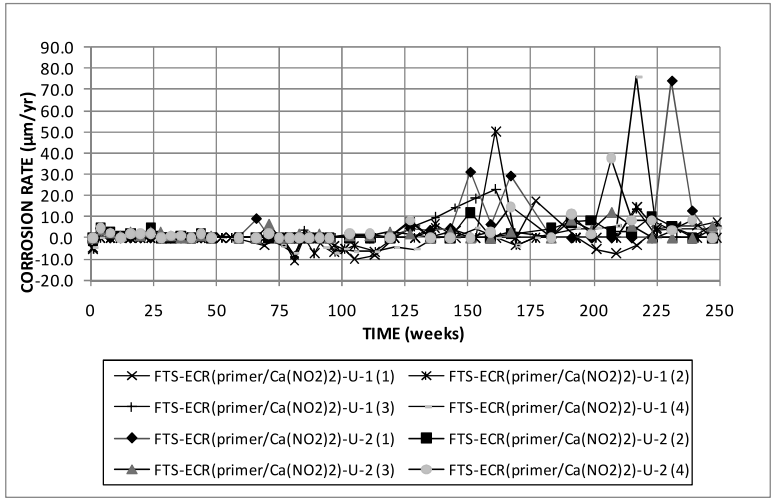

(a)

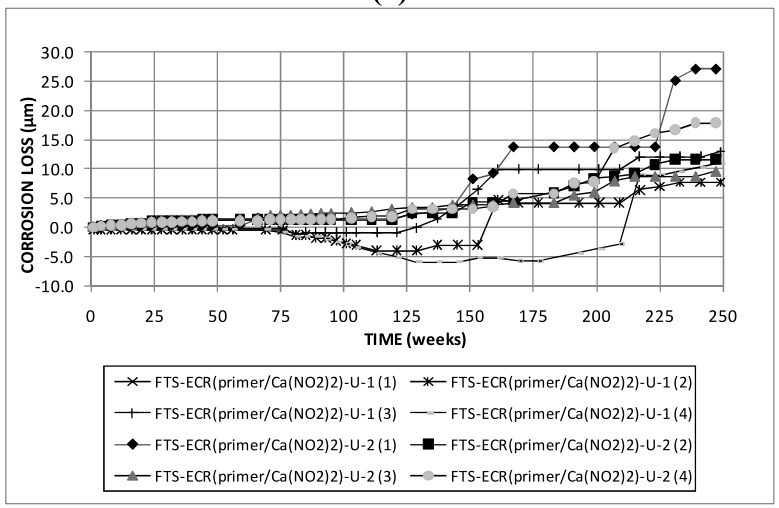

(b)

Figure A.49: (a) Corrosion rate and (b) corrosion losses based on exposed area for field test specimens with ECR with a calcium nitrite primer in uncracked concrete.

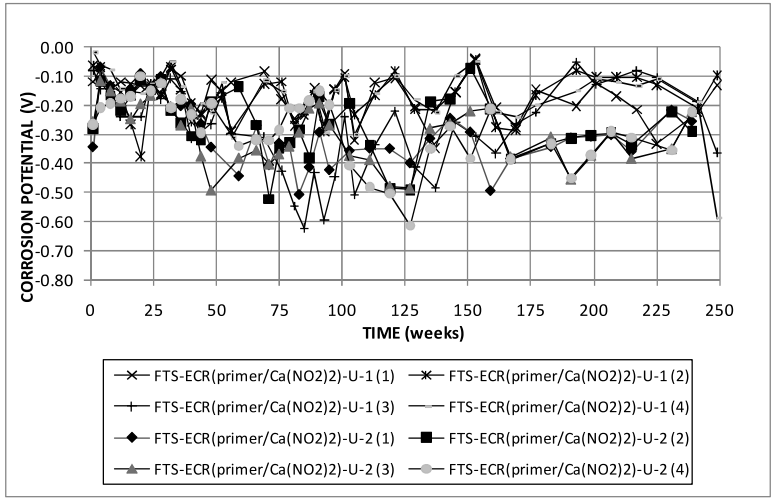

(a)

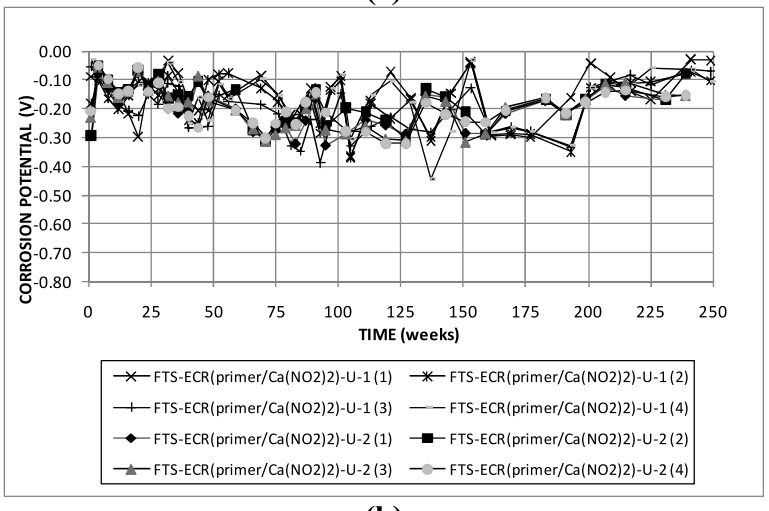

(b)

Figure A.50: (a) Top mat corrosion potentials and (b) bottom mat corrosion potentials for field test specimens with ECR with a calcium nitrite primer in uncracked concrete.

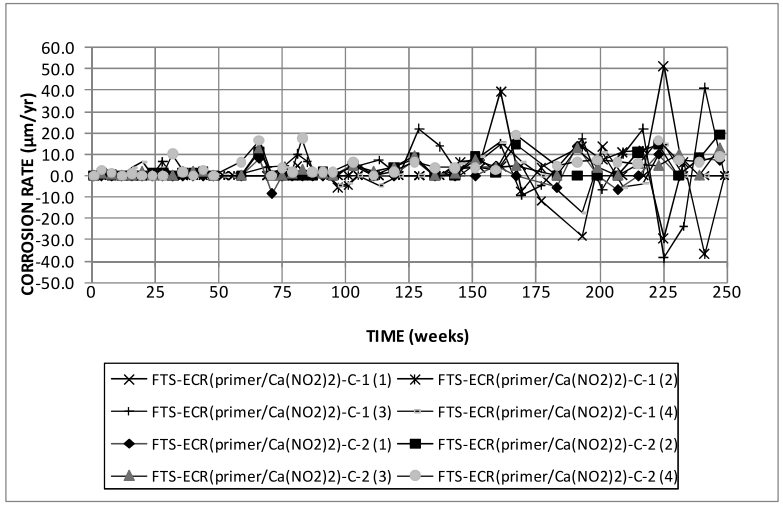

(a)

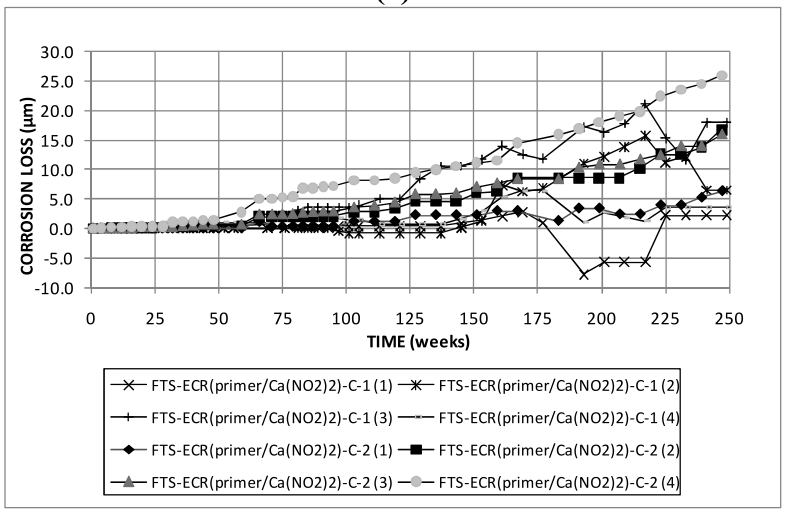

(b)

Figure A.51: (a) Corrosion rate and (b) corrosion losses based on exposed area for field test specimens with ECR with a calcium nitrite primer in cracked concrete.

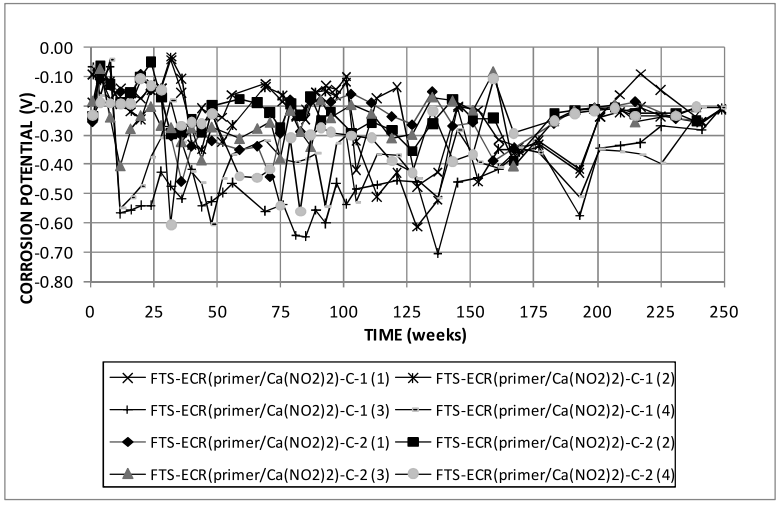

(a)

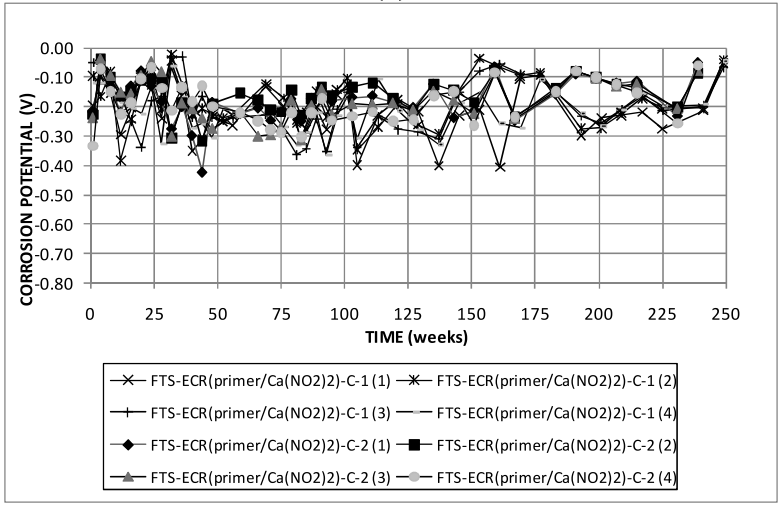

(b)

Figure A.52: (a) Top mat corrosion potentials and (b) bottom mat corrosion potentials for field test specimens with ECR with a calcium nitrite primer in cracked concrete.

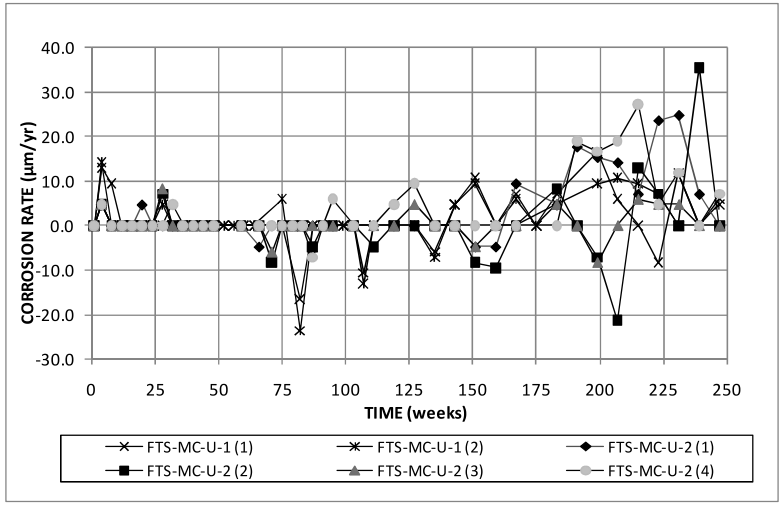

(a)

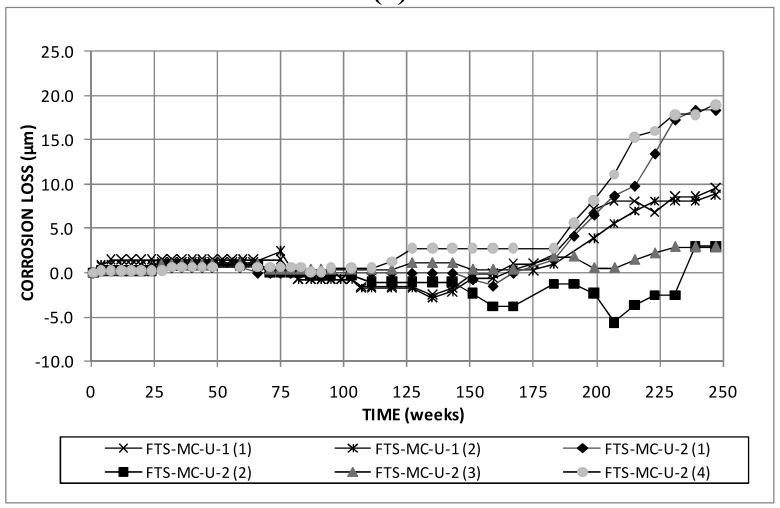

(b)

Figure A.53: (a) Corrosion rate and (b) corrosion losses based on exposed area for field test specimens with MC reinforcement in uncracked concrete.

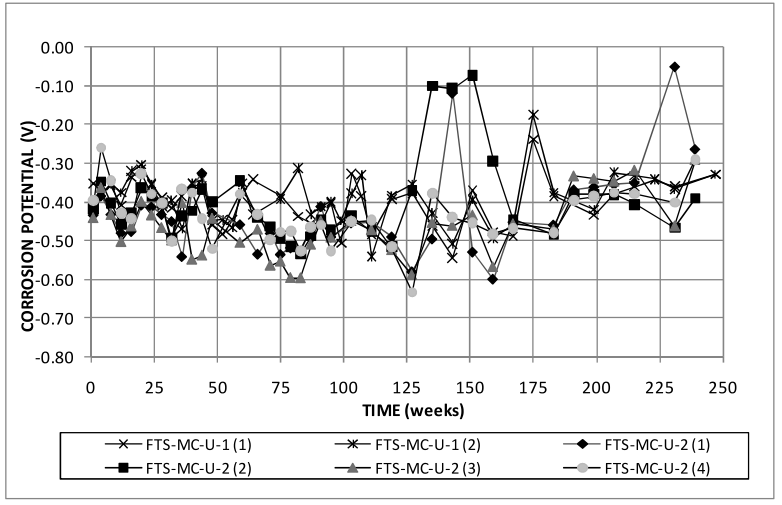

(a)

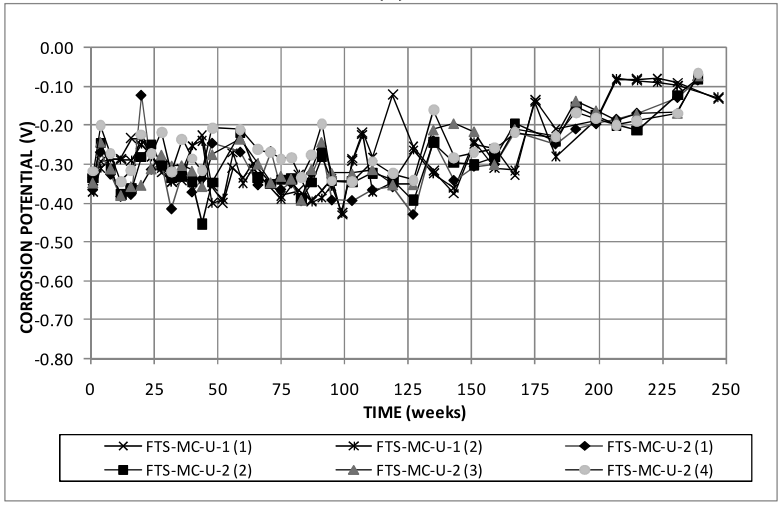

(b)

Figure A.54: (a) Top mat corrosion potentials and (b) bottom mat corrosion potentials for field test specimens with MC reinforcement in uncracked concrete.

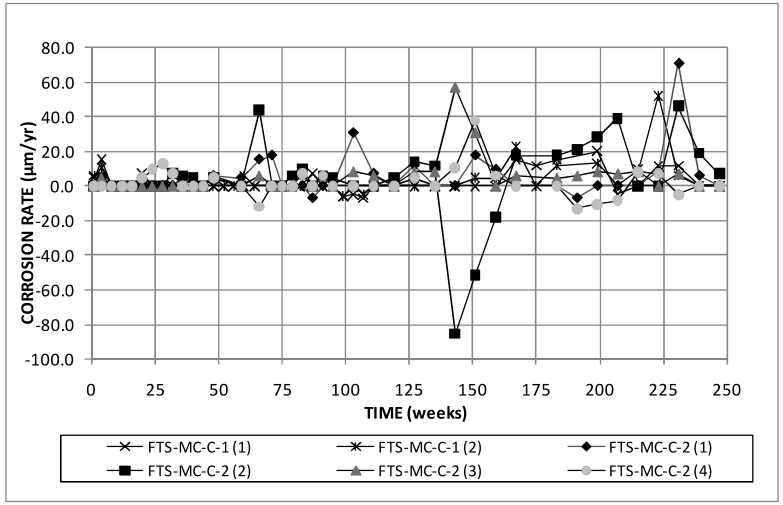

(a)

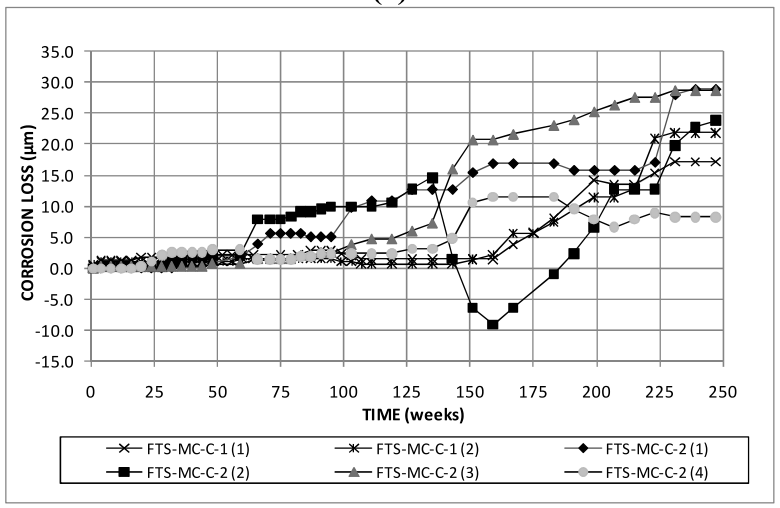

(b)

Figure A.55: (a) Corrosion rate and (b) corrosion losses based on exposed area for field test specimens with MC reinforcement in cracked concrete.

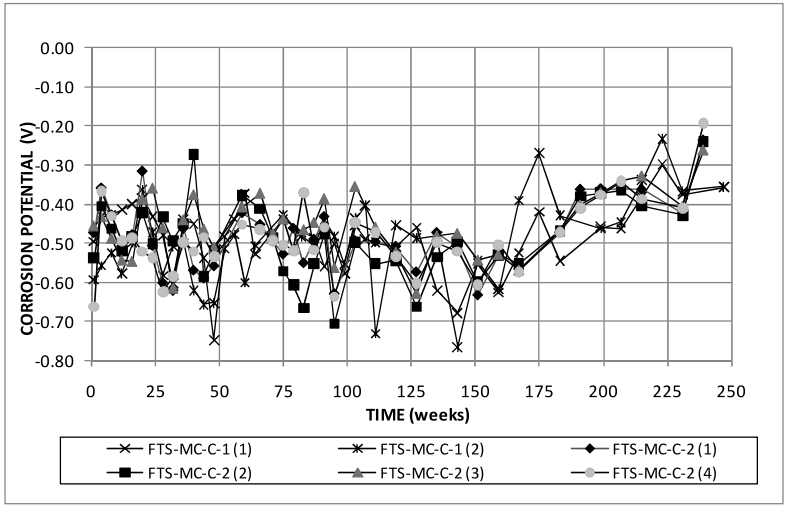

(a)

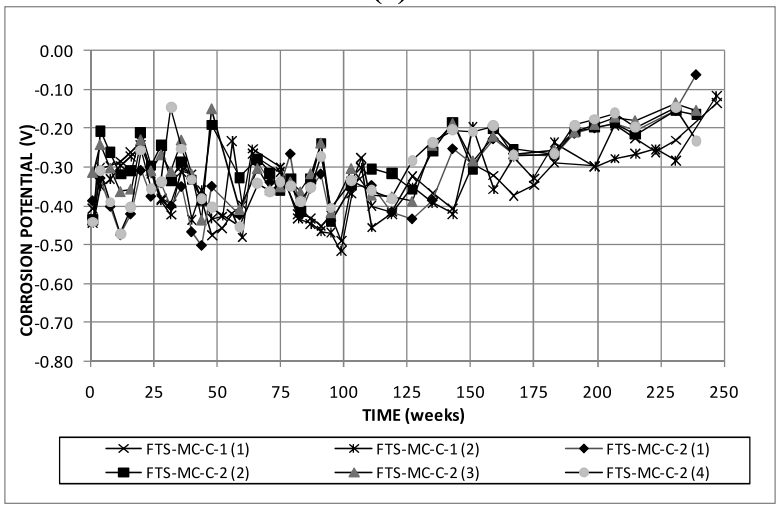

(b)

Figure A.56: (a) Top mat corrosion potentials and (b) bottom mat corrosion potentials for field test specimens with MC reinforcement in cracked concrete.

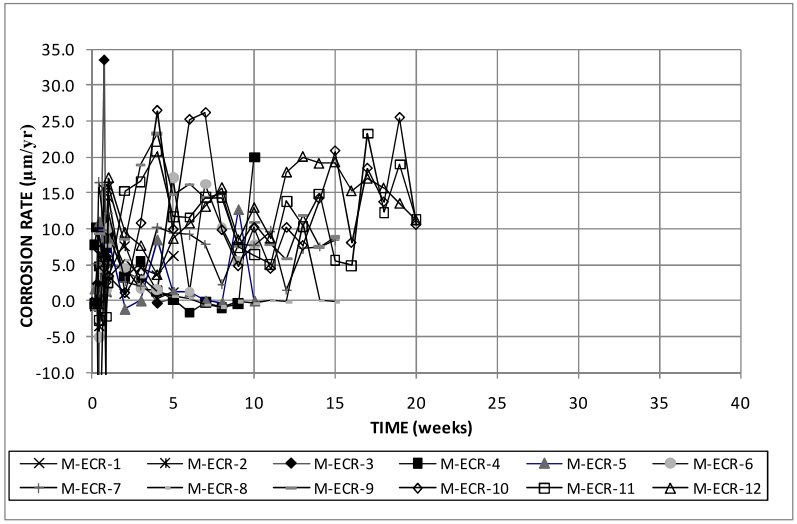

(a)

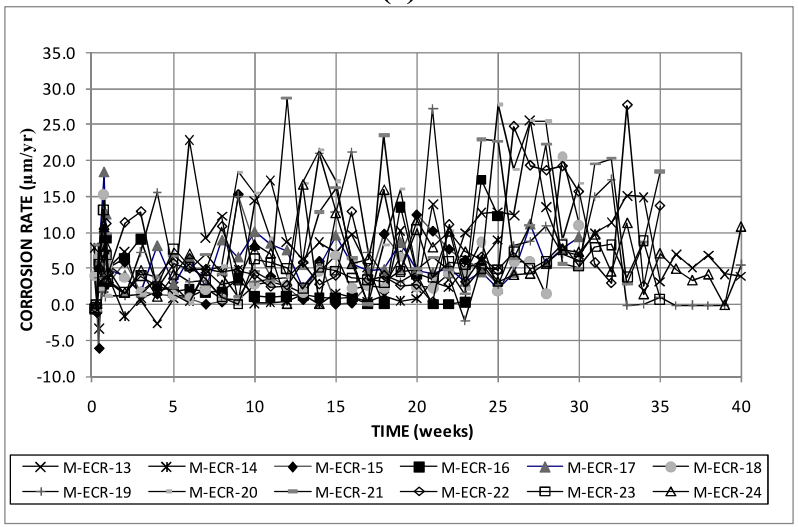

(b)

Figure A.57: Rapid macrocell test, ECR. Corrosion rate for (a) specimens 1-12 (b) specimens 13-24.

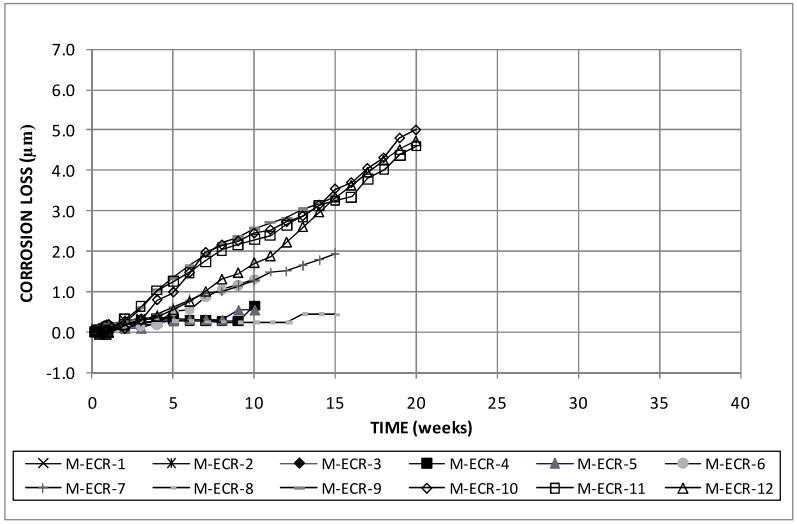

(a)

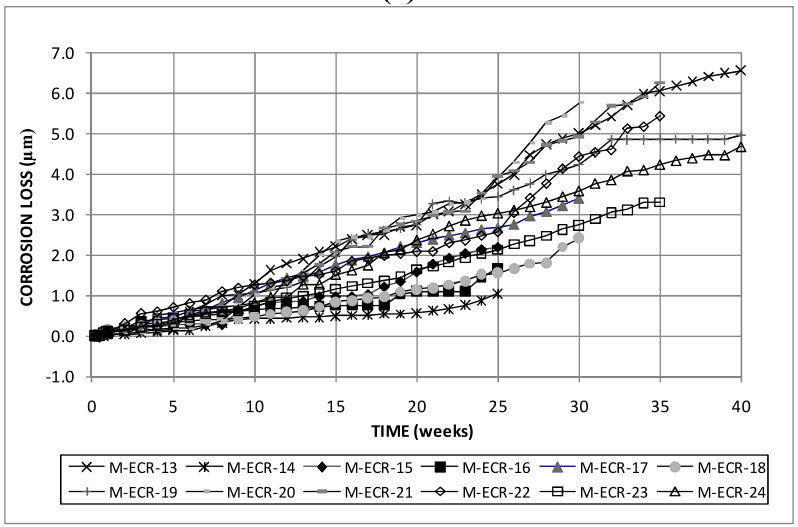

(b)

Figure A.58: Rapid macrocell test, ECR. Corrosion loss for (a) specimens 1-12 (b) specimens 13-24.

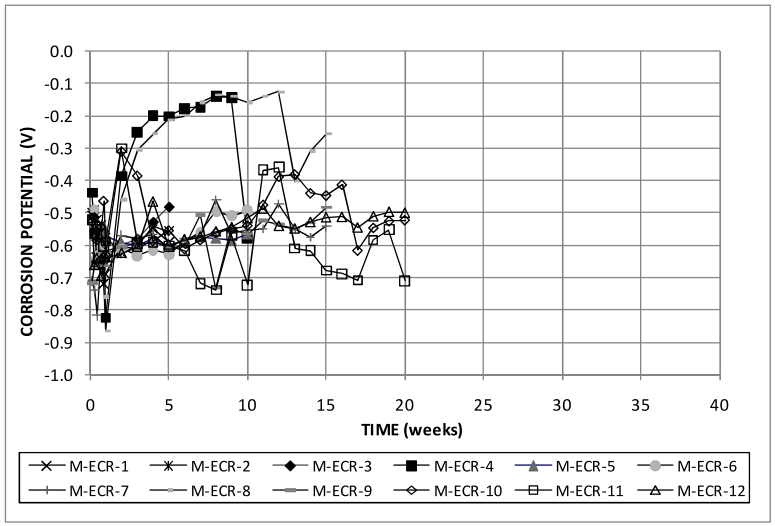

(a)

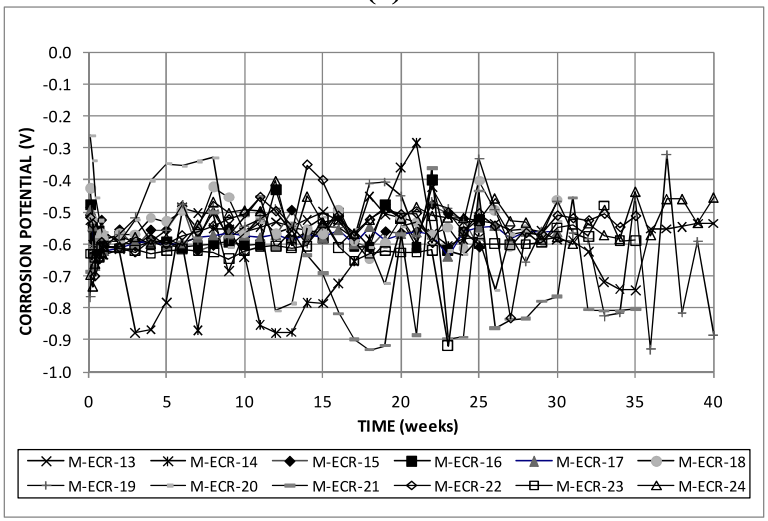

(b)

Figure A.59: Rapid macrocell test, ECR. Anode potential for (a) specimens 1-12 (b) specimens 13-24.

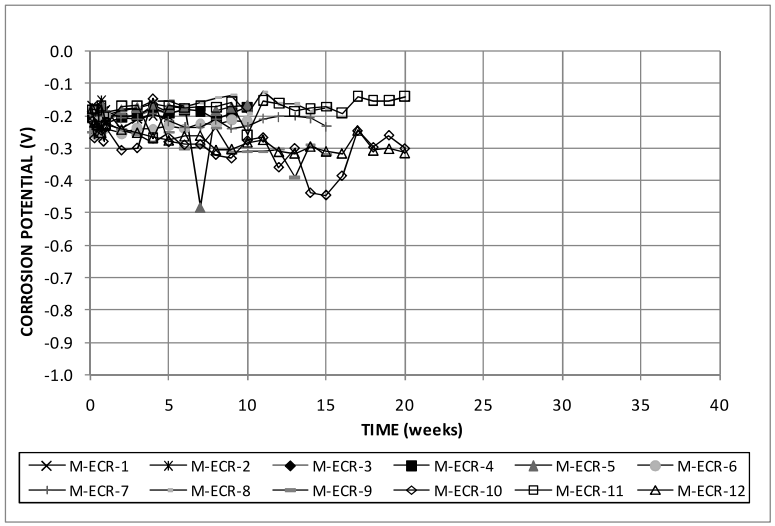

(a)

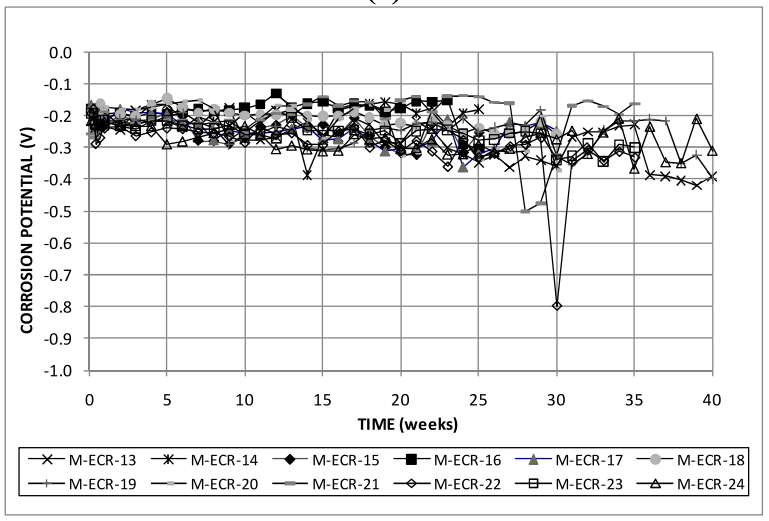

(b)

Figure A.60: Rapid macrocell test, ECR. Cathode potential for (a) specimens 1-12 (b) specimens 13-24.

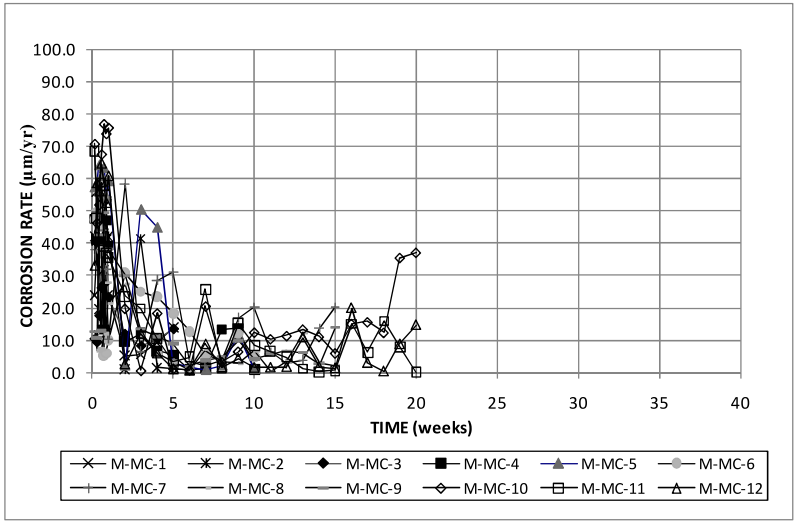

(a)

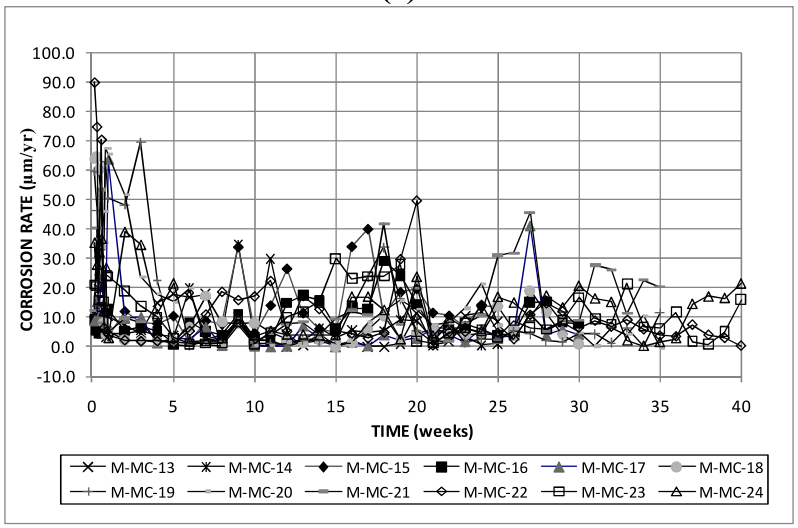

(b)

Figure A.61: Rapid macrocell test, MC. Corrosion rate for (a) specimens 1-12 (b) specimens 13-24.

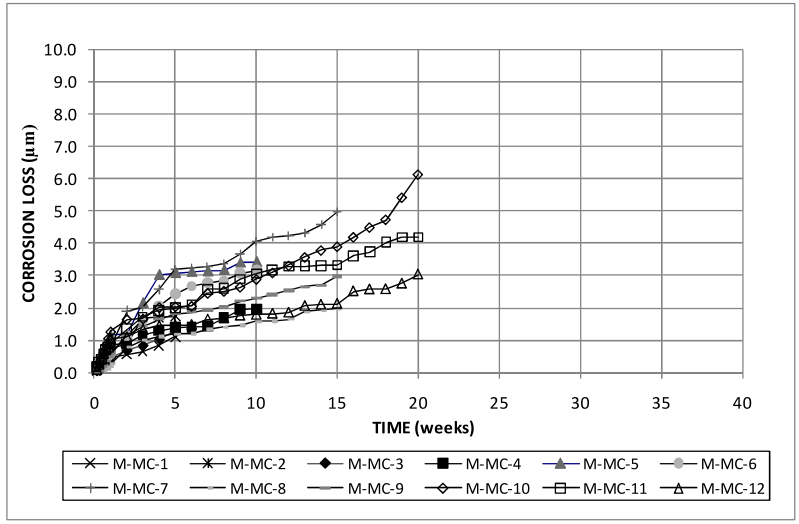

(a)

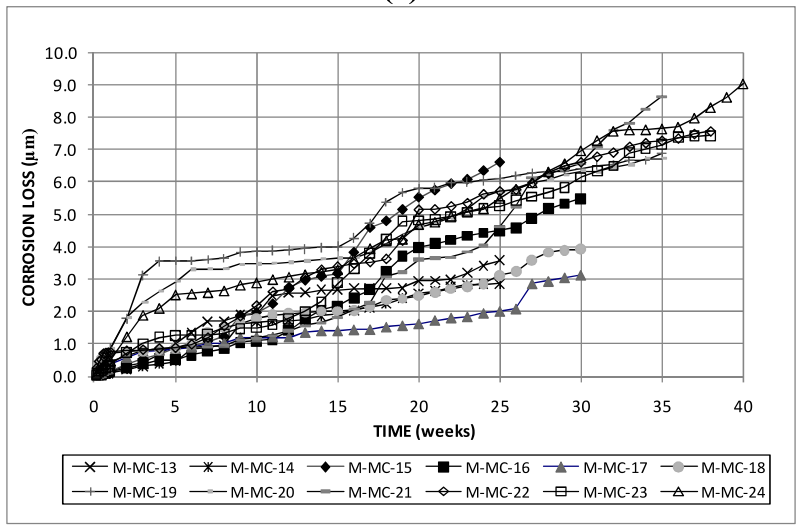

(b)

Figure A.62: Rapid macrocell test, MC. Corrosion loss for (a) specimens 1-12 (b) specimens 13-24.

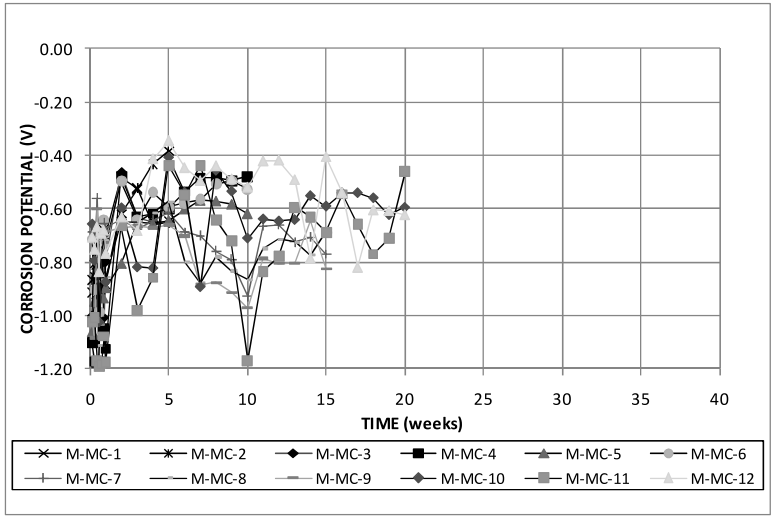

(a)

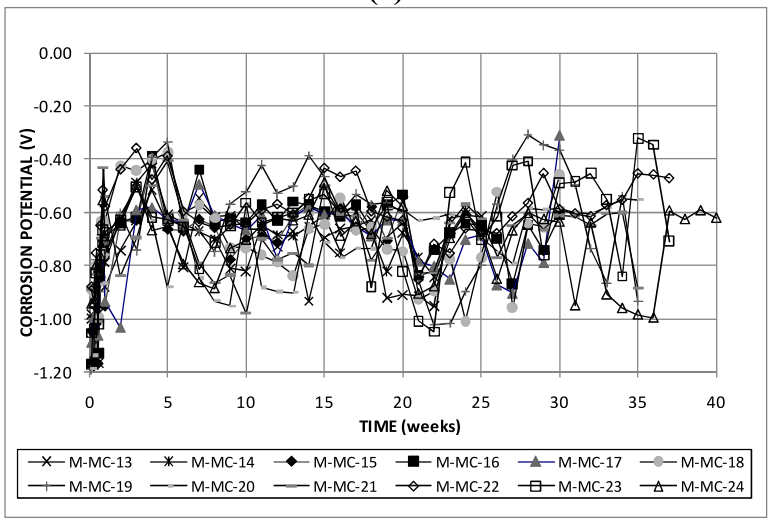

(b)

Figure A.63: Rapid macrocell test, MC. Anode potential for (a) specimens 1-12 (b) specimens 13-24.

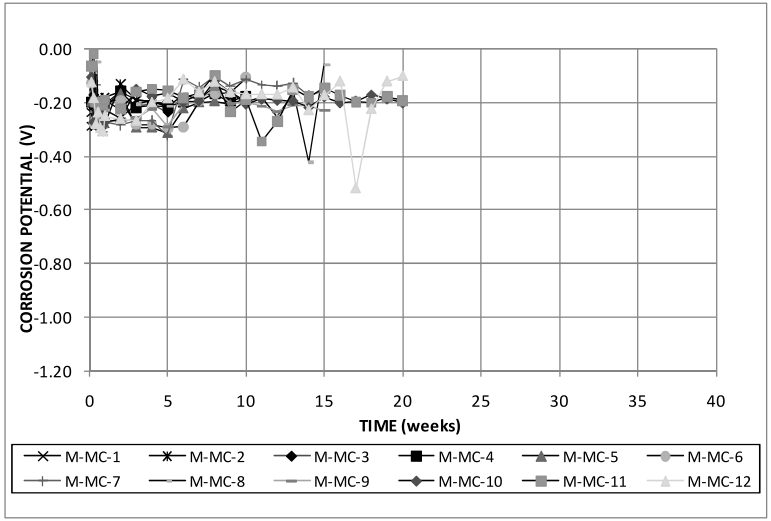

(a)

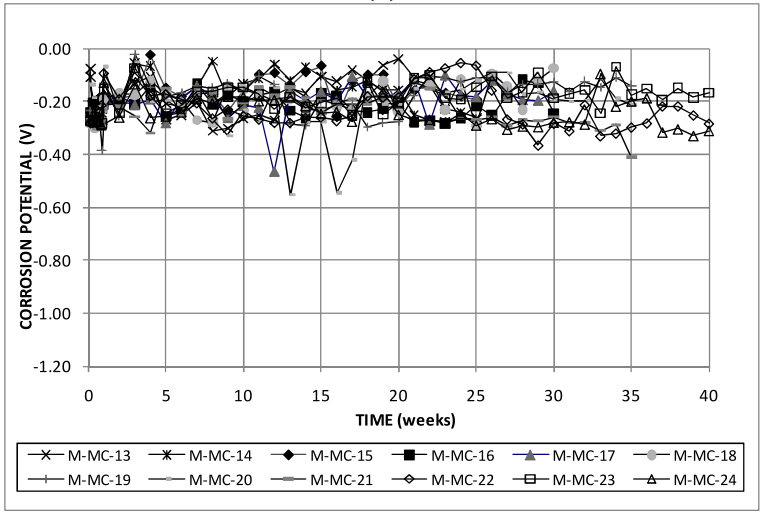

(b)

Figure A.64: Rapid macrocell test, MC. Cathode potential for (a) specimens 1-12 (b) specimens 13-24.

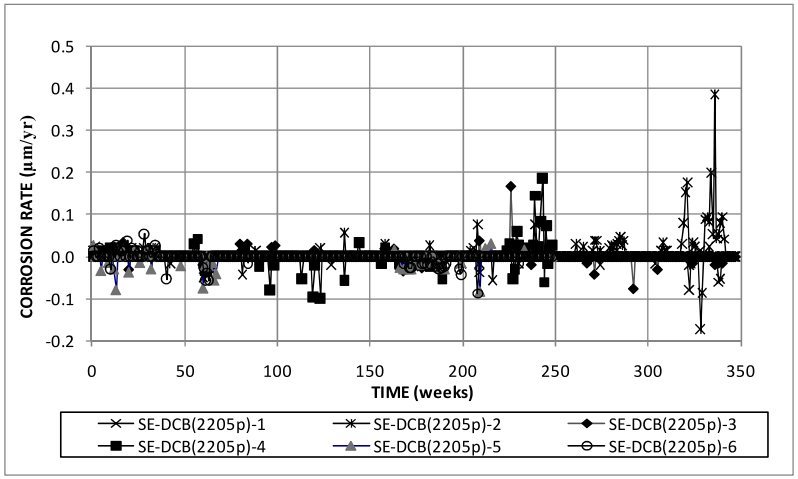

(a)

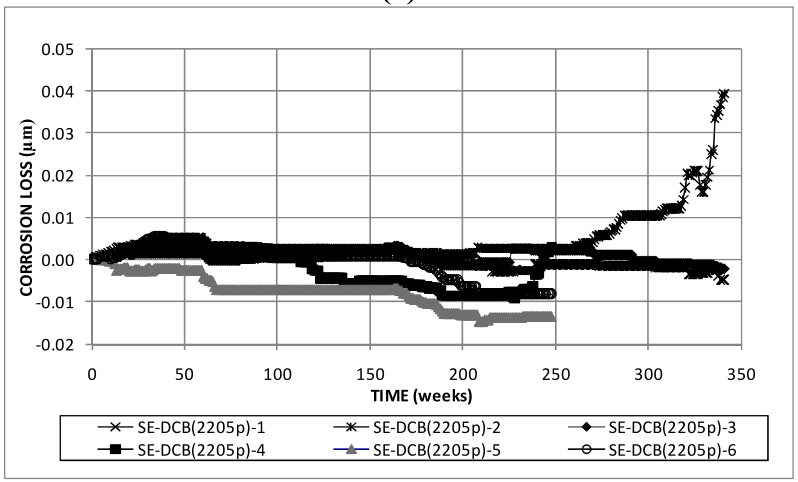

(b)

Figure A.65: (a) Corrosion rate and (b) corrosion losses for Southern Exposure DCB specimens with 2205p reinforcement.

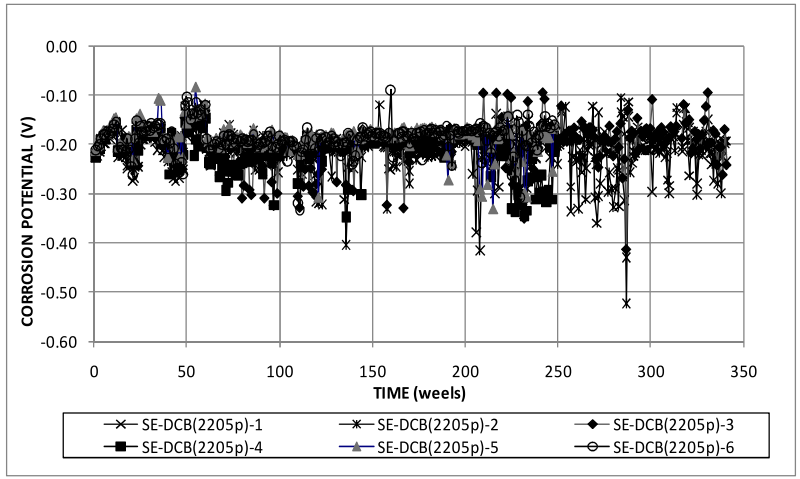

(a)

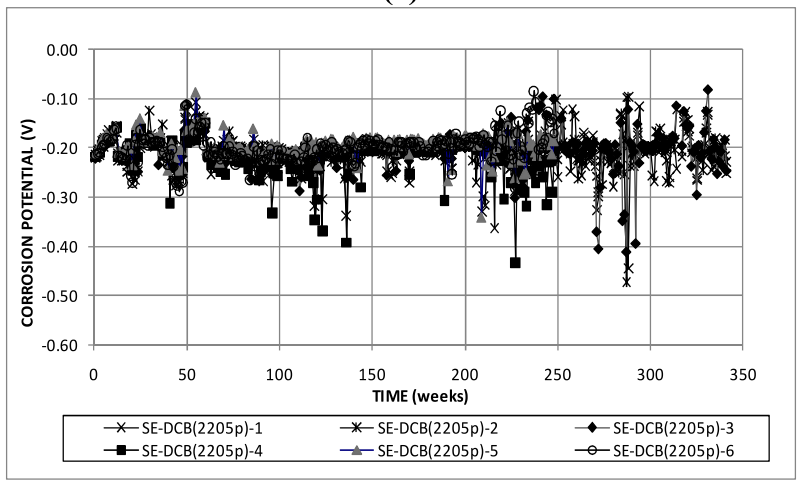

(b)

Figure A.66: (a) Top mat corrosion potentials and (b) bottom mat corrosion potentials for Southern Exposure DCB specimens with 2205p reinforcement.

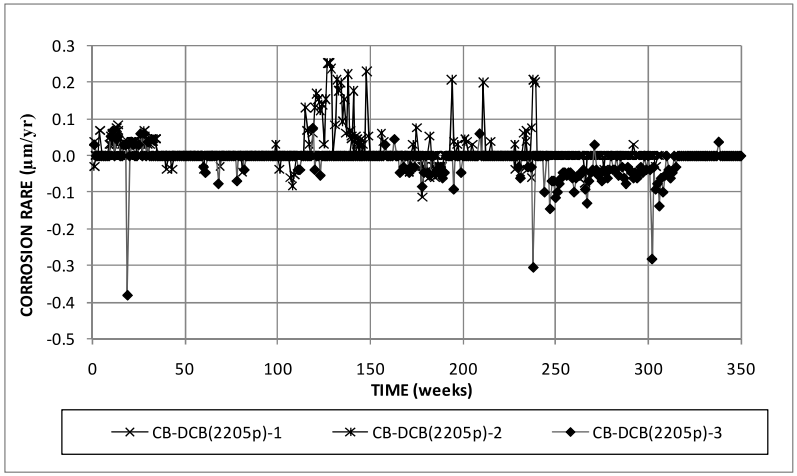

(a)

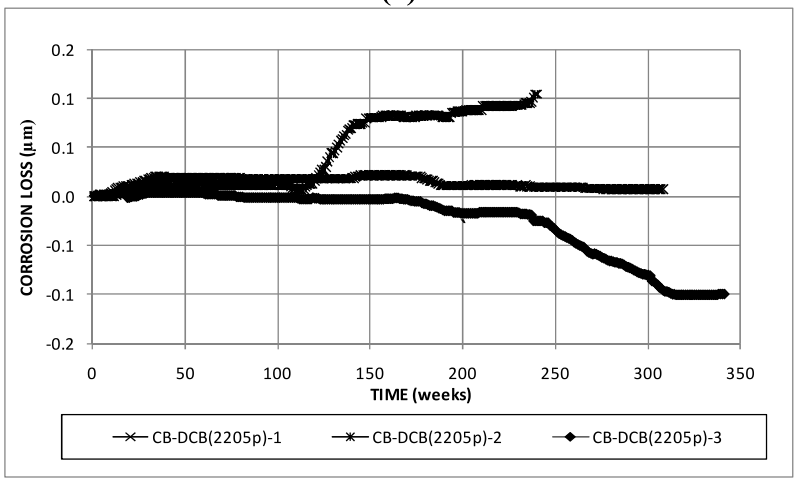

(b)

Figure A.67: (a) Corrosion rate and (b) corrosion losses for cracked beam DCB specimens with 2205p reinforcement.

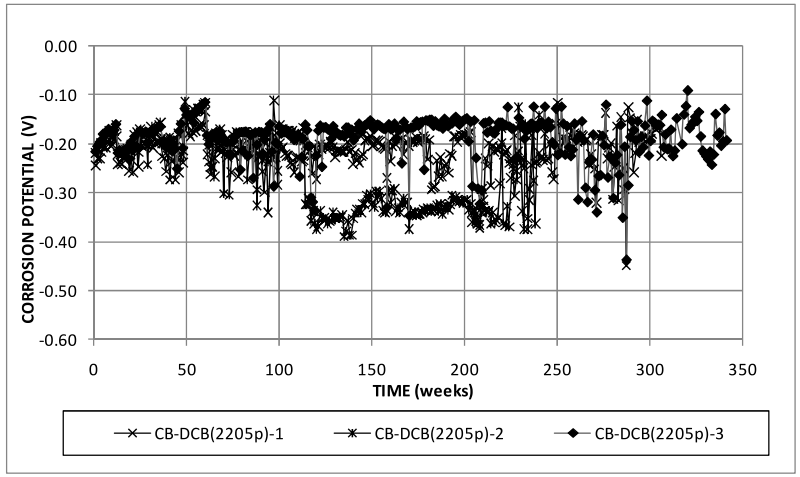

(a)

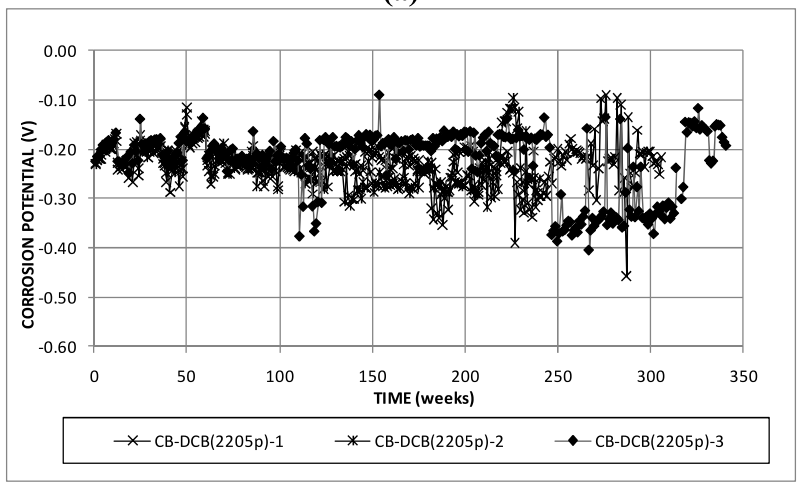

(b)

Figure A.68: (a) Top mat corrosion potentials and (b) bottom mat corrosion potentials for cracked beam DCB specimens with 2205p reinforcement.

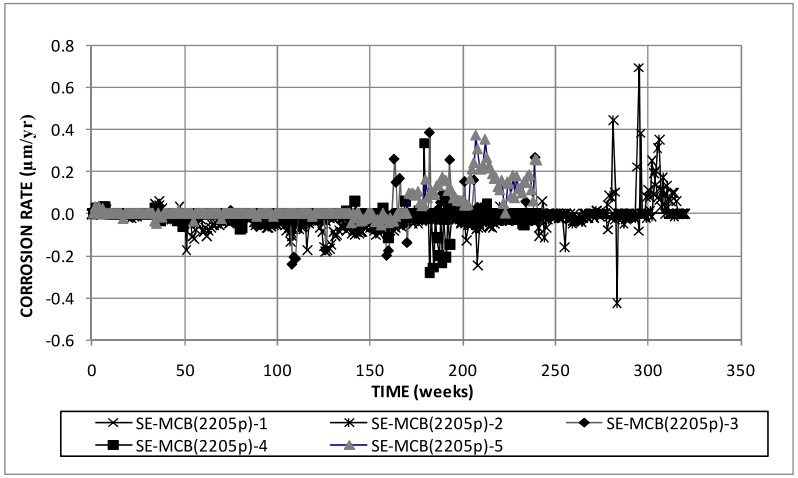

(a)

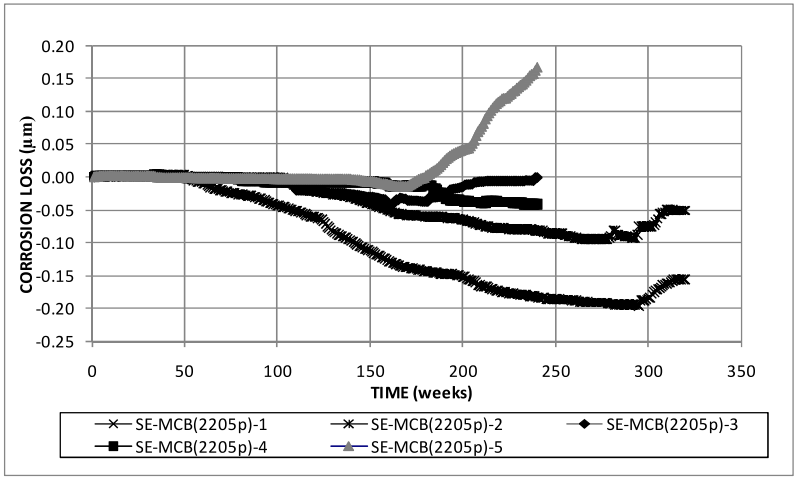

(b)

Figure A.69: (a) Corrosion rate and (b) corrosion losses for Southern Exposure MCB specimens with 2205p reinforcement.

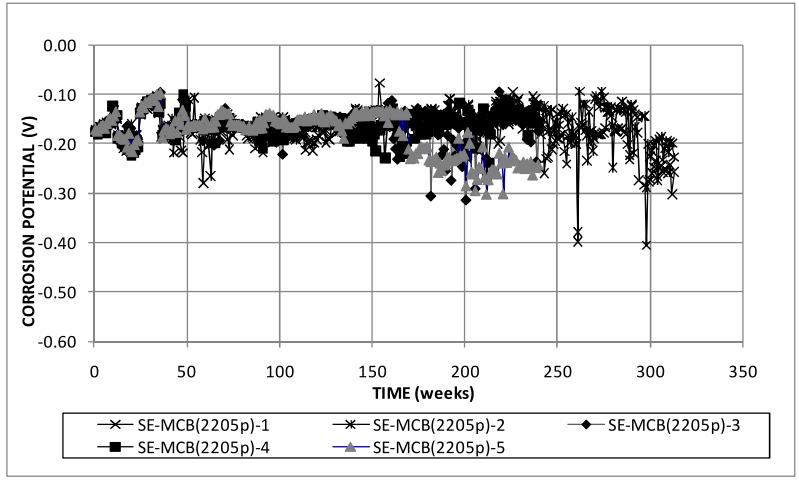

(a)

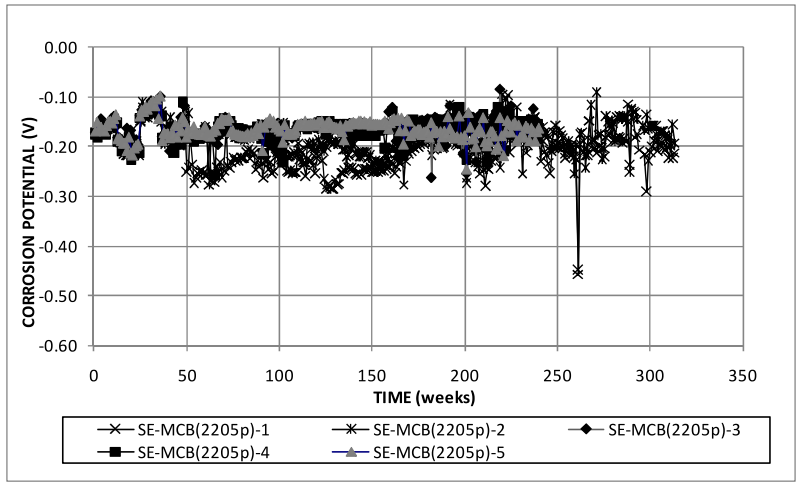

(b)

Figure A.70: (a) Top mat corrosion potentials and (b) bottom mat corrosion potentials for Southern Exposure MCB specimens with 2205p reinforcement.

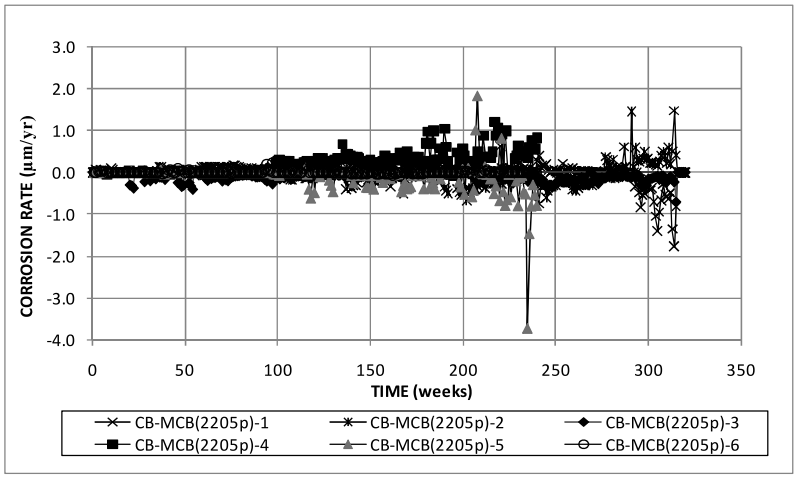

(a)

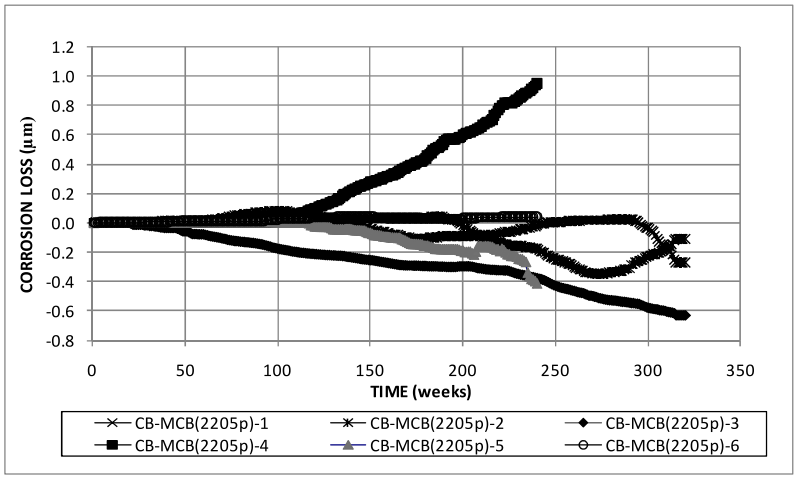

(b)

Figure A.71: (a) Corrosion rate and (b) corrosion losses for cracked beam MCB specimens with 2205p reinforcement.

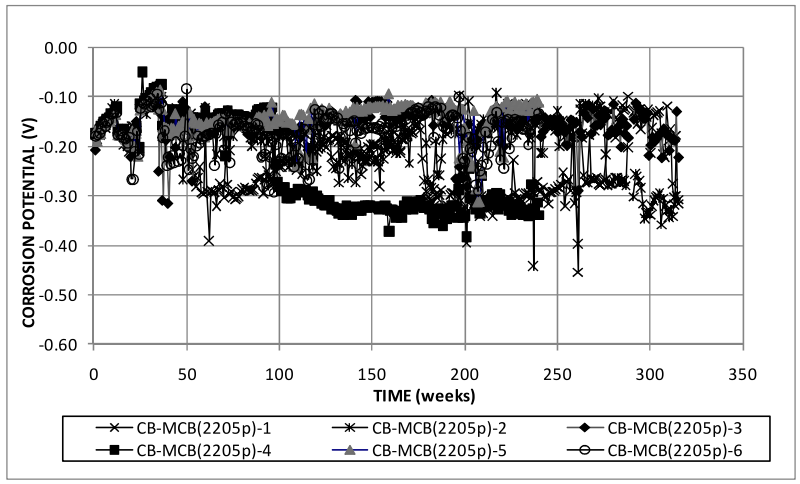

(a)

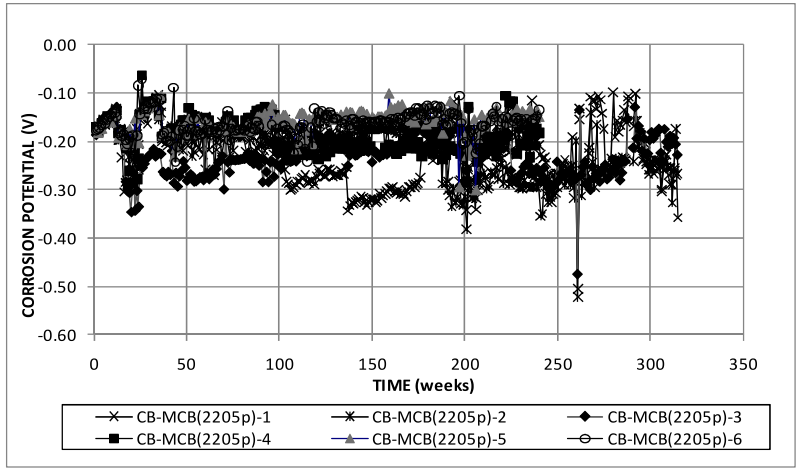

(b)

Figure A.72: (a) Top mat corrosion potentials and (b) bottom mat corrosion potentials for cracked beam MCB specimens with 2205p reinforcement.

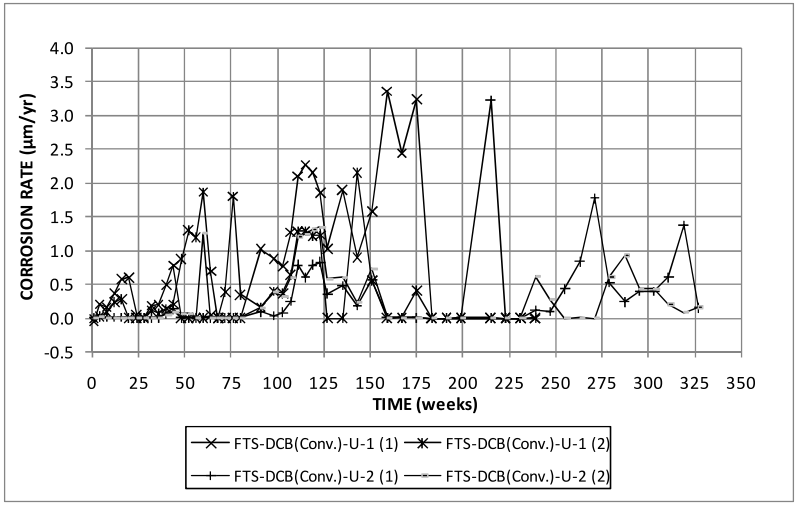

(a)

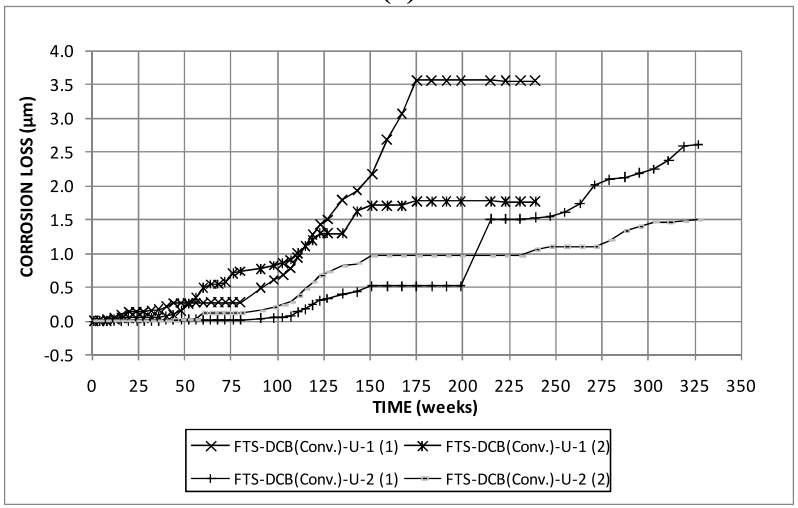

(b)

Figure A.73: (a) Corrosion rate and (b) corrosion losses for field test DCB specimens with conventional reinforcement.

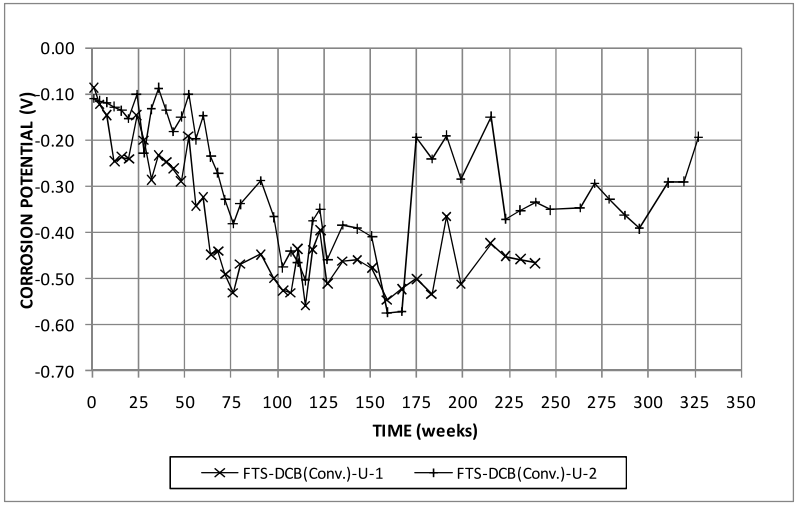

(a)

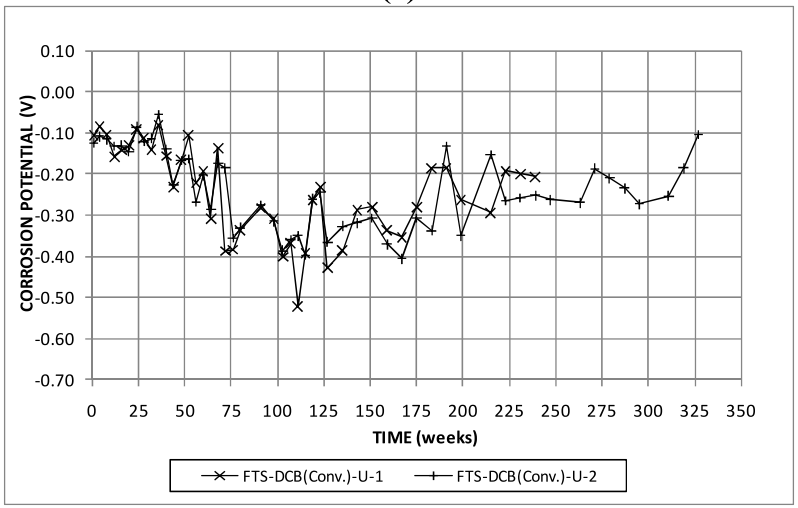

(b)

Figure A.74: (a) Top mat corrosion potentials and (b) bottom mat corrosion potentials for field test DCB specimens with conventional reinforcement.

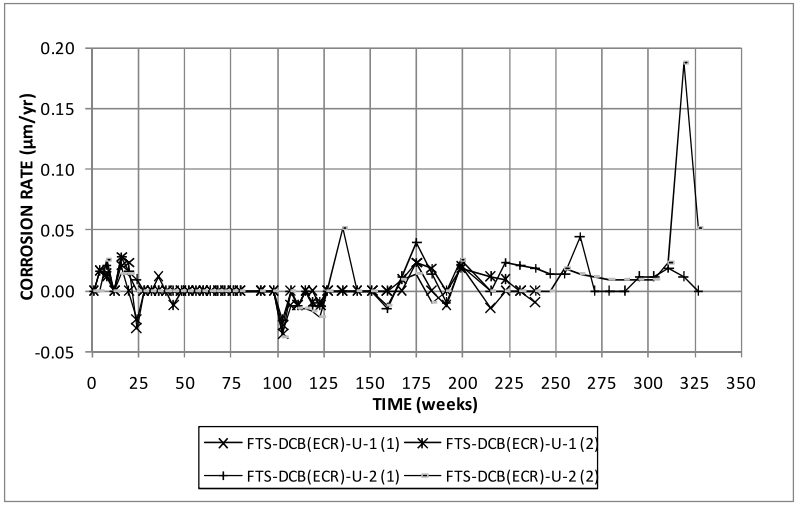

(a)

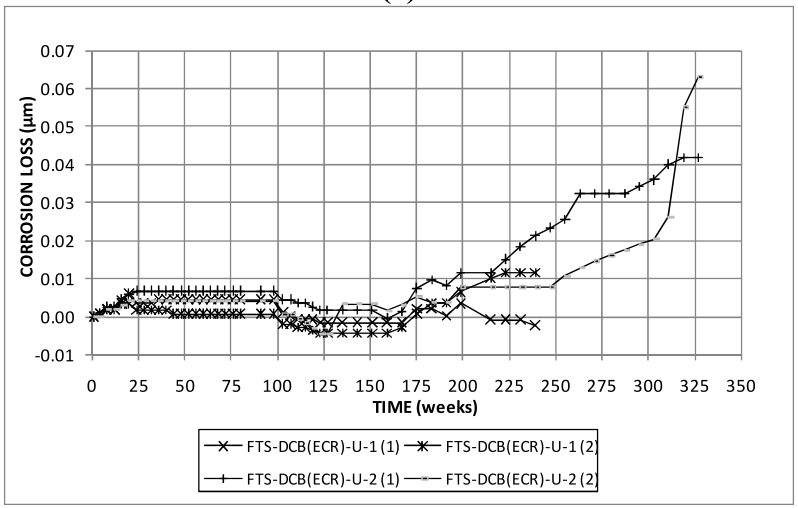

(b)

Figure A.75: (a) Corrosion rate and (b) corrosion losses for field test DCB specimens with ECR.

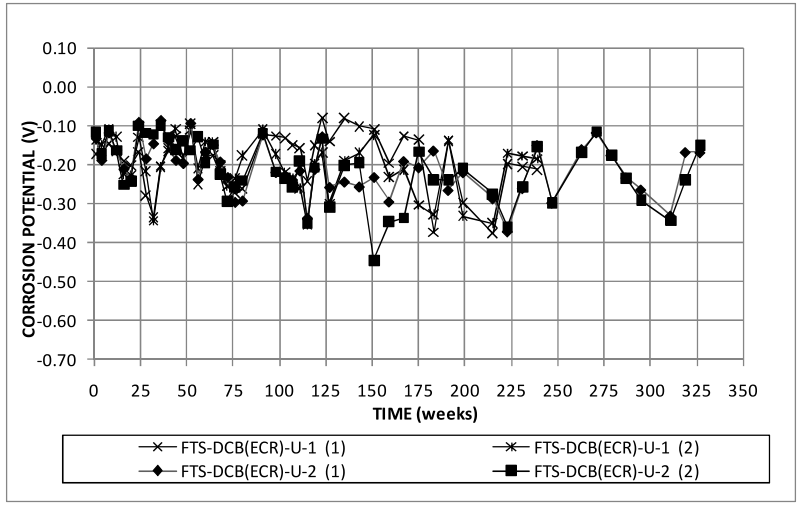

(a)

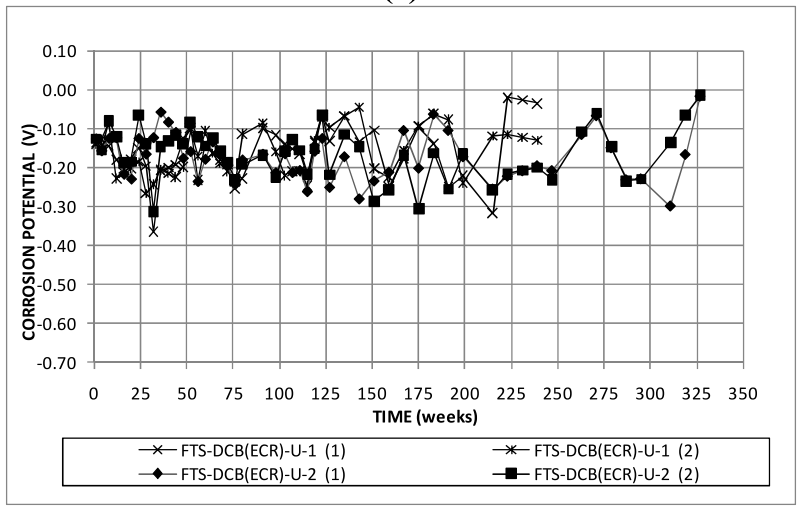

(b)

Figure A.76: (a) Top mat corrosion potentials and (b) bottom mat corrosion potentials for field test DCB specimens with ECR.

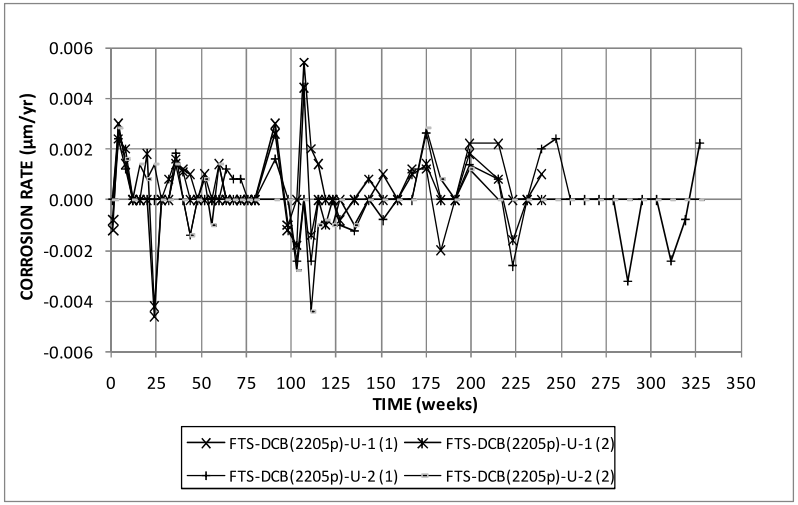

(a)

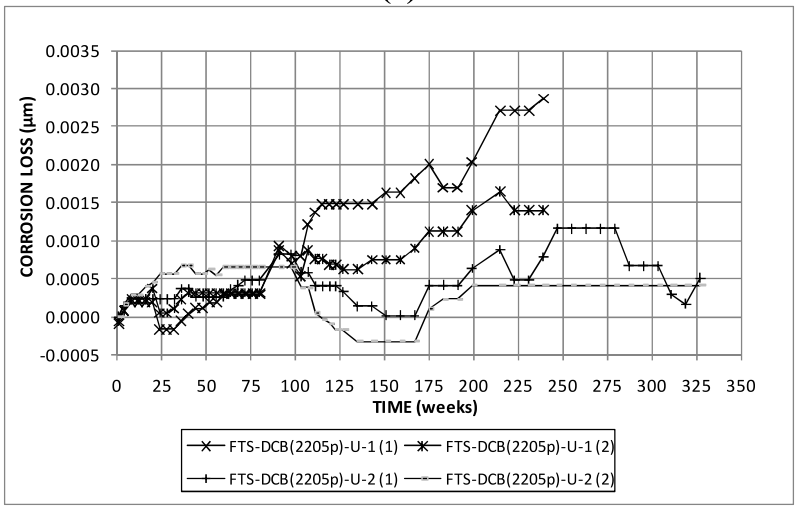

(b)

Figure A.77: (a) Corrosion rate and (b) corrosion losses for field test DCB specimens with 2205p reinforcement.

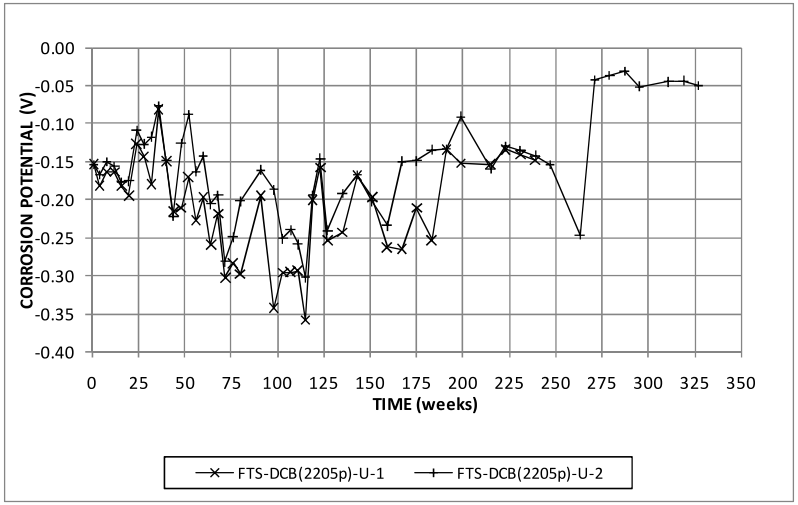

(a)

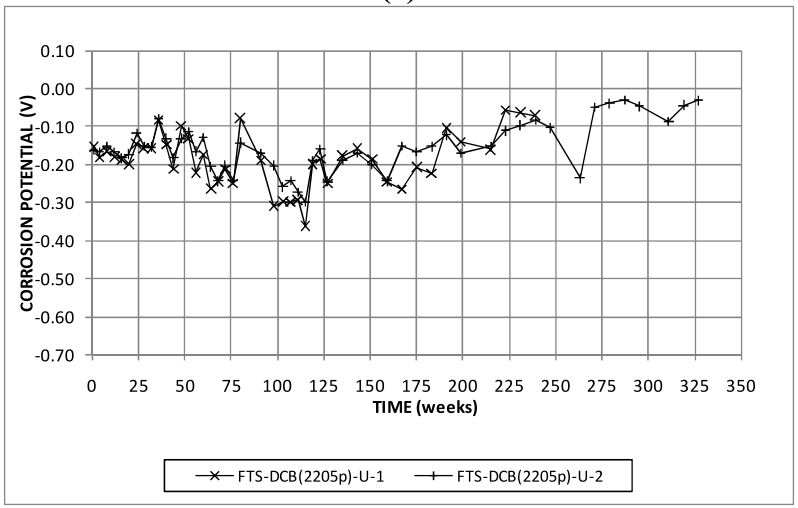

(b)

Figure A.78: (a) Top mat corrosion potentials and (b) bottom mat corrosion potentials for field test DCB specimens with 2205p reinforcement.

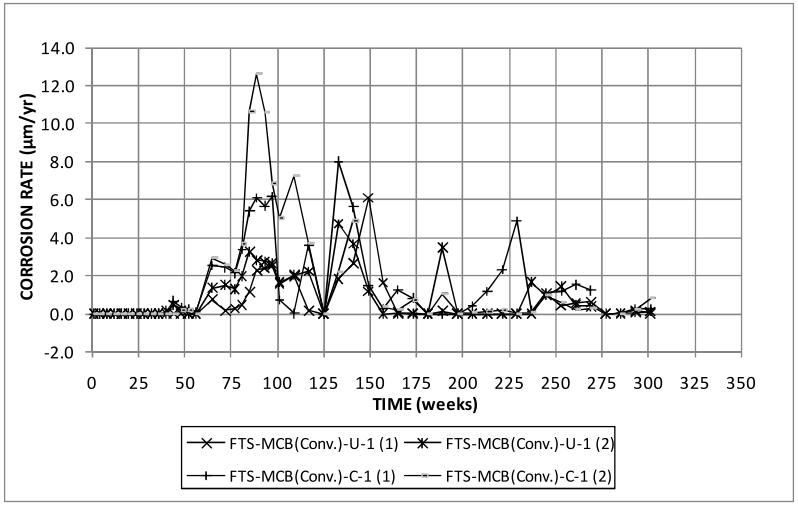

(a)

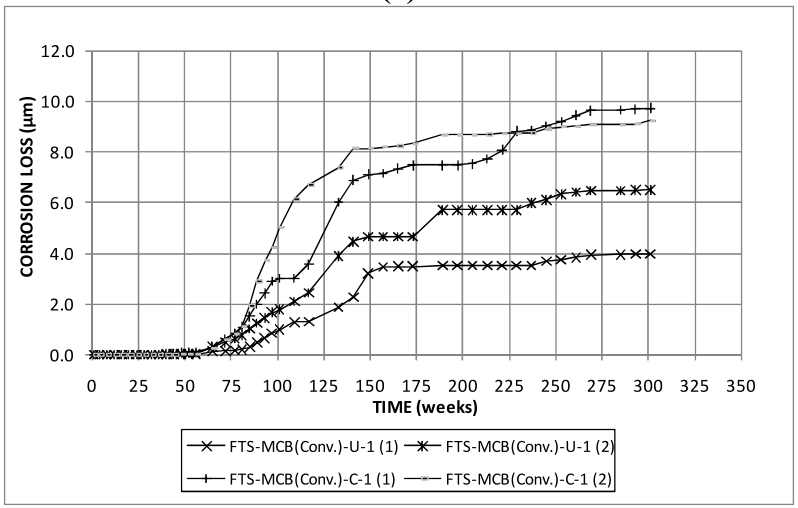

(b)

Figure A.79: (a) Corrosion rate and (b) corrosion losses for field test MCB specimens with conventional reinforcement.

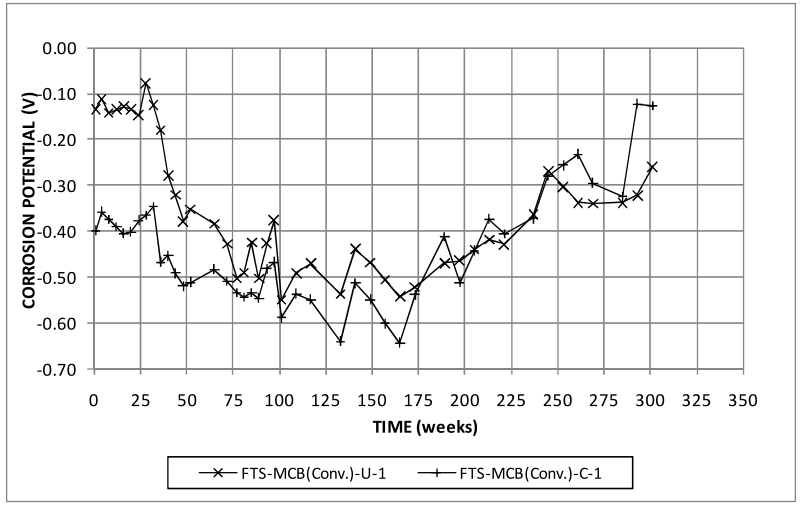

(a)

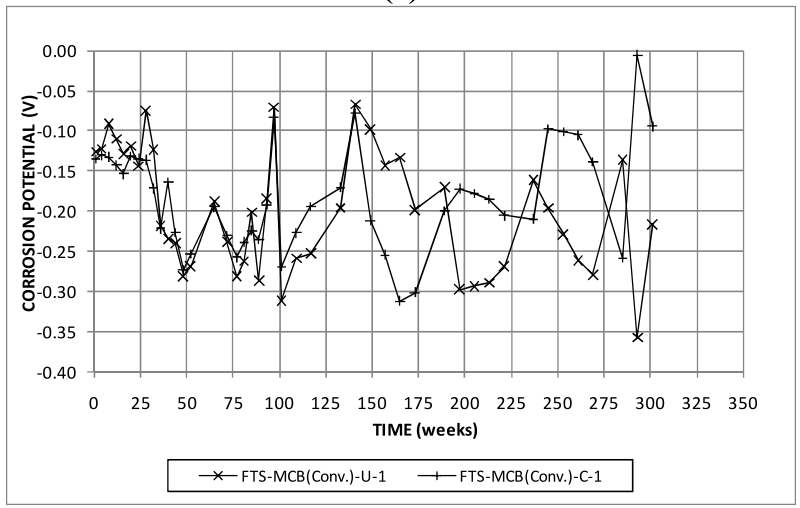

(b)

Figure A.80: (a) Top mat corrosion potentials and (b) bottom mat corrosion potentials for field test MCB specimens with conventional reinforcement.

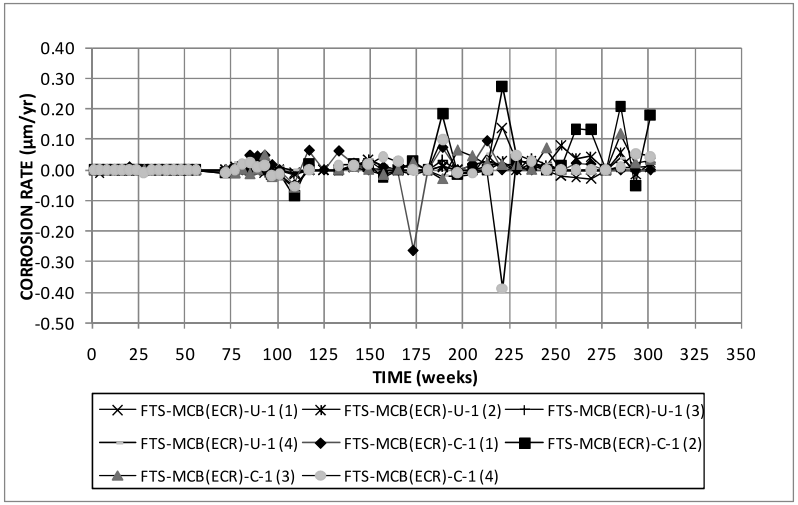

(a)

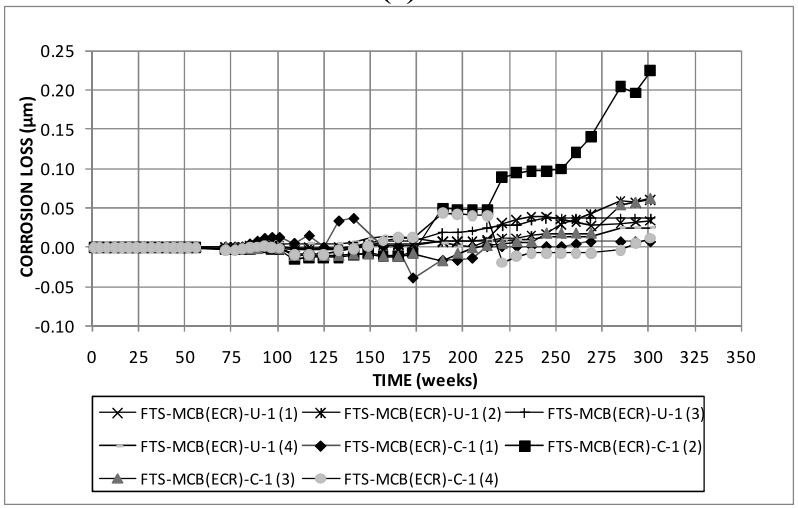

(b)

Figure A.81: (a) Corrosion rate and (b) corrosion losses for field test MCB specimens with ECR.

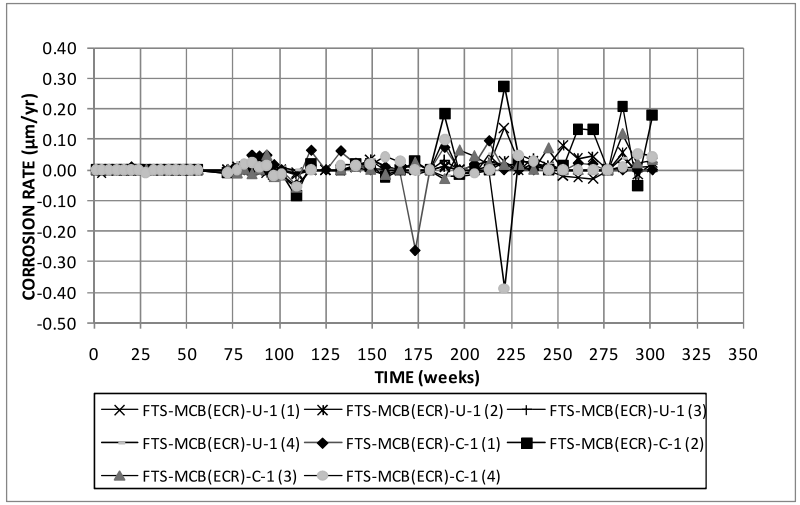

(a)

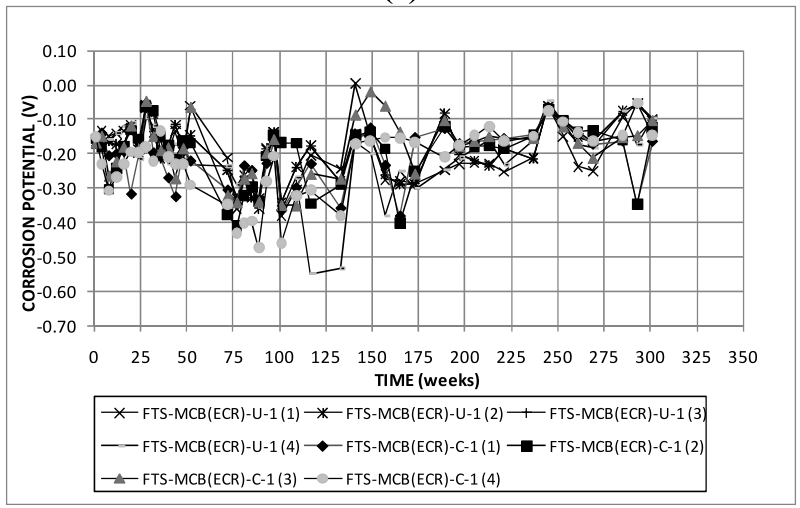

(b)

Figure A.82: (a) Top mat corrosion potentials and (b) bottom mat corrosion potentials for field test MCB specimens with ECR.

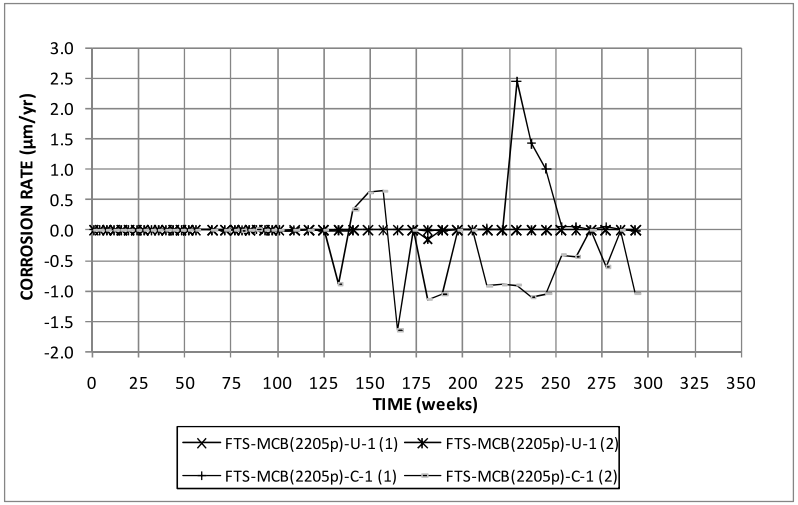

(a)

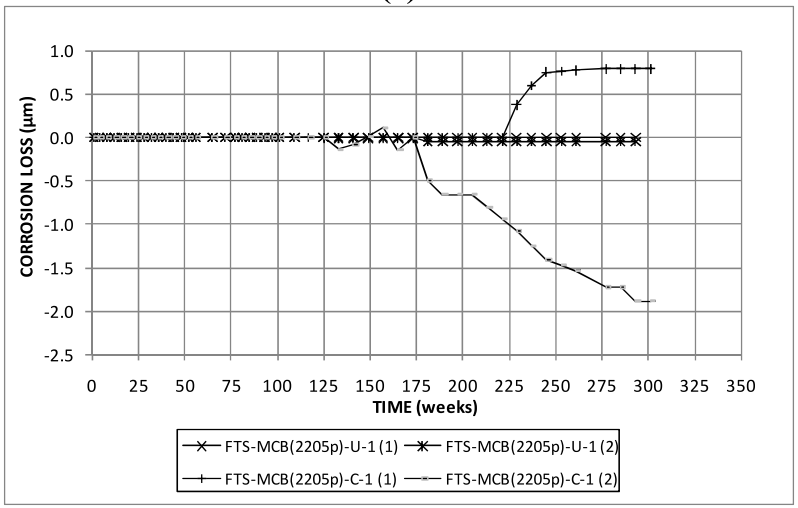

(b)

Figure A.83: (a) Corrosion rate and (b) corrosion losses for field test MCB specimens with 2205p reinforcement.

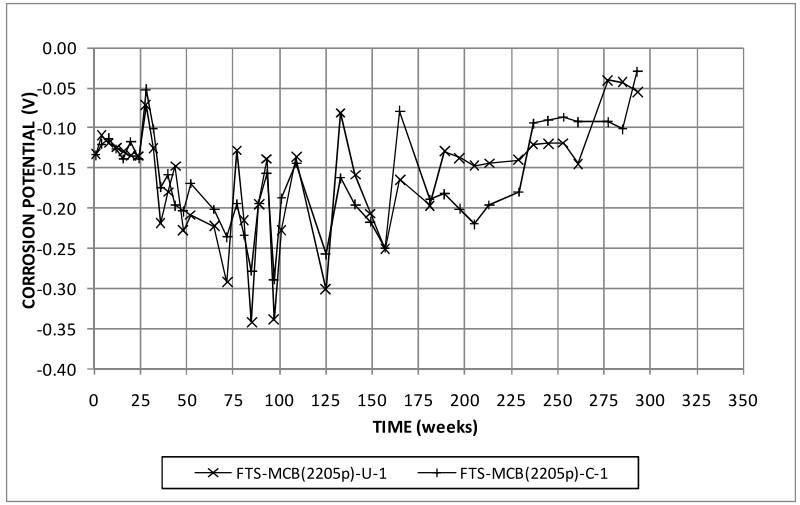

(a)

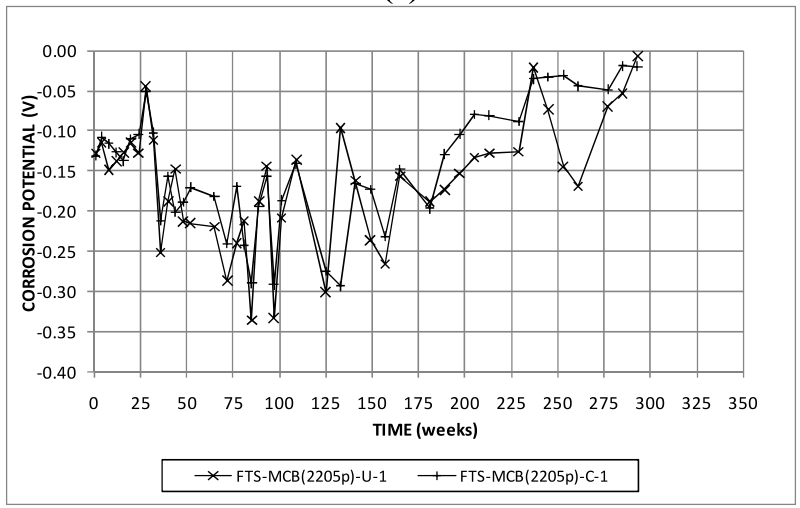

(b)

Figure A.84: (a) Top mat corrosion potentials and (b) bottom mat corrosion potentials for field test MCB specimens with 2205p reinforcement.

APPENDIX B

MAT-TO-MAT RESISTANCE OF LABORATORY SPECIMENS

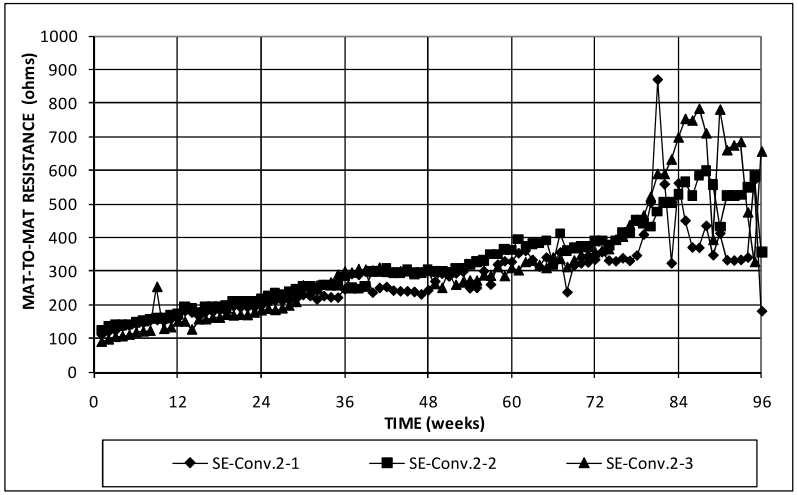

Figure B.1: Mat-to-mat resistance for Southern Exposure specimens with no corrosion inhibitor.

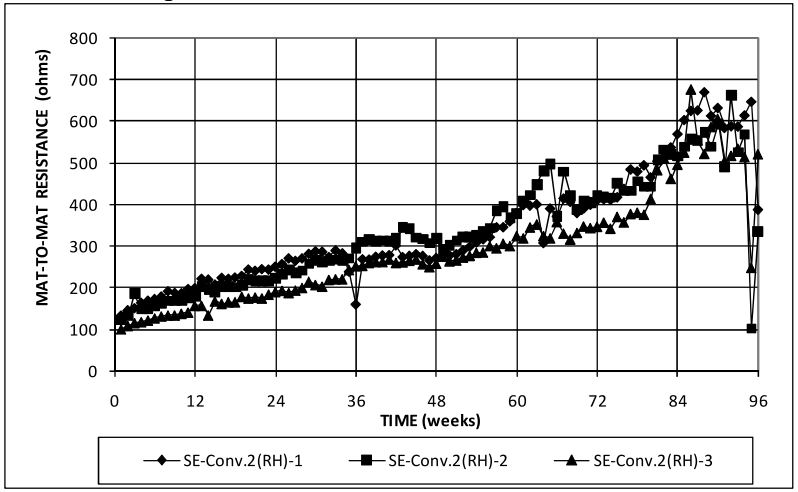

Figure B.2: Mat-to-mat resistance for Southern Exposure specimens containing Rheocrete.

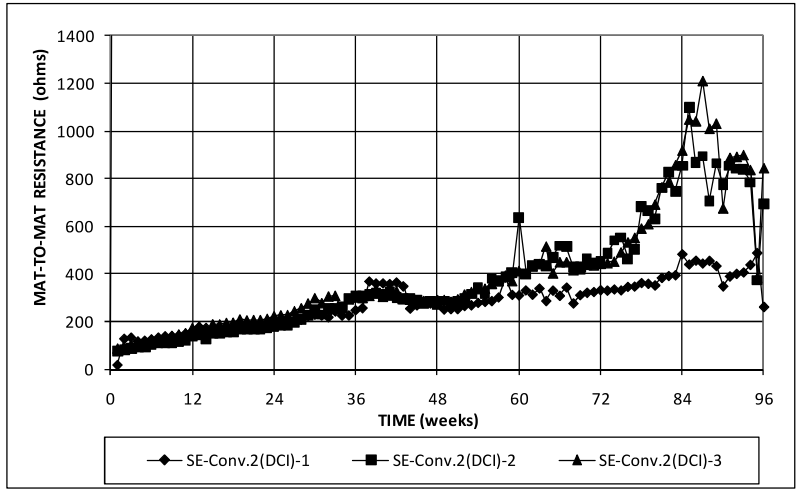

Figure B.3: Mat-to-mat resistance for Southern Exposure specimens containing DCI.

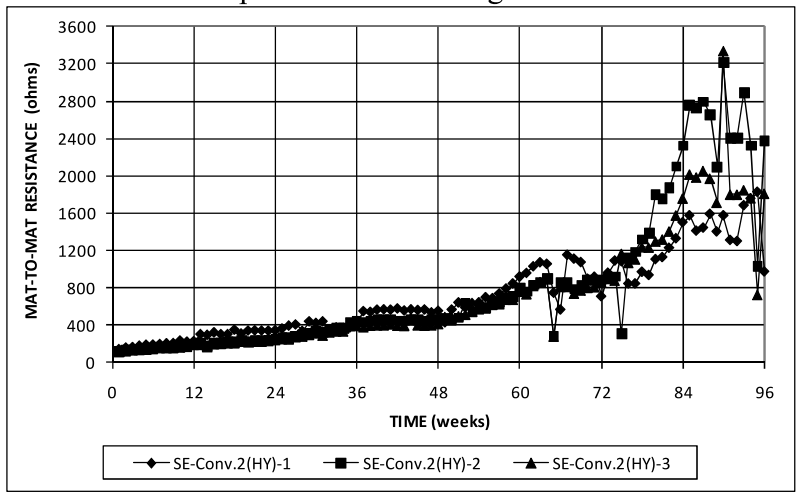

Figure B.4: Mat-to-mat resistance for Southern Exposure specimens containing Hycrete.

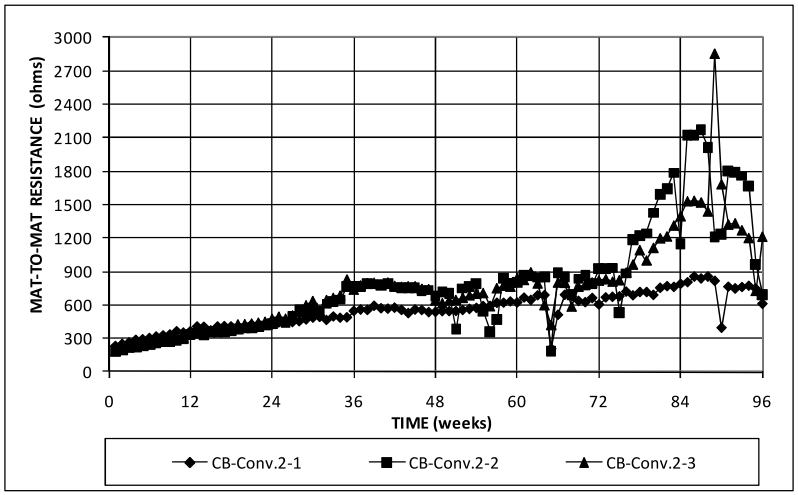

Figure B.5: Mat-to-mat resistance for cracked beam specimens with no corrosion inhibitor.

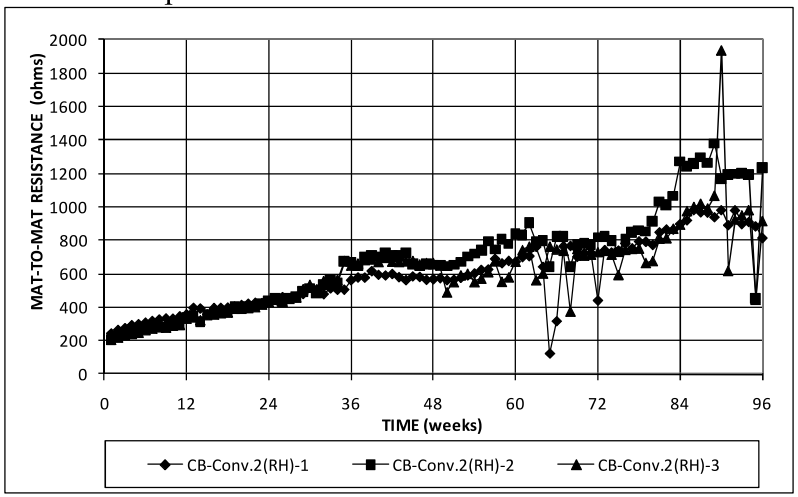

Figure B.6: Mat-to-mat resistance for cracked beam specimens containing Rheocrete.

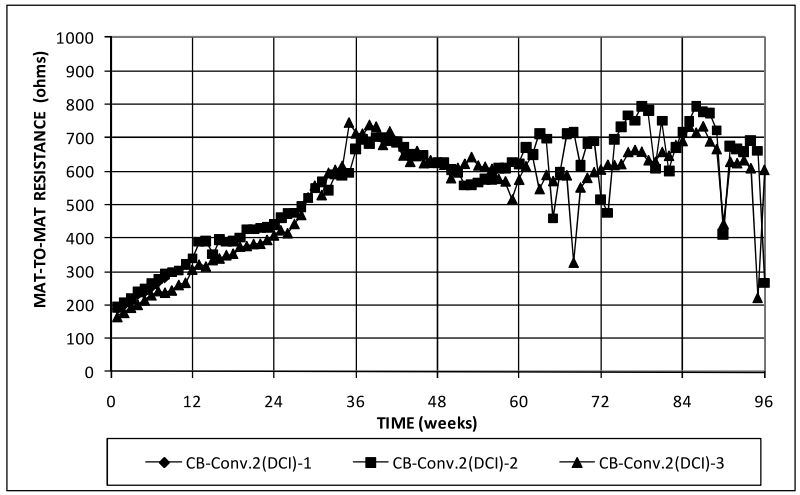

Figure B.7: Mat-to-mat resistance for cracked beam specimens containing DCI.

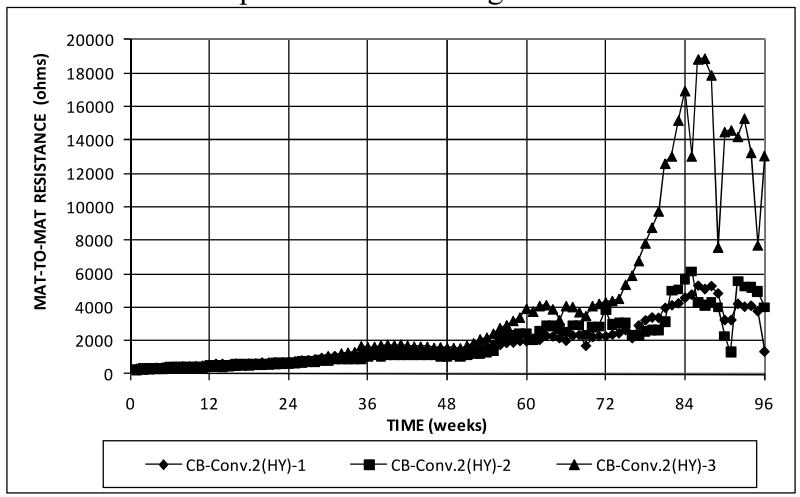

Figure B.8: Mat-to-mat resistance for cracked beam specimens containing Hycrete.

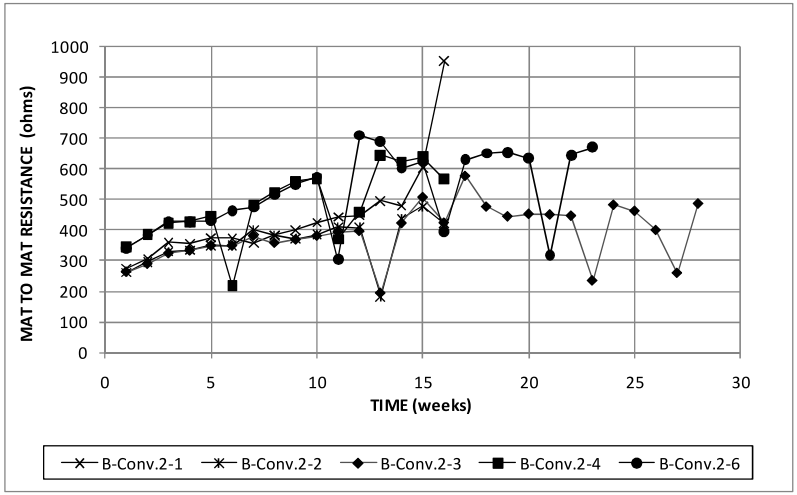

Figure B.9: Mat-to-mat resistance for corrosion initiation beam specimens containing no corrosion inhibitor.

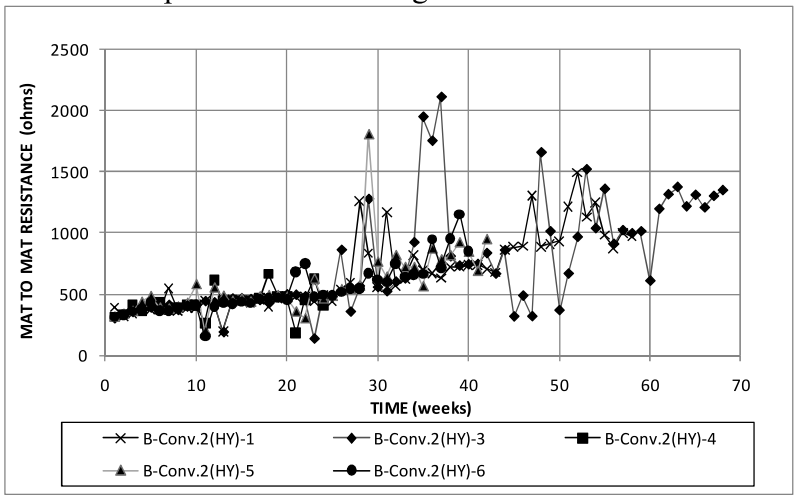

Figure B.10: Mat-to-mat resistance for corrosion initiation beam specimens containing Hycrete.

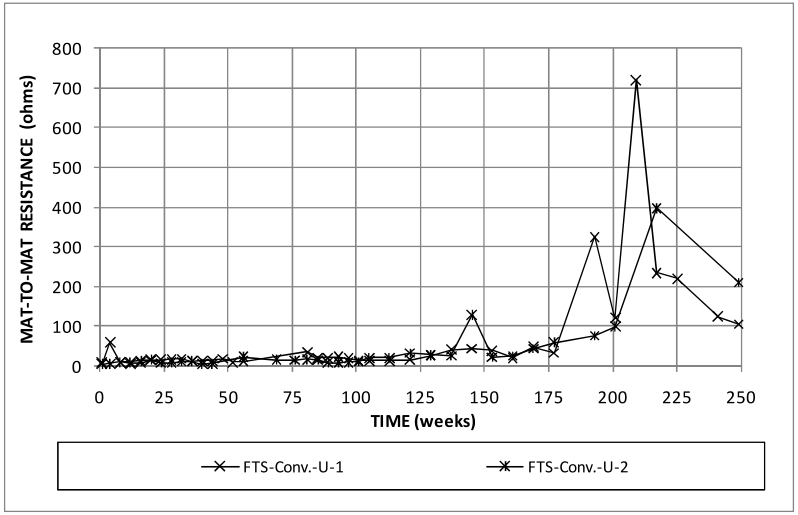

Figure B.11: Mat-to-mat resistance for field test specimens with conventional reinforcement in uncracked concrete.

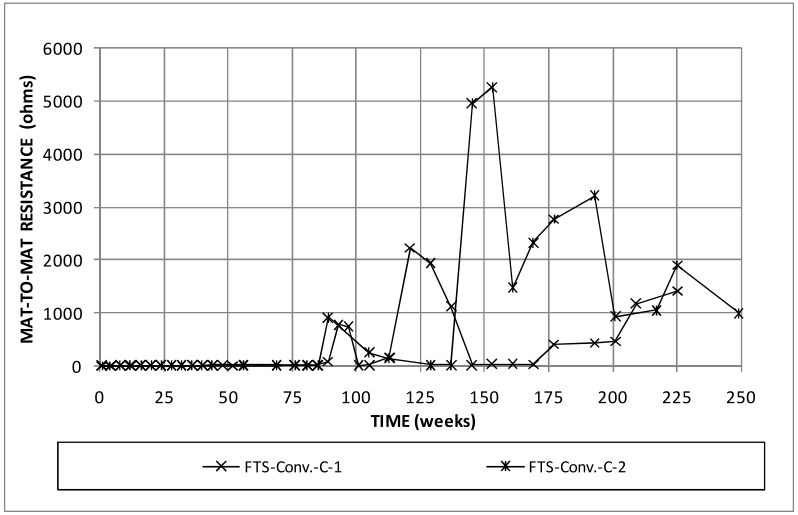

Figure B.12: Mat-to-mat resistance for field test specimens with conventional reinforcement in cracked concrete.

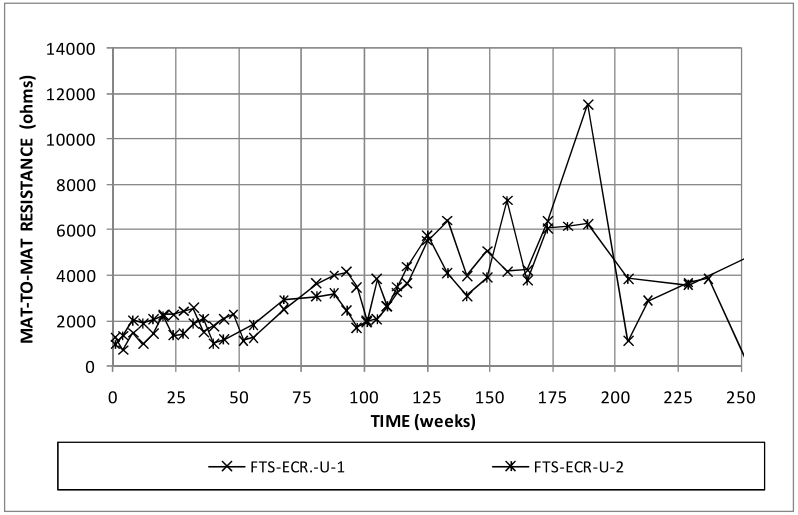

Figure B.13: Mat-to-mat resistance for field test specimens with ECR in uncracked concrete.

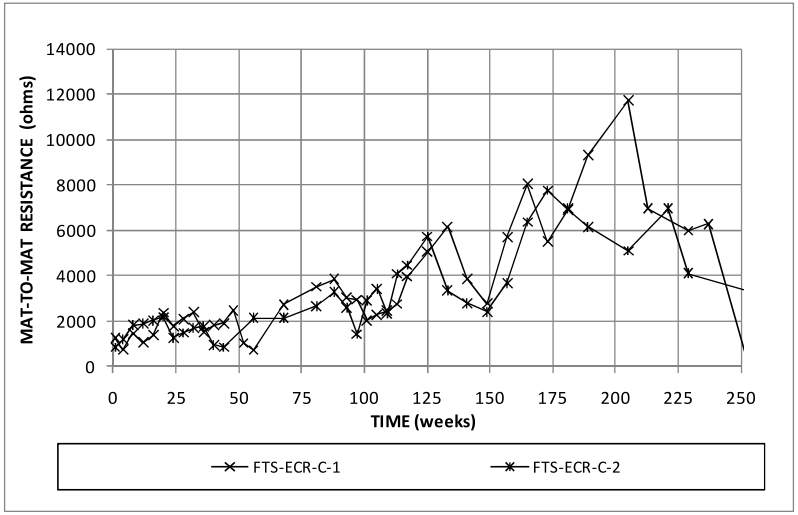

Figure B.14: Mat-to-mat resistance for field test specimens with ECR in cracked concrete.

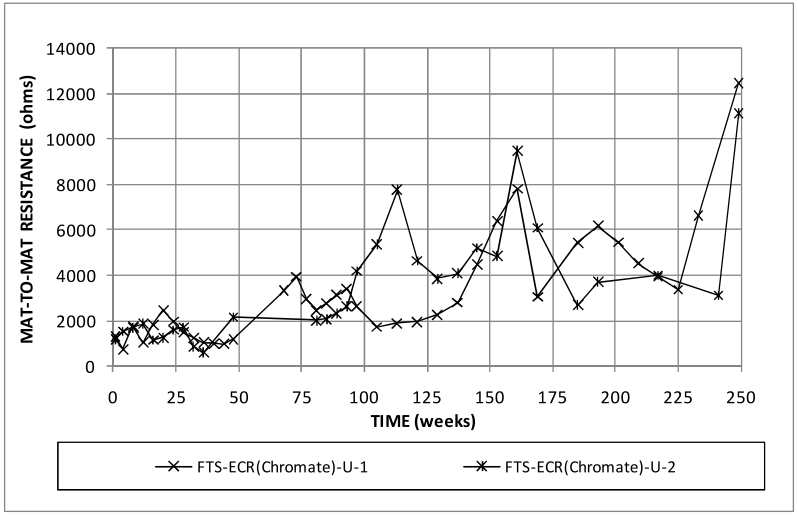

Figure B.15: Mat-to-mat resistance for field test specimens with ECR with chromate pretreatment in uncracked concrete.

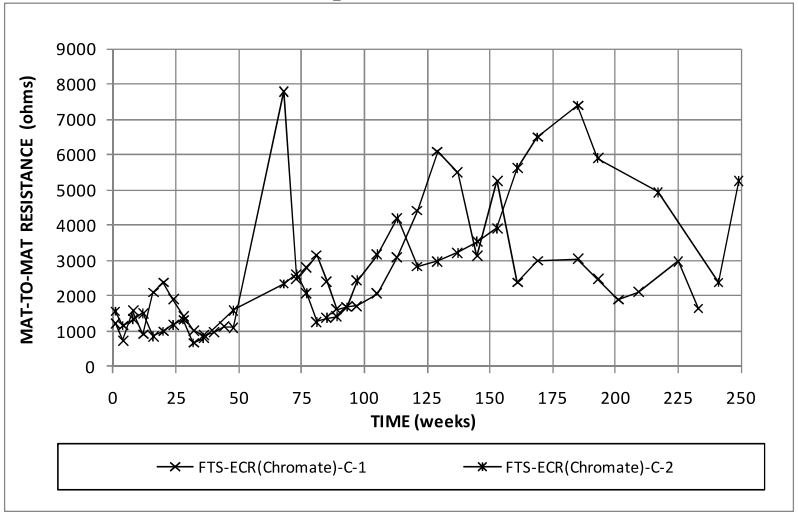

Figure B.16: Mat-to-mat resistance for field test specimens with ECR with chromate pretreatment in cracked concrete.

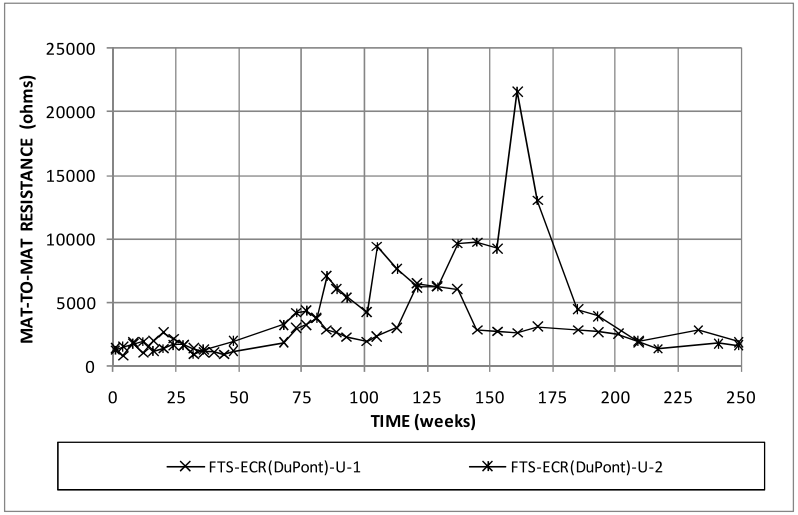

Figure B.17: Mat-to-mat resistance for field test specimens with ECR from DuPont in uncracked concrete.

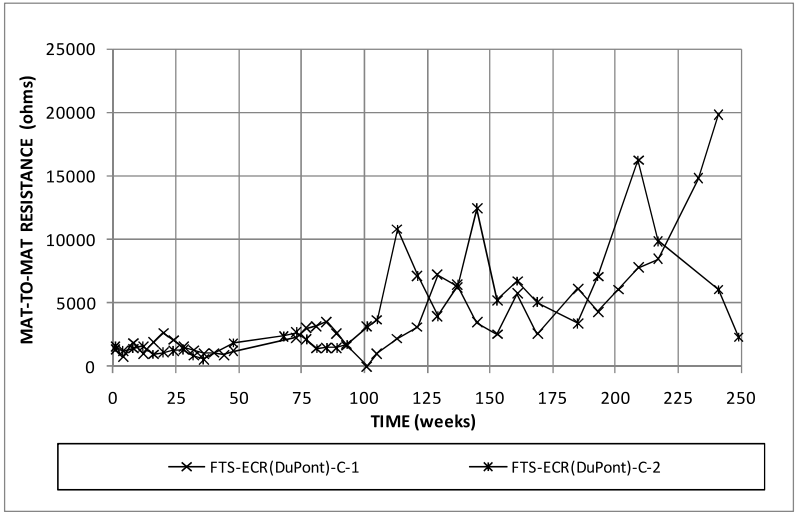

Figure B.18: Mat-to-mat resistance for field test specimens with ECR from DuPont in cracked concrete.

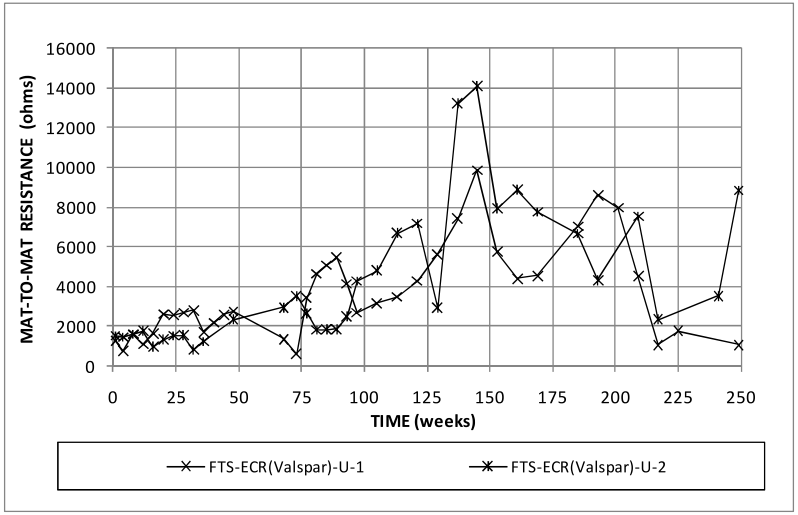

Figure B.19: Mat-to-mat resistance for field test specimens with ECR from Valspar in uncracked concrete.

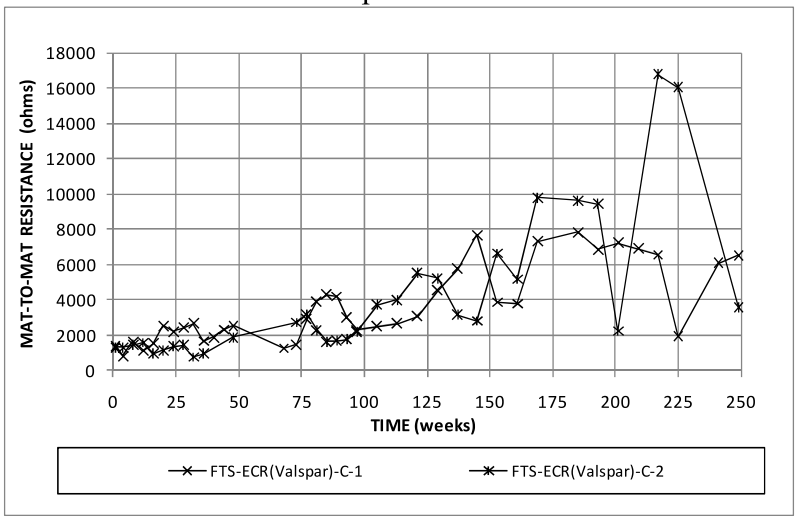

Figure B.20: Mat-to-mat resistance for field test specimens with ECR from Valspar in cracked concrete.

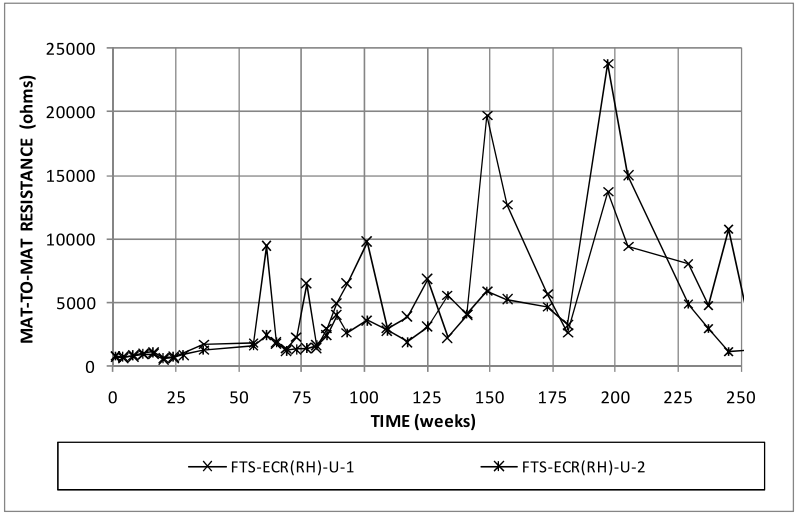

Figure B.21: Mat-to-mat resistance for field test specimens with ECR in uncracked concrete containing Rheocrete.

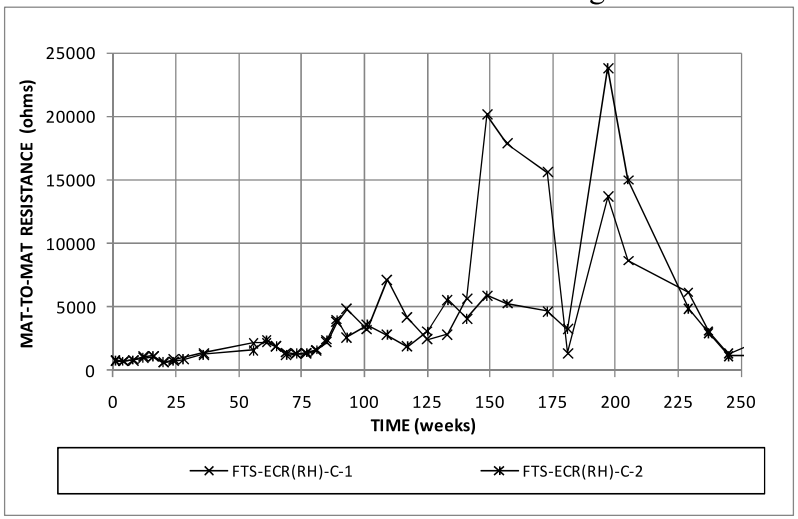

Figure B.22: Mat-to-mat resistance for field test specimens with ECR in cracked concrete containing Rheocrete.

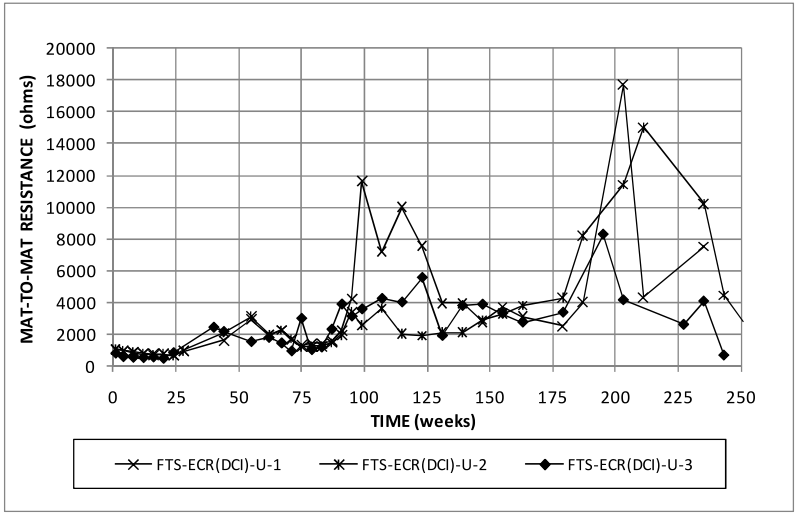

Figure B.23: Mat-to-mat resistance for field test specimens with ECR in uncracked concrete containing DCI.

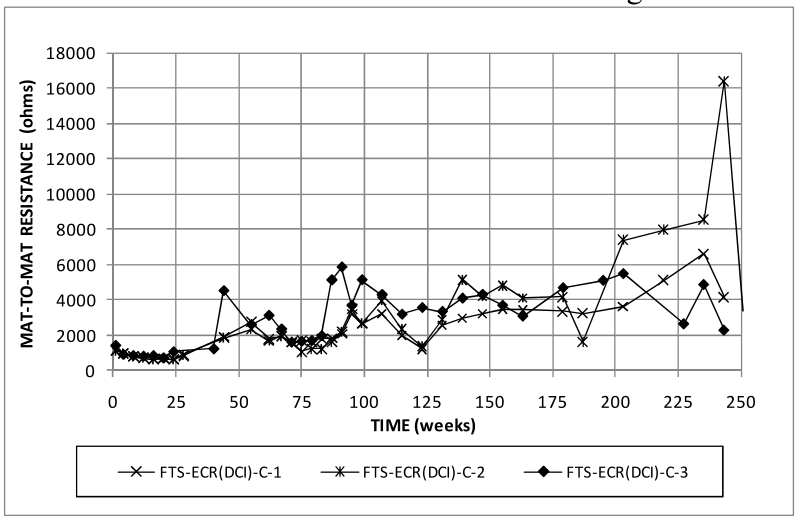

Figure B.24: Mat-to-mat resistance for field test specimens with ECR in cracked concrete containing DCI.

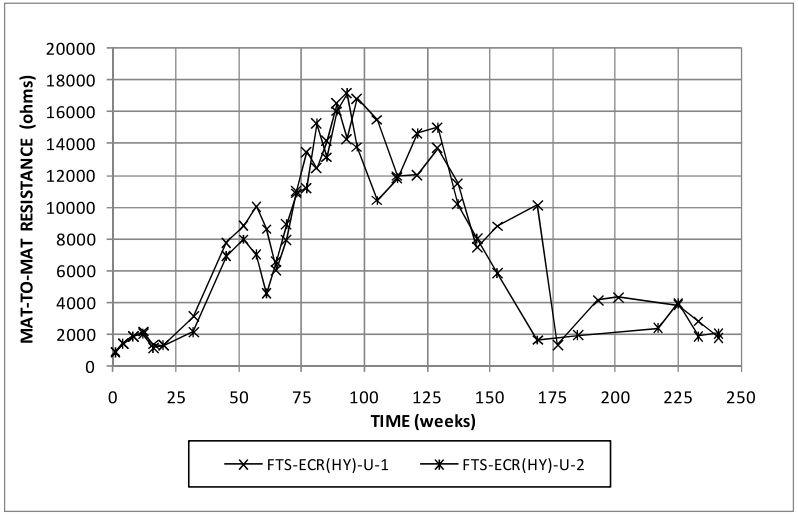

Figure B.25: Mat-to-mat resistance for field test specimens with ECR in uncracked concrete containing Hycrete.

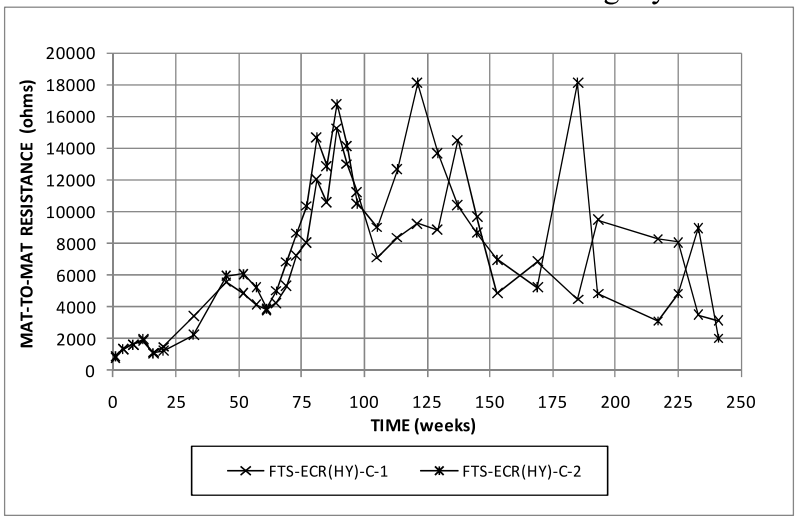

Figure B.26: Mat-to-mat resistance for field test specimens with ECR in cracked concrete containing Hycrete.

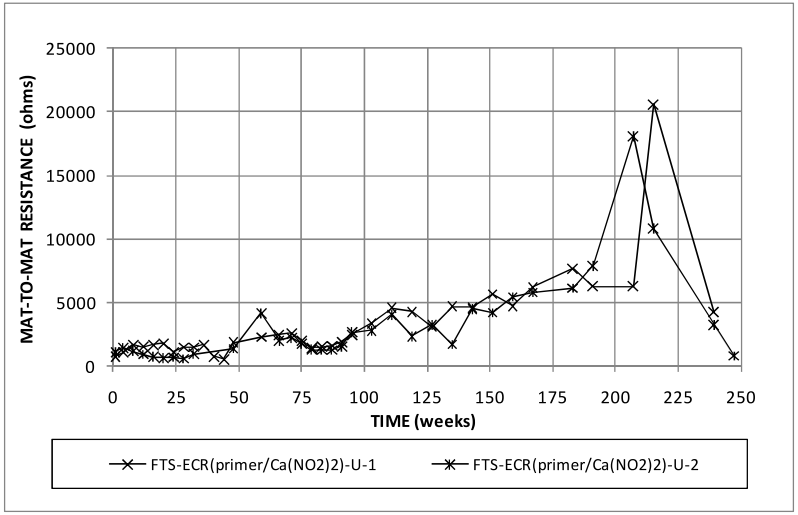

Figure B.27: Mat-to-mat resistance for field test specimens with ECR with calcium nitrite primer in uncracked concrete.

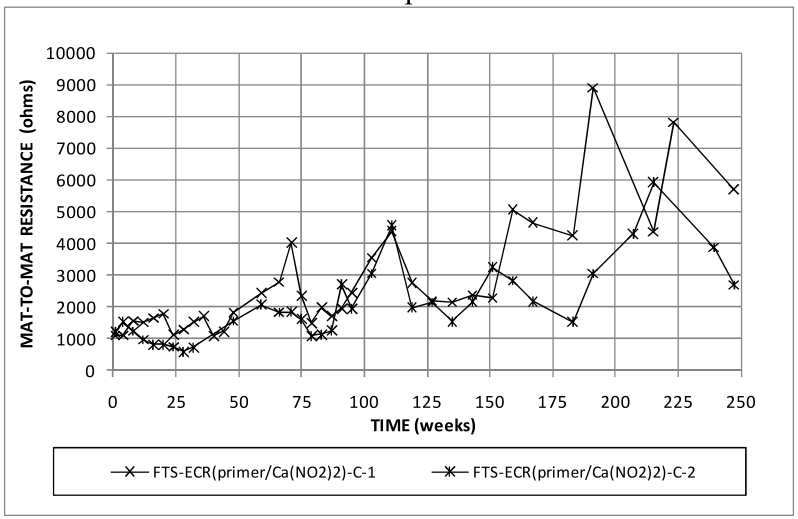

Figure B.28: Mat-to-mat resistance for field test specimens with ECR with calcium nitrite primer in cracked concrete.

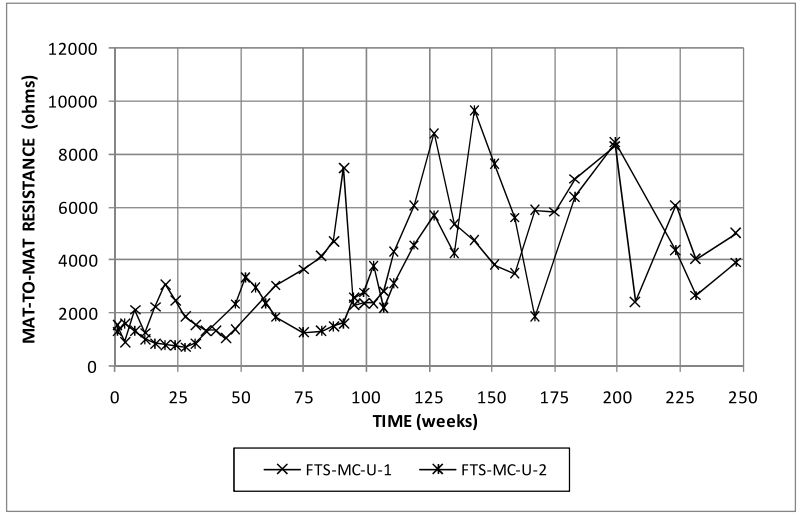

Figure B.29: Mat-to-mat resistance for field test specimens with MC reinforcement in uncracked concrete.

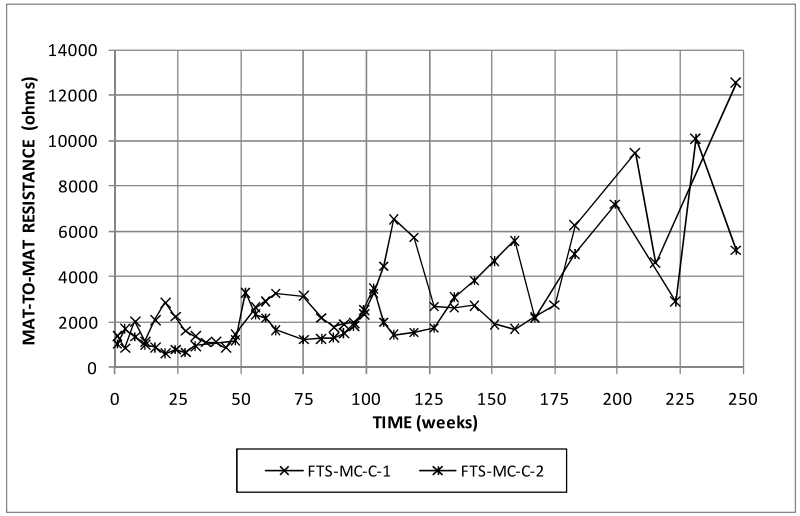

Figure B.30: Mat-to-mat resistance for field test specimens with MC reinforcement in cracked concrete.

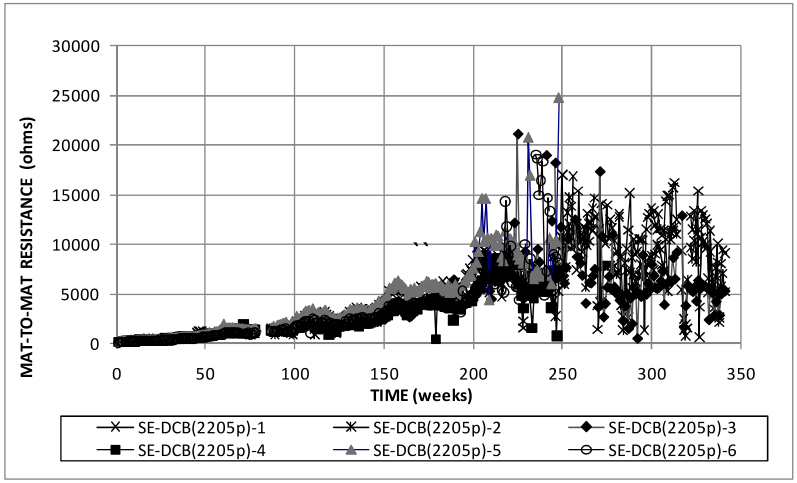

Figure B.31: Mat-to-mat resistance for Southern Exposure specimens, DCB 2205p reinforcement.

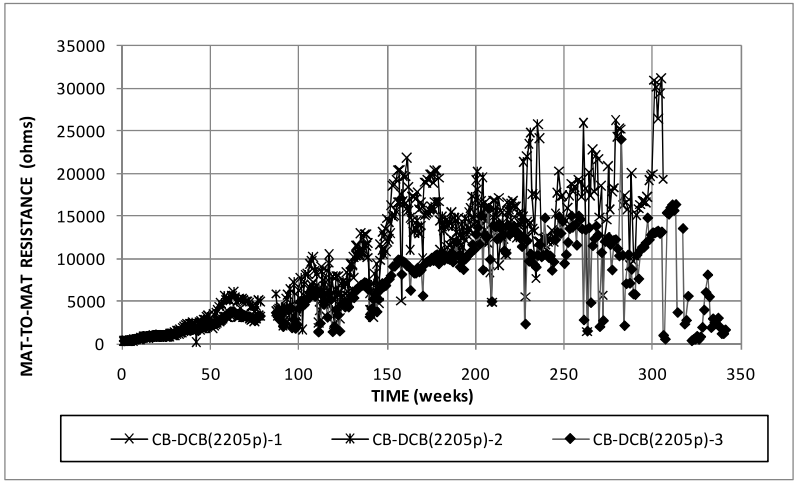

Figure B.32: Mat-to-mat resistance for cracked beam specimens, DCB 2205p reinforcement.

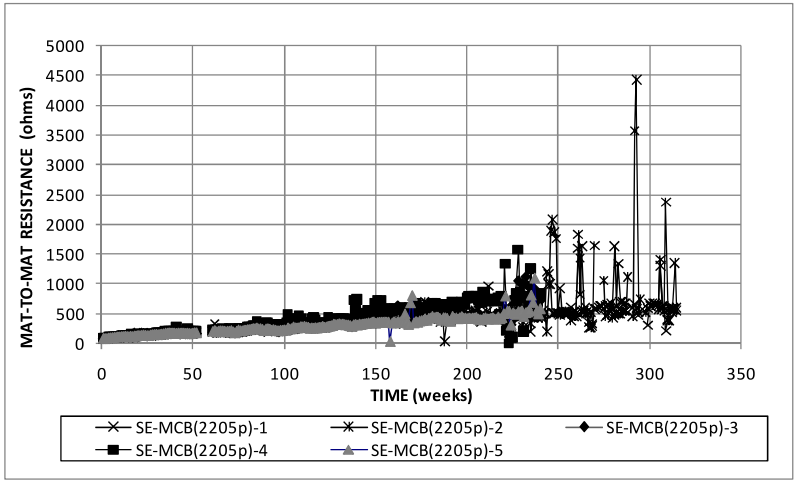

Figure B.33: Mat-to-mat resistance for Southern Exposure specimens, MCB 2205p reinforcement.

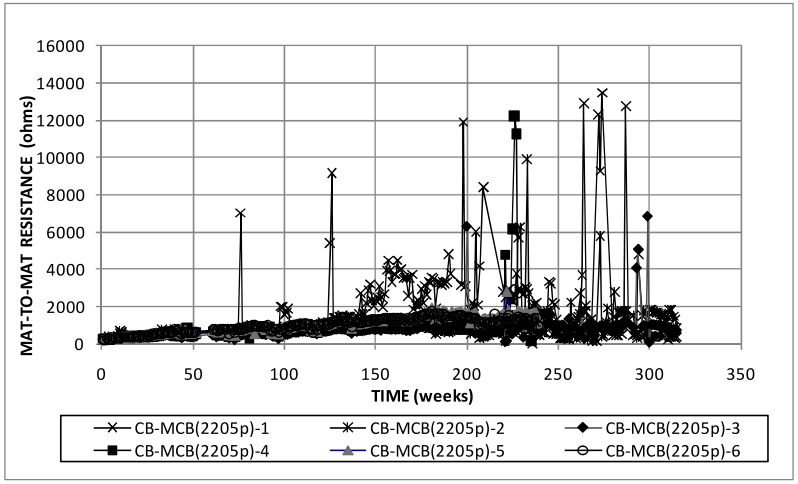

Figure B.34: Mat-to-mat resistance for cracked beam specimens, MCB 2205p reinforcement.

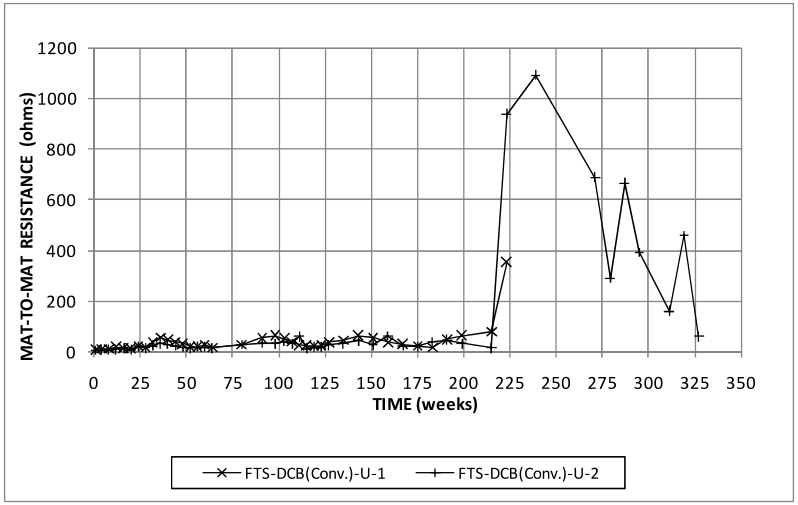

Figure B.35: Mat-to-mat resistance for field test specimens, DCB with conventional reinforcement.

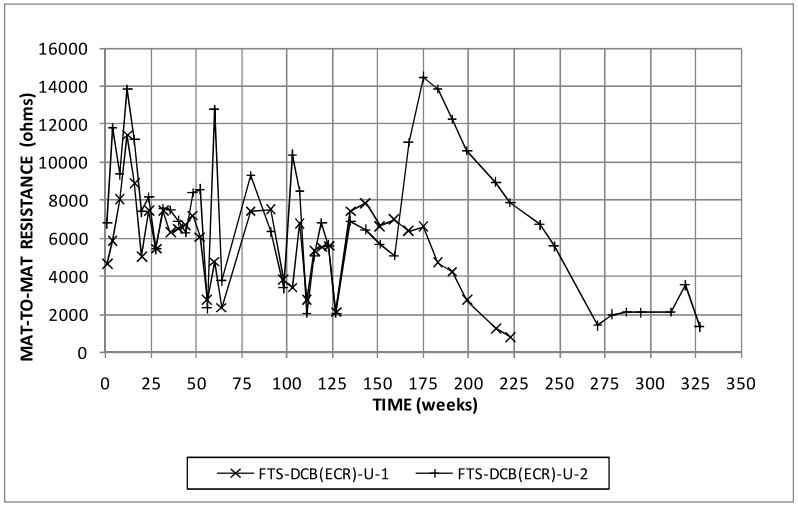

Figure B.36: Mat-to-mat resistance for field test specimens, DCB with ECR.

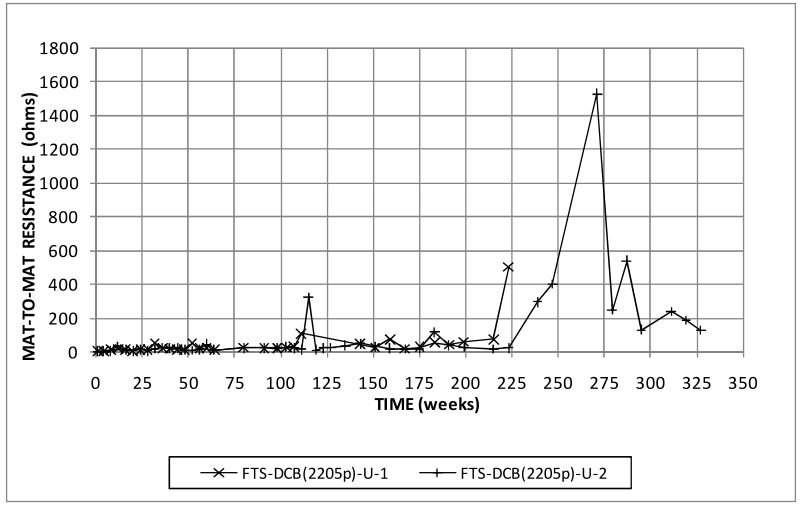

Figure B.37: Mat-to-mat resistance for field test specimens, DCB with 2205p reinforcement.

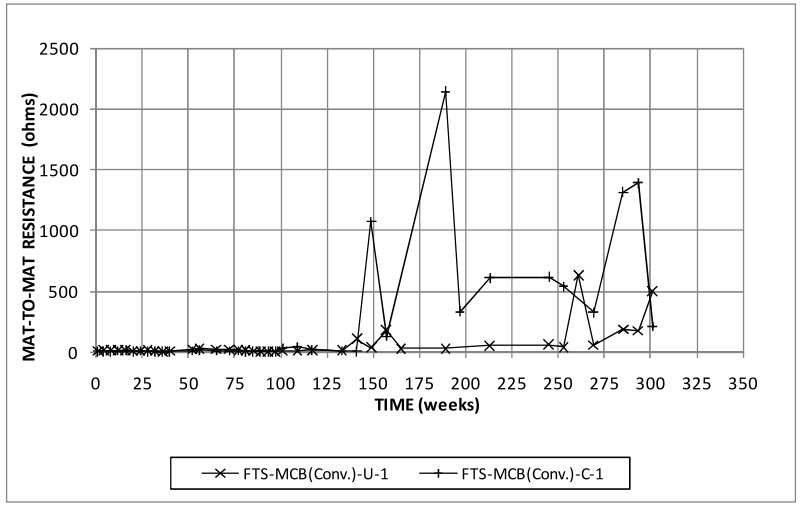

Figure B.38: Mat-to-mat resistance for field test specimens, MCB with conventional reinforcement.

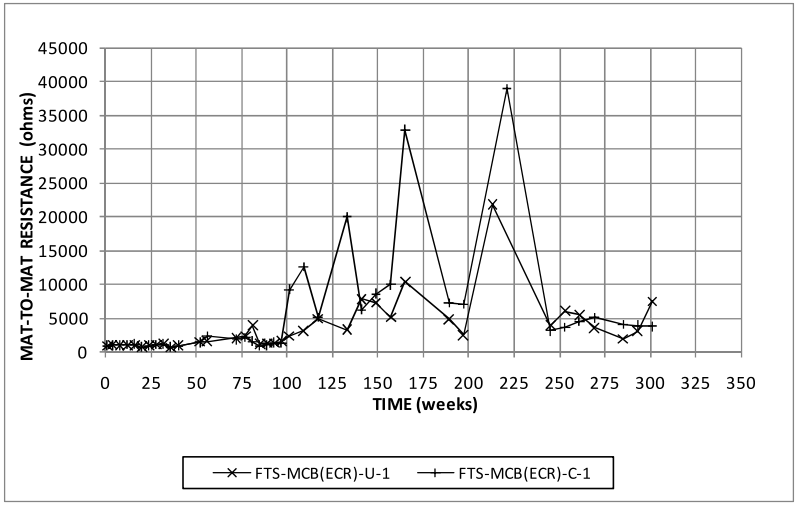

Figure B.39: Mat-to-mat resistance for field test specimens, DCB with ECR.

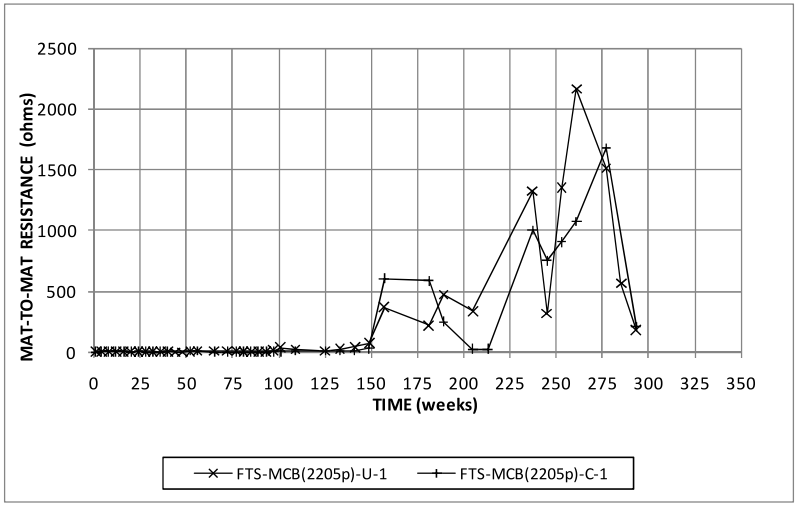

Figure B.40: Mat-to-mat resistance for field test specimens, MCB with 2205p reinforcement.

APPENDIX C

CHLORIDE CONCENTRATION DATA

Table C.1 Southern Exposure Test. Chloride Content at 48 Weeks.

Specimen	Water Soluble Cl^- Content, kg/m^3						Average	Standard Deviation	Coefficient of Variation
	1	2	3	4	5	6			
SE-Conv.2-45-1	3.94	3.38	4.09	6.30	3.49	6.00	4.53	1.29	0.28
SE-Conv.2-45-2	5.79	3.15	4.90	3.01	3.62	2.82	3.88	1.20	0.31
SE-Conv.2-45-3	5.08	6.30	5.50	5.76	3.90	9.56	6.02	1.91	0.32
					SE-Conv.2 Avg.		4.81	1.17	0.24
SE-Conv.2-RH-45-1	4.40	3.60	4.78	3.76	5.63	-	4.43	0.82	0.18
SE-Conv.2-RH-45-2	4.65	3.68	5.19	2.37	-	-	3.97	1.24	0.31
SE-Conv.2-RH-45-3	-	6.64	4.46	4.09	3.60	2.14	4.19	1.63	0.39
					SE-Conv.2-RH Avg.		4.20	1.19	0.28
SE-Conv.2-DCI-45-1	4.66	4.68	3.77	8.34	3.87	3.06	4.73	1.87	0.40
SE-Conv.2-DCI-45-2	10.93	9.06	7.96	8.91	8.82	7.54	8.87	1.17	0.13
SE-Conv.2-DCI-45-3	9.09	9.81	-	5.29	7.73	-	7.98	1.99	0.25
					SE-Conv.2-DCI Avg.		7.19	2.47	0.34
SE-Conv.2-HY-45-1	2.93	3.34	-	-	-	-	3.13	0.29	0.09
SE-Conv.2-HY-45-2	1.05	3.79	4.51	2.50	0.47	2.37	2.45	1.55	0.63
SE-Conv.2-HY-45-3	2.53	1.84	3.34	1.88	6.92	2.85	3.23	1.90	0.59
					SE-Conv.2-HY Avg.		2.93	1.57	0.53

Table C.2: Field Test Specimen FTS-Conv.-U-2. Chloride profile at end of test.

Cl^- Content (kg/m^3)							
Depth Range (mm)	3.8-7.6	7.6-12.7	12.7-19.1	19.1-25.4	25.4-28.6	28.6-31.8	38.1-41.3
Core A	7.16	6.00	4.13	2.85	1.95		
Core B	5.18	3.79	2.70	1.91	1.35	1.01	0.45

Table C.3: Field Test Specimen FTS-Conv.-C-2. Chloride profile at end of test.

Cl^- Content (kg/m^3)							
Depth Range (mm)	3.8-7.6	7.6-12.7	12.7-19.1	19.1-25.4	25.4-28.6	28.6-31.8	38.1-41.3
Core A	6.64	6.60	4.91	4.43	3.56	2.81	

Table C.4: Field Test Specimen FTS-ECR-U-2. Chloride profile at end of test.

Cl^- Content (kg/m^3)							
Depth Range (mm)	3.8-7.6	7.6-12.7	12.7-19.1	19.1-25.4	25.4-28.6	28.6-31.8	38.1-41.3
Core A	7.61	6.38	4.76	4.58	4.16	3.34	1.50
Core B	7.01	6.45	4.80	3.60	2.63	2.14	0.71
Core C	5.81	4.80	3.30	2.48	2.36	1.80	0.60

Table C.5: Field Test Specimen FTS-ECR-C-2. Chloride profile at end of test.

Cl^- Content (kg/m^3)							
Depth Range (mm)	3.8-7.6	7.6-12.7	12.7-19.1	19.1-25.4	25.4-28.6	28.6-31.8	38.1-41.3
Core A	5.29	4.65	2.33	1.73	1.11	0.53	0.15
Core B	6.49	6.60	4.91	3.45	2.33	0.00	0.94
Core C	6.15	4.69	3.79	2.93	2.25	1.76	0.68
Core D	6.43	6.45	3.64	3.00	2.40	2.85	0.56

Table C.6: Field Test Specimen FTS-ECR(Chromate)-U-2. Chloride profile at end of test.

Cl^- Content (kg/m^3)							
Depth Range (mm)	3.8-7.6	7.6-12.7	12.7-19.1	19.1-25.4	25.4-28.6	28.6-31.8	38.1-41.3
Core A	7.50	6.71	4.20	3.23	2.51	2.36	0.90
Core B	8.14	6.41	6.30	5.06	4.43	3.83	2.29
Core C	7.20	6.08	4.80	3.38	2.63	2.36	0.79
Core D	8.48	7.80	6.15	4.95	3.34	3.00	1.65

Table C.7: Field Test Specimen FTS-ECR(Chromate)-C-2. Chloride profile at end of test.

Cl^- Content (kg/m^3)							
Depth Range (mm)	3.8-7.6	7.6-12.7	12.7-19.1	19.1-25.4	25.4-28.6	28.6-31.8	38.1-41.3
Core A	10.76	9.45	7.01	6.34	5.59	4.91	3.34
Core B	8.74	7.46	6.71	4.73	3.08	2.93	2.21
Core C	9.90	9.64	7.76	5.81	5.40	4.84	3.00
Core D	11.59	9.04	6.90	4.88	4.39	4.01	2.21

Table C.8: Field Test Specimen FTS-ECR(DuPont)-U-2. Chloride profile at end of test.

Cl^- Content (kg/m^3)							
Depth Range (mm)	3.8-7.6	7.6-12.7	12.7-19.1	19.1-25.4	25.4-28.6	28.6-31.8	38.1-41.3
Core A	7.76	4.91	3.56	2.96	2.21	1.69	0.60
Core B	8.81	7.05	4.88	3.30	2.66	2.06	0.83
Core C	11.36	10.43	9.75	7.99	6.68	6.98	7.28
Core D	10.24	9.45	7.80	7.31	6.60	6.00	5.06

Table C.9: Field Test Specimen FTS-ECR(DuPont)-C-2. Chloride profile at end of test.

Cl^- Content (kg/m^3)							
Depth Range (mm)	3.8-7.6	7.6-12.7	12.7-19.1	19.1-25.4	25.4-28.6	28.6-31.8	38.1-41.3
Core A	8.89	6.90	6.30	4.61	3.98	3.75	2.18
Core B	9.98	9.19	7.50	5.36	4.46	3.86	2.29
Core C	9.73	6.56	6.15	4.58	4.09	3.26	1.89
Core D	9.86	7.88	5.74	5.18	4.16	3.68	2.29

Table C.10: Field Test Specimen FTS-ECR(Valspar)-U-2. Chloride profile at end of test.

Cl^- Content (kg/m^3)							
Depth Range (mm)	3.8-7.6	7.6-12.7	12.7-19.1	19.1-25.4	25.4-28.6	28.6-31.8	38.1-41.3
Core A	6.00	5.51	4.69	3.64	3.23	3.34	1.69
Core B	6.60	5.18	3.79	2.93	2.06	1.84	0.60
Core C	8.93	6.75	5.29	4.24	3.38	2.74	1.50
Core D	7.69	6.34	4.58	3.23	2.48	2.18	0.86

Table C.11: Field Test Specimen FTS-ECR(Valspar)-C-2. Chloride profile at end of test.

Cl^- Content (kg/m^3)							
Depth Range (mm)	3.8-7.6	7.6-12.7	12.7-19.1	19.1-25.4	25.4-28.6	28.6-31.8	38.1-41.3
Core A	9.56	7.95	6.64	5.25	4.80	4.09	2.78
Core B	7.61	9.98	6.49	4.58	3.68	3.19	1.61
Core C	10.09	9.41	7.28	5.74	0.00	0.00	0.00
Core D	7.80	8.51	7.28	5.89	5.36	4.39	2.78

Table C.12: Field Test Specimen FTS-ECR(RH)-U-1. Chloride profile at end of test.

Cl^- Content (kg/m^3)							
Depth Range (mm)	3.8-7.6	7.6-12.7	12.7-19.1	19.1-25.4	25.4-28.6	28.6-31.8	38.1-41.3
Core A	9.38	9.45	9.15	8.55	8.59	7.58	6.84
Core B	10.07	9.32	9.45	9.00	7.05	6.75	6.34
Core C	11.59	11.18	11.66	10.43	10.07	10.13	8.14
Core D	10.58	10.73	11.48	11.25	10.73	10.09	8.25

Table C.13: Field Test Specimen FTS-ECR(RH)-U-2. Chloride profile at end of test.

Cl^- Content (kg/m^3)							
Depth Range (mm)	3.8-7.6	7.6-12.7	12.7-19.1	19.1-25.4	25.4-28.6	28.6-31.8	38.1-41.3
Core A	8.59	8.03	8.48	6.79	7.28	6.00	6.04
Core B	8.81	8.81	8.48	8.14	6.79	5.85	5.33
Core C	8.03	6.11	6.04	5.33	5.49	4.76	3.79
Core D	7.76	7.24	6.08	5.55	4.91	4.73	4.39

Table C.14: Field Test Specimen FTS-ECR(RH)-C-1. Chloride profile at end of test.

Cl^- Content (kg/m^3)							
Depth Range (mm)	3.8-7.6	7.6-12.7	12.7-19.1	19.1-25.4	25.4-28.6	28.6-31.8	38.1-41.3
Core A	12.71	10.61	10.24	10.43	9.08	8.78	7.69
Core B	11.14	10.28	8.57	9.26	8.51	8.14	7.35
Core C	8.40	7.99	7.58	7.80	7.65	6.75	6.38
Core D	10.99	9.94	9.30	7.35	8.29	7.76	6.68

Table C.15: Field Test Specimen FTS-ECR(RH)-C-2. Chloride profile at end of test.

Cl^- Content (kg/m^3)							
Depth Range (mm)	3.8-7.6	7.6-12.7	12.7-19.1	19.1-25.4	25.4-28.6	28.6-31.8	38.1-41.3
Core A	10.24	8.33	7.65	7.80	7.50	7.24	6.08
Core B	9.38	10.54	9.41	8.12	7.50	6.83	6.38
Core C	9.15	9.45	7.99	6.90	8.01	7.86	6.79
Core D	10.73	8.85	8.55	7.31	7.29	6.90	6.79

Table C.16: Field Test Specimen FTS-ECR(DCI)-U-1. Chloride profile at end of test.

Cl^- Content (kg/m^3)							
Depth Range (mm)	3.8-7.6	7.6-12.7	12.7-19.1	19.1-25.4	25.4-28.6	28.6-31.8	38.1-41.3
Core A	11.25	11.03	9.34	8.55	9.04	7.09	6.64
Core B	9.98	9.19	8.33	7.43	7.88	8.27	7.05

Table C.17: Field Test Specimen FTS-ECR(DCI)-U-2. Chloride profile at end of test.

Cl^- Content (kg/m^3)							
Depth Range (mm)	3.8-7.6	7.6-12.7	12.7-19.1	19.1-25.4	25.4-28.6	28.6-31.8	38.1-41.3
Core A	11.96	11.21	11.12	10.09		7.50	5.49
Core B	9.19	10.09	9.41	8.89	7.31	6.75	6.64
Core C	13.00	11.23	10.99	8.55	8.33	8.70	4.61
Core D	14.85	12.49	11.55	11.89	11.03	10.01	7.76

Table C.18: Field Test Specimen FTS-ECR(DCI)-U-3. Chloride profile at end of test.

Cl^- Content (kg/m^3)							
Depth Range (mm)	3.8-7.6	7.6-12.7	12.7-19.1	19.1-25.4	25.4-28.6	28.6-31.8	38.1-41.3
Core A	9.34	9.60	7.76	7.76	7.13	6.41	4.20
Core B	11.81	11.78	10.28	9.45	8.63	8.03	6.60
Core C	10.46	9.75	10.31	9.30	8.29	7.84	5.85
Core D	9.34	8.36	8.55	8.81	7.88	6.79	5.48

Table C.19: Field Test Specimen FTS-ECR(DCI)-C-1. Chloride profile at end of test.

Cl^- Content (kg/m^3)							
Depth Range (mm)	3.8-7.6	7.6-12.7	12.7-19.1	19.1-25.4	25.4-28.6	28.6-31.8	38.1-41.3
Core A	11.63	11.18	12.38	10.20	10.76	9.94	7.09
Core B	10.09	10.56	9.34	9.60	9.41	8.72	6.21
Core C	13.88	10.95	11.14	9.34	8.18	8.03	7.09
Core D	13.35	14.03	11.29	10.65	9.75	9.15	7.44

Table C.20: Field Test Specimen FTS-ECR(DCI)-C-2. Chloride profile at end of test.

Cl^- Content (kg/m^3)							
Depth Range (mm)	3.8-7.6	7.6-12.7	12.7-19.1	19.1-25.4	25.4-28.6	28.6-31.8	38.1-41.3
Core A	7.95	8.63	8.40	8.81	9.30	8.44	
Core B		9.11	7.39	7.24	6.41	6.68	
Core C	16.50	14.66	12.53	11.89	10.09	9.04	8.06
Core D	13.09	9.75	9.38	10.43	9.53	8.10	5.51

Table C.21: Field Test Specimen FTS-ECR(DCI)-C-3. Chloride profile at end of test.

Cl^- Content (kg/m^3)							
Depth Range (mm)	3.8-7.6	7.6-12.7	12.7-19.1	19.1-25.4	25.4-28.6	28.6-31.8	38.1-41.3
Core A	8.81	7.43	6.68	4.91	3.94	2.93	0.79
Core B	7.69	7.76	7.54	6.56	5.55	4.76	2.85
Core C	11.51	10.43	8.51	5.93	5.33	4.35	1.73
Core D	11.18	10.99	8.33	6.19	4.61	3.83	1.46

Table C.22: Field Test Specimen FTS-ECR(HY)-U-1. Chloride profile at end of test.

Cl^- Content (kg/m^3)							
Depth Range (mm)	3.8-7.6	7.6-12.7	12.7-19.1	19.1-25.4	25.4-28.6	28.6-31.8	38.1-41.3
Core A	2.81	3.68	2.63	0.60	0.26	0.26	0.19
Core B	2.66	2.70	1.65	0.45	0.19	0.19	0.15
Core C	1.99	3.98	3.79	1.95	0.56	0.34	0.23
Core D	1.99	3.68	2.93	1.01	0.30	0.23	0.15

Table C.23: Field Test Specimen FTS-ECR(HY)-U-2. Chloride profile at end of test.

Cl^- Content (kg/m^3)							
Depth Range (mm)	3.8-7.6	7.6-12.7	12.7-19.1	19.1-25.4	25.4-28.6	28.6-31.8	38.1-41.3
Core A	1.91	3.45	2.74	0.49	0.19	0.15	0.19
Core B	2.18	2.66	1.56	0.34	0.26	0.08	0.08

Table C.24: Field Test Specimen FTS-ECR(HY)-C-1. Chloride profile at end of test.

Cl^- Content (kg/m^3)							
Depth Range (mm)	3.8-7.6	7.6-12.7	12.7-19.1	19.1-25.4	25.4-28.6	28.6-31.8	38.1-41.3
Core A	1.58	2.48	1.73	0.45	0.23	0.19	0.08
Core B	1.69	1.80	2.70	1.43	0.60	0.30	0.26
Core C	2.25	3.64	2.81	0.90	0.45	0.23	0.26
Core D	1.16	3.90	5.89	4.16	1.99	1.01	0.38

Table C.25: Field Test Specimen FTS-ECR(HY)-C-2. Chloride profile at end of test.

Cl^- Content (kg/m^3)							
Depth Range (mm)	3.8-7.6	7.6-12.7	12.7-19.1	19.1-25.4	25.4-28.6	28.6-31.8	38.1-41.3
Core A	1.54	1.31	1.01	0.45	0.19	0.19	0.19
Core B	2.10	4.46	5.36	2.21	0.83	0.41	0.15
Core C	3.30	7.20	5.44	2.89	1.16	0.71	0.26

Table C.26: Field Test Specimen FTS-ECR(primer/Ca(NO2)2)-U-2. Chloride profile at end of test.

Cl^- Content (kg/m^3)							
Depth Range (mm)	3.8-7.6	7.6-12.7	12.7-19.1	19.1-25.4	25.4-28.6	28.6-31.8	38.1-41.3
Core A	13.24	13.73	11.72	10.88	9.08	7.76	5.96
Core B	14.29	14.70	12.94	10.09	9.86	9.49	7.91
Core C	9.71	10.09	12.23	10.28	8.10	7.13	6.79
Core D	15.64	15.38	13.16	11.81	10.58	8.40	7.35

Table C.27: Field Test Specimen FTS-ECR(primer/Ca(NO2)2)-C-2. Chloride profile at end of test.

Cl^- Content (kg/m^3)							
Depth Range (mm)	3.8-7.6	7.6-12.7	12.7-19.1	19.1-25.4	25.4-28.6	28.6-31.8	38.1-41.3
Core A	11.66	9.83	9.94	7.73	7.05	7.01	5.98
Core B	10.24	9.86	8.36	7.05	6.68	6.00	4.95
Core C	12.30	11.78	12.19	10.84	11.10	10.35	7.50

Table C.28: Field Test Specimen FTS-MC-U-2. Chloride profile at end of test.

Cl^- Content (kg/m^3)							
Depth Range (mm)	3.8-7.6	7.6-12.7	12.7-19.1	19.1-25.4	25.4-28.6	28.6-31.8	38.1-41.3
Core A	10.58	9.75	9.90	9.41	8.93	7.91	7.05
Core B	12.71	12.75	12.90	11.51	10.20	9.56	6.83
Core C	10.09	8.74	8.10	7.54	7.01	6.68	5.06
Core D	12.64	13.31	11.74	9.75	8.25	7.82	5.40

Table C.29: Field Test Specimen FTS-MC-C-2. Chloride profile at end of test.

Cl^- Content (kg/m^3)							
Depth Range (mm)	3.8-7.6	7.6-12.7	12.7-19.1	19.1-25.4	25.4-28.6	28.6-31.8	38.1-41.3
Core A	12.26	11.81	10.54	8.51	7.84	8.25	6.86
Core B	13.26	11.81	9.90	9.30	9.84	8.78	7.73
Core C	14.51	13.35	9.75	8.63	8.63	8.70	6.38

Table C.30: Chloride data from samples taken with vacuum drill.

Specimen	**Age (Weeks)**	**Cl^- Content (kg/m^3)**	
		6.4-19.1 mm	**19.1-25.4.25 mm**
FTS-Conv-U-1	213	6.81	3.80
FTS-Conv-U-2	201	4.91	2.36
FTS-ECR-U-1	213	7.16	3.72
FTS-ECR-U-2	201	4.13	2.36

Table C.31: Chloride profile data from Southern Exposure KDOT Bridge project specimens.

Specimen	Depth (mm.)	Water Soluble Cl^- Content (kg/m^3)								Avg.	Std. Dev
		# 1	**# 2**	**# 3**	**# 4**	**# 5**	**# 6**	**# 7**	**# 8**		
MCB(2205p)-3	15.9	17.06	23.77	23.63	22.65	23.97	23.33	18.55	24.09	22.13	2.74
	28.6	19.16	18.11	18.71	18.99	21.53	16.88			18.90	1.53
	54.0	11.66	9.78	13.24	11.43	14.04	12.38	11.07	9.68	11.66	1.54
	79.4	1.99	3.24	3.96	2.59	4.22	4.69	4.46	6.34	3.94	1.35
	136.5	0.25	0.32	1.51	0.55	0.63	7.07	0.35	3.75	1.80	2.43
MCB(2205p)-4	15.9	17.80	21.69	23.05	21.67	23.14	19.05	27.86	24.22	22.31	3.11
	28.6	17.81	15.90	19.46	22.99	24.45				20.12	3.56
	54.0	11.81	10.99	9.04	8.63	12.45	15.96	13.09	13.51	11.93	2.41
	79.4	1.01	3.26	8.79	6.04	8.85	6.31	8.96	4.30	5.94	2.93
	136.5	1.39	9.29	1.49	4.30	7.82	0.23	0.19	0.35	3.13	3.62
MCB(2205p)-5	15.9	18.59	24.08	23.74	27.30	25.58	26.51	25.94	20.83	24.07	3.00
	28.6	16.58	15.71	17.14	21.50	16.37				17.46	2.31
	54.0	8.33	7.65	7.88	8.36	12.90	10.80	12.15	8.86	9.62	2.05
	79.4	2.03	3.42	2.59	2.66	4.42	4.99	5.36	6.00	3.94	1.46
	136.5	1.39	0.27	0.14	0.16	0.27	1.10	5.90	3.64	1.61	2.09

APPENDIX D

DISBONDMENT DATA

Table D.1: Disbondment data for FTS-ECR-U-1

	FTS-ECR-U-1		
	Top Hole 1	**Top Hole 2**	**Bottom Hole**
Specimen	**Area (in.^{2})**	**Area (in.^{2})**	**Area (in.^{2})**
Electrically Connected			
1	0.04	0.04	0
2	0.04	0	0
Electrically Isolated			
1	0.04	0	0
2	0	0	0
3	0	0	0
4	0	0	0
5	0	0	0
Bottom Bar			
1	0	0	0
2	0	0	0

Table D.2: Disbondment data for FTS-ECR-U-2

	FTS-ECR-U-2		
	Top Hole 1	**Top Hole 2**	**Bottom Hole**
Specimen	**Area (in.^{2})**	**Area (in.^{2})**	**Area (in.^{2})**
Electrically Connected			
1	0	0	0
2	0.04	0	0
3	0	0	0
4	0.04	0	0
Electrically Isolated			
1	0	0	0
2	0	0	0
3	0	0	0
Bottom Bar			
1	0.03	0.03	0
2	1.05	0.2	0.16
3	0.02	0	0
4	0.04	0	0

Table D.3: Disbondment data for FTS-ECR(Chromate)-U-1

	FTS-ECR(Chromate)-U-1		
	Top Hole 1	**Top Hole 2**	**Bottom Hole**
Specimen	**Area (in.^{2})**	**Area (in.^{2})**	**Area (in.^{2})**
Electrically Connected			
1	0.11	0.07	0
2	0.03	0	0
Electrically Isolated			
1	0.02	0	0
2	0	0	0
3	0	0	0
4	0	0	0
5	0	0	0
Bottom Bar			
1	0	0	0
2	0	0	0

Table D.4: Disbondment data for FTS-ECR(Chromate)-U-2

	FTS-ECR(Chromate)-U-2		
	Top Hole 1	**Top Hole 2**	**Bottom Hole**
Specimen	**Area (in.^{2})**	**Area (in.^{2})**	**Area (in.^{2})**
Electrically Connected			
1	0.06	0.04	0.02
2	0.05	0.05	0
3	0.03	0.04	0
4	0.03	0	0
Electrically Isolated			
1	0	0	0
2	0	0	0
3	0	0	0
Bottom Bar			
1	0.03	0.02	0
2	0.02	0	0
3	0	0	0
4	0	0	0

Table D.5: Disbondment data for FTS-ECR(DuPont)-U-1

	FTS-ECR(DuPont)-U-1		
	Top Hole 1	**Top Hole 2**	**Bottom Hole**
Specimen	**Area (in.^{2})**	**Area (in.^{2})**	**Area (in.^{2})**
Electrically Connected			
1	0.04	0.03	0
2	0.04	0.03	0
Electrically Isolated			
1	0	0	0
2	0	0	0
3	0	0	0
4	0	0	0
5	0	0	0
Bottom Bar			
1	0.17	0	0.04
2	0.05	0.04	0.04

Table D.6: Disbondment data for FTS-ECR(DuPont)-U-2

	FTS-ECR(DuPont)-U-2		
	Top Hole 1	**Top Hole 2**	**Bottom Hole**
Specimen	**Area (in.^{2})**	**Area (in.^{2})**	**Area (in.^{2})**
Electrically Connected			
1	0.03	0	0.02
2	0.06	0	0
3	0	0	0.03
4	0.04	0	0
Electrically Isolated			
1	0.03	0	0
2	0.03	0	0
3	0	0	0
Bottom Bar			
1	0	0	0
2	0	0	0
3	0	0	0
4	0	0	0

Table D.7: Disbondment data for FTS-ECR(Valspar)-U-1

	FTS-ECR(Valspar)-U-1		
	Top Hole 1	**Top Hole 2**	**Bottom Hole**
Specimen	**Area (in.^{2})**	**Area (in.^{2})**	**Area (in.^{2})**
Electrically Connected			
1	0.04	0.03	0.04
2	0.04	0.04	0
Electrically Isolated			
1	0	0	0
2	0	0	0
3	0	0	0
4	0	0	0
5	0	0	0
Bottom Bar			
1	0	0	0
2	0.03	0	0

Table D.8: Disbondment data for FTS-ECR(Valspar)-U-2

	FTS-ECR(Valspar)-U-2		
	Top Hole 1	**Top Hole 2**	**Bottom Hole**
Specimen	**Area (in.^{2})**	**Area (in.^{2})**	**Area (in.^{2})**
Electrically Connected			
1	0.03	0	0
2	0.04	0.03	0
3	0.04	0	0
4	0.04	0.03	0
Electrically Isolated			
1	0	0	0
2	0	0	0
3	0	0	0
Bottom Bar			
1	0	0	0
2	0	0	0
3	0.02	0	0
4	0	0	0

Table D.9: Disbondment data for FTS-ECR(primer/Ca(NO2)2)-U-1

	FTS-ECR(primer/Ca(NO2)2)-U-1		
	Top Hole 1	**Top Hole 2**	**Bottom Hole**
Specimen	**Area (in.^{2})**	**Area (in.^{2})**	**Area (in.^{2})**
Electrically Connected			
1	0.04	0	0.08
2	0	0	0
3	0.04	0.03	0
4	0.06	0	0
Electrically Isolated			
1	0	0	0
2	0	0	0.03
3	0	0	0
Bottom Bar			
1	0.14	0	0.03
2	0.14	0.1	0.08
3	0.89	0.07	0.15
4	0.13	0.11	0.07

Table D.10: Disbondment data for FTS-ECR(primer/Ca(NO2)2)-U-2

	FTS-ECR(primer/Ca(NO2)2)-U-2		
	Top Hole 1	**Top Hole 2**	**Bottom Hole**
Specimen	**Area (in.^{2})**	**Area (in.^{2})**	**Area (in.^{2})**
Electrically Connected			
1	1.05	0.95	0.61
2	0.66	0.49	0.4
3	0.68	0.55	0.28
4	0.85	0.42	0.58
Electrically Isolated			
1	0.82	0.16	0.23
2	0.29	0.23	0.3
3	0.5	0.23	0.17
Bottom Bar			
1	0.17	0.11	0.23
2	0.16	0.15	0.09
3	0.16	0.15	0.09
4	0.18	0.18	0.04

Table D.11: Disbondment data for FTS-ECR(RH)-U-1

	FTS-ECR(RH)-U-1		
	Top Hole 1	**Top Hole 2**	**Bottom Hole**
Specimen	**Area (in.^{2})**	**Area (in.^{2})**	**Area (in.^{2})**
Electrically Connected			
1	0.33	0.17	0.08
2	1.05	0.28	0.25
3	0.33	0.26	0.2
4	1.05	0.43	0.22
Electrically Isolated			
1	0.07	0.04	0.03
2	0.04	0.02	0
3	0.24	0.14	0.14
Bottom Bar			
1	0.07	0.06	0
2	0	0	0
3	0.06	0.04	0
4	0	0	0

Table D.12: Disbondment data for FTS-ECR(RH)-U-2

	FTS-ECR(RH)-U-2		
	Top Hole 1	**Top Hole 2**	**Bottom Hole**
Specimen	**Area (in.^{2})**	**Area (in.^{2})**	**Area (in.^{2})**
Electrically Connected			
1	1.05	0.88	0.13
2	0.14	0.14	0.11
3	0.41	0.3	0.15
4	0	0	0
Electrically Isolated			
1	0.03	0	0
2	0.07	0.07	0.05
3	0	0	0
Bottom Bar			
1	0.11	0.11	0.08
2	0.08	0.04	0.05
3	0.04	0	0
4	0.02	0	0

Table D.13: Disbondment data for FTS-ECR(DCI)-U-1

	FTS-ECR(DCI)-U-1		
	Top Hole 1	**Top Hole 2**	**Bottom Hole**
Specimen	**Area (in.^{2})**	**Area (in.^{2})**	**Area (in.^{2})**
Electrically Connected			
1	0.14	0.09	0.05
2	0.09	0.09	0.05
3	0.75	0.28	0.09
4	0.06	0.05	0.03
Electrically Isolated			
1	0.02	0.02	0.04
2	0.06	0	0
3	0	0	0
Bottom Bar			
1	0.03	0	0
2	0	0	0
3	0.04	0	0
4	0	0	0

Table D.14: Disbondment data for FTS-ECR(DCI)-U-2

	FTS-ECR(DCI)-U-2		
	Top Hole 1	**Top Hole 2**	**Bottom Hole**
Specimen	**Area (in.^{2})**	**Area (in.^{2})**	**Area (in.^{2})**
Electrically Connected			
1	0.43	0.45	0.04
2	1.05	0.5	0.18
3	0.93	0.22	0
Electrically Isolated			
1	0.1	0.09	0.13
2	0.03	0.05	0
3	0.05	0	0
Bottom Bar			
1	0	0	0
2	0	0	0
3	0	0	0
4	0	0	0

Table D.15: Disbondment data for FTS-ECR(DCI)-U-3

	FTS-ECR(DCI)-U-3		
	Top Hole 1	**Top Hole 2**	**Bottom Hole**
Specimen	**Area (in.^{2})**	**Area (in.^{2})**	**Area (in.^{2})**
Electrically Connected			
1	0.04	0.04	0.04
2	0.04	0.03	0.02
3	0.07	0.04	0.03
4	0.06	0.05	0
Electrically Isolated			
1	0.02	0	0
2	0	0	0
3	0	0	0
Bottom Bar			
1	0.03	0	0
2	0	0	0
3	0.07	0.08	0.04
4	0	0	0

Table D.16: Disbondment data for FTS-ECR(HY)-U-1

	FTS-ECR(HY)-U-1		
	Top Hole 1	**Top Hole 2**	**Bottom Hole**
Specimen	**Area (in.^{2})**	**Area (in.^{2})**	**Area (in.^{2})**
Electrically Connected			
1	0	0	0
2	0.05	0	0.04
3	0.03	0	0
4	0	0	0
Electrically Isolated			
1	0	0	0
2	0	0	0
3	0	0	0
Bottom Bar			
1	0	0	0
2	0.02	0	0
3	0	0	0
4	0.03	0	0

Table D.17: Disbondment data for FTS-ECR(HY)-U-2

	FTS-ECR(HY)-U-2		
	Top Hole 1	**Top Hole 2**	**Bottom Hole**
Specimen	**Area (in.^{2})**	**Area (in.^{2})**	**Area (in.^{2})**
Electrically Connected			
1	0.03	0.02	0
2	0.03	0.03	0
3	0	0	0
4	0	0	0
Electrically Isolated			
1	0	0	0
2	0	0	0
3	0	0	0
Bottom Bar			
1	0	0	0
2	0	0	0
3	0.04	0.03	0
4	0	0	0

Table D.18: Disbondment data for FTS-MC-U-1

	FTS-MC-U-1		
	Top Hole 1	**Top Hole 2**	**Bottom Hole**
Specimen	**Area (in.^{2})**	**Area (in.^{2})**	**Area (in.^{2})**
Electrically Connected			
1	0.14	0	0
2	0.1	0.04	0
Electrically Isolated			
1	0.1	0	0
2	0	0	0
3	0	0	0
4	0	0	0
5	0	0	0
Bottom Bar			
1	0	0	0
2	0	0	0

Table D.19: Disbondment data for FTS-MC-U-2

	FTS-MC-U-2		
	Top Hole 1	**Top Hole 2**	**Bottom Hole**
Specimen	**Area (in.^{2})**	**Area (in.^{2})**	**Area (in.^{2})**
Electrically Connected			
1	1.05	1.05	0.03
2	0.28	0.25	0.16
3	1.05	0.24	0
4	0.76	0.67	0.15
Electrically Isolated			
1	0.33	0.15	0.11
2	0.09	0.09	0
3	0.08	0.11	0.05
Bottom Bar			
1	0	0	0
2	0.02	0	0
3	0	0	0
4	0	0	0

Table D.20: Disbondment data for FTS-ECR-C-1

	FTS-ECR-C-1		
	Top Hole 1	**Top Hole 2**	**Bottom Hole**
Specimen	**Area (in.^{2})**	**Area (in.^{2})**	**Area (in.^{2})**
Top Bar			
1	1.05	0.89	0.58
2	0.77	0.24	0.28
Bottom Bar			
1	0.43	0.1	0.82
2	0.31	0.16	0.09

Table D.21: Disbondment data for FTS-ECR-C-2

	FTS-ECR-C-2		
	Top Hole 1	**Top Hole 2**	**Bottom Hole**
Specimen	**Area (in.^{2})**	**Area (in.^{2})**	**Area (in.^{2})**
Top Bar			
1	0.74	0.69	0.09
2	0.42	0.17	0.14
3	1.05	0.45	0.33
Bottom Bar			
1	0.05	0.04	0.05
2	0.04	0	0
3	0	0	0
4	0.11	0.05	0.07

Table D.22: Disbondment data for FTS-ECR(Chromate)-C-1

	FTS-ECR(Chromate)-C-1		
	Top Hole 1	**Top Hole 2**	**Bottom Hole**
Specimen	**Area (in.^{2})**	**Area (in.^{2})**	**Area (in.^{2})**
Top Bar			
1	1.05	1.05	0.37
2	1.03	0.66	0.73
Bottom Bar			
1	0.15	0.03	0.07
2	0.04	0	0.02

Table D.23: Disbondment data for FTS-ECR(Chromate)-C-2

	FTS-ECR(Chromate)-C-2		
	Top Hole 1	**Top Hole 2**	**Bottom Hole**
Specimen	**Area (in.^{2})**	**Area (in.^{2})**	**Area (in.^{2})**
Top Bar			
1	1.05	1.05	1.05
2	0.32	0.23	0.22
3	0.63	0.38	0.41
4	0.93	0.7	0.31
Bottom Bar			
1	0.04	0	0.03
2	0.14	0.05	0.11
3	0.03	0	0
4	0	0	0

Table D.24: Disbondment data for FTS-ECR(DuPont)-C-1

	FTS-ECR(DuPont)-C-1		
	Top Hole 1	**Top Hole 2**	**Bottom Hole**
Specimen	**Area (in.^{2})**	**Area (in.^{2})**	**Area (in.^{2})**
Top Bar			
1	1.05	1.05	1.05
2	1.05	1.05	1.05
Bottom Bar			
1	0	0	0
2	0.11	0.04	0

Table D.25: Disbondment data for FTS-ECR(DuPont)-C-2

	FTS-ECR(DuPont)-C-2		
	Top Hole 1	**Top Hole 2**	**Bottom Hole**
Specimen	**Area (in.^{2})**	**Area (in.^{2})**	**Area (in.^{2})**
Top Bar			
1	1.05	1.05	1.05
2	1.05	0.67	0.83
3	1.05	1.05	1.05
4	1.05	1.05	0.21
Bottom Bar			
1	0.04	0	0.03
2	0	0	0
3	0	0	0
4	0	0	0

Table D.26: Disbondment data for FTS-ECR(Valspar)-C-1

	FTS-ECR(Valspar)-C-1		
	Top Hole 1	**Top Hole 2**	**Bottom Hole**
Specimen	**Area (in.^{2})**	**Area (in.^{2})**	**Area (in.^{2})**
Top Bar			
1	1.05	1.05	1.05
2	1.05	1.05	1.05
Bottom Bar			
1	0.63	0.5	0.48
2	0.88	0.33	0.35

Table D.27: Disbondment data for FTS-ECR(Valspar)-C-2

	FTS-ECR(Valspar)-C-2		
	Top Hole 1	**Top Hole 2**	**Bottom Hole**
Specimen	**Area (in.^{2})**	**Area (in.^{2})**	**Area (in.^{2})**
Top Bar			
1	1.05	1.05	1.05
2	1.05	1.05	0.27
3	1.05	1.05	1.05
4	0.31	0.14	0.21
Bottom Bar			
1	0.56	0.23	0.41
2	0.19	0.15	0
3	0.21	0.05	0.1
4	0.06	0.04	0.04

Table D.28: Disbondment data for FTS-ECR(primer/Ca(NO2)2)-C-1

	FTS-ECR(primer/Ca(NO2)2)-C-1		
	Top Hole 1	**Top Hole 2**	**Bottom Hole**
Specimen	**Area (in.^{2})**	**Area (in.^{2})**	**Area (in.^{2})**
Top Bar			
1	1.05	1.05	1.05
2	0.74	0.17	0.33
3	0.49	0.13	0.3
4	0.24	0.06	0.19
Bottom Bar			
1	0.1	0.08	0.07
2	0.16	0.14	0.11
3	0.86	0.2	0.25
4	0.31	0.13	0

Table D.29: Disbondment data for FTS-ECR(primer/Ca(NO2)2)-C-2

	FTS-ECR(primer/Ca(NO2)2)-C-2		
	Top Hole 1	**Top Hole 2**	**Bottom Hole**
Specimen	**Area (in.^{2})**	**Area (in.^{2})**	**Area (in.^{2})**
Top Bar			
1	1.05	1.05	1.05
2	0.54	0.36	0.25
3	0.56	0.39	0.21
4	0.35	0.22	0.56
Bottom Bar			
1	0.26	0.2	0.14
2	0.18	0.11	0.06
3	0.1	0.08	0.09
4	0.04	0	0

Table D.30: Disbondment data for FTS-ECR(RH)-C-1

	FTS-ECR(RH)-C-1		
	Top Hole 1	**Top Hole 2**	**Bottom Hole**
Specimen	**Area (in.^{2})**	**Area (in.^{2})**	**Area (in.^{2})**
Top Bar			
1	1.05	1.05	1.05
2	1.05	1.05	1.05
3	1.05	1.05	1.05
4	1.05	1.05	1.05
Bottom Bar			
1	0.13	0.14	0.17
2	0.5	0.42	0.45
3	0.37	0.35	0.22
4	0.13	0.12	0.17

Table D.31: Disbondment data for FTS-ECR(RH)-C-2

	FTS-ECR(RH)-C-2		
	Top Hole 1	**Top Hole 2**	**Bottom Hole**
Specimen	**Area (in.^{2})**	**Area (in.^{2})**	**Area (in.^{2})**
Top Bar			
1	1.05	1.05	1.05
2	1.05	0.92	1.05
3	1.05	1.05	1.05
4	1.05	1.05	0.67
Bottom Bar			
1	0.28	0.25	0.1
2	0.24	0.17	0.15
3	0.37	0.24	0.13
4	0.29	0.27	0.15

Table D.32: Disbondment data for FTS-ECR(DCI)-C-1

	FTS-ECR(DCI)-C-1		
	Top Hole 1	**Top Hole 2**	**Bottom Hole**
Specimen	**Area (in.^{2})**	**Area (in.^{2})**	**Area (in.^{2})**
Top Bar			
1	1.05	1.05	1.05
2	1.05	1.05	1.05
3	1.05	1.05	1.05
4	1.05	1.05	1.05
Bottom Bar			
1	0.23	0.21	0.18
2	0.28	0.24	0.23
3	0.26	0.37	0.42
4	0.48	0.46	0.24

Table D.33: Disbondment data for FTS-ECR(DCI)-C-2

	FTS-ECR(DCI)-C-2		
	Top Hole 1	**Top Hole 2**	**Bottom Hole**
Specimen	**Area (in.^{2})**	**Area (in.^{2})**	**Area (in.^{2})**
Top Bar			
1	1.05	1.05	1.05
2	1.05	0.8	0.25
3	1.05	1.05	1.05
4	1.05	1.05	1.05
Bottom Bar			
1	0	0	0
2	0.09	0.07	0.11
3	0.31	0.25	0.2
4	0.13	0.12	0.08

Table D.34: Disbondment data for FTS-ECR(DCI)-C-3

	FTS-ECR(DCI)-C-3		
	Top Hole 1	**Top Hole 2**	**Bottom Hole**
Specimen	**Area (in.^{2})**	**Area (in.^{2})**	**Area (in.^{2})**
Top Bar			
1	1.05	0.57	0.37
2	0.3	0.15	0.11
3	1.05	1.05	1.05
4	1.05	1.05	1.05
Bottom Bar			
1	0.17	0.15	0.05
2	0.12	0.1	0.05
3	0.03	0.1	0.05
4	0.05	0.03	0

Table D.35: Disbondment data for FTS-ECR(HY)-C-1

	FTS-ECR(HY)-C-1		
	Top Hole 1	**Top Hole 2**	**Bottom Hole**
Specimen	**Area (in.^{2})**	**Area (in.^{2})**	**Area (in.^{2})**
Top Bar			
1	1.05	1.05	1.05
2	1.05	1.05	0.67
3	1.05	1.05	1.05
4	1.05	1.05	0.55
Bottom Bar			
1	0.14	0.14	0.09
2	0.21	0.18	0.16
3	0.07	0.07	0.03
4	0.14	0.14	0.12

Table D.36: Disbondment data for FTS-ECR(HY)-C-2

	FTS-ECR(HY)-C-2		
	Top Hole 1	**Top Hole 2**	**Bottom Hole**
Specimen	**Area (in.^{2})**	**Area (in.^{2})**	**Area (in.^{2})**
Top Bar			
1	1.05	1.05	1.05
2	1.05	1.05	1.05
3	1.05	1.05	1.05
4	1.05	1.05	1.05
Bottom Bar			
1	0.21	0.2	0.12
2	0.04	0.04	0
3	0.15	0.11	0.08
4	0.19	0.17	0.12

Table D.37: Disbondment data for FTS-MC-C-1

	FTS-MC-C-1		
	Top Hole 1	**Top Hole 2**	**Bottom Hole**
Specimen	**Area (in.^{2})**	**Area (in.^{2})**	**Area (in.^{2})**
Top Bar			
1	1.05	0.58	0.21
2	1.05	0.83	0.36
Bottom Bar			
1	0	0	0
2	0.03	0	0

Table D.38: Disbondment data for FTS-MC-C-2

	FTS-MC-C-2		
	Top Hole 1	**Top Hole 2**	**Bottom Hole**
Specimen	**Area (in.^{2})**	**Area (in.^{2})**	**Area (in.^{2})**
Top Bar			
1	1.05	1.05	1.05
2	1.05	0.23	1.05
3	1.05	1.05	1.05
4	1.05	1.01	1.05
Bottom Bar			
1	0	0	0
2	0.05	0	0
3	0	0	0
4	0	0	0

APPENDIX E

DONIPHAN COUNTY AND MISSION CREEK BRIDGE POTENTIAL MAPPINGS

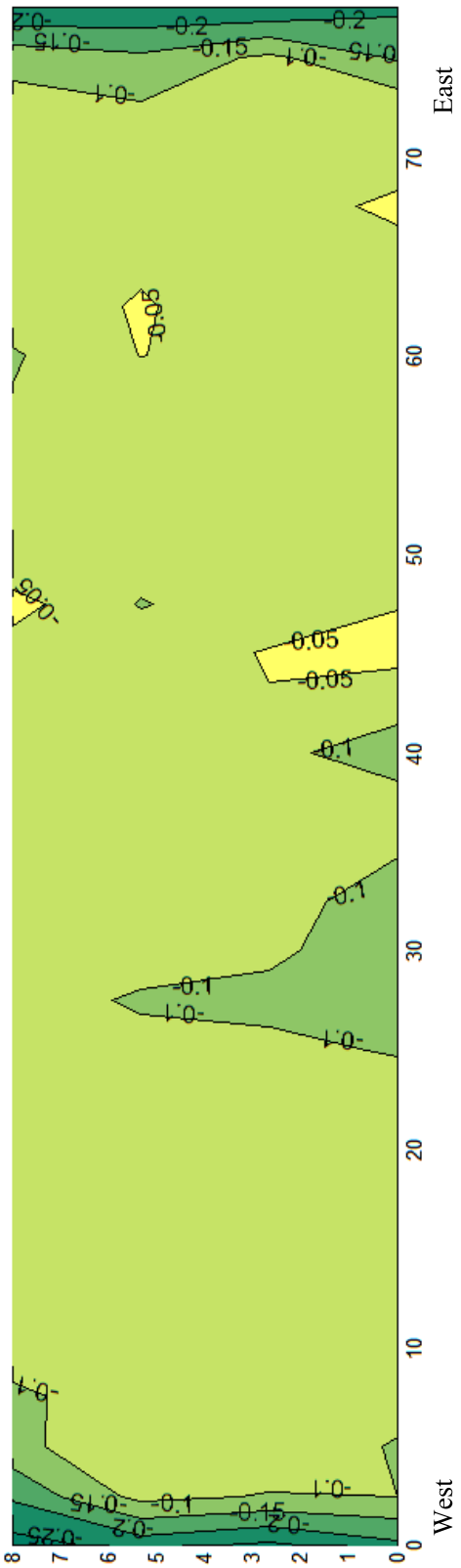

Figure E.1: Corrosion potential map for the Doniphan County Bridge (September 17, 2004)

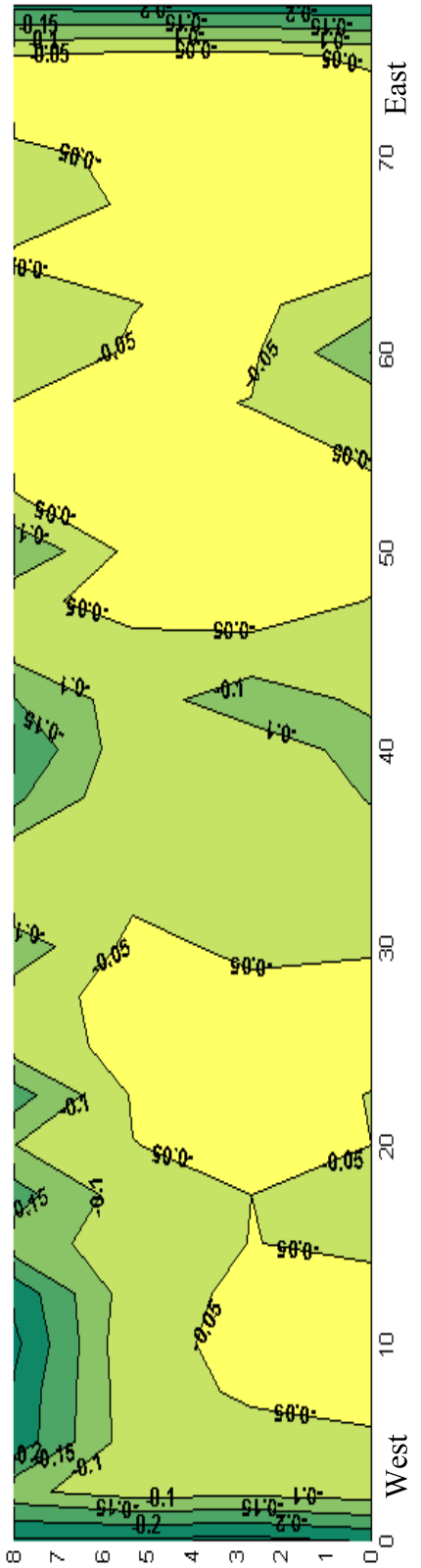

Figure E.2: Corrosion potential map for the Doniphan County Bridge (April 26, 2005)

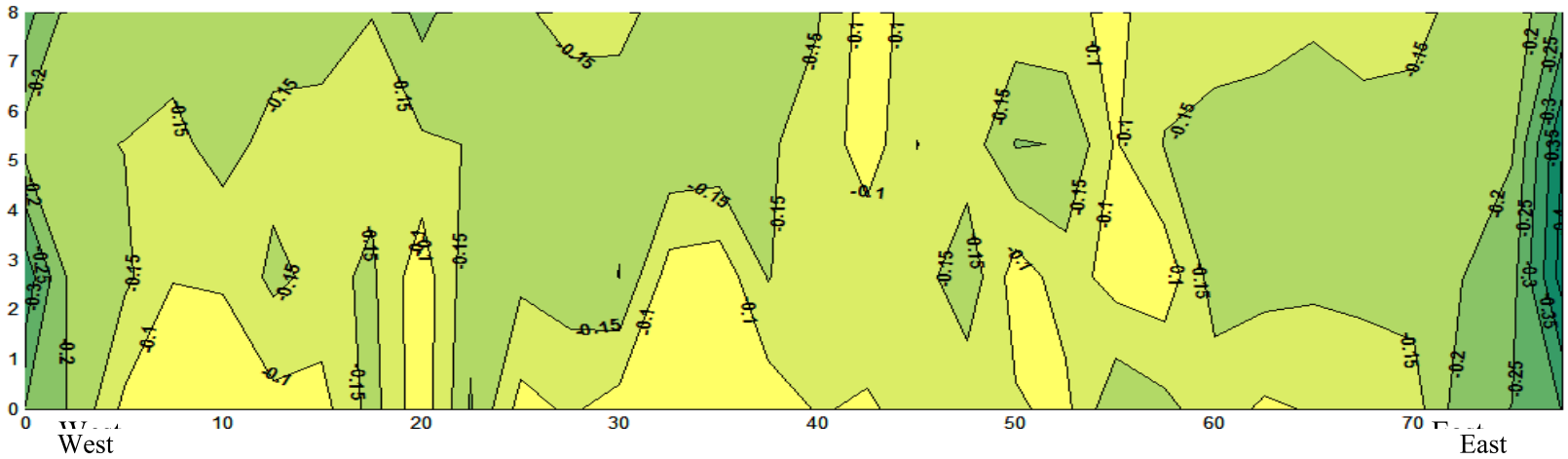

Figure E.3: Corrosion potential map for the Doniphan County Bridge (October 14, 2005)

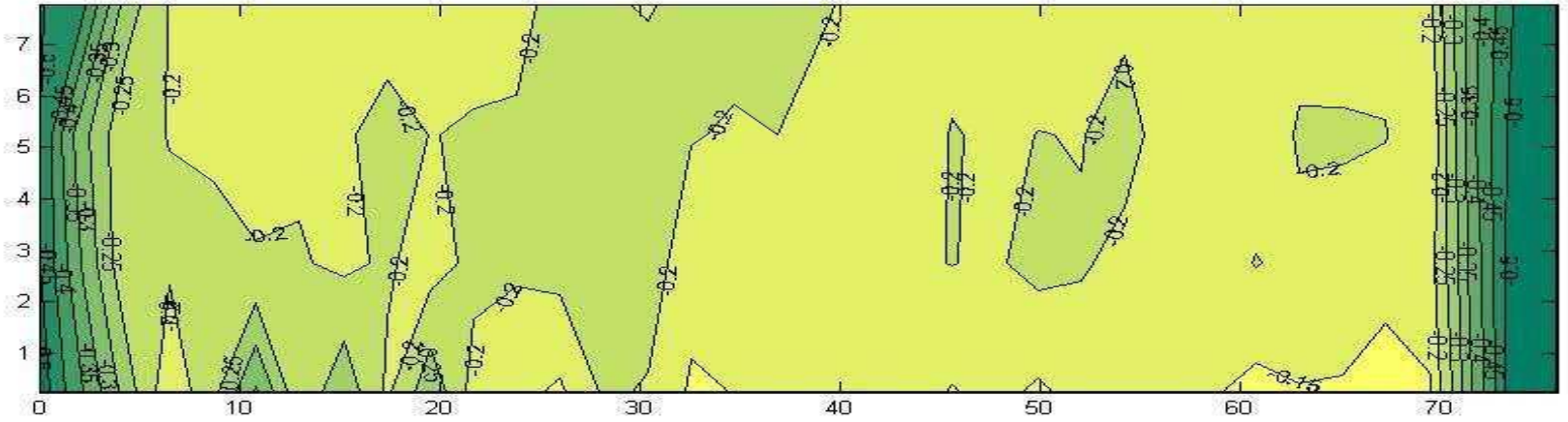

Figure E.4: Corrosion potential map for the Doniphan County Bridge (June 13, 2006)

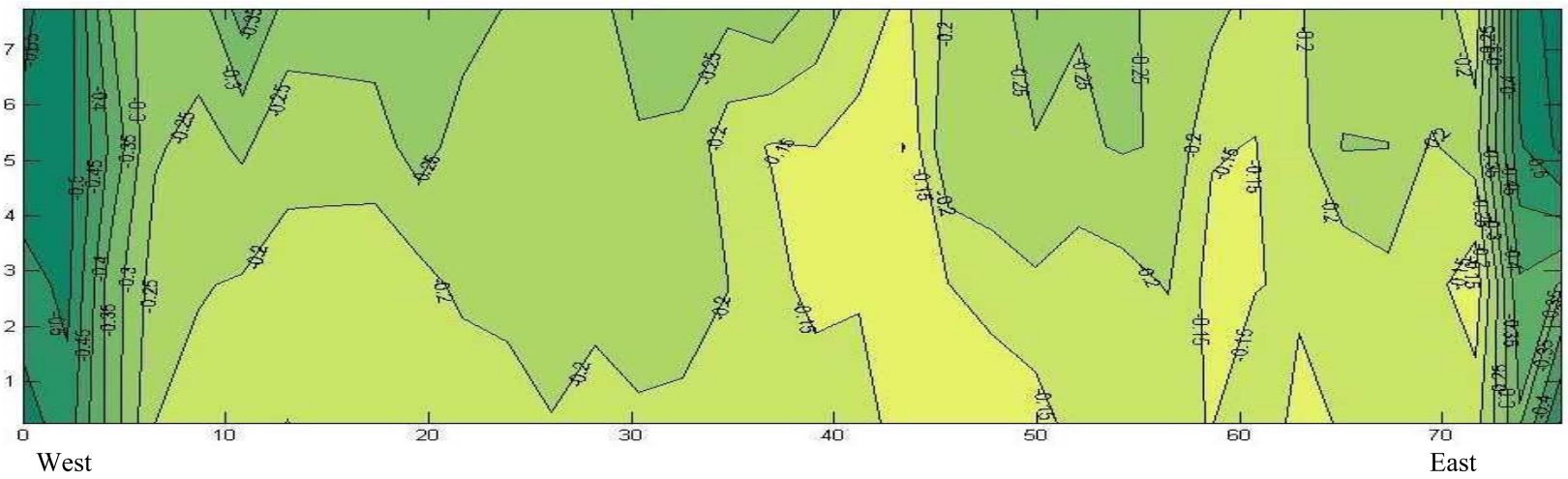

Figure E.5: Corrosion potential map for the Doniphan County Bridge (October 9, 2006)

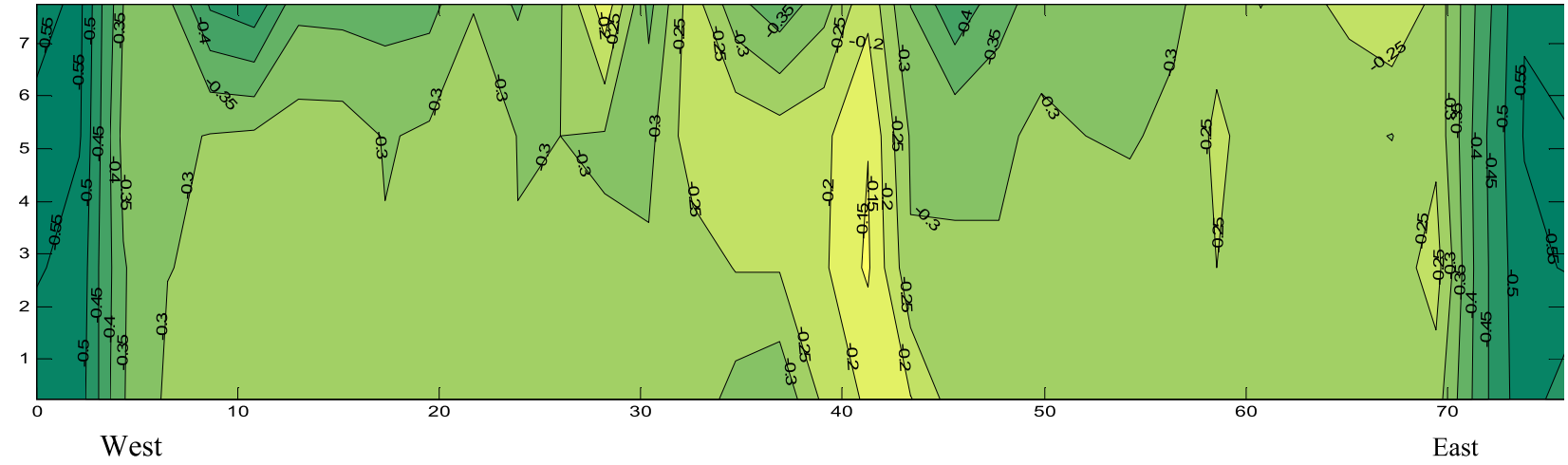

Figure E.6: Corrosion Potential Mapping for the Doniphan County Bridge (May 11, 2007)

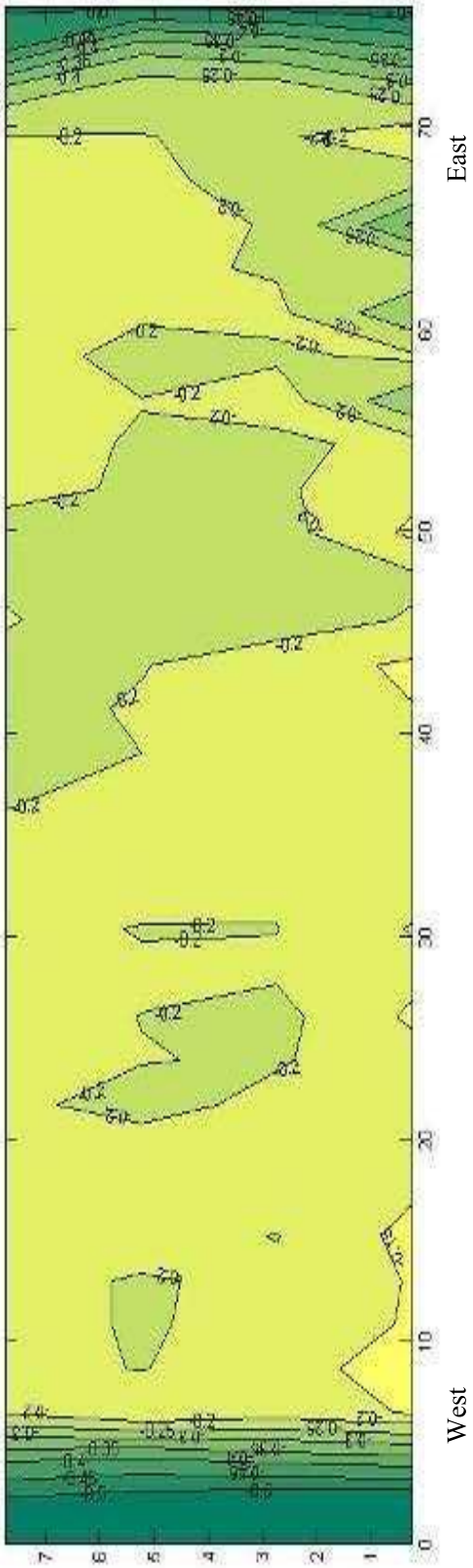

Figure E.7: Corrosion potential map for the Doniphan County Bridge (October 12, 2007)

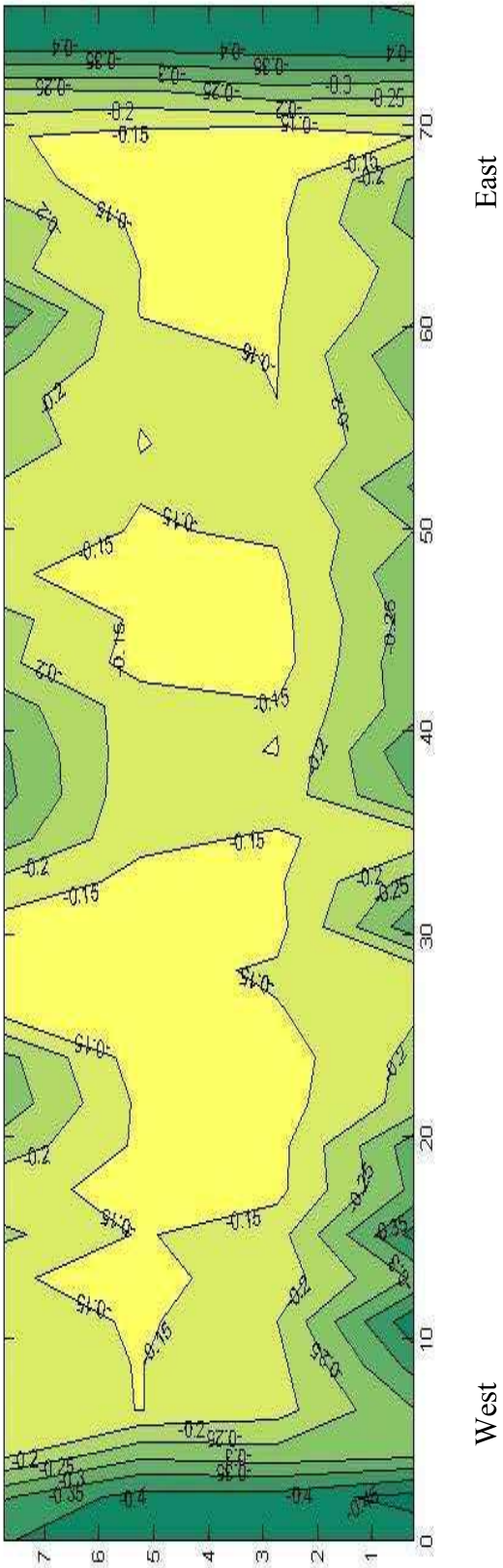

Figure E.8: Corrosion potential map for the Doniphan County Bridge (April 11, 2008)

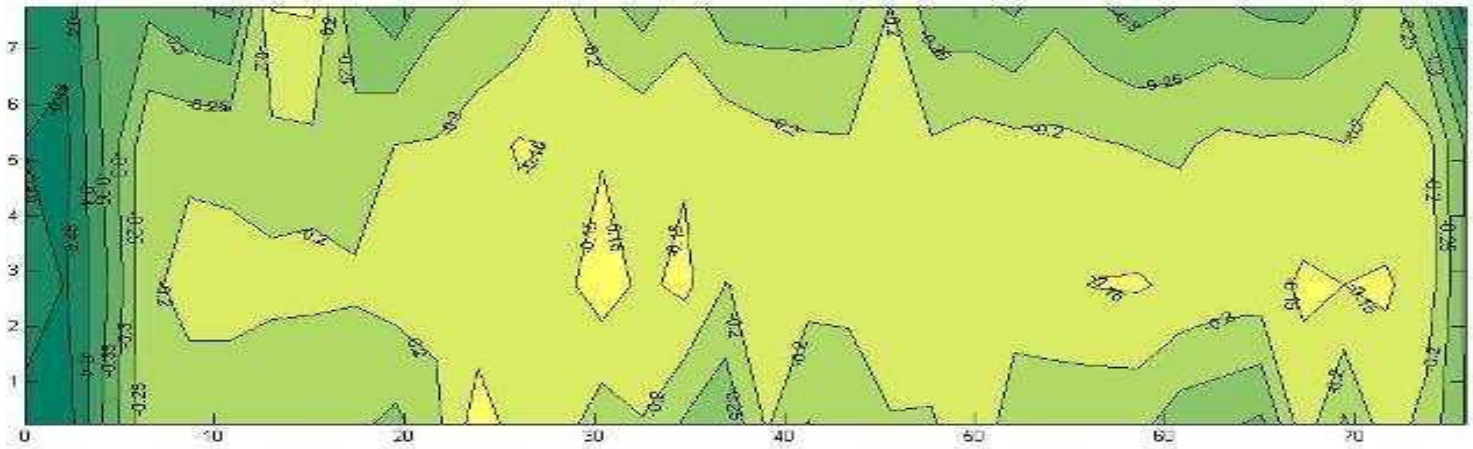

West East

Figure E.9: Corrosion potential map for the Doniphan County Bridge (October 16, 2008)

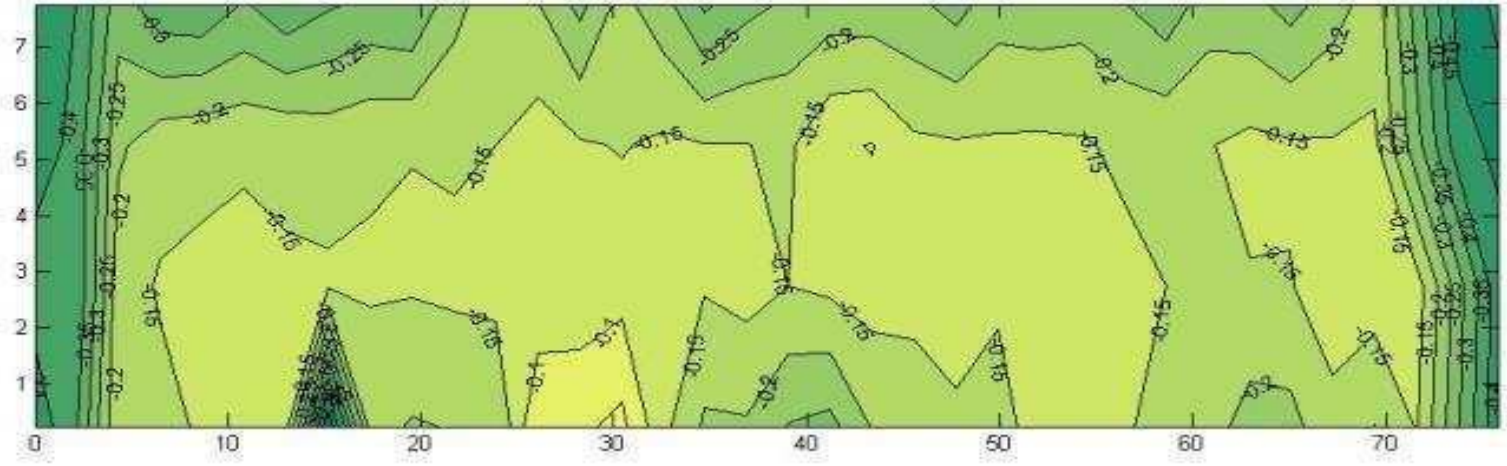

West East

Figure E.10: Corrosion potential map for the Doniphan County Bridge (May 8, 2009)

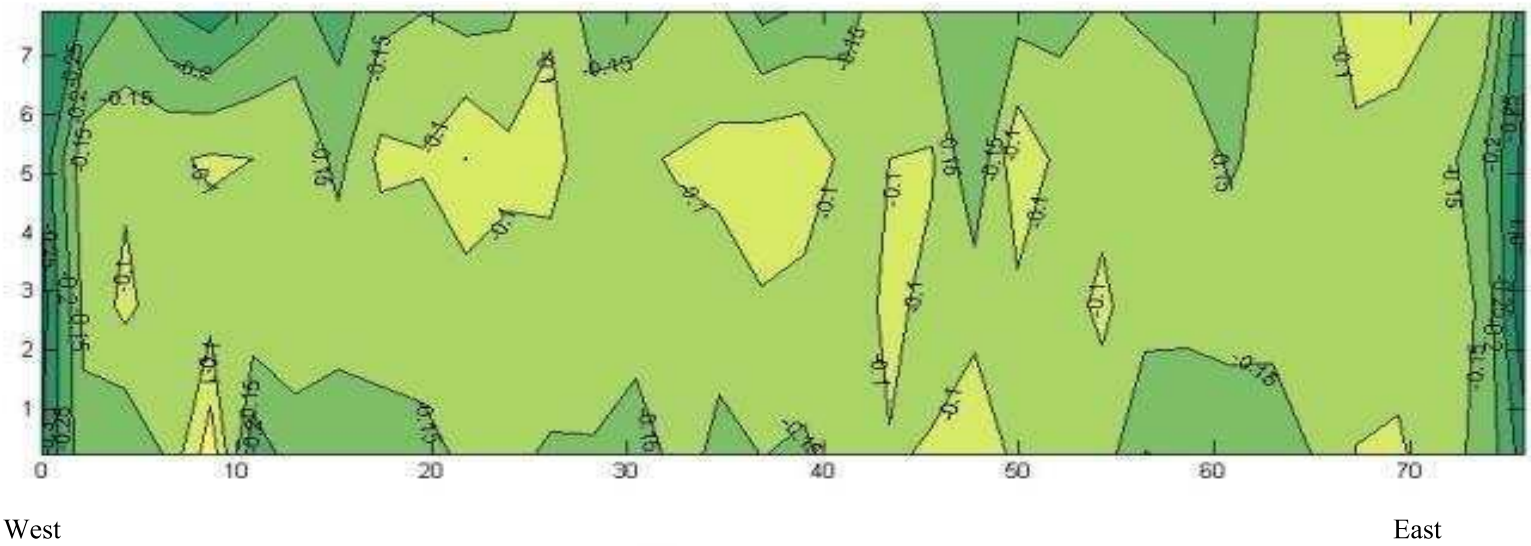

Figure E.11: Corrosion potential map for the Doniphan County Bridge (October 20, 2009)

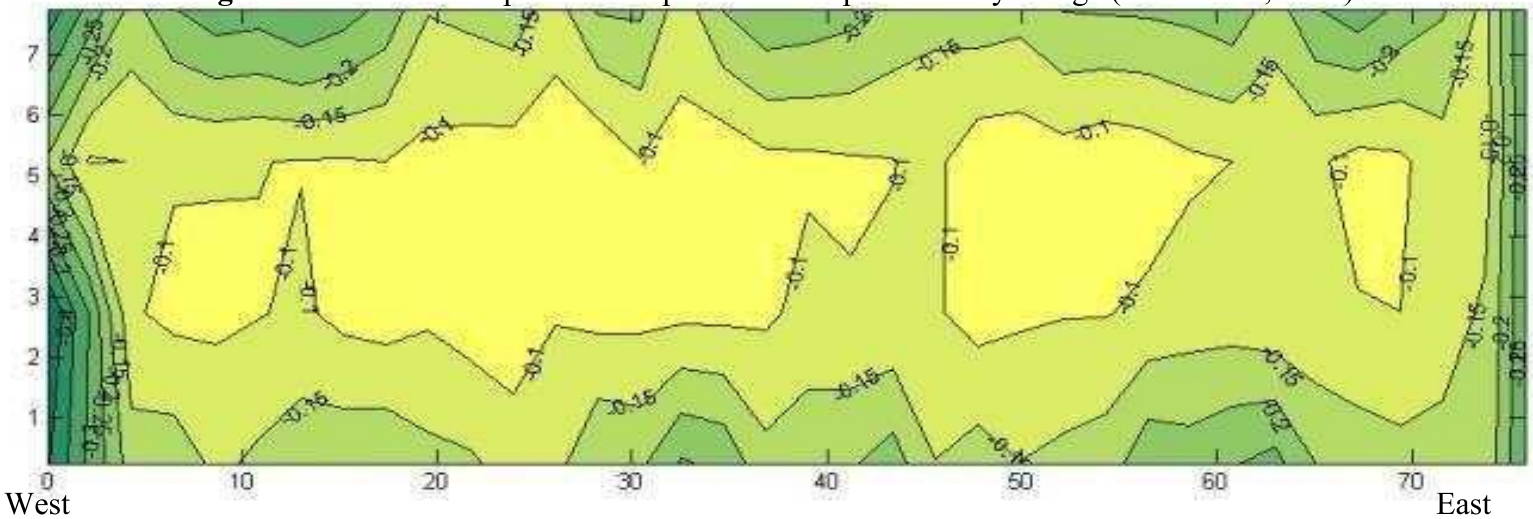

Figure E.12: Corrosion potential map for the Doniphan County Bridge (April 29, 2010)

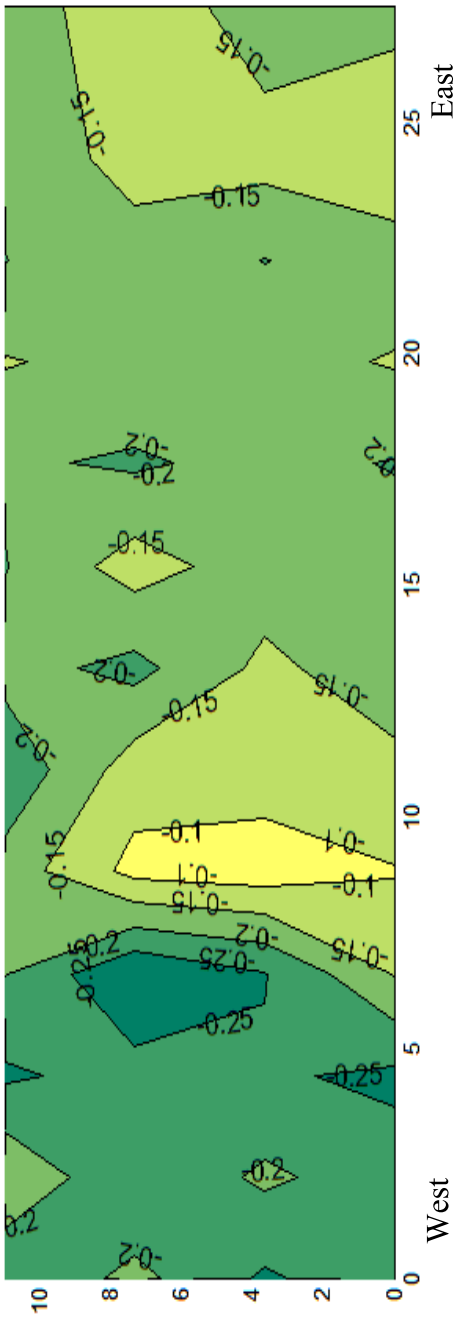

Figure E.13: Corrosion potential map for the Mission Creek Bridge (September 1, 2004)

Figure E.14: Corrosion potential map for the Mission Creek Bridge (April 1, 2005)

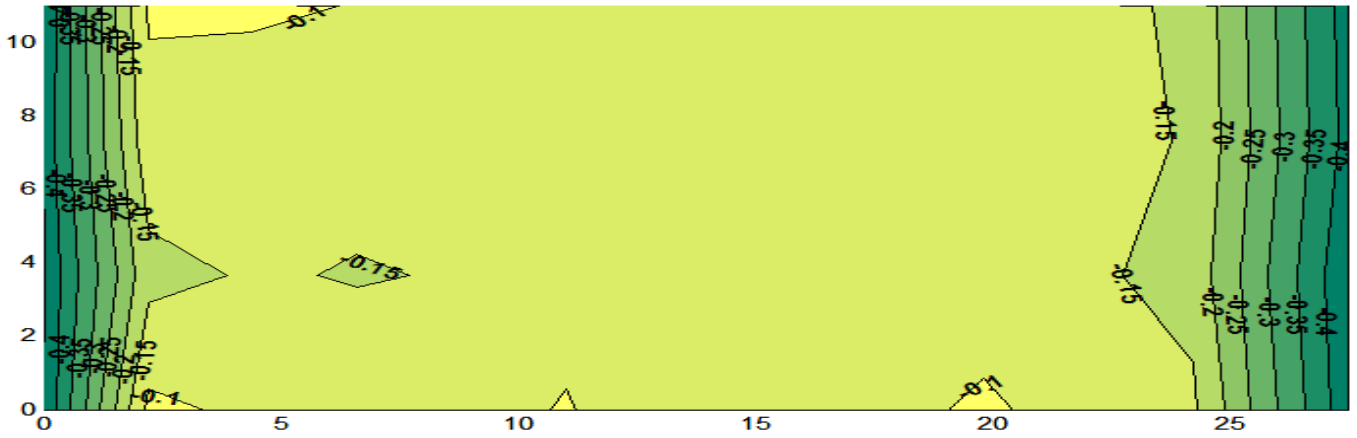

Figure E.15: Corrosion potential map for the Mission Creek Bridge (September 27, 2005)

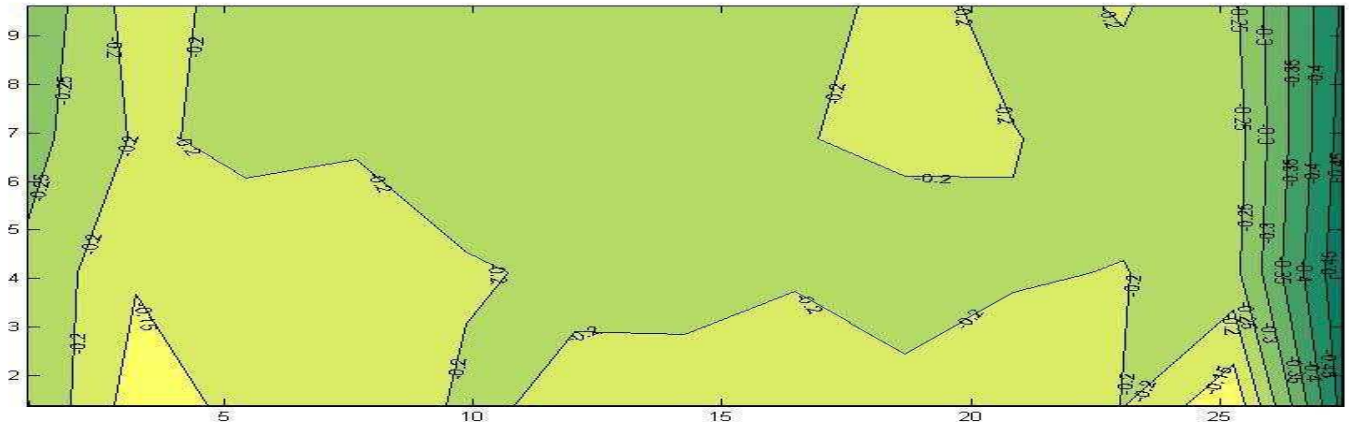

Figure E.16: Corrosion potential map for the Mission Creek Bridge (June 19, 2006)

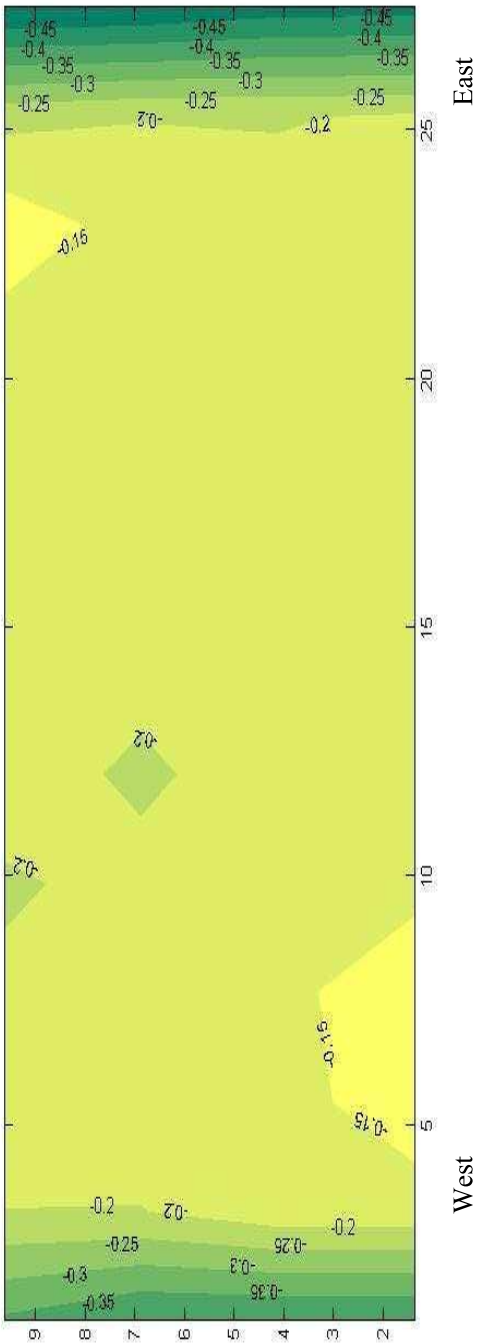

Figure E.17: Corrosion potential map for the Mission Creek Bridge (October 16, 2006)

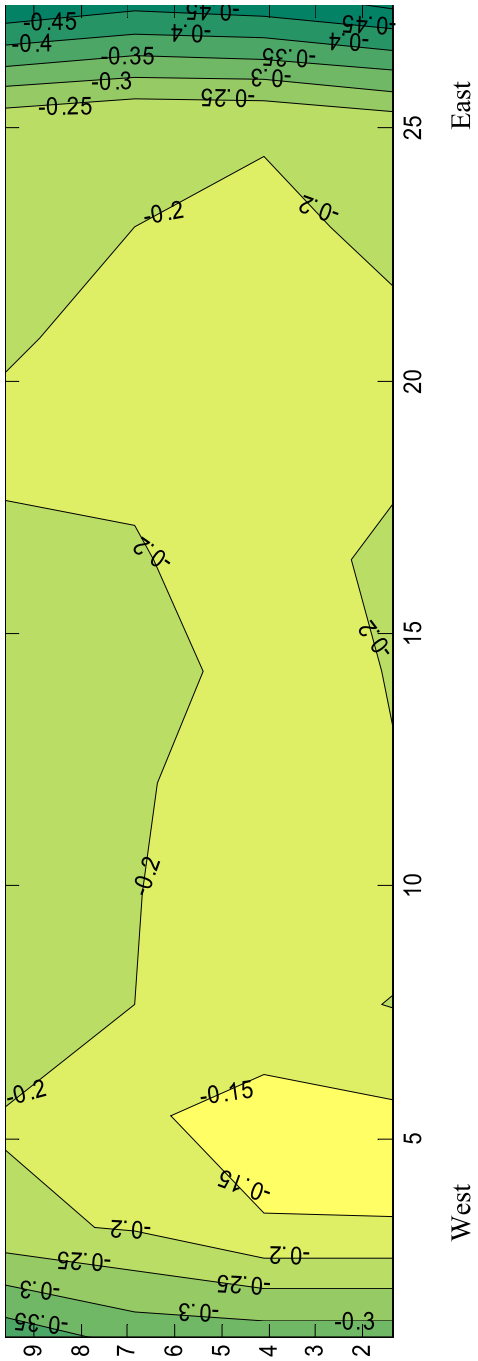

Figure E.18: Corrosion potential map for the Mission Creek Bridge (May 17, 2007)

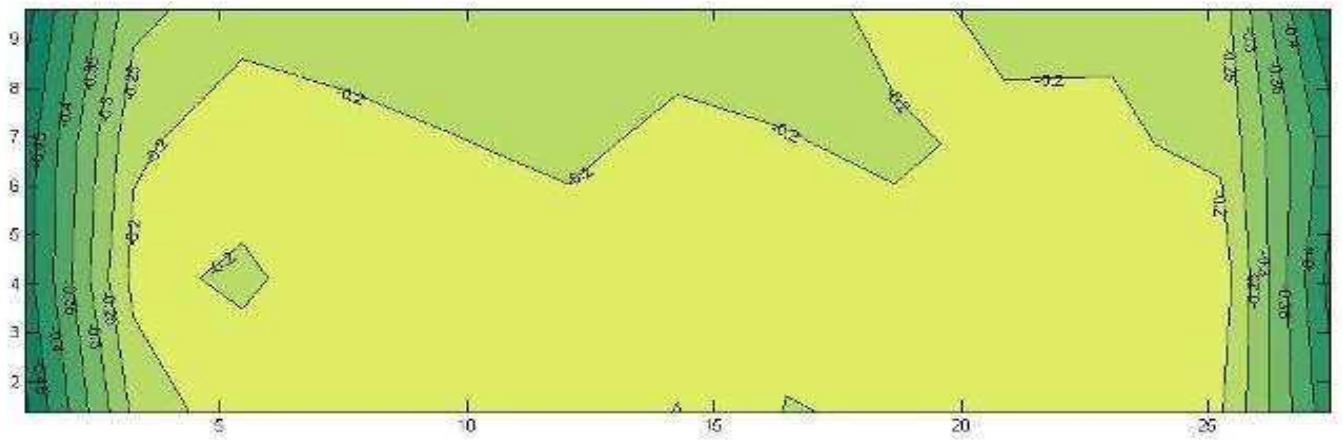

Figure E.19: Corrosion potential map for the Mission Creek Bridge (October 10, 2007)

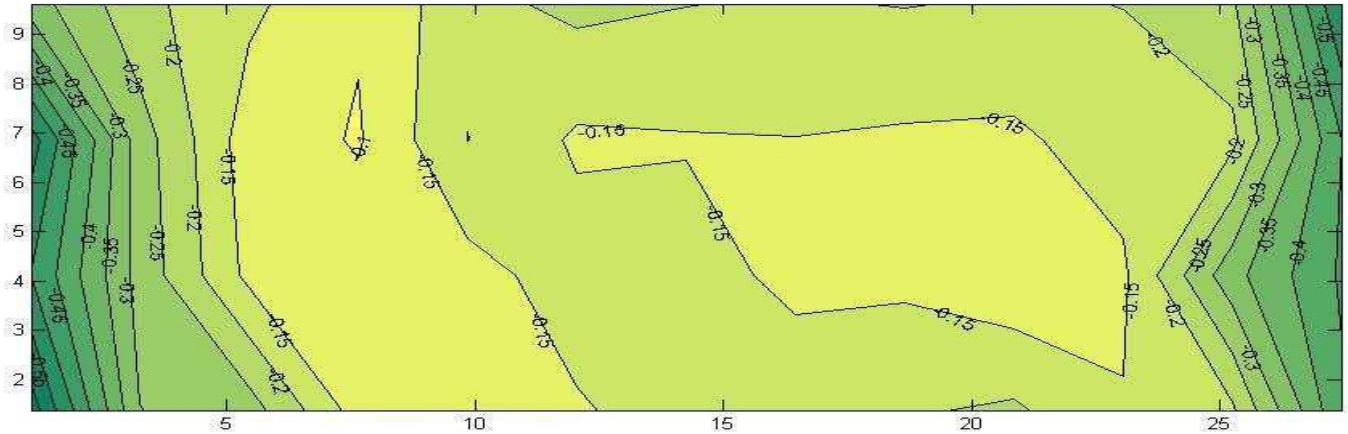

Figure E.20: Corrosion potential map for the Mission Creek Bridge (April 7, 2008)

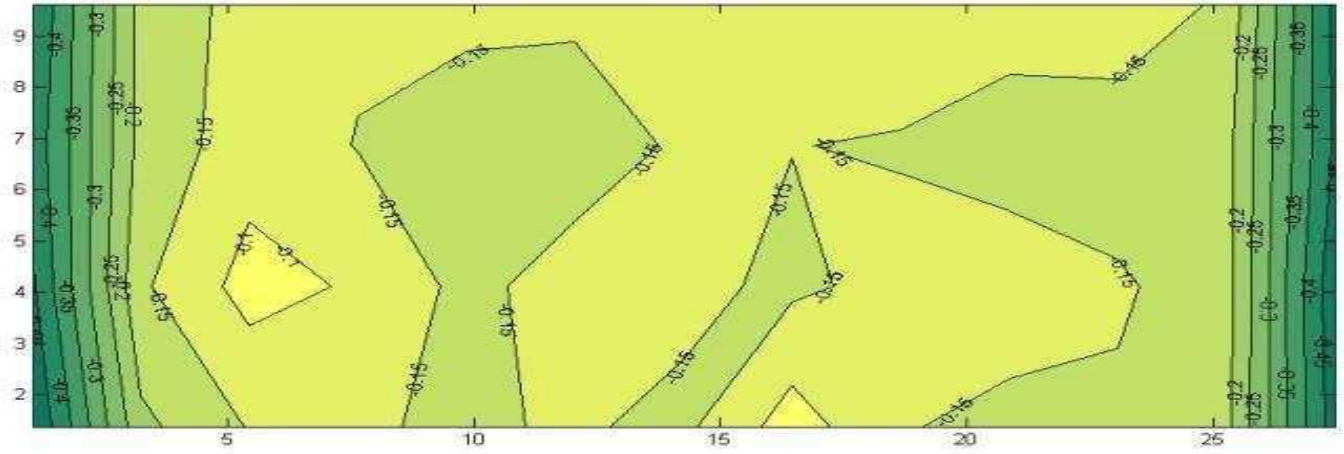

West East

Figure E.21: Corrosion potential map for the Mission Creek Bridge (October 19, 2008)

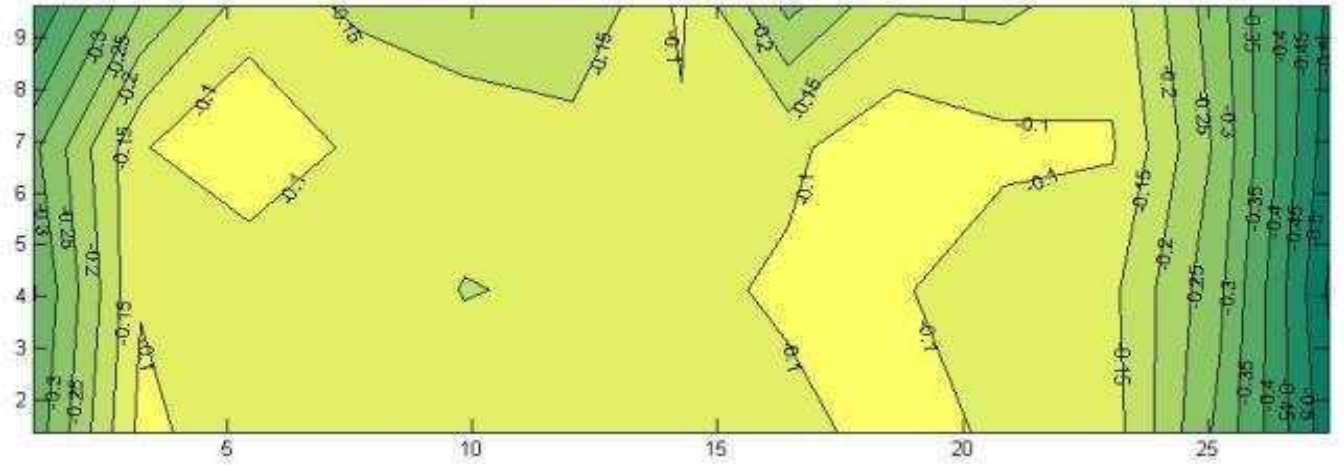

West East

Figure E.22: Corrosion potential map for the Mission Creek Bridge (May 15, 2009)

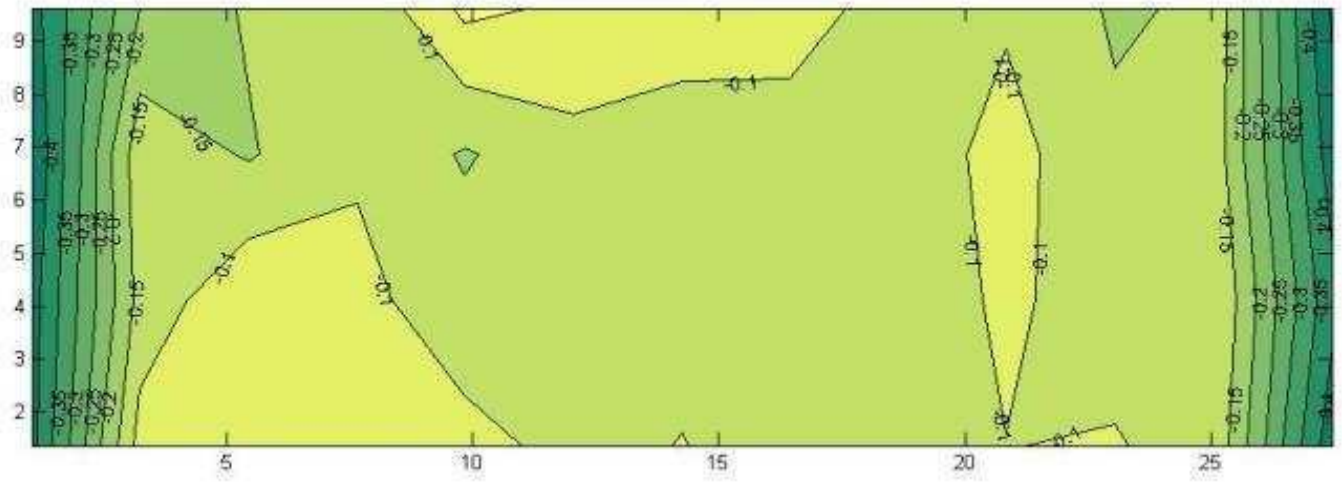

Figure E.23: Corrosion potential map for the Mission Creek Bridge (October 29, 2009)

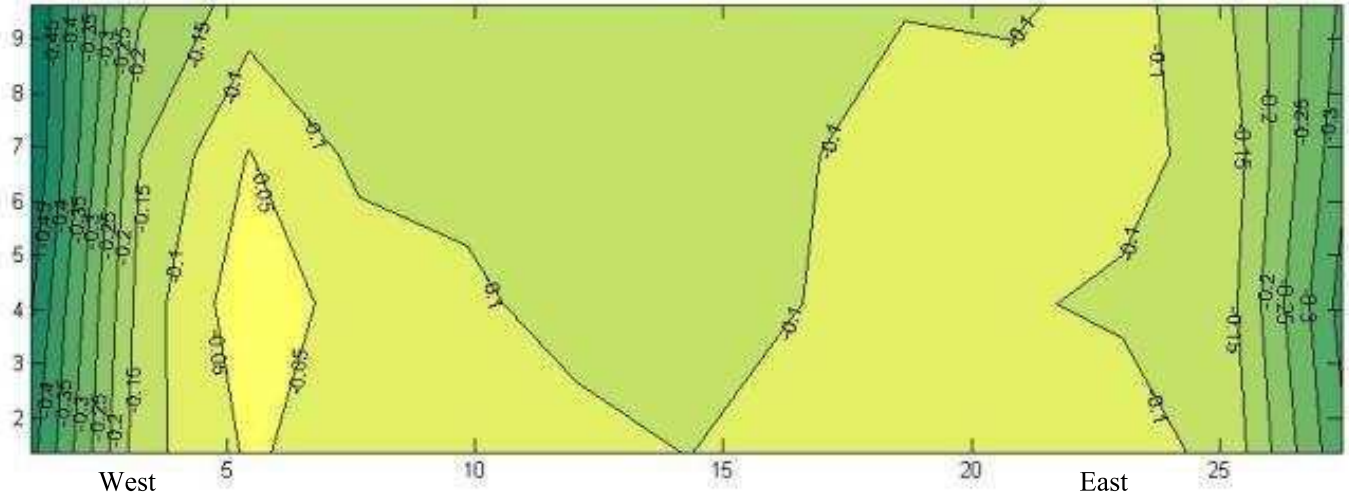

Figure E.24: Corrosion potential map for the Mission Creek Bridge (April 27, 2010)

APPENDIX F

CORROSION LOSSES FOR SPECIMENS IN THE CORROSION LOSS TO CAUSE CRACKING PROGRAM

Table F.1: Corrosion Loss, µm. Conventional and galvanized reinforcement, 12.7 mm (0.5 in.) cover.

	Specimen							
	Conv.-1	**Conv.-2**	**Conv.-3**	**Conv.-4**	**Zn-1**	**Zn-2**	**Zn-3**	**Zn-4**
Staining	4.53	6.57	10.47	5.37	58.26	32.36	23.59	27.54
Crack Initiation	8.93	9.59	14.72	8.98	70.84	40.36	32.27	40.23
Crack Width:								
0.25 mm (0.01 in.)	21.76	18.75	28.46	23.93	100.32	53.18	47.39	57.01
0.33 mm (0.013 in.)	29.62	29.00	46.12	31.82	115.90	73.57	63.80	73.22
0.41 mm (0.016 in.)	49.75	49.57	65.40	50.01	135.30	94.95	78.99	88.35
0.51 mm (0.02 in.)	62.00	71.70	101.10	57.21	167.75	111.27	92.76	109.64

Table F.2: Corrosion Loss, µm. Conventional and galvanized reinforcement, 25 mm (1 in.) cover.

	Specimen							
	Conv.-1	**Conv.-2**	**Conv.-3**	**Conv.-4**	**Zn-1**	**Zn-2**	**Zn-3**	**Zn-4**
Staining	12.31	32.79	12.97	17.59	45.99	48.60	124.19[a]	31.75
Crack Initiation	19.56	29.43	16.74	24.02	53.82	53.15	56.41	35.40
Crack Width:								
0.25 mm (0.01 in.)	30.15	43.03	42.02	39.81	83.71	60.66	77.12	42.55
0.33 mm (0.013 in.)	[b]	46.72	45.22	46.33	117.88	76.64	112.36	57.22
0.41 mm (0.016 in.)	43.54	60.05	55.82	55.59	140.77	118.77	127.80	84.10
0.51 mm (0.02 in.)	60.44	87.54	72.22	82.43	179.99	143.42	177.39	111.66

[a] Excluded from average (stastical outlier)
[b] Measurement missed

Table F.3: Corrosion Loss, µm. Conventional and galvanized reinforcement, 51 mm (2 in.) cover.

	Specimen							
	Conv.-1	**Conv.-2**	**Conv.-3**	**Conv.-4**	**Zn-1**	**Zn-2**	**Zn-3**	**Zn-4**
Staining	25.54	30.52	30.42	82.21[a]	[b]	[b]	87.11	[b]
Crack Initiation	25.54	30.52	26.89	35.91	75.93	62.20	36.11	73.77
Crack Width:								
0.25 mm (0.01 in.)	31.68	38.40	34.36	43.20	83.83	63.09	45.95	81.76
0.33 mm (0.013 in.)	42.28	50.16	42.98	60.19	102.89	82.43	51.75	90.14
0.41 mm (0.016 in.)	52.96	56.89	58.08	75.06	153.06	93.49	70.60	105.73
0.51 mm (0.02 in.)	58.94	74.93	70.27	94.54	204.68	111.74	78.55	135.77

[a] Excluded from average (stastical outlier)
[b] No surface staining observed

APPENDIX G

INDIVIDUAL PORE SOLUTION ANALYSIS DATA

Table G.1: Series 1-3 Pore Solution pH Results

Specimen	Series 1		Series 2		Series 3	
	Day 1	Day 7	Day 1	Day 7	Day 1	Day 7
Control	13.57	13.72	13.57	13.65	13.57	13.68
Rheocrete	13.76	13.90	13.65	13.76	13.68	13.81
DCI	13.24	13.44	13.18	13.35	13.18	13.40
Hycrete	13.53	13.74	13.57	13.69	13.6	13.68

Table G.2: Series 2 Pore Solution Analysis

Specimen		Ion Concentration (ppm)					
		Fluoride	Chloride	Nitrite	Sulfate	Nitrate	Phosphate
Day 1	Control	60	124	40	518	7	0
	Rheocrete	18	37	228	721	5	5
	DCI	32	77	9646	194	989	6
	Hycrete	96	59	199	2438	3	5
Day 7	Control	64	19	374	528	30	6
	Rheocrete	156	43	372	2364	9	13
	DCI	76	54	11927	908	993	0
	Hycrete	29	21	168	1403	23	5

Table G.3: Series 3 Pore Solution Analysis

Specimen		Ion Concentration (ppm)					
		Fluoride	Chloride	Nitrite	Sulfate	Nitrate	Phosphate
Day 1	Control	57	79	178	485	10	0
	Rheocrete	35	38	179	820	12	0
	DCI	15	62	9057	141	524	0
	Hycrete	22	54	311	2198	7	0
Day 7	Control	75	32	330	685	3	0
	Rheocrete	61	30	252	1140	25	0
	DCI	0	61	9597	439	663	0
	Hycrete	39	24	322	1595	26	0

Table G.4: Corrosion Inhibitor Analysis

Inhibitor	Ion Concentration (ppm)					
	Fluoride	Chloride	Nitrite	Sulfate	Nitrate	Phosphate
Rheocrete	47	0	29	3	0	0
DCI	17	0	49089*	11	0	0
Hycrete	8	0	64	5	6	0

*Extrapolated